UNIVERSIDADE FEDERAL DE MINAS GERAIS
Instituto de Geociências
Programa de Pós-Graduação em Geologia

Cristina Santos Araujo

MAGMATISMO OROGÊNICO BRASILIANO E SUAS RELAÇÕES COM O COMPLEXO NOVA VENÉCIA NO EXTREMO LESTE DO ORÓGENO ARAÇUAÍ, BRASIL

OROGENIC MAGMATIC EVENTS AND THEIR RELATIONS WITH THE NOVA VENÉCIA COMPLEX IN THE SOUTHEASTERN SECTOR OF THE ARAÇUAÍ OROGEN, BRAZIL

Belo Horizonte
2023

Cristina Santos Araujo

MAGMATISMO OROGÊNICO BRASILIANO E SUAS RELAÇÕES COM O COMPLEXO NOVA VENÉCIA NO EXTREMO LESTE DO ORÓGENO ARAÇUAÍ, BRASIL

OROGENIC MAGMATIC EVENTS AND THEIR RELATIONS WITH THE NOVA VENÉCIA COMPLEX IN THE SOUTHEASTERN SECTOR OF THE ARAÇUAÍ OROGEN, BRAZIL

Versão final de Tese apresentada ao Programa de Pós-Graduação em Geologia da Universidade Federal de Minas Gerais como requisito parcial para obtenção do título de Doutora em Geologia.

Área de concentração: Geologia Regional

Orientador: Prof. Dr. Antônio Carlos Pedrosa Soares (UFMG)

Coorientadora: Prof(a). Dr(a). Mahyra Ferreira Tedeschi (UFMG)

Belo Horizonte
2023

A663m
2023

Araujo, Cristina Santos.

Magmatismo Orogênico Brasiliano e suas relações com o Complexo Nova Venécia no extremo leste do Orógeno Araçuaí, Brasil = Orogenic Magmatic Events and their relations with the Nova Venécia complex in the southeastern sector of the Araçuaí Orogen, Brazil [manuscrito] / Cristina Santos Araujo. – 2023.

432 f., enc. il. (principalmente color.)

Orientador: Antônio Carlos Pedrosa Soares.

Coorientadora: Mahyra Ferreira Tedeschi.

Tese (doutorado) – Universidade Federal de Minas Gerais, Instituto de Geociências, 2023.

Área de concentração: Geologia Regional.

Bibliografia: f. 131-141.

Inclui apêndices.

1. Tempo geológico – Teses. 2. Isótopos – Teses. 3. Magmatismo – Brasil – Teses. I. Pedrosa-Soares, Antonio Carlos. II. Tedeschi, Mahyra. III. Universidade Federal de Minas Gerais. Instituto de Geociências. IV. Título.

CDU: 550.93(81)

Ficha catalográfica elaborada por Elisabete Quatrini Vieira – CRB6 2210
Biblioteca “Vitória Pedersoli”, Instituto de Geociências da UFMG

UNIVERSIDADE FEDERAL DE MINAS GERAIS

PROGRAMA DE PÓS-GRADUAÇÃO EM GEOLOGIA DO IGC-UFMG

FOLHA DE APROVAÇÃO

Magmatismo Orogênico Brasiliano e suas relações com o Complexo Nova Venécia no extremo leste do Orógeno Araçuaí, Brasil

CRISTINA SANTOS ARAUJO

Tese submetida à Banca Examinadora designada pela Coordenação do Colegiado do Programa de Pós-Graduação em GEOLOGIA do IGC-UFMG, como requisito para obtenção do grau de Doutor(a) em GEOLOGIA, área de concentração GEOLOGIA REGIONAL, pelo Programa de Pós-graduação em Geologia do Instituto de Geociências da Universidade Federal de Minas Gerais.

Aprovada* em 11 de maio de 2023, pela banca constituída pelos membros:

*Tese aprovada com distinção.

Prof. Dr. Antonio Carlos Pedrosa Soares – Orientador
UFMG

Prof. Dr. Tiago Amâncio Novo
UFMG

Profa. Dra. Valderez Pinto Ferreira
UFPE

Prof. Dr. Moacir José Buenano Macambira
UFPA

Profa. Dra. Caroline Cibele Vieira Soares
UFES

Belo Horizonte, 11 de maio de 2023.

Aos meus antepassados e família, em especial aos meus pais, Valter e Dalmes, e aos meus irmãos.
A minha querida sobrinha, Mariana.

AGRADECIMENTOS

Agradeço a todos que, de alguma forma, me ajudaram a realizar este trabalho, em especial:

A minha família, pela vida, apoio, incentivo e compreensão;

Ao meu eterno orientador, Antônio Carlos Pedrosa Soares, pela confiança, suporte, apoio, ajuda, amizade e, principalmente, pela oportunidade de trabalharmos juntos;

A minha coorientadora, Mahyra Ferreira Tedeschi, pela convivência, aprendizado, confiança e ajuda fornecidos;

Aos meus amigos e colegas da UFMG, pelos momentos de companheirismo, apoio, incentivo e discussões construtivas, em especial, à Mahyra Tedeschi, Paula Serrano, Raíssa Santiago, Laura Wisniowski, Jorge Roncato, Pedro Leonardo (Petrus), Leandro Amaral, Carolina Deluca, Ramon Aranda, Fernando Pacheco;

Aos colegas do Departamento de Geologia da Universidade Federal de Ouro Preto, pelo acolhimento, agradável convivência, compartilhamento de conhecimento e pela amizade construída durante os dias que estive em Ouro Preto, em especial, à Ana Alkmim, Débora Vasconcelos, Lorena Martins, Edgar Medeiros Júnior e Cristiano Lana;

Ao William Campos por sua paciência, auxílio, eficiência e cordialidade;

Aos amigos e funcionários do CPMTC/UFMG, em especial ao Carlos, Jhonny, Hélvio e Denise pela ajuda, amizade e disposição;

A todos os meus amigos e colegas que torceram por mim e me incentivaram, compreendendo minhas ausências;

Ao Programa de Pós-graduação de Geologia da Universidade Federal de Minas Gerais (UFMG);

À Pró-reitoria de Pós-graduação (PRPg) da UFMG;

À Companhia de Desenvolvimento de Minas Gerais (CODEMGE), ao Conselho Nacional de Desenvolvimento Científico e Tecnológico (CNPq) e ao Laboratório de Mapeamento Geológico e Geotectônica do Centro de Pesquisa Professor Manoel Teixeira da Costa (CPMTC-UFMG) pelo apoio financeiro;

Ao apoio financeiro vinculado ao projeto de pesquisa científica “Evolução e Recursos Minerais do Orógeno Araçuaí” da agência CNPq;

À Coordenação de Aperfeiçoamento de Pessoal de Nível Superior (CAPES) pela bolsa concedida. O presente trabalho foi realizado com apoio da Coordenação de Aperfeiçoamento de Pessoal de Nível Superior, Brasil - CAPES - Código de Financiamento 001

E, acima de tudo, agradeço à Deus!

ACKNOWLEDGEMENTS

I would like to thank everyone who helped me in one way or another to complete this work, especially:

My family, for life, support, encouragement, and understanding;

To my eternal supervisor, Antônio Carlos Pedrosa Soares, for his trust, support, help, friendship, and, mainly, for the opportunity to work together;

To my co-supervisor, Mahyra Ferreira Tedeschi, for the coexistence, learning, confidence, and help provided;

To my friends and colleagues at UFMG, for the moments of companionship, support, encouragement, and constructive discussions, especially Mahyra Tedeschi, Paula Serrano, Raíssa Santiago, Laura Wisniowski, Jorge Roncato, Pedro Leonardo (Petrus), Leandro Amaral, Carolina Deluca, Ramon Aranda, Fernando Pacheco;

To colleagues in the Department of Geology at the Federal University of Ouro Preto, for their welcome, pleasant coexistence, sharing of knowledge, and for the friendship built during the days I was in Ouro Preto, especially Ana Alkmim, Débora Vasconcelos, Lorena Martins, Edgar Medeiros Junior, and Cristiano Lana;

To William Campos for his patience, assistance, efficiency, and cordiality;

To friends and staff at CPMTC/UFMG, especially Carlos, Jhonny, Hélvio, and Denise for their help, friendship and disposition;

To all my friends and colleagues who cheered for me and encouraged me, understanding my absences;

To the Post-Graduate Program in Geology at the Federal University of Minas Gerais (UFMG);

To the Companhia de Desenvolvimento de Minas Gerais (CODEMGE), the Conselho Nacional de Desenvolvimento Científico e Tecnológico (CNPq), and the Laboratório de Mapeamento Geológico e Geotectônica do Centro de Pesquisa Professor Manoel Teixeira da Costa (CPMTC-UFMG) for financial support.

To the Coordenação de Aperfeiçoamento de Pessoal de Nível Superior (CAPES) for the scholarship granted. This work was also carried out with the support of the CAPES, Brazil - Financing Code 001.

And above all, I thank God!

"To reason without data is nothing but delusion."
James Hutton (1788)

"*Unraveling continental arc evolution from petrologic, geochemical, and tectonic perspectives is challenging and has great significance for understanding the formation and evolution of continental crust.*"
Mihai Ducea et al. (2015)

RESUMO

O Sistema Orogênico Araçuaí – Congo Ocidental constitui um orógeno confinado a um grande embainhamento do Cráton São Francisco – Congo, amalgamados no Paleocontinente Gondwana ao final do Neoproterozoico. Uma das características mais marcantes do orógeno Araçuaí é a longa sucessão de eventos magmáticos (ca. 630 - 480 Ma) associados aos estágios orogênicos. Localizada a extremo leste deste orógeno, a área em estudo inclui rochas dos estágios orogenéticos pré-, sin- e pós-colisionais que intrudem em migmatitos paragnáissicos do Complexo Nova Venécia, interpretada como representante da bacia de retroarco. Nova investigação petrológica, de química de rocha total e análises isotópicas (U-Th-Pb e Lu-Hf por LA-ICPMS em zircão e Sm-Nd em rocha total) foram realizadas em rochas desses estágios e em rochas do complexo Nova Venécia. Nesse contexto, as suítes Santa Tereza e Jequitibá representam a expressão mais oriental do magmatismo pré-colisional associado ao Arco Magmático Rio Doce, enquanto as rochas da suíte Ataléia representam o estágio sin-colisional e os plútons Aracê – Pedra Azul, Vitória e Mestre Álvaro registram o magmatismo pós-colisional. Com uma idade Concórdia de 612 ± 3 Ma para a suíte Santa Tereza e 594 ± 3 Ma para a suíte Jequitibá, os isotópicos representam o registro de magmatismo pré-colisional menos isotopicamente envolvido neste orógeno (suíte Santa Tereza: $\varepsilon Hf_{(612)}$ de +2,3 a -4,8 com T_{DM} de 1,33 a 1,65 Ga e $\varepsilon Nd_{(612Ma)}$ de -0,06 a -7,05 com T_{DM} de 1,4 a 2,04; suíte Jequitibá: $\varepsilon Hf_{(t)}$ de -1,7 a -36,4 com T_{DM} de 1,33 a 3,21 Ga e $\varepsilon Nd_{(594)}$ de -6,67 a -8,8 com T_{DM} de 1,64 a 1,87). Essas suítes consistem em intrusões do tipo I, intermediárias a ácidas, metaluminosas a levemente peraluminosas, com composições principalmente magnesianas e cálcicas a alcalino-cálcicas, com porções de rochas contendo ortopiroxênio e rochas gabroicas subordinadas. Os dados do granito Ataléia (583 ± 3 Ma; $\varepsilon Hf_{(t)}$ de -3,2 a -8,1, T_{DM} de 1,42 a 1,64 Ga) e dos paragnaisses migmatíticos do complexo Nova Venécia (582 ± 7 a 2363 ± 26 Ma – com picos de idades em 617 ± 4 Ma (68%), 719 ± 22 Ma (14%), 839 ± 46 Ma (8%) e 922 ± 31 Ma (10%); $\varepsilon Hf_{(t)}$ de +4,1 a -39,2, T_{DM} de 1,20 a 3,47 Ga) sugerem proximidade da bacia retroarco à margem continental e que essa bacia recebeu significativa quantidade de sedimentos do Arco Magmático Rio Doce. Além disso, dados das rochas pós-colisionais na área (Aracê – Pedra Azul: 523 ± 2 Ma, $\varepsilon Hf_{(t)}$ de -18,6 a -23,8, T_{DM} de 2,25 a 2,47 Ga; Vitória: 505 ± 1 Ma, $\varepsilon Hf_{(t)}$ de -7,4 a -10,3, T_{DM} de 1,58 a 1,71 Ga; Mestre Álvaro: 527 ± 2 Ma, $\varepsilon Hf_{(t)}$ de -0,7 a -8,8, T_{DM} de 1,27 a 1,66 Ga) indicam hibridização à altas temperaturas envolvendo as rochas encaixantes na petrogênese pós-colisional. As rochas estudadas refletem uma seção crustal composta de intrusões intermediárias a ácidas do tipo I, metagranitos do tipo S e rochas paragnaisses metamorfisados sob fácies anfibolito a granulito, comumente migmatizadas. Os resultados, comparados com uma vasta compilação bibliográfica, sugerem que um arco magmático provavelmente se desenvolveu na região com uma fase inicial extensional seguida por uma fase compressional e migração do arco para oeste.

Palavras-chave: Geocronologia U-Pb; Isotopos Hf-Nd; Margem ativa; Magmatismo orogênico; Orógeno Brasiliano; Orógeno Araçuaí.

ABSTRACT

The Araçuaí – West Congo Orogenic System constitutes a confined orogen to a large sheath of the São Francisco – Congo Craton, amalgamated into the Gondwana Paleocontinent at the end of the Neoproterozoic. A long-lasting succession of granite production events (ca. 630 – 480 Ma) associated to the orogenic stages is a remarkable feature of the Araçuaí orogen. Located in the easternmost sector, the study area includes rocks of pre-, sin-, and post-collisional orogenic stage intruded in the Nova Venécia migmatitic paragneisses, interpreted as an arc-related basin. The new petrological investigation, bulk-rock chemistry, and isotopic analyses (zircon U-Th-Pb and Lu-Hf by LA-ICPMS, and whole-rock Sm-Nd) were carried out in representative rocks from the orogenic magmatism and the Nova Venécia complex. In this context, Santa Tereza and Jequitibá suites represent the more eastern expression of pre-collisional magmatism associated with the Rio Doce magmatic arc, while Ataléia suite represent the syn-collisional rocks, and the Aracê – Pedra Azul, Vitória, and Mestre Álvaro plutons record the post-collisional event. The Santa Tereza and Jequitibá suites yield a concordant age of 612 ± 3 Ma and 594 ± 3 Ma, respectively. Their isotopic data represent the least evolved magmatism record in this orogen (Santa Tereza suite: $\varepsilon Hf_{(612)}$ of +2.3 to -4.8 with T_{DM} of 1.33 to 1.65 Ga and $\varepsilon Nd_{(612Ma)}$ of -0.06 to -7.05 with T_{DM} of 1.4 a 2.04; Jequitibá suite: $\varepsilon Hf_{(594)}$ of -1.7 to -36.4 with T_{DM} of 1.33 to 3.21 Ga and $\varepsilon Nd_{(594)}$ of -6.67 to -8.8 with T_{DM} of 1.64 to 1.87). These suites consist of I-type intermediate to acid intrusions, metaluminous to slightly peraluminous, mainly magnesian and calcic to alkali-calcic compositions, with portions of Opx-bearing and subordinate gabbroic rocks. Data from the S-type Ataléia granite (583 ± 3 Ma; $\varepsilon Hf_{(t)}$ -3.2 to -8.1, T_{DM} ages from 1.42 to 1.64 Ga) and Nova Venécia migmatitic paragneisses (582 ± 7 to 2363 ± 26 Ma - with age peaks at 617 ± 4 Ma (68%), 719 ± 22 Ma (14%), 839 ± 46 Ma (8%), and 922 ± 31 Ma (10%); $\varepsilon Hf_{(t)}$ +4.1 to -39.2, T_{DM} ages from 1.20 to 3.47 Ga) suggest the proximity of the Nova Venécia basin to the continental margin and that this basin received significant sediment from the Rio Doce magmatic arc. Furthermore, the dataset for the post-collisional intrusions (Aracê – Pedra Azul pluton: 523 ± 2 Ma, $\varepsilon Hf_{(t)}$ -18.6 to -23.8, T_{DM} ages from 2.25 to 2.47 Ga; Vitória pluton: 505 ± 1 Ma, $\varepsilon Hf_{(t)}$ -7.4 to -10.3, T_{DM} ages from 1.58 to 1.71 Ga; Mestre Álvaro pluton: 527 ± 2 Ma, $\varepsilon Hf_{(t)}$ -0.7 to -8.8, T_{DM} ages from 1.27 to 1.66 Ga) indicates magma hybridization at high temperature, involving country rocks in the petrogenesis of post-collisional intrusions. The rocks studied reflect a crustal section composed of I-type intermediate to acid intrusions, S-type metagranites, and paragneiss framework rocks metamorphosed under amphibolite to granulite facies, commonly migmatized. Compared to a wide compiled dataset, our data suggest that a magmatic arc is likely to have developed in the region with an initial extensional phase followed by a compressional phase and an arc migration westward.

Keywords: U-Pb geochronology; Hf-Nd isotopes; slab retreat; active margin; Brasiliano orogeny; Orogenic magmatism; Araçuaí orogen.

LIST OF ILLUSTRATIONS

Figure 1.1: Araçuaí orogen location and the region focused on this thesis (red rectangle) in the context of the Western Gondwana Paleocontinent (modified from Pedrosa-Soares et al. 2008). 20

Figure 1.2: Geotectonic Map of the State of Espírito Santo (Vieira and Menezes 2015). B) Study region focused on this thesis (modified from Vieira and Menezes 2015). 21

Figure 1.3: Studied area localization and main access roads. 23

Figure 2.1 Schematic cross section of extensional and compressional tectonic through a continental subduction system (from Ducea et al., 2015a).....29

Figure 2.2 (A) The Mantiqueira Province, other Brasiliano-Pan-African orogenic systems, and the related cratons in the context of West Gondwana (modified from Alkmim et al., 2006). (B) The Araçuaí – West Congo Orogenic System and adjacent cratons in the context of West Gondwana (modified from Alkmim et al., 2006). (C) Simplified geological map of the Araçuaí orogen (modified from Tedeschi et al., 2016). 32

Figure 2.3 Simplified geological map of the study area showing the local of samples (modified from Leite et al., 2004; Silva et al., 2004; Vieira and Menezes, 2015). 38

Figure 3.1 (A) Geotectonic setting of Araçuaí-Ribeira orogenic system (AROS), other Brasiliano-Pan-African orogenic systems, and the related cratons in West Gondwana (modified from Alkmim et al., 2006). (B) Brasiliano orogenic systems (blue color) exposed in the Brazilian territory and the related cratons (pink color) in the South American Platform context (modified from Cordani et al., 2016). Orogenic systems: Mantiqueira system - Araçuaí (Ar), Ribeira (Rb) and Dom Feliciano (DF) belts; Tocantins system (T) - Araguaia, Paraguai and Brasília (B) belts; Borborema system (Bo) - Rio Preto, Riacho do Pontal and Sergipano belts; Pan-African system – Damara (D), Gariep (G), Kaoko (K) and West Congo (WC). Cratons: Amazonian (Am), São Francisco (SFC), Paranapanema (Pp); Luís Alves (LA), Rio de La Plata (RP), São Luiz (SL); Parnaíba (Pr). (C) Simplified geological map of the AROS (modified from Santiago et al., 2020, after Pedrosa-Soares et al., 2011, Tedeschi et al., 2016, Degler et al., 2018; and Peixoto et al., 2017). Legend: 1 - Cenozoic cover (TQ); 2 - post-collisional plutonism (ca. 540–480 Ma); 3: collisional plutonism (ca. 585–540 Ma); 4: Rio Doce magmatic arc (ca. 630–585 Ma); 5: Neoproterozoic ophiolite-bearing rock assemblages; 6: Rio Negro – Serra da Prata arc domain (Rio Negro and Serra da Prata magmatic arcs, and related units; ca. 860 Ma–620

Ma); 7: Neoproterozoic metasedimentary and metavolcanic successions; 8: Tonian and Cryogenian rift-related magmatic rocks; 9: Southern Brasília belt; 10: Pre-Neoproterozoic units; CTB: Central Tectonic Boundary; CFTD: Cabo Frio tectonic domain.....47

Figure 3.2 Simplified geological map of the study area, showing the analyzed samples locations (modified from Leite et al., 2004; Silva et al., 2004; Vieira and Menezes, 2015). *Zircon U-Pb and Lu-Hf isotopic analyses by Araujo et al. (2020).....53

Figure 3.3 Photos and photomicrographs (under transmitted light and polarized light) showing mineralogical and textural features. CA-08 sample: A, B, C. (A) Greenish gray, coarse-grained biotite metagranodiorite, from Santa Tereza suite. (B and C) Photomicrographs showing the concentration of felsic minerals elongated according to bands and displaying undulatory extinction. Plagioclase displays irregular twinning and antiperthitic intergrowths (C); CA-14 sample: D, E, F. (A) Greenish gray, coarse-grained garnet-orthopyroxene-biotite-bearing charnockitic metagranodiorite from Santa Tereza suite. (E and F) Photomicrographs showing local concentration of biotite, orthopyroxene, amphibole, and garnet. Plagioclase displays irregular twinning and antiperthitic intergrowths (F). CA-03 sample: G, H, I. (G) Fine to coarse-grained garnet-biotite metagranodiorite from Jequitibá suite; (H and I) Photomicrographs showing stretched felsic minerals and poikiloblastic garnet. CA-31 sample: J, K, L. (J) Coarse-grained garnet-biotite metagranodiorite from Jequitibá suite. (K and L) Photomicrographs showing plagioclase with irregular twinning and antiperthitic intergrowths, and biotite oriented according to foliation.....59

Figure 3.4 Lithochemical data for the studied samples compared to the compiled dataset. A: FeOt / (FeOt + MgO) vs. SiO_2 (wt%) (Frost et al., 2001); B: $Na_2O + K_2O - CaO$ vs. SiO_2 (wt%) (Frost et al., 2001); C: Alumina saturation Index (Frost et al., 2001). Dashed line (ASI = 1.1) delimits the transition between I- and S-type granites according to Chappell and White (1974); D: R1-R2 diagram (De la Roche et al., 1980). Sources of data compilation in Supplementary file 3.A.....62

Figure 3.5 Lithochemical data for the studied samples compared to available data from G1 and G2 supersuites of Araçuaí orogen, Marceleza-Leopoldina-Serra da Bolívia complex and Rio Negro arc system from Ribeira orogen, and other classical continental magmatic arcs. A and C: Geotectonic discriminating diagrams by Pearce et al. (1984); B: AFM diagram (Irvine and Baragar, 1971); D: Hf-Rb/30-Ta*3 ternary diagram (Harris et al., 1986); E: $Na_2O + K_2O$ vs. SiO_2 (wt%); F: Source Diagram (Laurent et al., 2014). Meaning fields: ORG, Ocean Ridge

Granites; VAG or VA, Volcanic Arc Granites; WPG or WP, Within Plate Granites, COLG, Collision Granites; Group 2, Syn-collision peraluminous intrusions (leucogranites); Group 3, Late or post-collision calc-alkaline intrusions. Sources of data compilation in Supplementary file 3.A. 63

Figure 3.6 A) Multi-elemental diagram normalized to primitive mantle, according to Sun and McDonough (1989); B) Chondrite-normalized REE patterns, normalized according to Boynton (1984). Sources of data compilation in Supplementary file 3.A. 64

Figure 3.7 Average compositions from Santa Tereza and Jequitibá samples, and compiled data with SiO_2 > 54%. A) Multi-elemental diagram normalized to the primitive mantle, according to Sun and McDonough (1989); B) Chondrite-normalized REE patterns, according to Boynton (1984). Sources of data compilation in Supplementary file 3.A. 65

Figure 3.8 (A and B) Concordia diagrams, weighted mean ages, and representative zircons from Santa Tereza and Jequitibá samples. The U-Pb ages are reported as $^{206}Pb/^{238}U$ age in Ma, with errors at 2σ. 66

Figure 3.9 (A) Th vs U diagram, (B) Th/U vs U-Pb age (C and D) Lu-Hf data calculated for individual zircon ages, and (E and F) Lu-Hf data calculated for estimated crystallization ages from Santa Tereza and Jequitibá samples. (G and H) Diagrams comparing the Nd isotopic signature from studied samples with the compiled dataset. DM = depleted mantle; CHUR = chondrite uniform reservoir. T1: Concordia age; T2: Estimated crystallization ages. Sources of data compilation: De Campos et al. (2004)[1]; Figueiredo (2009)[1]; Gonçalves (2009)[1]; Gonçalves et al. (2016)[1]; Heilbron et al., (2013)[2]; Martins et al., (2004)[1]; Nalini Jr., (1997)[1]; Nalini et al. (2000)[1]; Novo et al. (2010)[1]; Pedrosa-Soares et al., (2011)[1]; Peixoto et al., (2017)[3,4]; Pereira et al., (2023)[1]; Santiago et al., (2020)[4]; Soares et al. (2020)[1]; Tedeschi et al. (2016)[1]; Tupinambá et al. (2012)[3]. 67

Figure 3.10 Diagrams comparing the U-Pb and Lu-Hf data from studied samples with the compiled dataset. Northern sector: North of 18°30'; Central sector from 18°30' to 20°; Southern sector: South of 20°; Western sector: West of 41°; Eastern sector: East of 41°; * Jequitibá and Santa Tereza data, respectively; DM = depleted mantle; CHUR = chondrite uniform reservoir. Black dashed lines classify fields of juvenile (0–5 ε-units below DM), moderately juvenile (5–12 ε-units below DM) and evolved (> 12 ε-units below DM) composition (Bahlburg et al., 2011). Sources of data compilation: Araujo et al. (2021)[8]; Araujo et al. (2020)[1,5]; Castro et al. (2020)[7]; Corrales et al. (2020)[3]; Degler et al. (2017, 2018)[7,8]; Gonçalves et al. (2016)[2]; Kuribara

et al. (2019)[8]; Narduzzi (2018)[2]; Pereira et al. (2023)[2]; Santiago et al. (2020)[4], (2022)[7]; Schannor et al. (2019)[2,6], (2020)[2,8]; Tedeschi et al. (2016)[2]. In A and B diagrams, only magmatic zircon grains were plotted.....68

Figure 3.11 Diagrams shown in-zircon Hf isotope data from Santa Tereza and Jequitibá samples, compared with compiled data from Nova Venécia paragneisses. B) Detail outlook showing the Hf signature spreading along approximately horizontal lines and indicating progressive Pb loss. 76

Figure 3.12 Histograms and probability density curves showing zircon U-Pb ages distribution. A: Studied samples and compiled dataset of the orogenic plutonism, metamorphism, and arc-related basins (Andrelândia and Rio Doce groups, Salinas formation, and Mpioka formation) from Araçuaí – West Conto orogen. B: Igneous zircon U-Pb ages from Rio Doce arc (including new data) for Northern to Southern sectors. C: Igneous zircon U-Pb ages from Rio Doce magmatic arc in Araçuaí orogen (including new data) for Western and Eastern sectors. Northern sector: North of 18°30'; Central sector from 18°30' to 20°; Southern sector: South of 20°; Western sector: West of 41°; Eastern sector: East of 41°. Sources of data compilation in Supplementary file 3.A.....78

Figure 3.13 Evolutionary model for the Rio Doce magmatic arc (modified from Tedeschi et al., 2016).....81

Figure 4.1: (A) The Araçuaí-West Congo orogenic system and the related cratons in the context of West Gondwana (modified from Alkmim et al., 2006). (B) Simplified geological map of the Araçuaí orogen (modified from Pedrosa-Soares et al., 2011). Local names of G5 intrusions: Cd, Caladão; Md, Medina; BSF, Barra de São Francisco; PE, Pedra do Elefante; Ct, Cotaché; SGB, São Gabriel da Baunilha; Am, Aimorés; VA, Várzea Alegre; SA, Santa Angélica; VN, Venda Nova; MA, Mestre Álvaro; Vt, Vitória; Ar, Aracê – Pedra Azul. See Supplementary file 4.A for further details. Data source references: (1) Noce et al., 2000; (2) Martins et al., 2004; (3) Serrano et al., 2018; (4) De Campos et al., 2016; (5) Belém, 2014; (6) Mello, 2000; (7) Gonçalves et al., 2016; (8) Aranda, 2018; (9) Gradim et al., 2014. 95

Figure 4.2: Photos and photomicrographs from the CA-02 (A, B), CA-04 (C, D, E), and CA-05 (F, G, H) samples. (A) Biotite granite sample. (B, G) Photomicrographs showing the main mineralogy. (C) CA-04 outcrop. (D, E, H) Rutile associated with biotite or as dark grains included in the biotite and (H) around zircons. (F) Biotite tonalite sample. 101

Figure 4.3: A) Ternary An-Ab-Or feldspar classification diagram; B) Ternary Al-Mg-Fe+Mn biotite classification diagram (Fedele et al., 2015); C) Mg# [Mg/(Fe+Mg)] vs. TiO2 (wt.%) for biotite. 102

Figure 4.4: Field photographs and photomicrographs showing the main mineralogy of the country rocks samples. (A-B) CA-06 sample: Crd granulite from Nova Venécia complex; (C-D) CA-07 sample: Grt-Bt metagranite from Ataléia suite; (E-F) CA-09 sample: Sil-Grt-Crd-Bt paragneiss from Nova Venécia complex; (G-H) CA-10 sample: Grt-Bt paragneiss from Nova Venécia complex. 104

Figure 4.5: Representative features of zircon crystals from G5 samples. (A, C, and E) Secondary electron images showing subtypes of external morphology by Pupin's typological classification. (B, D, and F) Textures on cathodoluminescence (left) and backscattered electron (right) images. The U-Pb ages are reported as $^{206}Pb/^{238}U$ age in Ma, with errors at 2σ..... 108

Figure 4.6: Morphological types of zircon grains found in the G5 samples and their petrogenetic classification based on Pupin (1980). 109

Figure 4.7: Representative features of zircon grains from country rocks on CL (left) and BSE (right) images. The U-Pb ages are reported as $^{206}Pb/^{238}U$ age in Ma, with errors at 2σ. NVC = Nova Venécia complex..... 110

Figure 4.8: Concordia diagrams, weighted mean ages, and Lu-Hf data for samples of G5 plutons. 112

Figure 4.9: Diagrams comparing the U-Th-Pb and Lu-Hf data from studied samples with the compiled dataset. DM = depleted mantle, CHUR = chondrite uniform reservoir. Sources of data compilation: Degler et al. (2018), Gonçalves et al. (2016), Tedeschi et al. (2016), Melo et al. (2017), and Aranda (2018). 113

Figure 4.10: Zircon isotopic data from country rocks. (A to D) U-Pb age histogram, distribution and probability density plots for samples of the Nova Venécia complex. (E) Concordia diagram for the Ataléia metagranite. (F) Lu-Hf data for Nova Venécia complex and Ataléia metagranite samples. (G) Compilation diagram showing zircon U-Pb ages for the orogenic supersuites G1 to G5 and the Nova Venécia complex, and data for metamorphism in the Araçuaí orogen (references in Supplementary file 4.A)..... 116

Figure 4.11: Schematic model for the evolution of the studied region (not to scale). 121

LIST OF TABLES

Table 1.1: Samples collected and the analytical methods used to study them. Analyses: Microscopic petrography (MP); Whole-rock and trace element chemistry (WR and TEC); zircon U-Pb and Lu-Hf isotopic analyses via LA-ICP-MS; whole-rock Sm-Nd. 24

Table 3.1 Main characteristics of the G1 to G5 plutonic supersuites of the Araçuaí orogen (Sources of data compilation in Supplementary file 3A, the present paper; and references therein). 48

Table 3.2 Summary of the main features of the studied from samples with whole rock Sm-Nd analyses. 70

Table 4.1: Summary of the main features of the studied samples. 100

Table 4.2: Summary of the main zircon characteristics for the studied samples. 107

SUMMARY

CHAPTER 1. INTRODUCTION 19

1.1 General Considerations 19

1.2 Characterization of the problem 21

1.3 Aim of this study 22

1.4 Studied area location and main access 22

1.5 Methodology 23

CHAPTER 2. LITERATURE REVIEW 28

2.1 Continental magmatic arcs and related back-arc zones 28

2.2 Regional context and general aspects of the Araçuaí-West Congo orogenic system 29

2.3 The crystalline core of the Araçuaí - West Congo orogenic system 35

CHAPTER 3. SCIENTIFIC CONTRIBUTION I 43

Article published by Journal of South American Earth Sciences (doi: 10.1016/j.jsames.2023.104490) 43

ABSTRACT 43

3.1 INTRODUCTION 44

3.2 GEOLOGICAL SETTING 46

3.3 MATERIALS AND METHODS 53

3.4 RESULTS 56

3.4.1 Petrography and textural relationships 57

3.4.1.1. Santa Tereza suite 57

3.4.1.1. Jequitibá suite 57

3.4.2. Lithochemistry, Geochronology and Isotope Geochemistry 60

3.4.2.1. Lithochemistry 60

3.4.2.2. Zircon U-Th-Pb and Lu-Hf data 60

3.4.2.2.1. Santa Tereza suite..... 60

3.4.2.2.2. Jequitibá suite 68

3.4.2.3. Sm-Nd data..... 69

3.5 DISCUSSION..... 71

3.5.1 Tectonic correlations along the Neoproterozoic Brasiliano belts of Brazil..... 71

3.5.2 Petrogenesis of Santa Tereza and Jequitibá suites 72

3.5.2. Isotopic correlations 74

3.5.3 Implications for Araçuaí geotectonic evolution 78

3.6 CONCLUSIONS..... 80

ACKNOWLEDGMENTS..... 81

REFERENCES 82

CHAPTER 4. SCIENTIFIC CONTRIBUTION II..... 91

Article published by Lithos Journal (doi: 10.1016/j.lithos.2019.105252) 91

ABSTRACT 91

4.1 INTRODUCTION 92

4.2 GEOLOGICAL SETTING..... 94

4.3 PETROGRAPHY AND MINERAL CHEMISTRY 98

4.3.1 G5 samples 98

4.3.1.1 Sample CA-02 (Aracê – Pedra Azul pluton) 98

4.3.1.2 Sample CA-04 (Vitória pluton) 102

4.3.1.3 Sample CA-05 (Mestre Álvaro pluton)..... 102

4.3.2 Country Rocks 103

4.3.2.1 Samples CA-06, CA-09, and CA-10 (Nova Venécia complex)..... 103

4.3.2.2 Sample CA-07 (Ataléia suite) 104

4.4 ZIRCON STUDY..... 104

4.4.1 Morphology and internal texture..... 105

4.4.1.1 G5 samples (CA-02, Aracê – Pedra-Azul granite; CA-04, Vitória granite; CA-05, Mestre Álvaro tonalite) 105

4.4.1.2 Country rocks (CA-06, CA-09, CA-10, Nova Venécia complex; CA-07, Ataléia suite) 109

4.4.2 Zircon U-Th-Pb and Lu-Hf data 110

4.4.2.1 Sample CA-02 (Aracê – Pedra Azul granite) 111

4.4.2.2 Sample CA-04 (Vitória pluton) 113

4.4.2.3 Sample CA-05 (Mestre Álvaro pluton) 114

4.4.2.4 Samples CA-06, CA-09, CA-10 (Nova Venécia migmatitic paragneisses) 114

4.4.2.5 Sample CA-07 (Ataléia metagranite) 115

4.5 LITHOCHEMISTRY 116

4.5.1 Zircon saturation geothermometry 117

4.6 DISCUSSION 118

4.6.1 Zircon morphology and internal textures as petrogenetic indicators for G5 samples 118

4.6.2 Implications of U-Th-Pb and Lu-Hf data 121

4.7 CONCLUSION 123

ACKNOWLEDGMENTS 124

REFERENCES 124

CHAPTER 5. CONCLUSIONS 129

CHAPTER 6. REFERENCES 131

APPENDIX A - Conference Abstracts 142

APPENDIX B - Supplementary File 3.A: Geochemistry Data 144

APPENDIX C - Supplementary File 3.B - Isotopic Data 154

APPENDIX D - Supplementary File 4.A - Compiled Data 175

APPENDIX E - Supplementary File 4.B - Materials and Methods 182

APPENDIX F - Supplementary File 4.C: Mineral Chemistry 192

APPENDIX G - Supplementary File 4.D - Geochemistry Data 218

APPENDIX H - Supplementary File 4.E - U-Pb and Lu-Hf Data 285

APPENDIX I - Petrographic Descriptions 351

APPENDIX J - Other contributions 406

CHAPTER 1. INTRODUCTION

1.1 General Considerations

Unraveling the development and evolution of continental magmatic arc provide significance key pieces for understanding the formation and the recycling of continental crusts through time. It is also a useful task for society because these geotectonic systems play an important role in the building of mountains, the formation of mineral resources and climate change (Paterson and Ducea, 2015).

The existence of a continental magmatic arc, namely Rio Doce arc, in the Araçuaí-West Congo Orogenic System (AWCO) building at the Neoproterozoic time has been indicated by several lithochemical and isotopic attributes. Its geotectonic situation confined to a cratonic embayment makes it increasingly necessary to investigate and test this hypothesis.

The AWCO characterizes a confined orogen to a large sheath of the São Francisco – Congo Craton, amalgamated into the Gondwana Paleocontinent in the end of the Neoproterozoic. Despite its peculiar geotectonic situation confined to a cratonic embayment (Figure 1.1), this orogenic system is considered as collisional orogen successor to an accretionary orogen of active continental margins (Alkmim et al., 2017; Pedrosa-Soares et al., 2020). The Rio Doce Magmatic arc represents the pre-collisional magmatism that consists mainly of tonalites and granodiorites, mafic to dioritic enclaves, and individual gabronoritic facies subordinate (Gonçalves et al., 2014, 2016, 2018; Gouvêa et al. 2020; Gradim et al., 2014; Pedrosa-Soares et al., 2011, 2020; Soares et al., 2020; Tedeschi et al., 2016).

This thesis presents a study about the orogenic magmatism in the easternmost sector of the Araçuaí orogen and its relationships with the Nova Venécia complex, one of the metavolcano-sedimentary units located in the arc-related setting (Figures 1.1 and 1.2). Such a study covers a region where rocks of pre-, sin-, and post-collisional orogenic stages intruded in the Nova Venécia migmatitic paragneisses.

Tonalitic and charnockitic rocks from Santa Tereza and Jequitibá suites are strong candidates to demonstrate the Rio Doce arc continuity in the easternmost region of the Araçuaí orogen (Figure 1.2) representing the pre-collisional magmatism. The Ataléia suite represent the syn-collisional magmatism associated with paragneisses anatexis, and the Aracê – Pedra Azul, Vitória, and Mestre Álvaro plutons record the post-collisional event.

This study may clarify the evolutionary history of this portion from the Araçuaí orogen mainly from the Rio Doce arc and its related basin.

This research was funded by CNPq and CODEMGE projects coordinated by A. Pedrosa Soares, in CPMTC-IGC-UFMG (Centro de Pesquisa Professor Manoel Teixeira da Costa of the Federal University of Minas Gerais). This work was also carried out with the support of the CAPES, Brazil - Financing Code 001 (O presente trabalho foi realizado com apoio da Coordenação de Aperfeiçoamento de Pessoal de Nível Superior, Brasil - CAPES - Código de Financiamento 001).

The obtained data, with their discussions, interpretations and conclusions are presented in the articles insert in Chapter 3, 4, and 5.

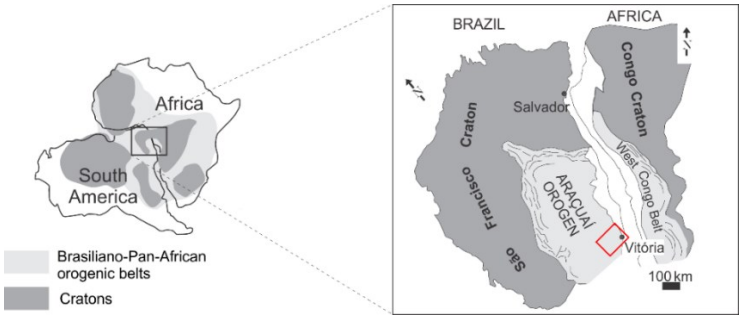

Figure 1.1: Araçuaí orogen location and the region focused on this thesis (red rectangle) in the context of the Western Gondwana Paleocontinent (modified from Pedrosa-Soares et al. 2008).

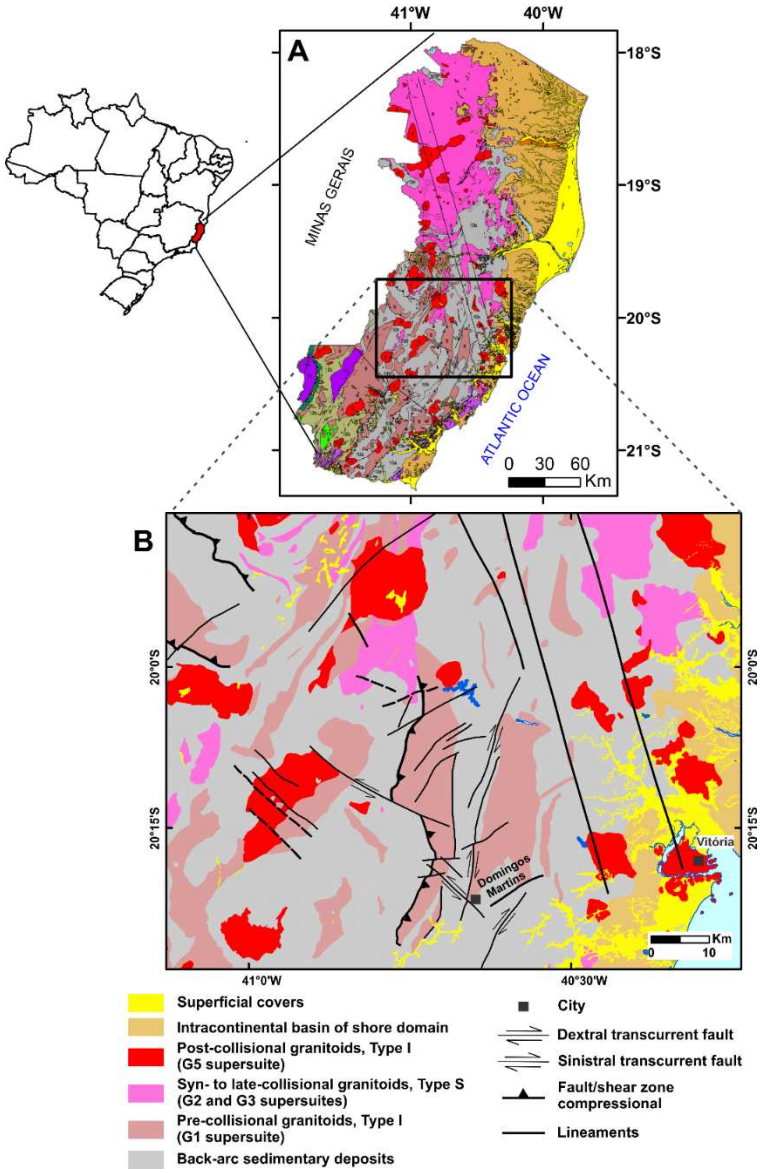

Figure 1.2: Geotectonic Map of the State of Espírito Santo (Vieira and Menezes 2015). B) Study region focused on this thesis (modified from Vieira and Menezes 2015).

1.2 Characterization of the problem

Rocks previously attributed to the post-collisional stage (G5 supersuite; 530 - 480 Ma; Vieira and Menezes 2015) in the easternmost sector of the Araçuaí orogen, have been shown to be older, with age compatible with the plutonic portion (G1 supersuite) of the Rio Doce magmatic arc (pre-collisional stage; 630 - 580 Ma). These U-Pb ages show solid evidence of the Rio Doce arc continuation to the east of its hitherto known limit, to the surroundings of Fundão, north of Vitória, Espírito Santo state. Those rocks are intruded in the Nova Venécia migmatitic paragneisses, and the relationship between these units needs to be further investigated.

In the last years, petrogenetic and petrochronological studies have been intensified through mineral chemistry, geochronology and isotopic signature of Lu-Hf, and trace elements in minerals such as zircon, monazite, and garnet from rocks of the Araçuaí orogen and its surroundings, with the increasing availability of data published. However, in this scenario, there is still an information gap in the region focused in this thesis, since there are no studies with an emphasis on Lu-Hf isotopic signature in zircons from the Nova Venécia complex and Ataleia rocks, and the studies that exist for rocks from G1 Supersuite are concentrated further north and/or west of the approached region (Gonçalves et al. 2016, Narduzzi et al., 2017, Tedeschi et al. 2016).

Thus, it is necessary to study in more detail the continuity of the Rio Doce magmatic arc in this region of the Araçuaí Orogen, integrating the results obtained with data already published and to investigate in more detail the provenance of the Nova Venécia complex, thus launching new contributions to the understanding of the geotectonic and geodynamic evolution of the Araçuaí-Congo orogen and its connection with the Ribeira orogen in the context of the Gondwana Paleocontinent.

1.3 Aim of this study

This PhD thesis project aims to improve and contribute to the understanding of the geotectonic evolution of the studied area in the context of the Araçuaí orogen through the characterization of the continuity of the Rio Doce Magmatic arc in the region and its relations with the genesis of the back-arc basin. Through new petrological investigation, bulk-rock chemistry, and isotopic analyses (zircon U-Th-Pb and Lu-Hf by LA-ICPMS, and whole-rock Sm-Nd), the data obtained in this study linked with the literature dataset can clarify issues of how the Rio Doce magmatic arc evolved over time, how was the evolution of orogen from subduction to post-collisional stage, and how the rocks of the Nova Venécia complex are related to the pre-, syn- and post-collisional rocks present in the region.

In addition, it is intended to bring data that contribute to the understanding of the connection between the Araçuaí and Ribeira orogens.

1.4 Studied area location and main access

The focused area in this project covers part of the Araçuaí orogen easternmost portion (Figure 1.1), located in the central region of the Espírito Santo state (Figures 1.2, 1.3, and 2.1).

Figure 1.3 shows the main access roads in the studied area and Table 1.1 shows the location of representative samples collected for petrographic characterization and further analyses.

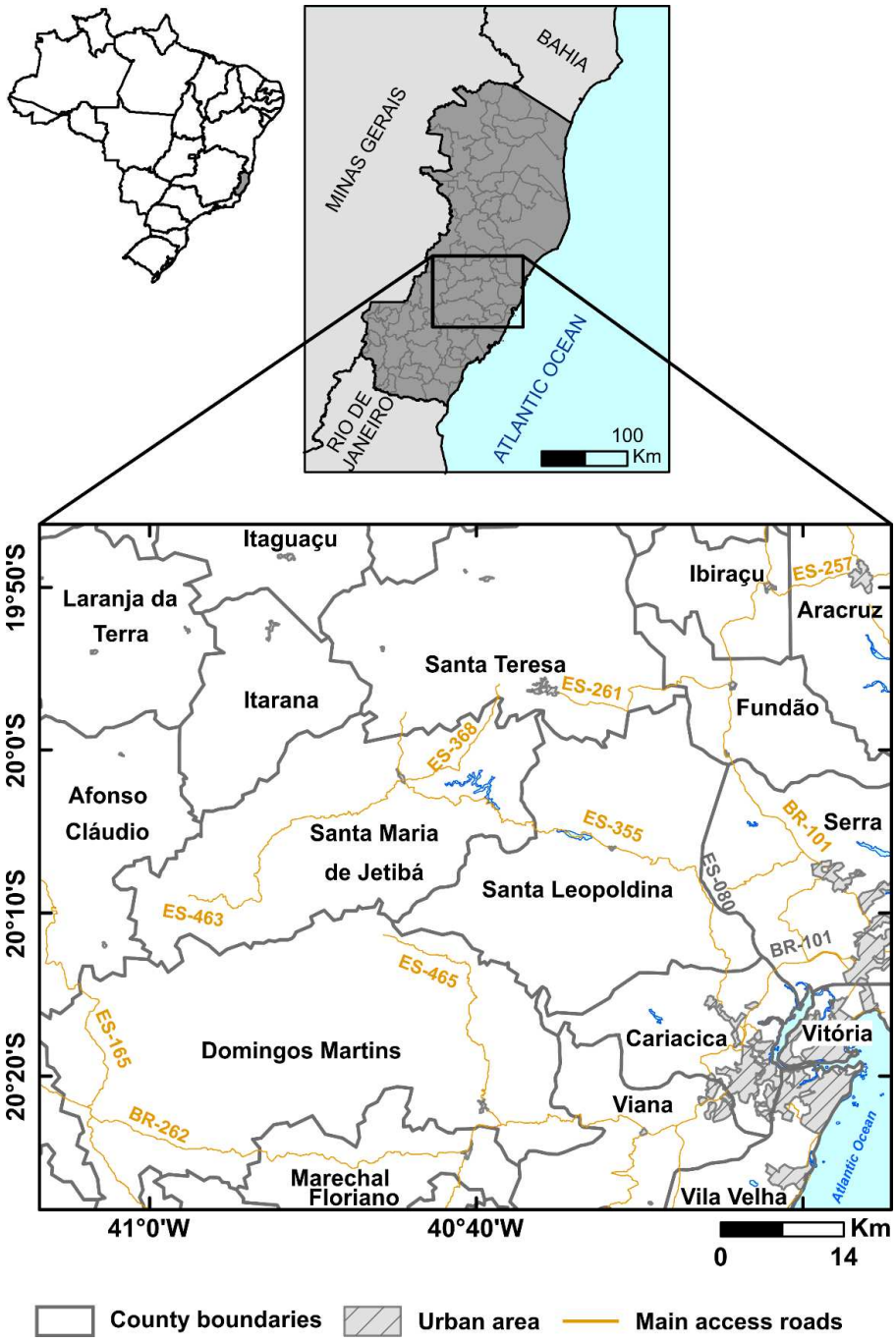

Figure 1.3: Studied area localization and main access roads.

1.5 Methodology

This thesis included fieldwork, petrographic description, lithochemical and isotopic (zircon U-Th-Pb and Lu-Hf by LA-ICPMS, and whole-rock Sm-Nd; Table 1.1) analyses in the candidates to represent the rocks of Rio Doce arc, the syn-collisional rocks (Ataléia suite), the

Aracê – Pedra Azul, Vitória, and Mestre Álvaro post-collisional plutons and in the Nova Venécia complex rocks. For a better interpretation of the obtained results, a large bibliographic compilation was necessary to compare and integrate the data presented in the literature with the data obtained in this project.

Fieldwork took place in the studied area during two periods. The aims were to obtain knowledge of the regional geology, to observe the relations between the granites and the metasedimentary rocks, detection and description of outcrop-scale features, as well collect representative samples for characterization of target lithological units. Sample localities and the methods used to study are indicated in Table 1.1 and Figure 2.1. See Supplementary file "Petrographic descriptions" for more details.

Table 1.1: Samples collected and the analytical methods used to study them. Analyses: Microscopic petrography (MP); Whole-rock and trace element chemistry (WR and TEC); zircon U-Pb and Lu-Hf isotopic analyses via LA-ICP-MS; whole-rock Sm-Nd.

Sample	County	Coordinates	Lithological unit	Local name	Lithotype	Method
CA-02	Domingos Martins	-20.38728/ -41.0174	G5 supersuite	Aracê – Pedra Azul	Titanite-allanite-biotite granite	MP, WR and TEC, U-Pb, Lu-Hf
CA-03	Marechal Floriano	-20,41225/ -40,85965	G1 supersuite, pre-collisional plutonism – Rio Doce arc	Jequitibá tonalite	Grt-Bt metagranodiorite	MP, WR and TEC, U-Pb, Lu-Hf; Sm-Nd
CA-04	Vila Velha	-20.33386 / -40.27305	G5 supersuite	Vitória	Biotite granite	MP, WR and TEC, U-Pb, Lu-Hf
CA-05	Serra	-20.1138 / -40.32152	G5 supersuite	Mestre Álvaro	Biotite tonalite	MP, WR and TEC, U-Pb, Lu-Hf
CA-06	Ibiraçu	-19,798133/ -40,36985	Nova Venécia complex, arc-related basin	Nova Venécia complex	Sil-Bt-Crd paragneiss (known as Crd granulite)	MP, WR and TEC, U-Pb, Lu-Hf
CA-07	Fundão	-19,932367/ -40,40955	G2 supersuite, collisional plutonism	Ataléia suite	Grt-Bt metatonalite	MP, WR and TEC, U-Pb, Lu-Hf
CA-08	Santa Teresa	-19,935167/ -40,498883	G1 supersuite, pre-collisional plutonism – Rio Doce arc	Santa Teresa orthogneiss	Bt metagranodiorite	MP, WR and TEC, U-Pb, Lu-Hf, Sm-Nd
CA-09	Santa Teresa	-19,92115/ -40,598183	Nova Venécia complex, arc-related basin	Nova Venécia complex	Sil-Grt-Crd-Bt paragneiss	MP, WR and TEC, U-Pb, Lu-Hf
CA-10	Santa Teresa	-19,814567/ -40,67865	Nova Venécia complex, arc-related basin	Nova Venécia complex	Grt-Bt paragneiss	MP, U-Pb, Lu-Hf
CA-11	Santa Teresa	-19,880528/ -40,540427	Nova Venécia complex, arc-related basin	Nova Venécia complex	Grt-Bt paragneiss	-

Sample	County	Coordinates	Lithological unit	Local name	Lithotype	Method
CA-12A	Santa Teresa	-19,876179/ -40,538724	Nova Venécia complex, arc-related basin	Nova Venécia complex	Grt-Bt-Crd paragneiss	MP
CA-12B	Santa Teresa	-19,876179/ -40,538724	Nova Venécia complex, arc-related basin	Nova Venécia complex	Calc-silicate rock	MP
CA-12C	Santa Teresa	-19,876179/ -40,538724	G2 supersuite, collisional plutonism	Ataléia suite	Grt-Bt metatonalite	MP
CA-13	Santa Teresa	-19,862764/ -40,528119	G1 supersuite, pre-collisional plutonism – Rio Doce arc	Santa Teresa orthogneiss	Bt metagranite	-
CA-14	Santa Teresa	-19,857562/ -40,516296	G1 supersuite, pre-collisional plutonism – Rio Doce arc	Santa Teresa orthogneiss	Grt-Opx-Bt metagranodiorite	MP, WR and TEC; Sm-Nd
CA-15	Santa Teresa	-19,857661/ -40,516316	G1 supersuite, pre-collisional plutonism – Rio Doce arc	Santa Teresa orthogneiss	Bt metagranite	-
CA-16	Santa Teresa	-19,832376/ -40,513975	G1 supersuite, pre-collisional plutonism – Rio Doce arc	Santa Teresa orthogneiss	Bt granite	-
CA-17	Fundão	-19,933009/ -40,465542	G1 supersuite, pre-collisional plutonism – Rio Doce arc	Santa Teresa orthogneiss	Opx-Bt metadiorite	MP, WR and TEC; Sm-Nd
CA-18A	Fundão	-19,933153/ -40,467836	G1 supersuite, pre-collisional plutonism – Rio Doce arc	Santa Teresa orthogneiss	Opx-Cpx-Bt metamonzogabbro	MP, WR and TEC; Sm-Nd
CA-18B	Fundão	-19,933153/ -40,467836	G2 supersuite, collisional plutonism	Ataléia suite	Grt-Bt granite	MP
CA-18C	Fundão	-19,933153/ -40,467836	G2 supersuite, collisional plutonism	Ataléia suite	Bt metagranite	MP, WR and TEC
CA-19	Santa Teresa	-19,936737/ -40,483412	G1 supersuite, pre-collisional plutonism – Rio Doce arc	Santa Teresa orthogneiss	Bt metagranodiorite	MP, WR and TEC; Sm-Nd
CA-20A	Santa Teresa	-19,934149/ -40,501071	G1 supersuite, pre-collisional plutonism – Rio Doce arc	Santa Teresa orthogneiss	Grt-Opx-Bt metagranodiorite	MP, WR and TEC; Sm-Nd
CA-20B	Santa Teresa	-19,934149/ -40,501071	G2 supersuite, collisional plutonism	Ataléia suite	Grt-Bt granite	-
CA-21A	Santa Teresa	-19,896408/ -40,517535	G1 supersuite, pre-collisional plutonism – Rio Doce arc	Santa Teresa orthogneiss	Grt-Opx-Bt metagranodiorite	MP, WR and TEC
CA-21B	Santa Teresa	-19,896408/ -40,517535	Nova Venécia complex, arc-related basin	Nova Venécia complex	Grt-Bt paragneiss	-
CA-22	Santa Teresa	-19,922514/ -40,465139	G2 supersuite, collisional plutonism	Ataléia suite	Grt-Bt metatonalite	-
CA-23	Santa Teresa	-19,957087/	G2 supersuite, collisional plutonism	Ataléia suite	Grt-Crd-Bt metatexite	MP, WR and TEC

Sample	County	Coordinates	Lithological unit	Local name	Lithotype	Method
		-40,517063				
CA-24	Santa Leopoldina	-19,994787/ -40,499017	G1 supersuite, pre-collisional plutonism – Rio Doce arc	Santa Teresa orthogneiss	Opx-Bt metatonalite	MP, WR and TEC
CA-25	Santa Leopoldina	-19,998492/ -40,506354	G1 supersuite, pre-collisional plutonism – Rio Doce arc	Santa Teresa orthogneiss	Opx-Bt metatonalite	WR and TEC
CA-27	Santa Leopoldina	-20,171016/ -40,500235	G1 supersuite, pre-collisional plutonism – Rio Doce arc	Jequitibá tonalite	Amphibolite	MP
CA-28A	Santa Teresa	-19,800573/ -40,683736	Nova Venécia complex, arc-related basin	Nova Venécia complex	Sil-Bt-Grt-Crd paragneiss	MP
CA-28B	Santa Teresa	-19,800573/ -40,683736	Nova Venécia complex, arc-related basin	Nova Venécia complex	Crd-Sil-Bt-Grt paragneiss	MP
CA-28C	Santa Teresa	-19,800573/ -40,683736	Nova Venécia complex, arc-related basin	Nova Venécia complex	Bt-Grt paragneiss	MP
CA-29	Santa Leopoldina	-20,09411/ -40,561507	G1 supersuite, pre-collisional plutonism – Rio Doce arc	Jequitibá tonalite	Opx-Cpx-Bt-Amp tonalite	MP
CA-30	Santa Leopoldina	-20,114662/ -40,577807	G1 supersuite, pre-collisional plutonism – Rio Doce arc	Jequitibá tonalite	Bt metadiorite	MP, WR and TEC
CA-31	Santa Leopoldina	-20,046944/ -40,699558	G1 supersuite, pre-collisional plutonism – Rio Doce arc	Jequitibá tonalite	Grt-Bt metagranodiorite	MP, WR and TEC; Sm-Nd
CA-32	Santa Maria de Jetibá	-20,045055/ -40,722958	G1 supersuite, pre-collisional plutonism – Rio Doce arc	Jequitibá tonalite	Grt-Bt metagranodiorite	WR and TEC; Sm-Nd

Petrographic characterization and lithochemistry analyses aim to know the study rocks and make inferences about the tectonic environment, sources and genetic processes (Frost et al. 2001; Rollinson 2007).

Isotopic studies using the methods of zircon isotopic analyses (U-Th-Pb and Lu-Hf) and whole-rock Sm-Nd is widely used to obtain petrogenetic and geochronological information for igneous and metamorphic rocks. These data can be used to investigate the chemical characteristics of the magma in which zircon crystallized, whether magma was derived from rock rework, the age of rock evolutionary processes and the detrital zircon grains provenance (Belousova et al. 2002, 2006; Corfu et al. 2003; Hoskin and Schaltegger, 2003; Kinny and Maas 2003, Tang et al. 2014).

Besides forthcoming chapters, the analytical methods descriptions of the petrography, whole-rock and trace element chemistry, zircons preparing, and isotopic analyses are available

in Supplementary file 4.B. The supplementary files 3.A, 4.A, and 4.B contain a thorough literature data compilation.

We use the name granite in a general sense, if not otherwise specified. Geographical coordinates refer to the present-day position of continents, even in relation to paleocontinental descriptions. Mineral abbreviations are in accordance to Whitney and Evans (2010).

CHAPTER 2. LITERATURE REVIEW

2.1 Continental magmatic arcs and related back-arc zones

Destructive plate margins involve boundaries where two plates are converging. The mechanism of the oceanic lithosphere of one of the plates being thrust under the continental lithosphere plate, eventually to become resorbed into the sub-lithospheric mantle, form continental magmatic arcs above subduction zones, that build an entire lithospheric section (Ducea et al., 2015a, b; Kearey et al., 2014; Paterson and Ducea, 2015). They are mixtures of fractional melting in the mantle and crustal materials, (Ducea et al., 2015a; Kohanpour et al., 2019) representing the most varied associations of igneous rocks on Earth.

Unraveling the development and evolution of continental magmatic arc provides significance key pieces for understanding the formation and the recycling of continental crusts through time (Castro et al., 2010, 2011; Moyen et al., 2017; Paterson and Ducea, 2015). The differentiation of a primitive mantle melt will contribute to continental crustal growth by subduction settings during lithospheric convergence (Moyen et al., 2017).

Continental magmatic arcs are mainly recognized based on their linear belts of calc-alkaline magmatism that are higher in silica, granitic batholiths with paired metamorphic belts, and possibly ophiolite bodies (Ducea et al., 2015a, b; Kearey et al., 2014). The geochemical signature of arc magmatism is characterized by expressive amounts of volatiles (H_2O, CO_2), mantle/crust hybrid isotopic signatures representing mixtures of fractional melting in the mantle and crustal materials, distinctive trace element patterns such as negative Nb-Ta-Ti anomaly, magnesian, a wide variety of silica contents, I-type granites, and much of the batholiths are tonalities and granodiorites (Best, 2003; Brown and Johnson, 2019; Castro et al., 2010; Castro, 2013; Ducea et al., 2015a, b; Frost et al., 2001; Frost and Frost, 2008; Kelemen et al., 2014).

In the continental arc, the tectonic setting can fluctuate from compressional to extensional (Castro, et al., 2010; Ducea et al., 2015a; Figure 2.1). Into compression, the arcs form under crustal and lithospheric shortening and thickening (~70 km thick), with the development of large plateaus in the back-arc areas and extensive magmatism (Ducea, 2015a; Kearey et al., 2014; Kohanpour et al., 2019; Figure 2.3B). The continuous increase of continental crust in the magmatic source leading to a decreasing of $^{176}Hf/^{177}Hf$ signature during compression and shortening of the continental crust (Kohanpour et al., 2019).

In contrast, the upper plate under extension develops basins, in back-arc and fore-arc areas, with crustal thickness remaining relatively small (~30 km thick). Back-arc basins form behind the volcanic arc in the upper plate of a subduction zone associated with extensional

tectonics and high heat flow as an effect of the weakening influence of mantle melting shared with slab pull (Ducea, 2015a; Kearey et al., 2014; Kohanpour et al., 2019; Figure 2.1A). The majority of back-arcs with oceanic affinity develops oceanic crust by seafloor spreading centers. During extension, there is a progressive addition of mantle-derived magma carrying to a more radiogenic Hf isotopic signature (Kohanpour et al., 2019).

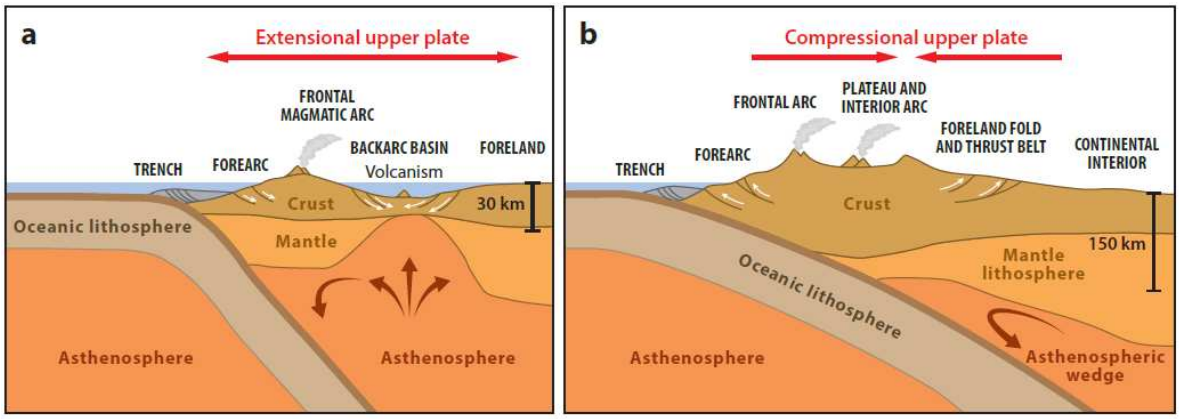

Figure 2.1 Schematic cross section of extensional and compressional tectonic through a continental subduction system (from Ducea et al., 2015a).

2.2 Regional context and general aspects of the Araçuaí-West Congo orogenic system

The studied region is located in the high-grade (crystalline) core of the Araçuaí-West Congo orogenic system - AWCO (Alkmim et al., 2006, 2017; Pedrosa-Soares et al., 2001, 2008; Figure 2.2). The AWCO comprises the northern sector of the Mantiqueira Province and is considered a confined orogen result of the amalgamation of the Western Gondwana in Neoproterozoic-Cambrian time, during the Brasiliano-Pan-African orogeny (Heilbron et al., 2004), constituting a confined orogenic system developed within an embayment surrounded by the São Francisco-Congo craton (Alkmim et al., 2006, 2017; Pedrosa-Soares et al., 2001, 2008, 2020). Long after that paleocontinental assemblage promoted by the Brasiliano - Pan-African orogeny, the AWCO was splitted apart in the Cretaceous, by the opening of the South Atlantic Ocean, leaving the Araçuaí orogen in South America, and the West Congo belt in Africa. The Araçuaí orogen connects with the Ribeira Belt in the south, forming the Araçuaí-Ribeira orogenic system (Figure 2.2). Its African correlates correspond to the Congo West and Kaoko orogenic systems, located on the west border of the Congo and Angola craton (Heilbron et al., 2008; Merdith et al., 2017).

According to Pedrosa-Soares et al. (2001), the Araçuaí Orogen is divided into two domains: the external, which comprises the W-verging basement-involved fold-thrust belt,

towards the São Francisco craton; and the internal domain, which comprises the metamorphic-anatectic core, where amount igneous bodies are exposed.

Geodynamic evolution of the AWCO comprises the closure of its precursor basin, the Macaúbas basin at Ediacaran Period, driven by convergence and collision of various plates that formed West Gondwana paleocontinent. The spatial and tectonic relations between the oceanic mafic-ultramafic slivers and the calc-alkaline granites, as well as their chemical signature and hybrid isotopic attributes, provide evidence of subduction of the oceanic lithosphere under a continental margin (Alkmim et al., 2006, 2007, 2017; Amaral et al., 2020; Araujo et al., 2019; Corrales et al., 2020; Gonçalves et al., 2014, 2016, 2018; Gradim et al., 2014; Pedrosa-Soares et al., 2001, 2008; Tedeschi et al., 2016). Despite numerous evidence supporting this geodynamic evolution of the AWCO, its singular geotectonic situation, as a confined orogenic system, makes many authors propose alternative evolutionary models (e.g. Cavalcante et al., 2019; Egydio-Silva et al., 2018; Fossen et al., 2017, Mondou et al., 2012; Petitgirard et al., 2009; Trompette, 1994, 1997; Vauchez et al., 2007, 2019) as a mainly collisional or an intracontinental belt.

The Araçuaí orogen stratigraphy can be grouped into 1) Archean-Paleoproterozoic basement originated from the São Francisco – Congo paleocontinent; 2) Statherian-Mesoproterozoic rocks related to the Espinhaço continental rift to rift-sag basins, and associated anorogenic plutonic rocks; 3) Two Neoproterozoic rifting stages comprised of Tonian and Cryogenian rocks successions of the Macaúbas Group and correlated units, representing the precursor basin system of the Araçuaí orogen and related Cryogenian ophiolite slivers; 4) Neoproterozoic pre- and orogenic-related rocks units, and syn- to post-collisional plutonic rocks (Alkmim et al., 2007, 2017; Amaral et al., 2020; Araujo et al., 2021; Castro et al., 2019, 2020; Deluca et al., 2019; Degler et al., 2017, 2018; Kuchenbecker, et al., 2015; Kuribara, et al., 2019; Magalhães, et al., 2018; Pedrosa-Soares, et al., 2001, 2008; Peixoto et al., 2015; Ricther et al., 2016; Souza et al., 2019, 2022).

Originated from the amalgamation of the São Francisco – Congo paleocontinent, the Archean-Paleoproterozoic basement consists of tonalite-trondhjemite-granodiorite (TTG) gneisses, granitoids and supracrustal units, and the remnants of greenstone belts. They are referred to as the Itarantim, Quadrilátero Ferrífero, Gavião, Mantiqueira, Guanhães, Gouveia, Porterinha, Juiz de Fora, Quirino, and Pocrane (in Brazil) and Kimezian (Africa) that constitute segments of Rhyacian-Orosirian orogenic systems (Alkmim et al., 2006, 2017; Brito-Neves et al., 2021; Degles et al., 2018; Heilbron et al., 2004; Kuchenbecker and Barbuena, 2023;

Pedrosa-Soares et al., 2020). Further east, in the crystalline core, the basement occurrences are made up of juvenile and associated supracrustals rocks from Paleoproterozoic magmatic arcs grouped in the Juiz de Fora, Pocrane, and Quirino complexes. They comprise banded ortho- and paragneisses interlayered with metamorphosed rocks with mafic to ultramafic compositions (Alkmim et al., 2017; Araujo et al., 2021; Degler et al., 2018; Kuribara et al., 2019; Noce et al., 2007a, b; Novo, 2013; Schannor et al., 2020).

The Juiz de Fora complex is composed predominantly of enderbitic to granodioritic orthogneisses and metabasites (mafic granulites) with metamafic enclaves and granitic leucosomes in NE-SW-trending. The Juiz de Fora rocks present crystallization ages from c. 2.45 to 1.77 Ga, Nd_{TDM} model ages of 2.6 to 2.03 Ga, $\varepsilon Nd_{(t)}$ from +7.7 to −3.5, Hf_{TDM} model ages of 3.5 to 2.0 Ga, $\varepsilon Hf_{(t)}$ from +8.4 to −11.7, and an Ediacaran metamorphism event related to the Brasiliano orogeny in upper amphibolite to lower granulite-facies. Due to their chemical and isotopic signatures, this unit was interpreted as a juvenile magmatic arc (Araujo et al., 2021; Degler et al., 2018; Kuribara et al., 2019; Noce et al., 2007a, b; Novo, 2013; Schannor et al., 2020; and references therein).

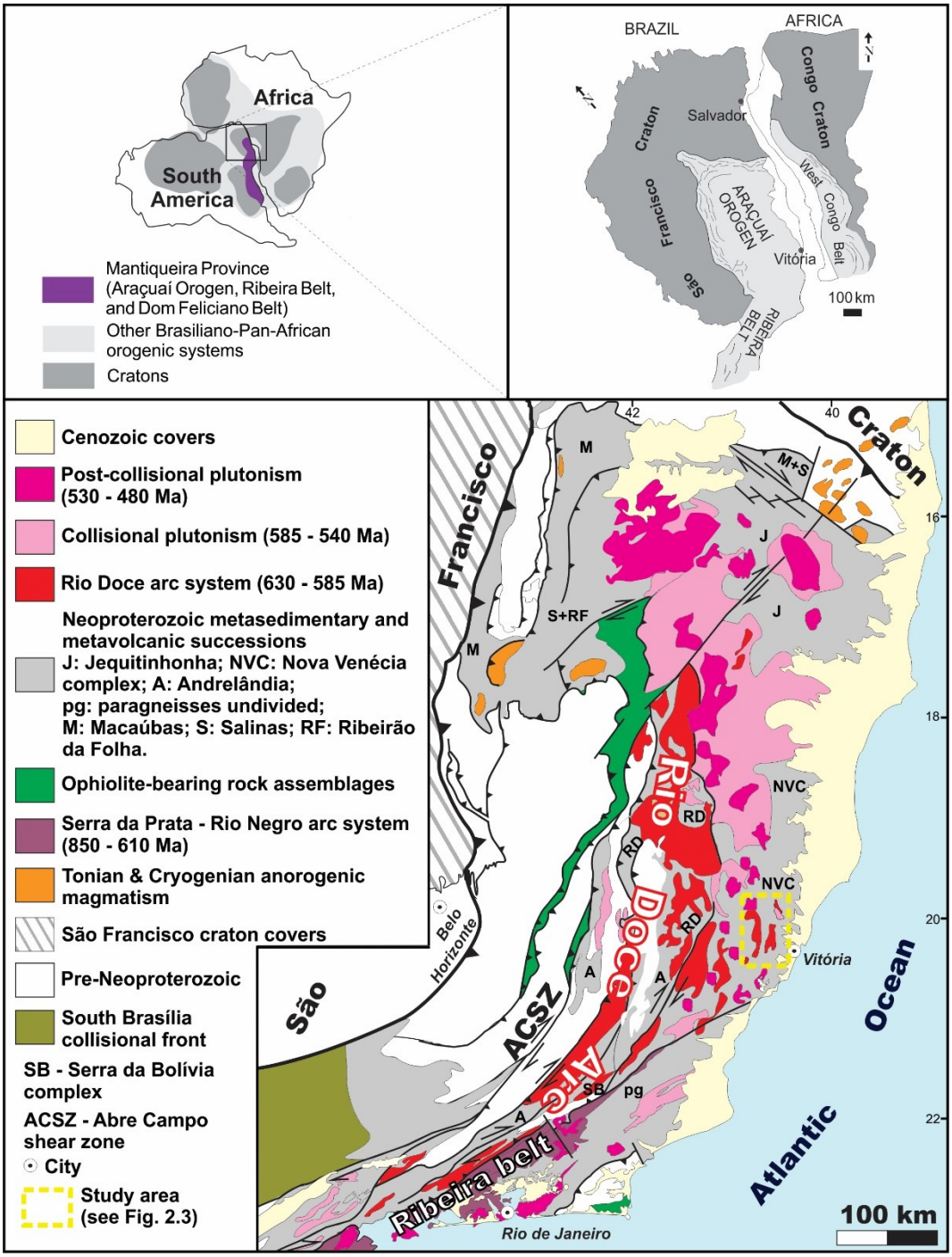

Figure 2.2 (A) The Mantiqueira Province, other Brasiliano-Pan-African orogenic systems, and the related cratons in the context of West Gondwana (modified from Alkmim et al., 2006). (B) The Araçuaí – West Congo Orogenic System and adjacent cratons in the context of West Gondwana (modified from Alkmim et al., 2006). (C) Simplified geological map of the Araçuaí orogen (modified from Tedeschi et al., 2016).

The Pocrane complex consists of orthogneisses, with intercalations of ortho-amphibolites and metasedimentary rocks metamorphosed in the high amphibolite facies. They have ages of c. 2.18 Ga to 2.08 Ga, with isotopic signature of Nd_{TDM} model ages of c. 2.3 Ga, $\varepsilon Nd_{(t)}$ of -0.43, Hf_{TDM} model ages from 2.8 to 2.02 Ga, and $\varepsilon Hf_{(t)}$ from +6.9 to −7.4 (Degler et al., 2018; Novo,

2013; and references therein). Degler et al. (2018) suggest that Pocrane and Juiz de Fora complexes form distinct crustal levels from only one magmatic arc system. The Juiz de Fora complex exhibits arc roots, and the Pocrane complex represents medium to uppermost (volcanic) arc sections.

The Quirino complex represents a Rhyacian continental magmatic arc. It encompasses tonalitic to granitic orthogneisses with intercalations of meta-mafic and meta-ultramafic rocks, metamorphosed in the high amphibolite facies in the Ediacaran. The Quirino orthogneisses have ages of c. 2.31 to 2.14 Ga, with isotopic signature of Nd_{TDM} model ages from c. 3.2 to c. 2.2 Ga, $\varepsilon Nd_{(t)}$ from +1.6 to −9.1, Hf_{TDM} model ages of 2.8 to 2.25 Ga, and $\varepsilon Hf_{(t)}$ from +3.8 to −7.3 (Degler et al., 2018; Novo, 2013; and references therein).

After the tectonic stabilization of the São Francisco-Congo paleocontinent, around 2.0 Ga, several episodes of the rift-type basin formation and intraplate magmatism happened. The first rifting event that affected the interior of the São Francisco-Congo was the Espinhaço rift in Statherian-Mesoproterozoic time. This episode represents an intracontinental basin filled with approximately 6 km thick of succession of sedimentary and volcanic rocks metamorphosed under greenschist facies conditions. The rift to rift-sag sequences crops out in the external fold-thrust belt on the western border of the orogen, mainly recorded at the Espinhaço ridge (Alkmim et al., 2006, 2020; Magalhães, et al., 2018; and references therein).

Next, two Neoproterozoic rifting stages developed forming the precursor basin system of the Araçuaí orogen and its related Cryogenian ophiolite slivers, which evolved mainly from a Cryogenian continental rift to a gulf-shaped inland-sea basin. Thrusts, reverse faults, and cratonward verging folds, developed between 575 Ma and 530 Ma, affected them. The Early Tonian extension that started at ca. 957 Ma and aborted around 875 Ma, named Rift I, includes the sedimentary and volcanic rocks of a lower unit free of diamictites from the Macaúbas Group, the anorogenic Borrachudos, Pedro Lessa, Salto da Divisa Suite, among others, and correlates rocks from of the Zadinian – Mayumbian groups in the West Congo Belt (Affton et al.; 2016; Alkmim et al., 2017; Bitencourt et al. 2019, Castro et al. 2019, 2020; Kuchenbecker et al., 2015; Kuchenbecker and Barbuena, 2023; Moreira et al, 2020; Silva et al., 2008; Souza et al. 2019; Thiéblemont et al., 2009; Victoria et al., 2019; and references therein). The second rift event, in the Tonian to Cryogenian includes deposition of the Upper Macaúbas Group, with the full development of precursor Macaúbas basin and the establishment of a continental passive margin and ocean-floor spreading marked by ophiolitic rocks from plagiogranites (ca. 645 Ma) of the Ribeirão da Folha formation, metagabbro (ca. 600 Ma) of the Santo Antônio do

Grama Suite, and accompanied by anorogenic magmatism registered by the Southern Bahia Alkaline Province, the Candonga suite and mafic volcanics in the West Congo belt (Amaral et al., 2020; Castro et al., 2020; Degler et al., 2017; Gonçalves-Dias et al., 2016; Kuchenbecker and Barbuena, 2023; Pacheco et al., 2021; Pedrosa-Soares et al., 2020; Rosa et al., 2007; Straathof, 2011; Thiéblemont et al., 2009; and references therein).

Summarizing, the AWCO precursor basin system is represented by the Metavolcano-sedimentary units from the Macaúbas Group, the anorogenic Salto da Divisa Suite, the Ribeirão da Folha Formation, the Santo Antônio do Grama Suite and its correlates such as the Dom Silvério group, the Jequitinhonha complex, and the Andrelândia group in the Brazilian counterpart, and the Zadinian and Mayumbian bimodal volcanic succession, and West Congolian group in the West Congo Belt. All these rifting events were ineffective in splitting the São Francisco-Congo paleocontinent that remained connected by the crustal bridge, namely Bahia-Gabon cratonic bridge, and was breakup by the Cretaceous Atlantic rifting (Alkmim et al., 2017; Pedrosa-Soares et al., 2020; and references therein).

The amalgamation of Western Gondwana in the Late Ediacaran to Early Cambrian, in the Araçuaí-West Congo orogenic system (AWCO), was probably developed by accretionary wedges in subduction zones, later evolving to suture zones in collisional settings. The Abre Campo shear zone (Figure 2.2C), a major AWCO structural and geophysical discontinuity, is interpreted as developed during the closure of the oceanic portion of the Macaúbas basin (Amaral et al., 2020; Alkmim et al., 2017; Pedrosa-Soares et al., 2020; Peixoto et al., 2015). This oceanic closure generated the Ediacaran Rio Doce magmatic arc, metavolcano-sedimentary units of the arc-related basins, the syn-orogenic assemblage of the Salinas basin and Jequitinhonha complex, and syn- to post-collisional plutonic rocks. Metavolcano-sedimentary and arc-related rocks, including pre- to post-collisional plutonic rocks, intra-arc, forearc, and retro-arc basins, forming the high-grade internal zone or the crystalline core of the AWCO (Alkmim et al., 2017; Araujo et al., 2020; Castro et al., 2020; Degler et al., 2017; Deluca et al., 2019; Gonçalves et al., 2018; Gradim et al., 2014; Noce et al., 2004; Novo et al., 2018; Pacheco et al., 2021; Paes et al., 2010; Pedrosa-Soares, et al., 2001, 2008, 2011, 2020; Peixoto et al., 2015; Ricther et al., 2016; Tedeschi et al., 2016; and references therein).

AWCO evolution includes three main orogenic stages: the pre-collisional stage (c. 630-585 Ma) related to the Rio Doce magmatic arc; the collisional stage (c. 585-540 Ma) associated with regional tectonics and metamorphism, and the production of a massive amount of peraluminous granites; and the post-collisional stage (c. 530-480 Ma) related to the AWCO

gravitational collapse, and the generation of a myriad of granitic and mafic intrusions associated with crustal decompression (Alkmim et al., 2017; Aranda et al., 2020; Araujo et al., 2020; De Campos et al., 2016; Deluca, 2018; Gonçalves et al., 2016, 2018; Gradim et al., 2014; Melo et al., 2017a, b, 2020; Pedrosa-Soares et al., 2008, 2011, 2020; Serrano et al., 2018; Tedeschi et al., 2016).

The Rio Doce magmatic arc extend to the Ribeira belt possibly through the Marceleza-Leopoldina-Serra da Bolívia complex (Figure 2.2) (Corrales et al., 2020; Heilbron et al., 2013, 2020; Tedeschi et al., 2016). The Ribeira belt comprises two different magmatic arc systems represented by Marceleza-Leopoldina-Serra da Bolívia complex, Rio Negro, and Serra da Prata arcs. The Marceleza-Leopoldina-Serra da Bolívia complex (εNd(t) -5.5 to -11; εHf(t) -0.9 to -3.75; Corrales et al., 2020; Heilbron et al., 2013, 2017, 2020) developed within a Paleoproterozoic microcontinent between ca. 650 Ma and 590 Ma, representing the Inner Continental Magmatic Arc System. Located to the east of Marceleza-Leopoldina-Serra da Bolívia complex, the correlated Rio Negro (790-605 Ma; εNd(t) +5 to -14; Heilbron and Machado, 2003; Lobato et al., 2015; Peixoto et al., 2017; Tupinambá, et al. 2012) and Serra da Prata (860-838 Ma; εNd(t) +6.4 to -3.7; εHf(t) +14 to +10; Ribeira orogen; Peixoto et al., 2017; Santiago et al., 2020) arcs make up an Outer Magmatic Arc System that evolved from an immature intra-oceanic arc setting, between 860 Ma and 750 Ma, to a continental primitive arc from ca. 660 to 605 Ma (Corrales et al., 2020; Heilbron et al., 2017, 2020).

2.3 The crystalline core of the Araçuaí - West Congo orogenic system

The crystalline core essentially encompasses amphibolite to granulite facies metavolcano-sedimentary rocks from Jequitinhonha orogenic basin and arc-related basins, and pre- to post-collisional plutonic bodies (Alkmim et al., 2017; Araujo et al., 2020; Castro et al., 2020; Degler et al., 2017; Deluca et al., 2019; Gonçalves et al., 2018; Gradim et al., 2014; Noce et al., 2004; Novo et al., 2018; Pacheco et al., 2021; Pedrosa-Soares, et al., 2001, 2008, 2011, 2020; Ricther et al., 2016; Tedeschi et al., 2016; and references therein). These igneous rocks represent a long-lasting succession of granite production events (ca. 630 - 480 Ma) and is one the most remarkable features of the Araçuaí orogen. All those orogenic granites and related rocks produced during the orogenic evolution stages have been grouped into five supersuites namely G1 up to G5 (Pedrosa-Soares and Wiedemann-Leonardos, 2000; Pedrosa-Soares et al., 2001, 2011). Supersuites include suites, batholiths, stocks, individual plutons, and other minor

igneous bodies. These supersuites have been related to the different tectonic episodes to the orogen: G1 supersuite (pre-collisional to early collisional, c. 630-580 Ma), G2 supersuite (late pre-collisional to syn-collisional stage, c. 585-540 Ma), G3 supersuite (late collisional to post-collisional, c. 540-500 Ma), G4 and G5 supersuites (post-collisional, c. 530-480 Ma). We use the name granite and granitoid in a general sense, if not otherwise specified.

The Ediacaran continental magmatic arc, namely Rio Doce arc, extends from the Northern sector of the Araçuaí orogen to the Ribeira belt, defining a roughly N–S-trending (Figure 2.2C). It includes the plutonic portion, represented by G1 supersuite rocks, (in the Araçuaí orogen) and Marceleza-Leopoldina-Serra da Bolívia complex (in the Ribeira orogen), and the arc-related supracrustal successions that comprise metavolcano-sedimentary units of the Rio Doce and Andrelândia groups, the Nova Venécia paragneiss complex, and mélange-related rock assemblages (Araujo et al., 2020; Corrales et al., 2020; Degler et al., 2017; Deluca et al., 2019; Gonçalves, 2009; Gonçalves et al., 2014, 2016, 2018; Gouvêa et al. 2020; Gradim et al., 2014; Heilbron et al., 2020; Noce et al., 2004; Novo, 2013; Novo et al., 2018; Pedrosa-Soares et al., 2020; Peixoto et al., 2015; Richter et al., 2016; Schannor et al., 2019; Soares et al., 2020; Tedeschi et al., 2016).

The Rio Doce magmatic arc evolution consists of oceanic lithosphere subduction from West to East under a continental margin, followed by slab retreating, subduction of the ridge, and slab break-off, with episodes of magmatic migrate from East to West (Tedeschi et al., 2016). Compared to the field, petrographic, geochemical, and isotopic attributes, the plutonic rocks of the Rio Doce arc have a good similarity with other classical continental magmatic arcs (Gonçalves et al., 2018; Narduzzi et al., 2017; Narduzzi, 2018), as Sierra del Valle Vértil (Argentina; Otamendi et al., 2012), North and South Patagonian Batholith (Chile-Argentina; Castro et al., 2011; Hervé et al., 2007; Pankhurst et al., 1999), Western and Eastern Peninsular Ranges (Western USA; Lee et al., 2007), Sierra Nevada Batholith (Western USA; Bateman et al., 1984; Cecil et al., 2012; Chapman et al., 2012; Dodge et al., 1982), Narsajuaq terrane (Canadá; Dunphy and Ludden, 1998), and Los Llanos-Ulapes batholith (Chile-Argentina Boundary; Pankhurst et al., 1998).

The G1 supersuite (c. 630 - 580 Ma; Figure 2.2C) encompasses the I-type, mostly magnesian, metaluminous to slightly peraluminous, calc-alkaline to alkali-calcic, and medium- to high-K granitic to mafic rocks of the Rio Doce magmatic arc, including magmas formed by crustal anatexis with minor involvement of mantle melts (e.g., Gonçalves et al., 2016, 2018; Tedeschi et al., 2016). It is represented by tonalites to granodiorites with mafic to dioritic

enclaves and facies, and minor gabbroic plutons showing ductile deformation and metamorphism, although well-preserved igneous features can be locally found (Pedrosa-Soares and Wiedemann-Leonardos, 2000; Pedrosa-Soares et al., 2001, 2011). U–Pb ages in magmatic zircon data constrain the crystallization of the rocks between ca. 630 Ma and 574 Ma, with metamorphic ages between ca. 592 Ma and 555 Ma, and isotopic signatures show wide variable for $^{87}Sr/^{86}Sr_{(t)}$ (0.703 to 0.723), $\varepsilon Nd_{(t)}$ (-4.8 to -13.6), Nd $_{TDM}$ model ages (1.36 Ga to 2.26 Ga), $\varepsilon Hf_{(t)}$ (-2 to -24.5), and Hf $_{TDM}$ (1.47 to 1.9 Ga) (Angelo et al., 2020; Araujo et al., 2019; De Campos et al., 2004; Figueiredo, 2009; Gonçalves-Dias, 2012; Gonçalves, 2009; Gonçalves et al., 2014; 2016; 2018; Gouvêa et al. 2020; Gradim et al., 2014; Martins el at., 2004; Mendes et al., 2010; Mondou et al., 2012; Nalini Jr., 1997; Nalini et al., 2000; Narduzzi, 2018; Narduzzi et al. 2017; Noce et al., 2000; Novo et al., 2010; Novo, 2013; Paes, 1999; Paes et al., 2010; Pedrosa-Soares et al., 2011; Petitgirard et al., 2009; Schannor et al., 2019; 2020; Silva et al., 2005; 2011; Soares et al., 2020; Tedeschi et al., 2016; Teixeira et al., 2020; and references therein). The chemical signature and hybrid isotopic attributes of the G1 rocks suggest an interaction between the Paleoproterozoic continental basement and minor mantle-derived magmas in a continental margin setting.

In the study area, G1 supersuite rocks form elongated intrusions namely Santa Tereza and Jequitibá suites (Figueiredo and Campos Neto, 1993; Leite et al., 2004; Silva et al., 2004; Tuller, 1993; Vieira and Menezes, 2015) intruding the Nova Venécia complex and contiguous to collisional and post-collisional granites (Figure 2.3). The Santa Tereza suite consists of gabbroic to granodioritic orthogneisses with or without orthopyroxene, garnet, and amphibole. The Jequitibá suite comprises of granodioritic to monzonitic orthogneisses with subordinate garnet and amphibole. They present metaluminous to slightly peraluminous (ASI < 1.1), calcic to alkali-calcic, predominantly magnesian, and calc-alkaline lithochemical signatures (Leite et al., 2004; Silva et al., 2004; Tuller, 1993).

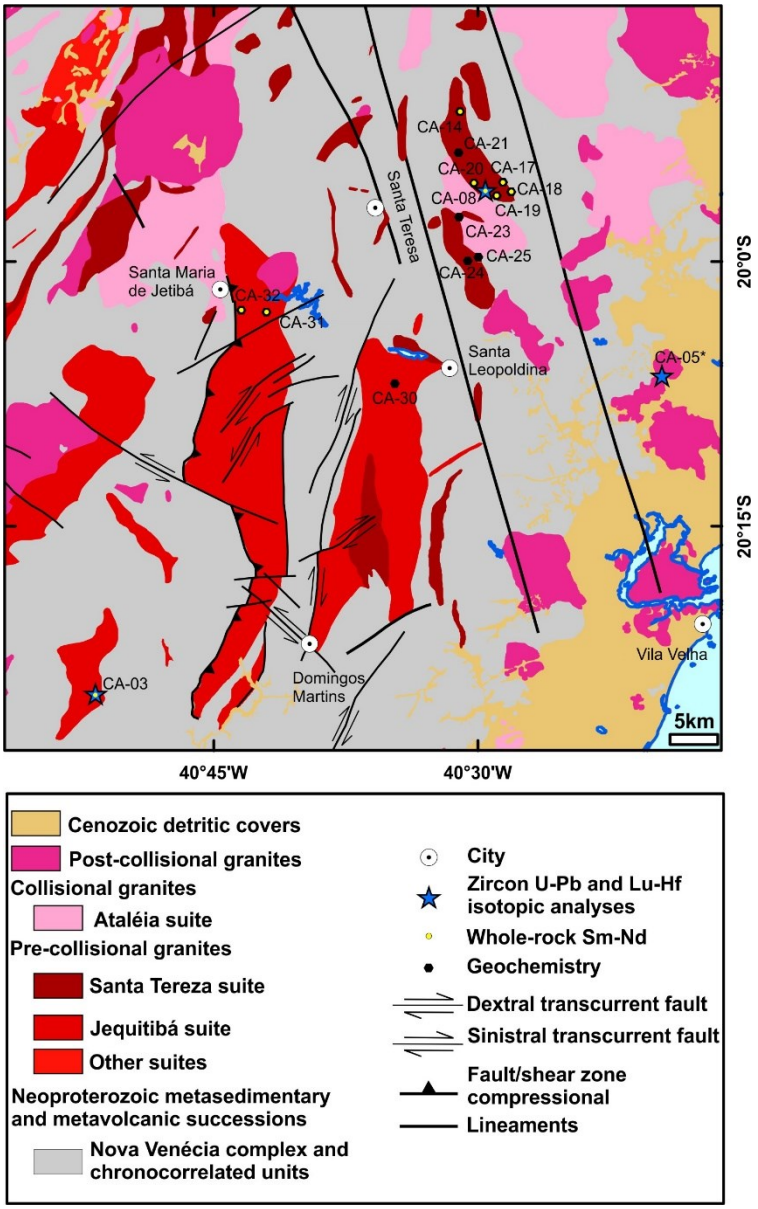

Figure 2.3 Simplified geological map of the study area showing the local of samples (modified from Leite et al., 2004; Silva et al., 2004; Vieira and Menezes, 2015).

The Nova Venécia complex (NVC; Figure 2.2C) consists of migmatitic Al-rich paragneisses and garnet-cordierite granulites, latest poor to free in biotite, and both with lenses of paraderived calc-silicate rocks, covering a large area in the focused region (Figures 2.2C and 2.3). Its protoliths were pelitic to wacky sediments (Gradim et al., 2014; Roncato, 2009; Uhlein et al., 2014). Quantitative data indicate a metamorphic peak of ca. 712 °C to ca. 970 °C at 4.4 kbar to 7.5 kbar, around 563 Ma, in an amphibolite to granulite facies (Gradim et al., 2014; Munhá et al., 2005; Pedrosa-Soares et al., 2020; Richter et al., 2016; Schiavetti, 2019; Vieira, 2007). Few analytical data for regional aluminous gneiss show $^{87}Sr/^{86}Sr_{(t)}$ between 0.708 and

0.7194, $\varepsilon Nd_{(t)}$ of -8.14, Nd_{TDM} of 1.88 Ga (De Campos et al., 2004; IBGE, 1987; Munhá et al., 2005; Tuller, 1993). U-Pb ages in detrital zircons suggest maximum sedimentation age at 590 to 640 Ma (Belém, 2014; Gradim et al., 2014; Noce et al., 2004; Richter et al., 2016). According to published U-Pb geochronological data from detrital grains of zircon, the Rio Doce arc has been considered one of the most significant sediment sources for the Nova Venécia complex (Araujo et al., 2020; Noce et al., 2004; Gradim et al., 2014; Richter et al., 2016). Besides, the obtained U-Pb age also indicate as probable sedimentary provenance the Marceleza-Leopoldina-Serra da Bolívia complex (620 - 590 Ma, εNd(t) -5.5 to -11; εHf(t) -0.9 to -3.75; Ribeira orogen; Heilbron et al., 2013; Corrales et al., 2020), the Rio Negro arc (790-605 Ma, εNd(t) +5 to -14, Ribeira orogen; Heilbron and Machado, 2003; Tupinambá, et al. 2012; Lobato et al., 2015), the Southern Bahia Alkaline Province (730-700 Ma; Rosa et al., 2007) and the Salto da Divisa Suite (ca. 880 Ma, Silva et al., 2008). Previous studies suggest that the NVC represents a back-arc basin related development over thin and hot lithospheric domains (Gradim et al., 2014; Richter et al., 2016). The NVC displays autochthonous melts (the G2 Ataléia and Carlos Chagas suites) intimately associated that were formed from paragneisses anatexis during the late pre-collisional to late-collisional stages (c. 585 - 540 Ma) of the Araçuaí orogen (Gradim et al., 2014). A post-collisional thermal episode (535 – 480 Ma) is recorded in the NVC rocks in response to the intrusion of large G5 igneous bodies post-collisional (Richter et al., 2016).

At the west of the Rio Doce magmatic arc, the arc-related supracrustal units encompass the Rio Doce and Andrelândia groups (Figure 2.2C) in the fore-arc to intra-arc domains (Degler et al., 2017; Novo et al., 2018; Tedeschi et al, 2016). The Rio Doce group includes metavolcano-sedimentary and meta-volcanoclastic rocks representing distal to proximal deposits concerning the volcanic arc front, with volcanic protoliths crystallization age of 595 ± 13 Ma to 584 ± 5 Ma, and maximum depositional age in the basin of ca. 594 Ma to 650 Ma (Novo et al., 2018). Strong positive $\varepsilon Hf_{(t)}$ values and zircon trace element data suggest deposition in an ocean or intra-oceanic arc basin distal to the continent for the detrital zircons with U-Pb ages from 650 to 900 Ma (Schannor et al., 2018). P-T quantitative estimations show values of ca. 440 °C to ca. 638 ºC at ca. 4 kbar to 9.3 kb (Novo et al., 2015; Vieira, 2007), constraining the metamorphic conditions from green schist and amphibolite transition to upper amphibolite facies.

Connecting the Araçuaí and Ribeira orogens, the Andrelândia Group located in the southeastern Rio Doce arc region (Figure 2.2C) records a complex sediment transport and mixture with the zircon U-Pb-Hf signature (ca. 592 – 1937 Ma; $\varepsilon Hf_{(t)}$ +14.9 to -25.3, Hf_{TDM}

0.72 to 3.53 Ga) suggesting a transference from passive to active margin settings, during the late amalgamation of Western Gondwana. P-T quantitative studies on migmatitic paragneiss show temperatures between 614 °C and 900 °C, at pressures from 4.2 kbar to 10 kbar (Degler et al., 2017; and references therein).

A vast amount of peraluminous autochthonous melts were formed in the late pre-collisional to syn-collisional stage (G2 Supersuite; c. 585 - 540 Ma) by the regional partial melting of Al-rich paragneisses (Gradim et al., 2014; Melo et al., 2017a, b; Pedrosa-Soares et al., 2011; Peixoto et al., 2015; Richter et al., 2016). This voluminous granite production is related to the maximum crustal stretching of the back-arc basin in the transition from the pre-collisional to collisional stages, the finish of the Rio Doce arc development, and the crustal thickening (Gradim et al., 2014, Melo et al., 2017a, b; Pedrosa-Soares et al., 2020; Richter et al., 2016).

The G2 supersuite (Figure 2.2C) encompasses (sillimanite)-(cordierite)-garnet-biotite granitic rocks, ranging in composition from tonalite to granite, rich in restites of paragneiss and calc-silicate rocks. Zircon and monazite U-Pb ages (ca. 546 Ma to ca. 597 Ma) show a higher period for the generation of the G2 Supersuite, with isotopic signatures variable for $^{87}Sr/^{86}Sr_{(t)}$ (0.70705 to 0.72633), $\varepsilon Nd_{(t)}$ (-4.05 to -15), Nd $_{TDM}$ model ages (1.33 Ga to 2.29 Ga), $\varepsilon Hf_{(t)}$ (-1.8 to -20.4), and Hf $_{TDM}$ (1.3 to 1.9 Ga) (Cavalcante et al. 2018; De Campos et al., 2004; Gonçalves-Dias, 2012; Gonçalves et al., 2016; Gradim et al., 2014; Martins et al., 2004; Mauri et al., 2021; Melo et al., 2017a, b; Nalini Jr., 1997; Nalini et al., 2000; Noce et al., 2000; Peixoto et al., 2015; Pedrosa-Soares et al., 2006; Petitgirard et al., 2009; Richter et al., 2016; Serrano et al., 2018; Silva et al., 2002, 2011; Tuller, 1993; Xavier, 2017; Vauchez et al., 2007). They display the regional solid-state foliation imprinted between 570 Ma - 550 Ma by the collisional tectono-metamorphic event under amphibolite to granulite facies, although some rocks preserve the magmatic textures (Gradim et al., 2014; Melo et al., 2017a, b; Petitgirard et al., 2009; Richter et al., 2016; Serrano et al., 2018). P–T quantitative conditions estimations suggest the metamorphic event at 680°C – 905 °C and 6 kbar – 10.5 kbar (Mauri et al., 2021; Melo et al., 2017a, b; Petitgirard et al., 2009). The post-collisional thermal event (535 – 480 Ma), related to the asthenospheric upwelling during gravitational collapse of the orogen, is also recorded in these rocks (Melo et al., 2017a, b; Richter et al., 2016; Serrano et al., 2018). The granites from Ataléia and Carlos Chagas suites are representatives of the G2 Supersuite formed by Nova Venécia paragneisses anatexis (Gradim et al., 2014; Pedrosa-Soares et al., 2006, 2011, 2020; Richter et al., 2016).

From the late to post-collisional stages (c. 540 - 500 Ma), mica-free peraluminous leucogranites of the G3 supersuite (Figure 2.2C) formed from dehydrating partial melting processes mainly on G2 granitic gneisses and supracrustal paragneisses (in veins, patches, and small plutons), under decompression conditions with the end of tangential efforts and the transition to the gravitational collapse, remaining until the climax of the post-collisional event (Gradim et al., 2014; Melo et al. 2017a, b, 2020; Pedrosa-Soares et al., 2011; Richter et al., 2016; Serrano et al., 2018). Poorly studied, these leucogranites are the least voluminous supersuite representing a long-lasting series of dehydrating melting processes, with crystallization conditions estimated between 750 °C and 840 °C at 2.4 to 5 kbar (Castañeda et al., 2007; Pedrosa-Soares et al., 2011; Serrano et al., 2018).

Lastly, during the late orogenic extensional collapse, mantle plume rising, probably related to delamination of lithospheric mantle and slab breakoff following the collisional stage, provided an important heat source for the production of several post-collisional intrusions grouped in the G4 and G5 supersuites (ca. 530 - 480 Ma) (Araujo et al., 2020; De Campos et al., 2004, 2016; Gradim et al., 2014; Pedrosa-Soares et al., 2011; Serrano et al., 2018). Formed at relatively shallow crustal levels in northern Araçuaí orogen, the G4 supersuite (Figure 2.2C) mostly comprises peraluminous, sub-alkaline, and S-type felsic granites. Hydrated two-mica granites with garnet and cordierite associated with pegmatitic granite and biotite granite represent them. They intrude the Ribeirão da Folha and Salinas formations, with common xenoliths from metasedimentary country rocks (Basílio et al., 2000; Deluca, 2018; Paes et al., 2010; Pedrosa-Soares et al., 2011, 2020; Silva Sá, 1977; Siga Jr., 1986; Silva et al., 2007). This Supersuite is poorly studied with few isotopic data available.

The G5 supersuite (Figure 2.2C) represents the most outstanding post-collisional plutonism of the Araçuaí orogen. They consist of I-type and A-type, metaluminous to slightly peraluminous, high K-Fe calc-alkaline to alkaline granitic rocks, and associated mafic terms, with granitic-charnockitic and/or gabbronoritic rocks displaying widespread evidence of magma mixing and mingling (Aranda et al., 2020, 2021; Araujo, 2019; Araujo et al., 2020; Baltazar et al., 2010; Belém, 2014; De Campos et al., 2004, 2016; Gradim et al., 2014; Macêdo et al. 2022; Mendes at al., 2005; Melo et al., 2020; Noce et al., 2000; Pedrosa-Soares et al., 2011, 2020; Serrano et al., 2018; Söllner et al., 2000; Teixeira et al., 2020; Temporim et al., 2020; Xavier, 2017; Wiedemann et al., 2002). At the south of latitude 18°30', some plutons show cores rich in gabbronoritic rocks surrounded by granitic-charnockitic rocks, with geothermobarometric quantitative data of crystallization pressures between 5.7 kbar and 11.5

kbar and temperatures from 503 ºC to 1000 ºC, suggesting emplacement at deeper crustal levels (Aranda et al., 2021; Ludka and Wiedemann-Leonardos, 2000; Medeiros et al., 2000; Mello, 2000; Mello et al., 2011; Mendes et al., 1999; Mendes and De Campos, 2012; Wiedemann et al., 2002). While to the north of latitude 18°30' S, they typically form composite batholiths with several microgranular enclaves and emplaced at estimated pressures of 2.4 kbar to 3.5 kbar and temperatures from 750 °C to 840 °C (Serrano et al., 2018), indicating exposure of higher crustal levels. They display isotopic attributes with wide variation ranges for $^{87}Sr/^{86}Sr$ (0.702 – 0.721), $\varepsilon Nd_{(t)}$ (-2.5 to -23.8), Nd $_{TDM}$ model ages (1.4 Ga to 3.29 Ga), as well as $\varepsilon Hf_{(t)}$ (+13.5 to -43.8), and Hf $_{TDM}$ model ages (0.6 Ga to 3.8 Ga) (Aranda et al., 2020; Araujo, 2019; Araujo et al., 2020; De Campos et al., 2016; Belém, 2014; Gonçalves-Dias, 2012; Martins et al., 2004; Macêdo et al. 2022; Mello, 2000; Melo et al., 2020; Mendes et al., 2005; Potratz, 2020; Santiago et al., 2020b; Xavier, 2017).

A wide compilation from monazite and zircon U-Pb geochronology from the basement, precursor and orogenic basins, and the granitic Supersuites point to (1) first metamorphism around 560 Ma, corresponding to the regional metamorphic peak of the collisional stage, with temporal overlap between the most productions of G2 granites; (2) second metamorphism around 505 Ma, a result of the thermal event post-cinematic to the regional foliation, matching with G4 and G5 plutonic intrusions; (3) a marked decrease in the production of orogenic magmatic rocks between 540 - 530 Ma, indicating magmatic quiescence and resumption of magma production around 530 Ma; (4) notable hydrothermalism between 515 Ma and 495 Ma due to the extensive production of fluids derived from the dehydration of metasedimentary rocks with delamination and upwelling of asthenospheric mantle (Araujo et al., 2020; Belém, 2014; Castro et al., 2019, 2020; Cutts et al., 2018; Degler et al. 2017; Figueiredo, 2009; Gonçalves et al., 2016; Gonçalves et al., 2019; Gradim et al., 2014; Kuribara et al.,2019; Lopes, 2016; Melo et al., 2017a, b; Monié et al., 2012; Noce et al., 2004, 2007a, b; Novo, 2013; Pedrosa-Soares et al., 2006, 2011, 2020; Peixoto et al., 2015; Richter et al., 2016, Schannor et al., 2018; Schiavetti, 2019; Serrano et al., 2018; Silva et al., 2002; 2011; Silveira-Braga et al., 2019; Söllner et al., 2000; Tedeschi et al., 2016).

CHAPTER 3. SCIENTIFIC CONTRIBUTION I

Article published by Journal of South American Earth Sciences (doi: 10.1016/j.jsames.2023.104490)

This article explores the more easterly expression of the Rio Doce arc through lithochemistry, literature compiled dataset, geochronological and Hf-Nd isotope that represent the least evolved magmatism record in this plutonic unit.

Tracking a magmatic arc within a confined orogen: new evidence from the Araçuaí Orogen (SE Brazil)

Cristina Araujo[1*], Antonio Pedrosa-Soares[1#], Cristiano Lana[2#], Mahyra Tedeschi[1#], Jorge Roncato[1], Ivo Dussin[3#], Paula Serrano[2#], Elton Dantas[4#]

[1]Universidade Federal de Minas Gerais, Programa de Pós-Graduação em Geologia, CPMTC-IGC, Campus Pampulha, Belo Horizonte, Brazil

[2]Universidade Federal de Ouro Preto, Departamento de Geologia, Morro do Cruzeiro, Ouro Preto, Brazil

[3]Universidade do Estado do Rio de Janeiro, Faculdade de Geologia, Rio de Janeiro, Brazil.

[4]Laboratório de Geocronologia, Instituto de Geociências, Universidade de Brasília, Brasília, DF, Brazil

Fellow of the Brazilian Research Council (CNPq)

https://doi.org/10.1016/j.jsames.2023.104490

*Corresponding author at: Universidade Federal de Minas Gerais, Programa de Pós-Graduação em Geologia, CPMTC-IGC, Av. Antônio Carlos, 6627 Belo Horizonte, Brazil. E-mail address: crisgeo@ufmg.br.

ABSTRACT

By comparison with igneous rock assemblages of well-exposed modern magmatic arcs and their typical calc-alkaline, magnesian, I-type signatures, many deeply eroded magmatic arcs have been characterized worldwide, unraveling ancient plate margins. Since the 1980's,

different assemblages of Ediacaran to Cambrian magmatic rocks have been systematically mapped and characterized according to their distinctive petrographic, structural, lithochemical, geochronologic, and isotopic features, allowing to establish the pre-collisional, collisional, and post-collisional stages of the Araçuaí orogen (SE Brazil). Among them, the tonalitic-granodioritic batholiths and stocks with calc-alkaline, magnesian, I-type signatures, rich in dioritic to mafic enclaves, and related metavolcano-sedimentary successions compose a magmatic arc formed in the early Ediacaran, the Rio Doce magmatic arc. Extending for more than 1000 km along the Araçuaí-Ribeira Orogenic System (AROS), the Rio Doce arc shows a hybrid isotopic signature and crustal inheritance, compatible with modern magmatic arcs built on continental active margins. We present new field, petrographic, and lithochemical studies, coupled with U-Pb (LA-ICPMS) geochronology and isotopic (in-zircon Lu-Hf and whole-rock Sm-Nd) analysis, unraveling the least evolved isotopic signatures ever found for tonalitic-granodioritic plutons of the Rio Doce magmatic arc, and a comprehensive data comparison with modern magmatic arcs. The studied Santa Tereza and Jequitibá suites comprise tonalitic-granodioritic and Opx-bearing charnockitic rocks, with calcic-to-alkali-calcic-magnesian I-type signature, associated with gabbroic rocks. Zircon U-Pb data yielded Concordia ages of 612 ± 3 Ma (Santa Tereza) and 594 ± 3 Ma (Jequitibá) for magmatic crystallization, and 580 ± 5 Ma to 571 ± 3 Ma for metamorphic recrystallization, with associated $\varepsilon Nd_{(612Ma)}$ values from -0.06 to -7.05 (T_{DM} model ages: 1.4–2.04 Ga), and $\varepsilon Nd_{(594Ma)}$ values from -6.67 to -8.8 (T_{DM} model ages: 1.64–1.87 Ga). The zircon $\varepsilon Hf_{(t)}$ (+2.3 to -4.8) and Hf T_{DM} model ages (1.33–1.65 Ga) assigned a moderately juvenile to evolved signature for the Santa Tereza suite, while the Jequitibá suite ($\varepsilon Hf_{(t)}$: -1.7 to -36.4; T_{DM} model ages: 1.33–3.21 Ga) shows a more evolved signature. Altogether, data from the Rio Doce arc are similar to typical continental-margin magmatic arcs with the involvement of mantle melts and/or melting of juvenile crust, suggesting a westward slab retreat during ocean-floor subduction within the Araçuaí confined orogen.

KEYWORDS: U-Pb geochronology; Hf-Nd isotopes; slab retreat; active margin; Brasiliano orogeny

3.1 INTRODUCTION

Melts from differentiation of primitive mantle magmas contribute to continental crustal growth in subduction-related settings along plate margins, either in intra-oceanic or continental

magmatic arcs of accretionary orogens (Cawood and Kröner, 2009; Condie, 2007; Moyen et al., 2017). Continental magmatic arcs provide key evidence to understand the formation and recycling of the continental crust through time because they are outcomes of intricate thermal-magmatic interactions involving subducted oceanic lithosphere, the overlain sub-continental mantle wedge, and the continental crust itself along an active plate margin (Castro et al., 2010, 2011; Ducea et al., 2015a, b; Kearey et al., 2014; Moyen et al., 2017; Paterson and Ducea, 2015). Thus, magmatic arcs comprise the most diversified associations of igneous rocks on Earth. After their volcano-sedimentary covers have been removed by erosion, continental magmatic arcs can be recognized by: i) short-to-long-lived, linear-shaped belts of calc-alkaline plutons relatively rich in silica, forming tonalite-granodiorite-rich batholiths, eventually associated with paired metamorphic belts and/or ophiolitic accretionary wedges; ii) common evidence of magma mingling-mixing processes involving mafic (gabbroic, noritic), intermediate (dioritic, tonalitic) and felsic (granodioritic, granitic) terms; and iii) typical petrographic and geochemical features, including wide-ranging silica contents (from acid and intermediate to basic terms), largely prevailing I-type granitic rocks with calc-alkaline-magnesian signature, distinctive trace element patterns (such as negative Nb-Ta-Ti anomaly), and hybrid isotopic attributes and zircon inheritance, reflecting variable thermal-magmatic interactions between continental crust and mantle components (Best, 2003; Brown and Johnson, 2019; Castro et al., 2010; Castro, 2013; Ducea et al., 2015a,b; Frost et al., 2001; Frost and Frost, 2008; Kearey et al., 2014; Kelemen et al., 2014).

By comparison with igneous rock assemblages of well-exposed modern magmatic arcs and their typical lithochemical signature, many deeply eroded magmatic arcs have been characterized worldwide, unraveling ancient plate margins. In the South American platform (Figure 3.1B) several orogenic belts of Brazil and Africa were shaped during the amalgamation of the supercontinent Gondwana (Figures 3.1A and B) as various plates converged and collided during Neoproterozoic/Cambrian times. The Brasiliano orogenic systems encompass distinct components of a Wilson cycle (rift-drift-subduction-collision-collapse) with the development of magmatic arcs from the Tonian to the early Ediacaran (Caxito et al., 2021, 2022; Cordani et al., 2016; Heilbron et al., 2004, 2017, 2020; Santiago et al., 2020; and references therein).

Since the 1980's, different assemblages of Ediacaran to Cambrian magmatic rocks have been systematically mapped in the Araçuaí orogen of southeastern Brazil (Figure 3.1), according to their distinctive field and structural relations, and petrographic, lithochemical, geochronologic, and isotopic features, resulting in the characterization of the major pre-

collisional, collisional and post-collisional igneous and metaigneous supersuites (Table 3.1). Among them, the N-S-trending range of tonalitic-granodioritic batholiths and stocks, crowded with dioritic to mafic enclaves, displaying calc-alkaline-magnesian I-type signatures, hybrid isotopic attributes, and crustal inheritance, locally associated with metavolcano-sedimentary successions, compose the Ediacaran Rio Doce magmatic arc (Figure 3.1), developed from ca. 630 Ma to ca. 585 Ma (Gonçalves et al., 2018; Novo et al., 2018; Pedrosa-Soares et al., 2011, 2020; Tedeschi et al., 2016).

Combined with petrographic and lithochemical studies, U–Pb ages coupled with Hf isotopic signatures from zircon grains are a powerful tool to unveil magmatic arc evolution (Ducea et al., 2015a; Milani et al., 2015; Moyen et al., 2017; Kohanpour et al., 2019). Moreover, in addition to magmatic arc rock studies, the sedimentary record of arc-related basins can provide additional evidence for the history of a magmatic arc, since detrital zircon grains may provide complementary information on old and eroded arc-related sediments (Ducea et al., 2015a, b; Gradim et al., 2014; Novo et al., 2018; Paterson and Ducea, 2015; Pedrosa-Soares et al., 2020; Richter et al., 2016).

Providing new data for understanding the Rio Doce magmatic arc evolution, we present additional bulk-rock chemistry and isotopic analyses (whole-rock Sm-Nd, and U-Pb and Lu-Hf in zircon) on samples collected from the Santa Tereza and Jequitibá suites in the Espírito Santo state, disclosing the easternmost expression of pre-collisional magmatism associated with the Araçuaí orogen (Figure 3.1). The studied rocks comprise charnockite, tonalite, and granodiorite, intruded in migmatitic paragneisses that represent an arc-related basin. The new results unravel the least evolved magmatism ever found in the Rio Doce magmatic arc. We also correlate our data with a thorough data compilation for arc-related rocks found in the Araçuaí and Ribeira orogens and, altogether, compare them with modern magmatic arcs. Finally, we discuss the geochronological and petrological implications of the Rio Doce magmatic arc evolution within the Araçuaí confined orogen in relation to the Adamastor Ocean closing and Western Gondwana amalgamation.

3.2 GEOLOGICAL SETTING

The Araçuaí orogen of southeastern Brazil together with the West Congo Belt of central-southwestern Africa (Figure 3.1) make up a Brasiliano – Pan-African confined orogenic system (the AWCO) developed within an embayment of the São Francisco – Congo paleocontinent (Alkmim et al., 2006, 2017; Pedrosa-Soares et al., 2001, 2008, 2020). To the south along the

Mantiqueira Province (or South Atlantic Brasiliano Orogenic System; Heilbron et al., 2020; Caxito et al., 2022) (Figure 3.1), the Araçuaí orogen connects with the Ribeira Orogen (or Belt; Corrales et al., 2020; Heilbron et al., 2013, 2020; Tedeschi et al., 2016).

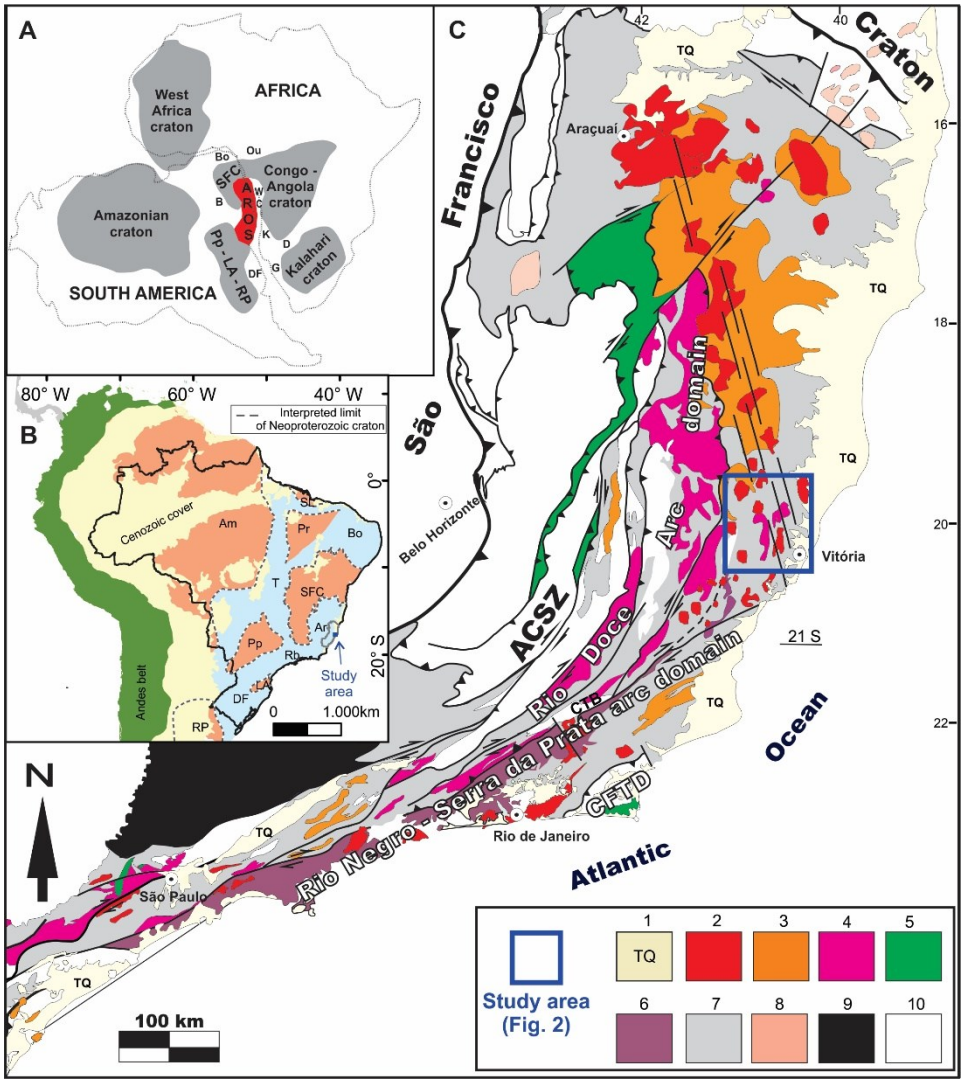

Figure 3.1 (A) Geotectonic setting of Araçuaí-Ribeira orogenic system (AROS), other Brasiliano-Pan-African orogenic systems, and the related cratons in West Gondwana (modified from Alkmim et al., 2006). (B) Brasiliano orogenic systems (blue color) exposed in the Brazilian territory and the related cratons (pink color) in the South American Platform context (modified from Cordani et al., 2016). Orogenic systems: Mantiqueira system - Araçuaí (Ar), Ribeira (Rb) and Dom Feliciano (DF) belts; Tocantins system (T) - Araguaia, Paraguai and Brasília (B) belts; Borborema system (Bo) - Rio Preto, Riacho do Pontal and Sergipano belts; Pan-African system – Damara (D), Gariep (G), Kaoko (K) and West Congo (WC). Cratons: Amazonian (Am), São Francisco (SFC), Paranapanema (Pp); Luís Alves (LA), Rio de La Plata (RP), São Luiz (SL); Parnaíba (Pr). (C) Simplified geological map of the AROS (modified from Santiago et al., 2020, after Pedrosa-Soares et al., 2011, Tedeschi et al., 2016, Degler et al., 2018; and Peixoto et al., 2017). Legend: 1 - Cenozoic cover (TQ); 2 - post-collisional plutonism (ca. 540–480 Ma); 3: collisional plutonism (ca. 585–540 Ma); 4: Rio Doce magmatic arc (ca. 630–585 Ma); 5: Neoproterozoic ophiolite-bearing rock assemblages; 6: Rio Negro – Serra da Prata arc domain (Rio Negro and Serra da Prata magmatic arcs, and related units; ca. 860 Ma–620 Ma); 7: Neoproterozoic metasedimentary and metavolcanic

successions; 8: Tonian and Cryogenian rift-related magmatic rocks; 9: Southern Brasília belt; 10: Pre-Neoproterozoic units; CTB: Central Tectonic Boundary; CFTD: Cabo Frio tectonic domain.

Table 3.1 Main characteristics of the G1 to G5 plutonic supersuites of the Araçuaí orogen (Sources of data compilation in Supplementary file 3A, the present paper; and references therein).

Supersuite	**G1**	**G2**	**G3**	**G4**	**G5**
U-Pb age (Ma)	630 – 585	585 – 540	540 – 500	530 – 480	530 – 480
Lithotypes	mostly tonalite to granodiorite, minor diorite to gabbronorite, with biotite, amphibole and/or pyroxenes; generally garnet-free	mostly biotite-garnet syenogranite to alkali feldspar granite, minor garnet-rich monzogranite to tonalite and garnet-two-mica granite	alkali feldspar granite to syenogranite rich in cordierite and/or garnet, generally biotite-free	garnet-bearing two-mica granite, pegmatoid granite, minor biotite granite	alkali feldspar granite to granodiorite, Opx-bearing charnockitic rocks, gabbro to norite, ultramafic rock
Field relations	tonalitic-granodioritic batholiths and stocks generally rich in dioritic to mafic enclaves, showing solid-state deformation, metamorphism and migmatization, locally with well-preserved igneous fabrics; few single mafic intrusions; associated with the metavolcano-sedimentary Rio Doce Group	granitic batholiths, stratoid bodies and stocks, showing solid-state deformation, metamorphism and migmatization, with restites and xenoliths of metasedimentary rocks; locally with well-preserved igneous fabrics	leucosomes in patches and veins, and minor single stocks, with restites and schlieren of host rocks; free of regional ductile deformation; mainly hosted by G2 metagranites	intrusive plutons and stratoid bodies; minor batholiths; mostly free of regional ductile deformation	intrusive balloon-shaped plutons (stocks) to batholith-size composite bodies, free of regional ductile deformation, rich in magma mingling-mixing features, locally with dioritic to mafic cores
Lithochemistry	metaluminous to slightly peraluminous (A/CNK < 1.1), magnesian, calcic to alkali-calcic, medium- to high-K, expanded calc-alkaline series	peraluminous, sub-alkaline to calc-alkaline	peraluminous, sub-alkaline to high-K alkaline	peraluminous sub-alkaline (K > Na) to alkaline (Na > K)	metaluminous to slightly peraluminous (A/CNK < 1.1), mostly ferroan, high-K calc-alkaline to alkaline; minor tholeiite
Isotopic signature	$\varepsilon Nd_{(t)}$: -0.06 to -13.6; Nd T_{DM}: 1.19 to 2.26 Ga; $^{87}Sr/^{86}Sr_{(i)}$: 0.703 to 0.723; $\varepsilon Hf_{(t)}$: +2.3 to -36.4; Hf T_{DM}: 1.1 to 3.21 Ga	$\varepsilon Nd_{(t)}$: -4.05 to -15; Nd T_{DM} ages: 1.33 to 2.29 Ga; $^{87}Sr/^{86}Sr_{(i)}$: 0.707 to 0.713; $\varepsilon Hf_{(t)}$: -1.8 to -20.4; Hf T_{DM}: 1.3 to 1.9 Ga	$\varepsilon Hf_{(t)}$: -4 to -10; Hf T_{DM}: 1.3 to 1.7 Ga	$^{87}Sr/^{86}Sr_{(i)}$: 0.713	$\varepsilon Nd_{(t)}$: -2.5 to -23.8; Nd T_{DM}: 1.4 to 3.29 Ga; $^{87}Sr/^{86}Sr_{(t)}$: 0.702 to 0.721; $\varepsilon Hf_{(t)}$: +13.5 to -43.8 Hf T_{DM}: 0.6 to 3.8 Ga
Genetic type	mostly metaluminous I-type, minor peraluminous I-type	mostly S-type, minor peraluminous I-type	S-type	S-type	A-type and I-type
Tectonic stage and setting	pre-collisional to early collisional, continental margin magmatic arc (Rio Doce arc)	late pre-collisional to late collisional	late collisional to post-collisional	late collisional to post-collisional	post-collisional

The Araçuaí orogen developed from a precursor basin system evolved from continental rifts to passive margin and ophiolitic rock assemblages, indicating ocean-floor spreading before the generation of a magmatic arc (the Rio Doce arc) triggered by subduction of the oceanic lithosphere during plate convergence, followed by continental collision and post-collisional

gravitational collapse (Alkmim et al., 2006, 2017; Amaral et al., 2020; Araujo et al., 2020; Caxito et al., 2022; Pedrosa-Soares et al., 2001, 2008, 2020; Serrano et al., 2018).

The basement comprises Archean and Paleoproterozoic infracrustal assemblages, including gneissic-migmatitic, granitoid, and granulitic rocks of the Mantiqueira, Guanhães, Gouveia, Porteirinha, Juiz de Fora, Quirino, and Pocrane complexes, as well as Statherian anorogenic granites, and supracrustal units, such as Archean greenstone belts, Siderian to Orosirian metavolcano-sedimentary and metasedimentary units, and the continental rift (aulacogen) to sag units of the Statherian to Stenian Espinhaço supergroup; all of them belonging to the São Francisco – Congo paleocontinent (Alkmim et al., 2017; Degler et al., 2018).

The Araçuaí orogen shows three distinct tectonic stages, disclosed by different rock assemblages: i) the pre-collisional stage (c. 630-585 Ma) mainly marked by the I-type tonalitic-granodioritic batholiths rich in mafic enclaves of the Rio Doce magmatic arc; iii) the collisional stage (c. 585-540 Ma) associated with the regional tectonics and metamorphism, and production of a huge amount of S-type granites; and iii) the post-collisional stage (c. 530-480 Ma) associated with the generation of a myriad of granitic-charnockitic and gabbronoritic intrusions, cutting across the regional tectonic framework (Figure 3.1 C). Accordingly, the orogenic plutonism has been grouped into five supersuites namely (Table 3.1): the G1 supersuite (c. 630-585 Ma), comprising the plutonic igneous rocks formed from pre-collisional to early collisional stages in the Rio Doce arc; the G2 supersuite (c. 585-540 Ma), mostly including the S-type, garnet – biotite ± cordierite ± sillimanite metagranites and granites formed from the late pre-collisional to tardi-collisional stages; the G3 supersuite (540-500 Ma), represented by cordierite-garnet leucogranites formed after the partial melting on G2 metagranites in the late collisional to post-collisional stages; and the G4 and G5 supersuites, encompassing a number of intrusions emplaced in the post-collisional stage (Aranda et al., 2020; Araujo et al., 2020; De Campos et al., 2016; Deluca, 2018; Gonçalves et al., 2016, 2018; Gradim et al., 2014; Melo et al., 2017, 2020; Pedrosa-Soares et al., 2011, 2020; Serrano et al., 2018; Soares et al., 2020; Tedeschi et al., 2016).

The Ediacaran Rio Doce magmatic arc and related orogenic basins extend at least 800 km from the northern sector of the Araçuaí orogen, at latitude 17°30’ N, to the central Ribeira Orogen (Figure 3.1). It includes plutonic rock assemblages and related orogenic basins (Pedrosa-Soares et al., 2020), represented by the G1 supersuite of the Araçuaí orogen (Gonçalves et al., 2014, 2016, 2018; Gouvêa et al. 2020; Pedrosa-Soares et al., 2011, Soares et

al., 2020; Tedeschi et al., 2016), and the Marceleza-Leopoldina-Serra da Bolívia complex of the Ribeira orogen (Corrales et al., 2020; Heilbron et al., 2013, 2020), as well as the arc-related supracrustal successions included in the Rio Doce and Andrelândia groups, the Nova Venécia complex, and mélange-related rock assemblages (Araujo et al., 2020; Degler et al., 2017; Gradim et al., 2014; Noce et al., 2004; Novo et al., 2018; Peixoto et al., 2015; Richter et al., 2016; Schannor et al., 2019). In the Araçuaí orogen, an evolution model for the Rio Doce arc includes oceanic lithosphere subduction from west to east, inducing arc plutons rising, followed by slab retreating driven magmatic migration from east to west, subduction of the oceanic ridge and, finally, slab break-off after continental collision (Tedeschi et al., 2016). Comparing field, petrographic, geochemical, and isotopic attributes, the Rio Doce magmatic arc shows great similarity with several continental magmatic arcs found elsewhere in the world (Gonçalves et al., 2018; Narduzzi et al., 2017; Narduzzi, 2018), such as the Famatinian magmatic arc (Chile-Argentina; Otamendi et al., 2012; Pankhurst et al., 1998), North and South Patagonian Batholith (Chile-Argentina; Castro et al., 2011; Hervé et al., 2007; Pankhurst et al., 1999), Western and Eastern Peninsular Ranges (Western USA; Lee et al., 2007), Sierra Nevada Batholith (Western USA; Bateman et al., 1984; Cecil et al., 2012; Chapman et al., 2012; Dodge et al., 1982), and Narsajuaq terrane (Canadá; Dunphy and Ludden, 1998).

The G1 supersuite mostly encompasses medium-to-high-K calc-alkaline, magnesian, metaluminous to slightly peraluminous I-type, calcic to alkali-calcic tonalitic to granodioritic rocks, generally with mafic to dioritic enclaves, representing granitic (*s.l.*) melts formed by deep crustal anatexis with minor involvement of mantle magmas. The magmatic arc comprises multiple plutons composed of tonalite and granodiorite, locally represented by Opx-bearing rocks (enderbitic to charnockitic rocks), with variable amounts of mafic to dioritic enclaves, and some gabbroic-noritic intrusions (Tedeschi et al., 2016; Gonçalves et al., 2018; Soares et al., 2020). All those rocks generally show ductile deformation and metamorphism, although well-preserved igneous fabrics and magma mingling-mixing features are also found elsewhere along the magmatic arc (Gonçalves et al., 2016, 2018; Gouvêa et al. 2020; Gradim et al., 2014; Narduzzi et al., 2017; Narduzzi, 2018; Pedrosa-Soares and Wiedemann-Leonardos, 2000; Pedrosa-Soares et al., 2011; Pereira et al., 2023; Soares et al., 2020; Tedeschi et al., 2016). Most U–Pb ages from magmatic zircon grains range from ca. 630 Ma to ca. 580 Ma, and zircon metamorphic ages cluster between ca. 592 Ma and ca. 560 Ma (Gonçalves et al., 2016, 2018; Gouvêa et al. 2020; Narduzzi et al., 2017; Narduzzi, 2018; Pedrosa-Soares et al., 2011, 2020; Pereira et al., 2023; Tedeschi et al., 2016;). Isotopic signatures, found in the literature prior to

the present paper, show wide variation for $^{87}Sr/^{86}Sr_{(t)}$ (0.703 to 0.723), $\varepsilon Nd_{(t)}$ (-4.8 to -13.6), Nd T_{DM} model ages (1.36 Ga to 2,26 Ga), $\varepsilon Hf_{(t)}$ (-2 to -24.5), and Hf T_{DM} (1.47 to 1.9 Ga) (Gonçalves et al., 2016; Narduzzi, 2018; Soares et al., 2020; Tedeschi et al., 2016; Pedrosa-Soares et al., 2020, Pereira et al., 2023, and references therein). Chemical signatures, zircon inheritances, and hybrid isotopic attributes for the G1 rocks suggest interactions between the Paleoproterozoic continental basement and variable mantle-derived magmas in a continental margin setting.

In the study area (Figure 3.2), the G1 supersuite rocks form elongated intrusions comprised in the Santa Tereza and Jequitibá suites (Féboli, 1993; Figueiredo and Campos Neto, 1993; Leite et al., 2004; Silva et al., 2004; Tuller, 1993; Vieira and Menezes, 2015), intruding the Nova Venécia complex (Figure 3.2). The Santa Tereza and Jequitibá suites consist of gabbroic to granodioritic orthogneisses (Figure 3.4D) with or without orthopyroxene, garnet, and amphibole.

The Nova Venécia complex covers a large area in the focused region (Figure 3.1, Figure 3.2), representing the sedimentary infill of an arc-related basin, largely located on the back-arc zone of the Rio Doce magmatic arc (Noce et al., 2004; Gradim et al., 2014; Richter et al., 2016; Tedeschi et al., 2016). Consisting of migmatitic Al-rich paragneisses, with intercalations of cordierite granulites and calc-silicate rocks, the Nova Venécia paragneisses represent pelitic to wacky sedimentary protoliths, and the calcsilicate rocks formed from pelite-carbonate (marl) deposits (Gradim et al., 2014). The cordierite granulites, generally bearing sillimanite, hercynite, and garnet, are poor to free in biotite, and represent the highest-grade metamorphic rocks from the metamorphism of Nova Venécia paragneisses (Gradim et al., 2014; Richter et al., 2016). Quantitative data constrain the regional (collisional) metamorphism on the Nova Venécia Complex from 712 °C to 930 °C at 5.0 kbar to 7.5 kbar, i.e., high-grade amphibolite facies to granulite facies, between 580-550 Ma (Gradim et al., 2014; Munhá et al., 2005; Richter et al., 2016). U-Pb analyses on detrital zircon grains from rocks of the Nova Venécia complex yield ages from 2597 Ma to 582 Ma, outlining a rather unimodal age spectrum with the main peak at 600 Ma, and $\varepsilon Hf_{(t)}$ from -39 to +4 with Hf_{TDM} from 3.5 Ga to 1.2 Ga (Araujo et al., 2020; Belém, 2014; Gradim et al., 2014; Noce et al., 2004; Pedrosa-Soares et al., 2020; Richter et al., 2016). Whole-rock samples from the peraluminous paragneisses show $^{87}Sr/^{86}Sr_{(t)}$ between 0.708 and 0.71938, and $\varepsilon Nd_{(t)}$ of -8.14 with Nd_{TDM} at 1.88 Ga (De Campos et al., 2004; IBGE, 1987; Munhá et al., 2005; Tuller, 1993). The available dataset suggests that the Rio Doce arc

is, indeed, the most important sediment source for the Nova Venécia complex, with minor contributions from older sources, such as the Serra da Prata and Rio Negro magmatic arcs of the Ribeira Orogen (Heilbron and Machado, 2003; Tupinambá, et al. 2012; Lobato et al., 2015; Peixoto et al., 2017, 2022; Heilbron et al., 2020), the Southern Bahia Alkaline Province (Rosa et al., 2007), the Salto da Divisa Suite (ca. 915-880 Ma, Silva et al., 2008; Victoria et al., 2022) and basement complexes (Degler et al., 2018).

Under high-amphibolite to granulite facies conditions, anatexis events on the Nova Venécia complex formed a huge amount of autochthonous to allochthonous peraluminous (S-type) granitic melts, crystallized as garnet-biotite granites comprised by the Ataléia and Carlos Chagas suites of the G2 supersuite, during the late pre-collisional to late collisional stages of the Araçuaí orogen (Araujo et al., 2020; Gradim et al., 2014; Melo et al., 2017; Mauri et al., 2021; Pedrosa-Soares et al., 2011, 2020; Richter et al., 2016).

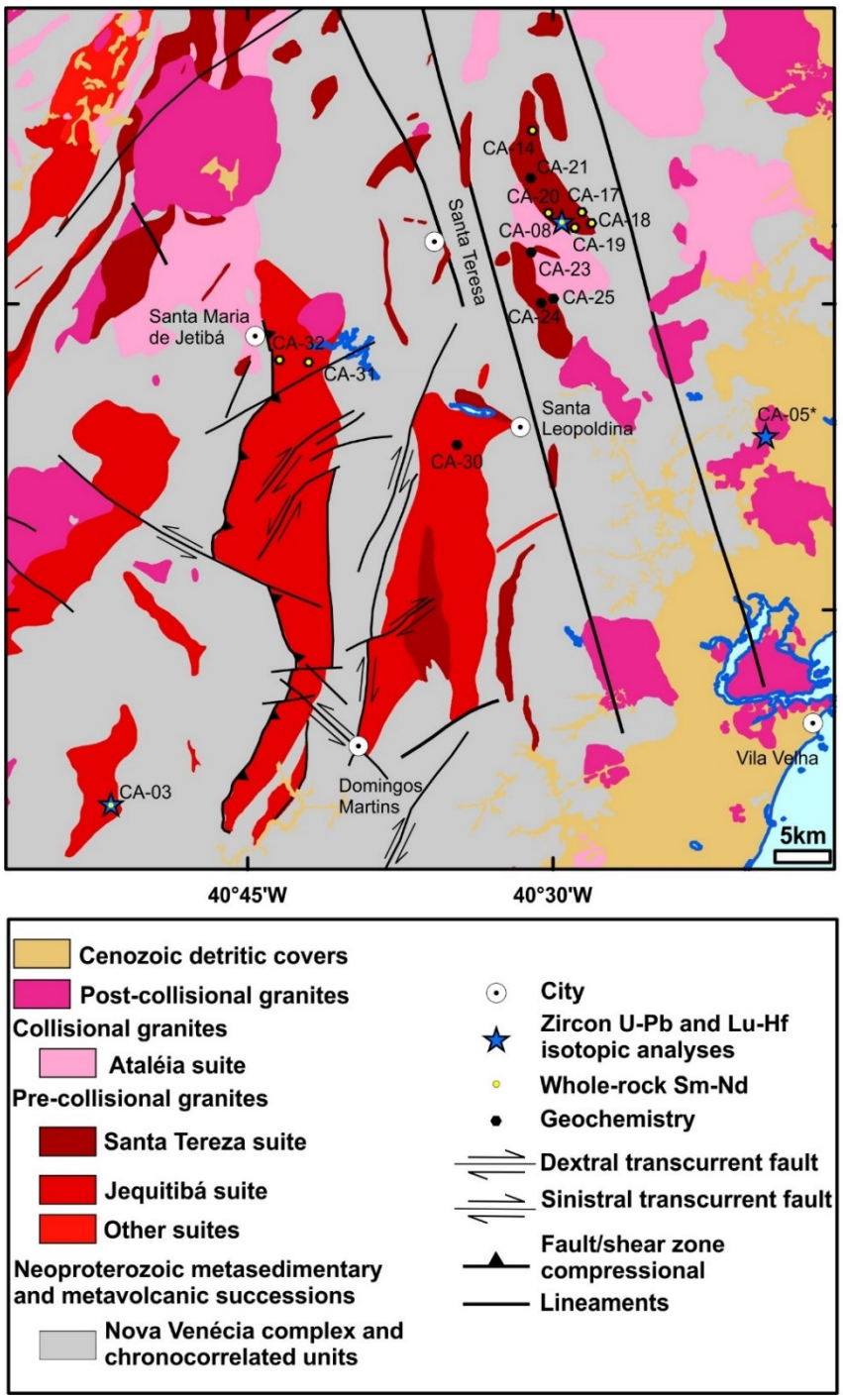

Figure 3.2 Simplified geological map of the study area, showing the analyzed samples locations (modified from Leite et al., 2004; Silva et al., 2004; Vieira and Menezes, 2015). *Zircon U-Pb and Lu-Hf isotopic analyses by Araujo et al. (2020).

3.3 MATERIALS AND METHODS

In this work, the Araçuaí orogen was divided into Northern (North of 18°30' S), Central (from 18°30' to 20° S) and Southern (South of 20° S) sectors, and Western (West of 41° W) and Eastern (East of 41° W) sectors. Geographical coordinates refer to the present-day position

of continents, even in relation to paleocontinental descriptions. Located in the Eastern and Southern-Central sectors, the study area includes rocks of the pre-collisional, collisional, and post-collisional orogenic stages, intruded in the Nova Venécia complex (Figure 3.2).

Our main focus is on intrusions comprised by the Santa Tereza and Jequitibá suites (Féboli, 1993; Figueiredo and Campos Neto, 1993; Leite et al., 2004; Silva et al., 2004; Tuller, 1993; Vieira and Menezes, 2015). Representative samples of these suites were selected, after field and petrographic studies, to be analyzed for bulk-rock chemistry and isotopic Sm-Nd, and zircon U-Pb and Lu-Hf methods. The terms granite and granitic rocks are used in a general sense for felsic igneous rocks rich in quartz unless otherwise specified. Mineral abbreviations are from Whitney and Evans (2010).

Our new analytical data are available in Supplementary Files 3.A and 3.B. The selected samples are homogenous and free of weathering coats, fracture fillings, veins, and any hydrothermal alteration evidence. All of them were properly cleaned before the analytical procedures. The samples were crushed and milled at the SEPURA laboratory of the CPMTC-UFMG research center, Federal University of Minas Gerais, Belo Horizonte, Brazil. Bulk-rock geochemistry (major and trace elements including Rare-Earth Elements - REE) analyses were performed in the SGS-Geosol Laboratories (Vespasiano, Brazil). Major elements were analyzed by X-Ray fluorescence (XRF79C) after fusion with lithium tetraborate, with detection limits of 0.01% to 0.1%. Trace element concentrations were analyzed via inductively coupled plasma mass spectrometry (ICP-MS) after fusion with lithium tetraborate and digestion with a multi-acid solution (HCl, HNO_3, HF, and $HClO_4$), and detection limits of 0.05 to 10 ppm. The loss on ignition (LOI) was calculated by weighting difference after 1000 ºC heating. The analytical results were organized, evaluated, and interpreted by using the GCDKit software (Janoušek et al., 2006). They are presented in Supplementary File 3.A, Table 3.2, and Figures 3.4 to 3.7.

For isotopic analyses on zircon grains, about 3 kg of each rock sample were prepared by crushing and milling, followed by heavy minerals concentration by conventional methods (e.g., dense liquid and magnetic separator) in the SEPURA laboratory (CPMTC-UFMG) and at the CPGeo of the University of São Paulo. Disregarding color, shape, or size, zircon grains were handpicked under a binocular microscope and mounted in epoxy mounts at the Isotopic Geochemistry Laboratory of UFOP (Federal University of Ouro Preto). After polishing the mounts to expose grain centers, they were imaged under cathodoluminescence (CL), secondary electron (SE), and the backscattered electron (BSE) in a JEOL 6510 Scanning Electron

Microscope hosted at Microscopy and Microanalysis Laboratory of the Federal University of Ouro Preto. These images were obtained to examine morphological features, internal textures, and the presence of inclusions, cracks, and damaged areas to assist in the discrimination of grain regions for locating the U-Pb and Lu-Hf spot analyses.

Zircon U-Pb isotopic analyses were carried out using a ThermoScientific Element II sector field coupled to a PhotonMachine ArF 193 mm laser ablation system (LA-SF-ICP-MS) at the Isotope Geochemistry Laboratory of the DEGEO-UFOP. Laser ablations were performed in peak jumping mode during 20s background measurement followed by 20s sample ablation, spot-size 30 μm, 1,9 J/cm^2 fluence, 6 Hz repetition rate, and carried out using He as a carrier gas mixed with Ar before introduction into the ICP-MS. As the primary standard was used the BB-9 zircon (Santos et al., 2017) and, for quality control, the Plesovice (Sláma et al., 2008) as a secondary standard. The software Glitter (van Achterbergh et al., 2001) was employed to reduce the signal data, and for correct background signal, common Pb, laser-induced elemental fractionation, instrumental mass discrimination, and time-dependent elemental fractionation of Pb/U was used a MS Excel spreadsheet program (Gerdes and Zeh, 2006). The common-Pb correction was based on the interference- and background-corrected ^{204}Pb signal and the Pb composition model (Stacey and Kramers, 1975). U-Pb spots cover grain rims and cores, with <1% of discordance, low common Pb, and suitable relations of isotopic ratios were selected for calculations and plotting to obtain the Concordia age distribution diagrams in Isoplot/Ex 4.15 (Ludwig, 2012). Unless otherwise indicated, we use the ^{206}Pb/^{238}U ages. The results are presented in Supplementary File 3.B, Table 3.2, Figures 3.8, and 3.9. Representative grains with different U-Pb ages, morphologies, and internal textures were selected for Lu-Hf isotope analyses.

Lu and Hf isotopic ratios were obtained at the Isotope Geochemistry Laboratory of the DEGEO-UFOP using a Thermo-Scientific Finnigan Neptune Multi-collector inductively coupled to a PhotonMachine ArF 193 mm laser ablation system (LA-MC-ICP-MS). The zircon spots were drilled on top of the previous U-Pb laser spot in order to analyze zircon domains with the same textures. Where this was not possible, care was taken to drill into the same zircon domain previously analyzed for U-Pb, characterized by the CL, SE, and BSE images. Data were collected in static mode during 60 s of ablation and the 50 μm spot-size laser was drilled with at 9 Hz repetition rate. The isotopes ^{172}Yb, ^{173}Yb, and ^{175}Lu were simultaneously monitored during each analysis step to allow for correction of isobaric interferences of Lu and Yb isotopes on 176 mass. Corrections for background signal, instrumental mass bias, and isobaric

interferences of Lu and Yb isotopes on 176 mass were done following the methods by Gerdes and Zeh (2006, 2009). The decay constant for ^{176}Lu is 1.865×10^{-11} a^{-1} (Söderlund et al., 2004) and the $^{176}Lu/^{177}Hf$ ratio is 0.0113 to the average crust in the Paleoproterozoic to Archean (Scherer et al., 2001). For accuracy and external reproducibility, the analyses were verified by BB-9 (Santos et al., 2017), GJ-1 (Jackson et al., 2004), and Plesovice (Sláma et al., 2008) standard zircon, which yielded ratios are in good agreement with the accepted values, with an average of $^{176}Hf/^{177}Hf$ of 0.281675 ± 0.000018 (n = 17), 0.282000 ± 0.000018 (n = 17), 0.282471 ± 0.000020 (n = 17) respectively (errors in ±2σ). The results are presented in Supplementary File 3.B, Table 3.2, Figures 3.9, 3.10, and 3.11.

Sm-Nd isotopic rations were obtained at the Isotope Geochemistry Laboratory of the University of Brasília, on a multi-collector TRITON – Thermo Finnigan mass spectrometer in static mode and methodology as described by Gioia and Pimentel (2000). Whole-rock samples (ca. 50 mg powdered) were mixed with ^{149}Sm-^{150}Nd spike solution and dissolved in HF, HNO_3, and HCl in Savillex capsules. Cation exchange techniques were employed for Sm and Nd extraction from dissolved whole-rock samples using Teflon columns containing LN-Spec resin (HDEHP-di- fractions ethylhexil phosphoric acid supported on PTFE powder). Sm and Nd were loaded in Re evaporation filaments in a double filament assembly. Uncertainties for Sm/Nd and $^{143}Nd/^{144}Nd$ ratios are better than ±0.5% (2σ) and ±0.005% (2σ), respectively, based on repeated analyses of international rock standards BHVO-2 and BCR-1. $^{143}Nd/^{144}Nd$ ratios were normalized to $^{146}Nd/^{144}Nd$ of 0.7219. The De Paolo (1981) model was used to calculate TDM ages. The results are presented in Supplementary File 3.B, Table 3.2, Figures 3.9G, and 3.9H.
In addition, we present a comparative study of our results with an updated and wide dataset, including isotopic U-Pb, Lu-Hf and Sm-Nd, and lithochemical data, compiled from previous studies on arc-related rocks from the Araçuaí and Ribeira orogens, as well as with other classical continental magmatic arcs found elsewhere around the world (Figures 3.4 to 3.12). The lithochemical from plutonic rocks of the Andean, North American, Cascades, Central American, Sierra Nevada, and the Trans-Mexican volcanic arcs were compiled from Castro et al. (2011), Cecil et al. (2012), Hervé et al. (2007), Pankhurst et al. (1999) and Rodríguez et al. (2018), as well as from the PetDB Database (www.earthchem.org/petdb) and GEOROC (http://georoc.mpch-mainz.gwdg.de/georoc/). The compiled dataset of zircon U-Pb ages encompasses spot zircon ages with less than 10% of concordance and excludes inherited zircon grains. When spot ages were not available, published Concordia ages were compiled.

3.4 RESULTS

3.4.1 Petrography and textural relationships

3.4.1.1. Santa Tereza suite

The Santa Tereza rocks have a greenish and, if somewhat weathered, a light gray color. They are medium- to coarse-grained with local alternations of compositional bands (Figures 3.3A and 3.3D). Most samples are garnet-bearing to garnet-free, locally biotite-bearing, foliated metacharnockitic rocks mostly with tonalitic to granodioritic compositions, and minor dioritic and monzogabbroic terms. They consist essentially of plagioclase (40-55%), quartz (20-35%), biotite (10-20%), and K-feldspar (5-10%), including orthopyroxene (5-10%), clinopyroxene (0-10%), amphibole (0-5%) and garnet (0-5%) in the charnockitic rocks. Accessory phases include opaque minerals, zircon, apatite, monazite, allanite, rutile, epidote, and titanite. Carbonate, amphibole, biotite, opaque minerals, sericite, rutile, epidote, muscovite, chlorite, and clay minerals are secondary minerals. Although magmatic features can be found, they mainly present granoblastic to granolepidoblastic textures, with the contacts between the grains being irregular, polygonal and straight, and interlobate. The foliation is given by the orientation of stretched minerals in both felsic and mafic minerals bands and laminae (Figures 3.3A to F). Quartz is anhedral and mostly interstitial, occurs in ribbons or polygonised sometimes. Some plagioclase crystals exhibit myrmekitic intergrowths, compositional zoning, and conspicuous to irregular deformed twins (Figure 3.3C). Antiperthitic texture is omnipresent in all samples (Figures 3.3C, 3.3F). Subgranulation and undulatory extinction are common in quartz and feldspars presented evidence of solid-state deformation. Commonly oriented, biotite presents dark brown to light greenish-brown pleochroism and occasionally is a product of pyroxene and/or amphibole breakdown (Figure 3.3E). K-feldspar is a microcline and trichinized orthoclase with a frequent perthitic texture. Pyroxene has colorless to light greenish-brown or pale pink to light green pleochroism, presenting intergrows with biotite and amphibole, as well as moderate uralitization (Figure 3.3E). Amphibole presents brown to greenish pleochroism and occasionally is a product of pyroxene breakdown. Garnet shows anhedral to subhedral habitus, light pink color, alteration into chlorite, and inclusions of quartz, biotite, zircon, plagioclase, and apatite (Figure 3.3E). There are also garnets free of inclusions.

3.4.1.1. Jequitibá suite

The Jequitibá rocks are light gray to greenish, fine to coarse-grained, isotropic to foliated (Figures 3.3G and 3.3J), and locally show small, coarse-grained, felsic patches with garnet up to 2 cm in diameter (Figure 3.3G). It is also possible to observe alternations of

compositional bands and the presence of mafic enclaves and xenoliths of migmatitic paragneiss. They comprise plagioclase (45-60%), quartz (15-30%), K-feldspar (5-15%), biotite (10-15%), and garnet (0-1%). Accessory phases include opaque minerals, zircon, apatite, monazite, and allanite. Carbonate, biotite, opaque minerals, sericite, muscovite, chlorite, and clay are secondary alteration minerals. The samples consist of foliated diorite to granodiorite, with granoblastic to granolepidoblastic textures and locally preserved magmatic fabrics. The foliation is defined by the orientation of stretched minerals along felsic and mafic bands (Figures 3.3I, 3.3K), with the contacts between the grains being irregular, polygonal and straight, and interlobate. Commonly, quartz and feldspars show elongated crystals with subgrain patterns and undulatory extinction (Figure 3.3I). Plagioclase exhibits antiperthitic and myrmekitic intergrowths, compositional zoning, and conspicuous to irregular, deformed twins (Figure 3.3L). K-feldspar is microcline and trichinized orthoclase, with a typical perthitic texture. Usually oriented along the foliation, the biotite presents dark brown to light greenish-brown pleochroism. Garnet has an anhedral habitus, light pink color, and inclusions of rounded quartz and monazite, and of elongated biotite and apatite (Figures 3.3H, 3.3K).

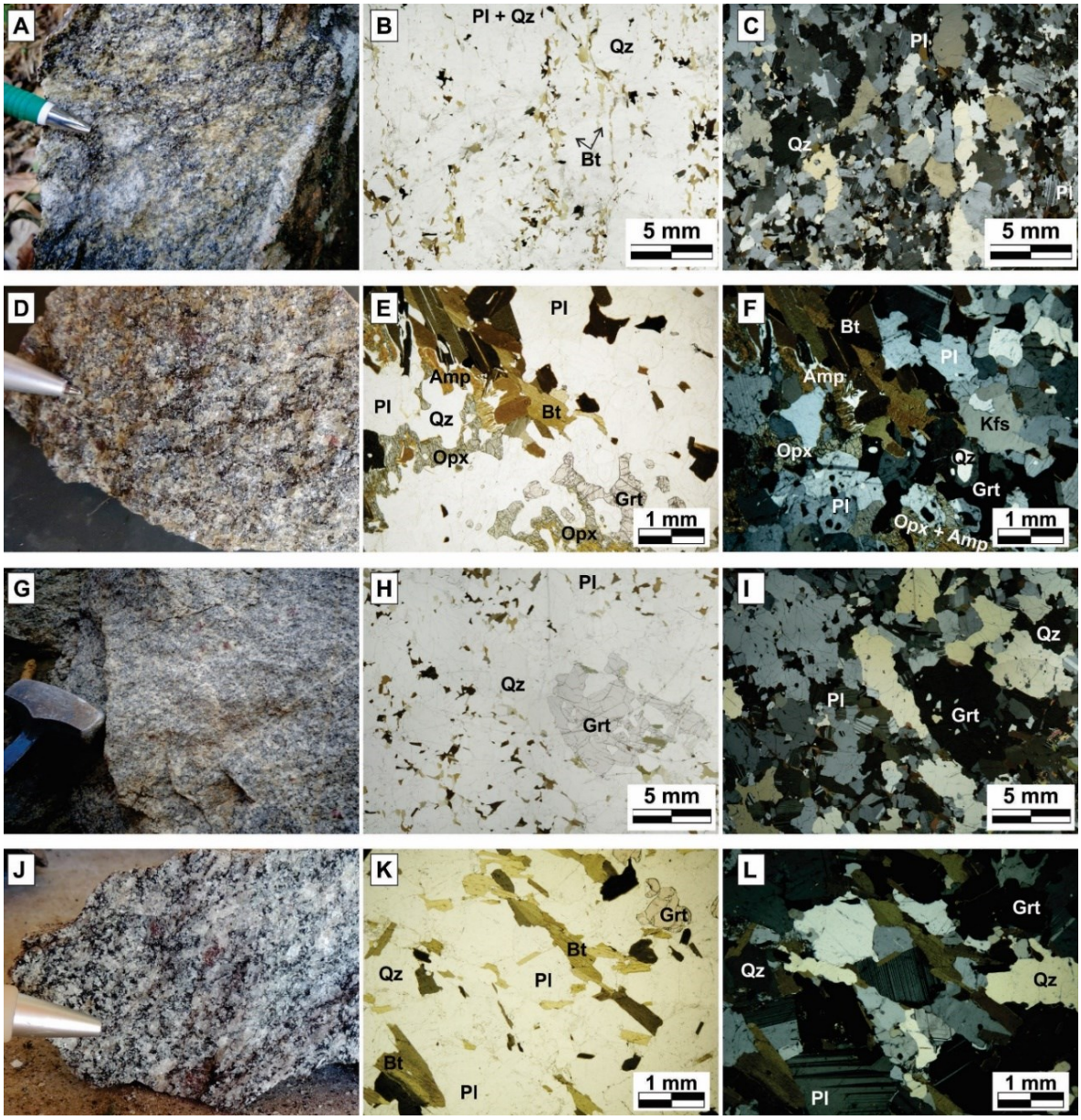

Figure 3.3 Photos and photomicrographs (under transmitted light and polarized light) showing mineralogical and textural features. CA-08 sample: A, B, C. (A) Greenish gray, coarse-grained biotite metagranodiorite, from Santa Tereza suite. (B and C) Photomicrographs showing the concentration of felsic minerals elongated according to bands and displaying undulatory extinction. Plagioclase displays irregular twinning and antiperthitic intergrowths (C); CA-14 sample: D, E, F. (A) Greenish gray, coarse-grained garnet-orthopyroxene-biotite-bearing charnockitic metagranodiorite from Santa Tereza suite. (E and F) Photomicrographs showing local concentration of biotite, orthopyroxene, amphibole, and garnet. Plagioclase displays irregular twinning and antiperthitic intergrowths (F). CA-03 sample: G, H, I. (G) Fine to coarse-grained garnet-biotite metagranodiorite from Jequitibá suite; (H and I) Photomicrographs showing stretched felsic minerals and poikiloblastic garnet. CA-31 sample: J, K, L. (J) Coarse-grained garnet-biotite metagranodiorite from Jequitibá suite. (K and L) Photomicrographs showing plagioclase with irregular twinning and antiperthitic intergrowths, and biotite oriented according to foliation.

3.4.2. Lithochemistry, Geochronology and Isotope Geochemistry

Besides lithochemical analyses on thirteen (13) bulk-rock samples of the Santa Tereza and Jequitibá suites, we also present U-Pb geochronology and isotopic Lu-Hf data for two (02) zircon concentrates and isotopic Sm-Nd results from nine (09) whole-rock samples, of both suites.

3.4.2.1. Lithochemistry

The samples from the Santa Tereza and Jequitibá suites have granodioritic to monzogabbroic compositions, with calc-alkaline, magnesian, calcic to alkali-calcic, I-type, and slightly peraluminous (ASI < 1.1) signatures, representing volcanic arc magmas related to mafic sources (Figures 3.4 and 3.5). They show enrichment in LILE (Large Ion Lithophile Elements), and negative Ba, Nb, Ti, and P anomalies, with positive Th anomalies in silica-rich (acid) samples, and negative Th-U and Ti anomalies in basic to intermediate samples (Figure 3.6). One sample with intermediate silica content from the Jequitibá suite presents a positive Ba anomaly (Figure 3.6). The REE patterns show LREE enrichment ($La_N/Yb_{N\ (intermediate\ to\ basic)}$ = 12 to 49; $La^N/Yb^N{}_{(acid)}$ = 8 – 87) with slightly negative to positive Eu anomalies (Eu/Eu* 0.76 and 1.12), except for the CA-08 sample presenting a prominent negative Eu anomaly (Eu/Eu* 0.32) (Figure 3.6B; Supplementary File 3.A).

3.4.2.2. Zircon U-Th-Pb and Lu-Hf data

3.4.2.2.1. Santa Tereza suite

A sample of a biotite metagranodiorite was selected for U-Pb and Lu-Hf in-zircon analyses (CA-08; Figures 3.2, 3.3A). The zircon population is light brown to colorless and translucent, exhibiting short to long prismatic habitus with subhedral to euhedral terminations (Figure 3.8A). Inclusions of apatite and plagioclase are common in zircon crystals. Grains range from 100 to 600 μm in length, with a length/width ratio from 2 to 11. CL-images display non-zoned to thin and parallel magmatic oscillatory zoning, prevailing medium to high luminescence (Figure 3.8A). Some crystals have a low to dark luminescence (Figures 3.8A, zircon grains 008, 066). Several crystals are surrounded by thin structureless domains of dissolution–recrystallization and overgrowth (Figure 3.8A, zircon grains 053, 059). Oscillatory zoning is absent in BSE images.

Fifty-three U-Pb spot data plot from 635 ± 9 Ma to 545 ± 7 Ma in the Concordia diagram, comprising two main age groups (Figures 3.8A, 3.9A, 3.9B). The older cluster

furnished ages ranging from 630 ± 8 Ma to 593 ± 8 Ma, with Th/U ratios from 1.8 to 0.1, resulting in a Concordia age of 612 ± 3 Ma (39 zircon spots; MSWD = 0.71) and a mean age of 612 ± 3.0 Ma (MSWD = 5.1). The younger cluster ages range from 587 ± 7 Ma to 545 ± 7 Ma with Th/U ratio from 1.4 to 0.2 from non-zoned zircon grains with low to dark CL luminescence (metamorphic domains), yielding a Concordia age of 580 Ma ± 5 Ma (9 zircon spots, MSWD = 0.24) and a mean age of 580 ± 4 Ma (MSWD = 1.6). Unmix age calculation routine (Isoplot/Ex 4.15, Ludwig, 2012) yields agreement age populations with peaks at 577 ± 2 Ma to 615 ± 1 Ma (relative misfit 0.436). One inherited zircon has a spot age of 796 ± 10 Ma.

Twenty- eight analyses on zircon crystals with ages from ca. 545 ± 7 Ma to 635 ± 9 show initial $^{176}Hf/^{177}Hf$ ratios ranging from 0.282457 to 0.282271, $\varepsilon Hf_{(t)}$ between +2.3 and - 4.8, and Hf_{TDM} model ages from ca. 1.13 Ga to ca. 1.5 Ga (Figures 3.9, 3.10, 3.11). The inherited zircon (796 ± 10 Ma) yield initial $^{176}Hf/^{177}Hf$ ratios of 0.282152, with $\varepsilon Hf_{(t)}$ -4.6 and Hf_{TDM} model ages of 1.65 Ga.

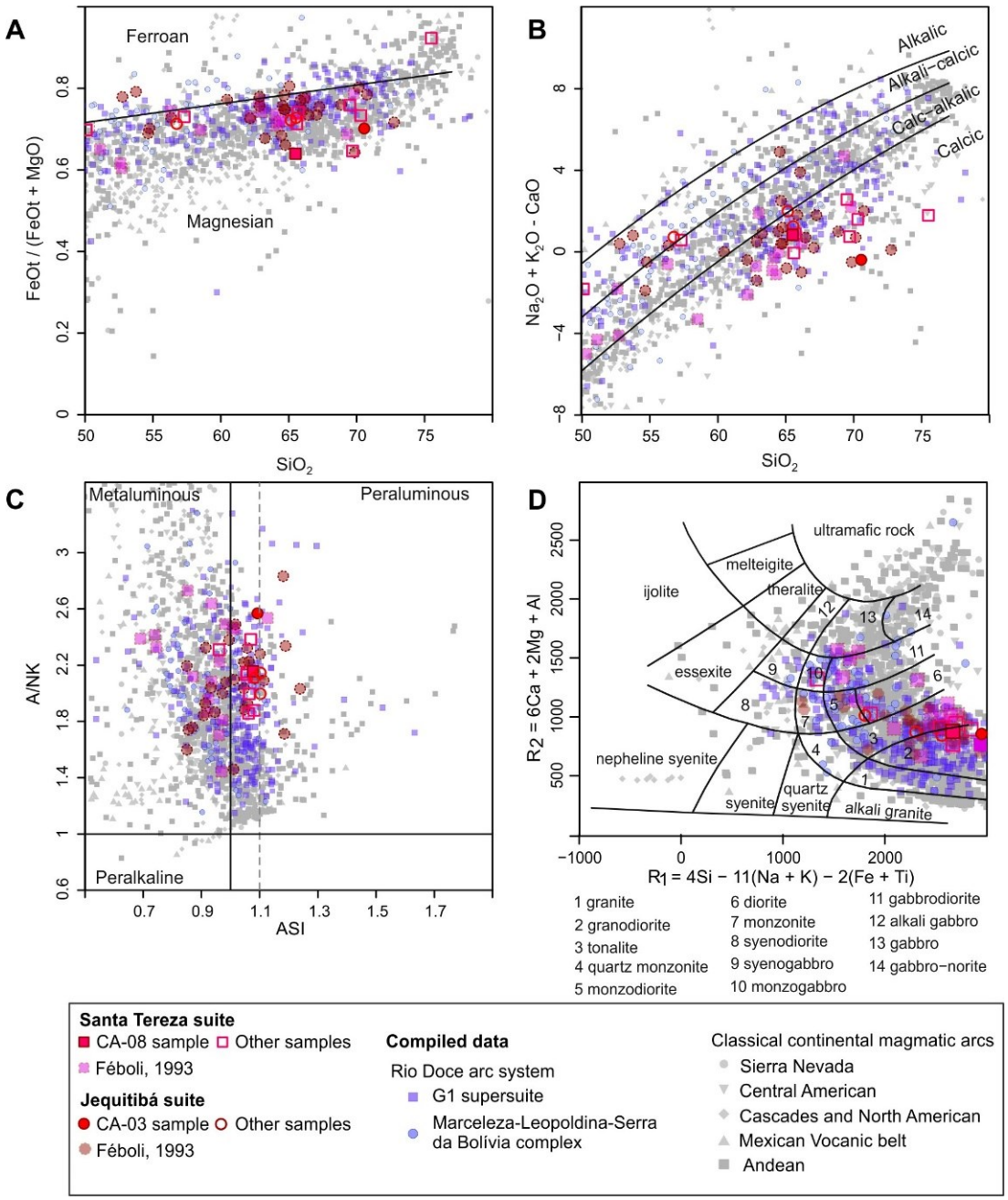

Figure 3.4 Lithochemical data for the studied samples compared to the compiled dataset. A: FeOt / (FeOt + MgO) vs. SiO_2 (wt%) (Frost et al., 2001); B: $Na_2O + K_2O – CaO$ vs. SiO_2 (wt%) (Frost et al., 2001); C: Alumina saturation Index (Frost et al., 2001). Dashed line (ASI = 1.1) delimits the transition between I- and S-type granites according to Chappell and White (1974); D: R1-R2 diagram (De la Roche et al., 1980). Sources of data compilation in Supplementary file 3.A.

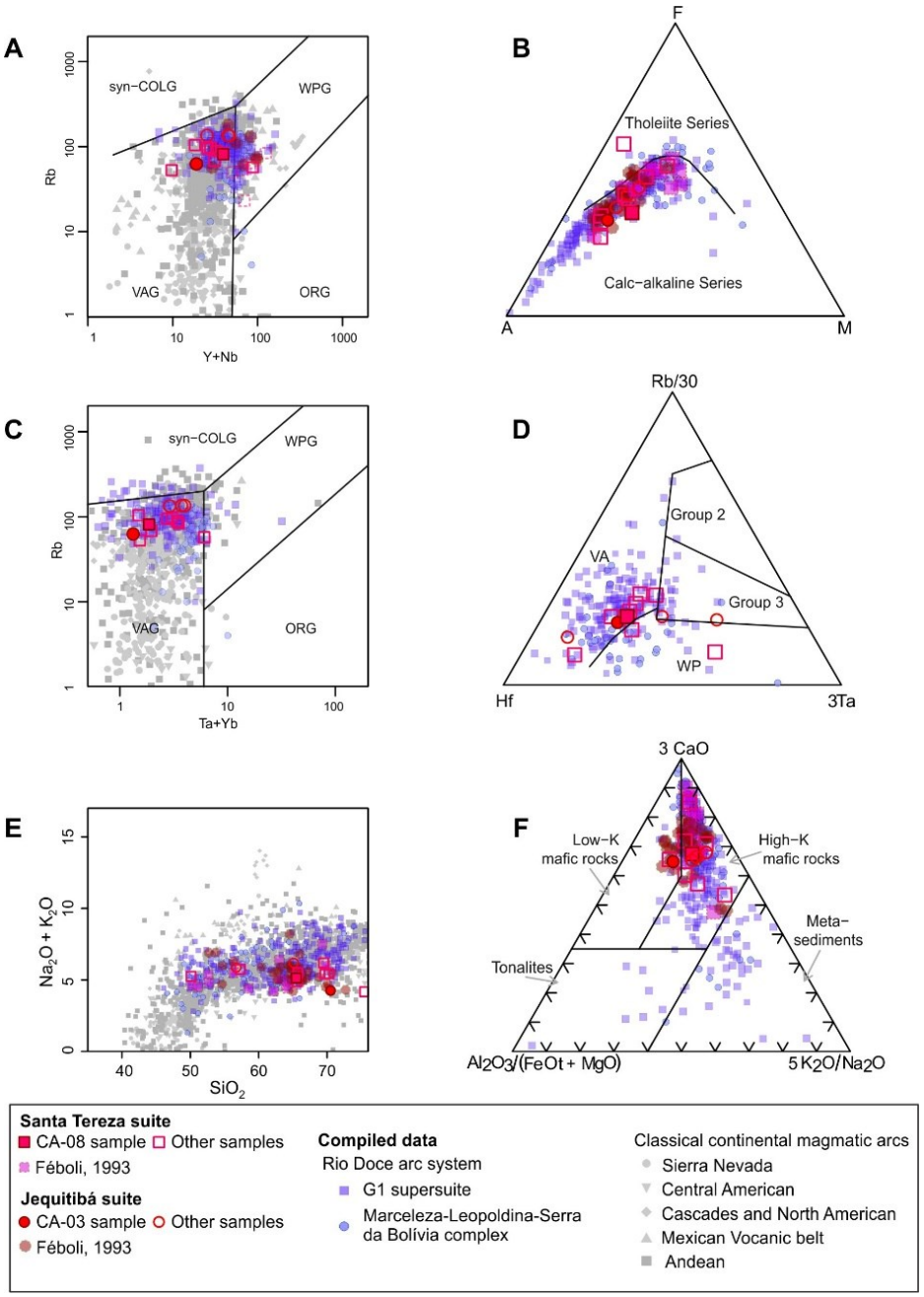

Figure 3.5 Lithochemical data for the studied samples compared to available data from G1 and G2 supersuites of Araçuaí orogen, Marceleza-Leopoldina-Serra da Bolívia complex and Rio Negro arc system from Ribeira orogen, and other classical continental magmatic arcs. A and C: Geotectonic discriminating diagrams by Pearce et al. (1984); B: AFM diagram (Irvine and Baragar, 1971); D: Hf-Rb/30-Ta*3 ternary diagram (Harris et al., 1986); E: $Na_2O + K_2O$ vs. SiO_2 (wt%); F: Source Diagram (Laurent et al., 2014). Meaning fields: ORG, Ocean Ridge Granites; VAG or VA, Volcanic Arc Granites; WPG or WP, Within Plate Granites, COLG, Collision Granites; Group 2, Syn-collision peraluminous intrusions (leucogranites); Group 3, Late or post-collision calc-alkaline intrusions. Sources of data compilation in Supplementary file 3.A.

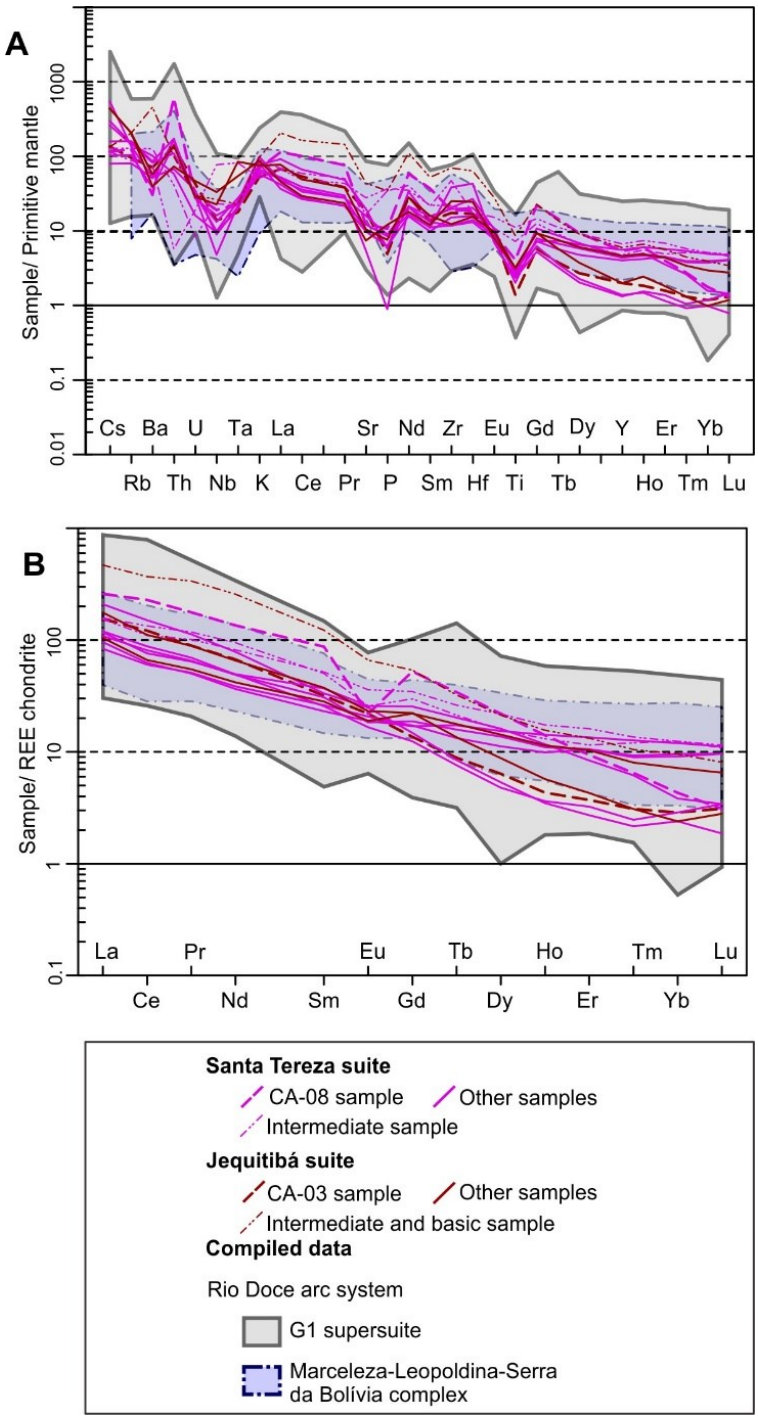

Figure 3.6 A) Multi-elemental diagram normalized to primitive mantle, according to Sun and McDonough (1989); B) Chondrite-normalized REE patterns, normalized according to Boynton (1984). Sources of data compilation in Supplementary file 3.A.

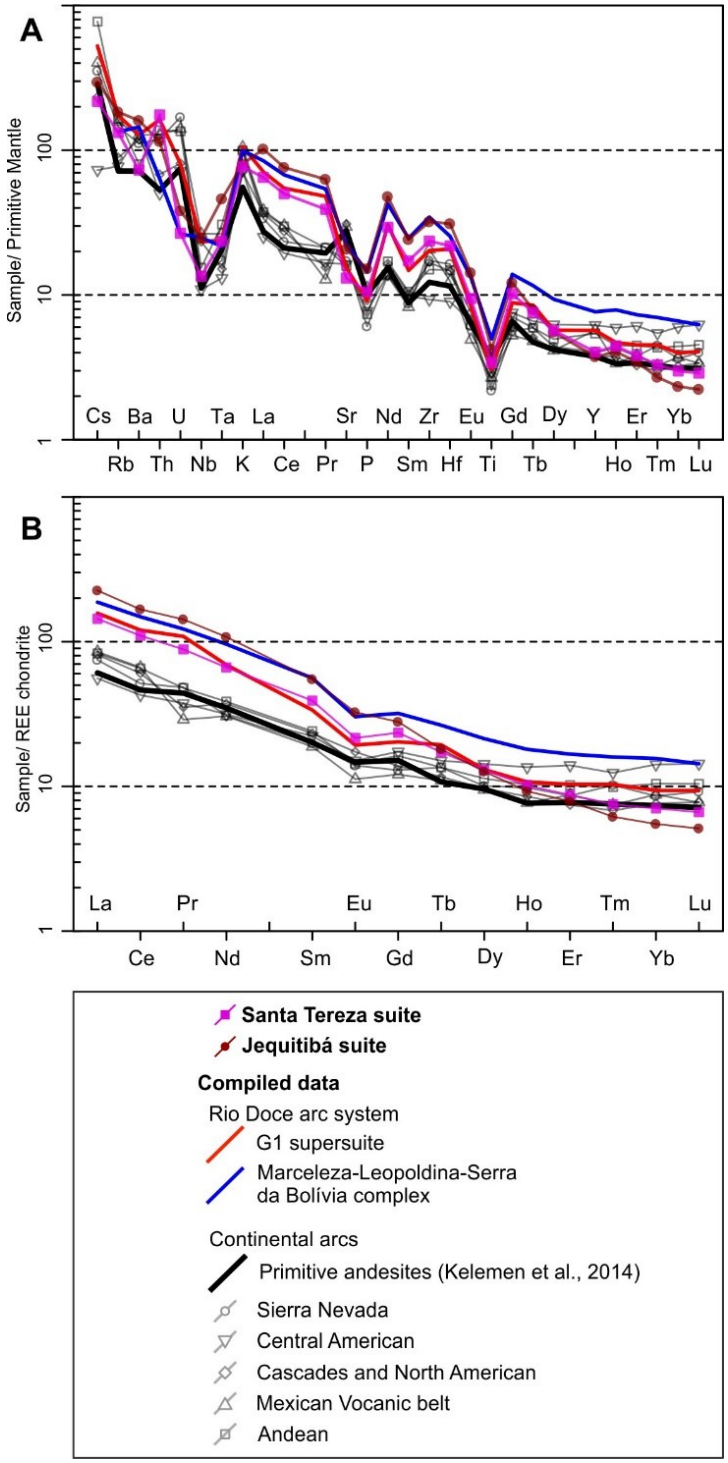

Figure 3.7 Average compositions from Santa Tereza and Jequitibá samples, and compiled data with SiO_2 > 54%. A) Multi-elemental diagram normalized to the primitive mantle, according to Sun and McDonough (1989); B)

Chondrite-normalized REE patterns, according to Boynton (1984). Sources of data compilation in Supplementary file 3.A.

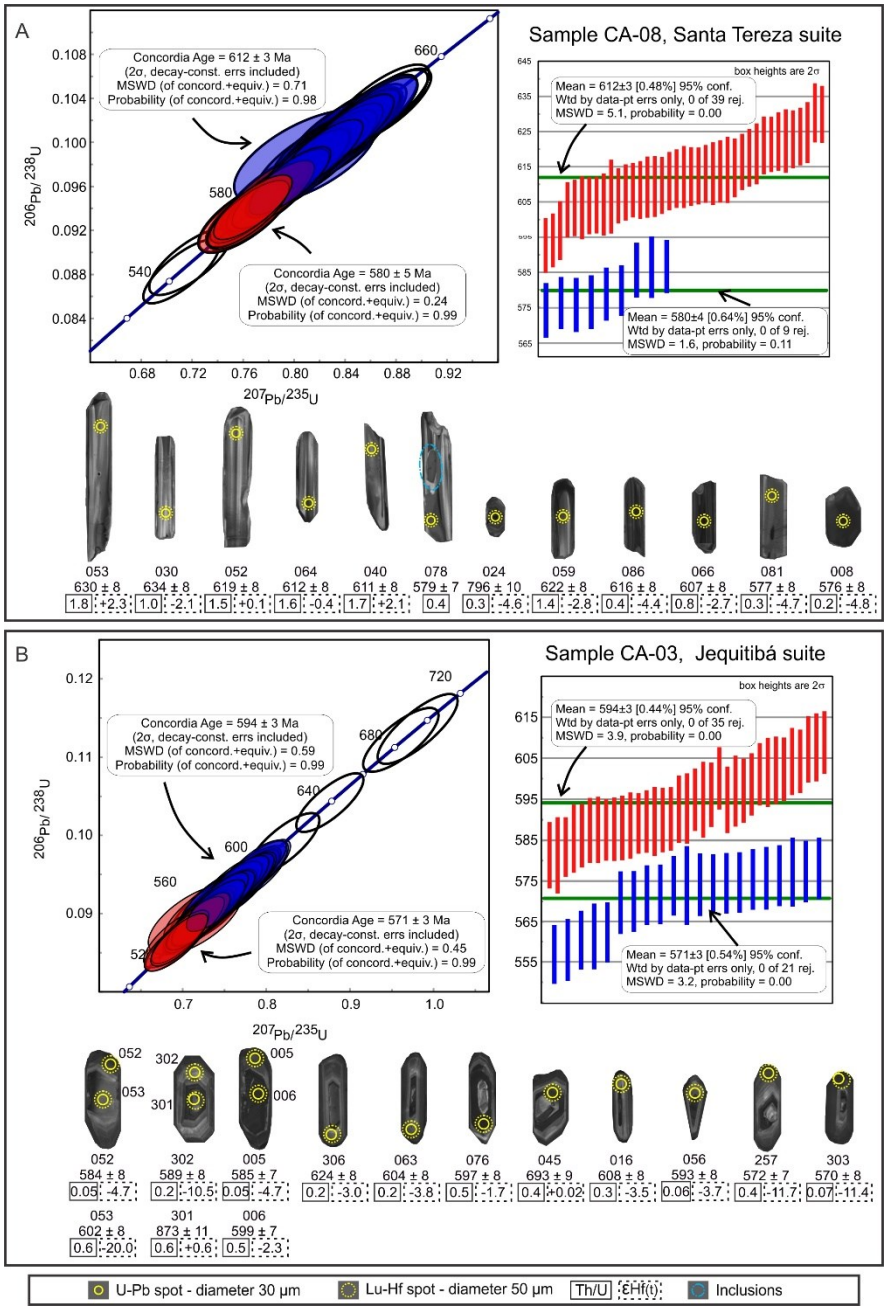

Figure 3.8 (A and B) Concordia diagrams, weighted mean ages, and representative zircons from Santa Tereza and Jequitibá samples. The U-Pb ages are reported as $^{206}Pb/^{238}U$ age in Ma, with errors at 2σ.

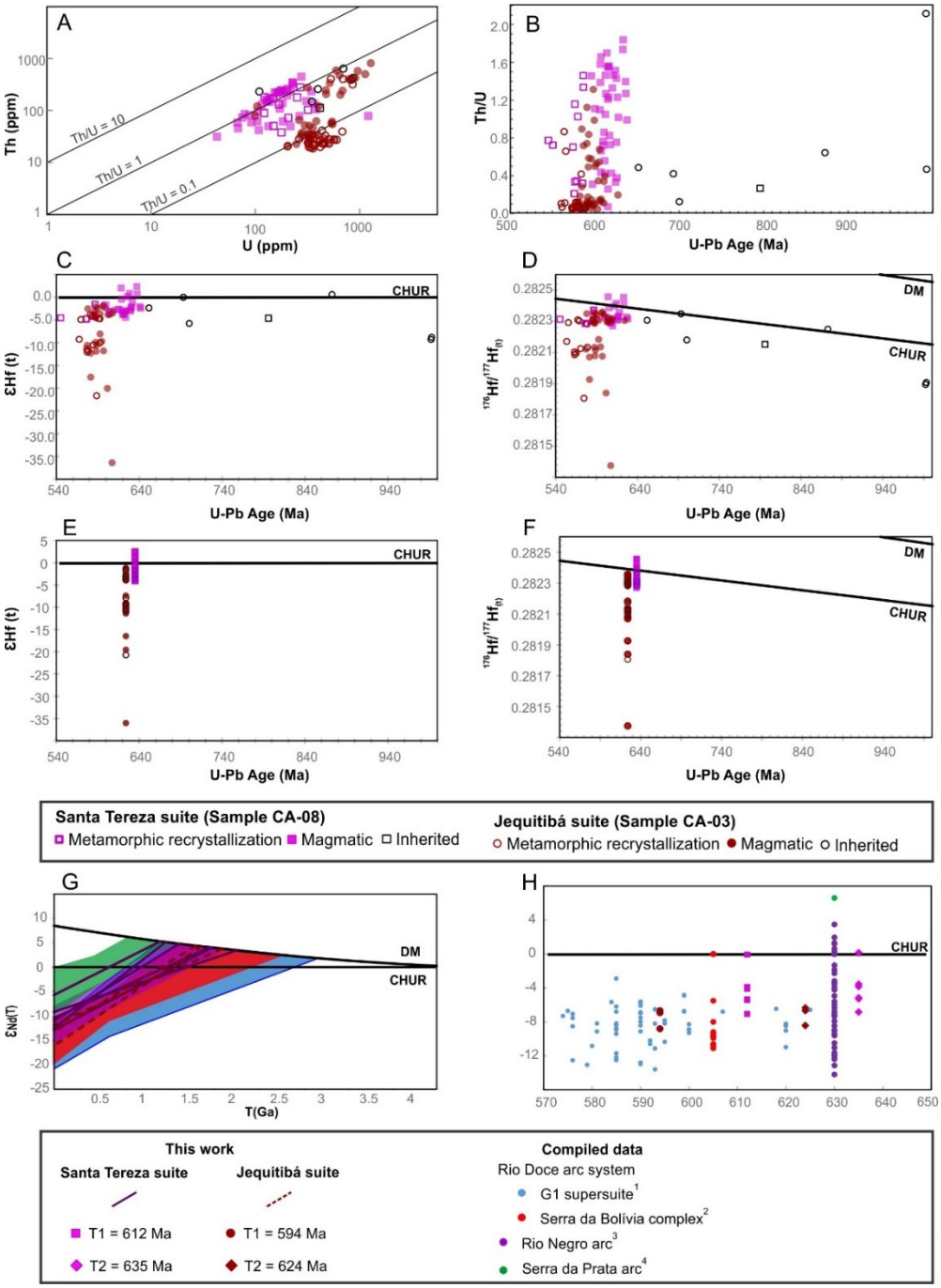

Figure 3.9 (A) Th vs U diagram, (B) Th/U vs U-Pb age (C and D) Lu-Hf data calculated for individual zircon ages, and (E and F) Lu-Hf data calculated for estimated crystallization ages from Santa Tereza and Jequitibá samples. (G and H) Diagrams comparing the Nd isotopic signature from studied samples with the compiled dataset. DM = depleted mantle; CHUR = chondrite uniform reservoir. T1: Concordia age; T2: Estimated crystallization ages. Sources of data compilation: De Campos et al. (2004)[1]; Figueiredo (2009)[1]; Gonçalves (2009)[1]; Gonçalves et al. (2016)[1]; Heilbron et al., (2013)[2]; Martins et al., (2004)[1]; Nalini Jr., (1997)[1]; Nalini et al. (2000)[1]; Novo et al. (2010)[1]; Pedrosa-Soares et al., (2011)[1]; Peixoto et al., (2017)[3,4]; Pereira et al., (2023)[1]; Santiago et al., (2020)[4]; Soares et al. (2020)[1]; Tedeschi et al. (2016)[1]; Tupinambá et al. (2012)[3].

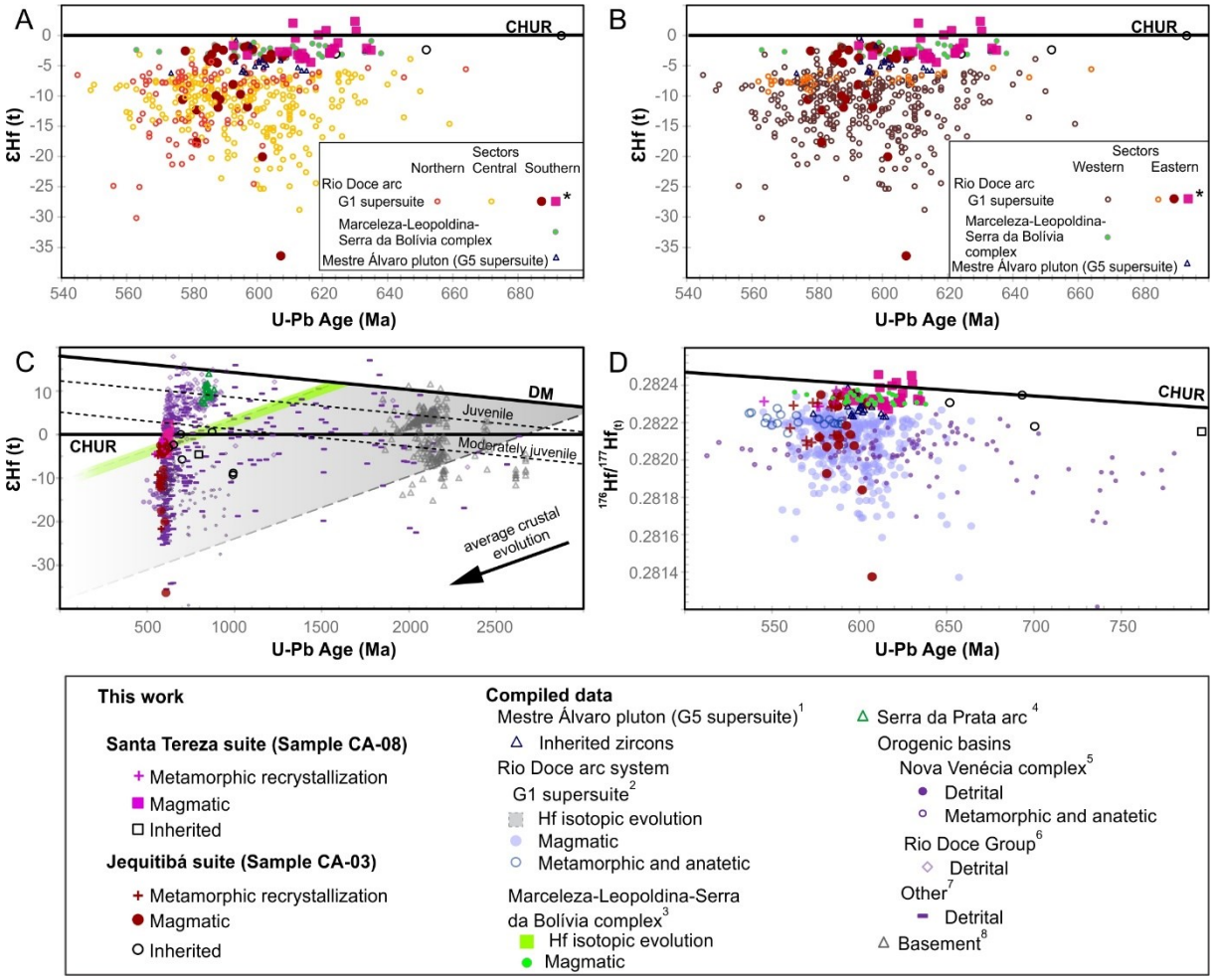

Figure 3.10 Diagrams comparing the U-Pb and Lu-Hf data from studied samples with the compiled dataset. Northern sector: North of 18°30'; Central sector from 18°30' to 20°; Southern sector: South of 20°; Western sector: West of 41°; Eastern sector: East of 41°; * Jequitibá and Santa Tereza data, respectively; DM = depleted mantle; CHUR = chondrite uniform reservoir. Black dashed lines classify fields of juvenile (0–5 ε-units below DM), moderately juvenile (5–12 ε-units below DM) and evolved (> 12 ε-units below DM) composition (Bahlburg et al., 2011). Sources of data compilation: Araujo et al. (2021)[8]; Araujo et al. (2020)[1,5]; Castro et al. (2020)[7]; Corrales et al. (2020)[3]; Degler et al. (2017, 2018)[7,8]; Gonçalves et al. (2016)[2]; Kuribara et al. (2019)[8]; Narduzzi (2018)[2]; Pereira et al. (2023)[2]; Santiago et al. (2020)[4], (2022)[7]; Schannor et al. (2019)[2,6], (2020)[2,8]; Tedeschi et al. (2016)[2]. In A and B diagrams, only magmatic zircon grains were plotted.

3.4.2.2.2. Jequitibá suite

Zircon grains from a garnet-biotite metagranodiorite were analyzed for U-Pb and Lu-Hf (Sample CA-03; Figures 3.2, 3.3G). The zircon population is light brown to colorless, translucent, exhibiting short to long prismatic and bipyramidal habitus with subhedral to euhedral terminations (Figure 3.8B). Inclusions are scarce. The grain lengths range from 70 to 550 µm, with length/width ratios from 2 to 10. CL-images show magmatic oscillatory zoning, prevailing medium to low luminescence, with inherited core in few crystals (Figure 3.8B). Several crystals are surrounded by domains of dissolution–recrystallization and overgrowth

rims (Figure 3.8B, zircon grains 052, 257, and 303). In BSE-images, magmatic oscillatory zoning is also present but absent in some crystals.

Forty analytical spots on igneous domains yield U-Pb ages from 624 ± 8 Ma to 574 ± 7 Ma, with Th/U ratios from 1.3 to 0.1 (Figures 3.8B, 3.9A, 3.9B). For better analytical accuracy, thirty-five spot data were selected to be plotted, resulting in a Concordia age and a mean age of 594 ± 3 Ma (MSWD = 0.55). Six spot analyses on inherited cores yield ages from 652 ± 8 Ma to 1051 ± 12 Ma. Twenty-seven spot analyses on structureless rims (metamorphic domains) yield U-Pb ages from 586 ± 8 Ma to 557 ± 7 Ma, with Th/U ratios ranging from 0.87 to 0.05. Twenty-one spots furnished a Concordia age and a mean age of 571 ± 3 Ma (MSWD = 0.45) (Figures 3.8B, 3.9A, 3.9B). Unmix age calculation routine (Isoplot/Ex 4.15; Ludwig, 2012) for zircon grains younger than 624 Ma yield age populations with peaks at 595 ± 2 Ma and 574 ± 2 Ma (relative misfit 0.622).

Forty-one analyses on zircon crystals with ages from ca. 624 Ma to 560 Ma show varied initial Hf isotopic signature, being separated into two groups. One group presents more clustered and less evolved Hf signatures with $^{176}Hf/^{177}Hf_{(t)}$ ratios ranging from 0.282359 to 0.282292, $\varepsilon Hf_{(t)}$ between -1.7 and -4.9, and Hf_{TDM} model ages from ca. 1.33 Ga to ca. 1.48 Ga. The other group shows greater values variation with $^{176}Hf/^{177}Hf_{(t)}$ ratios ranging from 0.282184 to 0.281375, $\varepsilon Hf_{(t)}$ between -8.0 and -36.4, and Hf_{TDM} model ages from ca. 1.33 Ga to ca. 1.48 Ga (Figures 3.9, 3.10, 3.11). Hf isotopic analyses on older zircon grains (six spots) yielded initial $^{176}Hf/^{177}Hf$ ratios ranging from 0.282348 to 0.281895, $\varepsilon Hf_{(t)}$ values between +0.6 and -9.3, and Hf_{TDM} model ages from ca. 1.31 Ga to ca. 2.04 Ga (Figures 3.9, 3.10, 3.11).

3.4.2.3. Sm-Nd data

Nine whole-rock samples were analyzed to obtain isotopic Sm–Nd compositions, including six from the Santa Tereza suite and three from the Jequitibá suite (Table 3.2). Initial $^{143}Nd/^{144}Nd$ ratios and $\varepsilon Nd_{(t)}$ values were calculated using the Concordia age at 612 Ma for the Santa Tereza rocks and 594 Ma for the Jequitibá. The results show $^{143}Nd/^{144}Nd$ ratios between 0.51234 to 0.51181, and Nd_{TDM} model ages from 1.19 Ga and 2.04 Ga with $\varepsilon Nd_{(t)}$ values ranging from -3.88 to -8.80 for metadiorite to metatonalite samples. The metamonzogabbro sample has $\varepsilon Nd_{(t)}$ of -0.06 and Nd_{TDM} model age of 1.19 Ga (Table 3.2). Garnet-bearing samples present more negative Nd signatures with $\varepsilon Nd_{(t)}$ from -5.42 to -8.8, and Nd_{TDM} model ages from 1.59 Ga to 2.04 Ga.

Table 3.2 Summary of the main features of the studied from samples with whole rock Sm-Nd analyses.

Suite	**Santa Tereza**						**Jequitibá**		
Sample	**CA- 08**	**CA -14**	**CA-17**	**CA-18 A**	**CA-19**	**CA-20 A**	**CA -03**	**CA-31**	**CA-32**
Coordinates	S19.935°/ W40.499°	S19.858°/ W40.516°	S19.933°/ W40.466°	S19.933°/ W40.468°	S19.937/ W40.483	S19.934/ W40.501	S20.412/ W40.859	S20.047/ W40.699	S20.045/ W40.723
Location	Santa Teresa, Espírito Santo state	Santa Teresa, Espírito Santo state	Fundão, Espírito Santo state	Fundão, Espírito Santo state	Santa Teresa, Espírito Santo state	Santa Teresa, Espírito Santo state	Marechal Floriano, Espírito Santo state	Santa Leopoldina, Espírito Santo state	Santa Maria de Jetibá, Espírito Santo state
Field Feature	Greenish gray rock, coarse-grained, composed of felsic and mafic bands	Greenish gray rock, coarse-grained, with millimetric garnet. Locally, the minerals are oriented	Greenish gray rock, coarse-grained, with high concentration of biotite. Locally, the minerals are oriented	Greenish gray rock, coarse-grained, with high concentration of biotite. Locally, the minerals are oriented.	Light gray, with fine to coarse-grained levels, with concentration of mafic minerals, and local small felsic patches very coarse-grained.	Greenish gray rock, coarse-grained, composed of felsic and mafic bands	Foliated with milimetric garnet, light gray, fine to coarse-grained, showing local small felsic patches with core of garnet up to 2 cm in diameter	Foliated with milimetric garnet, light gray, coarse-grained, showing local small felsic patches	Foliated with milimetric garnet, light gray, coarse-grained, showing local small felsic patches
Lithotype sample	Bt metagranodiorite	Grt-Opx-Bt metagranodiorite	Opx-Bt metadiorite	Opx-Cpx-Bt metamonzogabbro	Bt metagranodiorite	Grt-Opx-Bt metatonalite	Grt-Bt metagranodiorite	Grt-Bt metagranodiorite	Grt-Bt metatonalite
Lithochemical signature	Magnesian, calcic, slightly peraluminous, calc-alkaline serie	Magnesian, calcic, slightly peraluminous, calc-alkaline serie	Magnesian, calc-alkalic, metaluminous, high-K calc-alkaline serie	Magnesian, alkali-calcic, metaluminous, high-K calc-alkaline serie	Magnesian, calcic, slightly peraluminous, calc-alkaline serie	Magnesian, calcic, slightly peraluminous, calc-alkaline serie	Magnesian, calcic, slightly peraluminous, calc-alkaline serie	Magnesian, calcic, slightly peraluminous, calc-alkaline serie	Magnesian, calc-alkalic, slightly peraluminous, high-K calc-alkaline serie
Main mineralogy *	Pl-Qz-Bt-Kfs	Pl-Qz-Bt-Opx-Kfs-Grt	Pl-Qz-Bt-Opx-Kfs-Amp	Pl-Bt-Opx-Cpx-Qz-Amp	Pl-Qz-Bt-Kfs	Pl-Qz-Bt-Opx-Grt	Pl-Qz-Kfs-Bt-Grt	Pl-Qz-Kfs-Bt-Grt	Pl-Qz-Kfs-Bt-Grt
Acessory mineralogy	Opq-Zrn-Ap-Mnz-Ru-Aln	Zrn-Ap-Mnz-Aln-Ep	Zrn-Ap-Mnz	Zrn-Ap-Kfs	Zrn-Ap-Mnz	Opq-Kfs-Zrn-Ap-Mnz-Ttn	Zrn-Ap-Mnz-Aln	Zrn-Ap-Mnz-Aln-Opq	-
Secondary mineralogy	Ser-Ms-Chl-Cb-Ru	Amp-Opq-Sr-Ms-Bt-Chl-Cb	Amp-Opq-Sr-Ru-Bt-Chl-Cb	Amp-Opq-Bt-Chl-Cb	Ser-Ms-Opq-Chl-Cb-Ru	Amp-Opq-Bt-Chl	Ser-Ms-Chl-Opq	Ser-Ms-Chl	-
Sm (ppm)	13.429	5.656	11.819	10.340	4.401	5.321	3.999	7.126	5.319
Nd (ppm)	61.513	27.983	65.545	50.155	30.817	21.642	24.131	39.061	24.374
$^{147}Sm/^{144}Nd$	0.1320	0.1222	0.1090	0.1246	0.0863	0.1486	0.1002	0.1103	0.1319
$^{143}Nd/^{144}Nd$	0.512103	0.511976	0.512075	0.512344	0.511995	0.512166	0.51181	0.511958	0.512030
± 2SE	5	5	8	7	6	6	5	3	8
$T_{DM\ (Ga)}$	1.74	1.76	1.40	1.19	1.25	2.04	1.64	1.59	1.87
$\varepsilon_{Nd\ (T1)}$**	-5.34	-7.05	-4.09	-0.06	-3.87	-5.42	-8.8	-6.67	-6.91
$\varepsilon_{Nd\ (T2)}$***	-5.15	-6.84	-3.83	+0.16	-3.55	-5.27	-8.43	-6.34	-6.66

Suite	Santa Tereza						Jequitibá		
Sample	**CA- 08**	**CA -14**	**CA-17**	**CA-18 A**	**CA-19**	**CA-20 A**	**CA -03**	**CA-31**	**CA-32**
$^{176}Hf/^{177}Hf_{(T)}$	0.282457 to 0.282271 *(from 545 to 635 Ma)*	-	-	-	-	-	0.282359 to 0.282292 *(from 562 to 624 Ma)*[1] 0.282184 to 0.281375 *(from 560 to 607 Ma)*[2]	-	-
$^{176}Hf/^{177}Hf_{(T2)***}$	0.282456 to 0.282271	-	-	-	-	-	0.282359 to 0.282282 [1] 0.282183 to 0.281375 [2]	-	-
$\varepsilon Hf_{(T)}$	+2.3 to -4.8	-	-	-	-	-	-1.7 to -4.9 [1] -8.0 to -36.4 [2]	-	-
$\varepsilon Hf_{(T2)***}$	+2.5 to -4.6	-	-	-	-	-	-1.2 to -3.9 [1] -7.4 to -36.0 [2]	-	-
T1 (Ma)	612	612	612	612	612	612	594	594	594
T2 (Ma)	635	635	635	635	635	635	624	624	624

* in decreasing order of abundance

Aln: allanite; Amp: amphibole; Ap: apatite; Bt: biotite; Cb: carbonate; Chl: chlorite; Ep: epidote; Grt: garnet; Kfs: K-feldspar; Mnz: monazite; Ms: muscovite; Opq: opaques minerals; Opx: orthopyroxene; Cpx: clinopyroxene Pl: plagioclase; Qz: quartz; Ser: sericite; Ru: rutile; Ttn: titanite; Zrn: zircon

Lu-Hf data in zircon **T1: Concordia age ***T2 estimated crystallization age

1 - group (1); 2- group (2)

3.5 DISCUSSION

3.5.1 Tectonic correlations along the Neoproterozoic Brasiliano belts of Brazil

The orogenic belts of the Brasiliano Cycle surround the few cratonic areas that are tectonically stable at least since Neoproterozoic times when several continental masses were amalgamated to form West Gondwana (Figure 3.1 A e B), involving periods of accretion and collision (from the Tonian to the early Ediacaran) and including numerous arc-related volcanic-plutonic suites, high-grade metamorphic sequences, and occurrences of ophiolite slivers. Therefore, within all these orogenic belts, magmatic arcs were registered and presented rocks with typical magmatic arc geochemical and isotopic signatures generated in the supra-subduction region of the asthenospheric mantle from varied differentiation, mixing, and contamination processes. The Brasiliano orogenic belts were formed from consumed of two large oceanic realms by subduction-to-collision tectonic episodes (Cordani et al., 2016; Heilbron et al., 2004; 2017, 2020; and references therein).

The huge Goiás-Pharusian Ocean was closed after a long duration subduction phase, between ca. 900 and 600 Ma, that brought together the Amazonian and the West African cratons and the São Francisco-Congo, the Rio de La Plata and the African counterparts. As a result of this collision, the Tocantins orogenic system, the Borborema tectonic province, and the Trans-

Saharan belts in Africa were developed. This tectonic episode is related to the juvenile intra-oceanic island arcs roots of the Goiás Magmatic Arc, in Brasília belt (Tocantins orogenic system), and the magmatic arcs from the Santa Quitéria Arc and the Sergipano belt from Borborema tectonic province, where magmatic-arc related rocks, retro-eclogites, and dismembered ophiolites provide evidence of accretion (Cordani et al., 2016; Heilbron et al., 2004; 2017, 2020; Santos et al., 2022; Pimentel, 2016, and references therein) (Figure 3.1 A and B).

On the other hand, the Adamastor Ocean occupied an extended oceanic region that become the site of the amalgamation of smaller cratonic masses and massifs, such as the Rio de La Plata, Paranapanema, Luiz Alves, and Kalahari (Figure 3.1 A and B). With the closure of one of the Adamastor terminal segments, along the Brazilian and Uruguayan Atlantic coast, the Araçuaí, Ribeira, and Dom Feliciano orogenic belts were developed. The tectono-magmatic evolution was by the subduction-driven contraction phase taking place to a confined orogen with a pre-collisional continental-margin Andean-type arc (Araçuaí), connected, in turn, to complex accretionary-collisional orogens (Ribeira and Dom Feliciano) with accreted juvenile pre-collisional island arc terranes (Caxito et al., 2021, 2022; Cordani et al., 2016; De Toni et al., 2020; Heilbron et al., 2004; 2017, 2020; and references therein) (Figure 3.1 A and B). The Rio Doce, Rio Negro, and Serra da Prata magmatic arcs are formed in the Ribeira-Araçuaí Orogenic System (Southeast Brazil).

In this scenario, we discuss the Santa Tereza and Jequitibá suites from Araçuaí orogen through the correlation between new and compiled data, as well as their geological implications.

3.5.2 Petrogenesis of Santa Tereza and Jequitibá suites

Geochemical analyses coupled with field mapping and petrographic studies provide robust evidence to recognize distinct granitic rock assemblages (cf. Best, 2003; Frost and Frost, 2014), such as those from magmatic arcs (mostly calcic to calc-alkaline, magnesian, metaluminous), continental rifts (mostly ferroan, alkaline to alkali-calcic with anhydrous tendency), post-collisional settings (magnesian to ferroan, high-K calc-alkaline to alkali-calcic, I- and A-type), and collisional leucogranites (S-type, rich in peraluminous silicates, such as muscovite and/or almandine and/or cordierite and/or sillimanite). Indeed, the Araçuaí orogen is a good example of the successful application of that methodology (field mapping + petrographic studies + geochemistry) for clearly discriminating distinct anorogenic (e.g.,

Victoria et al., 2022) and orogenic granite suites (e.g., Araujo et al., 2020; Gradim et al., 2014; Pedrosa-Soares et al., 2011; Tedeschi et al., 2016; and references therein), as well the whole Mantiqueira Province of southeast and southern Brazil (Caxito et al., 2021, 2022; Heilbron et al., 2020; Santiago et al., 2020).

Overall, the Santa Tereza and Jequitibá suites present similar lithochemical signatures and fit well with those signatures recorded for rocks from the Rio Doce magmatic arc (Figures 3.4 to 3.7). Altogether, their geochemical attributes suggest a magmatic arc origin, with a well-defined calc-alkaline trend in the AFM diagram, and magnesian, calcic to alkali-calcic, metaluminous to slightly peraluminous I-type signatures, as well as negative Nb, Ta and, Ti anomalies, for a wide range of silica contents (Figures 3.4 to 3.7). The REE signatures are also compatible with magmatic arc settings. They plot mainly in volcanic arc fields, with predominantly mafic sources (Figure 3.5). All those chemical attributes also show remarkable similarities to signatures concerning other continental magmatic arcs around the world, remarkably in spidergram patterns (Figures 3.4 to 3.7).

Petrography from Santa Tereza and Jequitibá rocks also shows significant similarities with G1 rock associations described in the literature (Gonçalves et al., 2014, 2016, 2018; Gouvêa et al., 2020; Gradim et al., 2014; Narduzzi et al., 2017; Narduzzi, 2018; Pedrosa-Soares et al., 2011; Pereira et al., 2023; Soares et al., 2020; Tedeschi et al., 2016). Furthermore, charnockitic rocks found in the south and west of the Santa Tereza suite have been related to the granulitic root of the Rio Doce magmatic arc (Novo et al., 2010; Soares et al., 2020). As observed in the Santa Tereza suite, those charnockitic rocks can contain garnet that can be related to crustal contamination (Gouvêa et al., 2020; Novo et al., 2010; Soares et al., 2020) and/or partial melting of the very deep crust (Narduzzi et al., 2017; Narduzzi, 2018). Geothermobarometric calculations carried out on pre-collisional Opx-bearing metatonalite from the Araçuaí-Ribeira boundary records metamorphic conditions of high-amphibolite to granulite facies (670 °C to 860 °C) over a wide pressure range from 5 kbar to 10 kbar (Gouvêa et al., 2020).

Crystallized from hot CO_2-bearing magmas in deep arc levels, Opx-bearing granitic rocks form enderbitic to charnockitic series, generally associated with basic (noritic) terms displaying magnesian, calcic to calc-alkalic, metaluminous to slightly peraluminous I-type signatures (Frost and Frost, 2008). Orthopyroxene along with garnet even in slightly peraluminous magmas implies an increasing Al_2O_3 content that promotes the crystallization of Grt over Opx (Frost and Frost, 2008). Therefore, according to the geochemical signature, the

Santa Tereza charnockitic rocks would have been crystallized from CO_2-bearing magmas in deep arc levels after assimilation of a component enriched in Al and H_2O, producing garnet, amphibole, and more biotite. Such a crustal component could be a partial melt fraction derived from the regional paragneisses of the Nova Venécia complex.

In several rocks of the Rio Doce magmatic arc, garnet is relatively common as an accessory mineral (e.g., Gonçalves et al., 2016, 2018, Gouvêa et al., 2020; Narduzzi et al., 2017; Novo et al., 2010; Soares et al., 2020). After a thorough review and detailed studies, Narduzzi et al. (2017) concluded that garnet crystals found in tonalites and granodiorites of the Galiléia (G1) suite have a magmatic origin consistent with crystallization above 25 km depth and temperatures below 700 °C. Gouvêa et al. (2020) described a pressure of 10 kbar for calcium-rich garnet. The presence of magmatic orthopyroxene and the high contents of calcium in garnet crystals of metamorphosed tonalites and granodiorites of the Muriaé batholith suggest crystallization of arc-related magmas in the deep crust (Soares et al., 2020). Garnet can also be produced by contamination with peraluminous melts, intramagmatic metasomatism in late crystallization, and metamorphism by dehydration reactions involving biotite and hornblende, or plagioclase breakdown plus Opx in high amphibolite to granulite facies (Ducea et al., 2015a; Best, 2003). Indeed, samples from the Santa Tereza and Jequitibá suites show microstructures consistent with high equilibrium temperatures under upper amphibolite to granulite facies conditions, such as coexistence of antiperthite and perthite, conspicuous deformed to irregular twinning in feldspars, subgrain patterns and stretched fabrics (cf., Best, 2003; Kruhl, 1996; Yardley et al., 1996).

3.5.2. Isotopic correlations

A correlation of the presented geochronological data with the compiled Araçuaí dataset indicates that the Santa Tereza and Jequitibá suites, with Concordia ages at 612 ± 3 Ma and 594 ± 3 Ma, respectively, represent the easternmost part of the Rio Doce magmatic arc already found (Figures 3.1 and 3.12). The metamorphic ages from the samples of both suites also have a close correlation with the compiled metamorphic data from Araçuaí zircon grains (Figure 3.12A). Indeed, the U-Pb data spreading along the Concordia curve suggest post-crystallization disturbance under high-temperature conditions (Vervoort and Kemp, 2016; Tedeschi et al., 2018), which is consistent with the granulite facies features observed in the studied samples and described in previous articles on the regional metamorphism (Gradim et al., 2014; Richter et al., 2016). Furthermore, the Hf signatures of each sample are distributed roughly horizontally

(Figure 3.11) indicating progressive Pb loss (Vervoort and Kemp, 2016). Thus, the crystallization ages of these rocks may be older than the Concordia ages, and $\varepsilon Hf_{(t)}$ may be underestimated (Table 3.2; Figure 3.9E, 3.9F). By considering the older grains within the same Hf ratio ranges, the estimated crystallization ages of 635 ± 8 Ma for the Santa Tereza sample and 624 ± 8 for the Jequitibá sample seem to be reliable (Figure 3.11B). The recalculated Hf values are $\varepsilon Hf_{(635)}$ +2.5 to -4.6 for the Santa Tereza suite and $\varepsilon Hf_{(624)}$ -1.2 to -36.0 for the Jequitibá suite (Table 3.2).

The new Hf isotope data ($\varepsilon Hf_{(t)}$ +2.3 to -4.8 for Santa Tereza suite; $\varepsilon Hf_{(t)}$ -1.7 to -36.4 for Jequitibá suite) represent the most primitive signatures already found in the Rio Doce magmatic arc (Figures 3.9C to 3.9F, and 3.10). Nevertheless, the Jequitibá Hf signature shows the largest range, suggesting mixing between partial melting from the Nova Venécia or basement rocks and juvenile components, with the data of $\varepsilon Hf_{(t)}$ from -8 to -36 imply in crustal contamination (Figures 3.9C to 3.9F, 3.10). The presented isotopic data show a striking correlation with those from rocks of the Marceleza-Leopoldina-Serra da Bolívia complex. Conversely, they show minor isotopic correspondence with the migmatitic paragneiss of the Nova Venécia complex (Figure 3.10, 3.11).

Evaluating the overall Hf dataset in relation to samples locations from north to south and east to west in the Araçuaí orogen (Figures 3.10A, 3.10B), it is noteworthy that the progressive increase in $\varepsilon Hf_{(t)}$ from north to south and from west to east, i.e., the Hf signatures become more primitive to the south and east. The same tendencies are outlined by zircon U–Pb ages from the Rio Doce Arc which peaks of probability density curves become increasingly older from north to south and from west to east (Figures 3.12B, 3.12C).

Araujo et al. (2020) recorded Hf data from the border of a post-collisional intrusion (the Mestre Álvaro pluton, CA-05 sample; Figure 3.2) to the south and east of the Santa Tereza sampling localities, showing several inherited zircon grains with a Concordia age of 598 ± 1 Ma and $\varepsilon Hf_{(t)}$ between - 0.7 and -6.2, fitting well with Hf signatures from the Jequitibá, Santa Tereza, Marceleza, Leopoldina and Serra da Bolívia samples (Figure 3.10A, 3.10B, 3.10D). These data suggest the existence of (probably) non-exhumed arc-related intrusions further east of the studied area.

The new whole-rock Nd signatures ($\varepsilon Nd_{(t)}$ from -0.06 to -8.80) are among the least negative values ever reported for Rio Doce magmatic arc and fit well with the compiled data from G1 supersuite samples, especially the sample 18A ($\varepsilon Nd_{(t)}$ = -0.06), an Opx-Cpx-Bt

metamonzogabbro (Figure 3.9G, 3.9H). The Nd results recalculated for estimated crystallization ages show $\varepsilon Nd_{(635)}$ from +0.16 to -6.84 for the Santa Tereza suite and $\varepsilon Nd_{(624)}$ from -6.34 to -8.43 for the Jequitibá suite (Table 3.2). These slightly positive to moderately negative εNd values are expected for granitic rocks from continental magmatic arcs where interactions of mantle magmas with country rocks are common. The more negative signatures in samples with garnet ($\varepsilon Nd_{(t)}$ from -5.42 to -8.8) also suggest the assimilation of a crustal melt component.

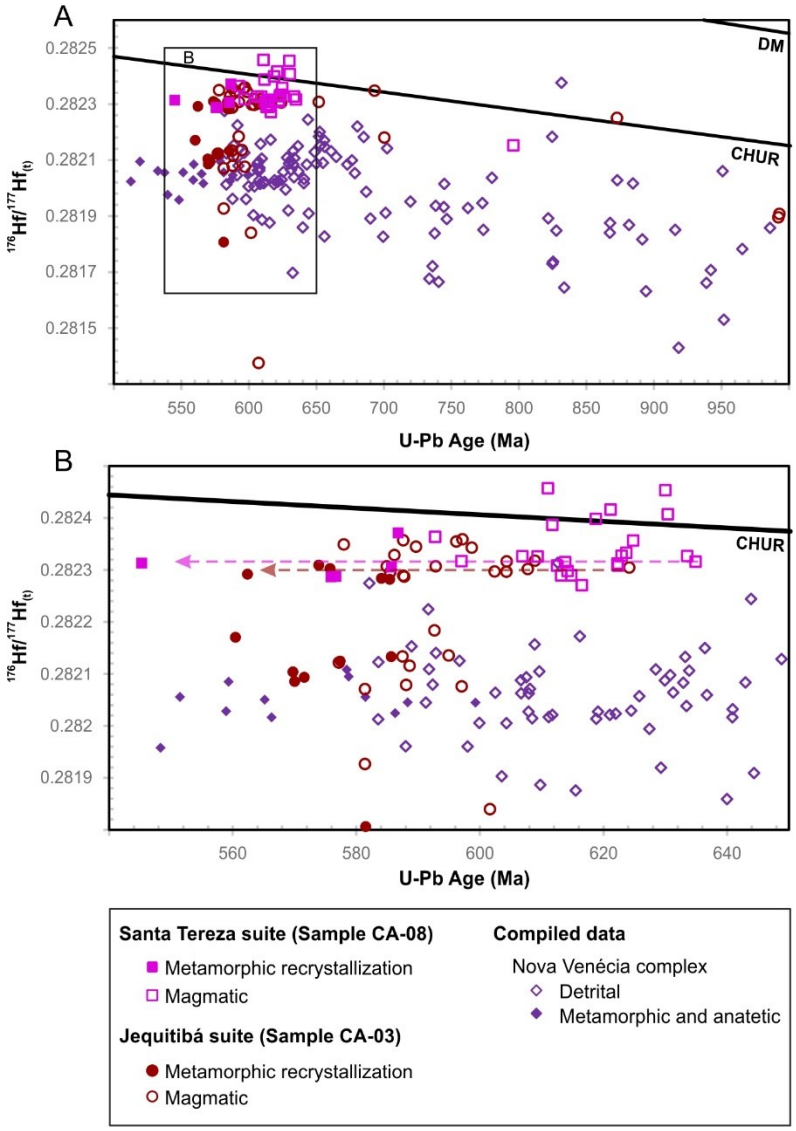

Figure 3.11 Diagrams shown in-zircon Hf isotope data from Santa Tereza and Jequitibá samples, compared with compiled data from Nova Venécia paragneisses. B) Detail outlook showing the Hf signature spreading along approximately horizontal lines and indicating progressive Pb loss.

From the compiled dataset, the G2 supersuite ages display a remarkable overlap with G1 supersuite ages between 600 Ma to 560 Ma (Figure 3.12A). However, though I-type

magmatism (G1 rocks) predominates from 600 Ma to 580 Ma, S-type magmatism (G2 rocks) predominates between 580 Ma and 560 Ma. The generation of I-type granites before S-type granites is further evidence for an orogeny driven by ocean subduction followed by continent collision (Best, 2003). The overlapping of age ranges is also consistent with the timing of magma generation in relation to tectonic stages which is pre-collisional to early collisional for G1 rocks and late pre-collisional to collisional for G2 rocks. However, the large number of zircon grains from G1 rocks aged between 580 Ma and 560 Ma may also be related to the opening of the U-Pb system during the collisional stage, although there is no evidence of this process in the CL images.

From the compiled literature is remarkable that zircon U–Pb ages from the Nova Venécia complex show an expressive number of zircon grains aged between 660 Ma and 580 Ma, even if compared with other arc-related basins (Figure 3.12A). However, detrital zircon grains with ages < 630 Ma could also reflect Pb-loss not detected by microstructural features shown in CL and BSE images. In fact, the available Hf signature for these rocks (Araujo et al., 2020) shows scattering along approximately horizontal lines (Figure 3.11), which is expected due to the high temperature and pressure conditions experimented for those samples. Thus, the ages younger than 630 Ma for detrital zircon grains may have been partially or completely reset by processes that triggered U-Pb zircon disturbances and could represent arc-related metamorphism followed by collisional metamorphism. Compared to other arc-related basins, the Nova Venécia complex has a more negative Hf signature and presents isotopic similarities with some zircon grains from the Andrelândia Group, while the Rio Doce Group shows great discrepancy, with juvenile zircon grains, which is also found in the Andrelândia Group (Figure 3.10C). The more evolved signatures given by Nova Venécia paragneisses indicate prevailing sediment provenance from sources rich in continental rocks, such as the Rio Doce magmatic arc and its basement (Araujo et al., 2020; Gradim et al., 2014; Richter et al., 2016).

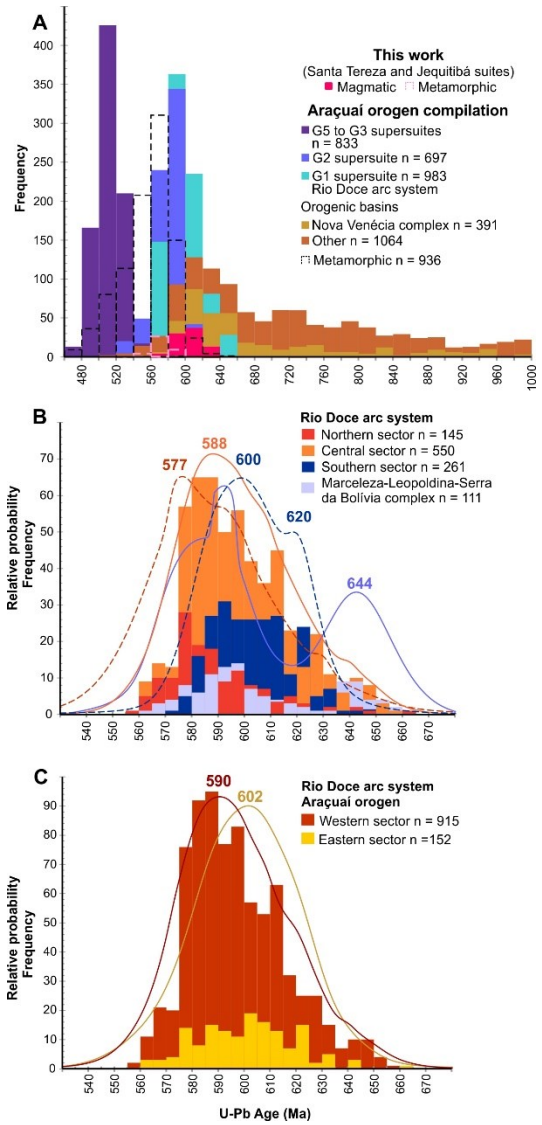

Figure 3.12 Histograms and probability density curves showing zircon U-Pb ages distribution. A: Studied samples and compiled dataset of the orogenic plutonism, metamorphism, and arc-related basins (Andrelândia and Rio Doce groups, Salinas formation, and Mpioka formation) from Araçuaí – West Conto orogen. B: Igneous zircon U-Pb ages from Rio Doce arc (including new data) for Northern to Southern sectors. C: Igneous zircon U-Pb ages from Rio Doce magmatic arc in Araçuaí orogen (including new data) for Western and Eastern sectors. Northern sector: North of 18°30'; Central sector from 18°30' to 20°; Southern sector: South of 20°; Western sector: West of 41°; Eastern sector: East of 41°. Sources of data compilation in Supplementary file 3.A.

3.5.3 Implications for Araçuaí geotectonic evolution

Together with a thorough information collection of field relations and petrographic features from the orogenic magmatic supersuites (e.g., Campos et al., 2016; Gonçalves et al., 2016, 2017; Melo et al., 2017; Pedrosa-Soares et al., 2011, 2020; Serrano et al., 2018; Tedeschi et al., 2016; Wisniowski et al., 2021), besides their tectonic relations with other geotectonic components (e.g., anorogenic magmatism related to continental rift and oceanic settings; cf. Amaral et al., 2020; Souza et al., 2022; Victoria et al., 2022) of the Araçuaí orogen, the

presented robust dataset of lithochemical and isotopic signatures point to an active continental margin for the Rio Doce magmatic arc development. In this scenario, the Marceleza-Leopoldina-Serra da Bolívia complex (650-590 Ma; $\varepsilon Nd_{(t)}$ = -5.5 to -11; $\varepsilon Hf_{(t)}$ = -0.9 to -3.75; Heilbron et al., 2013; Corrales et al., 2020), representing the Rio Doce arc in the northern Ribeira Orogen (Corrales et al., 2020; Tedeschi et al., 2016), have geochemical similarities with studied samples (Figures 3.4 to 3.7) and can be considered the best correlation with the Santa Tereza and Jequitibá suites.

The differences between Hf signatures of the Eastern and Western magmatic arc sectors are remarkable. The more juvenile signature in the Eastern sector indicates the involvement of mantle magma and/or juvenile crust in the melting processes that formed at least part of the Santa Tereza suite. Indeed, according to Hf data, the partial melting of basement or country supracrustal rocks would not explain the isotopic signature of Santa Tereza rocks without mixing with mantle melts (Figure 3.10C). Moreover, Nd_{TDM} model ages (between 1.2 and 2.0 Ga) are younger than the basement rocks of the Juiz de Fora, Quirino, and Pocrane complexes (cf., Degler et al., 2018; Novo, 2013; Schannor et al., 2020). In addition to basement units, juvenile Hf and Nd signatures are found in the Tonian to Cryogenian Serra da Prata and Rio Negro magmatic arcs of the Ribeira orogen (Heilbron and Machado, 2003; Tupinambá, et al. 2012; Lobato et al., 2015; Peixoto et al., 2017, 2022; Santiago et al., 2020). Indeed, melts from juvenile rocks of the Serra da Prata magmatic arc (860–838 Ma; $\varepsilon Nd_{(t)}$ +6.4 to -3.7; $\varepsilon Hf_{(t)}$ +14 to +10; cf. Peixoto et al., 2017; and Santiago et al., 2020) can be a potential source for the less evolved Santa Tereza melts (Figure 3.9G, 3.9H, 3.10C), if the Serra da Prata arc has a prolongation (not yet known) in the studied region.

That interpretation of sources for the Santa Tereza juvenile magmas can be also related to studies on the Rio Doce Group, the metavolcano-sedimentary cover of the Rio Doce magmatic arc (Novo et al., 2018). Whole-rock data and U-Pb age spectra, juvenile nature, and trace element composition recorded in detrital zircon grains from the Rio Doce Group suggest sediment sources in juvenile crustal setting, such as an intra-oceanic island arc (Schannor et al., 2019). Those U-Pb ages and Hf isotopic signatures from detrital zircon grains of the Rio Doce Group fit well with rocks from the Serra da Prata magmatic arc, which is typical of an intra-oceanic island arc setting (Peixoto et al., 2017, 2022; Santiago et al., 2020) (Figure 3.10C). Conversely, the isotopic signatures of zircon grains and whole-rock samples from Nova Venécia paragneisses indicate a continental setting for the basin, which has been largely

interpreted as a back-arc basin developed during most part of the Rio Doce Arc evolution (Araujo et al., 2020; Gradim et al., 2014; Noce et al., 2004; Pedrosa-Soares et al., 2011; Richter et al., 2016;).

Altogether, the new and compiled data provide further evidence for ocean subduction beneath a continental margin which includes the previous collage of juvenile crust, such as an island arc (the Serra da Prata magmatic arc), that could generate melts evolving from juvenile to evolved crustal melts, producing the Hf signatures shown by the rocks of the Santa Tereza suite and the Marceleza-Leopoldina-Serra da Bolívia complex (Degler et al., 2017; Corrales et al., 2020; Figure 3.10C). In a broad scenario, the data presented here also corroborate the consumption of the Neoproterozoic Adamastor Ocean, including its northern termination within a confined basin (an inland-sea basin, cf. Condie 2017), namely the Araçuaí – West Congo basin system, through a complete Wilson Cycle supported by wide evidence from several fields of the Geosciences (Caxito et al., 2022).

The new data provide robust evidence for a rather juvenile arc magmatism followed by more evolved magmatic activity in the easternmost portion of the Araçuaí orogen. This is also consistent with the evolutionary model, which suggests that the oldest plutons of the Rio Doce magmatic arc were emplaced to the east followed by migration of the magmatic front to the west (Tedeschi et al., 2016), owing to subduction retreat (Figure 3.13). The zircon U-Pb and Lu-Hf dataset record westward arc migration (Figure 3.12C), with increasing continental crust involvement (Figures 3.10A, 3.10B). Back-arc basin evolution in an initial and extensional phase followed by a compressional phase would explain older arc magmatism and less evolved isotopic compositions in the easternmost section (cf. Ducea et al., 2015a). Indeed, the studied region is related to the development of a back-arc basin on a hot and thin continental crust (Gradim et al., 2014; Richter et al., 2016).

3.6 CONCLUSIONS

New zircon U-Pb and Hf isotopic data for Santa Tereza and Jequitibá rocks, coupled with whole-rock Sm-Nd results, demonstrate the easternmost expression of pre-collisional, arc-related magmatism in the Araçuaí orogen. With Concordia ages of 612 ± 3 Ma and 594 ± 3 Ma, respectively, and estimated crystallization ages of 635 ± 8 Ma and 624 ± 8 Ma, the Lu-Hf and whole-rock Sm-Nd data show the least evolved magmatism in the Rio Doce magmatic arc. Together with a wide data compilation, our dataset indicates the involvement of juvenile crust and/or mantle melts in the Eastern sector of the Rio Doce arc, supporting a complete Wilson

Cycle for the orogenic evolution of the Araçuaí orogen, including the magmatic front migration owing to subduction retreat (Figure 3.13). The studied rocks can be correlated with the Marceleza-Leopoldina-Serra da Bolívia complex of the Ribeira Orogen, providing further evidence of the connection between both orogens during the evolution of the Rio Doce magmatic arc. The presented data also support the evolution of a continental-margin magmatic arc within a confined orogen, the Araçuaí - West Congo Orogen, formed by the closing of an inland-sea basin, providing an example of a singular geotectonic setting in the paleocontinental history, such as the Western Gondwana.

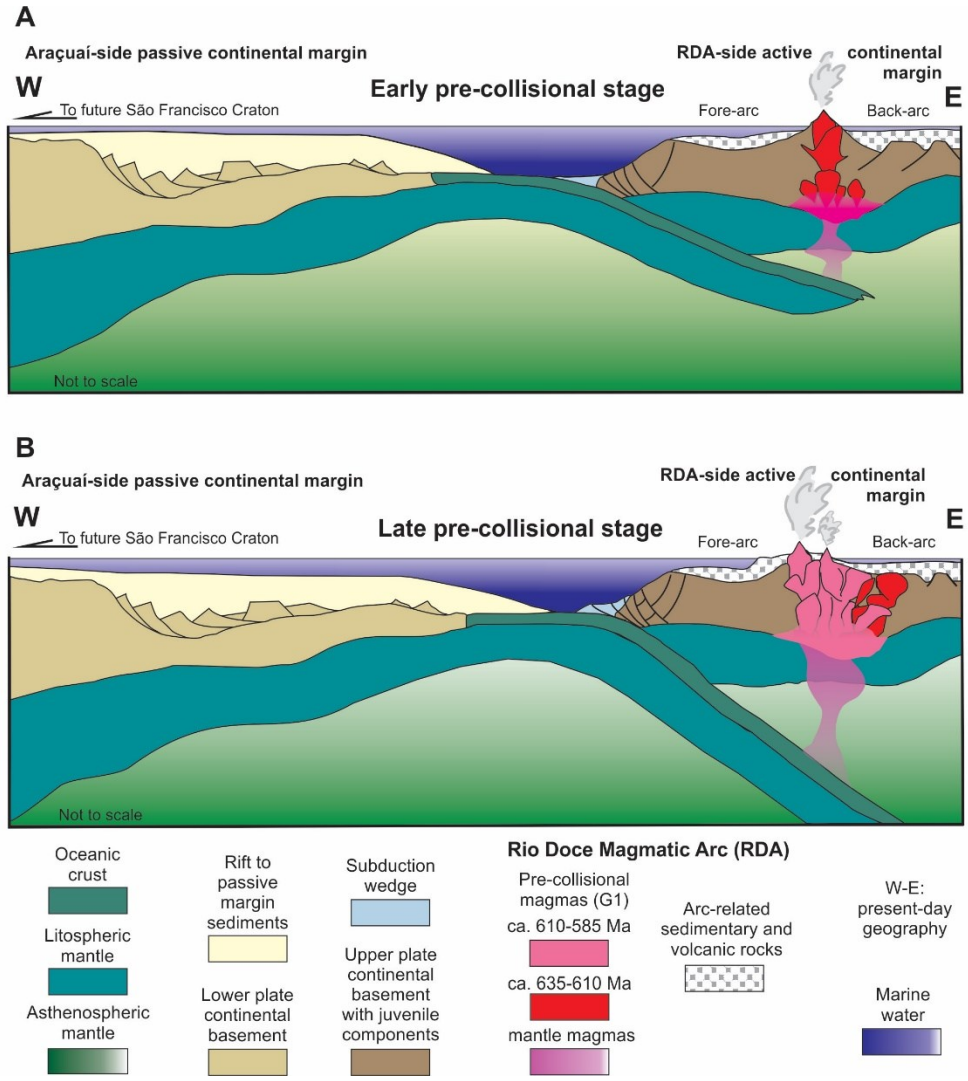

Figure 3.13 Evolutionary model for the Rio Doce magmatic arc (modified from Tedeschi et al., 2016).

ACKNOWLEDGMENTS

The authors acknowledge the financial support and scholarships provided by Brazilian research and development agencies (CNPq, CAPES, and CODEMIG-CODEMGE). We are

also grateful to the Microscopy and Microanalysis Laboratory (LMIc) of the Federal University of Ouro Preto, a member of the Microscopy and Microanalysis Network of Minas Gerais State/Brazil/FAPEMIG. For the use of the laboratories and analytical facilities from Minas Gerais (UFMG), and Ouro Preto (UFOP) universities and their staffs, we thank all people involved. Our gratitude to the editors and reviewers that greatly helped us to improve this paper.

REFERENCES

Alkmim, F.F., Marshak, S., Pedrosa-Soares, A.C., Peres, G.G., Cruz, S.C.P., Whittington, A., 2006. Kinematic evolution of the Araçuaí–West Congo orogen in Brazil and Africa: Nutcracker tectonics during the Neoproterozoic assembly of Gondwana. Precambrian Research 149, 43-64. https://doi.org/10.1016/j.precamres.2006.06.007

Alkmim, F.F., Kuchenbecker, M., Reis, H.L.S., Pedrosa-Soares, A.C., 2017. The Araçuaí belt. In: Heilbron, M., Cordani, U.G, Alkmim F.F. (Eds.), São Francisco Craton, Eastern Brazil. Regional Geology Reviews, Springer International Publishing Co., pp. 255–276. https://doi.org/10.1007/978-3-319-01715-0_14

Amaral, L., Caxito F.A., Pedrosa-Soares A., Queiroga G., Babinski, M., Trindade, R., Lana, C., Chemale, F., 2020. The Ribeirão da Folha ophiolite-bearing accretionary wedge (Araçuaí orogen, SE Brazil): New data for Cryogenian plagiogranite and metasedimentary rocks. Precambriam Research 336, 105522. https://doi.org/10.1016/j.precamres.2019.105522

Aranda, R.O., Chaves, A.O., Medeiros Júnior, E.B., Venturini Junior, R., 2020. Petrology of the Afonso Cláudio Intrusive Complex: New insights for the Cambro-Ordovician post-collisional magmatism in the Araçuaí-West Congo Orogen, Southeast Brazil. Journal of South American Earth Sciences 98, 102465. https://doi.org/10.1016/j.jsames.2019.102465

Araujo, L. E. A. B., Heilbron, M., Teixeira, W., Dussin, I., Valeriano, C.M., Henrique Bruno, Sato, K., Paravidini, G., Castro, M., 2021. Siderian to Rhyacian evolution of the Juiz de Fora Complex: Arc fingerprints and correlations within the Minas-Bahia Orogen and the Western Central Africa Belt. Precambrian Research, 359: 106118. https://doi.org/10.1016/j.precamres.2021.106118

Araujo C., Pedrosa-Soares A., Lana C., Dussin I., Queiroga G., Serrano P., Medeiros-Júnior E. 2020. Zircon in emplacement borders of post-collisional plutons compared to country rocks: A study on morphology, internal texture, U-Th-Pb geochronology and Hf isotopes (Araçuaí orogen, SE Brazil). Lithos, 352-353: 105252. https://doi.org/10.1016/j.lithos.2019.105252

Bahlburg, H., Vervoort, J.D., DuFrane, S.A., Carlotto, V., Reimann, C., Cárdenas, J., 2011. The U-Pb and Hf isotope evidence of detrital zircons of the Ordovician Ollantaytambo Formation, southern Peru, and the Ordovician provenance and paleogeography of southern Peru and northern Bolivia. Journal of South American Earth Sciences 32, 196–209. https://doi.org/10.1016/j.jsames.2011.07.002

Bateman, P.C., Dodge, F.C.W., Bruggman, P.E., 1984. Major oxide analyses, CIPW norms, modes, and bulk specific gravities of plutonic rocks from the Mariposa 1 degrees by 2 degrees sheet, central Sierra Nevada, California. US Geological Survey OF 84-0162, 59 pp. https://doi.org/10.3133/ofr84162

Belém, J., 2014. Geoquímica, geocronologia e contexto geotectônico do magmatismo máfico associado ao feixe de fraturas Colatina, Estado do Espírito Santo. Universidade Federal de Minas Gerais, Belo Horizonte (MS Dissertation, 138 p).

Best, M.G., 2003. Igneous and metamorphic petrology. Blackwell Science: Malden, 2° ed., 758p.

Boynton, W.V., 1984. Cosmochemistry of the rare earth elements: meteorites studies. In: Henderson, P. (Ed.), Rare Earth Element Geochemistry. Elsevier, pp. 63–114.

Brown, M., Johnson, T., 2019. Metamorphism and the evolution of subduction on Earth. American Mineralogist 104, 1065–1082. https://doi.org/10.2138/am-2019-6956

Castro, A., Gerya, T., Garcia-Casco, A., Fernandez, C., Diaz-Alvarado, J. Moreno-Ventas, I., Löw, I., 2010. Melting relations of MORB–sediment Mélanges in underplated mantle wedge plumes; implications for the origin of Cordilleran-type batholiths. Journal of Petrology 51,1267–1295. https://doi.org/10.1093/petrology/egq019

Castro, A., Moreno-Ventas, I., Fernández, C., Vujovich, G., Gallastegui, G., Heredia, N., Martino, R.D., Becchio, R., Corretgé, L.G., Díaz-Alvarado, J., Such, P., García-Arias, M., Liu D.Y., 2011. Petrology and SHRIMP U-Pb zircon geochronology of Cordilleran granitoids of the Bariloche area, Argentina. Journal of South American Earth Sciences 32, 508-530. https://doi.org/10.1016/j.jsames.2011.03.011

Castro, A., 2013. Tonalite-granodiorite suites as cotectic systems: A review of experimental studies with applications to granitoid petrogenesis, Earth-Science Reviews 124, 68-95. http://doi.org/10.1016/j.earscirev.2013.05.006

Castro, M.P., Queiroga, G.N., Martins, M., Pedrosa-Soares, A.C., Dias, L., Lana, C., Babinski, M., Alkmim, A.R., Silva, M., A., 2020. Provenance shift through time in superposed basins: From Early Cryogenian glaciomarine to Late Ediacaran orogenic sedimentations (Araçuaí Orogen, SE Brazil). Gondwana Research 87, 41–66. https://doi.org/10.1016/j.gr.2020.05.019

Cawood, P.A., Kröner, A. (eds) 2009. Earth accretionary systems in space and time. Geological Society, London, Special Publications, 318 (DOI: 10.1144/SP318)

Caxito, F.A., Heilbron, M., Valeriano, C.M., Bruno, H., Pedrosa-Soares, A., Alkmim, F.F., Chemale, F., Hartmann, L., Dantas, E., Basei, M.A.S., 2021. Integration of elemental and isotope data supports a Neoproterozoic Adamastor ocean realm. Geochemical Perspectives Letters 17, 6–10.

Caxito, F.A., Hartmann, L., Heilbron, M., Pedrosa-Soares, A., Bruno, H., Basei, M.A.S., Chemale, F., 2022. Multi-proxy evidence for subduction of the Neoproterozoic Adamastor Ocean and Wilson cycle tectonics in the South Atlantic Brasiliano Orogenic System of Western Gondwana. Precambrian Research 376, 106678. https://doi.org/10.1016/j.precamres.2022.106678

Cecil, M.R., Rotberg, G.L., Ducea, M.N., Saleeby, J.B., Gehrels, G.E., 2012. Magmatic growth and batholithic root development in the Northern Sierra Nevada, California. Geosphere 8, 592-606. https://doi.org/10.1130/GES00729.1

Chapman, A.D., Saleeby, J.B., Wood, D.J., Piasecki, A., Kidder, S., Ducea, M.N., Farley, K.A., 2012. Late Cretaceous gravitational collapse of the Southern Sierra Nevada batholith, California. Geosphere 8, 314–341. https://doi.org/10.1130/GES00740.1

Chappell, B.W., White, A.J.R., 2001. Two contrasting granite types: 25 years later. Australian Journal of Earth Sciences 48, 489–499. https://doi.org/10.1046/j.1440-0952.2001.00882.x

Condie, K.C., 2007. Accretionary orogens in space and time. In: Hatcher, R.D., Carlson, M.P., McBride, J H., Catalán, J.R. (eds), 4-D Framework of Continental Crust. Geological Society of America, Memoirs, 200, 1–14.

Corrales, F.F.P., Dussin, I.A., Heilbron, M., Bruno, H., Bersan, S.A., Valeriano, C.M., Pedrosa-Soares, A.C., Tedeschi, M., 2020. Coeval high Ba-Sr arc-related and OIB Neoproterozoic rocks linking pre-collisional magmatism of the Ribeira and Araçuaí orogenic belts, SE-Brazil. Precambriam Research 337, 105476. https://doi.org/10.1016/j.precamres.2019.105476

Cordani, U.G., Ramos, V.A., Fraga, L.M., Cegarra, M., Delgado, I., Souza, K.G., Gomes F.E.M., Schobbenhaus, C., 2016. Tectonic map of South America. Paris: Commission for the Geological Map of the World, Second edition, scale 1:5 000 000.

De Campos, C.P., Mendes, J.C., Ludka, I.P., Medeiros, S.R., Moura, J.C., Wallfass, C., 2004. A review of the Brasiliano magmatism in Southern Espírito Santo, Brazil, with emphasis on post-collisional magmatism. Journal of the Virtual Explorer 17, 1-35. https://doi.org/10.3809/jvirtex.2004.00106

De Campos, C.P, Medeiros, S.R., Mendes, J.C, Pedrosa-Soares, A.C., Dussin, I., Ludka, I.P., Dantas, E.L., 2016. Cambro-Ordovician magmatism in the Araçuaí Belt (SE Brazil): Snapshots from a post-collisional event. Journal of South American Earth Sciences 68, 248-268. http://doi.org/10.1016/j.jsames.2015.11.016

Degler, R., Pedrosa-Soares, A., Dussin, I., Queiroga, G., Schulz, B., 2017. Contrasting provenance and timing of metamorphism from paragneisses of the Araçuaí-Ribeira orogenic system, Brazil: Hints for Western Gondwana assembly. Gondwana Research 51, 30–50. http://doi.org/10.1016/j.gr.2017.07.004

Degler, R., Pedrosa-Soares, A., Novo, T., Tedeschi, M., Silva, L.C., Dussin, I., Lana, C. 2018. Rhyacian-Orosirian isotopic records from the basement of the Araçuaí-Ribeira orogenic system (SE Brazil): Links in the Congo-São Francisco palaeocontinent. Precambrian Research 317, 179-195. https://doi.org/10.1016/j.precamres.2018.08.018

De la Roche, H., Leterrier, J., Grandclaude, P., Marchal, M., 1980. A classification of volcanic and plutonic rocks using R1R2-diagram and major element analyses - Its relationships with current nomenclature. Chemical Geology 29, 183-210. https://doi.org/10.1016/0009-2541(80)90020-0

Deluca, C., 2018. Evolução do Batólito Itaporé e rochas encaixantes, Orógeno Araçuaí (MG): geoquímica, geocronologia e petrogênese. Universidade Federal de Minas Gerais, Belo Horizonte (MS Dissertation, 116 pp.).

Deluca C., Pedrosa-Soares A., Lima S., Cordani U., Sato K., 2019. Provenance of the Ediacaran Salinas Formation (Araçuaí Orogen, Brazil): Clues from lithochemical data and zircon U-Pb (SHRIMP) ages of volcanic clasts. Brazilian Journal of Geology 49, 1–19. https://doi.org/10.1590/2317-4889201920190017

De Paolo, D.J., 1981. A neodymium and strontium isotopic study of the Mesozoic calcalkaline granitic batoliths of the Sierra Nevada and Peninsular Rangers, California.

Journal of Geophysical Research 86, 10470–10488. https://doi.org/10.1029/JB086iB11p10470

De Toni, G.B., Bitencourt, M.F., Nardi, L.V.S., Florisbal, L.M., Almeida, B.S., Geraldes, M., 2020. Dom Feliciano Belt orogenic cycle tracked by its pre-collisional magmatism: The Tonian (ca. 800 Ma) Porto Belo Complex and its correlations in southern Brazil and Uruguay. Precambrian Research 342, 105702. https://doi.org/10.1016/j.precamres.2020.105702

Dodge, F.C.W., Millard, H.T., Elsheimer, H.N., 1982. Compositional variations and abundances of selected elements in granitoids rocks and constituent minerals, central Sierra Nevada batholiths, California. US Geological Survey Professional Paper, 1248.

Ducea, M.N., Saleeby, J.B., Bergantz, G., 2015a. The Architecture, Chemistry, and Evolution of Continental Magmatic Arcs. Annual Review of Earth and Planetary Sciences 43, 10.1-10.33. https://doi.org/10.1146/annurev-earth-060614-105049

Ducea, M.N., Paterson, S.R., DeCelles, P.G., 2015b. High-Volume Magmatic Events in Subduction Systems. Elements 11, 99-104. https://doi.org/ 10.2113/gselements.11.2.99

Dunphy, J.M., Ludden, J.N., 1998. Petrological and geochemical characteristics of a Paleoproterozoic magmatic arc (Narsajuaq terrane, Ungava Orogen, Canada) and comparisons to Superior Province granitoids. Precambriam Research 91, 109–142. https://doi.org/10.1016/S0301-9268(98)00041-2

Féboli, W.L., 1993 (Org.). Geologia da Folha Domingos Martins. Programa de Levantamentos Geológicos Básicos do Brasil, Folha SF.24-V-A-III – Domingos Martions. Brasília, DNPM/CPRM.

Figueiredo, M.C.H., Campos Neto, M.C., 1993. Geochemistry of the Rio doce magmatic arc, Southeastern Brazil. Anais da Academia Brasileira de Ciências. 65, 63-81.

Frost, B.R., Frost, C.D., 2008. On charnockites. Gondwana Reserach 13, 30-44. https://doi.org/10.1016/j.gr.2007.07.006

Frost, B.R., Barnes, C.G., Collins, W.J., Arculus, R.J., Ellis, D.J., Frost, C.D., 2001. A geochemical classification for granitic rocks. Journal of Petrology 42, 2033-2048. https://doi.org/10.1093/petrology/42.11.2033

Gerdes, A., Zeh, A., 2006. Combined U-Pb and Hf isotope LA-(MC)-ICP-MS analyses of detrital zircons: comparison with SHRIMP and new constraints for the provenance and age of an Armorican metasediment in Central Germany. Earth and Planetary Science Letters 249, 47-61. https://doi.org/10.1016/j.epsl.2006.06.039

Gerdes, A., Zeh, A., 2009. Zircon formation versus zircon alteration - new insights from combined U-Pb and Lu-Hf in-situ LA-ICP-MS analyses, and consequences for the interpretation of Archean zircon from the Central Zone of the Limpopo Belt. Chemical Geology 261, 230-243. https://doi.org/10.1016/j.chemgeo.2008.03.005

Gonçalves, L.E.S., 2009. Características gerais e história deformacional da Suíte Granítica G1, entre Governador Valadares e Ipanema, MG. Universidade Federal de Ouro Preto, Ouro Preto (MS Dissertation, 112 pp.).

Gonçalves, L., Farina, F., Lana, C., Pedrosa-Soares, A.C., Alkmim, F., Nalini, H.A.Jr., 2014. New U-Pb ages and lithochemical attributes of the Ediacaran Rio Doce magmatic arc, Araçuaí confined orogen, southeastern Brazil. Journal of South American Earth Sciences 52, 129–148. http://doi.org/10.1016/j.jsames.2014.02.008

Gonçalves, L., Alkmim, F.F., Pedrosa-Soares, A.C., Dussin, I.A., Valeriano, C.M., Lana, C., Tedeschi, M., 2016. Granites of the intracontinental termination of a magmatic arc: an example from the Ediacaran Araçuaí orogen, southeastern Brazil. Gondwana Research 36, 439-458. http://doi.org/10.1016/j.gr.2015.07.015

Gonçalves, L., Alkmim, F.F., Pedrosa-Soares, A.C., Gonçalves, C.C., Vieira V., 2018. From the plutonic root to the volcanic roof of a continental magmatic arc: a review of the Neoproterozoic Araçuaí orogen, southeastern Brazil. International Journal of Earth Science (Geologische Rundschau) 107, 337-358. http://doi.org/10.1007/s00531-017-1494-5

Gouvêa, L.P., Medeiros, S.R., Mendes, J.C., Soares, C., Marques, R., Melo, M., 2020. Magmatic activity period and estimation of P-T metamorphic conditions of pre-collisional Opx-metatonalite from Araçuaí-Ribeira orogens boundary, SE Brazil. Journal of South American Earth Sciences 99, 102506. https://doi.org/10.1016/j.jsames.2020.102506

Gradim, C., Roncato, J., Pedrosa-Soares, A.C., Cordani, U., Dussin, I., Alkmim, F.F., Queiroga, G., Jacobsohn, T., Silva, L.C., Babinski, M., 2014. The hot back-arc zone of the Araçuaí Orogen, Eastern Brazil: from sedimentation to granite generation. Brazilian Journal of Geology 44, 155-180. http://doi.org/10.5327/Z2317-4889201400010012

Gioia, S.M.C.L., Pimentel, M.M., 2000. The Sm-Nd isotopic method in the Geochronology Laboraty of the University of Brasília. Anais da Academia Brasília de Ciências 72, 2,

219–245.

Harris, N.B.W., Pearce, J.A., Tindle, A.G., 1986. Geochemical characteristics of collision-zone magmatism. In: Coward, M.P., Ries, A.C. (Eds.), Collision Tectonics. Geological Society London Special Publication 19, 67-81. https://doi.org/10.1144/GSL.SP.1986.019.01.04

Heilbron, M., Machado, N., 2003. Timing of terrane accretion in the Neoproterozoic-Eopaleozoic Ribeira Orogen (SE Brazil). Precambrian Research 125, 87-112. https://doi.org/10.1016/S0301-9268(03)00082-2

Heilbron, M., Pedrosa-Soares, A.C., Campos-Neto, M.C., Silva, L.C., Trouw, R., Janasi, V.A., 2004. Província Mantiqueira. In: V. Mantesso-Neto, A., Bartorelli, C.D.R., Carneiro, B.B., Brito-Neves (Org.). Geologia do Continente Sul-Americano. São Paulo, Editora Beca, XIII, 203-234.

Heilbron, M., Tupinambá, M., Valeriano, C., Armstrong, R., Silva, L.G.E., Melo, R.S., Simonetti, A., Pedrosa-Soares, A.C., Machado, N. 2013. The Serra da Bolívia complex: The record of a new Neoproterozoic arc-related unit at Ribeira belt. Precambrian Research 238, 158– 175. http://doi.org/10.1016/j.precamres.2013.09.014

Heilbron, M., Cordani, U.G, Alkmim F.F. The São Francisco Craton and Its Margins. In: Heilbron, M., Cordani, U.G, Alkmim F.F. (Eds.), São Francisco Craton, Eastern Brazil. Regional Geology Reviews, Springer International Publishing Co., pp. 255–276. https://doi.org/10.1007/978-3-319-01715-0_14

Heilbron, M., Valeriano, C.M., Peixoto, C., Tupinambá, M., Neubauer, F., Dussin, I., Corrales, F., Bruno, H., Lobato, M., Almeida, J.C.A., Silva L.G.E., 2020. Neoproterozoic magmatic arc systems of the central Ribeira belt, SE-Brazil, in the context of the West-Gondwana pre-collisional history: A review. Journal of South American Earth Sciences 103, 102710. https://doi.org/10.1016/j.jsames.2020.102710

Hervé, F., Pankurst, R.J., Fanning, C.M., Calderón, M., Yaxely, G.M., 2007. The South Patagonian batholith: 150 my of granite magmatism on a plate margin. Lithos 97, 373-394. http://doi.org/10.1016/j.lithos.2007.01.007

IBGE, 1987. Geologia. In: Projeto RADAMBRASIL. Folha SE 24 Rio Doce. IBGE, Rio de Janeiro, 548 pp.

Irvine, T.M., Baragar, W.R., 1971. A guide to the chemical classification of common volcanic rocks. Canadian Journal of Earth Sciences 8, 523-548. https://doi.org/10.1139/e71-055

Jackson, S.E., Pearson, N.J., Griffin, W.L., Belousova, E.A., 2004. The application of laser ablation-inductively coupled plasma-mass spectrometry to in situ U–Pb zircon geochronology. Chemical Geology 211, 47–69. https://doi.org/10.1016/j.chemgeo.2004.06.017

Janoušek, V., Farrow, C.M., Erban, V., 2006. Interpretation of whole-rock geochemical data in igneous geochemistry: Introducing Geochemical Data Toolkit (GCDkit). Journal of Petrology 47, 1255–1259. https://doi.org/10.1093/petrology/egl013

Kearey, P., Klepeis, K.A., Vine, F.J., 2014. Tectônica Global. 3° ed. Bookman, 436p.

Kelemen, P.B., Hanghoj, K., Greene, A.R., 2014. One view of the geochemistry of subduction-related magmatic arcs, with an emphasis on primitive andesite and lower crust. Treatise on Geochemistry 4, 749-806. http://doi.org/10.1016/B978-0-08-095975-7.00323-5.

Kohanpour, F., Kirkland. C.L., Gorczyk, C., Occhipinti, S., Lindsay, M.D., Mole, D., Vaillant, M., 2019. Hf isotopic fingerprinting of geodynamic settings: Integrating isotopes and numerical models. Gondwana Research 73, 190-199.

Kruhl, J.H., 1996. Prism- and basal-plane parallel subgrain boundaries in quartz: a microstructural geothermobarometer. Journal of Metamorphic Geology 14, 581–589. https://doi.org/10.1046/j.1525-1314.1996.00413.x

Kuribara, Y., Tsunogae, T., Santosh, M., Takamura, Y., Costa, A.G., Rosière, C.A., 2019. Eoarchean to Neoproterozoic crustal evolution of the Mantiqueira and the Juiz de Fora Complexes, SE Brazil: Petrology, geochemistry, zircon U-Pb geochronology and Lu-Hf isotopes. Precambrian Research 323, 82-101. https://doi.org/10.1016/j.precamres.2019.01.008

Laurent, O., Martin, H., Moyen, J.F., Doucelance, R., 2014. The diversity and evolution of late-Archean granitoids: evidence for the onset of 'modern-style' plate tectonics between 3.0 and 2.5 Ga. Lithos 205, 208-235. https://doi.org/10.1016/j.lithos.2014.06.012

Lee, C-T.A., Morton, D.M., Kistler, R.W., Baird, A.K. 2007. Petrology and tectonics of Phanerozoic continent formation: from island arcs to accretion and continental arc magmatism. Earth and Planetary Science Letters 263, 370-387. https://doi.org/10.1016/j.epsl.2007.09.025

Leite, C.A.S., Souza, J.D., Silva, S.L., Kosin, M., Silva, L.C., Bento, R.V., Santos Vieira, V.S., Camozzato, E., Paes, V.J.C., Netto, C., Junqueira, P.A., 2004. Folha Rio Doce (SE.24), escala 1:1.000.000. In: Schobbenhaus, C., Gonçalves, J.H., Santos, J.O.S., Abram, M.B., Leão Neto, R., Matos, G.M.M., Vidotti, R.M., Ramos, M.A.B., Jesus, J.D.A. de. (Eds.). Carta Geológica do Brasil ao Milionésimo. Programa Geologia do Brasil, CPRM–Serviço Geológico do Brasil, Brasília.

Lobato, M., Heilbron, M., Torós, T., Ragatky, D., Dantas, E., 2015. Provenance of the Neoproterozoic high-grade metasedimentary rocks of the arc-related Oriental Terrane of the Ribeira belt: Implications for Gondwana amalgamation. Journal of South American Earth Sciences 63, 260-278. http://doi.org/10.1016/j.jsames.2015.07.019

Ludwig, K.R., 2012. Isoplot/Ex Version 4.15: A Geochronological Toolkit for Microsoft Excel. Berkeley, Berkeley Geochronology Center 72 pp.

Martins, V.T.S, Teixeira, W., Noce, C.M., Pedrosa-Soares, A.C., 2004. Sr and Nd Characteristics of Brasiliano/Pan-African Granitoid Plutons of the Araçuai Orogen, Southeastern Brazil: Tectonic Implications. Gondwana Research 7, 75-89.

Mauri, S., Melo, M.G., Lana, C., Marques, R.A., 2021. Petrologic and geochronological constraints on the polymetamorphic evolution of the collisional granites, Araçuaí Orogen (SE Brazil). Anais da Academia Brasileira de Ciências 93(3), e20200639. https://doi.org/10.1590/0001-3765202120200639

Melo, M.G., Lana, C., Stevens, G., Pedrosa-Soares, A.C., Gerdes, A., Alkmin, L.A., Nalini Jr., H.A., Alkmim, F.F., 2017. Assessing the isotopic evolution of S-type granites of the Carlos Chagas batholith, SE Brazil: Clues from U-Pb, Hf isotopes, Ti geothermometry and trace element composition of zircon. Lithos 284-285, 730-750. http://doi.org/10.1016/j.lithos.2017.05.025

Melo, M.G., Lana, C., Stevens, G., Hartwig, M.E., Pimenta, M.E., Nalini Jr., H.A., 2020. Deciphering the source of multiple U–Pb ages and complex Hf isotope composition in zircon from post-collisional charnockite-granite associations from the Araçuaí orogen (southeastern Brazil). Journal of South American Earth Sciences 103, 102792. https://doi.org/10.1016/j.jsames.2020.102792

Milani, L., Kinnaird, J.A., Lehmann, J., Naydenov, K.V., Saalmann, K., Frei, D., Gerdes, A., 2015. Role of crustal contribution in the early stage of the Damara Orogen, Namibia: New constraints from combined U–Pb and Lu–Hf isotopes from the Goas Magmatic Complex. Gondwana Research 28, 961-986. http://doi.org/10.1016/j.gr.2014.08.007

Moyen, J.-F., Laurent, O., Chelle-Michou. C., Couzinié, S., Vanderhaeghe, O., Zeh, A., Villaros, A., Gardien, V., 2017. Collision vs. subduction-related magmatism: Two contrasting ways of granite formation and implications for crustal growth. Lithos 277, 154-177. http://doi.org/10.1016/j.lithos.2016.09.018

Munhá, J.M.U., Cordani, U.G., Tassinari, C.C.G., Palácios, T., 2005. Petrologia e termocronologia de Gnaisses Migmatíticos da Faixa de Dobramentos Araçuaí (Espírito Santo, Brasil). Revista Brasileira de Geociências 35, 123-134.

Nalini Jr., H.A., 1997. Caractérisation des suítes magmatiques néoprotérozoiques de la region de Conselheiro Pena et Galiléia (Minas Gerais, Brésil). Etude géochimique et structurale des suítes Galiléia et Urucum et relations avec les pegmatites à éléments rares associées. Ph.D. thesis. École des Mines de Saint Etienne et École des Mines de Paris, France, p. 237.

Nalini Jr., H.A., Bilal, E., Correia Neves, J.M., 2000. Syn-collisional peraluminous magmatism in the Rio Doce region: mineralogy, geochemistry and isotopic data of the Urucum suite (eastern Minas Gerais state, Brazil). Revista Brasileira de Geociências 30, 120–125.

Narduzzi, F., Farina F., Stevens, G., Lana, C., Nalini Jr, H.A., 2017. Magmatic garnet in the Cordilleran-type Galiléia granitoids of the Araçuaí belt (Brazil): Evidence for crystallization in the lower crust. Lithos, 282-283, 82-97. http://doi.org/10.1016/j.lithos.2017.02.017

Narduzzi, F., 2018 Genesis and evolution of a Neoproterozoic magmatic arc: the Cordilleran-type granitoids of the Araçuaí Belt, Brazil. PhD Thesis, Escola de Minas, Departamento de Geologia, Universidade Federal de Ouro Preto, 245p.

Noce, C.M., Pedrosa-Soares, A.C., Piuzana, D., Armstrong, R., Laux, J.H., De Campos, C.M., Medeiros, S.R. 2004. Ages of sedimentation of the kinzigitic complex and of a late orogenic thermal episode of the Araçuaí Orogen, Northern Espírito Santo State, Brazil: Zircon and monazite U-Pb SHRIMP and ID–TIMS data. Revista Brasileira de Geociências 34, 587-592.

Novo, T.A., Pedrosa-Soares, A.C., Noce, C.M., Alkmim, F.F., Dussin, I.A., 2010. Rochas charnockíticas do sudeste de Minas Gerais: a raiz granulítica do arco magmático do Orógeno Araçuaí. Revista Brasileira de Geociências 40, 573-592.

Novo, T.A., 2013. Caracterização do Complexo Pocrane, magmatismo básico Mesoproterozóico e unidades neoproterozóicas do Sistema Araçuaí-Ribeira, com ênfase em geocronologia U-Pb (SHRIMP e LA-ICP-MS). PhD Thesis, Instituto de Geociências, Universidade Federal de Minas Gerais, 177 p.

Novo, T.A., Pedrosa-Soares, A., Vieira, V.S., Dussin, I., Silva, L.C., 2018. The Rio Doce Group revisited: An Ediacaran arc-related volcano-sedimentary basin, Araçuaí orogen (SE Brazil). Journal of South American Earth Sciences 85, 345-361. https://doi.org/10.1016/j.jsames.2018.05.013

Otamendi, J.E., Ducea, M.N., Bergantz, G.W., 2012. Geological, petrological and geochemical evidence for progressive construction of an arc crustal section, Sierra de Valle Fértil, Famatinian Arc, Argentina. Journal of Petrology 53, 761–800. https://doi.org/10.1093/petrology/egr079

Pankhurst, R.J., Rapela, C.W., Saavedra, J., Baldo, E.G., Dahlquist, J., Pascua, I., Fanning, C.M., 1998. The Famatinian arc in the central Sierras Pampeanas: an early to mid-Ordovician continental arc on the Gondwana margin. In: Pankhurst, R.J., Rapela, C.W. (Eds.) The Proto-Andean Margin of Gondwana. Geological Society of London, Special Publications 142, 343–367. https://doi.org/10.1144/GSL.SP.1998.142.01.17

Pankhurst, R.J., Weaver, S.D., Hervé, F., Larrondo, P., 1999. Mesozoic-Cenozoic evolution of the North Patagonian Batholith in Aysen, Southern Chile. Journal of the Geological Society, London 156, 673-694. https://doi.org/10.1144/gsjgs.156.4.0673

Paterson, S.R., Ducea, M.N., 2015. Arc Magmatic Tempos: Gathering the Evidence. Elements 11, 91-98. https://doi.org/10.2113/gselements.11.2.91

Pearce, J.A., Harris, N.B.W., Tindle, A.G., 1984. Trace element diagrams for the tectonic interpretation of granitic rocks. Journal of Petrology 25, 956–983. https://doi.org/10.1093/petrology/25.4.956

Pedrosa Soares, A.C., Wiedemann-Leonardos, C.M., 2000. Evolution of the Araçuaí Belt and its connection to the Ribeira Belt, Eastern Brazil. In: Cordani, U.G., Milani, E.J., Thomaz Filho, A., Campo, D.A. (Eds.). Tectonic evolution of South America. Rio de Janeiro, 31st International Geological Congress, p. 265-285.

Pedrosa-Soares, A.C., Noce, C.M., Wiedemann, C., Pinto, C.P., 2001. The Araçuaí- West-Congo Orogen in Brazil: An overview of a confined orogen formed during Gondwanaland Assembly. Precambrian Research 110, 307-323. https://doi.org/10.1016/S0301-9268(01)00174-7

Pedrosa-Soares, A.C., Alkmim, F.F., Tack, L., Noce, C.M., Babinski, M., Silva, L.C., Martins-Neto, M.A., 2008. Similarities and differences between the Brazilian and African counterparts of the Neoproterozoic Araçuaí-West Congo orogen. In: Pankhurst, R.J., Trouw, R.A.J., Brito Neves, B.B., De Wit, M.J. (Eds.), West Gondwana: Pre-Cenozoic Correlations Across the South Atlantic Region. London, Geological Society of London, Special Publication 294, 153- 172. https://doi.org/10.1144/SP294.9

Pedrosa-Soares, A.C., De Campos, C.P., Noce, C.M., Silva, L.C., Novo, T., Roncato, J., Medeiros, S., Castañeda, C., Queiroga, G., Dantas, E., Dussin, I., Alkmim, F., 2011. Late Neoproterozoic-Cambrian Granitic Magmatism in the Araçuaí Orogen (Brazil), the Eastern Brazilian Pegmatite Province and Related Mineral Resources. In: Sial, A.N., Bettencourt, J.S., De Campos, C.P., Ferreira, V.P. (Eds.), Granite-Related Ore Deposits. London, Geological Society of London, Special Publication 350, 25–51. https://doi.org/10.1144/SP350.3

Pedrosa-Soares, A.C., Deluca, C., Araujo, C., Gradim, C., Lana, C., Dussin, I., Silva, L.C., Babinski, M., 2020. O Orógeno Araçuaí à luz da geocronologia: Um tributo a Umberto Cordani. In: Bartorelli, A., Teixeira, W., Brito Neves, B.B., Geocronologia e Evolução Tectônica do Continente Sul-Americano: a contribuição de Umberto Giuseppe Cordani. Solarias Edições Culturais, São Paulo, 728p.

Peixoto, E., Pedrosa-Soares, A.C., Alkmim, F.F., Dussin, I.A., 2015. A suture-related accretionary wedge formed in the Neoproterozoic Araçuaí orogen (SE Brazil) during Western Gondwanaland assembly. Gondwana Research 27, 878-896. http://doi.org/10.1016/j.gr.2013.11.010

Peixoto, C.A., Heilbron, M., Ragatky, D., Armstrong, R., Dantas, E., Valeriano, C.M., Simonetti, A. 2017. Tectonic evolution of the Juvenile Tonian Serra da Prata magmatic arc in the Ribeira belt, SE Brazil: Implications for early West Gondwana amalgamation. Precambrian Research 302, 221-254. http://doi.org/10.1016/j.precamres.2017.09.017

Peixoto, C.A., Lobato, M., Freitas, N.C., Heilbron, M., Dussin, I., Dantas, E. 2022. Geochronological constraints of high-grade metasedimentary rocks of the Italva and Costeiro basins: Reconstructing the Outer Magmatic Arc System of the Ribeira belt, SE Brazil. Precambrian Research 382, 106879. https://doi.org/10.1016/j.precamres.2022.106879

Pereira, V.H.M., Mendes, J.C, Carvalho, M.Q.T, Coelho, V.S.A., Medeiros, S.R., Valeriano, M. 2023. Petrogenesis of estrela granitoid and implications for the evolution of the rio doce magmatic arc: Araçuaí-Ribeira orogenic system, SE Brazil. Journal of South American Earth Sciences 126, 104337. https://doi.org/10.1016/j.jsames.2023.104337

Pimentel, M.M. 2016. The tectonic evolution of the Neoproterozoic Brasília Belt, central Brazil: a geochronological and isotopic approach. Brazilian Journal of Geology 46 (Suppl1): 67-82. https://doi.org/10.1590/2317-4889201620150004

Richter, F., Lana, C., Steven, G., Buick, I., Pedrosa-Soares, A.C., Alkmim, F.F., Cutts, K., 2016. Sedimentation, metamorphism and granite generation in a back-arc region: Records from the Ediacaran Nova Venécia Complex (Araçuaí Orogen, Southeastern Brazil). Precambrian Research 272, 78–100. http://doi.org/10.1016/j.precamres.2015.10.012

Rodríguez, N., Díaz-Alvarado J., Fernández C., Fuentes P., Breitkreuz C., Tassinari C.C.G., 2018. The significance of U-Pb zircon ages in zoned plutons – the case of the Flamenco pluton, Coastal Range batholith, northern Chile. Geoscience Frontiers 10, 1073-1099. https://doi.org/10.1016/j.gsf.2018.06.003

Roncato, J.G., 2009. As suítes graníticas tipo–S do norte do Espírito Santo na região das folhas Ecoporanga, Mantena, Montanha e Nova Venécia. Universidade Federal de Minas Gerais, Belo Horizonte (MS Dissertation, 102 p).

Rosa, M.d.L.d.S., Conceição, H., Macambira, M.J.B., Galarza, M.A., Cunha, M.P., Menezes, R.C.L., Marinho, M.M., Filho, B.E.d.C., Rios, D.C., 2007. Neoproterozoic anorogenic magmatism in the Southern Bahia Alkaline Province of NE Brazil: U–Pb and Pb-Pb ages of the blue sodalite syenites. Lithos 97, 88–97. https://doi.org/10.1016/j.lithos.2006.12.011

Santiago, R., Caxito, F.A., Pedrosa-Soares, A.C., Neves, M.A., Dantas, E.L., 2020. Tonian Island Arc Remnants in the Northern Ribeira Orogen of Western Gondwana: The Caxixe Batholith (ESPÍRITO SANTO, SE BRAZIL), Precambrian Research 105944 doi: https://doi.org/10.1016/j.precamres.2020.105944 Santiago, R., Caxito, F.A., Pedrosa-Soares, A.C., Neves, M.A., Calegari, S.S., Lana, C., 2022. Detrital zircon U–Pb and Lu–Hf constraints on the age, provenance and tectonic setting of arc-related high-grade units of the transition zone of the Araçuaí

and Ribeira orogens (SE Brazil). Journal of South American Earth Sciences 116, 103861. https://doi.org/10.1016/j.jsames.2022.103861

Santos, L.C.M.L, Caxito, F.A., Bouyo, M.H., Ouadahi, S., Araibia, K., Lages, G.A., Santos, G.L., Pitombeira, J.P.A., Cawood, P.A. 2022. Relics of ophiolite-bearing accretionary wedges in NE Brazil and NW Africa: connecting threads of western Gondwana´s ocean during Neoproterozoic times. Geosystems and Geoenvironment https://doi.org/10.1016/j.geogeo.2022.100148

Santos, M.M., Lana, C., Scholz, R., Buick, I., Schmitz, M.D., Kamo, S.L., Gerdes, A., Corfu, F., Tapster, S., Lancaster, P., Storey, C.D., Basei, M.A.S, Tohver, E., Alkmim, A., Nalini, H., Krambrock, K., Fantini, C., Wiedenbeck, M., 2017. A New appraisal of Sri Lankan BB zircon as reference material for LA-ICP-MS U-Pb geochronology and Lu-Hf isotope tracing. Geostandards and Geoanalytical Research 41, 335-358. https://doi.org/10.1111/ggr.12167

Schannor, M., Lana, C., Fonseca, M. 2019. São Francisco-Congo Craton break-up delimited by U-Pb-Hf isotopes and trace-elements of zircon from metasediments of the Araçuaí Belt. Geoscience Frontiers 10, 611-628. https://doi.org/10.1016/j.gsf.2018.02.011

Schannor, M., Lana, C., Mazoz, A., Narduzzi, F., Cutts, K., Fonseca, M. 2020. Paleoproterozoic sources for Cordilleran-type Neoproterozoic granitoids from the Araçuaí orogen (SE Brazil): Constraints from Hf isotope zircon composition. Lithos 378–379, 105815. https://doi.org/10.1016/j.lithos.2020.105815

Scherer, E., Münker, C., Mezger, K., 2001. Calibration of the Lutetium–Hafnium clock. Science 293, 683–687. https://doi.org/10.1126/science.1061372

Serrano, P., Pedrosa-Soares, A., Medeiros-Junior, E., Fonte-Boa, T., Araujo, C., Dussin, I., Queiroga, G., Lana, C., 2018. A-type Medina batholith and post-collisional anatexis in the Araçuaí orogen (SE Brazil). Lithos 320-321, 515-536. https://doi.org/10.1016/j.lithos.2018.09.009

Silva, M.A., Camozzato, E., Paes, V.J.C., Junqueira, P.A., Ramgrab, G. E. 2004. Folha SF.24-Vitoria. In: Schobbenhaus, C., Gonçalves, J.H., Santos, J.O.S., Abram, M.B., Leão Neto, R., Matos, G.M.M. , Vidotti, R.M., Ramos, M.A.B., Jesus, J.D.A. de. (Eds.). Carta Geológica do Brasil ao Milionésimo, Sistema de Informações Geográficas. Programa Geologia do Brasil. CPRM, Brasília.

Silva, L.C., Pedrosa-Soares, A.C., Teixeira, L.R., Armstrong, R., 2008. Tonian rift-related, A-type continental plutonism in the Araçuaí Orogen, Eastern Brazil: new evidence for the breakup stage of the São Francisco-Congo Paleocontinent. Gondwana Research 13, 527–537. https://doi.org/10.1016/j.gr.2007.06.002

Sláma, J., Košler, J., Condon, D.J., Crowley, J.L., Gerdes, A., Hanchar, J.M., Horstwood, M.S.A., Morris, G.A., Nasdala, L., Norberg, N., Schaltegger, U., Schoene, B., Tubrett, M.N., Whitehouse, M.J., 2008. Plešovice zircon – a new natural reference material for U–Pb and Hf isotopic microanalysis. Chemical Geology 249, 1–35. https://doi.org/10.1016/j.chemgeo.2007.11.005

Soares, C.C.V., Queiroga, G., Pedrosa-Soares, A.C., Gouvêa, L.P., Valeriano, C.M., Melo, M.G., Marques, R.A., Freitas, R.D.A., 2020. The Ediacaran Rio Doce magmatic arc in the Araçuaí – Ribeira boundary sector, southeast Brazil: Lithochemistry and isotopic (Sm–Nd and Sr) signatures. Journal of South American Earth Sciences 102880. https://doi.org/10.1016/j.jsames.2020.102880

Söderlund, U., Patchett, J.P., Vervoort, J.D., Isachsen, C.E., 2004. The 176Lu decay constant determined by Lu-Hf and U-Pb isotope systematics of Precambrian mafic intrusions. Earth and Planetary Science Letters 219, 311-324. https://doi.org/10.1016/S0012-821X(04)00012-3

Souza, M.E., Martins, M.S., Queiroga, G.N., Pedrosa-Soares, A.C., Dussin, I., Castro, M.P., Serrano, P., 2022. Time and isotopic constraints for Early Tonian basaltic magmatism in a large igneous province of the São Francisco – Congo paleocontinent (Macaúbas basin, Southeast Brazil). Precambrian Research 373, 106621. https://doi.org/10.1016/j.precamres.2022.106621

Stacey, J.S., Kramers, J.D., 1975. Approximation of terrestrial lead isotope evolution by a two-stage model. Earth and Planetary Science Letters 26, 207-221. https://doi.org/10.1016/0012-821X(75)90088-6

Sun S.S., McDonough W.F., 1989. Chemical and isotopic systematics of oceanic basalts: implications for mantle composition and processes. In: Saunders AD, Norry M (Eds.) Magmatism in Ocean Basins. Geological Society of London Special Publications 42, 313-345. http://doi.org/10.1144/GSL.SP.1989.042.01.19

Tedeschi, M., Novo, T., Pedrosa-Soares, A., Dussin, I., Tassinari, C., Silva, L.C., Gonçalves, L., Alkmim, F., Lana, C., Figueiredo, C., Dantas, E., Medeiros, S., De Campos, C., Corrales, F., Heilbron, M., 2016. The Ediacaran Rio

Doce magmatic arc revisited (Araçuaí-Ribeira orogenic system, SE Brazil). Journal of South American Earth Sciences 68, 167-186. http://doi.org/10.1016/j.jsames.2015.11.011

Tedeschi, M., Pedrosa-Soares, A., Dussin, I., Lanari, P., Novo, T., Pinheiro, M.A.P., Lana, C., Peters, D., 2018. Protracted zircon geochronological record of UHT garnet-free granulites in the Southern Brasília orogen (SE Brazil): Petrochronological constraints on magmatism and metamorphism. Precambrian Research 316, 103-126. https://doi.org/10.1016/j.precamres.2018.07.023

Tuller, M.P., 1993 (Org.). Geologia da Folha Colatina. Programa de Levantamentos Geológicos Básicos do Brasil, Folha SE.24-Y-C-VI - Colatina. Brasília, DNPM/CPRM.

Tupinambá, M., Heilbron, M., Valeriano, C.M., Porto Jr., R., Blanco de Dios, F., Machado, N., Silva, L.G.E., Almeida, J.C.H., 2012. Juvenile contribution of the Neoproterozoic Rio Negro magmatic arc (Ribeira Belt, Brazil): implications for Western Gondwana amalgamation. Gondwana Research 21, 422–438. https://doi.org/10.1016/j.gr.2011.05.012

Uhlein, A., Roncato, J., Egydio-Silva, M., Parizek-Silva, Y., Alves, M., 2014. Geologia, Petrologia e Contexto Geotectônico dos Gnaisses e Granitóides da Região de Colatina, Espírito Santo. Geonomos 22, 66-83. https://doi.org/10.18285/geonomos.v22i1.295

van Achterbergh, E., Ryan, C.G., Jackson, S.E., Griffin, W., 2001. Data reduction software for LA-ICP-MS. In: Sylvester, P. (Ed.), Laser-ablation-ICPMS in the Earth sciences, principles and applications. Mineralogical Association of Canada, Short Course Series 29, 239–243.

Vervoort, J.D., Kemp, A.I.S., 2016. Clarifying the zircon Hf isotope record of crust–mantle evolution. Chemical Geology 425, 65-75. http://doi.org/10.1016/j.chemgeo.2016.01.023

Victoria, A., Pedrosa-Soares, A., Cruz, S.C.P., Lana, C., Dantas, E., Dussin, I., Borges, R. 2022. Magmatic diversity in continental rifts: A case study on the Early Tonian, plutono-volcanic Salto da Divisa complex, Araçuaí Orogen, Eastern Brazil. Lithos 434-435, 106920 https://doi.org/10.1016/j.lithos.2022.106920

Vieira, V.S., Menezes, R.G. (Orgs.), 2015. Geologia e Recursos Minerais do Estado do Estado do Espírito Santo: texto explicativo do mapa geológico e de recursos minerais, escala 1:400.000. Programa Geologia do Brasil, CPRM - Serviço Geológico do Brasil, Belo Horizonte.

Whitney, D.L., Evans, B.W., 2010. Abbreviations for names of rock-forming minerals. American Mineralogist 95, 185-187. http://doi.org/10.2138/am.2010.3371

Wisniowski, L., Pedrosa-Soares, A., Medeiros-Junior, E., Belém, J., Dussin, I., Queiroga, G., 2021. Ultra-high temperature, mid-crustal level, contact metamorphism imprinted on granulite facies paragneisses by a norite intrusion (São Gabriel da Baunilha, Araçuaí orogen, southeast Brazil). Journal of Metamorphic Geology 00, 1-29.

Xavier, B.C., 2017. Relações tectônicas no setor central da Faixa Araçuaí: Análise Estrutural por ASM e Geocronologia U-Pb e Lu-Hf. Universidade de São Paulo, São Paulo (MS Dissertation, 123 p).

Yardley, B.W.D, Mackenzie, W.S., Guildford, C., 1996. Atlas de rocas metamórficas y sus texturas. Barcelona, Masson, 128p.

CHAPTER 4. SCIENTIFIC CONTRIBUTION II

Article published by Lithos Journal (doi: 10.1016/j.lithos.2019.105252)

This article presents the first data of Lu-Hf in zircon, together with their respective U-Pb ages, for representative rocks of the arc-related basin in the studied region, represented by Nova Venécia migmatitic paragneisses and a foliated granite of the Ataléia suite, one of their products of collisional anatexis. It also contains a detailed study of zircons (morphology, internal textures, and U-Th-Pb and Lu-Hf isotopic analyses) of post-collisional bodies that intruded this arc-related basin.

Zircon in emplacement borders of post-collisional plutons compared to country rocks: A study on morphology, internal texture, U-Th-Pb geochronology and Hf isotopes (Araçuaí orogen, SE Brazil)

Cristina Araujo[a*], Antonio Pedrosa-Soares[a#], Cristiano Lana[b#], Ivo Dussin[c#], Gláucia Queiroga[b#], Paula Serrano[b], Edgar Medeiros-Júnior[b]

[a]Universidade Federal de Minas Gerais, Programa de Pós-Graduação em Geologia, CPMTC-IGC, Campus Pampulha, Belo Horizonte, Brazil

[b]Universidade Federal de Ouro Preto, Departamento de Geologia, Morro do Cruzeiro, Ouro Preto, Brazil

[c] Universidade do Estado do Rio de Janeiro, Faculdade de Geologia, Rio de Janeiro, Brazil

https://doi.org/10.1016/j.lithos.2019.105252

Fellow of the Brazilian Research Council (CNPq)

*Corresponding author at: Universidade Federal de Minas Gerais, Programa de Pós-Graduação em Geologia, CPMTC-IGC, Av. Antônio Carlos, 6627 Belo Horizonte, Brazil. E-mail address: *crisgeo@ufmg.br*.

ABSTRACT

Zircon is a powerful tool to study the internal evolution of igneous bodies and their interactions with country rocks. At pluton borders, zircon may record the emplacement history from the crystallization onset to deuteric processes, as well as inheritance from country rocks. We present a detailed morphology and internal structure study coupled with isotopic analyses (U-

Th-Pb and Lu-Hf) on a great number of zircon grains extracted from samples collected at the borders of three distinct post-collisional intrusions of the Araçuaí orogen: granites from the Aracê – Pedra Azul and Vitória plutons, and a tonalite from the Mestre Álvaro pluton. For comparison, we also present mineral and bulk-rock chemistry data from these samples of post-collisional intrusions, as well as zircon U-Pb-Hf data from their country rocks (the Nova Venécia migmatitic paragneisses and Ataléia granites) and a wide dataset compilation. Zircon saturation geothermometry suggests igneous temperatures above 800 °C for pluton borders. Zircon geochronology resulted in crystallization ages for borders of the plutons at 523 ± 2 Ma (Aracê – Pedra Azul), 505 ± 1 Ma (Vitória), and 527 ± 2 Ma (Mestre Álvaro). Lu-Hf data (Aracê – Pedra Azul pluton: $\varepsilon Hf_{(t)}$ -18.6 to -23.8, T_{DM} ages from 2.25 to 2.47 Ga; Vitória pluton: $\varepsilon Hf_{(t)}$ -7.4 to -10.3, T_{DM} ages from 1.58 to 1.71 Ga; Mestre Álvaro pluton: $\varepsilon Hf_{(t)}$ -0.7 to -8.8, T_{DM} ages from 1.27 to 1.66 Ga; Nova Venécia migmatitic paragneiss: $\varepsilon Hf_{(t)}$ +4.1 to -39.2, T_{DM} ages from 1.20 to 3.47 Ga; and Ataléia granite: $\varepsilon Hf_{(t)}$ -3.2 to -8.1, T_{DM} ages from 1.42 to 1.64 Ga) indicate involvement of country rocks in the petrogenesis of post-collisional intrusions. Together, new and compiled data suggest: i) magma hybridization at high temperature, involving country rocks; ii) rapid growth of zircon crystals probably at rapid cooling rates; and iii) *in situ* dissolution–recrystallization and overgrowth processes in zircon crystals in response to interactions with residual (late-stage) melts and/or deuteric fluids.

KEYWORDS: zircon morphology; U-Pb geochronology; Hf isotope; post-collisional granites; Araçuaí orogen.

4.1 INTRODUCTION

Zircon is extensively studied in Earth sciences because it has a remarkable resistance to high-temperature diffusive re-equilibration and contains a wide spectrum of geochemically important trace elements, such as Y, Hf, U, Th, and the rare earth elements – REE (Bea et al., 2018a, 2018b; Belousova et al., 2006; Cherniak and Watson, 2003; Corfu et al., 2003; Hoskin and Schaltegger, 2003; Tang et al., 2014). The low diffusion rates of REE and tetravalent cations (U, Th, Hf) in zircon crystals suggest that they are essentially immobile under most geological conditions (Cherniak and Watson, 2003; Tang et al., 2014). Zircon is therefore widely used in geochronological and geochemical studies to investigate different evolution stages of igneous and metamorphic rocks (Bea et al., 2018a, 2018b; Belousova et al., 2006;

Cherniak and Watson, 2003; Corfu et al., 2003; Harley et al., 2007; Hoskin and Schaltegger, 2003; Tang et al., 2014).

The connection between zircon growth and granite petrogenesis has been widely studied, since zircon features may reflect the source characteristics of the host granite, such as crystallization temperature, alkalinity index, and the abundance of elements like U and REE (Belousova et al., 2006; Benisek and Finger, 1993; Köksal et al., 2008; Pupin, 1980; Vavra, 1990, 1994; Wang et al., 2002). Pupin (1980) established the fundamental basis for the study of zircon morphological populations, relating arrangements of prismatic and pyramidal crystal faces with a genetic classification of the host granite, and the crystallization temperature of the granitic magma (see Supplementary File 4.B). Although Pupin's scheme may be useful for several purposes, its principles were questioned by researchers who pointed out zircon morphologies as strongly dependent on magma chemistry among other factors and, thus, not necessarily reflect all stages of granite evolution (e.g., Benisek and Finger, 1993; Vavra, 1990, 1994).

At borders of granitic intrusions, zircon may record the emplacement history from the crystallization onset to deuteric processes, as well as inheritance from country rocks. During emplacement and cooling of plutons, their borders are subject to several processes that can affect magma crystallization, such as the country rocks assimilation and/or fluids release accompanied by chemical interchange (Corfu et al., 2003; Molina et al., 2012; Wang et al., 2018).

The Araçuaí orogen, Southeastern Brazil (Figure 4.1), exhibits a long-lasting magmatic activity, from the Early Ediacaran up to the Cambrian–Ordovician boundary, that produced a huge amount of distinct plutonic igneous rocks, covering about 200,000 km^2 along the orogen core (Pedrosa-Soares et al., 2001, 2011). Such a great amount and wide composition range of plutonic rocks record an evolutionary history from pre-collisional to post-collisional stages, showing countless fresh exposures of well-preserved rocks that make the hot core of the Araçuaí orogen a superb natural laboratory to study orogenic magmatism processes.

Here, we focus on zircon characterization from samples collected at the borders of three distinct post-collisional granitic intrusions (Aracê – Pedra Azul, Vitória, and Mestre Álvaro plutons; Figure 4.1B), reporting the results of a detailed study on zircon features associated with U-Th-Pb and Lu-Hf data from selected samples. To investigate the involvement of country rocks in the post-collisional plutonism, we also present new zircon U-Pb and Hf isotope data for representative samples of migmatitic paragneisses (Nova Venécia complex) and one of their

products of collisional anatexis (a foliated granite of the Ataléia suite). The results are compared with mineral and bulk-rock chemistry data of the studied samples from post-collisional granitic plutons, and with a compiled dataset from previous studies. Finally, we discuss geochronological and petrological implications of morphology, internal texture and isotopic chemistry of zircon crystals to help understanding on petrogenesis and emplacement of post-collisional plutons, as well as to add information on the late evolution of the Araçuaí orogen. Besides forthcoming sections, the supplementary files 4.A and 4.D contain a thorough literature data compilation. The analytical methods along with descriptions of the sampled plutons and studied materials are available in supplementary file 4.B. The new data are presented in Supplementary files 4.C, 4.D, and 4.E.

We use the name granite in a general sense, if not otherwise specified. Geographical coordinates refer to the present-day position of continents, even in relation to paleocontinental descriptions. Mineral abbreviations are in accordance to Whitney and Evans (2010).

4.2 GEOLOGICAL SETTING

The studied region is located in the high-grade (crystalline) core of the Araçuaí – West Congo orogenic system (AWCO; Figure 4.1). The AWCO represents the evolution of a confined orogenic system formed during the Western Gondwana amalgamation in Late Neoproterozoic time, within an embayment surrounded by the São Francisco – Congo craton (Alkmim et al., 2006, 2017; Pedrosa-Soares et al., 2001, 2008). Long after that paleocontinental assemblage promoted by the Brasiliano – Pan-African orogeny, the AWCO was split apart by the opening of the South Atlantic Ocean during the Cretaceous, leaving the Araçuaí orogen in South America and the West Congo belt in Africa.

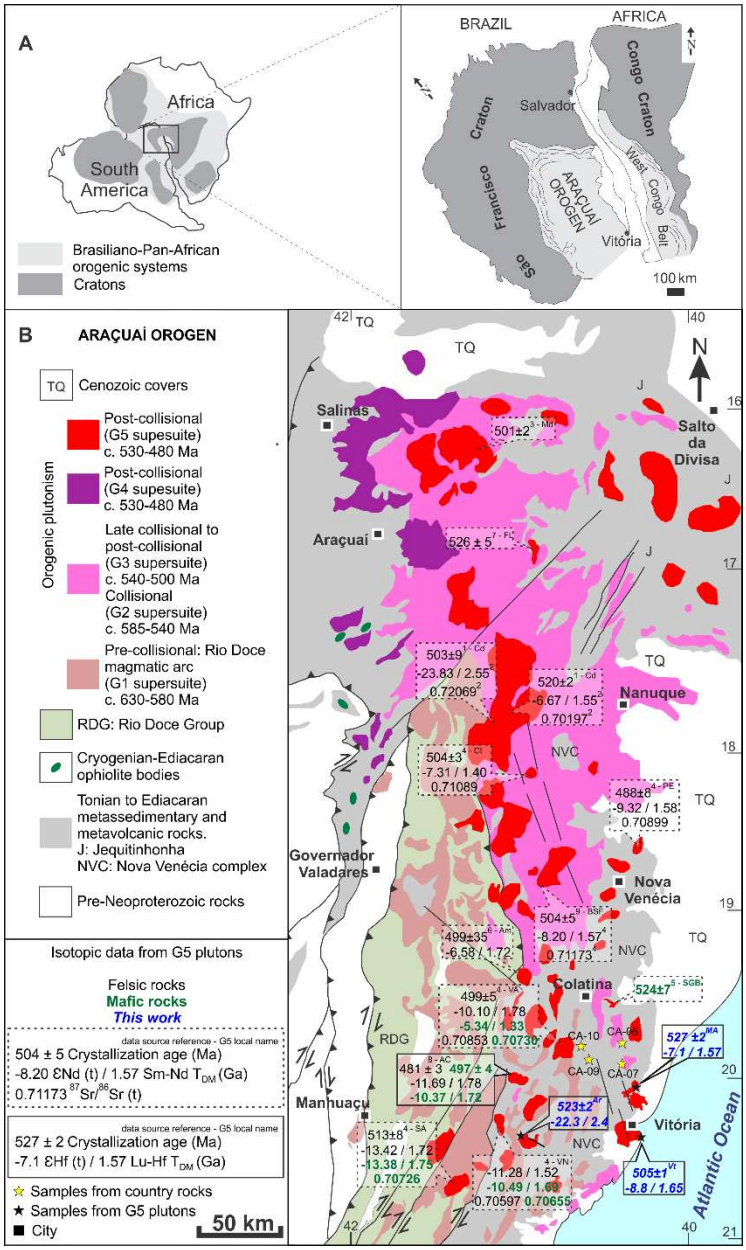

Figure 4.1: (A) The Araçuaí-West Congo orogenic system and the related cratons in the context of West Gondwana (modified from Alkmim et al., 2006). (B) Simplified geological map of the Araçuaí orogen (modified from Pedrosa-Soares et al., 2011). Local names of G5 intrusions: Cd, Caladão; Md, Medina; BSF, Barra de São Francisco; PE, Pedra do Elefante; Ct, Cotaché; SGB, São Gabriel da Baunilha; Am, Aimorés; VA, Várzea Alegre; SA, Santa Angélica; VN, Venda Nova; MA, Mestre Álvaro; Vt, Vitória; Ar, Aracê – Pedra Azul. See Supplementary file 4.A for further details. Data source references: (1) Noce et al., 2000; (2) Martins et al., 2004; (3) Serrano et al., 2018; (4) De Campos et al., 2016; (5) Belém, 2014; (6) Mello, 2000; (7) Gonçalves et al., 2016; (8) Aranda, 2018; (9) Gradim et al., 2014.

A long-lasting succession of granite production events (ca. 630 – 480 Ma) associated to the orogenic stages is one of the most remarkable features of the Araçuaí orogen (Gradim et al., 2014; De Campos et al., 2016; Gonçalves et al., 2016; Tedeschi et al., 2016; Melo et al., 2017;

Pedrosa-Soares et al., 2011; Serrano et al., 2018). All those orogenic granites and related rocks have been grouped into five supersuites (G1 to G5) by Pedrosa-Soares et al. (2011).

The G1 supersuite (ca. 630 - 580 Ma), formed from the pre-collisional to early collisional orogenic stages, represents the plutonic portion of the Rio Doce magmatic arc (Figure 4.1B). It mostly encompasses tonalitic to granodioritic rocks with calc-alkaline, magnesian and metaluminous signature, formed by crustal anatexis with minor involvement of mantle magmas. The latter is represented by countless mafic to dioritic enclaves, revealing magma mingling-mixing features in tonalite-granodioritic batholiths and stocks, and rare single plutons of mafic-dioritic composition. Chemical signature and hybrid isotopic attributes suggest an interaction between the Paleoproterozoic continental basement and minor mantle-derived magmas in a continental margin setting. The arc-related supracrustal successions comprise metavolcano-sedimentary units of the Rio Doce Group in the arc domain, the Nova Venécia paragneiss complex in the back-arc region, and mélange-related rock assemblages in the fore-arc zone (Araujo et al., 2019; Degler et al., 2017; Gonçalves et al., 2014, 2016; Gradim et al., 2014; Novo et al., 2018; Pedrosa-Soares et al., 2011; Peixoto et al., 2015; Richter et al., 2016; Tedeschi et al., 2016).

The Nova Venécia complex consists of migmatitic Al-rich paragneisses and garnet-cordierite granulites, which are poor to free in biotite, both with lenses of paraderived calc-silicate rocks, covering a large area in the focused region (Figure 4.1B). According to published geochronological data and our results from detrital grains of zircon, the Rio Doce arc has been considered to be one of the most important sediment sources for the Nova Venécia complex, located in a back-arc basin setting (Noce et al., 2004; Gradim et al., 2014; Richter et al., 2016).

A huge amount of peraluminous G2 granites (ca. 585 - 540 Ma) formed from the late pre-collisional to late-collisional stages by the regional anatexis of Al-rich paragneisses under amphibolite to granulite facies conditions (Gradim et al., 2014; Melo et al., 2017; Pedrosa-Soares et al., 2011; Peixoto et al., 2015; Richter et al., 2016). Accordingly, the Nova Venécia paragneisses were sources of great amounts of S-type granitic melts. Their autochthonous melts, encompassed by the Ataléia suite, formed garnet-biotite granitic rocks, ranging in composition from tonalite to granite, rich in restites of paragneiss and calc-silicate rocks. Those garnet-rich granitic rocks display the regional solid-state foliation imprinted by the collisional tectono-metamorphic event. The oldest Ataléia granites have been dated around 590 - 580 Ma and the related metamorphic peak, given by metamorphic zircon overgrowths, has been settled between 570 - 550 Ma (Gradim et al., 2014; Richter et al., 2016). From the late collisional to post-

collisional stages (ca. 540 - 500 Ma), mica-free peraluminous leucogranites of the G3 supersuite formed by dehydration partial melting of G2 granitic rocks during decompression (Gradim et al., 2014; Pedrosa-Soares et al., 2011; Serrano et al., 2018).

Lastly, upflow of asthenospheric mantle during the late orogenic extensional collapse, probably related to delamination of lithospheric mantle and slab breakoff following the collisional stage, provided an important heat source for the production of a number of post-collisional intrusions that have been grouped in the G4 and G5 supersuites (De Campos et al., 2004, 2016; Gradim et al., 2014; Pedrosa-Soares et al., 2011; Serrano et al., 2018). The G4 supersuite mostly comprises peraluminous, sub-alkaline to alkaline, two-mica granites, formed at relatively shallow crustal levels (Figure 4.1B).

The G5 supersuite (ca. 530 - 480 Ma), our focus in this work, consists of I-type and A-type, metaluminous to slightly peraluminous, high K-Fe calc-alkaline to alkaline granitic rocks and associated mafic terms, representing the most outstanding post-collisional magmatic event of the Araçuaí orogen. It includes balloon-shaped, inversely-zoned, circumscribed plutons mostly composed of granitic-charnockitic and/or gabbronoritic rocks, as well as batholiths encompassing several plutons, generally with widespread evidence of magma mixing and mingling (De Campos et al., 2004, 2016; Gradim et al., 2014; Pedrosa-Soares et al., 2011; Serrano et al., 2018; Wiedemann et al., 2002). Most G5 intrusions occur in the back-arc region of the Rio Doce magmatic arc (Figure 4.1B) and in the northern ensialic domain of the Araçuaí orogen (Pedrosa-Soares et al., 2011; Serrano et al., 2018). To the south of latitude 18°30’ S, the plutons, hosted by granulite-facies rocks, show relatively small exposure areas, and many of them display cores rich in gabbronoritic rocks surrounded by granitic-charnockitic rocks, disclosing their mafic roots and suggesting emplacement at deeper crustal levels (De Campos et al., 2004, 2016). Conversely, to the north of latitude 18°30’ S, the G5 bodies generally form composite batholiths, encompassing several single plutons, where microgranular enclaves are more common than mafic rocks, suggesting exposure of higher crustal levels in this sector of the orogen (Pedrosa-Soares et al., 2011). The available geothermobarometric quantitative data also suggest those crustal level relations. G5 plutons found to the south of latitude 18°30’ S have provided crystallization pressures in the range of 5.7 – 11.5 kbar (Ludka and Wiedemann-Leonardos, 2000; Mello et al., 2011; Mendes et al., 1999; Mendes and De Campos, 2012; Wiedemann et al., 2002), while the northern Medina batholith was emplaced at pressures around 2.4 – 3.5 kbar (Serrano et al., 2018). The quoted data suggest emplacement depths from ca. 9 km, in the region of the Medina batholith (Serrano et al., 2018), to 30 km, for the deeply

eroded G5 plutons hosted by granulites in the southeastern tip of the Araçuaí orogen (De Campos et al., 2016).

The crystallization temperatures estimated for G5 plutons range from 700 ºC to 1000 ºC (Ludka and Wiedemann-Leonardos, 2000; Mendes et al., 1999; Mendes and De Campos, 2012; Serrano et al., 2018; Wiedemann et al., 2002). Isotopic signatures show wide variation ranges for $^{87}Sr/^{86}Sr$ (0.702 – 0.721), $\varepsilon Nd_{(t)}$ (-4 to -15), Nd T_{DM} model ages (1.3 Ga to 3.3 Ga), as well as $\varepsilon Hf_{(t)}$ around -11, and Hf T_{DM} model ages around 1.7 Ga (Supplementary file 4.A and Figure 4.1B). Extremely negative εNd values (-20.4 to -23.7) with Neoarchean Nd T_{DM} ages (ca. 2.6 Ga) are reported by Martins et al. (2004). All those data imply an important crustal contribution for the generation of G5 granitic magmas, although the mantelic component is testified by the abundance of mafic components shown by mingling-mixing features and found in single gabbronorite plutons.

4.3 PETROGRAPHY AND MINERAL CHEMISTRY

Coordinates of the outcrops, their characteristics, mineralogy, and main features of each studied sample are presented in Table 1. Electron microprobe analyses of biotite, feldspars, allanite, titanite, rutile, zircon, and apatite from the G5 samples are available in Supplementary file 4.C.

4.3.1 G5 samples

4.3.1.1 Sample CA-02 (Aracê – Pedra Azul pluton)

A sample of titanite-allanite-biotite granite (Figure 4.2A) was collected in the northwest border of the pluton (Figure 4.1B). It presents K-feldspar (essentially perthitic microcline) with compositions ranging from Or_{89} to Or_{93} (Figure 4.3A). Plagioclase varies from oligoclase (An_{13}) to andesine (An_{31}; Figure 4.3A) with reverse and normal slight zonation, and calcic spike. Thin rims of albite surround some crystals (Figure 4.2B). Antiperthitic and myrmekitic intergrowths are also observed. Biotite presents annite-phlogopite composition and exhibits Mg# (Mg/Mg+Fe) ranging from 0.39 to 0.46, Ti from 0.22 to 0.38 a.p.f.u. (Figure 4.3B, 4.3C), ^{IV}Al from 2.1 to 2.4 a.p.f.u., and high contents of F (1.03 to 0.61 a.p.f.u.). Allanite, relatively rich in Ce (8.0 to 11.9%), occurs as zoned euhedral to subhedral crystals controlled by the abundance of light rare-earth elements (LREE), Fe, Ca, and Th, commonly showing an increase in LREE, Fe, and Ca from core to rim. Titanite is relatively coarse (up to 1 mm) and displays appreciable contents of Al (0.52 to 0.61 a.p.f.u.) and Fe (0.20 to 0.33 a.p.f.u.). The analyzed apatite crystals

have fluorapatite composition (F = 3.95 to 5.28%), with acicular shape coexisting with the usual stubby prismatic habit. Zircon commonly appears as inclusions in quartz, feldspars, biotite, allanite and titanite, showing slight increase of Fe from core to rim.

Table 4.1: Summary of the main features of the studied samples.

Unit	Aracê pluton	Vitória pluton	Mestre Álvaro pluton	Nova Venécia complex	Ataléia suite	Nova Venécia complex	Nova Venécia complex
Sample	CA-02	CA-04	CA-05	CA-06	CA-07	CA-09	CA-10
Coordinates	S20°23.237'/W41°01.044'	S20°20.032'/W40°16.383'	S20°06.828'/W40°19.291'	S19°47.888'/W40°22.191'	S19°55.942'/W40°24.573'	S19°55.269'/W40°35.891'	S19°48.874'/W40°40.719'
Location	Domingos Martins, Espírito Santo state	Vila Velha, Espírito Santo state	Serra, Espírito Santo state	Ibiraçu, Espírito Santo state	Fundão, Espírito Santo state	Santa Teresa, Espírito Santo state	Santa Teresa, Espírito Santo state
Field Feature	Light gray, medium to coarse-grained, isotropic	Light pink to gray, medium-grained, isotropic	Light green to gray, coarse-grained, isotropic	Metatexite, blue, coarse-grained, laminated to banded with variations in Crd+Grt+Bt and Qtz+Kfs+Pl.	Foliated granite in close spatial association with migmatitic paragneisses. Gray, medium to coarse-grained	Metatexite, banded with centimetric felsic and mafics bands. Fine to coaurse-grained. Poikiloblastic garnet is present in all lithotypes.	Metatexite, laminated to banded, with felsic and mafics bands. Fine to coarse-grained. Poikiloblastic garnet is present in all lithotypes.
Lithotype sample	Titanite-allanite-biotite granite	Biotite granite	Biotite tonalite	Sil-Bt-Crd paragneiss (known as Crd granulite)	Grt-Bt metagranite	Sil-Grt-Crd-Bt paragneiss	Grt-Bt paragneiss
Microtexture	Inequigranular	Inequigranular	Equigranular	Granoblastic	Granolepidoblastic	Granolepidoblastic	Granolepidoblastic
Main mineralogy*	Kfs-Qz-Pl-Bt	Kfs-Qz-Pl-Bt	Pl-Qz-Bt	Crd-Qz-Kfs-Bt-Pl	Pl-Qz-Bt-Kfs-Grt	Qz-Bt-Crd-Grt-Kfs-Sil-Pl	Qz-Bt-Kfs-Pl-Grt
Acessory mineralogy*	Aln-Ttn-Mag-Ap-Zrn-Ilm	Mag-Mnz-Zrn-Ap	Kfs-Mnz-Zrn-Ap-Mag	Grd-Opq-Hc-Ap-Zrn-Mnz	Opq-Mnz-Zrn-Ap	Opq-Mnz-Zrn-Ap	Opq-Mnz-Zrn-Ap
Secondary mineralogy	Ep-Ms-Chl-Ser	Ms-Chl-Ser-Ru-Cb-Mag-Ilm	Ms-Chl-Ser-Ru-Cb-Ilm	Ms-Chl-Ser-Cb	Ms-Chl-Ser-Cb	Ms-Chl-Ser	Ms-Chl-Ser

* in decreasing order of abundance

Aln: allanite; Ap: apatite; Bt: biotite; Cb: carbonate; Chl: chlorite; Crd: Cordierite; Ep: epidote; Grt: garnet; Hc: hercynite; Ilm: ilmenite; Kfs: K-feldspar; Mag: magnetite; Mnz: monazite; Ms: muscovite; Opq: opaques minerals; Pl: plagioclase; Qz: quartz; Ser: sericite; Sil: Sillimanite; Ru: rutile; Ttn: titanite; Zrn: zircon.

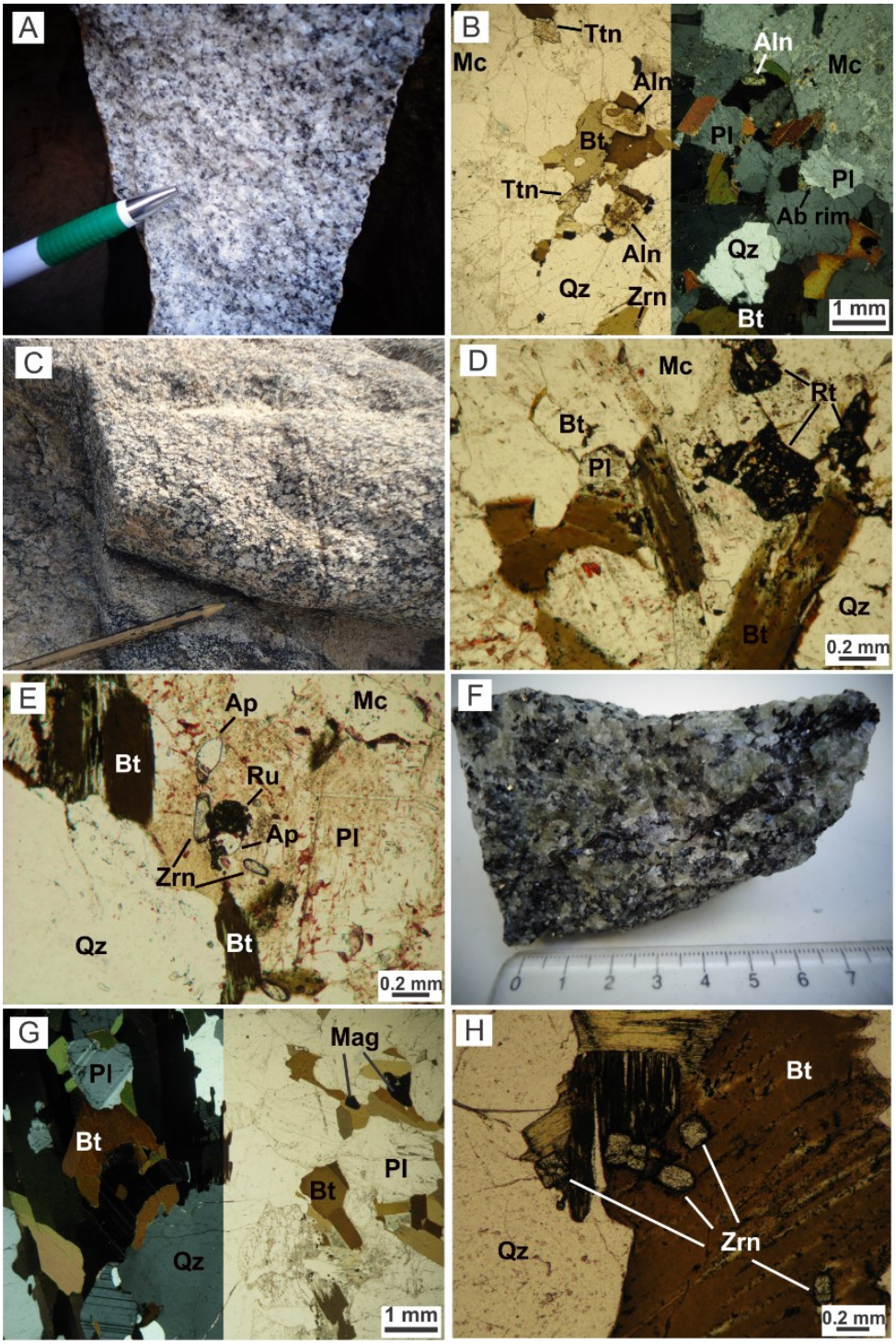

Figure 4.2: Photos and photomicrographs from the CA-02 (A, B), CA-04 (C, D, E), and CA-05 (F, G, H) samples. (A) Biotite granite sample. (B, G) Photomicrographs showing the main mineralogy. (C) CA-04 outcrop. (D, E, H) Rutile associated with biotite or as dark grains included in the biotite and (H) around zircons. (F) Biotite tonalite sample.

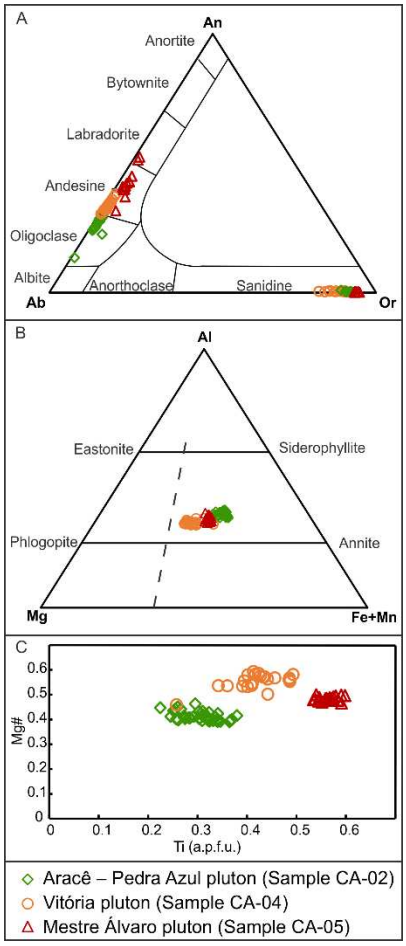

Figure 4.3: A) Ternary An-Ab-Or feldspar classification diagram; B) Ternary Al-Mg-Fe+Mn biotite classification diagram (Fedele et al., 2015); C) Mg# [Mg/(Fe+Mg)] vs. TiO2 (wt.%) for biotite.

4.3.1.2 Sample CA-04 (Vitória pluton)

A sample of biotite granite (Figure 4.2C) was collected in the east border of the pluton (Figure 4.1B). K-feldspar, essentially perthitic microcline, ranges from Or_{82} to Or_{92} (Figure 4.3A). Plagioclase has andesine composition (An_{30-38}; Figure 4.3A) and display slight normal zonation, with occasional antiperthitic and myrmekitic textures. Biotite shows annite-phlogopite composition and exhibits Mg# (Mg/Mg+Fe) ranging from 0.59 to 0.46, Ti from 0.34 to 0.49 a.p.f.u. (Figure 4.3B, 4.3C), ^{IV}Al from 2.4 to 2.7 a.p.f.u., and high contents of F (1.01 to 0.64 a.p.f.u.). Rutile occurs as dark inclusions in biotite or as granular aggregates frequently associated with biotite, feldspar, opaques, carbonate, zircon, and muscovite (Figure 4.2D, 4.2E). Apatite term is fluorapatite (F = 4.06 to 4.70%) with stubby prismatic and acicular habits. Zircon usually forms tiny inclusions in quartz, feldspars, and biotite.

4.3.1.3 Sample CA-05 (Mestre Álvaro pluton)

A sample of biotite tonalite (Figure 4.2F) was collected in the northeast border of the pluton (Figure 4.1B). Plagioclase varies from andesine (An_{32}) to labradorite (An_{52}) with predominance of andesine terms (An_{30-50}; Figure 4.3A), forming crystals with normal zonation and antiperthitic intergrowths. K-feldspar is essentially perthitic microcline with a mean composition of $Or_{94.}$ Biotite shows annite-phlogopite composition with mean Mg# (Mg/Mg+Fe) of 0.48 (2SD = 0.017), Ti from 0.56 to 0.60 a.p.f.u. (Figure 4.3B, 4.3C), ^{IV}Al from 2.3 to 2.5 a.p.f.u., and moderate contents of F (0.29 to 0.50 a.p.f.u.). Rutile appears as tiny granular aggregates included in biotite and plagioclase, being also associated with zircon, secondary muscovite, and chlorite. Sometimes, rutile appears as tiny dark grains around zircon and included in biotite (Figure 4.2H). Apatite term is also fluorapatite (F = 4.19 to 4.55%) with stubby prismatic and acicular forms. Zircon is commonly found as inclusions in quartz, feldspars, and biotite.

4.3.2 Country Rocks

4.3.2.1 Samples CA-06, CA-09, and CA-10 (Nova Venécia complex)

The sampled outcrops show stromatic metatexites whose paleosomes are laminated to banded paragneisses with variable contents of mafic and felsic minerals that may represent compositional changes of sedimentary protoliths (Figure 4.4A, 4.4E, 4.4G). Foliated, garnet-rich granites are parallel to the laminated to banded structure of the paragneiss, representing autochthonous leucosomes, which are correlated to granites of the Ataléia suite (Gradim et al., 2014). The paragneisses show a grano-lepidoblastic matrix composed of quartz, K-feldspar, plagioclase, cordierite and biotite, materializing the regional ductile foliation (Figure 4.4B, 4.4F, 4.4H). Garnet poikiloblasts, with subhedral habitus, containing rounded inclusions of quartz, and elongated biotite and sillimanite. Cordierite poikiloblasts (CA-06 and CA-09 samples) are subhedral to anhedral, presenting inclusions of biotite, opaque minerals, and abundant sillimanite oriented according to the regional foliation (Figure 4.4B, 4.4F). In CA-06 paragneiss sample, hercynite is commonly associated with opaque minerals (mostly magnetite and ilmenite) and cordierite (Figure 4.4B). K-feldspar is frequently perthitic while plagioclase is antiperthitic.

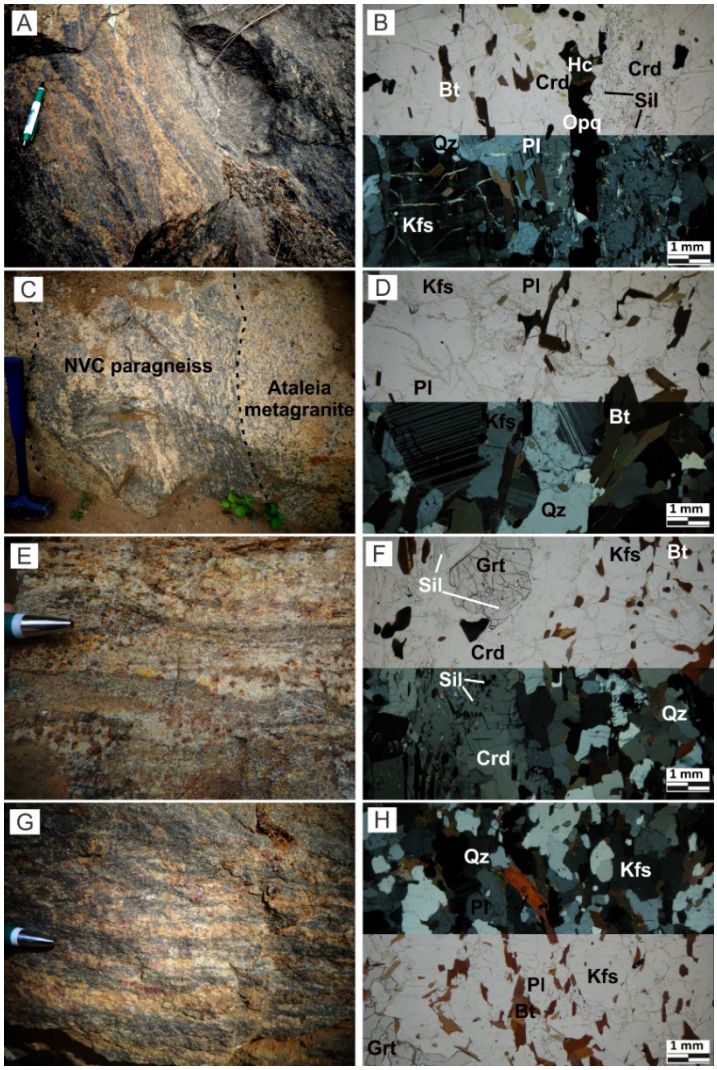

Figure 4.4: Field photographs and photomicrographs showing the main mineralogy of the country rocks samples. (A-B) CA-06 sample: Crd granulite from Nova Venécia complex; (C-D) CA-07 sample: Grt-Bt metagranite from Ataléia suite; (E-F) CA-09 sample: Sil-Grt-Crd-Bt paragneiss from Nova Venécia complex; (G-H) CA-10 sample: Grt-Bt paragneiss from Nova Venécia complex.

4.3.2.2 Sample CA-07 (Ataléia suite)

The outcrop shows a foliated garnet-biotite granite (Figure 4.4C, 4.4D) of the Ataléia suite in close spatial association with a migmatitic paragneiss of the Nova Venécia complex (Figure 4.4C). The regional foliation is defined by stretched quartz, K-feldspar, plagioclase, and biotite (Figure 4.4D). Garnet poikiloblasts have subhedral habitus and rounded quartz, biotite, and apatite inclusions.

4.4 ZIRCON STUDY

This article presents the first detailed study on morphological and textural features, and isotopic Lu-Hf data for a large number of zircon crystals recovered from samples collected in borders of post-collisional granites of the Araçuaí orogen, together with their U-Pb (LA-ICP-MS) ages (Figure 4.1B). To compare the results obtained for those intrusions with the predominant country rocks, we also present the first isotopic Lu-Hf data for zircon grains extracted from samples of migmatitic paragneisses (Nova Venécia complex) and foliated granite (Ataléia suite), along with their U-Pb (LA-ICP-MS) ages.

4.4.1 Morphology and internal texture

In order to compare the different populations and correlate them with petrogenetic indicators, we conducted a thorough study on the morphological and textural characteristics of a large number of zircon crystals and detrital grains on cathodoluminescence (CL), backscattered (BSE) and secondary electron (SE) images, after detailed examinations under optical microscope. The main characteristics are summarized in Table 4.2.

4.4.1.1 G5 samples (CA-02, Aracê – Pedra-Azul granite; CA-04, Vitória granite; CA-05, Mestre Álvaro tonalite)

Despite minor variations, the zircon crystals from selected G5 samples show similar morphologies and textures. The studied zircon populations are light brown and gray to colorless, translucent, displaying acicular and short to long-prismatic forms, with anhedral to euhedral terminations. Zircons from CA-05 sample commonly show rounded edges. Most zircon crystals have high elongation (length-to-width) ratios. External morphologies belong to subtypes S14-15, S18 to S20, S23 to S25, and P2 to P5 of Pupin's typological classification (Figures 4.5A, 4.5C, 4.5E, 4.6), with dominant well-developed {100} face. Inclusions are common in zircons from CA-02 and CA-04 granites and scarce in those from CA-05 tonalite (Figure 4.5B, 4.5D, 4.5F). CL images show non-zoned to magmatic oscillatory zoning, sometimes poorly developed, prevailing medium to low luminescence (Figure 4.5B, 4.5D). Several crystals are surrounded by structureless dissolution–recrystallization domains and overgrowth rims (e.g., Figure 4.5B, crystals 011, 046, 079; Figure 4.5D, crystals 114, 100, 059, 029; Figure 4.5F, crystals 041, 025, 102, 018-2) and/or show transgression of older zones by fronts of dissolution–recrystallization (e.g., Figure 4.5D, crystal 027; Figure 4.5F, crystals 030, 018-2, 041, 100). In some crystals of the CA-05 sample, oscillatory zoning is only disclosed by

bleached ghost-like relics (e.g., Figure 4.5F, zircons 011-2, 102, 007-2, 020-2). Oscillatory zoning is absent to weak in BSE images (Figure 4.5B, 4.5D, 4.5F).

Table 4.2: Summary of the main zircon characteristics for the studied samples.

Unit	Aracê pluton	Vitória pluton	Mestre Álvaro pluton	Nova Venécia complex	Ataléia suite	Nova Venécia complex	Nova Venécia complex
Sample	CA-02	CA-04	CA-05	CA-06	CA-07	CA-09	CA-10
Lithotype	Titanite-allanite-biotite granite	Biotite granite	Biotite tonalite	Cordierite granulite	Garnet-biotite metagranite	Sillimanite-garnet-cordierite-biotite paragneiss	Garnet-biotite paragneiss
Color	Light brown to colorless, translucent	Light brown to colorless, translucent	Light brown and gray to colorless, translucent	Brown to colorless, translucent	Light brown to colorless, translucent	Light brown to colorless, translucent	Light brown and gray to colorless, translucent
Form	Acicular to long-prisms with subhedral to euhedral terminations	Acicular and short to long-prisms with subhedral to euhedral terminations	Short to long-prisms with rounded edges and anhedral to euhedral terminations	Anhedral to euhedral and short to long prisms and bipyramids, often oval or stubby grains with rounded edges	Short to long-prisms with sub-rounded edges and subhedral to euhedral terminations.	Anhedral to euhedral and short prisms to bipyramids, often oval or stubby grains with rounded edges	Anhedral to euhedral and short prisms to bipyramids, often oval or stubby grains with rounded edges
Morphological type	S19-20, S24-25, P3 to P5	S14, S18 to S20, S23 to S25, P3 to P5	S14-15, S18 to S20, S23 to 25, P2 to P5	-	-	-	-
Size	130 to 600 µm	130 to 500 µm	100 to 550 µm	90 to 380 µm	80 to 400 µm	80 to 300 µm	80 to 280 µm
Length/width rations	4 to 11	2 to 11	2 to 8	1 to 6	1 to 6	2 to 4	2 to 6
Inclusions	Many. Apatite	Many. Apatite and monazite	Scarce. Apatite	Not observed	Not observed	Scarce. Quartz	Not observed
Internal Features in CL*	Unzoned to fine, sometimes weakly marked, magmatic oscillatory zoning. Medium to low luminescence (rarely high). Often surrounded by structureless and thin dark domains and present transgression of older zones	Unzoned to fined magmatic oscillatory zoning. Medium to low luminescence. Often surrounded by overgrowth, structureless domains and transgression of older zones	Zoned to little or no zoned and ghost-like relic. Medium to low luminescence. Often surrounded by overgrowth, structureless domains and transgression of older zones Commonly, the grain cores are dark and the edges are lighter	Zoned to no zoned. High to low luminescence. Often surrounded by overgrowth, structureless domains and transgression of older zones.	Zoned to no zoned. High to low luminescence. Often surrounded by overgrowth, structureless domains and transgression of older zones. Some grains present inherited cores	Zoned with high to low luminescence. Often surrounded by overgrowth, structureless domains and transgression of older zones. Some grains present inherited cores	Zoned with high to low luminescence. Often surrounded by overgrowth, structureless domains and transgression of older zones.
Internal Features in BSE*	Absence to weak magmatic oscillatory zoning	Absence to weak magmatic oscillatory zoning	Absence to weak magmatic oscillatory zoning	Absence to weak magmatic oscillatory zoning	Absence to weak magmatic oscillatory zoning	Absence to weak magmatic oscillatory zoning	Absence to weak magmatic oscillatory zoning
Th/U ratios	1.1 to 3.8	0.7 to 2.8 *0.6 to 2.2 (secondary domains)*	0.2 to 2.6 *0.2 to 1.3 (inherited grains)*	0.03 to 1.94 *0.01 to 1.55 (secondary domains)*	0.02 to 0.61 *0.01 to 0.74 (anatetic and metamorphic)*	0.01 to 1.87 *0.01 to 1.50 (secondary domains)*	0.02 to 2.27 *0.01 to 1.57 (secondary domains)*
U-Pb age (Ma)	522.9 ± 1.6**	505.0 ±1.3** *496.7 ± 3.0*****	526.6 ± 1.6** *598.2 ± 1.4***	585 ± 7 to 828 ± 11*** *478 ± 6 to 610 ± 7****	582.6 ± 3.2** *557.1 ± 1.4***	582 ± 7 to 2009 ± 25*** *486 ± 6 to 616 ± 7****	584 ± 7 to 2363 ± 26*** *498 ± 6 to 611 ± 7****
$^{176}Hf/^{177}Hf$ (t)	0.281882 to 0.281785	0.282248 to 0.282181 *0.282239 to 0.282186*	0.282290 to 0.282204 *0.282390 to 0.282234*	0.282173 to 0.281848 *0.282108 to 0.282025*	0.282314 to 0.282213 *0.282321 to 0.282241*	0.282314 to 0.281631 *0.282084 to 0.281958*	0.282374 to 0.281214 *0.282175 to 0.281976*
εHf(t)	-18.6 to -23.8	-7.4 to -10.1 *-8.3 to -10.3*	-5.7 to -8.8 *-0.7 to -6.2*	-7.1 to -15.0 *-11.0 to -15.5*	-3.2 to -7.7 *-4.0 to -8.1*	-2.9 to -22.9 *-11.7 to -17.0*	+4.1 to -39.2 *-16.6 to -10.5*
T_{DM} (Ga)	2.25 to 2.47	1.58 to 1.71 *1.61 to 1.71*	1.49 to 1.66 *1.27 to 1.57*	1.68 to 2.23 *1.83 to 1.98*	1.42 to 1.63 *1.42 to 1.64*	1.41 to 2.62 *1.87 to 2.13*	1.20 to 3.47 *1.73 to 2.10*

Figure 4.5: Representative features of zircon crystals from G5 samples. (A, C, and E) Secondary electron images showing subtypes of external morphology by Pupin's typological classification. (B, D, and F) Textures on cathodoluminescence (left) and backscattered electron (right) images. The U-Pb ages are reported as $^{206}Pb/^{238}U$ age in Ma, with errors at 2σ.

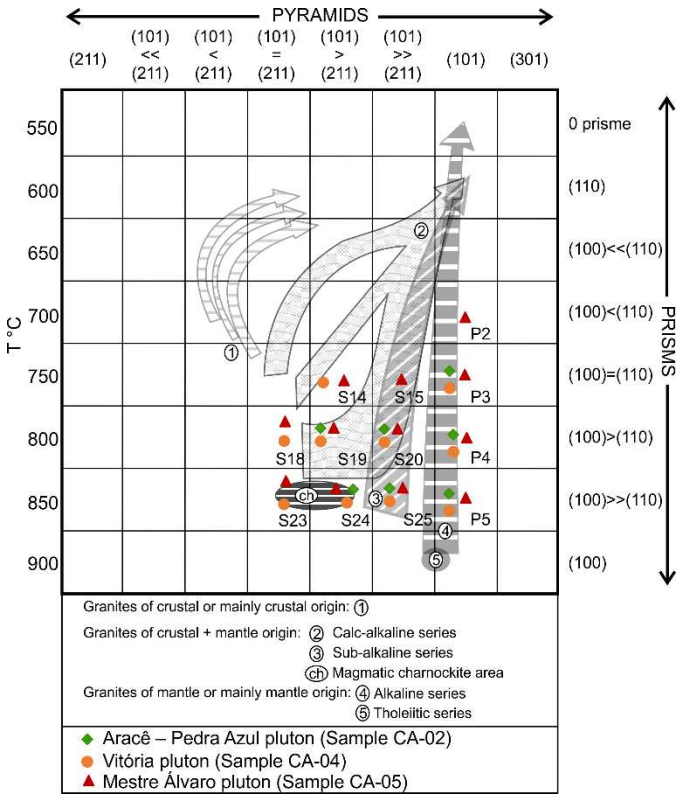

Figure 4.6: Morphological types of zircon grains found in the G5 samples and their petrogenetic classification based on Pupin (1980).

4.4.1.2 Country rocks (CA-06, CA-09, CA-10, Nova Venécia complex; CA-07, Ataléia suite)

In total, the zircon population from sampled country rocks is brown or gray to colorless, translucent, exhibiting anhedral to euhedral terminations, prevailing the short grains. Zircon grains from the Nova Venécia cordierite granulite and migmatitic paragneisses display variable morphologies with rounded edges, and oval, prismatic and bipyramidal shapes, while those from the Ataléia metagranite are largely prismatic with sub-rounded edges. Owing to the metamorphic nature of the samples, the typological classification of Pupin was not applied. CL images show a prevalence of medium to low luminescence domains, and cores with non-zoned to magmatic oscillatory zoning surrounded by structureless dissolution–recrystallization domains and overgrowth rims (e.g., Figure 4.7A, crystals 070, 146; Figure 4.7B, crystals 081, 091; Figure 4.7C, crystals 108, 053; Figure 4.7D, crystals 106, 030). Transgression of older zones by fronts of dissolution–recrystallization (e.g., Figure 4.7A, crystals 018, 031; Figure 4.7B, crystals 074, 072; Figure 4.7C, crystal 088; Figure 4.7D, crystal 063) and bleached ghost-like relics (e.g., Figure 4.7A, crystal 115; Figure 4.7B, crystal 176, Figure 4.7C; crystal 049; Figure 4.7D, crystal 033) are present in all samples. Oscillatory zoning is absent to weak in BSE images (Figure 4.7).

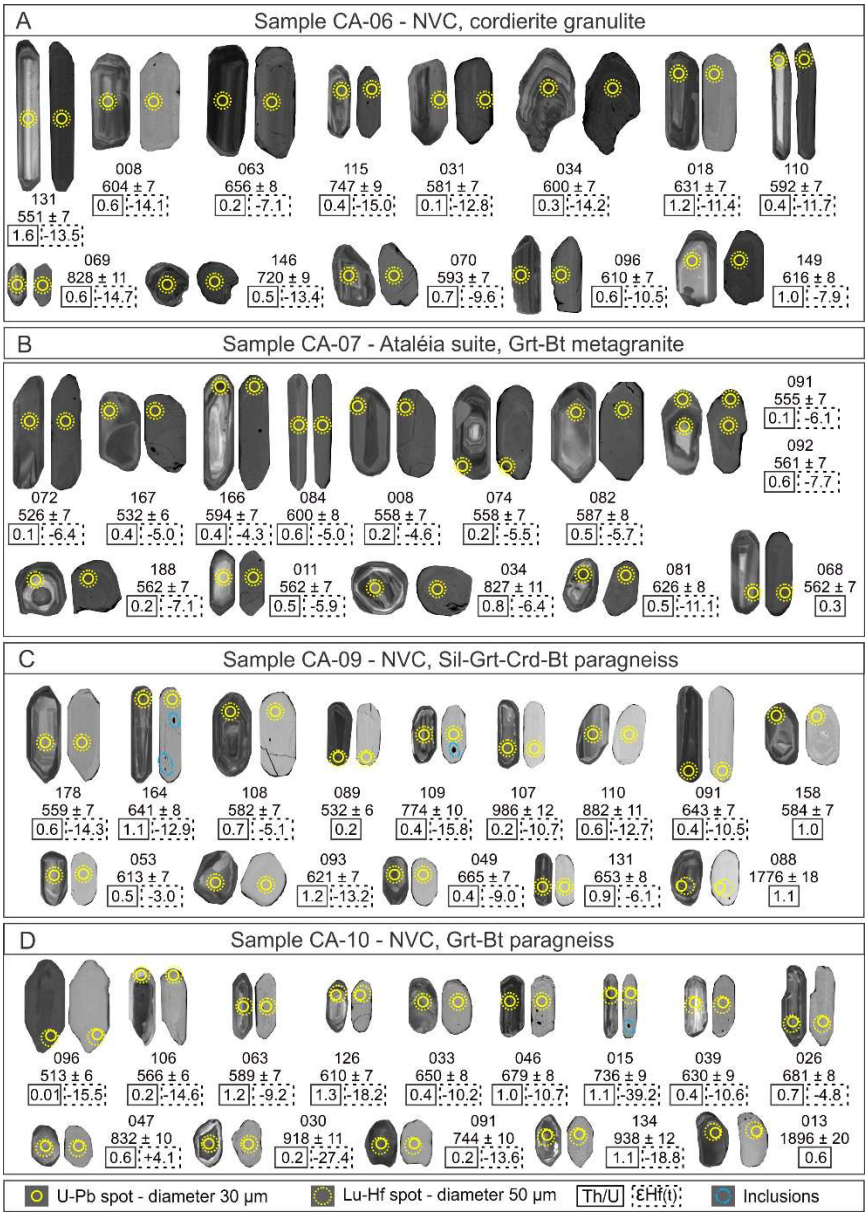

Figure 4.7: Representative features of zircon grains from country rocks on CL (left) and BSE (right) images. The U-Pb ages are reported as $^{206}Pb/^{238}U$ age in Ma, with errors at 2σ. NVC = Nova Venécia complex.

4.4.2 Zircon U-Th-Pb and Lu-Hf data

The analytical U-Th-Pb spots cover grain rims and cores. For calculations and plotting in Concordia diagrams, only data with discordance values less than 10%, low common Pb, and suitable relations of isotopic ratios were chosen. Representative grains with different U-Pb ages, morphologies, and internal textures were selected for Lu-Hf isotope analyses. If not otherwise indicated, we used the $^{206}Pb/^{238}U$ ages for all samples. LA-ICP-MS U-Pb ages (2σ error ellipses), U-Pb age histogram distribution, and probability density plots were achieved with

Isoplot/Ex 4.15 (Ludwig, 2012). The analytical results are presented in Supplementary file 4.E and summarized in Table 4.2, while plots are shown by Figures 4.8, 4.9 and 4.10.

4.4.2.1 Sample CA-02 (Aracê – Pedra Azul granite)

Thirty spot ages range from 513 ± 9 Ma to 530 ± 9 Ma, giving a Concordia age of 522.9 ± 1.6 Ma (MSWD = 0.86) virtually equal to the mean age of 522.9 ± 1.6 Ma (MSWD = 0.97), providing the best magmatic crystallization age (Figure 4.8A) for the northwestern border of the Aracê – Pedra Azul pluton (Figure 4.1B). The four grains with ages from 564 ± 9 Ma to 601 ± 9 Ma suggest inheritance from country rocks (cf. Gradim et al., 2014; Richter et al., 2016; Pedrosa-Soares et al., 2011; and this work). Overall, the Th/U ratios range from 1.1 to 3.8 (Figure 4.9A, 4.9B), tending to be greater in younger grains (Figure 4.9C, 4.9D).

Nineteen Lu-Hf isotopic analyses on zircon crystals ranging in age from ca. 513 Ma to ca. 530 Ma yielded initial $^{176}Hf/^{177}Hf$ ratios from 0.281852 to 0.281785, $\varepsilon Hf_{(t)}$ values between -21.3 and -23.8, and Hf T_{DM} model ages from ca. 2.34 Ga to ca. 2.47 Ga (Figures 4.8E, 4.9E, 4.9F). Seven analyses on the older grains (ca. 533 Ma to ca. 601 Ma) yielded initial $^{176}Hf/^{177}Hf$ ratios ranging from 0.281882 to 0.281783, $\varepsilon Hf_{(t)}$ values between -18.6 and -23.6, and Hf T_{DM} model ages from 2.25 Ga to 2.47 Ga (Figures 4.8E, 4.9E, 4.9F).

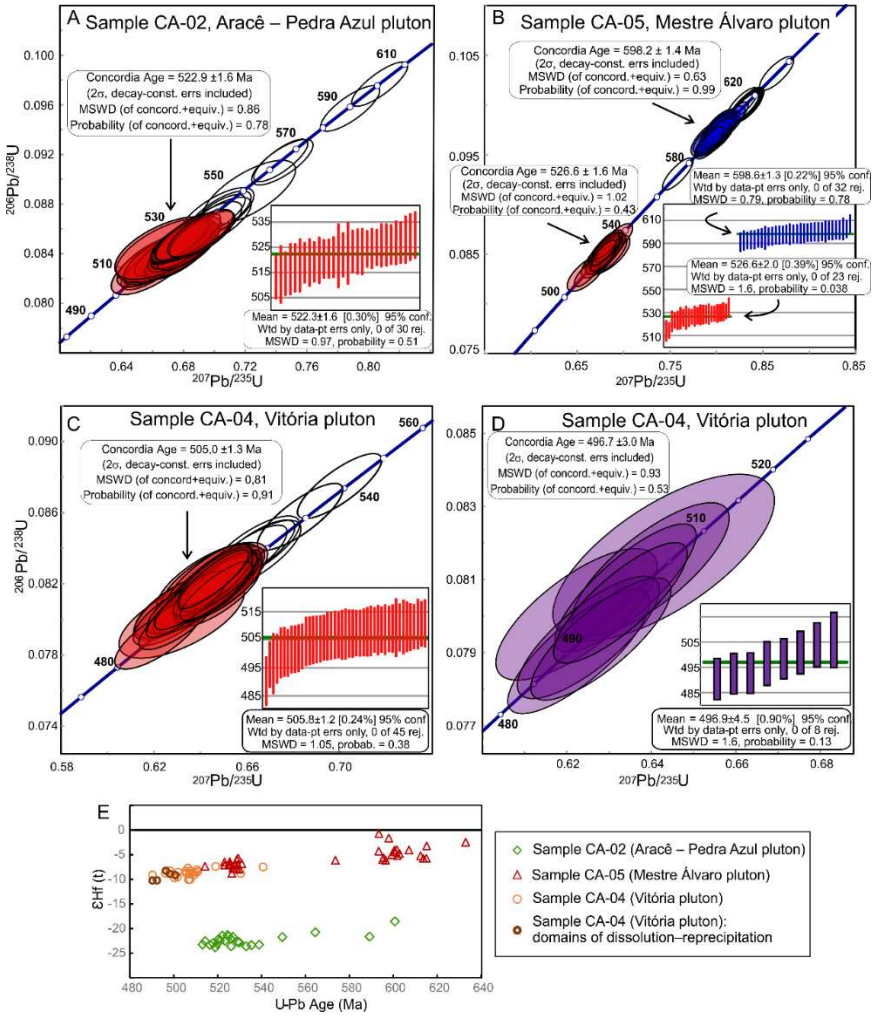

Figure 4.8: Concordia diagrams, weighted mean ages, and Lu-Hf data for samples of G5 plutons.

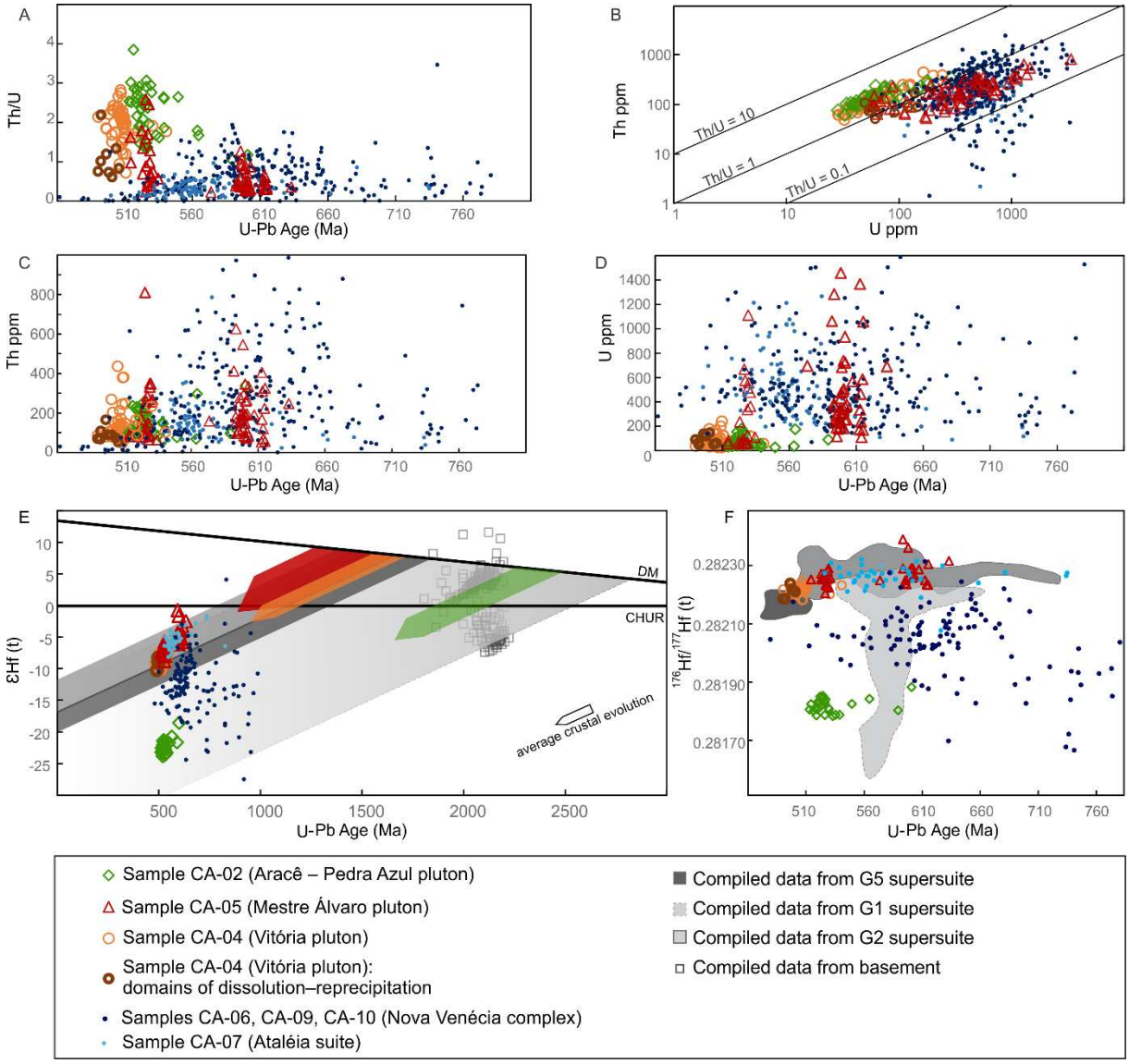

Figure 4.9: Diagrams comparing the U-Th-Pb and Lu-Hf data from studied samples with the compiled dataset. DM = depleted mantle, CHUR = chondrite uniform reservoir. Sources of data compilation: Degler et al. (2018), Gonçalves et al. (2016), Tedeschi et al. (2016), Melo et al. (2017), and Aranda (2018).

4.4.2.2 Sample CA-04 (Vitória pluton)

Fifty-one analytical spots on igneous crystals yield U-Pb ages from 490 ± 9 Ma to 541 ± 9 Ma, and Th/U ratios from 0.7 to 2.8 (Figures 4.8C, 4.9A, 4.9B). For better analytical consistency, forty-five spot data were selected to plot, resulting in a robust Concordia age of 505.0 ± 1.3 Ma (MSWD = 0.81) and the corresponding mean age of 505.8 ± 1.2 Ma (MSWD = 1.05), providing the best magmatic crystallization age (505 ± 1 Ma; Figure 4.8C) for the eastern border of the Vitória pluton (Figure 4.1B). Eight spots analyses on structureless rims furnished a Concordia age of 496.7 ± 3.0 Ma (MSWD = 0.93) and a mean age of 496.9 ± 4.5 Ma (MSWD = 1.6), with Th/U ratios ranging from 0.6 to 2.2 (Figures 4.8D, 4.9A, 4.9B).

Twenty-two analyses on zircon crystals with ages from ca. 490 Ma to 541 Ma show initial $^{176}Hf/^{177}Hf$ ratios ranging from 0.282248 to 0.282181, $\varepsilon Hf_{(t)}$ between -7.4 and -10.1, and Hf T_{DM} model ages from ca. 1.58 Ga to ca. 1.71 Ga (Figures 4.8E, 4.9E, 4.9F). Five Hf isotopic analyses on structureless rims with ages from ca. 490 Ma to ca. 501 Ma yielded initial $^{176}Hf/^{177}Hf$ ratios ranging from 0.282239 to 0.282186, $\varepsilon Hf_{(t)}$ values between -8.3 and -10.3, and Hf T_{DM} model ages from ca. 1.61 Ga to ca. 1.71 Ga (Figures 4.8E, 4.9E, 4.9F).

4.4.2.3 Sample CA-05 (Mestre Álvaro pluton)

Sixty-six analytical spots yield zircon U-Pb ages from 514 ± 9 to 633 ± 8 Ma, and Th/U ratios between 0.2 and 2.6 (Figures 4.8B, 4.9A, 4.9B), showing two age clusters, one related to the igneous crystallization and the other to inheritance from country rocks. Twenty-three younger spots yield a Concordia age of 526.6 ± 1.6 Ma (MSWD = 1.02), a mean age of 526.6 ± 2.0 Ma (MSWD = 1.6), and Th/U ratios from 0.24 to 2.6, providing the best magmatic crystallization age (527 ± 2 Ma) for the northern border of the Mestre Álvaro pluton. The thirty-two older spots provided a Concordia age of 598.2 ± 1.4 Ma (MSWD = 0.63), mean age of 598.6 ± 1.3 Ma (MSWD = 0.79), and Th/U ratios from 0.23 to 1.3, suggesting an age for the dominant primary source of the inherited zircon grains.

Seventeen isotopic Lu-Hf analyses were conducted on the younger zircon crystals (ca. 514 Ma to ca. 531 Ma), showing initial $^{176}Hf/^{177}Hf$ ratios from 0.282290 to 0.282204, $\varepsilon Hf_{(t)}$ between -5.7 and -8.8, and Hf T_{DM} model ages from ca. 1.49 Ga to ca. 1.66 Ga (Figures 4.8E, 4.9E, 4.9F). For the older zircon grains (ca.574 Ma to ca. 633 Ma), nineteen analyses yielded initial $^{176}Hf/^{177}Hf$ ratios from 0.282390 to 0.282234, $\varepsilon Hf_{(t)}$ between -0.7 and -6.2, and Hf T_{DM} model ages from 1.27 Ga to 1.57 Ga (Figures 4.8E, 4.9E, 4.9F).

4.4.2.4 Samples CA-06, CA-09, CA-10 (Nova Venécia migmatitic paragneisses)

Two hundred and forty analytical spots on detrital zircon grains show ages from 582 ± 7 to 2363 ± 26 Ma, and Th/U ratios from 0.01 to 2.27 (Figures 4.9, 4.10; Table 4.2). After using the Unmix age calculation routine provided by Isoplot/Ex 4.15 (Ludwig, 2012), four populations of detrital zircon grains were determined (Figure 10D) with age peaks at 617 ± 4 Ma (68%), 719 ± 22 Ma (14%), 839 ± 46 Ma (8%), and 922 ± 31 Ma (10%). One hundred and twelve spots on dissolution–recrystallization and overgrowth domains result in ages from 478 ± 6 to 616 ± 7 Ma, and Th/U ratios from 0.01 to 1.57 (Figures 4.9, 4.10; Table 4.2). Results from the Unmix age calculation routine (Ludwig, 2012) yield three main populations for the

younger zircon ages (Figure 4.10D) with peaks at 490 ± 21 Ma (5%), 527 ± 12 Ma (27%), and 565 ± 6 Ma (68%).

One hundred and thirteen Lu-Hf analyses on detrital zircon grains yielded variable isotopic signatures with initial $^{176}Hf/^{177}Hf$ ratios ranging from 0.282374 to 0.281214, $\varepsilon Hf_{(t)}$ values between +4.1 and -39.4, and Hf T_{DM} model ages from ca. 1.20 Ga to ca. 3.47 Ga (Figures 4.9E, 4.9F, 4.10F; Table 4.2). Nineteen analyses on dissolution–recrystallization and overgrowth domains yielded initial $^{176}Hf/^{177}Hf$ ratios ranging from 0.282175 to 0.281958, $\varepsilon Hf_{(t)}$ values between -11.0 and -17.0, and Hf T_{DM} model ages from 1.73 Ga to 2.13 Ga (Figures 4.9E, 4.9F, 4.10F; Table 4.2).

4.4.2.5 Sample CA-07 (Ataléia metagranite)

Thirty-four analytical spots on igneous crystals show ages from 561 ± 7 Ma to 609 ± 8 Ma, and Th/U ratios from 0.02 to 0.61 (Figures 4.9, 4.10; Table 4.2). For better analytical results, twenty-two spots analyses were selected resulting in a Concordia age of 582.6 ± 3.2 Ma (MSWD = 1.1), providing the best value for the igneous crystallization age (Figure 4.10E). Fifty spots in dissolution–recrystallization and overgrowth domains show ages from 496 ± 6 to 563 ± 8 Ma, with Th/U ratios ranging from 0.01 to 0.74 (Figures 4.9, 4.10E; Table 4.2). Among them, the oldest population (n = 26) provides a Concordia age of 557.1 ± 1.4 Ma (MSWD = 0.65), representing the peak age for the regional metamorphism related to the collisional stage. Ten analyses yield ages from ca. 620 Ma to 1184 Ma, indicating inherited zircon grains.

Twenty-eight analyses on igneous zircon crystals show initial $^{176}Hf/^{177}Hf$ ratios ranging from 0.282314 to 0.282213, $\varepsilon Hf_{(t)}$ between -3.2 and -7.7, and Hf T_{DM} model ages from ca. 1.42 Ga to ca. 1.63 Ga (Figures 4.9E, 4.9F, 4.10F). Twelve Hf isotopic analyses on structureless rim domains yielded initial $^{176}Hf/^{177}Hf$ ratios ranging from 0.282321 to 0.282241, $\varepsilon Hf_{(t)}$ values between -8.1 and -4.0, and Hf T_{DM} model ages from ca. 1.42 Ga to ca. 1.64 Ga (Figures 4.9E, 4.9F, 4.10F).

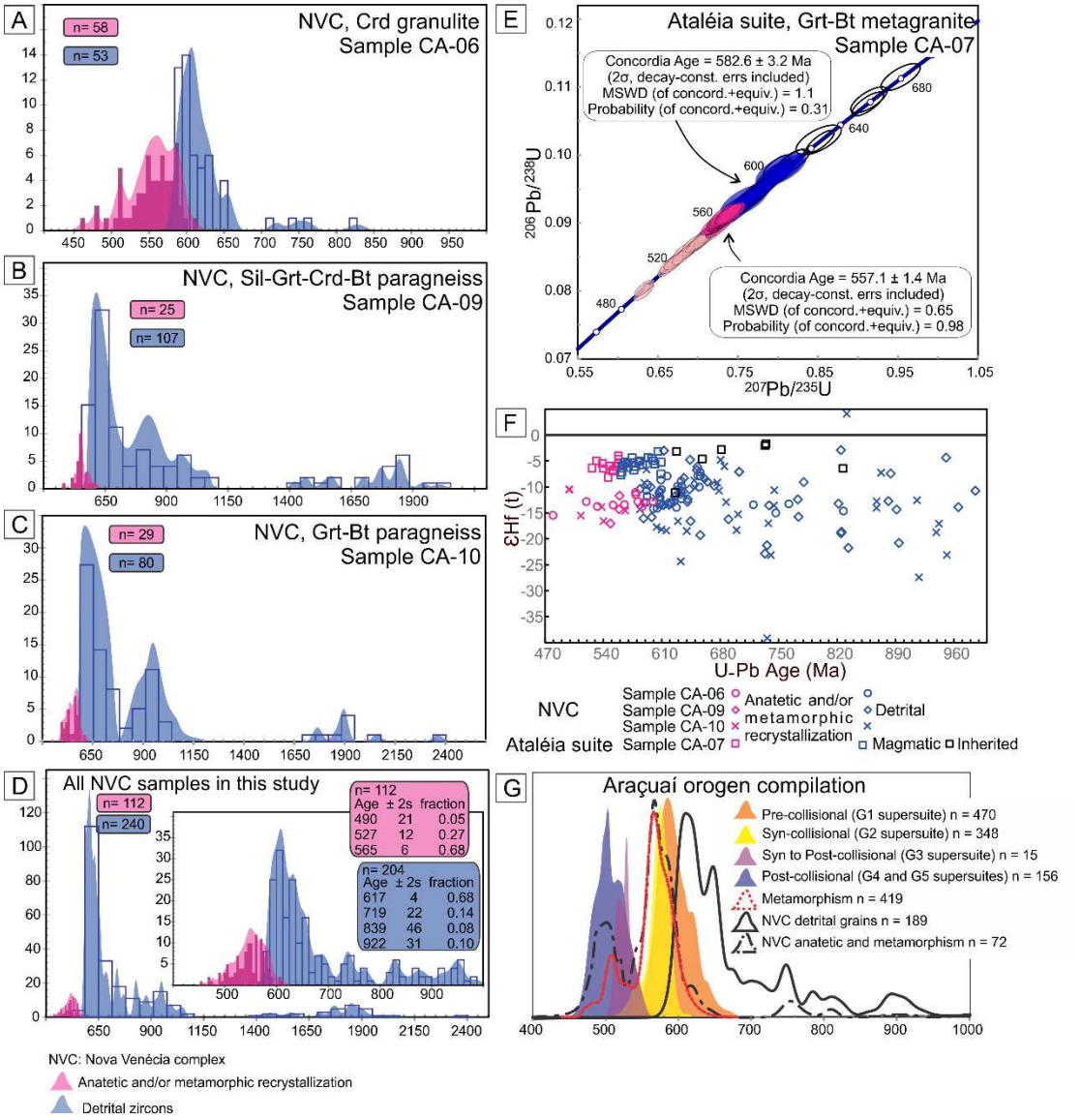

Figure 4.10: Zircon isotopic data from country rocks. (A to D) U-Pb age histogram, distribution and probability density plots for samples of the Nova Venécia complex. (E) Concordia diagram for the Ataléia metagranite. (F) Lu-Hf data for Nova Venécia complex and Ataléia metagranite samples. (G) Compilation diagram showing zircon U-Pb ages for the orogenic supersuites G1 to G5 and the Nova Venécia complex, and data for metamorphism in the Araçuaí orogen (references in Supplementary file 4.A).

4.5 LITHOCHEMISTRY

Aiming to provide further support to the zircon petrogenetic interpretations, chemical analysis on whole-rock samples were carried out and their results discussed in the context of a thorough compilation of the literature. The analytical results for lithochemical studies are shown in Supplementary file 4.D, and lithochemical diagrams are in Supplementary file 4.B.

The Aracê – Pedra Azul and Vitória granites (samples CA-02 and CA-04) show similar lithochemical patterns, both presenting ferroan, alkali-calcic, metaluminous to slightly peraluminous (A/CNK < 1.1) and high-K signatures (Figure 4.B1). In contrast, the Mestre

Álvaro tonalite (sample CA-05) displays a medium-K, magnesian, calcic, and slightly peraluminous (A/CNK 1.05) signature. In agreement with most G5 granites (Supplementary file 4.D), the studied samples are enriched in LREE with respect to HREE, and samples CA-02 and CA-04 show Eu negative anomalies (Figure 4.B1). The spider diagram (normalized to primitive mantle; cf. McDonough and Sun, 1995), shows enrichment in LILE compared to HFSE, and negative anomalies for Sr, P, and Ba. Sample CA-05 shows negative anomaly of Ta, while CA-02 and CA-04 samples display Ti and Nb anomalies (Figure 4.B1). A positive anomaly of Zr is remarkable in the Mestre Álvaro sample (CA-05). Th positive anomaly appears in all samples, being greater in the Vitória granite (CA-04).

The samples plot in the fields of post-collision to within-plate granites (cf. Pearce et al. 1984, 1996) and in the A-type granites field (cf. Whalen et al. 1987) (Figure 4.B2). Only the samples that plot in the within-plate granite field of Pearce et al. (1984) diagram and are A-type rocks in Whalen et al. (1987) diagram were tested in the A1-A2 types diagram of Eby (1992). Accordingly, around two thirds of the G5 granites plot in the A1-type field (Figure 4.B2), related to magma sources similar to those of oceanic-island basalts (cf. Eby 1992). However, the studied sample from the Aracê – Pedra Azul pluton belongs to the A2-type (Figure 4.B2), suggesting magma sources in continental crust or under-plated crust that had been involved in subduction and continent-continent collision settings (cf. Eby 1992).

The lithochemical data are in good agreement with the large dataset compiled from the literature on the G5 magmatism (Supplementary file 4.D, Figures 4.B1, 4.B2), demonstrating the greatest predominance of high-K, alkali-calcic, ferroan, A-type to I-type, within-plate, post-collisional granites.

4.5.1 Zircon saturation geothermometry

The Zr saturation temperature (T_{Zr}) was calculated for the studied plutons using the presented lithochemical data (see Supplementary file 4.B for details). This method (T_{Zr}), based on bulk-rock chemical data, is a simple and helpful instrument to estimate crystallization temperatures of magmatic rocks (Boehnke et al., 2013; Watson and Harrison, 1983).

Accordingly, T_{Zr} values calculated for the studied samples are 834 °C for the sample CA-05 (Mestre Álvaro tonalite), 860 °C for the sample CA-02 (Aracê – Pedra Azul granite), and 923 °C for the sample CA-04 (Vitória granite), bracketing a temperature range in very good agreement with published data from G5 plutons (De Campos et al., 2016; Mello et al., 2011; Mendes et al., 1999; Mendes and De Campos, 2012; Serrano et al., 2018; Wiedemann et al., 2002).

4.6 DISCUSSION

Here, we discuss the new data in the light of the local and regional geology, as well as in comparison with the compiled data presented in Supplementary data files. Our main focus is the emplacement and petrogenetic processes recorded by borders of post-collisional granitic intrusions.

4.6.1 Zircon morphology and internal textures as petrogenetic indicators for G5 samples

The morphological zircon types shown by the studied samples are characterized by the predominance of {100} and {101} faces over {110} and {211} faces (Figure 4.6). According to Pupin (1980), these morphologies may imply hybrid sources involving crustal and mantelic components, being more typical of zircon from charnockitic rocks, and calc-alkaline to sub-alkaline and alkaline granite series, with crystallization temperatures above 700°C and zircon crystals rich in inclusions. Accordingly, our samples show geochemical, T_{Zr} data (834 – 923 °C) and predominance of zircon crystals rich in inclusions, in agreement with the prevision by the Pupin's scheme (Figure 4.5, Table 4.2, Figure 4.B1).

Vavra (1994) described important compositional factors that control the morphologies of zircon crystals from different granites. High and constant growth rates of {100} face relatively to pyramidal forms and symmetric growth of {101} characterize zircon crystals from alkaline granites. Fluctuating or gradually decreasing relative growth rates of {100} face, the asymmetric and highly variable growth of {101}, and a tendency of {110} to become growth-inhibited are features of zircon crystals from calc-alkaline and anatectic granites. Selective adsorption of foreign elements on different faces may also control the development of zircon faces, such as restraining the growth of {211} and {110} faces (Vavra, 1990, 1994). These compositional controls are also indicated by our data, as quoted in previous sections.

Benisek and Finger (1993) found that low U(Th), Y(REE) and P contents relative to Zr in granite melts catalyze the development of {100} zircon face and inhibit the development of {110} face. Indeed, our samples have low U (except for CA-02 granite), Y, HREE, and P contents relatively to Zr content (Figure 4.B1), in agreement with observed zircon morphologies.

After statistical study on a comprehensive dataset, Kirkland et al. (2015) concluded that Th/U ratios in igneous zircon crystals are frequently less than 1. However, the analyzed zircons of the granites CA-02 (Aracê – Pedra Azul pluton) and CA-04 (Vitória pluton) show Th/U

ratios ranging from 1.1 to 3.8, with most values greater than 2, and only one value (0.72) lower than 1, thus predominantly presenting higher ratios in relation to most granites (cf. Kirkland et al., 2015); whilst the zircons of the tonalite CA-05 (Mestre Álvaro pluton) show Th/U ratios ranging from 0.2 to 2.6 with most values lower than 1, within the regular range for granites (Supplementary File 4.E). Generally, Th is more abundant than U in igneous rocks with a mean Th/U ratio of 3-4 (Ahrens, 1965; Kirkland et al., 2015). The Th/U ratios in zircon crystals are commonly less than 1 (Kirkland et al., 2015; Rubatto and Hermann, 2007; Wang et al., 2011) because U and Th contents in zircon are regulated by their melt availability and partition coefficients (D_U and D_{Th}; Harley et al., 2007; Tang et al., 2014; Wang et al., 2011). As ionic radii of U^{+4} is closer to that of Zr^{4+}, the uranium cation is more preferentially accepted in the zircon crystal lattice than Th^{+4} (Hoskin and Schaltegger, 2003; Shannon, 1976; Kirkland et al., 2015). However, Th becomes more compatible in zircon structure with increasing temperature owing to the expansion of crystal lattice that favors the substitution of Zr^{+4} by cations with larger ionic radii (Tang et al., 2014; Wang et al., 2011). According to Wang et al. (2002), conditions of rapid growth at undercooling may also facilitate the entry of significant amounts of Th into zircon lattice. These effects (i.e., high Th contents, high temperature, rapid growth, and undercooling) may explain the high Th/U ratios in the analyzed zircon crystals, especially in the CA-04 and CA-02 samples (Figure 4.9A to 4.9D; Table 4.2). This is consistent with the high temperatures provided by T_{Zr} data and with the Th positive anomaly observed in the studied samples. In addition, the high elongation (length-to-width) ratios observed in most zircon crystals (Table 4.2) may be further indication of rapid growth crystallization (Corfu et al., 2003).

The normal plagioclase zoning in all samples, the sodic rims in plagioclase crystals from the Aracê – Pedra Azul (CA-02) sample, and the relationship between biotite and rutile in the Vitória (CA-04) and Mestre Álvaro (CA-05) samples also provide evidence of cooling rates. Granular agglomerates of rutile included in biotite indicate Ti re-balancing within that mica during cooling. The absence of rutile in the Aracê – Pedra Azul granite may be related to a higher Ca activity in the melt, inducing the formation of allanite and titanite at the expenses of monazite and rutile (Angiboust and Harlov, 2017; Gieré and Sorensen, 2004). The acicular and mixed apatite morphologies found in all samples and the reverse plagioclase zonation in the Aracê – Pedra Azul granite are features related to magma mingling-mixing processes (Baxter and Feely, 2002; Hibbard, 1995, Molina et al., 2012). The presence of acicular apatite in all

samples and the development of calcic spike in plagioclase from the Aracê – Pedra Azul granite provide evidence of fast cooling (Baxter and Feely, 2002; Hibbard, 1995, Molina et al., 2012).

Processes that reflect high cooling rates and may explain rapid growth crystallization are mixing of magmas, rapid ascent of magma and release of volatile fluids (Belousova et al. 2006; Gill, 2010; Molina et al., 2012; Wang et al., 2002). Indeed, these are expected processes during a post-collisional stage because the crust is under extension and decompression related to gravitational collapse after ceasing the convergent stresses. Several authors have reported the bimodal (felsic-mafic) nature of G5 plutons with copious mingling-mixing features involving crustal and mantelic magmas, and geochemical and isotopic signatures associated with hybrid magma sources at high temperatures (> 700° to ca. 1000°C) (De Campos et al., 2016; Mello et al., 2011; Mendes et al., 1999; Mendes and De Campos, 2012; Pedrosa-Soares et al., 2011; Serrano et al., 2018; Wiedemann et al., 2002). In addition, the fast ascent to high crustal levels would have emplaced the plutons in contact with significantly colder host rocks, causing rapid crystallization of the magma at high temperatures along their borders. In fact, our samples, collected at borders of intrusions, show finer granulation than those frequently observed in G5 granitic plutons (cf. De Campos et al., 2016; Serrano et al., 2018). Moreover, decompression by pluton ascent reduces the solubility of dissolved volatile fluids in the magma, contributing to rapid crystallization (Gill, 2010). Indeed, high F contents in biotite and apatite in all samples suggest aqueous fluid release during magma evolution (Moreno et al., 2014; Wang et al. 2018).

Structureless rims are common in zircons of the studied samples of post-collisional intrusions, being more expressive in the Mestre Álvaro sample (CA-05; Figure 4.5). They show complex secondary textures characterized by transgression fronts over older zones, inward-penetrating, irregularly curved domains cutting across primary growth zones, overgrowth rims, and ghost bleached oscillatory zones still visible but blurred. These textures indicate the disequilibrium reactions of zircon crystals within the magma and may result from *in situ* zircon replacement by a combined dissolution–reprecipitation and overgrowth processes in response to interactions with residual (late-stage) silicatic melts and/or deuteric fluids (Geisler et al., 2007; Harley et al., 2007). Zirconium may have been released by the breakdown of minerals, such as biotite and rutile, during reactions associated with the late crystallization of magma, promoting growth of new zircon rims (Harley et al., 2007; Vavra et al., 1996). This may explain secondary textures of zircon crystals that are closely associated with rutile (Figure 4.2E, 4.2H) and show a slight increase in Fe from the core to rim.

4.6.2 Implications of U-Th-Pb and Lu-Hf data

The U-Pb (LA-ICP-MS) zircon ages from the Aracê – Pedra Azul (ca. 523 Ma), Vitória (ca. 505 Ma) and Mestre Álvaro (ca. 527 Ma) samples are in conformity with previously published ages for many G5 intrusions (Supplementary file 4.A, figure 4.1B). Together with those collected from literature, the presented ages suggest two main episodes during the G5 post-collisional magmatism in the Araçuaí orogen: ca. 530 - 515 Ma, and ca. 505 - 490 Ma.

Zircon crystals from G5 intrusions tend to present increasing Th/U ratios with age decrease (Figure 4.9A). Besides our samples, other G5 plutons also have high Th/U ratios (e.g., the São Gabriel da Baunilha norite, 524 ± 7 Ma, Th/U from 1.6 to 2.2, Belém, 2014; and the quartz monzonite and monzogabbro of Afonso Cláudio pluton, 481 ± 3 Ma and 497 ± 4 Ma, Th/U from 0.7 to 6.0, Aranda, 2018). The elevated Th/U ratios suggest a high thermal gradient to generate the magmas crystallized as G5 plutons, facilitating thorium entry into zircon structure (as mentioned above). The related heat source may be associated with asthenosphere up-flow after mantle delamination and slab breakoff during the gravitational collapse of the orogen (Figure 4.11A, 4.11B), and mantle plume upwelling at the late post-collisional stage (Figure 4.11C), similarly to models presented by De Campos et al. (2016), Gradim et al. (2014), and Serrano et al. (2018).

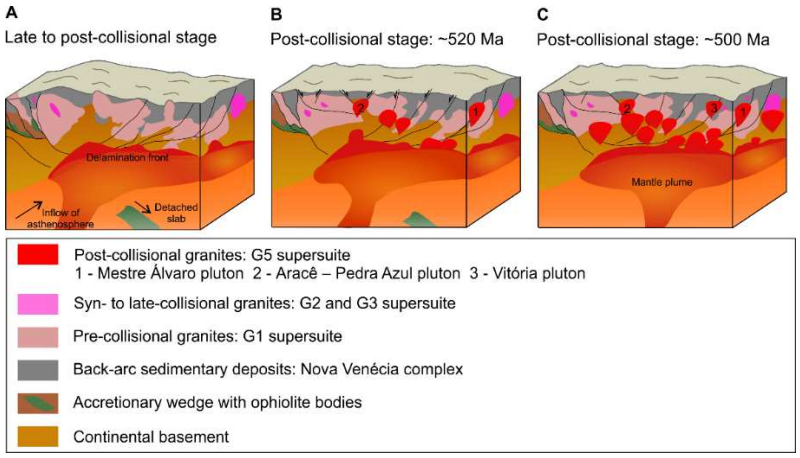

Figure 4.11: Schematic model for the evolution of the studied region (not to scale).

The Lu-Hf data from zircon crystals of the studied post-collisional intrusions implies a significant contribution of continental crust to the genesis of the plutons, as previously suggested by isotopic data from the literature (see Figure 4.1 and Supplementary file 4.A). Additionally, the Hf in-zircon signatures for the Mestre Álvaro tonalite ($\varepsilon Hf_{(t)}$: -0.7 to -8.8, Hf T_{DM} model ages: 1.27 Ga to 1.66 Ga) and Vitória granite ($\varepsilon Hf_{(t)}$: -7.4 to -10.3, Hf T_{DM} model

ages: 1.58 Ga to 1.71 Ga) show reliable correlations with those from the Nova Venécia paragneisses ($\varepsilon Hf_{(t)}$: +4.1 to -39.0, Hf T_{DM} model ages: 1.20 Ga to 3.47 Ga) and Ataléia metagranite ($\varepsilon Hf_{(t)}$: -3.2 to -8.1, Hf T_{DM} model ages: 1.42 Ga to 1.64 Ga), indicating a major role of the dominant country rocks in G5 magma genesis and/or contamination of pluton borders during intrusion ascent and emplacement (Figure 4.9E, 4.9F; Table 4.2). This is also consistent with the location of the sampled outcrops at pluton borders, favoring crustal contamination by country rocks like those studied here, the Nova Venécia complex and Ataléia suite. Accordingly, the available isotopic Nd and Sr data for mafic ($\varepsilon Nd_{(t)}$: -5.3 to -13.4, Nd T_{DM} model ages: 1.33 Ga to 1.75 Ga; Sr^{87}/Sr^{86}: 0.70655 – 0.70730) and granitic ($\varepsilon Nd_{(t)}$: -6.6 to -13.4, Nd T_{DM} model ages: 1.4 Ga to 1.78 Ga; Sr^{87}/Sr^{86}: 0.70197 – 0.72069) rocks from G5 plutons (see data and quoted references in Figure 4.1) also point to a large involvement of crustal melts in G5 magma genesis, although there is solid field and petrologic evidence of mingling-mixing processes, involving basaltic and granitic magmas, within several G5 plutons (De Campos et al., 2016, 2004; Mendes et al., 1999; Mendes and De Campos, 2012; Serrano et al., 2018; Wiedemann et al., 2002). However, the Hf in-zircon signatures for the Aracê – Pedra Azul granite ($\varepsilon Hf_{(t)}$: -18.6 to -23.8, Hf T_{DM} model ages: 2.25 Ga to 2.47 Ga) differ from the other studied post-collisional plutons, implying in contributions from older sources with Siderian to Early Rhyacian ages. As basement rocks with such older magmatic or inheritance ages are unknown in the focused area, the Hf signatures of the Aracê – Pedra Azul granite imply in inheritance from rocks hidden in depth, possibly related to basement complexes with evolved crustal signatures that crop out in the Ribeira belt, further to the south of the Araçuaí orogen (Degler et al., 2018).

It was only possible to perform isotopic analyses on structureless rims of zircons from the Vitória (CA-04) granite. The resulting age (497 ± 3 Ma) is slightly younger than that (505 ± 1.3 Ma) obtained from igneous zircons of the same sample. Overall, the structureless rims have preserved the Hf isotopic signature of the igneous zircons, although their $\varepsilon Hf_{(t)}$ values are more negative than those from the corresponding grain cores, indicating overgrowth process (Figure 4.5, crystals 100 and 107). Accordingly, these structureless domains may be associated with late-stage melts crystallized in the latest stage of pluton evolution.

The presented age spectra of detrital zircon grains for samples of the Nova Venécia complex matches well with previously published data (Figure 4.10D, 4.10G). Those age data together with Hf signatures (Figures 4.9E, 4.9F, 4.10D, 4.10G) corroborate prior interpretations

suggesting that this basin received significant sediment from the Rio Doce magmatic arc (Gradim et al., 2014; Richter et al., 2016). The youngest zircon populations with age peaks at 490 ± 21 Ma, 527 ± 12 Ma, and 565 ± 6 Ma (Figure 4.10D) represent dissolution–reprecipitation and overgrowth domains at zircon rims, formed during the regional metamorphism (565 ± 6 Ma) imprinted on the Nova Venécia complex during the collisional stage (Figure 4.10G) and thermal episodes (527 ± 12 Ma and 490 ± 21 Ma) related to the post-collisional plutonism (530 – 480 Ma). The two youngest ages (527 ± 12 Ma and 490 ± 21 Ma) are also in agreement with the two main episodes of post-collisional magmatism (ca. 530 – 515 Ma, and ca. 505 – 490 Ma).

The igneous crystallization age of the Ataléia metagranite (583 ± 3 Ma; Figure 4.10G) agrees with the transition from the pre-collisional to collisional stages, related to the final development of the Rio Doce magmatic arc and the onset of partial melting on Nova Venécia paragneisses (cf. Gradim et al., 2014; Richter et al., 2016). In fact, the Hf data of the inherited zircons from the Ataléia metagranite are consistent with those acquired for detrital zircon grains of the Nova Venécia samples (Figure 4.10F). In addition, our U-Pb and Lu-Hf data for the Ataléia metagranite are similar to those obtained from S-type granites of the Carlos Chagas batholith (Melo et al., 2017; Figure 4.9E, 4.9F), suggesting they record similar sources involved in the same partial melting process associated with the collisional stage of the Araçuaí orogen. That regional source of peraluminous melts are the fertile paragneisses of the Nova Venécia complex (Gradim et al., 2014; Pedrosa-Soares et al., 2011).

4.7 CONCLUSION

U-Pb (LA-ICP-MS) zircon geochronology yielded robust ages for the emplacements of the Mestre Álvaro (ca. 527 Ma ± 2), Aracê – Pedra Azul (ca. 523 ± 2 Ma), and Vitória (ca. 505 ± 1 Ma) plutons (Figure 4.8). Their Lu-Hf isotopic data indicate significant involvement of continental crust in magma evolution. The described zircon features and T_{Zr} calculated temperatures (ca. 834–923 °C) allow us to infer heat sources associated with asthenosphere up-flow and upwelling of mantle plume that triggered post-collisional crustal anatexis and formed the precursor granitic magmas recorded by the studied samples (Figure 4.11). These granitic rocks formed from hybrid magmas with significant contribution of country rocks. The studied zircons have crystallized from alkaline to calc-alkaline magmas with low U, Y, HREE, and P contents relatively to Zr, at temperatures above 800 °C and high cooling rates. These factors

are probably related to magma mixing processes, fast magma ascent and/or release of volatile fluids. After pluton emplacement, primary zircon crystals have been partially changed by *in situ* dissolution – recrystallization and overgrowth processes in response to zircon interactions with residual melts and/or deuteric fluids at the end of pluton crystallization.

ACKNOWLEDGMENTS

The authors acknowledge the financial support and scholarships provided by Brazilian research and development agencies (CNPq, CAPES, and CODEMIG-CODEMGE). We are also grateful to the Microscopy and Microanalysis Laboratory (LMIc) of the Federal University of Ouro Preto, a member of the Microscopy and Microanalysis Network of Minas Gerais State/Brazil/FAPEMIG. Our gratitude to Professor Xian-Hua Li, Editor-in-Chief of Lithos, and two anonymous reviewers for their suggestions, comments and corrections that greatly help us to improve this paper.

REFERENCES

Ahrens, L.H., 1965. Some observations on the uranium and thorium distributions in accessory zircon from granitic rocks. Geochimica et Cosmochimica Acta 29, 711-716.

Alkmim, F.F., Marshak, S., Pedrosa-Soares, A.C., Peres, G.G., Cruz, S.C.P., Whittington, A., 2006. Kinematic evolution of the Araçuaí–West Congo orogen in Brazil and Africa: Nutcracker tectonics during the Neoproterozoic assembly of Gondwana. Precambrian Research 149, 43-64.

Alkmim, F.F., Kuchenbecker, M., Reis, H.L.S., Pedrosa-Soares, A.C., 2017. The Araçuaí belt. In: Heilbron, M., Cordani, U.G, Alkmim F.F. (Eds.), São Francisco Craton, Eastern Brazil. Regional Geology Reviews, Springer International Publishing Co., pp. 255–276.

Angiboust, S., Harlov, D., 2017. Ilmenite breakdown and rutile-titanite stability in metagranitoids: Natural observations and experimental results. American Mineralogist 102, 1696-1708.

Aranda, R., 2018. Petrology of the Afonso Cláudio Intrusive Complex (Espírito Santo State, Araçuaí Orogen): Insights from Petrography, Lithogeochemistry, U-Pb Geochronology and Lu-Hf Isotopes. Instituto de Geociências, Universidade Federal de Minas Gerais, Belo Horizonte (MS Dissertation, 64pp.).

Araujo, C., Pedrosa-Soares, A., Lana, C., Tedeschi, M., Dussin, I., 2019. Primeiro registro de magmatismo juvenil no Arco Magmático Rio Doce, Orógeno Araçuaí Meridional. Anais do XVII Simpósio Nacional de Estudos Tectônicos p.105.

Baxter, S., Feely, M., 2002. Magma mixing and mingling textures in granitoids: examples from the Galway Granite, Connemara, Ireland. Mineralogy and Petrology 76, 63–74.

Bea, F., Montero, P., Molina, J.F., Scarrow, J.H., Cambeses, A., Moreno, J.A., 2018a. Lu-Hf ratios of crustal rocks and their bearing on zircon Hf isotope model ages: The effects of accessories. Chemical Geology 484, 179-190.

Bea, F., Montero, P., Molina Palma, J.F., 2018b. Experimental evidence for the preservation of U-Pb isotope ratios in mantle-recycled crustal zircon grains. Scientific Reports 8, 12904.

Belém, J., 2014. Geoquímica, geocronologia e contexto geotectônico do magmatismo máfico associado ao feixe de fraturas Colatina, Estado do Espírito Santo. Instituto de Geociências, Universidade Federal de Minas Gerais, Belo Horizonte (MS Dissertation, 138 pp.).

Belousova, E.A., Griffin, W.L., O'Reilly, S.Y., 2006. Zircon crystal morphology, trace element signatures and Hf isotope composition as a tool for petrogenetic modelling: examples from eastern Australian granitoids. Journal of Petrology 47, 329–353.

Benisek, A., Finger, F., 1993. Factors controlling the development of prism faces in granite zircons: a microprobe study. Contributions to Mineralogy and Petrology 114, 441-451.

Boehnke, P., Watson, E.B., Trail, D., Harrison, T.M., Schmitt, A.K., 2013. Zircon saturation re-revisited. Chemical Geology 351, 324-334.

Cherniak, D.J., Watson, E.B., 2003. Diffusion in zircon. In: Hanchar, J.M., Hoskin, P.W.O. (Eds.), Zircon. Reviews in Mineralogy and Geochemistry 53, 113-143.

Corfu, F., Hanchar, J.M., Hoskin, P.W.O., Kinny, P., 2003. Atlas of zircon textures. In: Hanchar, J.M., Hoskin, P.W.O. (Eds.), Zircon. Reviews in Mineralogy and Geochemistry, 53, 469–500.

De Campos, C.P., Mendes, J.C., Ludka, I.P., Medeiros, S.R., Moura, J.C., Wallfass, C., 2004. A review of the Brasilian magmatism in southern Espírito Santo, Brazil, with emphasis on post-collisional magmatism. Journal of the Virtual Explorer 17, 1-35.

De Campos, C.P, Medeiros, S.R., Mendes, J.C, Pedrosa-Soares, A.C., Dussin, I., Ludka, I.P., Dantas, E.L., 2016. Cambro-Ordovician magmatism in the Araçuaí Belt (SE Brazil): Snapshots from a post-collisional event. Journal of South American Earth Sciences 68, 248-268.

Degler, R., Pedrosa-Soares, A., Dussin, I., Queiroga, G., Schulz, B., 2017. Contrasting provenance and timing of metamorphism from paragneisses of the Araçuaí-Ribeira orogenic system, Brazil: Hints for Western Gondwana assembly. Gondwana Research 51, 30–50.

Degler, R., Pedrosa-Soares, A., Novo, T., Tedeschi, M., Silva, L.C., Dussin, I., Lana, C. 2018. Rhyacian-Orosirian isotopic records from the basement of the Araçuaí-Ribeira orogenic system (SE Brazil): Links in the Congo-São Francisco palaeocontinent. Precambrian Research 317, 179-195.

Eby, G.N., 1992. Chemical subdivision of A-type granitoids: petrogenetic and tectonic implications. Geology 20, 641-644.

Fedele, L., Lustrino, M., Melluso, L., Morra, V., Zanetti, A., Vannucci, R., 2015. Trace-element partitioning between plagioclase, alkali feldspar, Ti-magnetite, biotite, apatite, and evolved potassic liquids from Campi Flegrei (Southern Italy). American Mineralogist 100, 233–249.

Geisler, T., Schaltegger, U., Tomaschek, F., 2007. Re-equilibration of Zircon in Aqueous Fluids and Melts. Elements 3, 43-50.

Gieré, R., Sorensen, S.S., 2004. Allanite and Other REE-Rich Epidote-Group Minerals. Reviews in Mineralogy and Geochemistry 56, 431-493.

Gonçalves, L., Farina, F., Lana, C., Pedrosa-Soares, A.C., Alkmim, F., Nalini, H.A.Jr., 2014. New U-Pb ages and lithochemical attributes of the Ediacaran Rio Doce magmatic arc, Araçuaí confined orogen, southeastern Brazil. Journal of South American Earth Sciences 52, 129–148.

Gonçalves, L., Alkmim, F.F., Pedrosa-Soares, A.C., Dussin, I.A., Valeriano, C.M., Lana, C., Tedeschi, M., 2016. Granites of the intracontinental termination of a magmatic arc: an example from the Ediacaran Araçuaí orogen, southeastern Brazil. Gondwana Research 36, 439-458.

Gradim, C., Roncato, J., Pedrosa-Soares, A.C., Cordani, U., Dussin, I., Alkmim, F.F., Queiroga, G., Jacobsohn, T., Silva, L.C., Babinski, M., 2014. The hot back-arc zone of the Araçuaí Orogen, Eastern Brazil: from sedimentation to granite generation. Brazilian Journal of Geology 44, 155-180.

Gill, R., 2010. Igneous rocks and processes: a practical guide, first ed. Wiley-Blackwell.

Harley, S.L., Kelly, N.M., Möller, A., 2007. Zircon behaviour and the thermal histories of mountain chains. Elements 3, 25-30.

Hibbard, M.J., 1995. Petrography to petrogenesis. Prentice Hall, New Jersey, 587 p.

Hoskin, P.W.O., Schaltegger, U., 2003. The composition of zircon and igneous and metamorphic petrogenesis. In: Hanchar, J.M, Hoskin, P.W.O. (Eds.), Zircon. Reviews in Mineralogy and Geochemistry 53, 27-62.

Kirkland, C.L., Smithies, R.H., Taylor, R.J.M., Evans, N., McDonald, B., 2015. Zircon Th/U ratios in magmatic environs. Lithos 212-215, 397-414.

Köksal, S., Göncüoglu, M.C, Toksoy-Köksal, F., Möller, A., Kemnitz, H., 2008. Zircon typologies and internal structures as petrogenetic indicators in contrasting granitoid types from central Anatolia, Turkey. Mineralogy and Petrology 93, 185-211.

Ludka, I.P., Wiedemann-Leonardos, C.M., 2000. Further signs of an enriched mantle source under the Neoproterozoic Araçuaí-Ribeira Mobile Belt. Revista Brasileira de Geociências 30, 95-98.

Ludwig, K.R., 2012. Isoplot/Ex Version 4.15: A Geochronological Toolkit for Microsoft Excel. Berkeley, Berkeley Geochronology Center 72 pp.

Martins, V.T.S, Teixeira, W., Noce, C.M., Pedrosa-Soares, A.C., 2004. Sr and Nd Characteristics of Brasiliano/Pan-African Granitoid Plutons of the Araçuai Orogen, Southeastern Brazil: Tectonic Implications. Gondwana Research 7, 75-89.

McDonough, W.F., Sun, S.S., 1995. The composition of the Earth. Chemical Geology 120, 223–253.

Mello, F.M., 2000. Litogeoquímica e Química Mineral do Maciço Charnockítico Aimorés-MG. Universidade de São Paulo, São Paulo (Ph.D. Thesis, 167 pp.).

Mello, F.M., Machado, R., Bilal, E. 2011. Petrografia e Geoquímica do Complexo Charnockítico de Aimorés: Um Exemplo de Plutonismo Pós-orogênico do Cinturão Araçuaí/Ribeira. Revista do Instituto de Geociências – USP 11, 33-57.

Melo, M.G., Lana, C., Stevens, G., Pedrosa-Soares, A.C., Gerdes, A., Alkmin, L.A., Nalini Jr., H.A., Alkmim, F.F., 2017. Assessing the isotopic evolution of S-type granites of the Carlos Chagas batholith, SE Brazil: Clues from U-Pb, Hf isotopes, Ti geothermometry and trace element composition of zircon. Lithos 284-285, 730-750.

Mendes, J.C., Wiedemann, C.M., McReath, I., 1999. Conditions of formation of charnockitic magmatic rocks from the Várzea Alegre massif, Espírito Santo, southeast Brazil. Revista Brasileira de Geociências 29, 47-54.

Mendes, J.C., De Campos, C.M.P., 2012. Norite and charnockite from the Venda Nova Pluton, NE Brazil: intensive parameters and some petrogenetic constrains. Geoscience Frontiers 3, 789-800.

Molina, J.F., Montero, P., Bea, F., Scarrow, J.H., 2012. Anomalous xenocryst dispersion during tonalite-granodiorite crystal mush hybridization in the mid crust: mineralogical and geochemical evidence from Variscan appinites (Avila Batholith, Central Iberia). Lithos 153, 224-242.

Moreno, J.A, Molina, J.F., Montero, P., Anbar, M.A., Scarrow, J.H., Cambeses, A., Bea, F., 2014. Unraveling sources of A-type magmas in juvenile continental crust: Constraints from compositionally diverse Ediacaran post-collisional granitoids in the Katerina Ring Complex, southern Sinai, Egypt. Lithos 192-195, 56-85.

Noce, C.M., Macambira, M.J.B., Pedrosa-Soares, A.C., 2000. Chronology of Neoproterozoic–Cambrian granitic magmatism in the Araçuaí Belt, Eastern Brazil, based on single zircon evaporation dating. Revista Brasileira de Geociências 30, 25–29.

Noce, C.M., Pedrosa-Soares, A.C., Piuzana, D., Armstrong, R., Laux, J.H., De Campos, C.M., Medeiros, S.R. 2004. Ages of sedimentation of the kinzigitic complex and of a late orogenic thermal episode of the Araçuaí Orogen, northern Espírito Santo State, Brazil: Zircon and monazite U-Pb SHRIMP and ID–TIMS data. Revista Brasileira de Geociências 34, 587-592.

Novo, T.A., Pedrosa-Soares, A., Vieira, V.S., Dussin, I., Silva, L.C., 2018. The Rio Doce Group revisited: An Ediacaran arc-related volcano-sedimentary basin, Araçuaí orogen (SE Brazil). Journal of South American Earth Sciences 85, 345-361.

Pearce, J.A., Harris, N.B.W., Tindle, A.G., 1984. Trace element diagrams for the tectonic interpretation of granitic rocks. Journal of Petrology 25, 956–983.

Pearce, J., 1996. Sources and settings of granitic rocks. Episodes 19, 120-125.

Pedrosa-Soares, A.C., Noce, C.M., Wiedemann, C.M., Pinto, C.P., 2001. The Araçuaí-West-Congo Orogen in Brazil: An overview of a confined orogen formed during Gondwanaland assembly. Precambrian Research 110, 307-323.

Pedrosa-Soares, A.C., Alkmim, F.F., Tack, L., Noce, C.M., Babinski, M., Silva, L.C., Martins-Neto, M.A., 2008. Similarities and differences between the Brazilian and African counterparts of the Neoproterozoic Araçuaí-West Congo orogeny. In: Pankhurst, R.J., Trouw, R.A.J., Brito Neves, B.B., De Wit, M.J. (Eds.), West Gondwana: Pre-Cenozoic Correlations Across the South Atlantic Region. London, Geological Society of London, Special Publication 294, 153-172.

Pedrosa-Soares, A.C., De Campos, C.P., Noce, C.M., Silva, L.C., Novo, T., Roncato, J., Medeiros, S., Castañeda, C., Queiroga, G., Dantas, E., Dussin, I., Alkmim, F., 2011. Late Neoproterozoic-Cambrian Granitic Magmatism in the Araçuaí Orogen (Brazil), the Eastern Brazilian Pegmatite Province and Related Mineral Resources. In: Sial, A.N., Bettencourt, J.S., De Campos, C.P., Ferreira, V.P. (Eds.), Granite-Related Ore Deposits. London, Geological Society of London, Special Publication 350, 25–51.

Pedrosa-Soares 2020

Peixoto, E., Pedrosa-Soares, A.C., Alkmim, F.F., Dussin, I.A., 2015. A suture-related accretionary wedge formed in the Neoproterozoic Araçuaí orogen (SE Brazil) during Western Gondwanaland assembly. Gondwana Research 27, 878-896.

Pupin, J.P., 1980. Zircon and granite petrology. Contributions to Mineralogy and Petrology 73, 207-220.

Richter, F., Lana, C., Steven, G., Buick, I., Pedrosa-Soares, A.C., Alkmim, F.F., Cutts, K., 2016. Sedimentation, metamorphism and granite generation in a back-arc region: Records from the Ediacaran Nova Venécia Complex (Araçuaí Orogen, Southeastern Brazil). Precambrian Research 272, 78–100.

Rubatto, D., Hermann, J., 2007. Zircon behaviour in deeply subducted rocks. Elements 3, 31-35.

Serrano, P., Pedrosa-Soares, A., Medeiros-Junior, E., Fonte-Boa, T., Araujo, C., Dussin, I., Queiroga, G., Lana, C., 2018. A-type Medina batholith and post-collisional anatexis in the Araçuaí orogen (SE Brazil). Lithos 320-321, 515-536.

Shannon, R.D., 1976. Revised effective ionic radii and systematic studies of interatomic distances in halides and chalcogenides. Acta Crystallographica Section 32A, 751–767.

Tang, M., Wang, X.-L., Shu, X.-J., Wang, D., Yang, T., Gopon, P. 2014. Hafnium isotopic heterogeneity in zircons from granitic rocks: geochemical evaluation and modelling of "zircon effect" in crustal anatexis. Earth and Planetary Science Letters 389, 188-199.

Tedeschi, M., Novo, T., Pedrosa-Soares, A., Dussin, I., Tassinari, C., Silva, L.C., Gonçalves, L., Alkmim, F., Lana, C., Figueiredo, C., Dantas, E., Medeiros, S., De Campos, C., Corrales, F., Heilbron, M., 2016. The Ediacaran Rio Doce magmatic arc revisited (Araçuaí-Ribeira orogenic system, SE Brazil). Journal of South American Earth Sciences 68, 167-186.

Vavra, G., 1990. On the kinematics of zircon growth and its petrogenetic significance: a cathodeluminescence study. Contributions to Mineralogy and Petrology 106, 90-99.

Vavra, G., 1994. Systematics of internal zircon morphology in major Variscan granitoid types. Contributions to Mineralogy and Petrology 117, 331–344.

Vavra, G., Gebauer, D., Schmid, R., Compston, W., 1996. Multiple zircon growth and recrystallization during polyphase late Carboniferous to Triassic metamorphism in granulites of the Ivrea Zone (Southern Alps): an ion microprobe (SHRIMP) study. Contributions to Mineralogy and Petrology 122, 337-358.

Wang, X., Griffin, W.L., O'Reilly, S.Y., Zhou, X.M., Xu, X.S., Jackson, S.E., Pearson, N.J., 2002. Morphology and geochemistry of zircons from late Mesozoic igneous complexes in coastal SE China: implications for petrogenesis. Mineralogical Magazine 66, 235-251.

Wang, X., Griffin, W.L., Chen, J., Huang, P., Li, X., 2011. U and Th contents and Th/U rations of zircon in felsic and mafic magmatic rocks: improved zircon-melt distribution coefficients. Acta Geologica Sinica 85, 164-174.

Wang, L.X., Ma, C.Q., Zhang, C., Zhu, Y.X., Marks, M.A.W., 2018. Halogen geochemistry of I- and A-type granites from Jiuhuashan region (South China): Insights into the elevated fluorine in A-type granite. Chemical Geology 478, 164-182.

Watson, E.B., Harrison, T.M., 1983. Zircon saturation revisited: temperature and composition effects in a variety of crustal magma types. Earth and Planetary Science Letters 64, 295–304.

Wiedemann, C.M., Medeiros, S.R., Ludka, I.P., Mendes, J.C., Costa-de-Moura, J., 2002. Architecture of late orogenic plutons in the Araçuaí-Ribeira fold belt, Southeast Brazil. Gondwana Research 5, 381-399.

Whalen, J.B., Currie, K.L., Chappell, B.W., 1987. A-type granites, geochemical characteristics, discrimination and petrogenesis. Contributions to Mineralogy and Petrology 95, 407-419.

Whitney, D.L., Evans, B.W., 2010. Abbreviations for names of rock-forming minerals. American Mineralogist 95, 185-187.

CHAPTER 5. CONCLUSIONS

The integration of data obtained in plutonic and metasedimentary rocks from the north-central portion of the state of Espírito Santo, easternmost sector of the Araçuaí orogen, allowed to reach some conclusions for the rocks and the geotectonic evolution for the region:

- New zircon U-Pb and Hf isotopic data, coupled with whole-rock Sm-Nd results, for Santa Tereza (Concordia age of 612 ± 3 Ma) and Jequitibá (Concordia age 594 ± 3 Ma) rocks demonstrate the easternmost expression of pre-collisional, arc-related magmatism in the Araçuaí Orogen. The Lu-Hf and whole-rock Sm-Nd data show the least evolved magmatism in the Rio Doce Arc. The U-Pb data spreading along the Concordia curve and Hf signatures distributed roughly horizontally suggest post-crystallization disturbance under HT conditions indicating progressive Pb loss, consistent with the granulite facies observed in the samples and the studied region. Thus, based on the older zircons, the minimum crystallization ages are 635 ± 8 Ma for the Santa Tereza suite and 624 ± 8 Ma for the Jequitibá suite;
- Together with a wide data compilation, our dataset indicates involvement of juvenile crust and/or mantle melts in the Eastern sector of the Rio Doce Arc, supporting a complete Wilson Cycle for the orogenic evolution of the Araçuaí Orogen, including the magmatic front migration owing to subduction retreat;
- The pre-collisional studied rocks can be correlated with the Marceleza-Leopoldina-Serra da Bolívia complex of the Ribeira Orogen, providing further evidence of the connection between both orogens during the evolution of the Rio Doce Arc;
- The presented age spectra and Hf signatures of detrital zircon grains for samples of the Nova Venécia complex corroborate prior interpretations suggesting that this basin received significant sediment from the Rio Doce magmatic arc, with age peaks at 617 ± 4 Ma (68%), 719 ± 22 Ma (14%), 839 ± 46 Ma (8%), and 922 ± 31 Ma (10%). The youngest zircon populations, with age peaks at 490 ± 21 Ma (5%), 527 ± 12 Ma (27%), and 565 ± 6 Ma (68%), representing the regional metamorphism imprinted on the Nova Venécia complex during the collisional stage and thermal episodes related to the post-collisional plutonism (530 – 480 Ma);
- Nova Venécia Hf isotopic signature indicates continental proximity;
- U-Pb and Lu-Hf data for the Ataléia metagranite compared with those obtained from S-type granites of the Carlos Chagas batholith suggest similar sources involved in the same partial melting process associated with the collisional stage of the Araçuaí orogen;
- The dataset for the post-collisional intrusions indicate magma hybridization at high temperature, involving country rocks in their petrogenesis;

- The presented data also support the evolution of a continental-margin magmatic arc within a confined orogen, the Araçuaí - West Congo Orogen, formed by the closing of an inland-sea basin, providing an example of a singular geotectonic setting in the paleocontinental history, such as the Western Gondwana.

CHAPTER 6. REFERENCES

The references of the articles are at the end of their chapters (3, and 4) and in the Supplementary Files.

Affaton, P., Kalsbeek, F., Boudzoumou, F., Trompetted, R., Thrane K., Robert Frei, R., 2016. The Pan African West Congo belt in the Republic of Congo (CongoBrazzaville): Stratigraphy of the Mayombe and West CongoSupergroups studied by detrital zircon geochronology. Precambrian Research 272, 185–202.

Alkmim, F.F., Marshak, S., Pedrosa-Soares, A.C., Peres, G.G., Cruz, S.C.P., Whittington, A., 2006. Kinematic evolution of the Araçuaí–West Congo orogen in Brazil and Africa: Nutcracker tectonics during the Neoproterozoic assembly of Gondwana. Precambrian Research 149, 43-64.

Alkmim, F.F., Pedrosa-Soares, A.C., Noce, C.M., Cruz, S.C.P. 2007. Sobre a Evolução Tectônica do Orógeno Araçuaí-Congo Ocidental. Geonomos 15, 25 – 43.

Alkmim, F.F., Kuchenbecker, M., Reis, H.L.S., Pedrosa-Soares, A.C., 2017. The Araçuaí belt. In: Heilbron, M., Cordani, U.G, Alkmim F.F. (Eds.), São Francisco Craton, Eastern Brazil. Regional Geology Reviews, Springer International Publishing Co., pp. 255–276.

Angelo, T.V., Egydio-Silva, M., Temporim, F.A., Seraine, M., 2020. Midcrust deformation regime variations across the Neoproterozoic Araçuaí hot orogen (SE Brazil): Insights from structural and magnetic fabric analyses. Journal of Structural Geology 134, 104007.

Amaral, L., Caxito F.A., Pedrosa-Soares A., Queiroga G., Babinski, M., Trindade, R., Lana, C., Chemale, F., 2020. The Ribeirão da Folha ophiolite-bearing accretionary wedge (Araçuaí orogen, SE Brazil): New data for Cryogenian plagiogranite and metasedimentary rocks. Precambriam Research 336, 105522.

Aranda, R., 2018. Petrology of the Afonso Cláudio Intrusive Complex (Espírito Santo State, Araçuaí Orogen): Insights from Petrography, Lithogeochemistry, U-Pb Geochronology and Lu-Hf Isotopes. Instituto de Geociências, Universidade Federal de Minas Gerais, Belo Horizonte (MS Dissertation, 64pp.).

Aranda, R.O., Chaves, A.O., Medeiros Júnior, E.B., Venturini Junior, R., 2020. Petrology of the Afonso Cláudio Intrusive Complex: New insights for the Cambro-Ordovician post-collisional magmatism in the Araçuaí-West Congo Orogen, Southeast Brazil. Journal of South American Earth Sciences 98, 102465.

Aranda, R.O., Horn, A.H., Medeiros Júnior, E.B., Venturini Junior, R., 2021. Geothermobarometry of igneous rocks from Afonso Cl´audio Intrusive Complex (Espírito Santo state, Southeastern Brazil), Araçuaí-West Congo Orogen: Further evidence for deep emplacement levels. Journal of South American Earth Sciences 110, 103016. https://doi.org/10.1016/j.jsames.2020.103016

Araujo, C.S., 2019. Caracterização textural e respostas isotópicas U-Pb e Lu-Hf de zircão como indicador petrogenético de granitos pós-colisionais do Orógeno Araçuaí na região centro-sul do Estado do Espírito Santo. Instituto de Geociências, Universidade Federal de Minas Gerais, Belo Horizonte (MS Dissertation, 156pp.).

Araujo, C., Pedrosa-Soares, A., Lana, C., Tedeschi, M., Dussin, I., 2019. Primeiro registro de magmatismo juvenil no Arco Magmático Rio Doce, Orógeno Araçuaí Meridional. Anais do XVII Simpósio Nacional de Estudos Tectônicos p.105.

Araujo, L. E. A. B., Heilbron, M., Teixeira, W., Dussin, I., Valeriano, C.M., Henrique Bruno, Sato, K., Paravidini, G., Castro, M., 2021. Siderian to Rhyacian evolution of the Juiz de Fora Complex: Arc fingerprints and correlations within the Minas-Bahia Orogen and the Western Central Africa Belt. Precambrian Research, 359: 106118. https://doi.org/10.1016/j.precamres.2021.106118

Araujo C., Pedrosa-Soares A., Lana C., Dussin I., Queiroga G., Serrano P., Medeiros-Júnior E. 2020. Zircon in emplacement borders of post-collisional plutons compared to country rocks: A study on morphology, internal texture, U-Th-Pb geochronology and Hf isotopes (Araçuaí orogen, SE Brazil). Lithos, 352-353: 105252.

Baltazar, O.F., Zucchetti, M., Oliveira, S.A.M., Scandolara, J., Silva, L.C., 2010. Geologia das Folhas São Gabriel Da Palha e Linhares. Programa Geologia do Brasil, CPRM–Serviço Geológico do Brasil, Belo Horizonte.

Basílio, M., Pedrosa-Soares, A.C., Evangelista, H.J., 2000. Depósitos de alexandrita de Malacacheta. Minas Gerais. Geonomos 8, 47–54.

Bayer, P., Schmidt-Thomé, R., Weber-Diefenbach, K., Horn, H.A., 1987. Complex concentric granitoid intrusions in the Coastal Mobile Belt, Espírito Santo, Brazil: the Santa Angélica pluton - an example. Geologische Rundschau 76, 357-371.

Bateman, P.C., Dodge, F.C.W., Bruggman, P.E., 1984. Major oxide analyses, CIPW norms, modes, and bulk specific gravities of plutonic rocks from the Mariposa 1 degrees by 2 degrees sheet, central Sierra Nevada, California. U S Geological Survey OF 84-0162, 59 pp.

Belém, J., 2014. Geoquímica, geocronologia e contexto geotectônico do magmatismo máfico associado ao feixe de fraturas Colatina, Estado do Espírito Santo. Instituto de Geociências, Universidade Federal de Minas Gerais, Belo Horizonte (MS Dissertation, 138 pp.).

Belousova E.A., Walters S., Griffin W.L., O'Reilly S.Y., Fisher N.I., 2002. Zircon trace-element compositions as indicators of source rock type. Contributions to Mineralogy and Petrology 143, 602–622.

Belousova, E.A., Griffin, W.L., O'Reilly, S.Y., 2006. Zircon crystal morphology, trace element signatures and Hf isotope composition as a tool for petrogenetic modelling: examples from eastern Australian granitoids. Journal of Petrology 47, 329–353.

Best, M.G., 2003. Igneous and metamorphic petrology. Blackwell Science: Malden, 2° ed., 758p.

Carvalho, B.B., Janasi, V.A., Sawyer, E.W., 2017. Evidence for Paleoproterozoic anatexis and crustal reworking of Archean crust in the São Francisco Craton, Brazil: A dating and isotopic study of the Kinawa migmatite. Precambriam Research 291, 98-118.

Bitencourt, C.N., Cruz, S.C.P., dos Anjos Cruz, V., Pedrosa-Soares, A.C., Paquette, J.L., Alkmim A.R., Barbosa, J.S.F., 2019. Rifting events in the southern sector of the Paramirim Aulacogen, NE Brazil: new geochronological data and correlations for the São Francisco – Congo paleocontinent. Precambriam Research 326, 417–446.

Brito Neves, B.B., Fuck, R.A., Campanha, G.A.C., 2021. Basement inliers of the Brasiliano structural provinces of South America. Journal of South American Earth Sciences 110, 103392.

Brown, M., Johnson, T., 2019. Metamorphism and the evolution of subduction on Earth. American Mineralogist 104, 1065–1082.

Castañeda, C., Pedrosa-Soares, A.C., Belém, J., Dias, P.H.A., Gradim, C.T., Medeiros, S.R., Oliveira, L.F., 2007. Nota Explicativa da Folha Ecoporanga, 1:100.000. Programa Geologia do Brasil, CPRM–UFMG.

Castro, A., Gerya, T., Garcia-Casco, A., Fernandez, C., Diaz-Alvarado, J. Moreno-Ventas, I., Löw, I., 2010. Melting relations of MORB–sediment Mélanges in underplated mantle wedge plumes; implications for the origin of Cordilleran-type batholiths. Jounal of Petrology 51,1267–1295.

Castro, A., Moreno-Ventas, I., Fernández, C., Vujovich, G., Gallastegui, G., Heredia, N., Martino, R.D., Becchio, R., Corretgé, L.G., Díaz-Alvarado, J., García-Arias, M., Liu D., 2011. Petrology and SHRIMP U-Pb zircon geochronology of Cordilleran granitoids of the Bariloche area, Argentina. Journal of South American Earth Sciences 32, 508-530.

Castro, A., 2013. Tonalite-granodiorite suites as cotectic systems: A review of experimental studies with applications to granitoid petrogenesis, Earth-Science Reviews 124, 68-95.

Castro, M.P., Queiroga, G., Martins, M., Alkmim, F., Pedrosa-Soares, A., Dussin, I., Souza, M.E., 2019. An Early Tonian rifting event affecting the São Francisco-Congo paleocontinent recorded by the Lower Macaúbas Group, Araçuaí Orogen, SE Brazil. Precambriam Research 331, 105351.

Castro, M.P., Queiroga, G., Martins, M., Alkmim, F., Pedrosa-Soares, A., Dias, L., Lana, C., Babinski, M., Alkmim A.R., Silva M.A., 2020 Provenance shift through time in superposed basins: From Early Cryogenian glaciomarine to Late Ediacaran orogenic sedimentations (Araçuaí Orogen, SE Brazil). Gondwana Research 87, 41-66.

Cavalcante, C., Hollanda, M.H., Vauchez, A., Kawata, M., 2018. How long can the middle crust remain partially molten during orogeny? Geology 46, 839-842.

Cavalcante, C., Fossen, H., de Almeida, R.P., Hollanda, M.H.B.M., Egydio-Silva, M., 2019. Reviewing the puzzling intracontinental termination of the Araçuaí-West Congo orogenic belt and its implications for orogenic development. Precambriam Research 322, 85-98.

Cecil, M.R., Rotberg, G.L., Ducea, M.N., Saleeby, J.B., Gehrels, G.E., 2012. Magmatic growth and batholithic root development in the Northern Sierra Nevada, California. Geosphere 8, 592-606.

Chapman, A.D., Saleeby, J.B., Wood, D.J., Piasecki, A., Kidder, S., Ducea, M.N., Farley, K.A., 2012. Late Cretaceous gravitational collapse of the Southern Sierra Nevada batholith, California. Geosphere 8, 314–341.

Corrales, F.F.P., Dussin, I.A., Heilbron, M., Bruno, H., Bersan, S.A., Valeriano, C.M., Pedrosa-Soares, A.C., Tedeschi, M., 2020. Coeval high Ba-Sr arc-related and OIB Neoproterozoic rocks linking pre-collisional magmatism of the Ribeira and Araçuaí orogenic belts, SE-Brazil. Precambriam Research 337, 105476.

Corfu, F., Hanchar, J.M., Hoskin, P.W.O., Kinny, P., 2003. Atlas of zircon textures. In: Hanchar, J.M., Hoskin, P.W.O. (Eds.), Zircon. Reviews in Mineralogy and Geochemistry 53, 469–500.

Cutts, K., Lana, C., Alkmim, F., Peres, G.G., 2018. Metamorphic imprints on units of the southern Araçuaí belt, SE Brazil: The history of superimposed Transamazonian and Brasiliano orogenesis. Gondwana Research 58, 211–234.

De Campos, C.P., Mendes, J.C., Ludka, I.P., Medeiros, S.R., Moura, J.C., Wallfass, C., 2004. A review of the Brasilian magmatism in southern Espírito Santo, Brazil, with emphasis on post-collisional magmatism. Journal of the Virtual Explorer 17, 1-35.

De Campos, C.P., 2015. Chaotic flow patterns from a deep plutonic environment: a case study on natural magma mixing. Pure and Applied Geophysics 172, 1815–1833.

De Campos, C.P, Medeiros, S.R., Mendes, J.C, Pedrosa-Soares, A.C., Dussin, I., Ludka, I.P., Dantas, E.L., 2016. Cambro-Ordovician magmatism in the Araçuaí Belt (SE Brazil): Snapshots from a post-collisional event. Journal of South American Earth Sciences 68, 248-268.

Degler, R., Pedrosa-Soares, A., Dussin, I., Queiroga, G., Schulz, B., 2017. Contrasting provenance and timing of metamorphism from paragneisses of the Araçuaí-Ribeira orogenic system, Brazil: Hints for Western Gondwana assembly. Gondwana Research 51, 30–50.

Degler, R., Pedrosa-Soares, A., Novo, T., Tedeschi, M., Silva, L.C., Dussin, I., Lana, C. 2018. Rhyacian-Orosirian isotopic records from the basement of the Araçuaí-Ribeira orogenic system (SE Brazil): Links in the Congo-São Francisco palaeocontinent. Precambrian Research 317, 179-195.

Deluca, C., 2018. Evolução do Batólito Itaporé e rochas encaixantes, Orógeno Araçuaí (MG): geoquímica, geocronologia e petrogênese. Universidade Federal de Minas Gerais, Belo Horizonte (MS Dissertation, 116 pp.).

Deluca, C., Pedrosa-Soares, A., Lima, S., Cordani, U., Sato, K., 2019. Provenance of the Ediacaran Salinas Formation (Araçuaí Orogen, Brazil): Clues from lithochemical data and zircon U-Pb (SHRIMP) ages of volcanic clasts. Brazilian Journal of Geology 49, 1–19.

Dogde, F.C.W., Millard, H.T., Elsheimer, H.N., 1982. Compositional variations and abundances of selected elements in granitoids rocks and constituent minerals, central Sierra Nevada batholiths, California. US Geological Survey Professional Paper 1248.

Ducea, M.N., Saleeby, J.B., Bergantz, G., 2015a. The Architecture, Chemistry, and Evolution of Continental Magmatic Arcs. Annual Review of Earth and Planetary Sciences 43, 10.1-10.33.

Ducea, M.N., Paterson, S.R., DeCelles, P.G., 2015b. High-Volume Magmatic Events in Subduction Systems. Elements 11, 99-104.

Dunphy, J.M., Ludden, J.N., 1998. Petrological and geochemical characteristics of a Paleoproterozoic magmatic arc (Narsajuaq terrane, Ungava Orogen, Canada) and comparisons to Superior Province granitoids. Precambriam Research 91, 109–142.

Egydio-Silva, M., Vauchez, A., Fossen, H., Gonçalves Cavalcante, G.C., Xavier, B.C., 2018. Connecting the Araçuaí and Ribeira belts (SE – Brazil): Progressive transition from contractional to transpressive strain regime during the Brasiliano orogeny. Journal of South American Earth Sciences 86, 127–139.

Figueiredo, M.C.H., Campos Neto, M.C., 1993. Geochemistry of the Rio doce magmatic arc, Southeastern Brazil. Anais da Academia Brasileira de Ciências. 65, 63-81.

Figueiredo, C.M.S., 2009. O Arco Magmático Brasiliano na conexão entre os orógenos Araçuaí e Ribeira, Região de Muriaé-MG. Universidade Federal de Minas Gerais, Belo Horizonte, Brazil (Ph.D. Thesis, p. 103).

Fossen, H., Cavalcante, G.C., de Almeida, R.P., 2017. Hot Versus Cold Orogenic Behaviour: Comparing the Araçuaí-West Congo and the Caledonian Orogens. Tectonics 36, 2159-2178.

Frost, B.R., Frost, C.D., 2008. On charnockites. Gondwana Reserach 13, 30-44.

Frost, B.R., Barnes, C.G., Collins, W.J., Arculus, R.J., Ellis, D.J., Frost, C.D., 2001. A geochemical classification for granitic rocks. Journal of Petrology 42, 2033–2048.

Gonçalves-Dias, T., 2012. Caracterização Geoquímica e Geocronológica co Complexo Jequitinhonha na Área-Tipo, Orógeno Araçuaí. MS Dissertation, Universidade Federal de Minas Gerais, Belo Horizonte, 96 p.

Gonçalves-Dias, T., Caxito, F.A., Pedrosa-Soares, A.C., Stevenson, R., Dussin, I., Silva, L.C., Alkmim, F., Pimentel, M. 2016. Age, provenance and tectonic setting of the high-grade Jequitinhonha Complex, Araçuaí orogen, eastern Brazil. Brazilian Journal of Geology 46, 199–219.

Gonçalves, L.E.S., 2009. Características gerais e história deformacional da suíte granítica G1, entre governador valadares e ipanema, MG. MS Dissertation, Universidade Federal de Minas Gerais, Belo Horizonte, 212 p.

Gonçalves, L., Farina, F., Lana, C., Pedrosa-Soares, A.C., Alkmim, F., Nalini, H.A.Jr., 2014. New U-Pb ages and lithochemical attributes of the Ediacaran Rio Doce magmatic arc, Araçuaí confined orogen, southeastern Brazil. Journal of South American Earth Sciences 52, 129–148.

Gonçalves, L., Alkmim, F.F., Pedrosa-Soares, A.C., Dussin, I.A., Valeriano, C.M., Lana, C., Tedeschi, M., 2016. Granites of the intracontinental termination of a magmatic arc: an example from the Ediacaran Araçuaí orogen, southeastern Brazil. Gondwana Research 36, 439-458.

Gonçalves, L., Alkmim, F.F., Pedrosa-Soares, A.C., Gonçalves, C.C., Vieira V., 2018. From the plutonic root to the volcanic roof of a continental magmatic arc: a review of the Neoproterozoic Araçuaí orogen, southeastern Brazil. International Journal of Earth Science (Geologische Rundschau) 107, 337-358.

Gonçalves, G.O., Lana, C., Buick, I.S., Alkmim, F.F., Scholz, R, Queiroga, G., 2019. Twenty million years of post-orogenic fluid production and hydrothermal mineralization across the external Araçuaí orogen and adjacent São Francisco craton, SE Brazil. Lithos 342–343, 557–572.

Gouvêa, L.P., Medeiros, S.R., Mendes, J.C., Soares, C., Rodson Marques, R., Marilane Melo, M., 2020. Magmatic activity period and estimation of P-T metamorphic conditions of pre-collisional opx-metatonalite from Araçuaí-Ribeira orogens boundary, SE Brazil. Journal of South American Earth Sciences 99, 102506.

Gradim, C.T., 2013. Complexo Nova Venécia e magmatismo associado, Orógeno Araçuaí, Estado do Espírito Santo. MS Dissertation, Universidade Federal de Minas Gerais, Belo Horizonte, 123 p.

Gradim, C., Roncato, J., Pedrosa-Soares, A.C., Cordani, U., Dussin, I., Alkmim, F.F., Queiroga, G., Jacobsohn, T., Silva, L.C., Babinski, M., 2014. The hot back-arc zone of the Araçuaí Orogen, Eastern Brazil: from sedimentation to granite generation. Brazilian Journal of Geology 44, 155-180.

Heilbron, M., Machado, N., 2003. Timing of terrane accretion in the Neoproterozoic-Eopaleozoic Ribeira Orogen (SE Brazil). Precambrian Research 125,87-112.

Heilbron, M., Pedrosa-Soares, A.C., Campos-Neto, M.C., Silva, L.C., Trouw, R., Janasi, V.A., 2004. Província Mantiqueira. In: V. Mantesso-Neto, A., Bartorelli, C.D.R., Carneiro, B.B., Brito-Neves (org.). Geologia do Continente Sul-Americano. São Paulo, Editora Beca, XIII, 203-234.

Heilbron, M., Valeriano, C.M., Tassinari, C.C.G., Almeida, J., Tupinambá, M., Siga, O., Trouw, R., 2008. Correlation of Neoproterozoic terranes between the Ribeira Belt, SE Brazil and its African counterpart: comparative tectonic evolution and open questions. In: Pankhurst R.J., Trouw R.A.J., Brito Neves B.B., De Wit M.J. (Eds.). West Gondwana: Pre-Cenozoic Correlations Across The South Atlantic Region. London, Geological Society of London Special Publication 294, 211-237.

Heilbron, M., Tupinambá, M., Valeriano, C., Armstrong, R., Silva, L.G.E., Melo, R.S., Simonetti, A., Pedrosa-Soares, A.C., Machado, N. 2013. The Serra da Bolívia complex: The record of a new Neoproterozoic arc-related unit at Ribeira belt. Precambrian Research 238, 158– 175.

Heilbron, M., Ribeiro A., Valeriano, C.M., Paciullo, F.V., Almeida, J.C.H., Trouw, R.J.A., Tupinambá, M., Silva, L.G.E., 2017. The Riberia belt. In: Heilbron, M., Cordani, U.G, Alkmim F.F. (Eds.), São Francisco Craton, Eastern Brazil. Regional Geology Reviews, Springer International Publishing Co., pp. 277–302.

Heilbron, M., Valeriano, C.M., Peixoto, C., Tupinambá, M., Neubauer, F., Dussin, I., Corrales, F., Bruno, H., Lobato, M., Almeida, J.C.A., Silva L.G.E., 2020. Neoproterozoic magmatic arc systems of the central Ribeira belt, SE-Brazil, in the context of the West-Gondwana pre-collisional history: A review. Journal of South American Earth Sciences 103, 102710.

Hoskin, P.W.O., Schaltegger, U., 2003. The composition of zircon and igneous and metamorphic petrogenesis. In: Hanchar, J.M, Hoskin, P.W.O. (Eds.), Zircon. Reviews in Mineralogy and Geochemistry 53, 27-62.

Hervé, F., Pankurst, R.J., Fanning, C.M., Calderon, M., Yaxely, G.M., 2007. The south Patagonian batholith: 150 my of granite magmatism on a plate margin. Lithos 97, 373-394.

IBGE, 1987. Geologia. In: Projeto RADAMBRASIL. Folha SE 24 Rio Doce. IBGE, Rio de Janeiro, 548 pp.

Janasi, V.A., Andrade, S., Vasconcellos, A.C.B.C., Henrique-Pinto, R., Ulbrich, H.H.G.J., 2016. Timing and sources of granite magmatism in the Ribeira Belt, SE Brazil: Insights from zircon in situ U-Pb dating and Hf isotope geochemistry in granites from the São Roque Domain. Journal of South American Earth Sciences 68, 224-247.

Kearey, P., Klepeis, K.A., Vine, F.J., 2014. Tectônica Global. 3° ed. Bookman, 436p.

Kelemen, P.B., Hanghoj, K., Greene, A.R., 2014. One view of the geochemistry of subduction-related magmatic arcs, with an emphasis on primitive andesite and lower crust. Treatise on Geochemistry 4, 749-806.

Kinny, P.D., Mass, R., 2003. Lu–Hf and Sm–Nd isotope systems in zircon. In: Hanchar J.M, Hoskin P.W.O. (Eds.), Zircon. Reviews in Mineralogy and Geochemistry 53, 327–341.

Kohanpour, F., Kirkland. C.L., Gorczyk, C., Occhipinti, S., Lindsay, M.D., Mole, D., Vaillant, M., 2019. Hf isotopic fingerprinting of geodynamic settings: Integrating isotopes and numerical models. Gondwana Research 73, 190-199.

Kuchenbecker, M., Pedrosa-Soares, A.C., Babinski, M., Fanning, M., 2015. Detrital zircon age patterns and provenance assessment for pre-glacial to post-glacial successions of the Neoproterozoic Macaúbas Group, Araçuaí Orogen, Brazil. Precambriam Research 266, 12–26.

Kuchenbecker, M., Barbuena, D., 2012. Basement inliers of the Araçuaí-West Congo orogen: key pieces for understanding the evolution of the S˜ao Francisco-Congo paleocontinent. Journal of South American Earth Sciences 125, 104299.

Kuribara, Y., Tsunogae, T., Santosh, M., Takamura, Y., Costa, A.G., Rosière, C.A., 2019. Eoarchean to Neoproterozoic crustal evolution of the Mantiqueira and the Juiz de Fora Complexes, SE Brazil: Petrology, geochemistry, zircon U-Pb geochronology and Lu-Hf isotopes. Precambriam Research 323, 82-101.

Lee, C-T.A., Morton, D.M., Kistler, R.W., Baird, A.K. 2007. Petrology and tectonics of Phanerozoic continent formation: from island arcs to accretion and continental arc magmatism. Earth and Planetary Science Letters 263, 370-387.

Leite, C.A.S., Souza, J.D., Silva, S.L., Kosin, M., Silva, L.C., Bento, R.V., Santos Vieira, V.S., Camozzato, E., Paes, V.J.C., Netto, C., Junqueira, P.A., 2004. Folha Rio Doce (SE.24), escala 1:1.000.000. In: Schobbenhaus, C., Gonçalves, J.H., Santos, J.O.S., Abram, M.B., Leão Neto, R., Matos, G.M.M., Vidotti, R.M., Ramos, M.A.B., Jesus, J.D.A. de. (Eds.). Carta Geológica do Brasil ao Milionésimo. Programa Geologia do Brasil, CPRM–Serviço Geológico do Brasil, Brasília.

Lobato, M., Heilbron, M., Torós, T., Ragatky, D., Dantas, E., 2015. Provenance of the Neoproterozoic high-grade metasedimentary rocks of the arc-related Oriental Terrane of the Ribeira belt: Implications for Gondwana amalgamation. Journal of South American Earth Sciences 63, 260-278.

Lopes, R.G., 2016. Geologia da região de Colatina (ES): uma abordagem geocronológica, petrográfica e estrutural por ASM. Universidade de São Paulo, São Paulo, Brazil (MS Dissertation, 109p).

Ludka, I.P., Wiedemann, C.M., Töpfner, C., 1998. On the origin of incompatible element enrichment in the Venda Nova pluton, State of Espírito Santo, southeast Brazil. Journal of South America Earth Sciences 11, 473-486.

Ludka, I.P., Wiedemann-Leonardos, C.M., 2000. Further signs of an enriched mantle source under the Neoproterozoic Araçuaí-Ribeira Mobile Belt. Revista Brasileira de Geociências 30, 95-98.

Macêdo, I., M.L., Geraldes, M.C., Marques, R.A., Melo, M.G., Tavares., A.D., Martins, M.V.A., Oliveira, H.C., Rodrigues, R.D., 2022. New clues for magma-mixing processes using petrological and geochronological evidence

from the Castelo Intrusive Complex, Araçuaí Orogen (SE Brazil). Journal of South American Earth Sciences 115, 103758. https://doi.org/10.1016/j.jsames.2022.103758

Magalhães, J.R., Pedrosa-Soares, A., Dussin, I., Müntener, O., Pinheiro, M.A.P., Silva, L.C., Knauer, L.G., Bouvier, A.-S., Baumgartner, L., 2018. First Lu-Hf, δ18O and trace elements in zircon signatures from the Statherian Espinhaço anorogenic province (Eastern Brazil): geotectonic implications of a silicic large igneous province. Brazilian Journal of Geology 48, 735–759.

Martins, V.T.S, Teixeira, W., Noce, C.M., Pedrosa-Soares, A.C., 2004. Sr and Nd Characteristics of Brasiliano/Pan-African Granitoid Plutons of the Araçuai Orogen, Southeastern Brazil: Tectonic Implications. Gondwana Research 7, 75-89.

Mauri, S., Melo, M.G., Lana, C., Marques, R.A., 2021. Petrologic and geochronological constraints on the polymetamorphic evolution of the collisional granites, Araçuaí Orogen (SE Brazil). Anais da Academia Brasileira de Ciências 93(3), e20200639. https://doi.org/10.1590/0001-3765202120200639

Medeiros, S.R., Wiedemann-Leonardos, C.M., Mendes, J.C., 2000. Post-collisional multistage magmatism in the Ribeira mobile belt: geochemical and isotopic study of the Várzea Alegre intrusive complex, Espírito Santo, Brazil. Revista Brasileira de Geociências 30, 30-34.

Mello, F.M., 2000. Litogeoquímica e Química Mineral do Maciço Charnockítico Aimorés-MG. Universidade de São Paulo, São Paulo (Ph.D. Thesis, 167 pp.).

Mello, F.M., Machado, R., Bilal, E. 2011. Petrografia e Geoquímica do Complexo Charnockítico de Aimorés: Um Exemplo de Plutonismo Pós-orogênico do Cinturão Araçuaí/Ribeira. Revista do Instituto de Geociências – USP 11, 33-57.

Melo, M.G., Lana, C., Stevens, G., Pedrosa-Soares, A.C., Gerdes, A., Alkmin, L.A., Nalini Jr., H.A., Alkmim, F.F., 2017a. Assessing the isotopic evolution of S-type granites of the Carlos Chagas batholith, SE Brazil: Clues from U-Pb, Hf isotopes, Ti geothermometry and trace element composition of zircon. Lithos 284-285, 730-750.

Melo, M.G., Stevens, G., Lana, C., Pedrosa-Soares, A.C., Frei, D., Alkmim, F.F., Alkmin, L.A., 2017b. Two cryptic anatectic events within a syn-collisional granitoid from the Araçuaí orogen (southeastern Brazil): evidence from the polymetamorphic Carlos Chagas batholith. Lithos 277, 51–71.

Melo, M.G., Lana, C., Stevens, G., Hartwig, M.E., Pimenta, M.E., Nalini Jr., H.A., 2020. Deciphering the source of multiple U–Pb ages and complex Hf isotope composition in zircon from post-collisional charnockite-granite associations from the Araçuaí orogen (southeastern Brazil). Journal of South American Earth Sciences 103, 102792.

Mendes, J.C., McReath, I., Wiedemann, C.M., Figueiredo M.C.H., 1997. Charnockitóides do Maciço de Várzea Alegre: um novo exemplo do magmatismo cálcio-alcalino de alto-K no arco magmático do Espírito Santo. Revista Brasileira de Geociências 27, 13-24.

Mendes, J.C., Wiedemann, C.M., McReath, I., 2002. Norito e Charnoenderbitos da Borda do Maciço Intrusivo de Venda Nova, Espírito Santo. Anuário do Instituto de Geociências - UFRJ 25, 99-124.

Mendes, J.C., Medeiros, S.R., McReath, I., De Campos, C.M.P., 2005. Cambro-Ordovician magmatism in SE Brazil: U-Pb and Rb-Sr ages, combined with Sr and Nd isotopic data of Charnockitic rocks from the Várzea Alegre complex. Gondwana Research 8, 337-345.

Merdith, A.S., Collins, A., Williams, S.E., Pisarevsky, S., Foden, J.D., Archibald, D.B., Blades, M.L., Alessio, B.L., Armistead, S., Plavsa, D., Clark, C., Müller, R.D., 2017. A full-plate global reconstruction of the Neoproterozoic. Gondwana Research 50, 84-134.

Mondou, M., Egydio-Silva, M., Vauchez, A., Raposo, M.I.B., Bruiguier, O., Oliveira, A.F. 2012. Complex, 3D strain patterns in a synkinematic tonalite batholith from the Araçuaí Neoproterozoic orogen (Eastern Brazil): Evidence from combied magnetic and isotopic chronology studies. Journal of Structural Geology 39, 158-179.

Monié, P., Bosch, D., Bruguier, O., Vauchez, A., Rolland, Y., Nsungani, P., Buta Neto, A., 2012. The Late Neoproterozoic/Early Palaeozoic evolution of the West Congo Belt of NW Angola: geochronological (U-Pb and Ar-Ar) and petrostructural constraints. Terra Nova 24, 238–247.

Moreira, H.F., Danderfer, A., Costa A.F.O., Bersan, S.M., Lana, C.C., Queiroga, G.N., 2020 Record of Early Tonian mafic magmatism in the central Espinhaço (Brazil): New insights for break-up of the Neoproterozoic landmass ancestor of São Francisco-Congo paleocontinent. Geoscience Frontiers 11, 2323-2337.

Moyen, J.-F., Laurent, O., Chelle-Michou. C., Couzinié, S., Vanderhaeghe, O., Zeh, A., Villaros, A., Gardien, V., 2017. Collision vs. subduction-related magmatism: Two contrasting ways of granite formation and implications for crustal growth. Lithos 277, 154-177.

Munhá, J.M.U., Cordani, U.G., Tassinari, C.C.G., Palácios, T., 2005. Petrologia e termocronologia de Gnaisses Migmatíticos da Faixa de Dobramentos Araçuaí (Espírito Santo, Brasil). Revista Brasileira de Geociências 35, 123-134.

Nalini Jr., H.A., 1997. Caractérisation des suites magmatiques néoprotérozoiques de la region de Conselheiro Pena et Galiléia (Minas Gerais, Brésil). Etude géochimique et structurale des suites Galiléia et Urucum et relations avec les pegmatites à éléments rares associées. Ecole des Mines de Saint Etienne et Ecole des Mines de Paris (Ph.D. Thesis, 237 pp.).

Nalini Jr., H.A., Bilal, E., Correia Neves, J.M., 2000. Syn-collisional peraluminous magmatism in the Rio Doce region: mineralogy, geochemistry and isotopic data of the Urucum suite (eastern Minas Gerais state, Brazil). Revista Brasileira de Geociências 30, 120–125.

Narduzzi, F., Farina F., Stevens, Lana, C., Nalini Jr, H.A., 2017. Magmatic garnet in the Cordilleran-type Galiléia granitoids of the Araçuaí belt (Brazil): Evidence for crystallization in the lower crust. Lithos, 282-283, 82-97.

Narduzzi, F., 2018 Genesis and evolution of a Neoproterozoic magmatic arc: the Cordilleran-type granitoids of the Araçuaí Belt, Brazil. PhD Thesis, Escola de Minas, Departamento de Geologia, Universidade Federal de Ouro Preto, 245p.

Noce, C.M., Macambira, M.J.B., Pedrosa-Soares, A.C., 2000. Chronology of Neoproterozoic–Cambrian granitic magmatism in the Araçuaí Belt, Eastern Brazil, based on single zircon evaporation dating. Revista Brasileira de Geociências 30, 25–29.

Noce, C.M., Pedrosa-Soares, A.C., Piuzana, D., Armstrong, R., Laux, J.H., De Campos, C.M., Medeiros, S.R. 2004. Ages of sedimentation of the kinzigitic complex and of a late orogenic thermal episode of the Araçuaí Orogen, northern Espírito Santo State, Brazil: Zircon and monazite U-Pb SHRIMP and ID–TIMS data. Revista Brasileira de Geociências 34, 587-592.

Noce, C.M., Pedrosa-Soares, A.C., Silva, L.C., Alkmim, F.F., 2007a. O Embasamento Arqueano e Paleoproterozoico do Orógeno Araçuaí. Geonomos 15, 17 – 23.

Noce, C.M., Pedrosa-Soares, A.C., Silva, L.C., Armstrong, R., Piuzana, D., 2007b. Evolution of polycyclic basement complexes in the Araçuaí Orogen, based on U–Pb SHRIMP data: Implications for Brazil–Africa links in Paleoproterozoic time. Precambrian Research 159, 60–78.

Novo, T.A., Pedrosa-Soares, A.C., Noce, C.M., Alkmim, F.F., Dussin, I.A., 2010. Rochas charnockíticas do sudeste de Minas Gerais: a raiz granulítica do arco magmático do Orógeno Araçuaí. Revista Brasileira de Geociencias 40, 573–592.

Novo, T.A., 2013. Caracterização do Complexo Pocrane, magmatismo básico Mesoproterozóico e unidades neoproterozóicas do Sistema Araçuaí-Ribeira, com ênfase em geocronologia U-Pb (SHRIMP e LA-ICP-MS). PhD Thesis, Instituto de Geociências, Universidade Federal de Minas Gerais, 177 p.

Novo, T.A., Pedrosa-Soares, A., Vieira, V.S., Dussin, I., Silva, L.C., 2018. The Rio Doce Group revisited: An Ediacaran arc-related volcano-sedimentary basin, Araçuaí orogen (SE Brazil). Journal of South American Earth Sciences 85, 345-361.

Otamendi, J.E., Ducea, M.N., Bergantz, G.W., 2012., Geological, petrological and geochemical evidence for progressive construction of an arc crustal section, Sierra de Valle Fertil, Famatinian Arc, Argentina. Journal of Petrology 53,761–800.

Pacheco, F.E.R.C., Caxito, F.A., Pedrosa-Soares, A.C., Dussin, I.A., Gonçalves-Dias, T., 2021. Detrital zircon U-Pb and Lu-Hf data for a kinzigitic gneiss (Jequitinhonha Complex, Araçuaí Orogen, SE Brazil) constrain the age of a huge storage of Ediacaran carbon. Journal of South American Earth Sciences 105, 102709.

Paes, V.J.C., 1999. Geologia e Geoquímica da Região de Alvarenga, Minas Gerais: implicações geotectônicas e metalogenéticas, Universidade Federal de Minas Gerais, Belo Horizonte, MS Dissertation, 173p.

Paes, V.J.C., Raposo, F.O., Pinto, C.P., Oliveira, F.A.R. (Orgs.), 2010. Projeto Jequitinhonha, Estados de Minas Gerais e Bahia: texto explicativo. Geologia e Recursos Minerais das Folhas Comercinho, Jequitinhonha,

Almenara, Itaobim, Joaíma e Rio do Prado. Programa Geologia do Brasil. CPRM – Serviço Geológico do Brasil, Belo Horizonte.

Paterson, S.R., Ducea, M.N., 2015. Arc Magmatic Tempos: Gathering the Evidence. Elements 11, 91-98.

Pedrosa Soares, A.C., Wiedemann-Leonardos, C.M., 2000. Evolution of the Araçuaí Belt and its connection to the Ribeira Belt, eastern Brazil. In: Cordani, U.G., Milani, E.J., Thomaz Filho, A., Campo, D.A. (Eds.). Tectonic evolution of South America. Rio de Janeiro, 31st International Geological Congress, p. 265-285.

Pedrosa-Soares, A.C., Noce, C.M., Wiedemann, C., Pinto, C.P., 2001. The Araçuaí- West-Congo Orogen in Brazil: An overview of a confined orogen formed during Gondwanaland Assembly. Precambrian Research 110, 307-323.

Pedrosa-Soares, A.C., Queiroga, G.N., Gradim, C.T., Roncato, J.G., Novo, T.A., Jacobsohn, T., Silva, K.L., 2006. Nota Explicativa da Folha Mantena, 1:100.000. Programa Geologia do Brasil, CPRM–UFMG.

Pedrosa-Soares, A.C., Alkmim, F.F., Tack, L., Noce, C.M., Babinski, M., Silva, L.C., Martins- Neto, M.A., 2008. Similarities and differences between the Brazilian and African counterparts of the Neoproterozoic Araçuaí-West Congo orogeny. In: Pankhurst, R.J., Trouw, R.A.J., Brito Neves, B.B., De Wit, M.J. (Eds.), West Gondwana: Pre-Cenozoic Correlations Across the South Atlantic Region. London, Geological Society of London, Special Publication 294, 153- 172.

Pedrosa-Soares, A.C., De Campos, C.P., Noce, C.M., Silva, L.C., Novo, T., Roncato, J., Medeiros, S., Castañeda, C., Queiroga, G., Dantas, E., Dussin, I., Alkmim, F., 2011. Late Neoproterozoic-Cambrian Granitic Magmatism in the Araçuaí Orogen (Brazil), the Eastern Brazilian Pegmatite Province and Related Mineral Resources. In: Sial, A.N., Bettencourt, J.S., De Campos, C.P., Ferreira, V.P. (Eds.), Granite-Related Ore Deposits. London, Geological Society of London, Special Publication 350, 25–51.

Pedrosa-Soares, A.C., Deluca, C., Araujo, C., Gradim, C., Lana, C., Dussin, I., Silva, L.C., Babinski, M., 2020. O Orógeno Araçuaí à luz da geocronologia: Um tributo a Umberto Cordani. In: Bartorelli, A., Teixeira, W., Brito Neves, B.B., Geocronologia e Evolução Tectônica do Continente Sul-Americano: a contribuição de Umberto Giuseppe Cordani. Solarias Edições Culturais, São Paulo, 728p.

Peixoto, E., Pedrosa-Soares, A.C., Alkmim, F.F., Dussin, I.A., 2015. A suture-related accretionary wedge formed in the Neoproterozoic Araçuaí orogen (SE Brazil) during Western Gondwanaland assembly. Gondwana Research 27, 878-896.

Peixoto, C.A., Heilbron, M., Ragatky, D., Armstrong, R., Dantas, E., Valeriano, C.M., Simonetti, A. 2017. Tectonic evolution of the Juvenile Tonian Serra da Prata magmatic arc in the Ribeira belt, SE Brazil: Implications for early West Gondwana amalgamation. Precambrian Research 302, 221-254.

Petitgirard, S., Vauches, A., Egydio-Silva, M., Bruguier, O., Camps, P., Monié, P., Babinski, M., Mondou, M., 2009. Conflicting structural and geochronological data from the Ibituruna quartz-syenite (SE Brazil): effect of protracted “hot” orogeny and slow cooling rate? Tectonophysics 477, 174–196.

Potratz, G.L. 2020. Petrogênese e geocronologia U-Pb do Granito Sana, Faixa Ribeira, e dos Complexos Intrusivos de Santa Angélica e Várzea Alegre, Faixa Araçuaí. Universidade do Estado do Rio de Janeiro (MS Dissertation, 256p.).

Richter, F., Lana, C., Steven, G., Buick, I., Pedrosa-Soares, A.C., Alkmim, F.F., Cutts, K., 2016. Sedimentation, metamorphism and granite generation in a back-arc region: Records from the Ediacaran Nova Venécia Complex (Araçuaí Orogen, Southeastern Brazil). Precambrian Research 272, 78–100.

Rollinson H.R. 2007. Early Earth systems: a geochemical approach. Oxford, Blackwell. 285p. ISBN: 978-1-405-12255-9.

Roncato, J.G., 2009. As suítes graníticas tipo–S do norte do Espírito Santo na região das folhas Ecoporanga, Mantena, Montanha e Nova Venécia. MS Dissertation, Universidade Federal de Minas Gerais, Belo Horizonte, 102 p.

Rosa, M.d.L.d.S., Conceição, H., Macambira, M.J.B., Galarza, M.A., Cunha, M.P., Menezes, R.C.L., Marinho, M.M., Filho, B.E.d.C., Rios, D.C., 2007. Neoproterozoic anorogenic magmatism in the Southern Bahia Alkaline Province of NE Brazil: U–Pb and Pb-Pb ages of the blue sodalite syenites. Lithos 97, 88–97.

Santiago, R., Caxito, F.A., Pedrosa-Soares, A.C., Neves, M.A., Dantas, E.L., 2020a. Tonian Island Arc Remnants in the Northern Ribeira Orogen of Western Gondwana: The Caxixe Batholith (ESPÍRITO SANTO, SE BRAZIL), Precambrian Research 351, 105944

Santiago, R., Caxito, F.A., Neves, M., A., Dantas, E.L., Medeiros Júnior, E.B., Queiroga, G.N., 2020b. Two generations of mafic dyke swarms in the Southeastern Brazilian coast: reactivation of structural lineaments during the gravitational collapse of the Araçuaí-Ribeira Orogen (500 Ma) and West Gondwana breakup (140 Ma). Precambrian Research 340, 105344.

Schannor, M., Lana, C., Fonseca, M. 2019. São Francisco-Congo Craton break-up delimited by U-Pb-Hf isotopes and trace-elements of zircon from metasediments of the Araçuaí Belt. Geoscience Frontiers 10, 611-628.

Schannor, M., Lana, C., Mazoz, A., Narduzzi, F., Cutts, K., Fonseca, M. 2020. Paleoproterozoic sources for Cordilleran-type Neoproterozoic granitoids from the Araçuaí orogen (SE Brazil): Constraints from Hf isotope zircon composition. Lithos 378–379, 105815.

Serrano, P., Pedrosa-Soares, A., Medeiros-Junior, E., Fonte-Boa, T., Araujo, C., Dussin, I., Queiroga, G., Lana, C., 2018. A-type Medina batholith and post-collisional anatexis in the Araçuaí orogen (SE Brazil). Lithos 320-321, 515-536.

Schiavetti, L., 2019. Metamorfismo e geocronologia em orógenos quentes – o caso do Complexo Nova Venécia, Orógeno Araçuaí. Universidade Estadual de Campinas, Campinas (MS Dissertation, 174p.).

Serrano, P., Pedrosa-Soares, A., Medeiros-Junior, E., Fonte-Boa, T., Araujo, C., Dussin, I., Queiroga, G., Lana, C., 2018. A-type Medina batholith and post-collisional anatexis in the Araçuaí orogen (SE Brazil). Lithos 320-321, 515-536.

Siga-Júnior O., 1986. A evolução geocronológica da porção nordeste de Minas Gerais, com base em interpretações geocronológicas. MS Dissertation, IG-USP, São Paulo.

Silva, L.C., Armstrong, R., Noce, C.M., Carneiro, M., Pimentel,M., Pedrosa-Soares, A.C., Leite, C., Vieira, V.S., Silva, M., Paes, V., Cardoso-Filho, J., 2002. Reavaliação da evolução geológica em terrenos pré-cambrianos brasileiros com base em novos dados U–Pb SHRIMP, parte II: Orógeno Araçuaí, Cinturão Móvel Mineiro e Cráton São Francisco Meridional. Revista Brasileira de Geociências 32, 513–528.

Silva, M.A., Camozzato, E., Paes, V.J.C., Junqueira, P.A., Ramgrab, G. E. 2004. Folha SF.24-Vitoria. In: Schobbenhaus, C., Gonçalves, J.H., Santos, J.O.S., Abram, M.B., Leão Neto, R., Matos, G.M.M., Vidotti, R.M., Ramos, M.A.B., Jesus, J.D.A. de. (Eds.). Carta Geológica do Brasil ao Milionésimo, Sistema de Informações Geográficas. Programa Geologia do Brasil. CPRM, Brasília.

Silva, L.C., McNaughton, N.J., Armstrong, R., Hartmann, L.A., Fletcher, I.R., 2005. The Neoproterozoic Mantiqueira Province and its African connections: a zircon-based U-Pb geochronologic subdivision for the Brasiliano/Pan-African systems of orogens. Precambrian Research 136, 203–240.

Silva, L.C., Pinto, C.P., Gomes, A.C., Paes, V.C., Chemale, F., 2007. Granitogenesis at the northern tip of the Araçuaí Orogen, SE Brazil: LA-ICP-MS U–Pb zircon geochronology, and tectonic significance. In: Simpósio de Geologia do Sudeste.Diamantina, Anais, pp. 20–21.

Silva, L.C., Pedrosa-Soares, A.C., Teixeira, L.R., Armstrong, R., 2008. Tonian rift-related, A-type continental plutonism in the Araçuaí Orogen, eastern Brazil: new evidence for the breakup stage of the São Francisco-Congo Paleocontinent. Gondwana Research 13, 527–537.

Silva, L.C., Pedrosa-Soares, A.C., Armstrong, R., Noce, C.M., 2011. Determinando a duração do período colisional do Orógeno Araçuaí com base em geocronologia U–Pb de alta resolução emzircão: uma contribuição para a história da amalgamação do Gondwana Ocidental. Geonomos 19, 180–197.

Silva Sá, J.H., 1977. Pegmatitos Litiníferos da região de Itinga-Araçuaí, Minas Gerais. PhD Thesis, Universidade de São Paulo, São Paulo.

Silveira-Braga, F.C., Rosière, C.A., Santos, J.O.S., Hagemann, S.G., McNaughtone, N.J., Salles, P.V., 2019. The Horto-Baratinha itabirite-hosted iron ore: A basal fragment of the Espinhaço basin in the eastern São Francisco Craton. Journal of South American Earth Sciences 90, 12–33.

Soares, C.C.V., Queiroga, G., Pedrosa-Soares, A.C., Gouvêa, L.P., Valeriano, C.M., Melo, M.G., Marques, R.A., Freitas, R.D.A., 2020. The Ediacaran Rio Doce magmatic arc in the Araçuaí – Ribeira boundary sector, southeast Brazil: Lithochemistry and isotopic (Sm–Nd and Sr) signatures. Journal of South American Earth Sciences 102880.

Söllner, F., Lammerer, B., Weber-Diefenbach, K., 1991. Die Krustenentwicklung in Der Küstenregion Nördlich Von Rio de Janeiro, Brasilien. Münchener Geowis-senschaftliche Hefte 11. Friedrich Pfeil Verlag, München, pp. 4.

Söllner, F., Lammerer, B., Wiedemann-Leonardos, C., 2000. Dating the Ribeira Mobile Belt of Brazil. In: Sonderheft, Zeitschrift Angwandte Geologie pp. 245-255.

Souza, M.E., Martins, M.S., Queiroga, G.N., Leite, M., Oliveira, R.G., Dussin, I., Pedrosa-Soares, A.C., 2019. Paleoenvironment, sediment provenance and tectonic setting of Tonian basal deposits of the Macaúbas basin system, Araçuaí orogen, southeast Brazil. Journal of South American Earth Sciences 96, 102393.

Souza, M.E., Martins, M.S., Queiroga, G.N., Pedrosa-Soares, A.C., Dussin, I., Castro, M.P., Serrano, P., 2022. Time and isotopic constraints for Early Tonian basaltic magmatism in a large igneous province of the São Francisco – Congo paleocontinent (Macaúbas basin, Southeast Brazil). Precambrian Research 373, 106621. https://doi.org/10.1016/j.precamres.2022.106621

Straathof, G.B., 2011. Neoproterozoic Low Latitude Glaciations: An African Perspective. Ph.D. Thesis, Universidade de Edinburgo, Edinburgo.

Tang, M., Wang, X.-L., Shu, X.-J., Wang, D., Yang, T., Gopon, P. 2014. Hafnium isotopic heterogeneity in zircons from granitic rocks: geochemical evaluation and modelling of "zircon effect" in crustal anatexis. Earth and Planetary Science Letters 389, 188-199.

Tedeschi, M., Novo, T., Pedrosa-Soares, A., Dussin, I., Tassinari, C., Silva, L.C., Gonçalves, L., Alkmim, F., Lana, C., Figueiredo, C., Dantas, E., Medeiros, S., De Campos, C., Corrales, F., Heilbron, M., 2016. The Ediacaran Rio Doce magmatic arc revisited (Araçuaí-Ribeira orogenic system, SE Brazil). Journal of South American Earth Sciences 68, 167-186.

Teixeira, P.A.D., Fernandes, C.M., Mendes, J.C., Medeiros, S.R., Rocha, I.S., 2020. U-PB LA-ICP-MS and geochemical data of the Alto Chapéu Pluton: Contributions on bimodal post-collisional magmatism in the Araçuaí belt (SE Brazil). Journal of South American Earth Sciences 103, 102724.

Temporim, F.A., Trindade, R.I.F., Tohver, E., Soares, C.C., Gouvêa, L.P., Egydio-Silva, M., Amaral, C.A.D., Souza Jr., G.F., 2020. Magnetic fabric and geochronology of a Cambrian “isotropic” pluton in the Neoproterozoic Araçuaí orogen. Tectonics.

Thiéblemont D., Castaing C., Billa M., Bouton P., Préat A. 2009. Notice explicative de la carte géologique et des ressources minérales de la République gabonaise à 1/1,000,000. Editions DGMG - Ministère des Mines, du Pétrole, des Hydrocarbures, Libreville, 384 p.

Trompette R. 1994. Geology of Western Gondwana (2000–500 Ma). In: Pan-African/Brasiliano aggregation of South America and Africa. A.A. Balkema, Rotterdam, 350 p.

Trompette R. 1997. Neoproterozoic (~600 Ma) aggregation of Western Gondwana: a tentative scenario. Precambrian Research. 82: 101–112.

Tuller, M.P., 1993. Geologia da Folha Colatina. In: Tuller M.P. (eds.) Programa de Levantamentos Geológicos Básicos do Brasil, Folha SE.24-Y-C-VI - Colatina. Brasília, DNPM/CPRM, p. 3-143.

Tupinambá, M., Heilbron, M., Valeriano, C.M., Porto, Jr. R., Blanco de Dios, F., Machado, N., Silva, L.G.E., Almeida, J.C.H., 2012. Juvenile contribution of the Neoproterozoic Rio Negro magmatic arc (Ribeira Belt, Brazil): implications for western Gondwana amalgamation. Gondwana Research 21, 422–438.

Uhlein, A., Roncato, J., Egydio-Silva, M., Parizek-Silva, Y., Alves, M., 2014. Geologia, Petrologia e Contexto Geotectônico dos Gnaisses e Granitóides da Região de Colatina, Espírito Santo. Geonomos 22, 66-83.

Vauchez, A., Egydio-Silva, M., Babinski, M., Tommasi, A., Uhlein, A., Liu D., 2007. Deformation of a pervasively molten middle crust: insights from the Neoproterozoic Ribeira-Araçuaí orogen (SE Brazil). Terra Nova 19, 278-286.

Vauchez, A., Hollanda, M.H.B.M, Monié, M., Mondou, M., Egydio-Silva, M., 2019. Slow cooling and crystallization of the roots of the Neoproterozoic Araçuaí hot orogen (SE Brazil): Implications for rheology, strain distribution, and deformation analysis. Tectonophysics 766, 500-518.

Victoria, A.M., Pedrosa-Soares, A., Cruz, S.C.P. 2019. Os riftes neoproterozoicos precursores ao Orógeno Araçuaí – Congo Ocidental: atualização dos limites de tempo com base em idades (U-Pb e Pb-Pb) do magmatismo anorogênico. In: XVII Simpósio Nacional de Estudos Tectônicos, SBG, Bento Gonçalves, Anais..., p. 111.

Vieira, V.S., 2007. Significado do Grupo Rio Doce no Contexto do Orógeno Araçuaí. Ph.D. Thesis, Universidade Federal de Minas Gerais, Belo Horizonte, 117 p.

Vieira, V.S., Menezes, R.G. (Orgs.), 2015. Geologia e Recursos Minerais do Estado do Estado do Espírito Santo: texto explicativo do mapa geológico e de recursos minerais, escala 1:400.000. Programa Geologia do Brasil, CPRM - Serviço Geológico do Brasil, Belo Horizonte.

Xavier B.C. 2017. Relações tectônicas no setor central da Faixa Araçuaí: Análise Estrutural por ASM e Geocronologia U-Pb e Lu-Hf. MS Dissertation, Universidade de São Paulo, São Paulo, 123 p.

Whalen, J.B., Hildebrand, R.S., 2019. Trace element discrimination of arc, slab failure, and A-type granitic rocks. Lithos 348-349, 105179.

Whitney, D.L., Evans, B.W., 2010. Abbreviations for names of rock-forming minerals. American Mineralogist 95, 185-187.

Wiedemann, C.M., Medeiros, S.R., Ludka, I.P., Mendes, J.C., Costa-de-Moura, J., 2002. Architecture of late orogenic plutons in the Araçuaí-Ribeira fold belt, Southeast Brazil. Gondwana Research 5, 381-399.

Zanon, M.L., Chaves, A.O., Rangel, C.V.G.T., Gaburo, L., Pires, C.R., 2015. Os aspectos geológicos do Maciço Santa Angélica (ES): uma nova abordagem. Brazilian Journal of Geology 45, 609-633.

APPENDIX A - Conference Abstracts

XVII SIMPÓSIO NACIONAL DE ESTUDOS TECTÔNICOS
XI INTERNATIONAL SYMPOSIUM ON TECTONICS
XI SIMPÓSIO SUL-BRASILEIRO DE GEOLOGIA
26 a 29 de maio de 2019 | Bento Gonçalves - RS - Brasil

PRIMEIRO REGISTRO DE MAGMATISMO JUVENIL NO ARCO MAGMÁTICO RIO DOCE, ORÓGENO ARAÇUAÍ MERIDIONAL

Araujo, C.[1*]; Pedrosa-Soares, A.[1]; Lana, C.[2]; Tedeschi, M.[1]; Dussin, I.[3]

[1]Universidade Federal de Minas Gerais, Programa de Pós-Graduação em Geologia, CPMTC-IGC, *crisgeo@ufmg.br

[2]Universidade Federal de Ouro Preto, Departamento de Geologia

[3]Universidade do Estado do Rio de Janeiro, Faculdade de Geologia

RESUMO

O sistema orogênico Araçuaí – Congo Ocidental constitui um orógeno confinado a um grande embainhamento do Cráton São Francisco – Congo, amalgamados no Paleocontinente Gondwana ao final do Neoproterozoico. Mesmo nessa singular situação geotectônica, o Orógeno Araçuaí registra uma sucessão de eventos de magmatismo orogênico que são típicos dos estágios pré-colisional, colisional e pós-colisional dos orógenos de margem continental ativa, diretamente relacionados à subducção de litosfera oceânica, sucedida por colisão de margens continentais. O magmatismo pré-colisional está materializado no Arco Rio Doce, cujo plutonismo é majoritariamente constituído por tonalitos e granodioritos, portadores a ricos em enclaves máficos a dioríticos, com fácies e plútons individuais gabronoríticos subordinados. As rochas do Arco Rio Doce geralmente mostram a foliação dúctil regional e enclaves estirados, mas há partes localmente preservadas da deformação regional. As assinaturas litoquímicas de mais de 300 amostras de rochas plutônicas e vulcânicas demonstram a consistente assinatura magnesiana, metaluminosa (tipo I) e cálcio-alcalina expandida do Arco Rio Doce, ao passo que os atributos isotópicos (de Nd, Sr e Hf) e zircões herdados evidenciam sua evolução em margem continental ativa, com marcante contribuição do embasamento riaciano na geração dos magmas. Datações U-Pb em zircão de mais de 50 amostras demonstram que o período pré-colisional e a consequente edificação do Arco Rio Doce se deu entre ca. 630 Ma e ca. 580 Ma. Para o presente trabalho, foram realizados estudos petrográficos, litoquímicos e análises isotópicas U-Pb e Lu-Hf (LA-ICP-MS) em zircão sobre amostras (CA-03 e CA-08) de dois corpos granodioríticos que representam o Arco Rio Doce na região centro-norte do Estado do Espírito Santo. Sua assinatura litoquímica (tipo I, magnesiana, cálcio-alcalina, de médio K) enquadra-se no conjunto do Arco Rio Doce. Os dados U-Pb obtidos em zircões ígneos forneceram idades concórdia de 593 +/- 5 Ma (MSWD = 0,62; 32 grãos) para CA-03, e de 610 +/- 5 Ma (MSWD = 0,72; 27 grãos) para CA-08. A assinatura isotópica Lu-Hf (25 grãos de zircão) para a amostra CA-03, com epsilon Hf(t) entre -1,7 e -21,6, e idades-modelo TDM de ca. 1,3 a ca. 2,4 Ga, sugere envolvimento de magma essencialmente crustal. Entretanto, assinatura moderadamente juvenil é marcante nos zircões (21 grãos) da amostra CA-08, que revelam valores de epsilon Hf(t) entre +2,3 e -4,4, com idades-modelo TDM de ca. 1,1 Ga a ca. 1,5 Ga. Essas são, portanto, as primeiras evidências isotópicas do envolvimento de magmas juvenis na geração de rochas graníticas do Arco Rio Doce. Isto, somado à presença de rochas gabronoríticas e dioríticas, é mais uma evidência do envolvimento de subducção de litosfera oceânica na edificação do Arco Rio Doce. A descoberta de componentes juvenis também indica que os magmas quimicamente menos evoluídos e mais antigos do Arco Rio Doce se colocaram a leste e que a subducção sofreu retração para oeste, como aventado em modelo anterior.

28 a 30 | *junho de 2021* | *Brasília - DF*

287 ISBN | 978-65-992688-1-6

CARACTERIZAÇÃO TEXTURAL E ISOTÓPICA (U-Pb E Lu-Hf) DE ZIRCÃO COMO INDICADOR PETROGENÉTICO EM BORDAS DE PLÚTONS PÓS-COLISIONAIS (ORÓGENO ARAÇUAÍ, ESTADO DO ESPÍRITO SANTO)

Araujo, C.[1]; Pedrosa-Soares, A.[1]; Lana, C.[2]*; Dussin I.[3]*; Queiroga, G.[2]*; Serrano, P.[2]; Medeiros-Júnior, E.[2]*

[1]Universidade Federal de Minas Gerais, Programa de Pós-graduação em Geologia, CPMTC-IGC; [2]Universidade Federal de Ouro Preto; [3]Universidade do Estado do Rio de Janeiro, *Pesquisadores do CNPQ

RESUMO: O zircão é um mineral particularmente útil para investigações da evolução da litosfera, sendo amplamente utilizado para obter informações geocronológicas e petrogenéticas. Nas bordas de plútons graníticos, esse mineral pode registrar diferentes estágios da história ígnea, desde o alojamento da intrusão até a cristalização tardia do magma, bem como eventual assimilação das rochas encaixantes. Além do completo mapeamento geológico sistemático, o Orógeno Araçuaí também conta com grande quantidade de dados analíticos que permitem caracterizar sua diversidade de rochas ígneas e meta-ígneas, as quais, em decorrência de associações litológicas típicas distribuídas no espaço e no tempo, remetem a diferentes estágios orogênicos, incluindo o Arco Magmático Rio Doce formado no estágio pré-colisional (630 – 585 Ma), grande quantidade de granitos tipo S originados no estágio colisional (585 – 540 Ma) e de intrusões pós-colisionais (530 – 480 Ma). As diferentes associações litológicas originadas nesses estágios evolutivos requerem distintos processos tectônicos e térmicos, cuja explicação mais plausível inclui subducção de litosfera oceânica (registrada por corpos ofiolíticos localizados a oeste do Arco Rio Doce), sucedida por colisão de margens continentais, e processos de desestabilização do manto astenosférico durante colapso gravitacional do edifício orogênico. Com o intuito de entender processos petrogeneticos em intrusões pós-colisionais do Orógeno Araçuaí, realizou-se um estudo focalizado na caracterização textural e isotópica (U-Th-Pb e Lu-Hf) de zircões em amostras coletadas nas bordas de três plutons graníticos distintos (Aracê - Pedra Azul, Vitória e Mestre Álvaro), localizados na região centro-sul do Estado do Espírito Santo, e em rochas regionais, como paragnaisses migmatíticos do Complexo Nova Venécia e metagranitos tipo-S, colisionais, da Suíte Ataléia. Também foram realizadas análises litoquímicas, além de um estudo detalhado da morfologia dos zircões das amostras pós-colisionais. Os zircões das bordas das intrusões apresentam formas prismáticas longas, cristais não-zonados a fracamente zonados, frequentemente rodeados por domínios de dissolução–recristalização ou finas bordas de sobrecrescimento e elevada razão Th/U. Idades U-Pb (LA-ICP-MS) indicam cristalização magmática nas bordas dos plútons em 523 +/- 2 Ma (Aracê - Pedra Azul), 505 +/- 1 Ma (Vitória) e 527 +/- 2 Ma (Mestre Álvaro). Os parâmetros épsilon Hf(t) e idades-modelo TDM resultantes das análises Lu-Hf (Aracê: -18,6 a -23,8 e 2,25 a 2,47 Ga; Vitória: 7,4 a -10,3 e 1,58 a 1,71 Ga; Mestre Álvaro: -0,7 a -8,8 e 1,27 a 1,66 Ga; paragnaisses Nova Venécia: +4,1 a -39,2 e 1,20 a 3,47 Ga; e metagranito Ataléia: -3,2 a -8,1 e 1,42 a 1,64 Ga) apontam uma importante participação de rochas encaixantes na gênese dos plutons. Geotermometria de saturação de zircão indica temperaturas acima de 800 °C nas bordas dos plútons. Em conclusão, os zircões estudados cristalizaram-se a partir de magmas alcalinos a cálcio-alcalinos com baixos teores de U, Y, HREE e P, em relação a Zr, sob altas taxas de resfriamento. Após a colocação dos plútons, as alterações nos zircões por processos de dissolução - recristalização e sobrecrescimento ocorreram em resposta a interações com fluidos deutéricos ao final da cristalização magmática.

PALAVRAS-CHAVE: GEOQUÍMICA ISOTÓPICA U-Pb-Hf; GRANITOS PÓS-COLISIONAIS; ORÓGENO ARAÇUAÍ

APPENDIX B - Supplementary File 3.A: Geochemistry Data

Geochemistry data

Local name	Rock-type*	Sample	SiO_2	TiO_2	Al_2O_3	FeO(t)[a]	Fe_2O_3	MnO	MgO	CaO	Na_2O	K_2O	P_2O_5	Ba	Rb	Sr	Zn	Zr	V	Ce	Co	Cs	Cu	Dy	Er	Eu	Ga	Gd
Jequitibá	Grt-Bt metagranodiorite	CA-03	70.6	0.31	15.6	2.58	2.87	0.03	1.1	4.64	2.62	1.63	0.11	512	62.5	405	128	201	21	98	86.8	1.1	<5	2.05	0.78	1.61	20.3	3.53
Santa Tereza	Bt metagranodiorite	CA-08	65.5	0.91	15.6	3.96	4.4	0.03	2.23	4.3	2.99	2.14	0.24	219	81.4	266	85	217	75	184.5	112	0.94	16	7.07	1.97	1.61	17.2	13.56
Santa Tereza	Grt-Opx-Bt metagranodiorite	CA-14	69.5	0.45	15.9	3.77	4.19	0.06	1.2	3.62	3.13	3.06	0.14	593	98	217	71	136	23	65.4	102	2.42	<5	4.41	2.22	1.35	17	4.86
Santa Tereza	Opx-Bt metadiorite	CA-17	57.3	1.61	16.7	7.87	8.75	0.14	2.91	5.16	2.99	2.75	0.77	908	83.8	359	157	544	109	108.1	42.1	1.04	18	5.07	2.42	1.89	15.8	7.72
Santa Tereza	Opx-Cpx-Bt metamonzogabbro	CA-18A	50.1	2.49	17.9	10.35	11.5	0.2	4.48	7.07	3.67	1.58	0.82	538	57.2	604	134	252	165	88.9	41.4	0.94	55	7.01	3.38	2.64	22.9	8.96
Santa Tereza	Bt metagranodiorite	CA-19	70.3	0.56	15.2	3.05	3.39	0.02	1.11	3.84	3.06	2.38	0.13	613	104.3	428	56	237	26	121.5	86	1.29	20	1.72	0.57	1.83	18	3.83
Santa Tereza	Grt-Opx-Bt metagranodiorite	CA-20A	69.7	0.56	16.7	2.39	2.66	0.02	1.31	4.66	3.51	1.9	0.2	274	68.1	345	27	226	126	61.4	99.5	0.84	<5	5.19	1.76	1.89	20.5	6.59
Santa Tereza	Grt-Opx-Bt metagranodiorite	CA-21A	75.5	0.52	10.6	6.95	7.72	0.06	0.58	2.38	2.12	2.05	0.02	366	52.8	118	97	443	178	71	122.9	0.65	<5	1.54	0.68	1.22	20.6	3.22
Santa Tereza	Opx-Bt metatonalite	CA-24	65.7	0.66	16.5	5.13	5.7	0.09	1.79	4.62	3.03	2.48	0.19	731	94.8	264	77	136	61	48.7	73.5	2.12	7	3.61	2.21	1.52	18.7	4.46
Santa Tereza	Opx-Bt metatonalite	CA-25	65.6	0.64	16.7	4.44	4.93	0.08	1.79	4.92	3.08	1.79	0.14	378	89.1	213	44	175	113	50.5	69.8	4.44	10	4.95	2.83	1.39	19.6	4.4
Jequitibá	Bt metadiorite	CA-30	56.8	1.92	17.1	6.78	7.54	0.07	2.73	5.14	2.87	3	0.77	3272	133.9	952	127	805	125	298.6	54.7	1.09	34	6.86	2.78	4.86	25.2	13.93
Jequitibá	Grt-Bt metagranodiorite	CA-31	65.6	0.7	15.9	5.23	5.81	0.05	1.96	4.13	3.04	2.34	0.17	412	134.9	228	91	142	99	89.9	76	3.55	12	2.83	0.9	1.7	24.1	5.77
Jequitibá	Grt-Bt metagranodiorite	CA-32	65.2	0.72	17.3	4.71	5.24	0.07	1.82	4.2	3.49	2.7	0.27	284	135.3	161	88	288	87	53.5	66.1	3.59	16	4.59	2.17	1.39	24.4	5.71

[a] $FeO(t)=Fe_2O_3$ (analysis)×0.8998

[b] Normalized elements for chondrite (Boynton, 1984).

$Eu/Eu^* = Eu_N / [(Sm_N) + (Gd_N)]^{1/2}$

* Mineral abbreviations, in accordance to Whitney and Evans (2010): Bt, biotite; Crd, cordierite; Grt, garnet; Opx, orthopyroxene; Cpx, clinopyroxene

Local name	Rock-type*	Sample	Hf	Ho	La	Lu	Mo	Nb	Nd	Ni	Pr	Sm	Sn	Ta	Tb	Th	Tl	Tm	U	Y	Yb	LOI
Jequitibá	Grt-Bt metagranodiorite	CA-03	5.4	0.31	47.8	0.1	4	10.13	40.2	6	10.88	6.2	<0,3	0.75	0.42	11.8	0.6	0.1	0.93	9.34	0.6	0.63
Santa Tereza	Bt metagranodiorite	CA-08	6.07	1.01	80.3	0.1	3	14.02	81.1	40	21.61	17	1.1	0.96	1.62	53.1	<0,5	0.21	0.65	25.28	0.9	0.71
Santa Tereza	Grt-Opx-Bt metagranodiorite	CA-14	4.17	0.79	33.7	0.31	4	7.26	29.3	9	7.96	6	1.2	1.05	0.75	9.6	<0,5	0.3	0.68	20.51	2	0.21
Santa Tereza	Opx-Bt metadiorite	CA-17	5.59	0.94	48.9	0.35	<2	17.12	56.8	16	14.38	9.8	1.3	0.91	1.01	3.6	<0,5	0.39	0.18	22.17	2.6	0.57
Santa Tereza	Opx-Cpx-Bt metamonzogabbro	CA-18A	5.58	1.25	47.6	0.37	2	56.54	49	20	12.34	10.1	4.5	3.46	1.24	0.5	<0,5	0.44	0.41	31.3	2.6	0.16
Santa Tereza	Bt metagranodiorite	CA-19	8.53	0.25	64.8	0.06	3	11.83	47	12	13.74	6.5	1.5	0.99	0.4	15.1	<0,5	0.07	0.59	6.48	0.5	1.33
Santa Tereza	Grt-Opx-Bt metagranodiorite	CA-20A	6.47	0.84	36.3	0.11	6	9.72	29.7	17	7.84	7.2	0.5	1.16	0.96	12.6	<0,5	0.2	0.64	21.28	0.8	0.43
Santa Tereza	Grt-Opx-Bt metagranodiorite	CA-21A	13.7	0.26	37.1	0.11	5	3.52	29.5	28	8.48	5	3.8	0.93	0.36	14.4	<0,5	0.08	0.64	6.21	0.6	0.11
Santa Tereza	Opx-Bt metatonalite	CA-24	4.45	0.71	25.9	0.31	3	6.99	23.1	13	6.23	5.1	2.3	0.83	0.63	5.1	<0,5	0.29	0.35	18.83	1.9	0.26
Santa Tereza	Opx-Bt metatonalite	CA-25	5.01	1.02	29.7	0.36	4	6.58	21.9	14	6.12	4.5	3	0.89	0.82	5.9	<0,5	0.41	0.76	26.08	2.5	0.24
Jequitibá	Bt metadiorite	CA-30	20.29	1.12	145.1	0.26	3	19.41	154.1	19	41.13	23.9	2.8	0.95	1.53	8.7	<0,5	0.34	0.64	27.99	2	0.94
Jequitibá	Grt-Bt metagranodiorite	CA-31	4.91	0.41	54.6	0.09	6	16.62	39.3	20	10.82	7.3	3.2	3.57	0.64	12.2	0.7	0.1	0.62	9.33	0.5	0.65
Jequitibá	Grt-Bt metagranodiorite	CA-32	7.81	0.82	32.4	0.21	3	24.36	25.1	19	6.68	5.5	1.3	2.29	0.84	6.4	0.5	0.26	1.01	21.61	1.5	0.43

Local name	Rock-type*	Sample	Eu/Eu*[b]	La_N/Yb_N[b]	La_N/Sm_N[b]	Ce_N/Yb_N[b]	Ce_N/Sm_N[b]	Eu_N/Yb_N[b]
Jequitibá	Grt-Bt metagranodiorite	CA-03	1.05	53.71	4.85	42.25	3.81	7.63
Santa Tereza	Bt metagranodiorite	CA-08	0.32	60.15	2.97	53.03	2.62	5.09
Santa Tereza	Grt-Opx-Bt metagranodiorite	CA-14	0.76	11.36	3.53	8.46	2.63	1.92
Santa Tereza	Opx-Bt metadiorite	CA-17	0.66	12.68	3.14	10.75	2.66	2.07
Santa Tereza	Opx-Cpx-Bt metamonzogabbro	CA-18A	0.85	12.34	2.96	8.84	2.12	2.89
Santa Tereza	Bt metagranodiorite	CA-19	1.12	87.38	6.27	62.86	4.51	10.41
Santa Tereza	Grt-Opx-Bt metagranodiorite	CA-20A	0.84	30.59	3.17	19.85	2.06	6.72
Santa Tereza	Grt-Opx-Bt metagranodiorite	CA-21A	0.93	41.69	4.67	30.61	3.43	5.78
Santa Tereza	Opx-Bt metatonalite	CA-24	0.97	9.19	3.19	6.63	2.30	2.27
Santa Tereza	Opx-Bt metatonalite	CA-25	0.96	8.01	4.15	5.22	2.71	1.58
Jequitibá	Bt metadiorite	CA-30	0.81	48.91	3.82	38.62	3.02	6.91
Jequitibá	Grt-Bt metagranodiorite	CA-31	0.80	73.62	4.70	46.51	2.97	9.67
Jequitibá	Grt-Bt metagranodiorite	CA-32	0.76	14.56	3.71	9.23	2.35	2.64

[a] $FeO(t)=Fe_2O_3$ (analysis)×0.8998

[b] Normalized elements for chondrite (Boynton, 1984).

$Eu/Eu^* = Eu_N / [(Sm_N) + (Gd_N)]^{1/2}$

REFERENCES

Boynton, W.V., 1984. Cosmochemistry of the rare earth elements: meteorites studies. In: Henderson, P. (Ed.), Rare Earth Element Geochemistry. Elsevier, pp. 63–114.

Whitney, D.L., Evans, B.W., 2010. Abbreviations for names of rock-forming minerals. American Mineralogist 95, 185-187.

REFERENCES OF FIGURES 4, 5, 6, 7, 12 AND TABLE 1

Figure / Table Reference

12 Affaton, P., Kalsbeek, F., Boudzoumou, F., Trompette, R., Thrane, K., Frei, R., 2016. The Pan-African West Congo belt in the Republic of Congo (Congo Brazzaville): Stratigraphy of the Mayombe and West Congo Supergroups studied by detrital zircon geochronology. Precambriam Research 272, 185-202.

12, Table 1 Angelo, T.V., Egydio-Silva, M., Temporim, F.A., Seraine, M., 2020 Midcrust deformation regime variations across the Neoproterozoic Araçuaí hot orogen (SE Brazil): Insights from structural and magnetic fabric analyses. Journal of Structural Geology 134, 104007."

12, Table 1 Aranda, R.O., Chaves, A.O., Medeiros Júnior, E.B., Venturini Junior, R., 2020. Petrology of the Afonso Cláudio Intrusive Complex: New insights for the Cambro-Ordovician post-collisional magmatism in the Araçuaí-West Congo Orogen, Southeast Brazil. Journal of South American Earth Sciences 98, 102465.

12 Araujo, L. E. A. B., Heilbron, M., Teixeira, W., Dussin, I., Valeriano, C.M., Henrique Bruno, Sato, K., Paravidini, G., Castro, M., 2021. Siderian to Rhyacian evolution of the Juiz de Fora Complex: Arc fingerprints and correlations within the Minas-Bahia Orogen and the Western Central Africa Belt. Precambrian Research, 359: 106118.

4, 5, 6, 7, 12, Table 1 Araujo, C.S., Pedrosa-Soares, A., Lana, C., Dussin, I., Queiroga, G., Serrano, P., Medeiros-Júnior, E., 2020. Zircon in emplacement borders of post-collisional plutons compared to country rocks: A study on morphology, internal texture, U-Th-Pb geochronology and Hf isotopes (Araçuaí orogen, SE Brazil). Lithos 352-353, 105252.

4, 5, 6, 7, Table 1 Baltazar, O.F., Zucchetti, M., Oliveira, S.A.M., Scandolara, J., Silva, L.C., 2010. Geologia das Folhas São Gabriel Da Palha e Linhares. Programa Geologia do Brasil, CPRM–Serviço Geológico do Brasil, Belo Horizonte.

12, Table 1 Basílio, M., Pedrosa-Soares, A.C., Evangelista, H.J., 2000. Depósitos de alexandrita de Malacacheta. Minas Gerais. Geonomos 8, 47–54.

12 Belém, J., Pedrosa-Soares, A.C., Noce, C.M., Silva, L.C., Armstrong, R., Fleck, A., Gradim, C., Queiroga, G., 2011. Bacia precursora versus bacias orogênicas: exemplos do Grupo Andrelândia com base em datações U-Pb (LA-ICP-MS) em zircão e análises litoquímicas. Geonomos 19, 224-243.

12, Table 1 Belém, J., 2014. Geoquímica, geocronologia e contexto geotectônico do magmatismo máfico associado ao feixe de fraturas Colatina, Estado do Espírito Santo. Universidade Federal de Minas Gerais, Belo Horizonte, (MS Dissertation, 138 p).

4, 5, 7 Castro, A., Moreno-Ventas, I., Fernández, C., Vujovich, G., Gallastegui, G., Heredia, N., Martino, R.D., Becchio, R., Corretgé, L.G., Díaz-Alvarado, J., García-Arias, M., Liu D., 2011. Petrology and SHRIMP U-Pb zircon geochronology of Cordilleran granitoids of the Bariloche area, Argentina. Journal of South American Earth Sciences 32, 508-530.

4, 5, 7 Castro, A., 2013. Tonalite-granodiorite suites as cotectic systems: A review of experimental studies with applications to granitoid petrogenesis, Earth Science Reviews 124, 68-95.

12 Castro, M.P., Queiroga, G., Martins, M., Alkmim, F., Pedrosa-Soares, A., Dussin, I., Souza, M.E. 2019. An Early Tonian rifting event affecting the São Francisco-Congo paleocontinent recorded by the Lower Macaúbas Group, Araçuaí Orogen, SE Brazil. Precambriam Research, 331.

12 Castro, M.P., Queiroga, G.N., Martins, M., Pedrosa-Soares, A.C., Dias, L., Lana, C., Babinski, M., Alkmim, A.R., Silva, M., A., 2020. Provenance shift through time in superposed basins: From Early Cryogenian glaciomarine to Late Ediacaran orogenic sedimentations (Araçuaí Orogen, SE Brazil). Gondwana Research 87, 41–66. https://doi.org/10.1016/j.gr.2020.05.019

Table 1 Cavalcante, C.G.C., Vauchez, A., Egydio-Silva, M., Hollanda, M.H.B., Boyer, B., 2014.Thermal conditions during deformation of partially molten crust from TitaniQ geothermometry: rheological implications for the anatectic domain of the Araçuaí belt, eastern Brazil. Solid Earth, 5, 1223–1242."

12, Table 1 Cavalcante, C., Hollanda, M.H., Vauchez, A., Kawata, M., 2018. How long can the middle crust remain partially molten during orogeny? Geology 46, 839-842.

4, 5, 7 Cecil, M.R., Rotberg, G.L., Ducea, M.N., Saleeby, J.B., Gehrels, G.E., 2012. Magmatic growth and batholithic root development in the northern Sierra Nevada, California. Geosphere 8, 592-606.

4, 5, 6, 7, 12 Corrales, F.F.P., Dussin, I.A., Heilbron, M., Bruno, H., Bersan, S.A., Valeriano, C.M., Pedrosa-Soares, A.C., Tedeschi, M., 2020. Coeval high Ba-Sr arc-related and OIB Neoproterozoic rocks linking pre-collisional magmatism of the Ribeira and Araçuaí orogenic belts, SE-Brazil. Precambriam Research 337, 105476.

Table 1 De Campos, C.P., Mendes, J.C., Ludka, I.P., Medeiros, S.R., Moura, J.C., Wallfass, C., 2004. A review of the Brasilian magmatism in southern Espírito Santo, Brazil, with emphasis on post-collisional magmatism. Journal of the Virtual Explorer 17, 1-35.

12, Table 1 De Campos, C.P, Medeiros, S.R., Mendes, J.C, Pedrosa-Soares, A.C., Dussin, I., Ludka, I.P., Dantas, E.L., 2016. Cambro-Ordovician magmatism in the Araçuaí Belt (SE Brazil): Snapshots from a post-collisional event. Journal of South American Earth Sciences 68, 248-268.

12 Degler, R., Pedrosa-Soares, A., Dussin, I., Queiroga, G., Schulz, B., 2017. Contrasting provenance and timing of metamorphism from paragneisses of the Araçuaí-Ribeira orogenic system, Brazil: Hints for Western Gondwana assembly. Gondwana Research 51, 30–50.

12 Degler, R., Pedrosa-Soares, A., Novo, T., Tedeschi, M., Silva, L.C., Dussin, I., Lana, C. 2018. Rhyacian-Orosirian isotopic records from the basement of the Araçuaí-Ribeira orogenic system (SE Brazil): Links in the Congo-São Francisco palaeocontinent. Precambrian Research 317, 179-195.

12, Table 1 Deluca, C., 2018. Evolução do Batólito Itaporé e rochas encaixantes, Orógeno Araçuaí (MG): geoquímica, geocronologia e petrogênese. Universidade Federal de Minas Gerais, Belo Horizonte (MS Dissertation, 116 pp.).

12, Table 1 Deluca C., Pedrosa-Soares A., Lima S., Cordani U., Sato K. 2019. Provenance of the Ediacaran Salinas Formation (Araçuaí Orogen, Brazil): Clues from lithochemical data and zircon U-Pb (SHRIMP) ages of volcanic clasts. Brazilian Journal of Geology, 49:1–19.

4, 5, 7 Dunphy, J.M., Ludden, J.N., 1998. Petrological and geochemical characteristics of a Paleoproterozoic magmatic arc (Narsajuaq terrane, Ungava Orogen, Canada) and comparisons to Superior Province granitoids. Precambriam Research 91, 109–142.

4, 5, 6, 7, Table 1 Féboli, W.L., 1993 (Org.). Geologia da Folha Domingos Martins. Programa de Levantamentos Geológicos Básicos do Brasil, Folha SF.24-V-A-III – Domingos Martions. Brasília, DNPM/CPRM.

4, 5, 6, 7, Table 1 Figueiredo, M.C.H., Campos Neto, M.C., 1993. Geochemistry of the Rio doce magmatic arc, Southeastern Brazil. Anais da Academia Brasileira de Ciências. 65, 63-81.

12, Table 1 Figueiredo, C.M.S., 2009. O Arco Magmático Brasiliano na conexão entre os orógenos Araçuaí e Ribeira, Região de Muriaé-MG. Universidade Federal de Minas Gerais, Belo Horizonte, Brazil (Ph.D. Thesis, p. 103).

4, 5, 7 GEOROC Database (http://georoc.mpch-mainz.gwdg.de/georoc/)

4, 5, 6, 7, Table 1 Gonçalves, L.E.S., 2009. Características gerais e história deformacional da Suíte Granítica G1, entre Governador Valadares e Ipanema, MG. Universidade Federal de Ouro Preto, Ouro Preto (MS Dissertation, 112 pp.).

4, 5, 6, 7, 12, Table 1 Gonçalves, L., Farina, F., Lana, C., Pedrosa-Soares, A.C., Alkmim, F., Nalini, H.A.Jr., 2014. New U-Pb ages and lithochemical attributes of the Ediacaran Rio Doce magmatic arc, Araçuaí confined orogen, southeastern Brazil. Journal of South American Earth Sciences 52, 129–148.

4, 5, 6, 7, 12, Table 1 Gonçalves, L., Alkmim, F.F., Pedrosa-Soares, A.C., Dussin, I.A., Valeriano, C.M., Lana, C., Tedeschi, M., 2016. Granites of the intracontinental termination of a magmatic arc: an example from the Ediacaran Araçuaí orogen, southeastern Brazil. Gondwana Research 36, 439-458.

12, Table 1 Gouvêa, L.P., Medeiros, S.R., Mendes, J.C., Soares, C., Marques, R., Melo, M., 2020. Magmatic activity period and estimation of P-T metamorphic conditions of pre-collisional opx-metatonalite from Araçuaí-Ribeira orogens boundary, SE Brazil. Journal of South American Earth Sciences 99, 102506.

4, 5, 6, 7, 12, Table 1 Gradim, C., Roncato, J., Pedrosa-Soares, A.C., Cordani, U., Dussin, I., Alkmim, F.F., Queiroga, G., Jacobsohn, T., Silva, L.C., Babinski, M., 2014. The hot back-arc zone of the Araçuaí Orogen, Eastern Brazil: from sedimentation to granite generation. Brazilian Journal of Geology 44, 155-180.

4, 5, 6, 7, 12 Heilbron, M., Tupinambá, M., Valeriano, C., Armstrong, R., Silva, L.G.E., Melo, R.S., Simonetti, A., Pedrosa-Soares, A.C., Machado, N. 2013. The Serra da Bolívia complex: The record of a new Neoproterozoic arc-related unit at Ribeira belt. Precambrian Research 238, 158– 175.

4, 5, 7 Hervé, F., Pankurst, R.J., Fanning, C.M., Calderon, M., Yaxely, G.M., 2007. The south Patagonian batholith: 150 my of granite magmatism on a plate margin. Lithos 97, 373-394.

12 Kuchenbecker, M., 2014. Relações entre coberturas do Cráton do São Francisco e bacias situadas em orógenos marginais: O registro de datações U-Pb de grãos detríticos de zircão e suas implicações geotectônicas. PhD Thesis, Universidade Federal de Minas Gerais, Belo Horizonte, 173 p.

12 Kuribara, Y., Tsunogae, T., Santosh, M., Takamura, Y., Costa, A.G., Rosière, C.A., 2019. Eoarchean to Neoproterozoic crustal evolution of the Mantiqueira and the Juiz de Fora Complexes, SE Brazil: Petrology, geochemistry, zircon U-Pb geochronology and Lu-Hf isotopes. Precambrian Research 323, 82-101.

12, Table 1 Lopes, R.G., 2016. Geologia da região de Colatina (ES): uma abordagem geocronológica, petrográfica e estrutural por ASM. Universidade de São Paulo, São Paulo, Brazil (MS Dissertation, 109p).

12, Table 1 Macêdo, I., M., L., Geraldes, M., C., Marques, R., A., Melo, M., G., Tavares., A., D., Martins, M., V., A., Oliveira, H., C., Rodrigues, R., D., 2022. New clues for magma-mixing processes using petrological and geochronological evidence from the Castelo Intrusive Complex, Araçuaí Orogen (SE Brazil). Journal of South American Earth Sciences 115, 103758.

Table 1 Martins, V.T.S, Teixeira, W., Noce, C.M., Pedrosa-Soares, A.C., 2004. Sr and Nd Characteristics of Brasiliano/Pan-African Granitoid Plutons of the Araçuai Orogen, Southeastern Brazil: Tectonic Implications. Gondwana Research 7, 75-89.

12, Table 1 Mauri, S., Melo, M., G., Lana, C., Marques, R., A., 2021. Petrologic and geochronological constraints on the polymetamorphic evolution of the collisional granites, Araçuaí Orogen (SE Brazil). Anais da Academia Brasileira de Ciências 93(3), e20200639. https://doi.org/10.1590/0001-3765202120200639

12, Table 1 Mello, F.M., 2000. Litogeoquímica e Química Mineral do Maciço Charnockítico Aimorés-MG. Universidade de São Paulo, São Paulo (Ph.D. Thesis, 167 pp.).

12, Table 1 Mendes, J.C., Medeiros, S.R., McReath, I., De Campos, C.M.P., 2005. Cambro-Ordovician magmatism in SE Brazil: U-Pb and Rb-Sr ages, combined with Sr and Nd isotopic data of Charnockitic rocks from the Várzea Alegre complex. Gondwana Research 8, 337-345.

12, Table 1 Melo, M.G., Lana, C., Stevens, G., Pedrosa-Soares, A.C., Gerdes, A., Alkmin, L.A., Nalini Jr., H.A., Alkmim, F.F., 2017. Assessing the isotopic evolution of S-type granites of the Carlos Chagas batholith, SE Brazil: Clues from U-Pb, Hf isotopes, Ti geothermometry and trace element composition of zircon. Lithos 284-285, 730-750.

4, 5, 12, Table 1 Melo, M.G., Stevens, G., Lana, C., Pedrosa-Soares, A.C., Frei, D., Alkmim, F.F., Alkmin, L.A., 2017. Two cryptic anatectic events within a syn-collisional granitoid from the Araçuaí orogen (southeastern Brazil): evidence from the polymetamorphic Carlos Chagas batholith. Lithos 277, 51–71.

12, Table 1 Melo, M.G., Lana, C., Stevens, G., Hartwig, M.E., Pimenta, M.S., Nalini Jr., H.A., 2020. Deciphering the source of multiple U–Pb ages and complex Hf isotope composition in zircon from post-collisional charnockite-granite associations from the Araçuaí orogen (southeastern Brazil). Journal of South American Earth Sciences 103, 102792.

12 Mondou, M., Egydio-Silva, M., Vauchez, A., Raposo,M.I.B., Bruguier, O., Oliveira, A.F., 2012. Complex, 3D strain patterns in a synkinematic tonalite batholith from the Araçuaí Neoproterozoic orogen (Eastern Brazil): evidence from combined magnetic and isotopic chronology studies. Journal of Structural Geology 39, 158–179.

12 Monié, P., Bosch, D., Bruguier, O., Vauchez, A., Rolland, Y., Nsungani, P., Buta Neto, A., 2012. The Late Neoproterozoic/Early Palaeozoic evolution of the West Congo Belt of NW Angola: geochronological (U-Pb and Ar-Ar) and petrostructural constraints. Terra Nova 24, 238–247.

4, 5, 6, 7, 12, Table 1 Nalini Jr., H.A., 1997. Caractérisation des suítes magmatiques néoprotérozoiques de la region de Conselheiro Pena et Galiléia (Minas Gerais, Brésil). Etude géochimique et structurale des suítes Galiléia et Urucum et relations avec les pegmatites à éléments rares associées. Ph.D. thesis. École des Mines de Saint Etienne et École des Mines de Paris, France, p. 237.

Table 1 Nalini Jr., H.A., Bilal, E., Correia Neves, J.M., 2000. Syn-collisional peraluminous magmatism in the Rio Doce region: mineralogy, geochemistry and isotopic data of the Urucum suite (eastern Minas Gerais state, Brazil). Revista Brasileira de Geociências 30, 120–125.

4, 5, 6, 7, Table 1 Narduzzi, F., Farina F., Stevens, Lana, C., Nalini Jr, H.A., 2017. Magmatic garnet in the Cordilleran-type Galiléia granitoids of the Araçuaí belt (Brazil): Evidence for crystallization in the lower crust. Lithos, 282-283, 82-97.

4, 5, 6, 7, 12, Table 1 Narduzzi, F., 2018 Genesis and evolution of a Neoproterozoic magmatic arc: the Cordilleran-type granitoids of the Araçuaí Belt, Brazil. PhD Thesis, Escola de Minas, Departamento de Geologia, Universidade Federal de Ouro Preto, 245p.

12, Table 1 Noce, C.M., Macambira, M.J.B., Pedrosa-Soares, A.C., 2000. Chronology of Neoproterozoic–Cambrian granitic magmatism in the Araçuaí Belt, Eastern Brazil, based on single zircon evaporation dating. Revista Brasileira de Geociências 30, 25–29.

12 Noce, C.M., Pedrosa-Soares, A.C., Piuzana, D., Armstrong, R., Laux, J.H., De Campos, C.M., Medeiros, S.R. 2004. Ages of sedimentation of the kinzigitic complex and of a late orogenic thermal episode of the Araçuaí Orogen, northern Espírito Santo State, Brazil: Zircon and monazite U-Pb SHRIMP and ID–TIMS data. Revista Brasileira de Geociências 34, 587-592.

12 Noce, C.M., Pedrosa-Soares A.C., Silva, L.C., Armstrong, R., Piuzana, D., 2007. Evolution of polycyclic basement complexes in the Araçuaí Orogen, based on U–Pb SHRIMP data: Implications for Brazil–Africa links in Paleoproterozoic time. Precambriam Research 159, 60-78.

4, 5, 6, 7, 12, Table 1 "Novo, T., Pedrosa-Soares, A.C., Noce, C.M., Alkmim, F.F., Dussin, I., 2010. Rochas charnockíticas do sudeste de Minas Gerais: a raiz granulítica do arco Magmático do Orógeno Araçuaí. Revista Brasileira de Geociências 40, 573-592.

12 Novo, T.A., 2013. Caracterização do Complexo Pocrane, magmatismo básico mesoproterozóico e unidades neoproterozóicas do sistema Araçuaí-Ribeira, com ênfase em geocronologia U-Pb (SHRIMP e LA-ICP-MS). Universidade Federal de Minas Gerais, Belo Horizonte (MS Dissertation, 211 p.).

12, Table 1 Novo, T.A., Pedrosa-Soares, A., Vieira, V.S., Dussin, I., Silva, L.C., 2018. The Rio Doce Group revisited: An Ediacaran arc-related volcano-sedimentary basin, Araçuaí orogen (SE Brazil). Journal of South American Earth Sciences 85, 345-361.

4, 5, 7 Otamendi, J.E., Ducea, M.N., Bergantz, G.W., 2012. Geological, petrological and geochemical evidence for progressive construction of an arc crustal section, Sierra de Valle Fertil, Famatinian Arc, Argentina. Journal of Petrology, 53:761–800.

12, Table 1 Paes, V.J.C.,1999. Geologia e Geoquímica da Região de Alvarenga, Minas Gerais: implicações geotectônicas e metalogenéticas, Universidade Federal de Minas Gerais, Belo Horizonte, (MS Dissertation, 173p.).

4, 5, 6, 7, 12, Table 1 Paes, V.J.C., Raposo, F.O., Pinto, C.P., Oliveira, F.A.R. (Orgs.), 2010. Projeto Jequitinhonha, Estados de Minas Gerais e Bahia: texto explicativo. Geologia e Recursos Minerais das Folhas Comercinho, Jequitinhonha, Almenara, Itaobim, Joaíma e Rio do Prado. Programa Geologia do Brasil. CPRM – Serviço Geológico do Brasil, Belo Horizonte.

4, 5, 7 Pankhurst, R.J., Weaver, S.D., Hervé, F., Larrondo, P., 1999. Mesozoic-Cenozoic evolution of the North Patagonian Batholith in Aysen, southern Chile. Journal of the Geological Society, London 156, 673-694.

12 Peixoto, E., Pedrosa-Soares, A.C., Alkmim, F.F., Dussin, I.A., 2015. A suture-related accretionary wedge formed in the Neoproterozoic Araçuaí orogen (SE Brazil) during Western Gondwanaland assembly. Gondwana Research 27, 878-896.

4, 5, 7 Peixoto, C.A., Heilbron, M., Ragatky, D., Armstrong, R., Dantas, E., Valeriano, C.M., Simonetti, A. 2017. Tectonic evolution of the Juvenile Tonian Serra da Prata magmatic arc in the Ribeira belt, SE Brazil: Implications for early West Gondwana amalgamation. Precambrian Research 302, 221-254.

Table 1 Pedrosa Soares, A.C., Wiedemann-Leonardos, C.M., 2000. Evolution of the Araçuaí Belt and its connection to the Ribeira Belt, eastern Brazil. In: Cordani, U.G., Milani, E.J., Thomaz Filho, A., Campo, D.A. (Eds.). Tectonic evolution of South America. Rio de Janeiro, 31st International Geological Congress, p. 265-285.

Table 1 Pedrosa-Soares, A.C., Noce, C.M., Wiedemann, C., Pinto, C.P., 2001. The Araçuaí- West-Congo Orogen in Brazil: An overview of a confined orogen formed during Gondwanaland Assembly. Precambrian Research 110, 307-323. https://doi.org/10.1016/S0301-9268(01)00174-7

4, 5, 6, 7, 12, Table 1 Pedrosa-Soares, A.C., Queiroga, G.N., Gradim, C.T., Roncato, J.G., Novo, T.A., Jacobsohn, T., Silva, K.L., 2006. Nota Explicativa da Folha Mantena, 1:100.000. Programa Geologia do Brasil, CPRM–UFMG.

12, Table 1 Pedrosa-Soares, A.C., De Campos, C.P., Noce, C.M., Silva, L.C., Novo, T., Roncato, J., Medeiros, S., Castañeda, C., Queiroga, G., Dantas, E., Dussin, I., Alkmim, F., 2011. Late Neoproterozoic-Cambrian Granitic Magmatism in the Araçuaí Orogen (Brazil), the Eastern Brazilian Pegmatite Province and Related Mineral Resources. In: Sial, A.N., Bettencourt, J.S., De Campos, C.P., Ferreira, V.P. (Eds.), Granite-Related Ore Deposits. London, Geological Society of London, Special Publication 350, 25–51.

Table 1 Pedrosa-Soares, A.C., Deluca, C., Araujo, C., Gradim, C., Lana, C., Dussin, I., Silva, L.C., Babinski, M., 2020. O Orógeno Araçuaí à luz da geocronologia: Um tributo a Umberto Cordani. In: Bartorelli, A., Teixeira, W., Brito Neves, B.B., Geocronologia e Evolução Tectônica do Continente Sul-Americano: a contribuição de Umberto Giuseppe Cordani. Solarias Edições Culturais, São Paulo, 728p.

4, 5, 7 PetDB Database (http://earthchem.org/petdb)

12, Table 1 Petitgirard, S., Vauches, A., Egydio-Silva, M., Bruguier, O., Campos, P., Monié P., Babinski M., Mondou, M., 2009. Conflicting structural and geochronological data from the Ibituruna quartz-syenite (SE Brazil): effect of protracted “hot” orogeny and slow cooling rate? Tectonophysics 477, 174–196.

Table 1 "Pinto C.P., Drumond J.B.V., Féboli W.L. (coord.) 2001. Projeto Leste, Etapas 1 e 2. Belo Horizonte, CPRM-COMIG, CD-ROM.

12, Table 1 Potratz, G.L. 2020. Petrogênese e geocronologia U-Pb do Granito Sana, Faixa Ribeira, e dos Complexos Intrusivos de Santa Angélica e Várzea Alegre, Faixa Araçuaí. Universidade do Estado do Rio de Janeiro (MS Dissertation, 256p.)

10, 12, Table 1 "Potratz, G.L., Geraldes, M.C., Medeiros-Júnior, E., Temporim, F., A., Martins, M.V.A., Almeida, B.S., 2022. A Juvenile Component in the Pre- and Post-Collisional Magmatism in the Transition Zone between the Araçuaí and Ribeira Orogens (SE Brazil) (Rio de Janeiro, SE Brazil)"

12, Table 1 Richter, F., Lana, C., Steven, G., Buick, I., Pedrosa-Soares, A.C., Alkmim, F.F., Cutts, K., 2016. Sedimentation, metamorphism and granite generation in a back-arc region: Records from the Ediacaran Nova Venécia Complex (Araçuaí Orogen, Southeastern Brazil). Precambrian Research 272, 78–100.

4, 5, 7 Rodríguez, N., Díaz-Alvarado J., Fernández C., Fuentes P., Breitkreuz C., Tassinari C.C.G., 2018. The significance of U-Pb zircon ages in zoned plutons – the case of the Flamenco pluton, Coastal Range batholith, northern Chile. Geoscience Frontiers 10, 1073-1099.

4, 5, 6, 7, 12, Table 1 Roncato, J.G., 2009. As suítes graníticas tipo–S do norte do Espírito Santo na região das folhas Ecoporanga, Mantena, Montanha e Nova Venécia. Universidade Federal de Minas Gerais, Belo Horizonte, (MS Dissertation, 102 p).

12 "Santiago, R., Caxito, F.A., Neves, M., A., Dantas, E.L., Medeiros Júnior, E.B., Queiroga, G.N., 2020. Two generations of mafic dyke swarms in the Southeastern Brazilian coast: reactivation of structural lineaments during the gravitational collapse of the Araçuaí-Ribeira Orogen (500 Ma) and West Gondwana breakup (140 Ma). Precambrian Research 340, 105344."

12 Santiago, R., Caxito, F.A., Pedrosa-Soares, A.C., Neves, M.A., Calegari, S.S., Lana, C., 2022. Detrital zircon U–Pb and Lu–Hf constraints on the age, provenance and tectonic setting of arc-related high-grade units of the transition zone of the Araçuaí and Ribeira orogens (SE Brazil). Journal of South American Earth Sciences 116, 103861. https://doi.org/10.1016/j.jsames.2022.103861

12 Schannor, M., Lana, C., Fonseca, M. 2019. São Francisco-Congo Craton break-up delimited by U-Pb-Hf isotopes and trace-elements of zircon from metasediments of the Araçuaí Belt. Geoscience Frontiers 10, 611-628.

12, Table 1 Schannor, M., Lana, C., Mazoz, A., Narduzzi, F., Cutts, K., Fonseca, M. 2020. Paleoproterozoic sources for Cordilleran-type Neoproterozoic granitoids from the Araçuaí orogen (SE Brazil): Constraints from Hf isotope zircon composition. Lithos 378–379, 105815. https://doi.org/10.1016/j.lithos.2020.105815

12 Schiavetti, L., 2019. Metamorfismo e geocronologia em orógenos quentes – o caso do Complexo Nova Venécia, Orógeno Araçuaí. Universidade Estadual de Campinas, Campinas (MS Dissertation, 174p.).

4, 5, 6, 7, 12, Table 1 Serrano, P., Pedrosa-Soares, A., Medeiros-Junior, E., Fonte-Boa, T., Araujo, C., Dussin, I., Queiroga, G., Lana, C., 2018. A-type Medina batholith and post-collisional anatexis in the Araçuaí orogen (SE Brazil). Lithos 320-321, 515-536.

12 Silva L.C., Armstrong R., Noce C.M., Carneiro M., Pimentel M., Pedrosa-Soares A.C., Leite C., Vieira V.S., Silva M., Paes V., Cardoso-Filho J. 2002. Reavaliação da evolução geológica em terrenos pré-cambrianos brasileiros com base em novos dados U–Pb SHRIMP, parte II: Orógeno Araçuaí, Cinturão Móvel Mineiro e Cráton São Francisco Meridional. Revista Brasileira de Geociências, 32:513–528.

12 Silva L.C., McNaughton N.J., Armstrong R., Hartmann L.A., Fletcher I.R. 2005. The Neoproterozoic Mantiqueira Province and its African connections: a zircon-based U-Pb geochronologic subdivision for the Brasiliano/Pan-African systems of orogens. Precambrian Research, 136:203–240.

12, Table 1 Silva L.C., Pedrosa-Soares A.C., Armstrong R., Noce C.M. 2011. Determinando a duração do período colisional do Orógeno Araçuaí com base em geocronologia U–Pb de alta resolução em zircão: uma contribuição para a história da amalgamação do Gondwana Ocidental. Geonomos, 19:180–197.

12 Silveira Braga, F.C., Rosière, C.A., Santos, J.O.S., Hagemann, S.G., McNaughtone, N.J., Salles, P.V., 2019. The Horto-Baratinha itabirite-hosted iron ore: A basal fragment of the Espinhaço basin in the eastern São Francisco Craton. Journal of South American Earth Sciences 90, 12–33.

Table 1 Soares, C.C.V., Queiroga, G., Pedrosa-Soares, A.C., Gouvêa, L.P., Valeriano, C.M., Melo, M.G., Marques, R.A., Freitas, R.D.A., 2020. The Ediacaran Rio Doce magmatic arc in the Araçuaí – Ribeira boundary sector, southeast Brazil: Lithochemistry and isotopic (Sm–Nd and Sr) signatures. Journal of South American Earth Sciences 102880.

12, Table 1 Söllner F., Lammerer B., Weber-Diefenbach K. 1991. Die Krustenentwicklung in Der Küstenregion Nördlich Von Rio de Janeiro, Brasilien. Münchener Geowis-senschaftliche Hefte 11. Friedrich Pfeil Verlag, München, p. 4.

12, Table 1 Söllner, F., Lammerer, B., Wiedemann-Leonardos, C., 2000. Dating the Ribeira Mobile Belt of Brazil. In: Sonderheft, Zeitschrift Angwandte Geologie, p. 245-255.

12 Straathof, G.B., 2001. Neoproterozoic low latitude glaciations: An African Perspective. PhD Thesis. University of Edinburgh, 296p.

4, 5, 6, 7, 12, Table 1 Tedeschi, M., Novo, T., Pedrosa-Soares, A., Dussin, I., Tassinari, C., Silva, L.C., Gonçalves, L., Alkmim, F., Lana, C., Figueiredo, C., Dantas, E., Medeiros, S., De Campos, C., Corrales, F., Heilbron, M., 2016. The Ediacaran Rio Doce magmatic arc revisited (Araçuaí-Ribeira orogenic system, SE Brazil). Journal of South American Earth Sciences 68, 167-186.

12, Table 1 Teixeira, P.A.D., Fernandes, C.M., Mendes, J.C., Medeiros, S.R., Rocha, I.S., 2020. U-PB LA-ICP-MS and geochemical data of the Alto Chapéu Pluton: Contributions on bimodal post-collisional magmatism in the Araçuaí belt (SE Brazil). Journal of South American Earth Sciences 103, 102724.

12, Table 1 "Temporim, F.A., Trindade, R.I.F., Tohver, E., Soares, C.C., Gouvêa, L.P., Egydio-Silva, M., Amaral, C.A.D., Souza Jr., G.F., 2020. Magnetic fabric and geochronology of a Cambrian “isotropic” pluton in the Neoproterozoic Araçuaí orogen. Tectonics "

4, 5, 6, 7, 12, Table 1 Uhlein, A., Roncato, J., Egydio-Silva, M., Parizek-Silva, Y., Alves, M., 2014. Geologia, Petrologia e Contexto Geotectônico dos Gnaisses e Granitóides da Região de Colatina, Espírito Santo. Geonomos 22, 66-83.

12, Table 1 Vauchez, A., Egydio-Silva, M., Babinski, M., Tommasi, A., Uhlein, A., Liu, D., 2007. Deformation of a pervasely molten middle crust: insights from the Neoproterozoic Ribeira-Araçuaí orogen (SE Brazil). Terra Nova 19, 278–286.

12 Vieira, V.S., 2007. Significado do Grupo Rio Doce no Contexto do Orógeno Araçuaí. PhD Thesis, Universidade Federal de Minas Gerais, Belo Horizonte, 117 p.

12, Table 1 Xavier B.C. 2017. Relações tectônicas no setor central da Faixa Araçuaí: Análise Estrutural por ASM e Geocronologia U-Pb e Lu-Hf. MS Dissertation, Universidade de São Paulo, São Paulo, 123 p.

12; Table 1 Wiedemann, C.M., Medeiros, S.R., Ludka, I.P., Mendes, J.C., Costa-de-Moura, J., 2002. Architecture of late orogenic plutons in the Araçuaí-Ribeira fold belt, Southeast Brazil. Gondwana Research 5, 381-399.

Table 1 Wisniowski, L., Pedrosa-Soares, A., Medeiros-Junior, E., Belém, J., Dussin, I., Queiroga, G. 2020. Ultra-high temperature, mid-crustal level, contact metamorphism imprinted on granulite facies paragneisses by a norite intrusion (São Gabriel da Baunilha, Araçuaí orogen, southeast Brazil). Journal of Metamorphic Geology 00:1-29.

4, 5, 6, 7, 12; Table 1 Zanon, M.L., Chaves, A.O., Rangel, C.V.G.T., Gaburo, L., Pires, C.R., 2015. Os aspectos geológicos do Maciço Santa Angélica (ES): uma nova abordagem. Brazilian Journal of Geology 45, 609-633.

APPENDIX C - Supplementary File 3.B - Isotopic Data

Zircon U-Pb

LA(SF)-ICP-MS U-Pb zircon results data from Jequitibá pluton (Sample CA-03)

Identifier	Lu-Hf identifier	f206[a]	207Pb	206Pb	U	Th[b]/U	206Pb/204Pb	Ratios[c]									Ages (Ma)[c]									% conc[e]
								207Pb/206Pb	2s (%)	207Pb/235U	2s (%)	206Pb/238U	2s (%)	Rho[d]	208Pb/232Th	2s (%)	207Pb/206Pb	2s abs	206Pb/238U	2s abs	207Pb/235U	2s abs	208Pb/232Th	2s abs	
		(%)	CPS	CPS	(ppm)			Data for Wetherill plot																		
5.sSMPABC287	-	**0.00**	**144785**	**8568**	**478.45**	**0.12**	**0**	**0.059**	**2.163**	**0.760**	**3.464**	**0.093**	**2.706**	**0.781**	**0.033**	**7.470**	**574**	**24**	**574**	**7**	**574**	**8**	**660**	**24**	**100.0**
5.sSMPABC256	seq0061	**0.00**	**79430**	**4708**	**285.98**	**0.12**	**0**	**0.059**	**2.430**	**0.765**	**3.886**	**0.094**	**3.032**	**0.780**	**0.035**	**14.314**	**577**	**26**	**577**	**8**	**577**	**9**	**705**	**50**	**100.0**
5.sSMPABC297	seq0044	**0.00**	**55600**	**3307**	**182.42**	**0.12**	**0**	**0.059**	**2.287**	**0.769**	**3.693**	**0.094**	**2.900**	**0.785**	**0.044**	**11.969**	**584**	**25**	**578**	**8**	**579**	**8**	**879**	**52**	**99.8**
5.sSMPABC034	-	**0.00**	**95508**	**5641**	**342.52**	**0.18**	**0**	**0.059**	**2.337**	**0.766**	**3.752**	**0.094**	**2.935**	**0.782**	**0.035**	**10.118**	**569**	**25**	**579**	**8**	**577**	**8**	**691**	**34**	**100.4**
5.sSMPABC265	**seq0069**	**0.00**	**71782**	**4263**	**234.07**	**0.28**	**0**	**0.059**	**2.155**	**0.773**	**3.565**	**0.094**	**2.840**	**0.797**	**0.033**	**6.293**	**581**	**23**	**581**	**8**	**581**	**8**	**657**	**20**	**100.0**
5.sSMPABC281	**seq0065**	**0.00**	**27252**	**1610**	**88.86**	**0.89**	**0**	**0.059**	**2.911**	**0.769**	**4.373**	**0.094**	**3.263**	**0.746**	**0.029**	**7.263**	**570**	**32**	**581**	**9**	**579**	**10**	**582**	**21**	**100.4**
5.sSMPABC044	-	0.00	320544	19053	1141.18	0.72	0	0.059	2.153	0.776	3.325	0.095	2.534	0.762	0.028	4.536	583	23	583	7	583	7	562	12	100.0
5.sSMPABC035	**seq0031**	**0.00**	**125384**	**7375**	**445.16**	**0.06**	**0**	**0.059**	**2.312**	**0.770**	**3.583**	**0.095**	**2.737**	**0.764**	**0.013**	**53.782**	**560**	**25**	**585**	**8**	**580**	**8**	**263**	**70**	**100.9**
5.sSMPABC070	seq0032	0.19	99332	5902	352.33	0.10	1406	0.059	2.665	0.779	3.935	0.095	2.894	0.736	0.045	11.517	582	29	585	8	585	9	893	50	100.1
5.sSMPABC048	seq0041	0.04	115059	6856	407.60	0.07	6898	0.060	2.198	0.782	3.477	0.095	2.694	0.775	0.043	11.715	589	24	586	8	587	8	851	49	99.9
5.sSMPABC285	seq0057	0.08	142635	8489	460.08	0.74	3406	0.060	2.185	0.783	3.509	0.095	2.746	0.783	0.030	4.046	586	24	587	8	587	8	591	12	100.1
5.sSMPABC024	seq0022	0.00	68963	4112	243.69	0.13	0	0.060	2.315	0.784	3.639	0.095	2.808	0.772	0.037	14.082	590	25	588	8	588	8	738	51	99.9
5.sSMPABC031	seq0029	0.00	150018	8889	530.11	1.12	0	0.059	2.093	0.780	3.337	0.095	2.599	0.779	0.027	3.758	576	23	588	7	585	7	531	10	100.4
5.sSMPABC066	seq0036	0.00	85459	5035	301.89	0.09	0	0.059	2.410	0.776	3.606	0.095	2.682	0.744	0.028	21.360	564	26	588	8	583	8	560	59	100.8
5.sSMPABC267	seq0067	0.00	68340	4069	220.21	0.10	0	0.060	2.150	0.784	3.469	0.096	2.722	0.785	0.041	10.404	587	23	588	8	588	8	815	41	100.0
5.sSMPABC302	seq0071	0.00	91542	5445	294.66	0.18	0	0.059	2.253	0.784	3.596	0.096	2.803	0.779	0.030	9.121	585	24	589	8	588	8	603	27	100.1
5.sSMPABC009	-	0.00	120658	7188	425.16	0.49	0	0.060	2.182	0.786	3.356	0.096	2.550	0.760	0.030	4.976	588	24	589	7	589	8	592	15	100.0
5.sSMPABC072	seq0043	0.00	119808	7141	421.81	0.59	0	0.060	2.248	0.787	3.461	0.096	2.631	0.760	0.030	5.643	589	24	590	7	590	8	593	16	100.0
5.sSMPABC074	-	0.00	162345	9686	571.57	0.84	0	0.060	2.380	0.788	3.770	0.096	2.923	0.775	0.028	6.349	591	26	590	8	590	8	565	18	99.9
5.sSMPABC071	-	0.12	89395	5315	289.50	0.11	2352	0.059	2.544	0.786	3.721	0.096	2.715	0.730	0.018	27.687	584	28	590	8	589	8	356	49	100.2

LA(SF)-ICP-MS U-Pb zircon results data from Jequitibá pluton (Sample CA-03)

Identifier	Lu-Hf identifier	f206[a]	^{207}Pb	^{206}Pb	U	Th[b]/U	^{206}Pb/^{204}Pb	Ratios[c]									Ages (Ma)[c]								% conc[e]
								^{207}Pb/^{206}Pb	2s (%)	^{207}Pb/^{235}U	2s (%)	^{206}Pb/^{238}U	2s (%)	Rho[d]	^{208}Pb/^{232}Th	2s (%)	^{207}Pb/^{206}Pb	2s abs	^{206}Pb/^{238}U	2s abs	^{207}Pb/^{235}U	2s abs	^{208}Pb/^{232}Th	2s abs	
		(%)	CPS	CPS	(ppm)			Data for Wetherill plot																	
5.sSMPABC055	-	0.00	82782	4921	291.12	0.10	0	0.059	2.355	0.786	3.560	0.096	2.670	0.750	0.022	32.066	584	26	590	8	589	8	437	69	100.2
5.sSMPABC011	**-**	**0.00**	**128696**	**7638**	**502.71**	**0.06**	**0**	**0.059**	**2.359**	**0.788**	**3.744**	**0.096**	**2.908**	**0.777**	**0.037**	**19.376**	**580**	**26**	**593**	**8**	**590**	**8**	**725**	**69**	**100.4**
5.sSMPABC012	seq0021	0.00	179679	10775	701.86	0.58	0	0.060	2.234	0.796	3.602	0.096	2.825	0.784	0.029	5.296	602	24	593	8	595	8	572	15	99.7
5.sSMPABC056	seq0042	0.00	90306	5389	316.16	0.15	0	0.060	2.480	0.792	3.853	0.096	2.949	0.765	0.035	15.704	592	27	593	8	593	9	688	53	100.0
5.sSMPABC025	-	0.00	89997	5354	318.67	0.10	0	0.059	2.252	0.793	3.445	0.097	2.607	0.757	0.028	18.628	585	24	595	7	593	8	561	52	100.3
5.sSMPABC262	seq0059	0.00	29183	1745	92.90	1.31	0	0.060	2.675	0.797	4.160	0.097	3.186	0.766	0.028	5.363	597	29	595	9	595	9	565	15	99.9
5.sSMPABC065	seq0035	0.00	81280	4849	282.89	0.99	0	0.060	2.280	0.797	3.521	0.097	2.683	0.762	0.029	5.292	591	25	596	8	595	8	572	15	100.2
5.sSMPABC019	-	0.00	115329	6905	398.59	0.05	0	0.060	2.205	0.805	3.396	0.098	2.583	0.761	0.050	15.409	599	24	600	7	600	8	978	74	100.0
5.sSMPABC294	-	0.00	90788	5430	289.00	0.09	0	0.060	2.207	0.797	3.543	0.097	2.772	0.782	0.039	11.813	597	24	595	8	595	8	772	45	99.9
5.sSMPABC292	seq0056	0.26	103565	6183	328.45	0.11	1053	0.060	2.786	0.799	4.066	0.097	2.962	0.728	0.044	9.031	593	30	597	8	596	9	876	39	100.1
5.sSMPABC076	seq0024	0.00	291041	17433	1011.16	0.50	0	0.060	2.204	0.802	3.469	0.097	2.679	0.772	0.032	5.521	600	24	597	8	598	8	634	17	99.9
5.sSMPABC006	seq0026	0.11	233355	13916	808.58	0.53	2552	0.060	2.200	0.800	3.395	0.097	2.586	0.762	0.030	3.876	590	24	599	7	597	8	596	11	100.3
5.sSMPABC054	-	0.00	168620	10109	581.76	0.35	0	0.060	2.202	0.808	3.391	0.098	2.578	0.760	0.031	5.896	602	24	601	7	601	8	608	18	100.0
5.sSMPABC053	seq0038	0.00	215940	12933	744.41	0.55	0	0.060	2.237	0.808	3.633	0.098	2.862	0.788	0.030	5.873	600	24	602	8	601	8	597	17	100.1
5.sSMPABC013	-	0.00	71242	4266	245.37	0.14	0	0.060	2.405	0.808	3.674	0.098	2.778	0.756	0.033	12.771	599	26	602	8	602	8	660	42	100.1
5.sSMPABC069	seq0033	0.00	247950	14894	853.62	0.68	0	0.060	2.131	0.811	3.372	0.098	2.614	0.775	0.030	4.792	606	23	602	8	603	8	598	14	99.9
5.sSMPABC063	seq0037	0.00	79822	4807	252.11	0.15	0	0.060	2.458	0.816	3.702	0.098	2.768	0.748	0.038	11.940	611	27	604	8	606	8	758	45	99.7
5.sSMPABC050	seq0040	0.00	141618	8489	485.92	0.13	0	0.060	2.269	0.812	3.454	0.098	2.605	0.754	0.032	11.223	601	25	604	8	604	8	631	35	100.1
5.sSMPABC075	seq0028	0.00	143366	8621	489.42	0.11	0	0.060	2.262	0.819	3.532	0.099	2.713	0.768	0.017	24.005	608	24	607	8	607	8	337	40	100.0
5.sSMPABC016	seq0019	0.00	105941	6379	361.37	0.34	0	0.060	2.259	0.821	3.591	0.099	2.792	0.777	0.038	6.080	611	24	608	8	608	8	757	23	99.9
5.sSMPABC015	seq0020	0.07	179265	10745	610.24	0.40	3956	0.060	2.152	0.819	3.344	0.099	2.559	0.765	0.032	4.361	601	23	609	7	607	8	639	14	100.3
5.sSMPABC306	**seq0027**	**0.08**	**878865**	**5327**	**266.06**	**0.20**	**3480**	**0.061**	**2.335**	**0.850**	**3.684**	**0.102**	**2.850**	**0.773**	**0.039**	**8.305**	**626**	**25**	**624**	**8**	**624**	**9**	**764**	**31**	**100.0**
5.sSMPABC028	**seq0023**	**0.00**	**276724**	**16960**	**877.03**	**0.49**	**0**	**0.061**	**2.056**	**0.899**	**3.280**	**0.106**	**2.556**	**0.779**	**0.035**	**3.894**	**649**	**22**	**652**	**8**	**651**	**8**	**694**	**13**	**100.1**

LA(SF)-ICP-MS U-Pb zircon results data from Jequitibá pluton (Sample CA-03)

Identifier	Lu-Hf identifier	f206[a] (%)	^{207}Pb CPS	^{206}Pb CPS	U (ppm)	Th[b]/U	^{206}Pb/^{204}Pb	Ratios[c] Data for Wetherill plot									Ages (Ma)[c]								% conc[e]
								^{207}Pb/^{206}Pb	2s (%)	^{207}Pb/^{235}U	2s (%)	^{206}Pb/^{238}U	2s (%)	Rho[d]	^{208}Pb/^{232}Th	2s (%)	^{207}Pb/^{206}Pb	2s abs	^{206}Pb/^{238}U	2s abs	^{207}Pb/^{235}U	2s abs	^{208}Pb/^{232}Th	2s abs	
5.sSMPABC045	**seq0030**	**0.00**	**119306**	**7435**	**354.37**	**0.42**	**0**	**0.062**	**2.182**	**0.976**	**3.400**	**0.114**	**2.607**	**0.767**	**0.032**	**5.881**	**685**	**23**	**693**	**9**	**691**	**9**	**636**	**18**	**100.3**
5.sSMPABC280	**seq0074**	**0.00**	**107276**	**6736**	**287.66**	**0.13**	**0**	**0.063**	**2.134**	**0.994**	**3.539**	**0.115**	**2.823**	**0.798**	**0.061**	**7.087**	**701**	**23**	**700**	**9**	**701**	**9**	**1196**	**41**	**100.0**
5.sSMPABC301	**seq0070**	**0.00**	**190747**	**12996**	**404.93**	**0.64**	**0**	**0.068**	**2.084**	**1.362**	**3.436**	**0.145**	**2.732**	**0.795**	**0.045**	**4.220**	**873**	**22**	**873**	**11**	**873**	**10**	**881**	**18**	**100.0**
5.sSMPABC286	**seq0060**	**0.00**	**60014**	**4330**	**110.99**	**2.12**	**0**	**0.072**	**2.245**	**1.655**	**3.618**	**0.166**	**2.836**	**0.784**	**0.050**	**3.619**	**990**	**23**	**992**	**13**	**992**	**12**	**981**	**17**	**100.1**
5.sSMPABC279	**seq0073**	**0.08**	**456800**	**32927**	**844.13**	**0.47**	**3558**	**0.072**	**2.018**	**1.655**	**3.465**	**0.167**	**2.817**	**0.813**	**0.040**	**4.200**	**988**	**21**	**993**	**13**	**992**	**11**	**793**	**16**	**100.1**
5.sSMPABC062	**-**	**0.00**	**371766**	**28001**	**708.24**	**0.91**	**0**	**0.075**	**2.071**	**1.838**	**3.305**	**0.177**	**2.576**	**0.779**	**0.055**	**4.405**	**1077**	**21**	**1051**	**12**	**1059**	**11**	**1090**	**23**	**99.2**
5.sSMPABC033	-	0.00	113985	6701	388.73	0.11	0	0.059	2.347	0.731	3.581	0.090	2.704	0.755	0.034	10.865	559	26	557	7	557	8	673	36	99.9
5.sSMPABC254	-	0.00	106716	6273	363.22	0.07	0	0.059	2.144	0.733	3.551	0.090	2.831	0.797	0.044	10.918	559	23	558	8	558	8	877	47	100.0
5.sSMPABC273	seq0066	0.00	139518	8211	472.72	0.87	0	0.059	2.073	0.737	3.393	0.091	2.686	0.792	0.027	3.608	562	23	560	7	561	7	531	9	100.0
5.sSMPABC299	-	0.00	53811	3153	182.00	0.11	0	0.059	2.697	0.735	4.026	0.091	2.989	0.743	0.032	19.549	552	29	561	8	560	9	635	61	100.3
5.sSMPABC293	seq0046	0.00	183090	10751	618.11	0.66	0	0.059	2.078	0.738	3.423	0.091	2.720	0.795	0.024	4.102	557	23	562	7	561	7	487	10	100.2
5.sSMPABC303	seq0064	0.00	87406	5161	291.12	0.07	0	0.059	2.235	0.752	3.594	0.092	2.814	0.783	0.034	16.851	569	24	570	8	570	8	684	57	100.0
5.sSMPABC264	seq0068	0.00	161565	9544	537.83	0.05	0	0.059	2.065	0.753	3.420	0.092	2.726	0.797	0.046	8.773	570	22	570	7	570	7	910	39	100.0
5.sSMPABC257	seq0062	0.00	122526	7231	406.73	0.06	0	0.059	2.067	0.754	3.381	0.093	2.675	0.791	0.045	9.509	568	22	572	7	571	7	882	41	100.1
5.sSMPABC266	-	0.00	121566	7191	403.41	0.06	0	0.059	2.130	0.756	3.419	0.093	2.674	0.782	0.046	9.877	573	23	572	7	572	8	912	44	100.0
5.sSMPABC282	seq0034	0.00	184450	10921	609.66	0.07	0	0.059	2.060	0.760	3.367	0.093	2.664	0.791	0.038	7.989	575	22	574	7	574	7	745	29	100.0
5.sSMPABC298	-	0.51	116929	6865	386.44	0.06	538	0.059	4.140	0.754	5.426	0.093	3.507	0.646	0.042	12.701	556	45	574	10	570	12	823	51	100.6
5.sSMPABC295	-	0.00	88251	5217	291.57	0.08	0	0.059	2.233	0.759	3.574	0.093	2.791	0.781	0.042	11.698	572	24	574	8	574	8	839	48	100.1
5.sSMPABC008	-	0.00	84404	4998	305.39	0.11	0	0.059	2.196	0.761	3.417	0.093	2.618	0.766	0.026	14.889	575	24	574	7	575	8	520	38	100.0
5.sSMPABC255	-	0.00	119880	7096	395.81	0.06	0	0.059	2.061	0.761	3.400	0.093	2.704	0.795	0.040	10.127	574	22	574	7	574	7	798	40	100.0
5.sSMPABC263	-	0.00	71024	4188	234.43	0.12	0	0.059	2.137	0.758	3.445	0.093	2.703	0.784	0.041	8.226	566	23	575	7	573	8	819	33	100.3
5.sSMPABC278	-	0.00	98100	5816	323.34	0.07	0	0.059	2.125	0.763	3.435	0.093	2.699	0.786	0.045	10.076	578	23	575	7	576	8	887	44	99.9
5.sSMPABC296	seq0045	0.03	100213	5914	330.13	0.06	9147	0.059	2.280	0.760	3.600	0.093	2.786	0.774	0.035	14.794	568	25	576	8	574	8	703	51	100.3

LA(SF)-ICP-MS U-Pb zircon results data from Jequitibá pluton (Sample CA-03)

Identifier	Lu-Hf identifier	f206[a] (%)	^{207}Pb CPS	^{206}Pb CPS	U (ppm)	Th[b]/U	$^{206}Pb/^{204}Pb$	Ratios[c] Data for Wetherill plot									Ages (Ma)[c]								% conc[e]
								$^{207}Pb/^{206}Pb$	2s (%)	$^{207}Pb/^{235}U$	2s (%)	$^{206}Pb/^{238}U$	2s (%)	Rho[d]	$^{208}Pb/^{232}Th$	2s (%)	$^{207}Pb/^{206}Pb$	2s abs	$^{206}Pb/^{238}U$	2s abs	$^{207}Pb/^{235}U$	2s abs	$^{208}Pb/^{232}Th$	2s abs	
5.sSMPABC258	-	0.07	96575	5726	317.77	0.07	3690	0.059	2.117	0.765	3.441	0.094	2.713	0.788	0.045	9.498	578	23	576	7	577	8	883	41	100.0
5.sSMPABC300	-	0.30	127425	7500	418.61	0.08	923	0.059	3.011	0.760	4.285	0.094	3.049	0.712	0.030	13.414	562	33	577	8	574	9	594	39	100.5
5.sSMPABC274	seq0063	0.00	86503	5128	284.12	0.09	0	0.059	2.159	0.766	3.482	0.094	2.732	0.785	0.036	11.183	577	23	577	8	577	8	710	39	100.0
5.sSMPABC277	-	0.00	96750	5730	317.33	0.06	0	0.059	2.128	0.766	3.460	0.094	2.728	0.789	0.037	12.598	575	23	578	8	578	8	737	46	100.1
5.sSMPABC073	-	0.00	104477	6231	375.12	0.07	0	0.060	2.280	0.772	3.521	0.094	2.683	0.762	0.040	14.604	591	25	579	7	581	8	793	57	99.6
5.sSMPABC043	**-**	**0.00**	**126852**	**7526**	**454.34**	**0.05**	**0**	**0.059**	**2.191**	**0.770**	**3.394**	**0.094**	**2.592**	**0.764**	**0.027**	**23.759**	**579**	**24**	**580**	**7**	**580**	**8**	**531**	**62**	**100.0**
5.sSMPABC268	**-**	**0.06**	**233647**	**13843**	**762.93**	**0.42**	**4886**	**0.059**	**2.127**	**0.770**	**3.359**	**0.094**	**2.600**	**0.774**	**0.030**	**4.088**	**576**	**23**	**581**	**7**	**580**	**7**	**604**	**12**	**100.2**
5.sSMPABC305	**seq0058**	**0.00**	**93252**	**5507**	**304.01**	**0.06**	**0**	**0.059**	**2.168**	**0.769**	**3.538**	**0.094**	**2.797**	**0.790**	**0.058**	**11.476**	**569**	**24**	**582**	**8**	**579**	**8**	**1137**	**64**	**100.4**
5.sSMPABC052	**seq0039**	**0.00**	**143388**	**8544**	**509.89**	**0.05**	**0**	**0.060**	**2.182**	**0.779**	**3.504**	**0.095**	**2.742**	**0.783**	**0.050**	**14.180**	**589**	**24**	**584**	**8**	**585**	**8**	**990**	**68**	**99.8**
5.sSMPABC005	**seq0025**	**0.00**	**105130**	**6257**	**372.94**	**0.05**	**0**	**0.060**	**2.151**	**0.780**	**3.381**	**0.095**	**2.609**	**0.772**	**0.048**	**12.728**	**586**	**23**	**585**	**7**	**586**	**8**	**943**	**59**	**100.0**
5.sSMPABC027	**seq0072**	**0.00**	**127821**	**7610**	**453.24**	**0.06**	**0**	**0.060**	**2.318**	**0.781**	**3.780**	**0.095**	**2.986**	**0.790**	**0.072**	**12.629**	**587**	**25**	**586**	**8**	**586**	**8**	**1397**	**85**	**100.0**

[a] *percentage of the common Pb on the ^{206}Pb*

[b] *Th/U ratios are calculated relative to BB reference zircon*

[c] *data corrected for background, within-run Pb/U fractionation (in case of $^{206}Pb/^{238}U$) and common Pb using Stacey and Kramers (1975) model Pb composition*

[d] *Rho is the error correlation defined as the quotient of the propagated errors of the $^{206}Pb/^{238}U$ and the $^{207}Pb/^{235}U$ ratio*

[e] *Concordance calculated as (^{206}Pb-^{238}U age/^{207}Pb-^{206}Pb age)*100*

CPS = count per second

Spots in domains of dissolution–recrystallization, overgrowth or Pb lost rims are in red letter

Zircon grains not used for concordia age are in bold letter

LA(SF)-ICP-MS U-Pb zircon results data from Santa Tereza pluton (Sample CA-08)

Identifier	Lu-Hf identifier	f206[a]	^{207}Pb	^{206}Pb	U	Th[b]/U	$^{206}Pb/^{204}Pb$	Ratios[c]									Ages (Ma)[c]									% conc[e]
								$^{207}Pb/^{206}Pb$	2s (%)	$^{207}Pb/^{235}U$	2s (%)	$^{206}Pb/^{238}U$	2s (%)	Rho[d]	$^{208}Pb/^{232}Th$	*2s (%)*	$^{207}Pb/^{206}Pb$	2s abs	$^{206}Pb/^{238}U$	2s abs	$^{207}Pb/^{235}U$	2s abs	$^{208}Pb/^{232}Th$	2s abs		
		(%)	CPS	CPS	(ppm)			Data for Wetherill plot																		
5.sSMPABC036	seq0217	0.00	110102	6590	182.66	1.46	0	0.060	2.072	0.795	3.370	0.096	2.658	0.789	0.028	2.827	598	22	593	8	594	8	564	8	99.8
5.sSMPABC010	-	0.00	207270	12403	343.00	0.31	0	0.060	2.005	0.797	3.291	0.097	2.610	0.793	0.031	3.328	598	22	594	7	595	7	622	10	99.9
5.sSMPABC080	seq0230	0.00	40458	2426	66.62	1.11	0	0.060	2.335	0.802	3.680	0.097	2.844	0.773	0.030	3.850	602	25	597	8	598	8	600	11	99.8
5.sSMPABC016	-	0.00	110299	6611	179.77	1.10	0	0.060	2.035	0.810	3.343	0.098	2.652	0.793	0.029	2.901	601	22	603	8	603	8	577	8	100.1
5.sSMPABC082	-	0.00	108852	6525	177.25	1.39	0	0.060	2.069	0.811	3.394	0.098	2.691	0.793	0.029	2.886	601	22	603	8	603	8	580	8	100.1
5.sSMPABC056	-	0.27	97536	5841	158.81	1.58	1012	0.060	2.848	0.810	4.151	0.098	3.020	0.728	0.029	3.224	600	31	603	9	603	9	569	9	100.1
5.sSMPABC039	-	0.00	59302	3563	96.46	0.44	0	0.060	2.264	0.814	3.545	0.098	2.728	0.770	0.030	4.868	606	24	604	8	605	8	605	14	99.9
5.sSMPABC058	-	0.08	83974	5028	136.55	1.66	3326	0.060	2.207	0.811	3.493	0.098	2.707	0.775	0.028	2.970	599	24	604	8	603	8	564	8	100.2
5.sSMPABC038	-	0.00	57369	3447	93.26	0.66	0	0.060	2.463	0.814	3.859	0.098	2.971	0.770	0.031	5.100	607	27	604	9	605	9	609	15	99.9
5.sSMPABC084	-	0.57	94576	5623	153.15	0.72	477	0.059	4.399	0.809	5.648	0.099	3.543	0.627	0.030	3.490	584	48	607	10	602	13	593	10	100.8
5.sSMPABC066	seq0212	0.00	189847	11408	307.29	0.77	0	0.060	1.964	0.818	3.285	0.099	2.634	0.802	0.029	2.722	607	21	607	8	607	8	586	8	100.0
5.sSMPABC050	-	0.00	100387	6038	162.23	0.86	0	0.060	2.095	0.820	3.394	0.099	2.670	0.787	0.030	3.099	609	23	608	8	608	8	591	9	100.0
5.sSMPABC011	-	0.00	170161	10237	274.68	0.56	0	0.060	1.995	0.821	3.266	0.099	2.586	0.792	0.031	2.868	609	22	608	8	609	8	611	9	100.0
5.sSMPABC012	-	0.00	73771	4438	119.07	0.42	0	0.060	2.261	0.821	3.558	0.099	2.748	0.772	0.030	4.914	609	24	608	8	609	8	600	14	100.0
5.sSMPABC083	seq0227	0.00	48395	2920	78.00	1.05	0	0.060	2.387	0.825	3.760	0.099	2.905	0.773	0.028	4.228	615	26	609	8	611	9	566	12	99.8
5.sSMPABC051	-	0.22	74855	4492	120.61	1.46	1228	0.060	2.654	0.820	3.921	0.099	2.886	0.736	0.030	3.215	604	29	609	8	608	9	595	9	100.2
5.sSMPABC069	-	0.00	72103	4339	116.12	1.27	0	0.060	2.160	0.823	3.459	0.099	2.701	0.781	0.029	3.202	610	23	610	8	610	8	573	9	100.0
5.sSMPABC040	seq0215	0.14	127364	7650	204.68	1.70	1896	0.060	2.277	0.823	3.576	0.099	2.757	0.771	0.029	2.775	606	25	611	8	610	8	574	8	100.2
5.sSMPABC064	seq0214	0.19	97114	5835	155.88	1.56	1420	0.060	2.458	0.825	3.698	0.100	2.763	0.747	0.029	2.891	607	27	612	8	611	9	579	8	100.2
5.sSMPABC013	-	0.00	77363	4680	124.08	1.21	0	0.061	2.380	0.831	3.776	0.100	2.931	0.776	0.031	3.927	622	26	612	9	614	9	608	12	99.7
5.sSMPABC026	-	0.02	673067	40402	1079.28	0.07	12434	0.060	2.038	0.825	3.440	0.100	2.771	0.806	0.040	5.343	605	22	612	8	611	8	801	21	100.3
5.sSMPABC087	seq0224	0.00	120884	7303	193.78	0.26	0	0.060	2.086	0.830	3.403	0.100	2.689	0.790	0.032	4.317	618	23	612	8	614	8	627	13	99.8
5.sSMPABC068	-	0.00	88554	5342	141.81	1.55	0	0.060	2.255	0.830	3.538	0.100	2.726	0.771	0.029	3.447	615	24	613	8	613	8	578	10	99.9

LA(SF)-ICP-MS U-Pb zircon results data from Santa Tereza pluton (Sample CA-08)

Identifier	Lu-Hf identifier	f206[a]	207Pb	206Pb	U	Th[b]/U	206Pb/204Pb	Ratios[c]								Ages (Ma)[c]								% conc[e]
								207Pb/206Pb	2s (%)	207Pb/235U	2s (%)	206Pb/238U	2s (%)	Rho[d]	208Pb/232Th	2s (%)	207Pb/206Pb	2s abs	206Pb/238U	2s abs	207Pb/235U	2s abs	208Pb/232Th	2s abs	
		(%)	CPS	CPS	(ppm)			Data for Wetherill plot																
5.sSMPABC073	seq0232	0.00	43880	2642	70.26	1.23	0	0.060	2.591	0.828	3.938	0.100	2.967	0.753	0.030	4.444	611	28	613	9	613	9	592	13	100.1
5.sSMPABC071	seq0233	0.22	127851	7704	204.50	1.56	1258	0.060	2.595	0.830	3.918	0.100	2.935	0.749	0.028	3.121	613	28	614	9	614	9	562	9	100.0
5.sSMPABC028	seq0223	0.00	23908	1442	38.21	0.83	0	0.060	2.818	0.831	4.205	0.100	3.121	0.742	0.032	5.786	615	30	614	9	614	10	633	18	100.0
5.sSMPABC037	seq0216	0.00	51116	3082	81.62	0.73	0	0.060	2.223	0.832	3.542	0.100	2.758	0.779	0.029	4.024	614	24	615	8	615	8	575	11	100.0
5.sSMPABC086	seq0231	0.00	203575	12296	324.13	0.43	0	0.060	2.020	0.836	3.317	0.100	2.631	0.793	0.030	3.289	618	22	616	8	617	8	605	10	99.9
5.sSMPABC054	-	0.00	80207	4841	127.45	1.33	0	0.060	2.087	0.837	3.417	0.101	2.705	0.792	0.030	2.941	617	23	618	8	617	8	596	9	100.0
5.sSMPABC052	seq0211	0.26	101900	6135	161.62	1.47	1060	0.060	2.705	0.836	3.930	0.101	2.851	0.725	0.030	2.899	611	29	619	8	617	9	605	9	100.3
5.sSMPABC070	seq0209	0.00	96126	5809	151.84	1.51	0	0.060	2.052	0.843	3.383	0.101	2.689	0.795	0.029	2.851	619	22	621	8	621	8	587	8	100.1
5.sSMPABC017	-	0.00	149333	9039	235.77	0.33	0	0.061	2.016	0.845	3.265	0.101	2.569	0.787	0.031	3.590	623	22	621	8	622	8	621	11	100.0
5.sSMPABC059	seq0213	0.00	72377	4391	114.11	1.43	0	0.061	2.275	0.848	3.548	0.101	2.724	0.768	0.030	3.508	628	25	622	8	623	8	591	10	99.8
5.sSMPABC079	seq0229	0.00	38560	2330	60.78	0.76	0	0.060	2.615	0.844	3.949	0.101	2.960	0.749	0.030	5.523	619	28	622	9	622	9	606	16	100.1
5.sSMPABC027	seq0218	0.00	104278	6316	164.23	0.38	0	0.061	2.245	0.847	3.497	0.101	2.681	0.767	0.031	4.853	624	24	623	8	623	8	623	15	100.0
5.sSMPABC067	seq0208	0.00	123354	7467	194.02	1.23	0	0.061	2.049	0.848	3.371	0.102	2.678	0.794	0.028	3.004	623	22	624	8	623	8	557	8	100.0
5.sSMPABC045	seq0234	0.00	59971	3634	94.15	1.02	0	0.061	2.277	0.850	3.632	0.102	2.830	0.779	0.030	3.816	625	25	625	8	625	9	605	11	100.0
5.sSMPABC042	seq0226	0.10	158237	9608	246.11	1.84	2724	0.061	2.147	0.860	3.461	0.103	2.715	0.784	0.030	2.689	629	23	630	8	630	8	593	8	99.8
5.sSMPABC053	seq0210	0.00	129924	7910	202.21	1.74	0	0.061	2.070	0.862	3.331	0.103	2.611	0.784	0.030	2.824	635	22	630	8	631	8	592	8	100.0
5.sSMPABC029	**-**	**0.00**	**73651**	**4493**	**114.01**	**1.40**	**0**	**0.061**	**2.164**	**0.868**	**3.440**	**0.103**	**2.674**	**0.777**	**0.030**	**3.080**	**640**	**23**	**633**	**8**	**635**	**8**	**595**	**9**	**99.8**
5.sSMPABC044	**seq0235**	**0.00**	**66473**	**4063**	**102.84**	**1.27**	**0**	**0.061**	**2.192**	**0.870**	**3.487**	**0.103**	**2.711**	**0.778**	**0.031**	**3.278**	**644**	**24**	**634**	**8**	**636**	**8**	**608**	**10**	**99.6**
5.sSMPABC030	**seq0219**	**0.00**	**38799**	**2358**	**59.90**	**0.99**	**0**	**0.061**	**2.337**	**0.867**	**3.663**	**0.104**	**2.821**	**0.770**	**0.032**	**3.833**	**631**	**25**	**635**	**9**	**634**	**9**	**644**	**12**	**100.1**
5.sSMPABC024	**seq0221**	**0.00**	**347917**	**22862**	**422.99**	**0.27**	**0**	**0.066**	**2.009**	**1.191**	**3.275**	**0.131**	**2.587**	**0.790**	**0.047**	**3.646**	**797**	**21**	**796**	**10**	**796**	**9**	**932**	**17**	**100.0**
5.sSMPABC015	**seq0222**	**0.00**	**94527**	**5526**	**171.12**	**0.77**	**0**	**0.058**	**2.121**	**0.711**	**3.413**	**0.088**	**2.674**	**0.783**	**0.027**	**3.285**	**547**	**23**	**545**	**7**	**546**	**7**	**534**	**9**	**99.9**
5.sSMPABC031	**-**	**0.14**	**69022**	**4034**	**123.72**	**0.73**	**1995**	**0.058**	**2.381**	**0.718**	**3.646**	**0.089**	**2.761**	**0.757**	**0.028**	**3.564**	**547**	**26**	**550**	**7**	**550**	**8**	**559**	**10**	**100.1**
5.sSMPABC072	-	0.20	148867	8812	255.24	0.70	1398	0.059	2.590	0.761	3.807	0.093	2.790	0.733	0.027	4.148	574	28	574	8	574	8	539	11	100.0

LA(SF)-ICP-MS U-Pb zircon results data from Santa Tereza pluton (Sample CA-08)

Identifier	Lu-Hf identifier	f206[a] (%)	^{207}Pb CPS	^{206}Pb CPS	U (ppm)	Th[b]/U	$^{206}Pb/^{204}Pb$	Ratios[c] $^{207}Pb/^{206}Pb$	2s (%)	$^{207}Pb/^{235}U$	2s (%)	$^{206}Pb/^{238}U$	2s (%)	Rho[d]	$^{208}Pb/^{232}Th$	2s (%)	Ages (Ma)[c] $^{207}Pb/^{206}Pb$	2s abs	$^{206}Pb/^{238}U$	2s abs	$^{207}Pb/^{235}U$	2s abs	$^{208}Pb/^{232}Th$	2s abs	% conc[e]
								Data for Wetherill plot																	
5.sSMPABC055	-	0.00	88028	5216	150.36	1.16	0	0.059	2.127	0.764	3.399	0.094	2.651	0.780	0.027	3.208	576	23	576	7	576	8	547	9	100.0
5.sSMPABC008	seq0236	0.00	105671	6277	180.67	0.21	0	0.059	2.256	0.765	3.549	0.093	2.739	0.772	0.032	6.196	582	24	576	8	577	8	642	20	99.8
5.sSMPABC081	seq0228	0.00	88860	5261	151.72	0.34	0	0.059	2.196	0.764	3.508	0.094	2.736	0.780	0.029	4.873	575	24	577	8	576	8	573	14	100.1
5.sSMPABC078	-	0.00	123659	7311	210.26	0.35	0	0.059	2.097	0.766	3.405	0.094	2.682	0.788	0.029	4.006	572	23	579	7	577	8	577	11	100.3
5.sSMPABC022	-	0.00	161399	9545	273.93	1.03	0	0.059	2.063	0.768	3.279	0.094	2.549	0.777	0.029	2.947	572	22	580	7	578	7	568	8	100.3
5.sSMPABC025	seq0220	0.00	192935	11468	324.11	0.32	0	0.059	2.052	0.779	3.418	0.095	2.734	0.800	0.032	3.912	583	22	586	8	585	8	631	12	100.1
5.sSMPABC041	-	0.00	74184	4409	124.44	1.46	0	0.059	2.456	0.781	3.928	0.095	3.066	0.780	0.026	4.143	583	27	587	9	586	9	520	11	100.1
5.sSMPABC043	seq0225	0.00	100573	5998	168.63	1.34	0	0.060	2.079	0.784	3.364	0.095	2.645	0.786	0.027	2.914	591	23	587	7	588	8	547	8	99.9

[a] *percentage of the common Pb on the ^{206}Pb*

[b] *Th/U ratios are calculated relative to BB reference zircon*

[c] *data corrected for background, within-run Pb/U fractionation (in case of $^{206}Pb/^{238}U$) and common Pb using Stacey and Kramers (1975) model Pb composition*

[d] *Rho is the error correlation defined as the quotient of the propagated errors of the $^{206}Pb/^{238}U$ and the $^{207}Pb/^{235}U$ ratio*

[e] *Concordance calculated as (^{206}Pb-^{238}U age/^{207}Pb-^{206}Pb age)*100*

CPS = count per second

Spots in domains of dissolution–recrystallization, overgrowth or Pb lost rims are in red letter

Zircon grains not used for concordia age are in bold letter

PRIMARY REFERENCE STANDARD

LA(SF)-ICP-MS U-Pb zircon results data from BB-09 primary standard of the Jequitibá pluton (Sample CA-03)

Identifier	f206[a] (%)	^{207}Pb CPS	^{206}Pb CPS	U (ppm)	Th[b]/U	$^{206}Pb/^{204}Pb$	Ratios[c] $^{207}Pb/^{206}Pb$	2s (%)	$^{207}Pb/^{235}U$	2s (%)	$^{206}Pb/^{238}U$	2s (%)	Rho[d]	$^{208}Pb/^{232}Th$	2s (%)	Ages (Ma)[c] $^{207}Pb/^{206}Pb$	2s abs	$^{206}Pb/^{238}U$	2s abs	$^{207}Pb/^{235}U$	2s abs	$^{208}Pb/^{232}Th$	2s abs	% conc[e]
									Data for Wetherill plot															
5.sSMPABC269	0.00	178976	10488	605	0.61	0	0.059	2.048	0.735	3.339	0.091	2.637	0.790	0.027	3.537	552	22	561	7	560	7	541	10	100

PRIMARY REFERENCE STANDARD

LA(SF)-ICP-MS U-Pb zircon results data from BB-09 primary standard of the Jequitibá pluton (Sample CA-03)

Identifier	f206[a]	^{207}Pb	^{206}Pb	U	Th[b]/U	^{206}Pb/^{204}Pb	Ratios[c]									Ages (Ma)[c]								% conc[e]
							^{207}Pb/^{206}Pb	2s (%)	^{207}Pb/^{235}U	2s (%)	^{206}Pb/^{238}U	2s (%)	Rho[d]	^{208}Pb/^{232}Th	2s (%)	^{207}Pb/^{206}Pb	2s abs	^{206}Pb/^{238}U	2s abs	^{207}Pb/^{235}U	2s abs	^{208}Pb/^{232}Th	2s abs	
	(%)	CPS	CPS	(ppm)			Data for Wetherill plot																	
5.sSMPABC270	0.35	121026	7148	412	0.46	787	0.059	3.169	0.736	4.435	0.090	3.102	0.700	0.030	4.284	569	34	558	8	560	10	595	13	100
5.sSMPABC288	0.19	120775	7136	407	0.43	1406	0.059	2.591	0.744	3.847	0.091	2.844	0.739	0.030	5.279	570	28	564	8	565	8	589	15	100
5.sSMPABC289	0.44	123776	7228	416	0.45	623	0.058	3.712	0.737	4.976	0.092	3.314	0.666	0.028	4.973	545	41	565	9	561	11	561	14	101
5.sSMPABC307	0.00	126262	7355	422	0.45	0	0.058	2.163	0.740	3.555	0.092	2.821	0.794	0.027	5.106	539	24	568	8	562	8	547	14	101
5.sSMPABC308	0.00	129218	7646	432	0.46	0	0.059	2.467	0.751	3.950	0.092	3.084	0.781	0.028	6.916	573	27	568	8	569	9	565	19	100
5.sSMPABC001	0.00	94972	5604.3	353	0.45	0	0.059	2.203	0.739	3.407	0.091	2.599	0.763	0.029	5.141	567	24	560	7	562	7	574	15	100
5.sSMPABC002	0.00	98660	5887	364	0.45	0	0.060	2.112	0.752	3.369	0.091	2.625	0.779	0.029	4.851	592	23	564	7	570	7	575	14	99
5.sSMPABC039	0.00	114498	6831	422	0.45	0	0.060	2.213	0.753	3.396	0.092	2.576	0.759	0.027	5.852	591	24	565	7	570	7	545	16	99
5.sSMPABC040	0.00	111045	6591.6	411	0.44	0	0.059	2.358	0.746	3.535	0.091	2.634	0.745	0.030	6.669	580	26	562	7	566	8	597	20	99
5.sSMPABC059	0.00	129760	7670.1	478	0.43	0	0.059	2.267	0.746	3.433	0.092	2.578	0.751	0.028	6.039	571	25	565	7	566	7	568	17	100
5.sSMPABC077	0.00	113685	6650.6	416	0.44	0	0.059	2.359	0.742	3.548	0.092	2.651	0.747	0.027	6.994	549	26	568	7	564	8	536	19	101
5.sSMPABC078	0.00	123870	7328.1	459	0.45	0	0.059	2.502	0.743	3.796	0.091	2.855	0.752	0.030	7.643	573	27	562	8	564	8	594	22	100

LA(SF)-ICP-MS U-Pb zircon results data from BB-09 primary standard of the Santa Tereza pluton (Sample CA-08)

Identifier	f206[a]	^{207}Pb	^{206}Pb	U	Th[b]/U	^{206}Pb/^{204}Pb	Ratios[c]									Ages (Ma)[c]								% conc[e]
							^{207}Pb/^{206}Pb	2s (%)	^{207}Pb/^{235}U	2s (%)	^{206}Pb/^{238}U	2s (%)	Rho[d]	^{208}Pb/^{232}Th	2s (%)	^{207}Pb/^{206}Pb	2s abs	^{206}Pb/^{238}U	2s abs	^{207}Pb/^{235}U	2s abs	^{208}Pb/^{232}Th	2s abs	
	(%)	CPS	CPS	(ppm)			Data for Wetherill plot																	
5.sSMPABC001	0.03	235662	13735	408	0.45	8686	0.058	1.001	0.741	1.626	0.092	1.282	0.788	0.029	1.473	540	22	568	7	563	7	568	8	101
5.sSMPABC006	0.00	242798	14332	426	0.45	0	0.059	0.983	0.740	1.610	0.091	1.275	0.792	0.028	1.408	568	21	561	7	563	7	566	8	100
5.sSMPABC007	0.00	238488	14281	418	0.45	0	0.060	0.985	0.752	1.610	0.091	1.273	0.791	0.028	1.477	599	21	562	7	570	7	567	8	99
5.sSMPABC018	0.00	234730	13877	409	0.44	0	0.059	0.981	0.748	1.618	0.092	1.286	0.795	0.028	1.490	572	21	566	7	567	7	562	8	100
5.sSMPABC019	0.00	230643	13569	403	0.45	0	0.059	0.986	0.741	1.625	0.091	1.292	0.795	0.028	1.497	561	21	563	7	563	7	559	8	100

LA(SF)-ICP-MS U-Pb zircon results data from BB-09 primary standard of the Santa Tereza pluton (Sample CA-08)

Identifier	f206 [a]	^{207}Pb	^{206}Pb	U	Th[b]/U	$^{206}Pb/^{204}Pb$	Ratios[c]									Ages (Ma)[c]								% conc[e]
							$^{207}Pb/^{206}Pb$	2s (%)	$^{207}Pb/^{235}U$	2s (%)	$^{206}Pb/^{238}U$	2s (%)	Rho[d]	$^{208}Pb/^{232}Th$	2s (%)	$^{207}Pb/^{206}Pb$	2s abs	$^{206}Pb/^{238}U$	2s abs	$^{207}Pb/^{235}U$	2s abs	$^{208}Pb/^{232}Th$	2s abs	
	(%)	CPS	CPS	(ppm)			Data for Wetherill plot																	
5.sSMPABC032	0.00	234051	13622	408	0.45	0	0.058	0.997	0.736	1.627	0.092	1.286	0.790	0.028	1.505	537	22	566	7	560	7	556	8	101
5.sSMPABC033	0.02	233958	13736	412	0.46	17527	0.059	0.989	0.735	1.617	0.091	1.279	0.791	0.028	1.446	556	22	560	7	559	7	552	8	100
5.sSMPABC046	0.16	231227	13618	409	0.45	1656	0.059	1.147	0.734	1.759	0.090	1.333	0.758	0.028	1.489	563	25	558	7	559	8	562	8	100
5.sSMPABC047	0.12	231763	13662	403	0.45	2240	0.059	1.083	0.746	1.701	0.092	1.313	0.771	0.029	1.465	565	24	566	7	566	7	571	8	100
5.sSMPABC060	0.00	233183	13700	406	0.45	0	0.059	1.004	0.743	1.649	0.092	1.307	0.793	0.028	1.545	558	22	566	7	564	7	568	9	100
5.sSMPABC061	0.00	234750	13827	409	0.46	0	0.059	1.002	0.744	1.649	0.092	1.310	0.794	0.027	1.540	563	22	565	7	565	7	544	8	100
5.sSMPABC074	0.00	236341	13902	411	0.44	0	0.059	1.003	0.745	1.646	0.092	1.305	0.793	0.028	1.551	560	22	567	7	566	7	565	9	100
5.sSMPABC075	0.00	233316	13663	407	0.45	0	0.059	1.008	0.740	1.652	0.092	1.309	0.793	0.028	1.570	551	22	565	7	562	7	559	9	101
5.sSMPABC088	0.00	242681	14364	426	0.45	0	0.059	1.014	0.743	1.662	0.091	1.317	0.792	0.028	1.576	574	22	562	7	564	7	556	9	100
5.sSMPABC089	0.27	242144	14281	425	0.44	998	0.059	1.375	0.741	1.996	0.091	1.447	0.725	0.029	1.578	566	30	562	8	563	9	581	9	100

[a] percentage of the common Pb on the ^{206}Pb

[b] Th/U ratios are calculated relative to BB reference zircon

[c] data corrected for background, within-run Pb/U fractionation (in case of $^{206}Pb/^{238}U$) and common Pb using Stacey and Kramers (1975) model Pb composition

[d] Rho is the error correlation defined as the quotient of the propagated errors of the $^{206}Pb/^{238}U$ and the $^{207}Pb/^{235}U$ ratio

*[e] Concordance calculated as (^{206}Pb-^{238}U age/^{207}Pb-^{206}Pb age)*100*

CPS = count per second

SECONDARY REFERENCE STANDARD

LA(SF)-ICP-MS U-Pb zircon results data from Plesovice secondary standard of the Jequitibá pluton (Sample CA-03)

Identifier	f206[a]	^{207}Pb	^{206}Pb	U	Th[b]/U	^{206}Pb/^{204}Pb	Ratios[c]									Ages (Ma)[c]								% conc[e]
							^{207}Pb/^{206}Pb	2s (%)	^{207}Pb/^{235}U	2s (%)	^{206}Pb/^{238}U	2s (%)	Rho[d]	^{208}Pb/^{232}Th	2s (%)	^{207}Pb/^{206}Pb	2s abs	^{206}Pb/^{238}U	2s abs	^{207}Pb/^{235}U	2s abs	^{208}Pb/^{232}Th	2s abs	
	(%)	CPS	CPS	(ppm)			Data for Wetherill plot																	
5.sSMPABC252	0.00	**2E+05**	**11526**	1255	0.11	0	0.053	1.075	0.390	1.756	0.053	1.389	0.791	0.019	2.703	331	24	335	5	334	5	385	10	100
5.sSMPABC271	0.00	173086	9160	1001	0.11	0	0.053	1.077	0.388	1.729	0.053	1.353	0.782	0.017	2.725	325	24	334	4	333	5	338	9	100
5.sSMPABC272	0.00	163292	8679	938	0.11	0	0.053	1.072	0.392	1.691	0.054	1.307	0.773	0.018	2.624	335	24	336	4	336	5	351	9	100
5.sSMPABC290	0.00	172540	9176	996	0.11	0	0.053	1.072	0.391	1.754	0.053	1.389	0.792	0.017	2.759	336	24	335	5	335	5	349	10	100
5.sSMPABC291	0.00	164147	8734	948	0.11	0	0.053	1.071	0.391	1.724	0.053	1.351	0.784	0.016	2.841	338	24	335	4	335	5	325	9	100
5.sSMPABC309	0.05	184324	9802	1050	0.11	5832	0.053	1.197	0.396	1.912	0.054	1.491	0.780	0.016	3.783	336	27	339	5	339	6	329	12	100
5.sSMPABC310	0.00	125649	6680	724	0.10	0	0.053	1.354	0.392	2.019	0.053	1.497	0.742	0.017	5.284	336	31	336	5	336	6	349	18	100
5.sSMPABC003	0.00	187751	10003	1167	0.10	0	0.053	1.089	0.398	1.717	0.054	1.327	0.773	0.017	3.114	341	25	341	4	341	5	348	11	100
5.sSMPABC004	0.00	153185	8111	951	0.11	0	0.053	1.152	0.397	1.813	0.054	1.399	0.772	0.017	3.919	327	26	341	5	339	5	338	13	101
5.sSMPABC022	0.00	177814	9445.5	1108	0.12	0	0.053	1.167	0.396	1.883	0.054	1.478	0.785	0.016	4.326	334	26	340	5	339	5	315	14	100
5.sSMPABC023	0.00	169819	9098.9	1058	0.10	0	0.054	1.213	0.400	1.912	0.054	1.478	0.773	0.015	6.362	353	27	340	5	342	6	303	19	99
5.sSMPABC041	0.00	151426	8016.5	935	0.10	0	0.053	1.247	0.399	1.923	0.055	1.464	0.761	0.019	4.818	326	28	343	5	341	6	374	18	101
5.sSMPABC042	0.00	206320	10914	1274	0.09	0	0.053	1.248	0.398	1.815	0.055	1.319	0.726	0.018	4.530	325	28	343	4	340	5	354	16	101
5.sSMPABC060	0.00	215744	11432	1339	0.11	0	0.053	1.227	0.397	1.945	0.054	1.509	0.776	0.017	4.403	328	28	341	5	339	6	346	15	100
5.sSMPABC079	0.00	152155	8102.3	949	0.11	0	0.053	1.239	0.397	1.901	0.054	1.442	0.758	0.016	5.102	339	28	340	5	340	6	315	16	100
5.sSMPABC080	0.32	139465	7359.6	870	0.09	836	0.053	1.771	0.393	2.513	0.054	1.783	0.710	0.014	6.197	319	40	339	6	337	7	285	18	101

LA(SF)-ICP-MS U-Pb zircon results data from Plesovice secondary standard of the Santa Tereza pluton (Sample CA-08)

Identifier	f206[a]	^{207}Pb	^{206}Pb	U	Th[b]/U	$^{206}Pb/^{204}Pb$	Ratios[c]									Ages (Ma)[c]								% conc[e]
							$^{207}Pb/^{206}Pb$	2s (%)	$^{207}Pb/^{235}U$	2s (%)	$^{206}Pb/^{238}U$	2s (%)	Rho[d]	$^{208}Pb/^{232}Th$	2s (%)	$^{207}Pb/^{206}Pb$	2s abs	$^{206}Pb/^{238}U$	2s abs	$^{207}Pb/^{235}U$	2s abs	$^{208}Pb/^{232}Th$	2s abs	
	(%)	CPS	CPS	(ppm)			Data for Wetherill plot																	
5.sSMPABC003	0.15	235927	12535	700	0.20	1803	0.053	1.177	0.394	1.812	0.054	1.378	0.761	0.018	2.160	334	27	338	5	338	5	352	7	100
5.sSMPABC004	0.00	236576	12588	694	0.21	62799	0.053	0.996	0.399	1.627	0.054	1.286	0.791	0.017	1.804	338	23	342	4	341	5	333	6	100
5.sSMPABC005	0.00	133443	7096	397	0.13	0	0.053	1.053	0.394	1.676	0.054	1.304	0.778	0.017	3.037	336	24	337	4	337	5	343	11	100
5.sSMPABC020	0.03	133380	7079	395	0.12	7713	0.053	1.045	0.395	1.669	0.054	1.302	0.780	0.018	3.057	332	24	339	4	338	5	367	11	100
5.sSMPABC021	0.00	147195	7831	431	0.13	0	0.053	1.034	0.400	1.648	0.055	1.284	0.779	0.015	3.230	337	23	342	4	342	5	298	10	100
5.sSMPABC034	0.09	156059	8295	461	0.14	2861	0.053	1.075	0.396	1.718	0.054	1.340	0.780	0.017	2.593	335	24	339	4	339	5	340	9	100
5.sSMPABC035	0.00	117048	6228	347	0.13	0	0.053	1.090	0.395	1.754	0.054	1.375	0.784	0.015	4.186	338	25	338	5	338	5	297	12	100
5.sSMPABC048	0.00	116070	6182	344	0.13	0	0.053	1.014	0.396	1.675	0.054	1.334	0.796	0.018	2.710	340	23	339	4	339	5	370	10	100
5.sSMPABC049	0.00	119927	6384	356	0.13	0	0.053	1.146	0.395	1.760	0.054	1.336	0.759	0.018	3.906	339	26	338	4	338	5	359	14	100
5.sSMPABC062	0.05	223413	11857	662	0.20	5386	0.053	1.016	0.395	1.659	0.054	1.311	0.790	0.017	1.928	332	23	339	4	338	5	333	6	100
5.sSMPABC063	0.00	188955	10049	558	0.16	0	0.053	1.034	0.397	1.656	0.054	1.293	0.781	0.017	2.358	336	23	340	4	339	5	340	8	100
5.sSMPABC076	0.00	177426	9437	528	0.14	0	0.053	1.034	0.393	1.665	0.054	1.305	0.784	0.017	2.487	337	23	337	4	337	5	339	8	100
5.sSMPABC077	0.00	173331	9223	515	0.15	0	0.053	1.015	0.395	1.650	0.054	1.301	0.788	0.016	2.441	338	23	338	4	338	5	329	8	100

[a] percentage of the common Pb on the ^{206}Pb

[b] Th/U ratios are calculated relative to BB reference zircon

[c] data corrected for background, within-run Pb/U fractionation (in case of $^{206}Pb/^{238}U$) and common Pb using Stacey and Kramers (1975) model Pb composition

[d] Rho is the error correlation defined as the quotient of the propagated errors of the $^{206}Pb/^{238}U$ and the $^{207}/^{235}U$ ratio

[c] *Concordance calculated as (^{206}Pb-^{238}U age/^{207}Pb-^{206}Pb age)*100*

CPS = count per second

LA-(MC)ICP-MS Lu-Hf zircon results data from Jequitibá pluton (Sample CA-03)

Identifier	^{176}Yb/^{177}Hf [a]	±2s	^{176}Lu/^{177}Hf [a]	±2s	^{178}Hf/^{177}Hf	^{180}Hf/^{177}Hf	Sig_{Hf} [b] (V)	^{176}Hf/^{177}Hf	±2s [c]	^{176}Hf/^{177}Hf$_{(t)}$ [d]	eHf(t) [d]	±2s [c]	T_{DM} [e] (Ga)	T_{DM} [f] (Ga)	T_{DM} [g] (Ga)	U-Pb identifier	Age (Ma)[h]	±2σ
seq0019	0.019645	18.1	0.000471	3.2	1.467245	1.886764	10.0	0.282307	14.7	0.282302	-3.5	0.85	1.44	1.67	1.41	5.sSMPABC016	608	8
seq0020	0.047024	40.4	0.000957	7.2	1.467243	1.886827	16.5	0.282329	21.6	0.282318	-2.9	0.92	1.41	1.64	1.37	5.sSMPABC015	609	7
seq0021	0.066241	95.0	0.001394	18.3	1.467243	1.886881	12.4	0.282199	15.6	0.282184	-8.0	1.26	1.67	1.91	1.64	5.sSMPABC012	593	8
seq0022	0.008839	8.5	0.000204	1.6	1.467154	1.886862	14.5	0.282292	14.7	0.282289	-4.4	0.83	1.47	1.70	1.44	5.sSMPABC024	588	8
seq0023	**0.042447**	**37.0**	**0.000856**	**6.0**	**1.467227**	**1.886922**	**14.3**	**0.282318**	**19.5**	**0.282307**	**-2.3**	**0.91**	**1.41**	**1.64**	**1.38**	**5.sSMPABC028**	**652**	**8**
seq0024	0.076030	65.6	0.001496	10.8	1.467247	1.886869	15.6	0.282376	14.3	0.282359	-1.7	1.06	1.33	1.56	1.30	5.sSMPABC076	597	8
seq0025	**0.033564**	**29.7**	**0.000669**	**4.7**	**1.467220**	**1.886821**	**13.8**	**0.282290**	**14.9**	**0.282282**	**-4.7**	**0.88**	**1.49**	**1.72**	**1.45**	**5.sSMPABC005**	**585**	**7**
seq0026	0.067649	56.8	0.001387	10.1	1.467224	1.886941	14.5	0.282359	13.9	0.282343	-2.3	1.00	1.36	1.59	1.33	5.sSMPABC006	599	7
seq0027	**0.010159**	**8.3**	**0.000217**	**1.3**	**1.467187**	**1.886835**	**14.4**	**0.282308**	**15.6**	**0.282305**	**-3.0**	**0.83**	**1.43**	**1.66**	**1.39**	**5.sSMPABC306**	**624**	**8**
seq0028	0.033335	43.2	0.000732	8.4	1.467187	1.886907	12.1	0.281383	20.4	0.281375	-36.4	0.93	3.21	3.44	3.18	5.sSMPABC075	607	8
seq0029	0.052131	58.4	0.001047	9.3	1.467210	1.886851	8.8	0.282369	15.924685	0.282357	-2.0	1.01	1.34	1.57	1.31	5.sSMPABC031	588	7
seq0030	**0.069820**	**58.7**	**0.001499**	**9.8**	**1.467183**	**1.886962**	**12.3**	**0.282367**	**14.08959**	**0.282348**	**0.0**	**1.02**	**1.31**	**1.54**	**1.28**	**5.sSMPABC045**	**693**	**9**
seq0031	0.026763	23.6	0.000537	3.8	1.467218	1.886909	13.1	0.282313	18.929631	0.282307	-3.9	0.86	1.44	1.67	1.41	5.sSMPABC035	585	8
seq0032	0.024548	19.8	0.000518	3.1	1.467190	1.886845	13.5	0.282301	14.943596	0.282296	-4.2	0.85	1.46	1.69	1.43	5.sSMPABC070	585	8
seq0033	0.037201	36.2	0.000753	6.2	1.467242	1.886988	13.1	0.282306	13.076787	0.282298	-3.8	0.90	1.45	1.68	1.42	5.sSMPABC069	602	8
seq0034	**0.033720**	**27.8**	**0.000654**	**4.2**	**1.46718805**	**1.886849**	**16.5**	**0.282317**	**12.50368**	**0.282310**	**-3.8**	**0.87**	**1.43**	**1.67**	**1.40**	**5.sSMPABC282**	**574**	**7**
seq0035	0.035469	28.7	0.000718	4.5	1.467224768	1.886816	13.8	0.282363	15.869174	0.282355	-1.9	0.88	1.34	1.57	1.31	5.sSMPABC065	596	8
seq0036	0.016159	14.1	0.000335	2.6	1.467200898	1.886913	14.7	0.282291	26.850299	0.282287	-4.5	0.84	1.48	1.71	1.44	5.sSMPABC066	588	8
seq0037	0.004594	3.8	0.000094	0.6	1.46725718	1.886841	12.7	0.282298	17.402215	0.282297	-3.8	0.83	1.45	1.68	1.42	5.sSMPABC063	604	8
seq0038	0.046671	40.8	0.000947	10.0	1.467256423	1.886866	13.5	0.281851	22.665171	0.281840	-20.0	0.92	2.33	2.56	2.30	5.sSMPABC053	602	8
seq0039	**0.004383**	**3.5**	**0.000096**	**0.6**	**1.4672088**	**1.886740**	**15.9**	**0.282285**	**15.07779**	**0.282284**	**-4.7**	**0.83**	**1.48**	**1.72**	**1.45**	**5.sSMPABC052**	**584**	**8**
seq0040	0.044195	36.4	0.000880	5.5	1.467213109	1.886810	13.5	0.282327	14.622759	0.282317	-3.1	0.90	1.41	1.64	1.38	5.sSMPABC050	604	8

LA-(MC)ICP-MS Lu-Hf zircon results data from Jequitibá pluton (Sample CA-03)

Identifier	$^{176}Yb/^{177}Hf$ [a]	±2s	$^{176}Lu/^{177}Hf$ [a]	±2s	$^{178}Hf/^{177}Hf$	$^{180}Hf/^{177}Hf$	Sig_{Hf} [b] (V)	$^{176}Hf/^{177}Hf$	±2s [c]	$^{176}Hf/^{177}Hf_{(t)}$ [d]	eHf(t) [d]	±2s [c]	T_{DM} [e] (Ga)	T_{DM} [f] (Ga)	T_{DM} [g] (Ga)	U-Pb identifier	Age (Ma)[h]	±2σ
seq0041	0.042663	34.3	0.000858	5.2	1.467207491	1.886836	10.2	0.282338	15.493719	0.282329	-3.1	0.90	1.40	1.63	1.36	5.sSMPABC048	586	8
seq0042	0.042593	34.6	0.000879	5.4	1.467255769	1.886903	17.2	0.282317	17.563442	0.282307	-3.7	0.90	1.43	1.67	1.40	5.sSMPABC056	593	8
seq0043	0.054087	44.9	0.001133	7.0	1.467162863	1.886868	12.0	0.282357	13.6	0.282345	-2.4	0.94	1.36	1.60	1.33	5.sSMPABC072	590	7
seq0044	**0.052313**	**43.8**	**0.001128**	**7.7**	**1.46717769**	**1.886877**	**13.6**	**0.282362**	**17.0**	**0.282350**	**-2.5**	**0.94**	**1.36**	**1.59**	**1.33**	**5.sSMPABC297**	**578**	**8**
seq0045	**0.005986**	**4.8**	**0.000119**	**0.7**	**1.46719479**	**1.886793**	**13.4**	**0.282304**	**19.3**	**0.282303**	**-4.2**	**0.83**	**1.45**	**1.68**	**1.42**	**5.sSMPABC296**	**576**	**8**
seq0046	**0.026337**	**21.1**	**0.000541**	**3.2**	**1.46726343**	**1.886848**	**13.1**	**0.282298**	**18.9**	**0.282292**	**-4.9**	**0.85**	**1.48**	**1.71**	**1.45**	**5.sSMPABC293**	**562**	**7**
seq0056	0.010461	10.0	0.000220	1.8	1.467223497	1.886871	17.1	0.282079	24.0	0.282076	-11.8	0.83	1.88	2.11	1.85	5.sSMPABC292	597	8
seq0057	0.039882	34.9	0.000810	5.8	1.467172753	1.886760	16.3	0.282143	21.8	0.282134	-9.9	0.90	1.77	2.00	1.74	5.sSMPABC285	587	8
seq0058	**0.030093**	**32.6**	**0.000719**	**6.2**	**1.467267**	**1.886748**	**12.6**	**0.281814**	**16.3**	**0.281807**	**-21.7**	**0.89**	**2.40**	**2.63**	**2.37**	**5.sSMPABC305**	**582**	**8**
seq0059	0.035387	28.8	0.000860	5.3	1.467192	1.886770	14.5	0.282145	16.1	0.282136	-9.7	0.88	1.77	2.00	1.73	5.sSMPABC262	595	9
seq0060	**0.040580**	**33.2**	**0.000971**	**6.1**	**1.467206**	**1.886767**	**14.0**	**0.281913**	**18.7**	**0.281895**	**-9.3**	**0.89**	**2.07**	**2.29**	**2.02**	**5.sSMPABC286**	**992**	**13**
seq0061	**0.014851**	**13.1**	**0.000345**	**2.5**	**1.467262**	**1.886839**	**17.4**	**0.282126**	**21.9**	**0.282122**	**-10.6**	**0.84**	**1.80**	**2.03**	**1.77**	**5.sSMPABC256**	**577**	**8**
seq0062	**0.002767**	**3.1**	**0.000061**	**0.6**	**1.467216**	**1.886783**	**14.7**	**0.282095**	**19.6**	**0.282094**	**-11.7**	**0.83**	**1.86**	**2.09**	**1.83**	**5.sSMPABC257**	**572**	**7**
seq0063	**0.033261**	**36.4**	**0.000711**	**6.8**	**1.467242**	**1.886854**	**17.3**	**0.282133**	**19.7**	**0.282125**	**-10.5**	**0.90**	**1.79**	**2.03**	**1.76**	**5.sSMPABC274**	**577**	**8**
seq0064	**0.039282**	**44.2**	**0.000800**	**8.3**	**1.467262**	**1.886856**	**9.9**	**0.282113**	**19.0**	**0.282104**	**-11.4**	**0.94**	**1.84**	**2.07**	**1.81**	**5.sSMPABC303**	**570**	**8**
seq0065	0.014917	13.9	0.000380	3.0	1.467223	1.886888	10.6	0.281931	15.9	0.281927	-17.6	0.84	2.18	2.41	2.15	5.sSMPABC281	581	9
seq0066	**0.053981**	**45.6**	**0.001105**	**7.4**	**1.467253**	**1.886864**	**12.0**	**0.282182**	**17.0**	**0.282171**	**-9.2**	**0.94**	**1.71**	**1.95**	**1.68**	**5.sSMPABC273**	**560**	**7**
seq0067	0.017958	14.7	0.000403	2.5	1.467219	1.886864	15.5	0.282084	27.6	0.282079	-11.9	0.84	1.88	2.11	1.85	5.sSMPABC267	588	8
seq0068	**0.005545**	**8.9**	**0.000161**	**2.5**	**1.467236**	**1.886700**	**13.0**	**0.282088**	**19.5**	**0.282086**	**-12.0**	**0.83**	**1.87**	**2.10**	**1.84**	**5.sSMPABC264**	**570**	**7**
seq0069	0.041282	62.5	0.000949	13.3	1.467267	1.886890	13.9	0.282081	19.8	0.282071	-12.3	1.04	1.90	2.13	1.87	5.sSMPABC265	581	8
seq0070	**0.040744**	**41.7**	**0.000936**	**8.7**	**1.467196**	**1.886802**	**12.7**	**0.282265**	**15.3**	**0.282250**	**0.6**	**0.93**	**1.43**	**1.65**	**1.39**	**5.sSMPABC301**	**873**	**11**
seq0071	0.025878	24.3	0.000567	4.7	1.467194	1.886895	17.4	0.282122	21.9	0.282116	-10.5	0.86	1.81	2.04	1.78	5.sSMPABC302	589	8
seq0072	**0.050398**	**43.2**	**0.000994**	**6.5**	**1.467178**	**1.886861**	**19.6**	**0.282144**	**19.1**	**0.282133**	**-10.0**	**0.93**	**1.77**	**2.01**	**1.74**	**5.sSMPABC027**	**586**	**8**
seq0073	**0.038169**	**38.2**	**0.000842**	**7.4**	**1.467261**	**1.886755**	**13.8**	**0.281924**	**14.9**	**0.281908**	**-8.8**	**0.91**	**2.04**	**2.26**	**2.00**	**5.sSMPABC279**	**993**	**13**
seq0074	**0.099805**	**126.2**	**0.002030**	**22.1**	**1.467245**	**1.886866**	**17.1**	**0.282207**	**16.2**	**0.282181**	**-5.7**	**1.51**	**1.64**	**1.87**	**1.60**	**5.sSMPABC280**	**700**	**9**

LA-(MC)ICP-MS Lu-Hf zircon results data from Santa Tereza pluton (Sample CA-08)

Identifier	$^{176}Yb/^{177}Hf$ [a]	±2s	$^{176}Lu/^{177}Hf$ [a]	±2s	$^{178}Hf/^{177}Hf$	$^{180}Hf/^{177}Hf$	Sig_{Hf} [b] (V)	$^{176}Hf/^{177}Hf$	±2s [c]	$^{176}Hf/^{177}Hf_{(t)}$ [d]	eHf(t) [d]	±2s [c]	T_{DM} [e] (Ga)	T_{DM} [f] (Ga)	T_{DM} [g] (Ga)	U-Pb identifier	Age (Ma)[h]	±2σ
seq0208	0.045517	36.5	0.000949	5.7	1.467202	1.886891	11.2	0.282344	16.5	0.282333	-2.1	0.90	1.37	1.60	1.34	5.sSMPABC067	624	8
seq0209	0.077995	63.0	0.001600	9.6	1.467161	1.886786	10.7	0.282435	19.8	0.282416	0.8	1.04	1.21	1.44	1.18	5.sSMPABC070	621	8
seq0210	0.107635	86.6	0.002212	13.3	1.467163	1.886812	11.0	0.282480	15.1	0.282454	2.3	1.20	1.13	1.37	1.10	5.sSMPABC053	630	8
seq0211	0.080573	64.8	0.001681	10.1	1.467213	1.886816	11.0	0.282418	17.5	0.282399	0.1	1.05	1.25	1.48	1.21	5.sSMPABC052	619	8
seq0212	0.053097	43.9	0.001131	7.3	1.467219	1.886818	15.5	0.282340	17.0	0.282327	-2.7	0.94	1.39	1.62	1.36	5.sSMPABC066	607	8
seq0213	0.047866	39.3	0.001015	6.6	1.467222	1.886954	14.3	0.282324	22.7	0.282312	-2.8	0.92	1.41	1.64	1.38	5.sSMPABC059	622	8
seq0214	0.082461	92.0	0.001712	16.4	1.467237	1.886923	12.0	0.282407	27.5	0.282387	-0.4	1.24	1.27	1.50	1.24	5.sSMPABC064	612	8
seq0215	0.121431	100.1	0.002563	16.1	1.467182	1.886903	8.3	0.282487	16.8	0.282457	2.1	1.30	1.13	1.37	1.10	5.sSMPABC040	611	8
seq0216	0.034740	38.1	0.000757	7.6	1.467225	1.886759	12.4	0.282299	14.7	0.282290	-3.8	0.91	1.46	1.69	1.43	5.sSMPABC037	615	8
seq0217	0.060103	50.2	0.001279	8.1	1.467200	1.886761	11.9	0.282378	17.3	0.282364	-1.7	0.97	1.32	1.56	1.29	5.sSMPABC036	593	8
seq0218	0.044457	38.6	0.000950	8.9	1.467235	1.886920	12.5	0.282339	22.8	0.282328	-2.3	0.91	1.38	1.61	1.35	5.sSMPABC027	623	8
seq0219	**0.042586**	**39.1**	**0.000904**	**6.3**	**1.467226**	**1.886925**	**11.9**	**0.282327**	**19.4**	**0.282316**	**-2.4**	**0.92**	**1.40**	**1.63**	**1.37**	**5.sSMPABC030**	**635**	**9**
seq0220	**0.029724**	**25.2**	**0.000670**	**4.6**	**1.467187**	**1.886790**	**14.5**	**0.282313**	**16.6**	**0.282306**	**-3.9**	**0.86**	**1.44**	**1.67**	**1.41**	**5.sSMPABC025**	**586**	**8**
seq0221	**0.098042**	**80.1**	**0.001867**	**11.8**	**1.467248**	**1.886887**	**7.5**	**0.282180**	**14.0**	**0.282152**	**-4.6**	**1.15**	**1.65**	**1.88**	**1.61**	**5.sSMPABC024**	**796**	**10**
seq0222	**0.037716**	**35.0**	**0.000816**	**5.8**	**1.467248**	**1.886738**	**12.3**	**0.282322**	**20.8**	**0.282313**	**-4.5**	**0.90**	**1.44**	**1.68**	**1.41**	**5.sSMPABC015**	**545**	**7**
seq0223	0.026132	22.3	0.000559	4.7	1.467190	1.886876	12.1	0.282305	18.0	0.282298	-3.5	0.86	1.44	1.68	1.41	5.sSMPABC028	614	9
seq0224	0.035886	30.2	0.000775	5.7	1.467292	1.886798	11.3	0.282317	17.9	0.282309	-3.2	0.88	1.42	1.66	1.39	5.sSMPABC087	612	8
seq0225	**0.073287**	**63.3**	**0.001569**	**11.0**	**1.467186**	**1.886699**	**9.0**	**0.282389**	**14.3**	**0.282372**	**-1.5**	**1.04**	**1.31**	**1.54**	**1.28**	**5.sSMPABC043**	**587**	**7**
seq0226	0.089382	73.5	0.001870	11.5	1.467191	1.886822	11.8	0.282430	18.9	0.282408	0.7	1.11	1.22	1.46	1.19	5.sSMPABC042	630	8
seq0227	0.049610	41.4	0.001031	6.8	1.467205	1.886846	13.4	0.282338	17.3	0.282326	-2.6	0.93	1.39	1.62	1.36	5.sSMPABC083	609	8
seq0228	**0.024264**	**20.2**	**0.000543**	**4.0**	**1.467196**	**1.886823**	**13.5**	**0.282294**	**14.7**	**0.282288**	**-4.7**	**0.85**	**1.48**	**1.71**	**1.45**	**5.sSMPABC081**	**577**	**8**
seq0229	0.053833	79.6	0.001128	14.1	1.467121	1.886864	8.6	0.282322	31.7	0.282309	-3.0	1.15	1.42	1.65	1.39	5.sSMPABC079	622	9
seq0230	0.028326	23.2	0.000620	4.0	1.467254	1.886932	13.5	0.282324	23.8	0.282317	-3.2	0.86	1.41	1.65	1.38	5.sSMPABC080	597	8
seq0231	0.041341	34.4	0.000896	5.7	1.467185	1.886963	11.9	0.282281	16.8	0.282271	-4.4	0.90	1.50	1.73	1.46	5.sSMPABC086	616	8

seq0232	0.024309	21.4	0.000520	3.3	1.467236	1.886942	11.9	0.282296	15.7	0.282290	-3.8	0.85	1.46	1.69	1.43	5.sSMPABC073	613	9
seq0233	0.039698	44.6	0.000828	8.0	1.467180	1.886777	12.2	0.282325	20.2	0.282315	-2.9	0.94	1.41	1.64	1.38	5.sSMPABC071	614	9
seq0234	0.075705	66.9	0.001610	11.7	1.467244	1.886889	8.0	0.282376	16.1	0.282357	-1.2	1.06	1.32	1.56	1.29	5.sSMPABC045	625	8
seq0235	**0.042256**	**34.9**	**0.000916**	**5.9**	**1.467233**	**1.886824**	**8.4**	**0.282338**	**20.1**	**0.282327**	**-2.1**	**0.90**	**1.38**	**1.61**	**1.35**	**5.sSMPABC044**	**634**	**8**
seq0236	**0.023719**	**22.2**	**0.000527**	**4.0**	**1.467237**	**1.886774**	**15.3**	**0.282293**	**17.1**	**0.282287**	**-4.8**	**0.86**	**1.48**	**1.71**	**1.45**	**5.sSMPABC008**	**576**	**8**

(a) $^{176}Yb/^{177}Hf = (^{176}Yb/^{173}Yb)_{true} \times (^{173}Yb/^{177}Hf)_{meassured} \times (M_{173(Yb)}/M_{177(Hf)})^{b(Hf)}$, $b(Hf) = \ln(^{179}Hf/^{177}Hf_{true} / {}^{179}Hf/^{177}Hf_{measured}) / \ln (M_{179(Hf)}/M_{177(Hf)})$

M=mass of respective isotope. The $^{176}Lu/^{177}Hf$ were calculated in a similar way by using the $^{175}Lu/^{177}Hf$ and b(Yb)

(b) Mean Hf signal in volt

(c) Uncertainties are quadratic additions of the within-run precision and the daily reproducibility of the zircon standards. Uncertainties for the standard quoted at 2SD (2 standard deviation)

(d) Initial $^{176}Hf/^{177}Hf$ and ƐHf calculated using the apparent Pb-Pb ages of respective zircon domains, and the CHUR parameters: $^{176}Lu/^{177}Hf = 0.0336$, and $^{176}Hf/^{177}Hf = 0.282785$ (Bouvier et al., 2008)

(e) Two stage model age in billion years using the measured $^{176}Lu/^{177}Lu$ of each spot (first stage = age of zircon), a value of 0.0113 for the average continental crust (second stage), and a average MORB (DM) $^{176}Lu/^{177}Hf$ and $^{176}Hf/^{177}Hf$ of 0.0384 and 0.283164

(f) Two stage model age in billion years using the measured $^{176}Lu/^{177}Lu$ of each spot (first stage = age of zircon), a value of 0.0113 for the average continental crust (second stage), and a $^{176}Lu/^{177}Hf$ and $^{176}Hf/^{177}Hf$ of 0.03933 and 0.283294 (Blichert-Toft et al., 2010)

(g) Two stage model age in billion years using the measured $^{176}Lu/^{177}Lu$ of each spot (first stage = age of zircon), a value of 0.0113 for the average continental crust (second stage), and a $^{176}Lu/^{177}Hf$ and $^{176}Hf/^{177}Hf$ of 0.03933 and 0.283158 (Dhuime et al., 2011)

(h) $^{206}Pb/^{238}U$ age determined by LA-ICP-MS

Spots in domains of dissolution–recrystallization, overgrowth or Pb lost rims are in red letter

Zircon grains not used for concordia age are in bold letter

STANDARDS FOR ANALYSIS OF JEQUITIBÁ PLUTON (SAMPLE CA-03) AND SANTA TEREZA PLUTON (SAMPLE CA-08)

LA-(MC)ICP-MS Lu-Hf zircon results data from BB-09 standard

Identifier	$^{176}Yb/^{177}Hf$ [a]	±2s	$^{176}Lu/^{177}Hf$ [a]	±2s	$^{178}Hf/^{177}Hf$	$^{180}Hf/^{177}Hf$	Sig_{Hf} [b] (V)	$^{176}Hf/^{177}Hf$	±2s [c]	$^{176}Hf/^{177}Hf_{(t)}$ [d]	eHf(t) [d]	±2s [c]	T_{DM} [e] (Ga)	T_{DM} [f] (Ga)	T_{DM} [g] (Ga)	Age (Ma)	±2σ
seq0001	0.007438	6.0	0.000157	1.0	1.465871	1.882641	10.4	0.281698	14.7	0.281697	-26.0	0.83	2.62	2.85	2.6	560	1
seq0002	0.007419	6.0	0.000156	1.0	1.465850	1.882457	10.4	0.281686	17.2	0.281685	-26.5	0.83	2.64	2.87	2.6	560	1
seq0003	0.007374	5.9	0.00015553	0.9	1.465884	1.882695	10.3	0.281677	18.2	0.281675	-26.8	0.83	2.66	2.89	2.6	560	1
seq0004	0.007402	5.9	0.00015529	0.9	1.465800	1.882613	10.4	0.281673	21.1	0.281671	-26.9	0.83	2.67	2.90	2.6	560	1
seq0005	0.007490	6.0	0.00015683	0.9	1.465865	1.882701	10.7	0.281687	20.9	0.281685	-26.4	0.83	2.64	2.87	2.6	560	1
seq0047	0.007415	6.0	0.00015755	0.9	1.467208	1.886886	9.7	0.281680	18.1	0.281679	-26.7	0.83	2.66	2.88	2.6	560	1
seq0048	0.007496	6.1	0.00015787	1.0	1.467231	1.886934	10.5	0.281671	14.0	0.281670	-27.0	0.83	2.67	2.90	2.6	560	1
seq0049	0.007478	6.2	0.0001576	1.0	1.467204	1.886834	10.4	0.281679	15.8	0.281678	-26.7	0.83	2.66	2.89	2.6	560	1
seq0075	0.007439	11.0	0.00015707	2.2	1.467246	1.886837	10.7	0.281691	23.0	0.281690	-26.3	0.83	2.64	2.86	2.6	560	1
seq0076	0.007034	5.9	0.0001477	0.9	1.467239	1.886883	10.8	0.281668	19.4	0.281667	-27.1	0.83	2.68	2.91	2.6	560	1
seq0077	0.007172	6.4	0.00015136	1.1	1.467252	1.886935	10.8	0.281680	17.1	0.281678	-26.7	0.83	2.66	2.89	2.6	560	1
seq0199	0.007186	7.0	0.00015087	1.6	1.467255	1.886915	10.3	0.281668	21.5	0.281666	-27.1	0.83	2.68	2.91	2.7	560	1
seq0200	0.007175	5.8	0.00015062	1.0	1.467196	1.886820	10.2	0.281679	14.4	0.281678	-26.7	0.83	2.66	2.89	2.6	560	1
seq0201	0.007277	6.3	0.00015218	1.0	1.467219	1.886832	10.2	0.281650	16.0	0.281648	-27.7	0.83	2.71	2.94	2.7	560	1
seq0237	0.007598	6.7	0.00015921	1.1	1.467214	1.886817	10.8	0.281650	24.8	0.281649	-27.7	0.83	2.71	2.94	2.7	560	1
seq0238	0.007514	6.3	0.0001578	1.0	1.467194	1.886828	10.6	0.281657	18.0	0.281655	-27.5	0.83	2.70	2.93	2.7	560	1
seq0239	0.007061	7.6	0.00014965	1.4	1.467229	1.886867	10.2	0.281688	15.0	0.281686	-26.4	0.83	2.64	2.87	2.6	560	1

BB (560Ma): $^{176}Hf/^{177}Hf$=0.2816713±0.0000028 **Average:** 0.281675 18.18

LA-(MC)ICP-MS Lu-Hf zircon results data from Gj-1 standard

Identifier	$^{176}Yb/^{177}Hf$ [a]	±2s	$^{176}Lu/^{177}Hf$ [a]	±2s	$^{178}Hf/^{177}Hf$	$^{180}Hf/^{177}Hf$	Sig_{Hf} [b] (V)	$^{176}Hf/^{177}Hf$	±2s [c]	$^{176}Hf/^{177}Hf_{(t)}$ [d]	eHf(t) [d]	±2s [c]			T_{DM} [e] (Ga)	Age (Ma)	±2σ
seq0011	0.011309	10.2	0.000269	2.0	1.465758	1.881975	9.5	0.282013	16.5	0.282010	-14.0	0.83	2.01	2.24	2.0	602	1
seq0012	0.011225	9.3	0.000269	1.7	1.465695	1.882028	9.4	0.281997	19.5	0.281994	-14.6	0.83	2.04	2.27	2.0	602	1
seq0013	0.011336	9.5	0.000270	1.8	1.465637	1.881886	9.2	0.281984	16.3	0.281981	-15.0	0.83	2.06	2.29	2.0	602	1
seq0014	0.011298	11.3	0.000269	3.2	1.465662	1.881934	9.0	0.282001	21.1	0.281998	-14.4	0.83	2.03	2.26	2.0	602	1
seq0015	0.011257	9.3	0.000269	1.7	1.465628	1.881848	9.1	0.281980	17.7	0.281977	-15.2	0.83	2.07	2.30	2.0	602	1
seq0053	0.010785	8.7	0.000266	1.6	1.467258	1.886862	9.5	0.282015	22.0	0.282012	-13.9	0.83	2.00	2.23	2.0	602	1
seq0054	0.010845	10.7	0.000265	2.1	1.467268	1.886922	9.6	0.282004	22.7	0.282001	-14.3	0.83	2.02	2.25	2.0	602	1
seq0055	0.010683	10.3	0.000266	2.1	1.467224	1.886834	9.4	0.281992	20.1	0.281989	-14.7	0.83	2.05	2.28	2.0	602	1
seq0081	0.010847	13.9	0.000264	3.0	1.467217	1.886813	9.7	0.281981	18.7	0.281978	-15.1	0.84	2.07	2.30	2.0	602	1
seq0082	0.010834	15.9	0.000264	3.6	1.467188	1.886990	9.7	0.281995	15.7	0.281992	-14.6	0.84	2.04	2.27	2.0	602	1
seq0083	0.010677	8.6	0.000265	1.6	1.467153	1.886710	9.8	0.281985	16.7	0.281982	-15.0	0.83	2.06	2.29	2.0	602	1
seq0205	0.010708	8.6	0.000267	1.6	1.467219	1.886925	9.3	0.281994	20.6	0.281991	-14.7	0.83	2.04	2.27	2.0	602	1
seq0206	0.010648	8.8	0.000267	1.7	1.467190	1.886852	9.1	0.282017	14.5	0.282014	-13.8	0.83	2.00	2.23	2.0	602	1
seq0207	0.010605	8.5	0.000265	1.6	1.467184	1.886827	9.2	0.281999	17.9	0.281996	-14.5	0.83	2.03	2.26	2.0	602	1
seq0243	0.011109	13.7	0.000266	2.9	1.467240	1.886887	9.5	0.282027	17.1	0.282024	-13.5	0.84	1.98	2.21	1.9	602	1
seq0244	0.011000	9.6	0.000264	1.9	1.467226	1.886900	9.5	0.282003	19.8	0.282000	-14.3	0.83	2.03	2.25	2.0	602	1
seq0245	0.011115	9.1	0.000265	1.6	1.467190	1.886831	9.8	0.282010	16.2	0.282007	-14.1	0.83	2.01	2.24	2.0	602	1
GJ-1(602Ma): $^{176}Hf/^{177}Hf$=0.282000±0.000005							**Average:**	0.282000	18.42								

LA-(MC)ICP-MS Lu-Hf zircon results data from Plesovice standard

Identifier	$^{176}Yb/^{177}Hf$ [a]	±2s	$^{176}Lu/^{177}Hf$ [a]	±2s	$^{178}Hf/^{177}Hf$	$^{180}Hf/^{177}Hf$	Sig_{Hf} [b] (V)	$^{176}Hf/^{177}Hf$	±2s [c]	$^{176}Hf/^{177}Hf_{(t)}$ [d]	eHf(t) [d]	±2s [c]			T_{DM} [e] (Ga)	Age (Ma)	±2σ
seq0006	0.016086	14.2	0.000241	1.6	1.465725	1.882163	14.7	0.282450	22.9	0.282448	-4.4	0.84	1.26	1.51	1.2	337	1
seq0007	0.006720	6.5	0.000103	1.1	1.465710	1.882113	15.4	0.282474	21.4	0.282473	-3.5	0.83	1.22	1.46	1.2	337	1
seq0008	0.010149	8.6	0.000155	1.0	1.465889	1.882486	15.4	0.282481	14.6	0.282480	-3.3	0.83	1.20	1.44	1.2	337	1
seq0009	0.014646	12.5	0.000218	1.5	1.465684	1.882064	14.9	0.282460	23.7	0.282459	-4.0	0.84	1.24	1.48	1.2	337	1
seq0010	0.009750	8.2	0.000151	1.0	1.465656	1.882023	15.2	0.282449	13.9	0.282448	-4.4	0.83	1.26	1.51	1.2	337	1
seq0050	0.007622	6.2	0.000117	0.7	1.467241	1.886811	15.0	0.282473	15.0	0.282472	-3.6	0.83	1.22	1.46	1.2	337	1
seq0051	0.008625	6.9	0.000133	0.8	1.467210	1.886896	14.2	0.282480	21.9	0.282479	-3.3	0.83	1.21	1.45	1.2	337	1
seq0052	0.015146	12.2	0.000234	1.4	1.467223	1.886842	14.5	0.282507	18.8	0.282505	-2.4	0.84	1.15	1.40	1.1	337	1
seq0078	0.014180	14.4	0.000219	1.7	1.467194	1.886787	14.3	0.282490	16.8	0.282489	-3.0	0.84	1.19	1.43	1.2	337	1
seq0079	0.005851	9.0	0.000090	1.2	1.467210	1.886931	15.2	0.282465	21.2	0.282465	-3.8	0.83	1.23	1.47	1.2	337	1
seq0080	0.013917	13.9	0.000221	2.1	1.467227	1.886904	14.0	0.282485	21.6	0.282484	-3.2	0.84	1.20	1.44	1.2	337	1
seq0202	0.007035	5.7	0.000109	0.7	1.467214	1.886786	15.4	0.282450	20.4	0.282449	-4.4	0.83	1.26	1.50	1.2	337	1
seq0203	0.007047	5.7	0.000107	0.6	1.467243	1.886854	15.3	0.282456	16.7	0.282456	-4.1	0.83	1.25	1.49	1.2	337	1
seq0204	0.007533	6.1	0.000117	0.7	1.467191	1.886877	15.4	0.282461	23.8	0.282460	-4.0	0.83	1.24	1.48	1.2	337	1
seq0240	0.009856	8.3	0.000148	0.9	1.467257	1.886774	16.3	0.282478	18.9	0.282477	-3.4	0.83	1.21	1.45	1.2	337	1
seq0241	0.007340	8.4	0.000109	1.2	1.467226	1.886859	16.6	0.282467	24.9	0.282466	-3.8	0.83	1.23	1.47	1.2	337	1
seq0242	0.008990	12.1	0.000135	1.4	1.467217	1.886773	15.8	0.282474	26.9	0.282474	-3.5	0.84	1.22	1.46	1.2	337	1

Plesocvice (337Ma): $^{176}Hf/^{177}Hf$=0.282482±0.000013 **Average:** 0.282471 20.20

[a] $^{176}Yb/^{177}Hf = (^{176}Yb/^{173}Yb)_{true} \times (^{173}Yb/^{177}Hf)_{meassured} \times (M_{173(Yb)}/M_{177(Hf)})^{b(Hf)}$, $b(Hf) = \ln(^{179}Hf/^{177}Hf_{true} / {}^{179}Hf/^{177}Hf_{measured}) / \ln(M_{179(Hf)}/M_{177(Hf)})$

M=mass of respective isotope. The $^{176}Lu/^{177}Hf$ were calculated in a similar way by using the $^{175}Lu/^{177}Hf$ and b(Yb)

[b] Mean Hf signal in volt

(c) Uncertainties are quadratic additions of the within-run precision and the daily reproducibility of the zircon standards. Uncertainties for the standard quoted at 2SD (2 standard deviation)

(d) Initial $^{176}Hf/^{177}Hf$ and ƐHf calculated using the apparent Pb-Pb ages of respective zircon domains, and the CHUR parameters: $^{176}Lu/^{177}Hf = 0.0336$, and $^{176}Hf/^{177}Hf = 0.282785$ (Bouvier et al., 2008)

(e) Two stage model age in billion years using the measured $^{176}Lu/^{177}Lu$ of each spot (first stage = age of zircon), a value of 0.0113 for the average continental crust (second stage), and a average MORB (DM) $^{176}Lu/^{177}Hf$ and $^{176}Hf/^{177}Hf$ of 0.0384 and 0.283164

(f) Two stage model age in billion years using the measured $^{176}Lu/^{177}Lu$ of each spot (first stage = age of zircon), a value of 0.0113 for the average continental crust (second stage), and a $^{176}Lu/^{177}Hf$ and $^{176}Hf/^{177}Hf$ of 0.03933 and 0.283294 (Blichert-Toft et al., 2010)

(g) Two stage model age in billion years using the measured $^{176}Lu/^{177}Lu$ of each spot (first stage = age of zircon), a value of 0.0113 for the average continental crust (second stage), and a $^{176}Lu/^{177}Hf$ and $^{176}Hf/^{177}Hf$ of 0.03933 and 0.283158 (Dhuime et al., 2011)

Sm-Nd Data

Sample	Suite	Sm (ppm)	Nd (ppm)	$^{147}Sm/^{144}Nd$	$^{143}Nd/^{144}Nd$	± 2SE	$e_{Nd(0)}$	$T_{DM\ (Ga)}$	$e_{Nd\ (T1)}$	T1*	$e_{Nd\ (T2)}$	T2**
CA- 08	Santa Tereza	13.429	61.513	0.1320	0.512103	5	-10.43	1.74	-5.3410224	0.612	-5.1503017	0.635
CA -14	Santa Tereza	5.656	27.983	0.1222	0.511976	5	-12.92	1.76	-7.0551703	0.612	-6.83566	0.635
CA-17	Santa Tereza	11.819	65.545	0.1090	0.512075	8	-10.99	1.40	-4.0885346	0.612	-3.8299675	0.635
CA-18 A	Santa Tereza	10.340	50.155	0.1246	0.512344	7	-5.73	1.19	-0.0575947	0.612	0.155088	0.635
CA-19	Santa Tereza	4.401	30.817	0.0863	0.511995	6	-12.53	1.25	-3.8752	0.612	-3.5497215	0.635
CA-20 A	Santa Tereza	5.321	21.642	0.1486	0.512166	6	-9.21	2.04	-5.4162961	0.612	-5.2747705	0.635
CA -03	Jequitibá	3.999	24.131	0.1002	0.51181	5	-16.15	1.64	-8.7979714	0.594	-8.4271997	0.624
CA-31	Jequitibá	7.126	39.061	0.1103	0.511958	3	-13.26	1.59	-6.6743907	0.594	-6.3423169	0.624
CA-32	Jequitibá	5.319	24.374	0.1319	0.512030	8	-11.85	1.87	-6.9126063	0.594	-6.6637982	0.624
BHVO 2	Padrão	6.342	25.711	0.1491	0.512970	2	6.47	0.22				

*T1: Concordia age

**T2 maximum crystallization age

TDM model ages after DePaolo (1981)

REFERENCES

Stacey, J.S., Kramers, J.D., 1975. Approximation of terrestrial lead isotope evolution by a two-stage model. Earth and Planetary Science Letters 26, 207-221.

Blichert-Toft, J., Puchtel, I.S., 2010. Depleted mantle sources through time: Evidence from Lu–Hf and Sm–Nd isotope systematics of Archean komatiites. Earth and Planetary Science Letters 297, 298-606.

Bouvier, A., Vervoort, J.D., Patchett, P.J., 2008. The Lu-Hf and Sm-Nd isotopic composition of CHUR: constraints from unequilibrated chondrites and implications for the bulk composition of terrestrial planets. Earth and Planetary Science Letters 273, 48-57.

De Paolo, D.J., 1981. A neodymium and strontium isotopic study of the Mesozoic calcalkaline granitic batoliths of the Sierra Nevada and Peninsular Rangers, California. Journal of Geophysical Research 86, 10470–10488.

Dhuime, B., Hawkesworth, C.J., Cawood, P., 2011. When continents formed. Science 331, 154–155

APPENDIX D - Supplementary File 4.A - Compiled Data

G5 plutons ages obtained from literature					
G5 local name	**Rock-type**	**Locality**	**Age (Ma)**	**Details**	**Data source**
Caladão	Megaporphyritic granite	Minas Gerais state (between Teófilo Otoni and Ataléia)	520 ± 2	Pb-evaporation, zircon, n: 4. Sample: MU-1c	Noce et al. 2000
	Fine-grained granite vein		503 ± 9	Pb-evaporation, zircon, n: 2. Sample: MU-10b	Noce et al., 2000
Padre Paraíso	Charnockite	Minas Gerais state (between Teófilo Otoni and Ataléia)	516 ± 3	Pb-evaporation, zircon, n: 1. Sample: MU-2	Noce et al., 2000
Santa Angélica	Porphyric granite	Southern region of Espírito Santo state	513 ± 8	ID-TIMS, zircon, upper intercept. Sample: St A-51	Söller et al., 1991 in De Campos et al., 2016
	Titanite Granite		492 ± 15	Zircon	Wiedemann et al., 2002
Mimoso do Sul	Titanite Granite	Southern region of Espírito Santo state	480 ± 4	Zircon. Sample: BU-11	Söller et al., 2000
	Monzosyenite		495 ± 5	ID-TIMS, zircon. Sample: MS-11	Söller et al., 2000
Medina	Sienogranite	Medina, Minas Gerais state	501 ± 2	LA-ICPMS, zircon, n: 21. Sample: R13A	Serrano et al., 2018
	Sienogranite		497 ± 2	LA-ICPMS, monazite, n: 28. Sample: R13A	Serrano et al., 2018
Várzea Alegre	Charnockite	Central region of Espírito Santo state	499 ± 5	TIMS, zircon, n: 4. Sample: VA-04	Mendes at al., 2005
Aimorés	Hypersthene granitoid	Central region of Espírito Santo state	513	LA-ICPMS, zircon. Sample: 2107-LC-168	Baltazar et al., 2010
	Hypersthene granitoid		502	LA-ICPMS, zircon. Sample: OF-172A	Baltazar et al., 2010
	Charnockite		499 ± 35	TIMS, zircon, lower intercept, n: 14. Sample: FAM10	Mello, 2000
Intrusive in Muniz Freire batolith	Granitoid	Southern region of Espírito Santo state	500 ± 4	Zircon	Silva et al., 2005
Barra de São Francisco	Charnockite	Central region of Espírito Santo state	523 ± 3	LA-ICPMS, zircon, n: 4. Sample: SC-01B	De Campos et al., 2016
	Charnockite	Barra de São Francisco, Espírito Santo state	504 ± 5	SHRIMP, zircon, n: 7. Sample: 470	Gradim et al., 2014
Pedra do Elefante	Granite	Northern region of Espírito Santo state	531 ± 34	LA-ICPMS, zircon, n: 4. Sample: SC-18B	De Campos et al., 2016
	Charnockite		488 ± 8	LA-ICPMS, zircon, n: 4. Sample: SC-18A	De Campos et al., 2016
Cotaché	Granite	Northern region of Espírito Santo state	504 ± 3	TIMS, zircon, n: 7, intecept. Sample: SC-13	De Campos et al., 2016

G5 plutons ages obtained from literature					
G5 local name	**Rock-type**	**Locality**	**Age (Ma)**	**Details**	**Data source**
São Gabriel da Baunilha	Norite	Baunilha, Colatina, Espírito Santo state	524 ± 7	SHRIMP, zircon, n: 8. Sample: JB21B	Belém, 2014
Suíte Fundão	Gabronorite dike	João Neiva, Espírito Santo state	498 ± 16	SHRIMP, zircon, n: 4. Sample: D15	Belém, 2014
	Porphyritic olivine-basalt dike	Pendanga, Espírito Santo state	509 ± 16	SHRIMP, zircon, n: 6. Sample: JB16	Belém, 2014
	Enderbitic-norite dike	Alto de Santa Maria, Espírito Santo state	525 ± 10	SHRIMP, zircon, n: 6. Sample: JF120	Belém, 2014
Fazenda Liberdade	Granodiorite	Fonteira dos Vales, Minas Gerais state	526 ± 5	LA-MC-ICPMS, zircon, n: 31. Sample: LG29	Gonçalves et al., 2016
Afonso Cláudio	Quartz monzonite	Central region of Espírito Santo state	481 ± 3	LA-ICP-MS, zircon, n: 5. Sample: P98	Aranda, 2018
	Monzogabbro		497 ± 4	LA-ICP-MS, zircon, n: 5. Sample: P246-A	Aranda, 2018

n: number of grains

Sm-Nd, Rb-Sr, and Lu-Hf data of the G5 plutons obtained from literature								
G5 local name	**Rock-type**	**Sample**	**Locality**	**Ɛ Nd (t)**	**Sm-Nd TDM (Ga)**	**$^{87}Sr/^{86}Sr$ (t)**	**t (Ma)**	**Data source**
Caladão	Aplite fine granite	MU-10b	Minas Gerais (between Teófilo Otoni and Ataléia)	-20.47	2.57	0.710652	505	Martins et al., 2004
		MU-13		-23.83	2.55	0.720693	505	Martins et al., 2004
	Granite	MU-01A		-6.67	1.55	0.70197	520	Martins et al., 2004
Padre Paraíso	Charnockite	MU-08A	Minas Gerais (between Teófilo Otoni and Ataléia)	-6.85	1.48	0.70978	520	Martins et al., 2004
Barra de São Francisco	Charnockite	SC-01B	Northern region of Espírito Santo	-8.20	1.57	0.71173	500	De Campos et al., 2016
	Granite	SC-01A		-14.44	1.58	0.71312	500	De Campos et al., 2016
Pedra do elefante	Charnockite	SC-18A	Northern region of Espírito Santo	-9.32	1.58	0.70899	500	De Campos et al., 2016
	Granite	SC-18B		-10.67	1.70	0.70948	500	De Campos et al., 2016
Cotaché	Granite	SC-14A	Northern region of Espírito Santo	-6.04	1.55	0.71291	500	De Campos et al., 2016
	Granite	SC-13		-7.31	1.40	0.71089	500	De Campos et al., 2016

Sm-Nd, Rb-Sr, and Lu-Hf data of the G5 plutons obtained from literature								
G5 local name	**Rock-type**	**Sample**	**Locality**	**Ɛ Nd (t)**	**Sm-Nd TDM (Ga)**	**$^{87}Sr/^{86}Sr$ (t)**	**t (Ma)**	**Data source**
Suíte Fundão	Gabronorite dike	D15	João Neiva, Espírito Santo	-6.93	1.96	0.7077*	500	Belém, 2014
	Porphyritic olivine-basalt dike	JB-16-3	Pendanga, Espírito Santo	-11.74	1.53	0.7066*	500	Belém, 2014
Aimorés	Charnockite	FAM-4	Central region of Espírito Santo state	-7.05	1.51	0.71756*	500	Mello, 2000
	Porphyritic granite	FAM-25		-6.58	1.72	0.71686*	500	Mello, 2000
	Granodiorite	FAM-21		-7.77	1.66	0.71962*	500	Mello, 2000
Várzea Alegre	Qtz-diorite	VA-06	Central region of Espírito Santo	-7.90	1.53	0.70726	500	De Campos et al., 2016
	Opx-gabbro	VA-218		-5.34	1.33	0.70730	500	De Campos et al., 2016
	Charnockite	VA-90		-8.38	1.63	0.70852	500	Mendes et al., 2005
	Charnockite	VA-261		-10.10	1.78	0.70853	500	Mendes et al., 2005
	Charnockite	VA-125		-8.89	1.67	0.71223	500	Mendes et al., 2005
	Granite	VA-176		-7.93	1.72	0.70847	500	De Campos et al., 2016
Santa Angélica	Gabbro/diorite	St A-63	Southern region of Espírito Santo	-13.07	1.76	0.70699	500	De Campos et al., 2016
	Gabbro/diorite	St A-71A		-13.38	1.75	0.70726	500	De Campos et al., 2016
	Gabbro/diorite	St A-72		-13.55	1.82	0.70711	500	De Campos et al., 2016
	Allanite-granite	St A-50		-12.73	1.65	0.71688	500	De Campos et al., 2016
	Allanite-granite	St A-51		-13.42	1.72	-	500	De Campos et al., 2016
Venda Nova	Alkali gabro	VNI-3	Southern region of Espírito Santo	-10.49	1.69	0.70655	500	De Campos et al., 2016
	Alkali gabro	VNI-12		-9.28	1.45	-	500	De Campos et al., 2016
	Charnockite	VN-13		-7.33	1.44	0.70753	500	De Campos et al., 2016
	Charnockite	VN-23		-11.28	1.52	0.70597	500	De Campos et al., 2016
Mimoso do Sul	Monzonite	M24	Southern region of Espírito Santo	-12.20	1.66	0.70672	500	De Campos et al., 2016
	Monzonite	M-81		-14.58	1.93	0.70681	500	De Campos et al., 2016
Jacutinga	Gabbro	M475	Southern region of Espírito Santo	-14.10	3.29	0.70712	500	De Campos et al., 2016
	Gabbro	M470(2)		-10.39	2.21	0.70813	500	De Campos et al., 2016
Itaoca	Gabbro	MHW-31	Southern region of Espírito Santo	-8.05	2.35	0.70604	500	De Campos et al., 2016
	Gabbro	PS-32		-3.83	2.65	0.70499	500	De Campos et al., 2016
G5 local name	**Rock-type**	**Sample**	**Locality**	**ƐHf (t)**	**Lu-Hf TDM (Ga)**	**-**	**t (Ma)**	**Data source**
Afonso Cláudio	Quartz monzonite	P-98	Central region of Espírito Santo state	-11.70	1.78	-	481	Aranda, 2018
	Monzogabbro	P-246A		-10.37	1.72	-	497	Aranda, 2018

* (t) not cited

REFERENCES

Aranda, R., 2018. Petrology of the Afonso Cláudio Intrusive Complex (Espírito Santo State, Araçuaí Orogen): Insights from Petrography, Lithogeochemistry, U-Pb Geochronology and Lu-Hf Isotopes. Instituto de Geociências, Universidade Federal de Minas Gerais, Belo Horizonte (MS Dissertation, 64 pp.).

Baltazar, O.F., Zucchetti, M., Oliveira, S.A.M., Scandolara, J., Silva, L.C., 2010. Geologia das Folhas São Gabriel Da Palha e Linhares. Programa Geologia do Brasil, CPRM–Serviço Geológico do Brasil, Belo Horizonte.

Belém, J., 2014. Geoquímica, geocronologia e contexto geotectônico do magmatismo máfico associado ao feixe de fraturas Colatina, Estado do Espírito Santo. Instituto de Geociências, Universidade Federal de Minas Gerais, Belo Horizonte (MS Dissertation, 138 pp.).

De Campos, C.P, Medeiros, S.R., Mendes, J.C, Pedrosa-Soares, A.C., Dussin, I., Ludka, I.P., Dantas, E.L., 2016. Cambro-Ordovician magmatism in the Araçuaí Belt (SE Brazil): Snapshots from a post-collisional event. Journal of South American Earth Sciences 68, 248-268.

Gradim, C., Roncato, J., Pedrosa-Soares, A.C., Cordani, U., Dussin, I., Alkmim, F.F., Queiroga, G., Jacobsohn, T., Silva, L.C., Babinski, M., 2014. The hot back-arc zone of the Araçuaí Orogen, Eastern Brazil: from sedimentation to granite generation. Brazilian Journal of Geology 44, 155-180.

Martins, V.T.S, Teixeira, W., Noce, C.M., Pedrosa-Soares, A.C., 2004. Sr and Nd Characteristics of Brasiliano/Pan-African Granitoid Plutons of the Araçuai Orogen, Southeastern Brazil: Tectonic Implications. Gondwana Research 7, 75-89.

Mello, F.M., 2000. Litogeoquímica e Química Mineral do Maciço Charnockítico Aimorés-MG. Universidade de São Paulo, São Paulo (Ph.D. Thesis, 167 pp.).

Mendes, J.C., Medeiros, S.R., McReath, I., De Campos, C.M.P., 2005. Cambro-Ordovician magmatism in SE Brazil: U-Pb and Rb-Sr ages, combined with Sr and Nd isotopic data of Charnockitic rocks from the Várzea Alegre complex. Gondwana Research 8, 337-345.

Noce, C.M., Macambira, M.J.B., Pedrosa-Soares, A.C., 2000. Chronology of Neoproterozoic–Cambrian granitic magmatism in the Araçuaí Belt, Eastern Brazil, based on single zircon evaporation dating. Revista Brasileira de Geociências 30, 25–29.

Serrano, P., Pedrosa-Soares, A., Medeiros-Junior, E., Fonte-Boa, T., Araujo, C., Dussin, I., Queiroga, G., Lana, C., 2018. A-type Medina batholith and post-collisional anatexis in the Araçuaí orogen (SE Brazil). Lithos 320-321, 515-536.

Silva, L.C., McNaughton, N.J., Armstrong, R., Hartmann, L.A., Fletcher, I.R., 2005. The Neoproterozoic Mantiqueira Province and its African connections: a zircon-based U-Pb geochronologic subdivision for the Brasiliano/Pan-African systems of orogens. Precambrian Research 136, 203–240.

Söllner, F., Lammerer, B., Wiedemann-Leonardos, C., 2000. Dating the Ribeira Mobile Belt of Brazil. In: Sonderheft, Zeitschrift Angwandte Geologie pp. 245-255.

Wiedemann, C.M., Medeiros, S.R., Ludka, I.P., Mendes, J.C., Costa-de-Moura, J., 2002. Architecture of late orogenic plutons in the Araçuaí-Ribeira fold belt, Southeast Brazil. Gondwana Research 5, 381-399.

REFERENCES OF ARAÇUAÍ OROGEN COMPILATION IN FIGURE 10G

Aranda, R., 2018. Petrology of the Afonso Cláudio Intrusive Complex (Espírito Santo State, Araçuaí Orogen): Insights from Petrography, Lithogeochemistry, U-Pb Geochronology and Lu-Hf Isotopes. Instituto de Geociências, Universidade Federal de Minas Gerais, Belo Horizonte (MS Dissertation, 64 pp.).

Basílio, M., Pedrosa-Soares, A.C., Evangelista, H.J., 2000. Depósitos de alexandrita de Malacacheta. Minas Gerais. Geonomos 8, 47–54.

Belém, J., 2014. Geoquímica, geocronologia e contexto geotectônico do magmatismo máfico associado ao feixe de fraturas Colatina, Estado do Espírito Santo. Instituto de Geociências, Universidade Federal de Minas Gerais, Belo Horizonte (MS Dissertation, 138 pp.).

Cavalcante, C., Hollanda, M.H., Vauchez, A., Kawata, M., 2018. How long can the middle crust remain partially molten during orogeny? Geology 46, 839-842.

De Campos, C.P, Medeiros, S.R., Mendes, J.C, Pedrosa-Soares, A.C., Dussin, I., Ludka, I.P., Dantas, E.L., 2016. Cambro-Ordovician magmatism in the Araçuaí Belt (SE Brazil): Snapshots from a post-collisional event. Journal of South American Earth Sciences 68, 248-268.

Degler, R., Pedrosa-Soares, A., Dussin, I., Queiroga, G., Schulz, B., 2017. Contrasting provenance and timing of metamorphism from paragneisses of the Araçuaí-Ribeira orogenic system, Brazil: Hints for Western Gondwana assembly. Gondwana Research 51, 30–50.

Degler, R., Pedrosa-Soares, A., Novo, T., Tedeschi, M., Silva, L.C., Dussin, I., Lana, C. 2018. Rhyacian-Orosirian isotopic records from the basement of the Araçuaí-Ribeira orogenic system (SE Brazil): Links in the Congo-São Francisco palaeocontinent. Precambrian Research 317, 179-195.

Figueiredo, C.M.S., 2009. O Arco Magmático Brasiliano na conexão entre os orógenos Araçuaí e Ribeira, Região de Muriaé-MG. Universidade Federal de Minas Gerais, Belo Horizonte, Brazil (Ph.D. Thesis, p. 103).

Gonçalves, L., Farina, F., Lana, C., Pedrosa-Soares, A.C., Alkmim, F., Nalini Jr., H.A., 2014. New U–Pb ages and lithochemical attributes of the Ediacaran Rio Doce magmatic arc, Araçuaí confined orogen, Southeastern Brazil. Journal of South American Earth Sciences 52, 129–148.

Gonçalves, L., Alkmim, F.F., Pedrosa-Soares, A.C., Dussin, I.A., Valeriano, C.M., Lana, C., Tedeschi, M., 2016. Granites of the intracontinental termination of a magmatic arc: an example from the Ediacaran Araçuaí orogen, southeastern Brazil. Gondwana Research 36, 439-458.

Gradim, C., Roncato, J., Pedrosa-Soares, A.C., Cordani, U., Dussin, I., Alkmim, F.F., Queiroga, G., Jacobsohn, T., Silva, L.C., Babinski, M., 2014. The hot back-arc zone of the Araçuaí Orogen, Eastern Brazil: from sedimentation to granite generation. Brazilian Journal of Geology 44, 155-180.

Mondou, M., Egydio-Silva, M., Vauchez, A., Raposo, M.I.B., Bruguier, O., Oliveira, A.F., 2012. Complex, 3D strain patterns in a synkinematic tonalite batholith from the Araçuaí Neoproterozoic orogen (Eastern Brazil): evidence from combined magnetic and isotopic chronology studies. Journal of Structural Geology 39, 158–179.

Melo, M.G., Lana, C., Stevens, G., Pedrosa-Soares, A.C., Gerdes, A., Alkmin, L.A., Nalini Jr., H.A., Alkmim, F.F., 2017. Assessing the isotopic evolution of S-type granites of the Carlos Chagas batholith, SE Brazil: Clues from U-Pb, Hf isotopes, Ti geothermometry and trace element composition of zircon. Lithos 284-285, 730-750.

Mello, F.M., 2000. Litogeoquímica e Química Mineral do Maciço Charnockítico Aimorés-MG. Universidade de São Paulo, São Paulo (Ph.D. Thesis, 167 pp.).

Mendes, J.C., Medeiros, S.R., McReath, I., De Campos, C.M.P., 2005. Cambro-Ordovician magmatism in SE Brazil: U-Pb and Rb-Sr ages, combined with Sr and Nd isotopic data of Charnockitic rocks from the Várzea Alegre complex. Gondwana Research 8, 337-345.

Nalini Jr., H.A., 1997. Caractérisation des suites magmatiques néoprotérozoiques de la region de Conselheiro Pena et Galiléia (Minas Gerais, Brésil). Etude géochimique et structurale des suites Galiléia et Urucum et relations avec les pegmatites à éléments rares associées. Ecole des Mines de Saint Etienne et Ecole des Mines de Paris (Ph.D. Thesis, 237 pp.).

Nalini Jr., H.A., Bilal, E., Correia Neves, J.M., 2000. Syn-collisional peraluminous magmatism in the Rio Doce region: mineralogy, geochemistry and isotopic data of the Urucum suite (eastern Minas Gerais state, Brazil). Revista Brasileira de Geociências 30, 120–125.

Noce, C.M., Macambira, M.J.B., Pedrosa-Soares, A.C., 2000. Chronology of Neoproterozoic–Cambrian granitic magmatism in the Araçuaí Belt, Eastern Brazil, based on single zircon evaporation dating. Revista Brasileira de Geociências 30, 25–29.

Noce, C.M., Pedrosa-Soares, A.C., Piuzana, D., Armstrong, R., Laux, J.H., Campos, C.M., Medeiros, S.R., 2004. Ages of sedimentation of the kinzigitic complex and of alate orogenic thermal episode in the Araçuaí orogen, Northern Espírito Santo State, Brazil: Zircon and monazite U–Pb SHRIMP and ID-TIMS data. Revista Brasileira de Geociências 34, 587–592.

Novo, T.A., Pedrosa-Soares, A.C., Noce, C.M., Alkmim, F.F., Dussin, I.A., 2010. Rochas charnockíticas do sudeste de Minas Gerais: a raiz granulítica do arco magmático do Orógeno Araçuaí. Revista Brasileira de Geociencias 40, 573–592.

Novo, T.A., 2013. Caracterização do Complexo Pocrane, magmatismo básico mesoproterozóico e unidades neoproterozóicas do sistema Araçuaí-Ribeira, com ênfase em geocronologia U-Pb (SHRIMP e LA-ICP-MS). Universidade Federal de Minas Gerais, Belo Horizonte, pp. 193.

Pedrosa-Soares, A.C., De Campos, C.P., Noce, C.M., Silva, L.C., Novo, T., Roncato, J., Medeiros, S., Castañeda, C., Queiroga, G., Dantas, E., Dussin, I., Alkmim, F., 2011. Late Neoproterozoic-Cambrian Granitic Magmatism in the Araçuaí Orogen (Brazil), the Eastern Brazilian Pegmatite Province and Related Mineral Resources. In: Sial, A.N., Bettencourt, J.S., De Campos, C.P., Ferreira, V.P. (Eds.), Granite-Related Ore Deposits. London, Geological Society of London, Special Publication 350, 25–51.

Petitgirard, S., Vauches, A., Egydio-Silva, M., Bruguier, O., Camps, P., Monié, P., Babinski, M., Mondou, M., 2009. Conflicting structural and geochronological data from the Ibituruna quartz-syenite (SE Brazil): effect of protracted “hot” orogeny and slow cooling rate? Tectonophysics 477, 174–196.

Richter, F., Lana, C., Steven, G., Buick, I., Pedrosa-Soares, A.C., Alkmim, F.F., Cutts, K., 2016. Sedimentation, metamorphism and granite generation in a back-arc region: Records from the Ediacaran Nova Venécia Complex (Araçuaí Orogen, Southeastern Brazil). Precambrian Research 272, 78–100.

Roncato, J.G., 2009. As suítes graníticas tipo-s do norte do Espírito Santo na região das folhas Ecoporanga, Mantena, Montanha e Nova Venécia. Instituto de Geociências, Universidade Federal de Minas Gerais, Minas Gerais (MSc Dissertation 102 pp.).

Serrano, P., Pedrosa-Soares, A., Medeiros-Junior, E., Fonte-Boa, T., Araujo, C., Dussin, I., Queiroga, G., Lana, C., 2018. A-type Medina batholith and post-collisional anatexis in the Araçuaí orogen (SE Brazil). Lithos 320-321, 515-536.

Silva, L.C., Armstrong, R., Noce, C.M., Carneiro,M., Pimentel,M., Pedrosa-Soares, A.C., Leite, C., Vieira, V.S., Silva, M., Paes, V., Cardoso-Filho, J., 2002. Reavaliação da evolução geológica em terrenos pré-cambrianos brasileiros com base em novos dados U–Pb SHRIMP, parte II: Orógeno Araçuaí, Cinturão Móvel Mineiro e Cráton São Francisco Meridional. Revista Brasileira de Geociências 32, 513–528.

Silva, L.C., McNaughton, N.J., Armstrong, R., Hartmann, L.A., Fletcher, I.R., 2005. The Neoproterozoic Mantiqueira Province and its African connections: a zircon-based U-Pb geochronologic subdivision for the Brasiliano/Pan-African systems of orogens. Precambrian Research 136, 203–240.

Silva, L.C., Pinto, C.P., Gomes, A.C., Paes, V.C., Chemale, F., 2007. Granitogenesis at the northern tip of the Araçuaí Orogen, SE Brazil: LA-ICP-MS U–Pb zircon geochronology, and tectonic significance. In: Simpósio de Geologia do Sudeste.Diamantina, Anais, pp. 20–21.

Silva, L.C., Pedrosa-Soares, A.C., Armstrong, R., Noce, C.M., 2011. Determinando a duração do período colisional do Orógeno Araçuaí com base em geocronologia U–Pb de alta resolução emzircão: uma contribuição para a história da amalgamação do Gondwana Ocidental. Geonomos 19, 180–197.

Söllner, F., Lammerer, B., Weber-Diefenbach, K., 1991. Die Krustenentwicklung in Der Küstenregion Nördlich Von Rio de Janeiro, Brasilien. Münchener Geowis-senschaftliche Hefte 11. Friedrich Pfeil Verlag, München, pp. 4.

Söllner, F., Lammerer, B., Wiedemann-Leonardos, C., 2000. Dating the Ribeira Mobile Belt of Brazil. In: Sonderheft, Zeitschrift Angwandte Geologie pp. 245-255.

Tedeschi, M., Novo, T., Pedrosa-Soares, A., Dussin, I., Tassinari, C., Silva, L.C., Gonçalves, L., Alkmim, F., Lana, C., Figueiredo, C., Dantas, E., Medeiros, S., De Campos, C., Corrales, F., Heilbron, M., 2016. The Ediacaran Rio Doce magmatic arc revisited (Araçuaí-Ribeira orogenic system, SE Brazil). Journal of South American Earth Sciences 68, 167-186.

Vauchez, A., Egydio Silva, M., Babinski, M., Tommasi, A., Uhlein, A., Liu, D., 2007. Deformation of a pervasely molten middle crust: insights from the Neoproterozoic Ribeira-Araçuaí orogen (SE Brazil). Terra Nova 19, 278–286.

Wiedemann, C.M., Medeiros, S.R., Ludka, I.P., Mendes, J.C., Costa-de-Moura, J., 2002. Architecture of late orogenic plutons in the Araçuaí-Ribeira fold belt, Southeast Brazil. Gondwana Research 5, 381-399.

APPENDIX E - Supplementary File 4.B - Materials and Methods

B. MATERIALS AND METHODS

B.1 Sampled plutons

The Aracê pluton (sample CA-02, figure 4.1B), also called Pedra Azul, is an intrusion hosted by the peraluminous migmatites of the Nova Venécia complex. The pluton has a large volume of hybrid rocks, being an inversely-zoned pluton constituted by mingling and mixing of contrasting magmas mainly represented by tonalite to granodiorite and granite (Costa-de-Moura et al., 1999; Costa-Nascimento et al., 1996; De Campos et al., 2004, 2016). Whole-rock Rb-Sr isotopic data suggest a crystallization age of 536 ± 31 Ma (Platzer, 1997, in De Campos et al., 2004). Geochemical signature points to high-K calc-alkaline magmatism (Wiedemann et al., 2002; De Campos et al., 2004). The emplacement depth estimated for this pluton is c. 15 km (Wiedemann et al., 2002).

The Vitória pluton (sample CA-04, figure 4.1B) also intrudes the migmatitic paragneisses of the Nova Venécia complex, showing several magma pulses under different H_2O/CO_2 fluid conditions (De Campos et al., 2004). It is predominantly composed of porphyritic biotite granite to diorite and pink granite. The pluton shows both isotropic and anisotropic fabrics, the latter with striking magmatic flow outlined by the orientation of euhedral K-feldspar megacrysts and of mafic enclaves (De Campos et al., 2004; Vieira and Menezes, 2015). Several granite and basalt dikes cut the massif.

The Mestre Álvaro pluton (sample CA-05, figure 1B) is an irregularly-shaped intrusive body also hosted by the Nova Venécia paragneissic complex. It consists of porphyritic biotite granite to diorite, generally displaying isotropic fabrics, but locally with igneous flow features (Vieira and Menezes, 2015).

B.2 Petrography

The thin sections were made in CPMTC-UFMG (Centro de Pesquisa Professor Manoel Teixeira da Costa of the Federal University of Minas Gerais) and examined under transmitted and reflected light microscopy at the CPMTC-UFMG and DEGEO-UFOP (Geology Department of Federal University of Ouro Preto).

Mineral abbreviations, in accordance to Whitney and Evans (2010), are: Ab, albite; Aln, allanite; Ap, apatite; Bt, biotite; Cb, carbonate; Chl, chlorite; Crd, Cordierite; Ep, epidote; Grt, garnet; Hc, hercynite; Ilm, ilmenite; Kfs, K-feldspar; Mag, magnetite; Mc, microcline; Mnz, monazite; Ms, muscovite; Opq, opaques minerals; Pl, plagioclase; Qz, quartz; Ser, sericite; Sil; Sillimanite; Ru, rutile; Ttn, titanite; Zrn, zircon.

B.3 Mineral chemistry

Microprobe data were obtained from feldspars, biotite, allanite, zircon, apatite, titanite, and rutile using an electron microprobe JEOL JXA-8230 at the Microscopy and Microanalysis Laboratory (LMIc), Federal University of Ouro Preto. For silicates (except allanite) and oxides, the column conditions were performed under an accelerating voltage of 15 kV, a beam current of 20 nA, and a spot diameter of 5 μm. Quartz (Si), CaF_2 (F), anorthoclase (Na), zircon (Zr), olivine (Mg), corundum (Al), magnetite (Fe), fluor-apatite (Ca and P), rutile (Ti), MnO (Mn), microcline (K), chromite (Cr_2O_3), diopside (CaO), barite (Ba), scapolite (Cl) and strontianite (Sr) were used as standards. For allanite, the accelerating voltage was of 20 kV, with a beam current of 150 nA, and a spot diameter of 5 μm; the standards used were YPO_4 (Y), quartz (Si), corundum (Al), olivine (Mg), U glass (U), monazite MADMON (Th and Ce), magnetite (Fe), lead sulphide (Pb), fluor-apatite (Ca and P), rutile (Ti), $GdPO_4$ (Gd), $SmPO_4$ (Sm), MnO (Mn), $NdPO_4$ (Nd), $PrPO_4$ (Pr), $LaPO_4$ (La). Common matrix ZAF corrections were applied. All Fe is present as Fe^{2+}. Counting times on the peak/background were 10/5 s for most of the elements, except for U and Pb (40/20 s), and for Cl (30/5 s). Background intensities were collected at higher and lower energies relative to the corresponding Kα and Lα lines. Analytical errors are within 0.27 and 0.98%.

The chemical formulas (a.p.f.u. - atoms per formula unit) for all minerals were calculated according to Deer et al. (2013).

The feldspar end-member concentrations were calculated in percent as An = 100*Ca/(Ca + Na + K), Ab = 100*Na/(Ca + Na + K), Or = 100*K/(Ca + Na + K).

The results are presented in Supplementary File 4.C.

B.4 Whole-rock chemistry

The samples were carefully examined to select only fresh and homogenous parts, free of weathering superficies, fracture fillings, veins or hydrothermal alteration signs. Then the samples were cleaned, crushed and milled at the SEPURA laboratory (Laboratório de Separação Mineral de Alta Pureza) of the Federal University of Minas Gerais, Brazil.

They were analyzed by whole-rock chemistry (majors, traces, and rare-earth elements - REE) in SGS Geosol Laboratories (Brazil). Major elements were analyzed by X-Ray fluorescence (XRF79C) after fusion with lithium tetraborate. Trace elements and REE concentrations were analyzed via inductively coupled plasma mass spectrometry (ICP-MS) after fusion with lithium tetraborate and digestion with a multi-acid solution (HCl, HNO_3, HF, and $HClO_4$). Detection limits are 0.01% for oxides and 0.1–0.01 ppm for most trace, and rare earth elements. The loss on ignition (LOI) was calculated by the weighting difference after 1000 ºC heating. The results were analyzed by GCDKit software (Janoušek et al., 2006). They are presented in Supplementary File 4.D.

B.4.1 Lithochemical diagrams

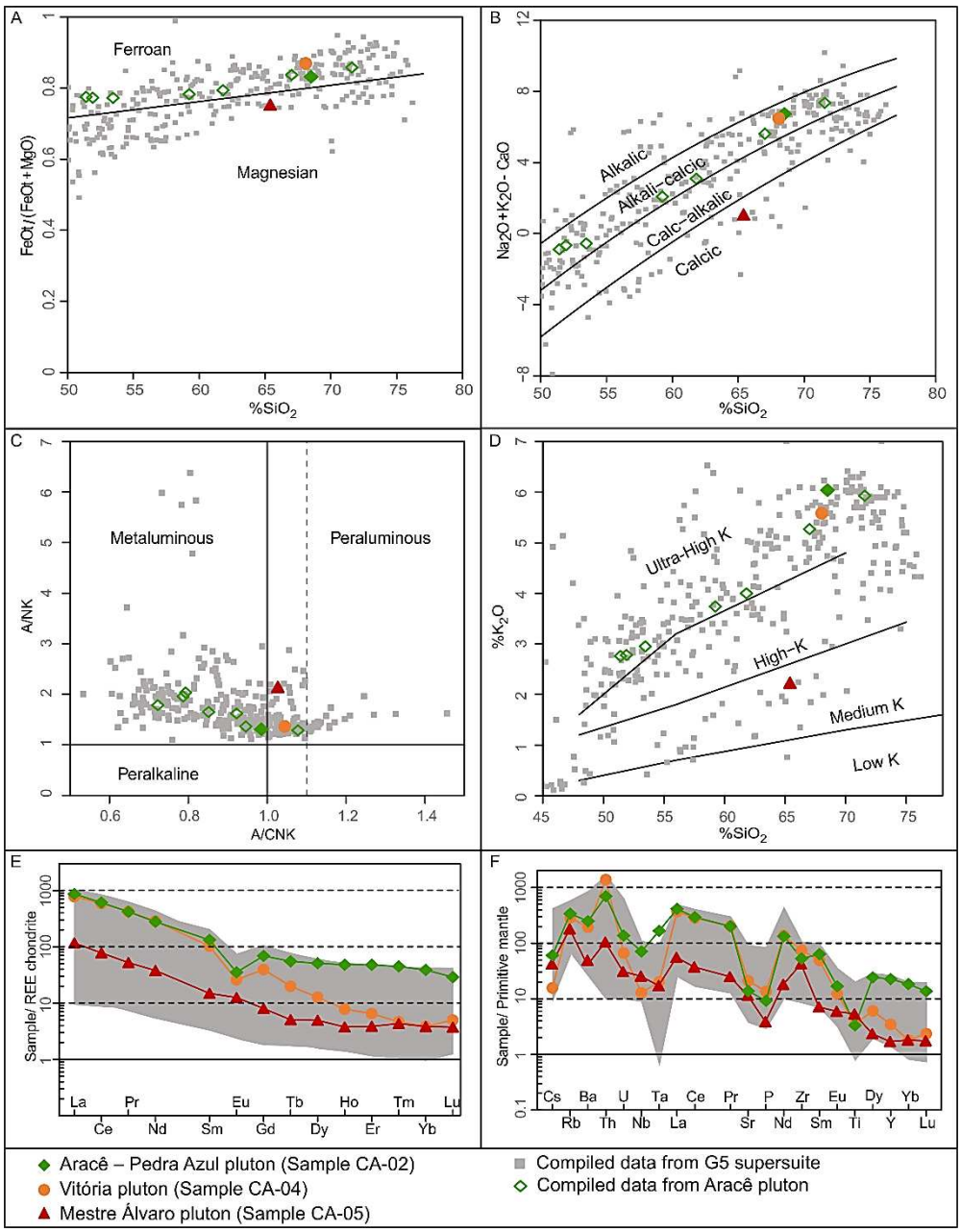

Figure B 1: Lithochemical data for the studied samples compared with the available data for G5 rocks (see Supplementary file D). A) FeOt / (FeOt + MgO) vs. SiO2 (wt%) (Frost et al., 2001); B) Na2O + K2O – CaO vs. SiO2 (wt%) (Frost et al., 2001); C) Alumina saturation Index. Dashed line (A/CNK < 1.1) delimits the transition between I- and S-type granites according to Chappell and White (1974); D) K2O vs. SiO2 (wt%); E) Chondrite-normalized REE patterns, normalized according to Boynton (1984); F) Multi-elemental diagram normalized to the primitive mantle, according to McDonough and Sun (1995).

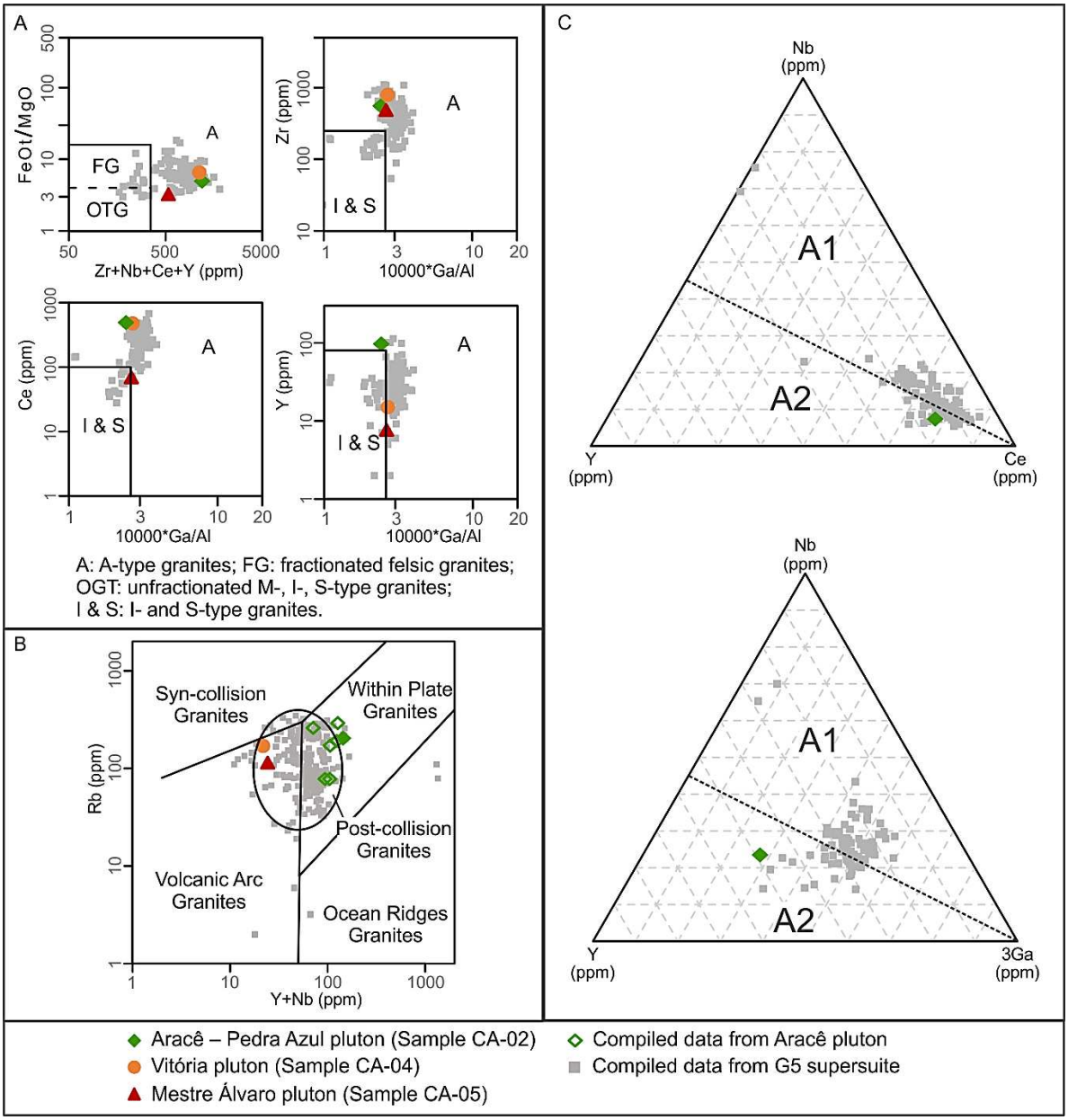

Figure B 2: G5 granites in (A) the discrimination diagrams by Whalen et al. (1987), in (B) the tectonic discriminating diagrams by Pearce et al. (1984) and Pearce (1996), and in (C) the discrimination diagrams for A-type granites by Eby (1992).

B.4.2 Zr saturation temperature (T_{Zr})

Watson and Harrison (1983) established that the crystallization temperatures of the melts are related to zircon solubility, temperature, and major element composition of melt through the following relationship:

$$\ln D_{Zr} = (- 3.80 - [0.85(M - 1)]) + 12900/T$$

Where:

-T is temperature provided in kelvin;

-M value is a compositional factor calculated by the relation [(Na + K + 2*Ca)/(Al*Si)] with all elements in cation fraction. This factor takes into account the dependence of zircon solubility with SiO_2 and melt aluminosity;

-D_{Zr} is partition coefficient of Zr between zircon and melt.

Using modern experimental techniques, Boehnke et al. (2013) re-evaluated the zircon saturation geothermometer proposed by Watson and Harrison (1983) expanding the results for pressures up to 25 kbar and temperatures decreasing up to 700ºC. They concluded that the new relationship is not present significantly different from the original study of Watson and Harrison (1983) and provided the following equation:

$$\ln D_{Zr} = (10108/T) - 1.16\,(M-1)\,1.48$$

This geothermometer proposed by Boehnke et al. (2013) was applied in the crystallization temperatures calculation for the studied G5 samples.

B.5 Zircons preparing

About 3 kg of each rock sample were prepared for analyses. First, the samples were cleaned for removal of weathering layers and any other contaminants in SEPURA laboratory in CPMTC-UFMG, then concentrate to zircon in laboratories at USP (University of São Paulo). Zircon grains were handpicked (disregarding color, shape or size) under a binocular microscope and mounted in epoxy mounts at the DEGEO-UFOP (Geology Department of Federal University of Ouro Preto). After polished the mounts to expose grain centers, they were imaged under cathodoluminescence (CL) and the Backscattered electron (BSE) in a JEOL 6510 Scanning Electron Microscope hosted at Microscopy and Microanalysis Laboratory (LMIc) of the Federal University of Ouro Preto. These images were obtained to examine morphologic features, internal structures, and the possible presence of inclusions, cracks or damaged areas to help discriminating regions spot allocation. After observing all available zircon crystals in the concentrates of zircon, only the euhedral crystals representative of the zircon populations were separated and mounted in a carbon adhesive tape for typological investigations of the external morphology and imaged, without polishing, under secondary electron (SE) in a JEOL 6510 Scanning Electron Microscope hosted at CPMTC-UFMG.

B.5.1 Zircon morphology

The most common zircon crystals are morphologically constituted by two prismatic crystalline forms {100} and {110}, and two pyramidal forms {101} and {211} (Figure B3).

Pupin (1980) proposed a scheme in which an arrangement of given prismatic and pyramidal crystal faces constitutes population types and relating the external zircon morphology to a genetic

classification of the host-granite, the source Al/alkaline ration, and the temperature of crystallization of the magma (Figure B3 and B4).

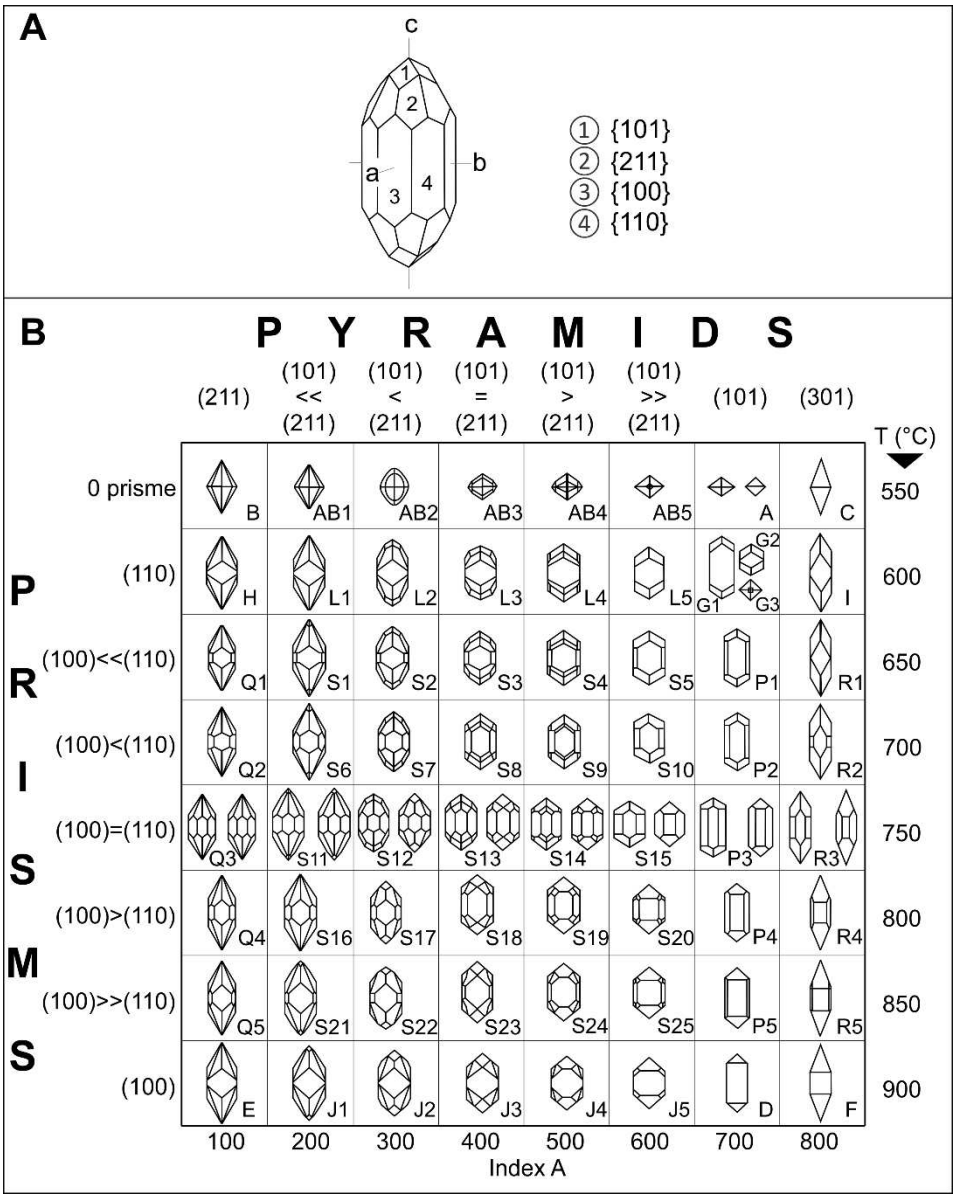

Figure B 3: (A) Zircon morphology schemes showing the combination of {100}, {110}, {211}, and {101} faces in S12 zircon type. Modified from Wang et al. (2002). (B) Zircon typological classification proposed by Pupin (1980). Index A reflects the Al/(Na+K) ratio, controlling the development of zircon pyramids. T (°C) reflects temperature of the medium crystallization that affects the development of different zircon prisms. Modified from Pupin (1980).

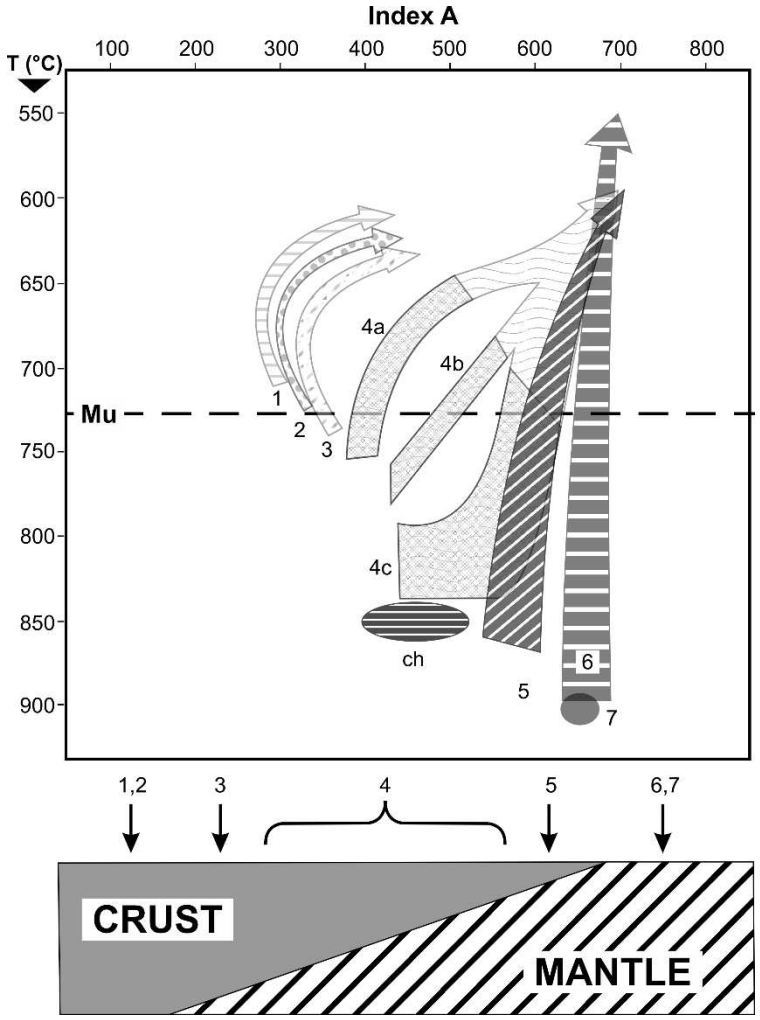

Figure B 4: Petrogenetic classification proposed by Pupin (1980) based in zircon populations from: Granites of crustal or mainly crustal origin (orogenic granites): (1) aluminous leucogranites; (2) (sub) autochthonous monzogranites and granodiorites; (3) intrusive aluminous monzogranites and granodiorites. Granites of crustal + mantle origin, hybrid granites (orogenic granites): (4a–c) calc-alkaline series granites (dark area: granodiorites + monzogranites; clear area: monzogranites + alkaline granites); (5) sub-alkaline series granites. Granites of the mantle or mainly mantle origin (anorogenic granites); (6) alkaline series granites; (7) tholeiitic series granites. Ch: magmatic charnockite area; Mu, limit of muscovite granites (T <725°C). Modified from Belousova et al. (2006).

B.6 U-Pb analyses

U-Pb isotopic analyses were carried out using a ThermoScientific Element II sector field coupled to a PhotonMachine ArF 193 mm laser ablation system (LA-SF-ICP-MS) at the Isotope Geochemistry Laboratory of the DEGEO-UFOP. Laser ablations were performed in peak jumping mode during 20s background measurement followed by 20s sample ablation, spot-size 30 μm, 1,9 J/cm^2 fluence, 6 Hz repetition rate, and carried out using He as a carrier gas mixed with Ar prior to introduction into the ICP-MS. As primary standard was used the BB-9 zircon (Santos et al., 2017) and, for quality control, the Plesovice (Sláma et al., 2008) or GJ-1 zircons (Jackson et al., 2004) were used as a secondary standard. Signal data were reduced using the software Glitter (van Achterbergh et al., 2001) and

corrected for background signal, common Pb, laser-induced elemental fractionation, instrumental mass discrimination, and time-dependent elemental fractionation of Pb/U using a MS Excel spreadsheet program (Gerdes and Zeh, 2006). The common-Pb correction was based on the interference- and background-corrected ^{204}Pb signal and on the Pb composition model (Stacey and Kramers, 1975). Zircons that were >2% discordant and with high error were discarded. The Concordia diagram and age distribution diagrams were obtained with the software Isoplot/Ex (Ludwig, 2012). The results are presented in Supplementary File 4.E.

B.7 Lu-Hf isotopes analyses

After U-Pb isotopic determinations, Lu and Hf isotopic ratios were obtained at the Isotope Geochemistry Laboratory of the DEGEO-UFOP using a Thermo-Scientific Finnigan Neptune multi-collector inductively coupled to a PhotonMachine ArF 193 mm laser ablation system (LA-MC-ICP-MS). The Lu-Hf laser spot was drilled on top of the previous U-Pb laser spot in order to analyze zircons domains with the same isotopic characteristics. Where this was not possible, care was taken to drill into the same zircon domain previously analyzed for U-Pb, characterized by the CL image. Data were collected in static mode during 60 s of ablation and the 50 μm spotsize laser was drilled with at 9 Hz repetition rate. The isotopes ^{172}Yb, ^{173}Yb, and ^{175}Lu were simultaneously monitored during each analysis step to allow for correction of isobaric interferences of Lu and Yb isotopes on mass 176. Corrections for background signal, instrumental mass bias and isobaric interferences of Lu and Yb isotopes on mass 176 were done following the methods by Gerdes and Zeh (2006, 2009). In this work, it was adopted the decay constant for ^{176}Lu of 1.865×10^{-11} a^{-1} (Söderlund et al., 2004) and the ^{176}Lu/^{177}Hf ratio for 0.0113 to the average crust in the Paleoproterozoic to Archean (Scherer et al., 2001). The accuracy and external reproducibility were verified by analyses of the reference zircons BB-9 (Santos et al., 2017), GJ-1 (Jackson et al., 2004), and Plesovice (Sláma et al., 2008) which yielded an average ^{176}Hf/^{177}Hf of 0.281672 ± 0.000019 (n = 35), 0.282001 ± 0.000018 (n = 26), 0.282468 ± 0.000019 (n = 33) respectively (all errors are ±2σ). These ratios are in good agreement with the accepted values (Jackson et al., 2004; Santos et al., 2017; Sláma et al., 2008). The results are presented in Supplementary File 4.E.

REFERENCES

Belousova, E.A., Griffin, W.L., O'Reilly, S.Y., 2006. Zircon crystal morphology, trace element signatures and Hf isotope composition as a tool for petrogenetic modelling: examples from eastern Australian granitoids. Journal of Petrology 47, 329–353.

Boehnke, P., Watson, E.B., Trail, D., Harrison, T.M., Schmitt, A.K., 2013. Zircon saturation re-revisited. Chemical Geology 351, 324-334.

Boynton, W.V., 1984. Cosmochemistry of the rare earth elements: meteorites studies. In: Henderson, P. (Ed.), Rare Earth Element Geochemistry. Elsevier, pp. 63–114.

Chappell, B.W., White, A.J.R., 2001. Two contrasting granite types: 25 years later. Australian Journal of Earth Sciences 48, 489–499.

Costa-de-Moura, J., Wiedemann, C.M., Wallfass, C.M., Van Westrenen, W., 1999. O Plúton de Pedra Azul: a estrutura do maciço intrusivo e de suas rochas encaixantes – Domingos Martins, Espirito Santo, Brasil. In: VII Simpósio Nacional de Estudos Tectônicos, SBG. Lençóis, Anais, p. 129-131.

Costa-Nascimento, R.C., Costa-de-Moura, J., Wiedemann, C.M., Da Silva, D.B.M., 1996. Geologia e petrografia do maciço intrusivo da Pedra Azul e suas rochas encaixantes - ES. In: 39º Congresso Brasileiro Geologia, SBG. Salvador, Anais 1, 96-99.

De Campos, C.P., Mendes, J.C., Ludka, I.P., Medeiros, S.R., Moura, J.C., Wallfass, C., 2004. A review of the Brasilian magmatism in southern Espírito Santo, Brazil, with emphasis on post-collisional magmatism. Journal of the Virtual Explorer 17, 1-35.

De Campos, C.P, Medeiros, S.R., Mendes, J.C, Pedrosa-Soares, A.C., Dussin, I., Ludka, I.P., Dantas, E.L., 2016. Cambro-Ordovician magmatism in the Araçuaí Belt (SE Brazil): Snapshots from a post-collisional event. Journal of South American Earth Sciences 68, 248-268.

Deer, W.A., Howie, R.A., Zussman, J., 2013. An Introduction to the Rock-Forming Minerals. London, Mineralogical Society of Great Britain and Ireland 3rd ed., 549.

Eby, G.N., 1992. Chemical subdivision of A-type granitoids: petrogenetic and tectonic implications. Geology 20, 641-644.

Frost, B.R., Barnes, C.G., Collins, W.J., Arculus, R.J., Ellis, D.J., Frost, C.D., 2001. A geochemical classification for granitic rocks. Journal of Petrology 42, 2033–2048.

Geisler, T., Schaltegger, U., Tomaschek, F., 2007. Re-equilibration of zircon in aqueous fluids and melts. Elements 3, 43-50.

Gerdes, A., Zeh, A., 2006. Combined U-Pb and Hf isotope LA-(MC)-ICP-MS analyses of detrital zircons: comparison with SHRIMP and new constraints for the provenance and age of an Armorican metasediment in Central Germany. Earth and Planetary Science Letters 249, 47-61.

Gerdes, A., Zeh, A., 2009. Zircon formation versus zircon alteration - new insights from combined U-Pb and Lu-Hf in-situ LA-ICP-MS analyses, and consequences for the interpretation of Archean zircon from the Central Zone of the Limpopo Belt. Chemical Geology 261, 230-243.

Jackson, S.E., Pearson, N.J., Griffin, W.L., Belousova, E.A., 2004. The application of laser ablation-inductively coupled plasma-mass spectrometry to in situ U–Pb zircon geochronology. Chemical Geology 211, 47–69.

Janoušek, V., Farrow, C.M., Erban, V., 2006. Interpretation of whole-rock geochemical data in igneous geochemistry: Introducing Geochemical Data Toolkit (GCDkit). Journal of Petrology 47, 1255–1259.

Ludwig, K.R., 2012. Isoplot/Ex Version 3.75: A Geochronological Toolkit for Microsoft Excel. Berkeley, Berkeley Geochronology Center 72 pp.

McDonough, W.F., Sun, S.S., 1995. The composition of the Earth. Chemical Geology 120, 223–253.

Pupin, J.P., 1980. Zircon and granite petrology. Contributions to Mineralogy and Petrology 73, 207-220.

Pearce, J.A., Harris, N.B.W., Tindle, A.G., 1984. Trace element diagrams for the tectonic interpretation of granitic rocks. Journal of Petrology 25, 956–983.

Pearce, J., 1996. Sources and settings of granitic rocks. Episodes 19, 120-125.

Platzer, S., 1997. Whole rock geochemistry of the Aracê/Pedra Azul pluton. University of Utrecht (MS Dissertation - unpublished, 58 pp).

Santos, M.M., Lana, C., Scholz, R., Buick, I., Schmitz, M.D., Kamo, S.L., Gerdes, A., Corfu, F., Tapster, S., Lancaster, P., Storey, C.D., Basei, M.A.S, Tohver, E., Alkmim, A., Nalini, H., Krambrock, K., Fantini, C., Wiedenbeck, M., 2017. A New appraisal of Sri Lankan BB zircon as reference material for LA-ICP-MS U-Pb geochronology and Lu-Hf isotope tracing. Geostandards and Geoanalytical Research 41, 335-358.

Scherer, E., Münker, C., Mezger, K., 2001. Calibration of the Lutetium–Hafnium clock. Science 293, 683–687.

Shand, S.J., 1943. Eruptive rocks. Their genesis, composition, classification, and their relation to ore-deposits with a chapter on meteorite. New York: John Wiley & Sons.

Sláma, J., Košler, J., Condon, D.J., Crowley, J.L., Gerdes, A., Hanchar, J.M., Horstwood, M.S.A., Morris, G.A., Nasdala, L., Norberg, N., Schaltegger, U., Schoene, B., Tubrett, M.N., Whitehouse, M.J., 2008. Plešovice zircon – a new natural reference material for U–Pb and Hf isotopic microanalysis. Chemical Geology 249, 1–35.

Stacey, J.S., Kramers, J.D., 1975. Approximation of terrestrial lead isotope evolution by a two-stage model. Earth and Planetary Science Letters 26, 207-221.

van Achterbergh, E., Ryan, C.G., Jackson, S.E., Griffin, W., 2001. Data reduction software for LA-ICP-MS. In: Sylvester, P. (Ed.), Laser-ablation-ICPMS in the Earth sciences, principles and applications. Mineralogical Association of Canada, Short Course Series 29, 239–243.

Vieira, V.S., Menezes, R.G. (Orgs.), 2015. Geologia e Recursos Minerais do Estado do Estado do Espírito Santo: texto explicativo do mapa geológico e de recursos minerais, escala 1:400.000. Programa Geologia do Brasil, CPRM - Serviço Geológico do Brasil, Belo Horizonte.

Wang, X., Griffin, W.L., O'Reilly, S.Y., Zhou, X.M., Xu, X.S., Jackson, S.E., Pearson, N.J., 2002. Morphology and geochemistry of zircons from late Mesozoic igneous complexes in coastal SE China: implications for petrogenesis. Mineralogical Magazine 66, 235-251.

Watson, E.B., Harrison, T.M., 1983. Zircon saturation revisited: temperature and composition effects in a variety of crustal magma types. Earth and Planetary Science Letters 64, 295–304.

Whalen, J.B., Currie, K.L., Chappell, B.W., 1987. A-type granites, geochemical characteristics, discrimination and petrogenesis. Contributions to Mineralogy and Petrology 95, 407-419.

Whitney, D.L., Evans, B.W., 2010. Abbreviations for names of rock-forming minerals. American Mineralogist 95, 185-187.

Wiedemann, C.M., Medeiros, S.R., Ludka, I.P., Mendes, J.C., Costa-de-Moura, J., 2002. Architecture of late orogenic plutons in the Araçuaí-Ribeira fold belt, Southeast Brazil. Gondwana Research 5, 381-399.

APPENDIX F - Supplementary File 4.C: Mineral Chemistry

Spot	SiO_2	Al_2O_3	TiO_2	FeO	Cr_2O_3	MnO	MgO	CaO	Na_2O	K_2O	F	Cl	ZrO_2	Total	Position
Electron-microprobe analyses of biotite from Sample CA-02															
Major element compositions (wt%)															
A-1	35.765	14.884	2.743	22.832	0.008	0.312	8.301	0.053	0.100	9.793	1.684	0.319	0.000	96.794	Rim
A-2	35.629	14.679	2.709	22.611	0.000	0.335	8.275	0.025	0.124	9.659	1.812	0.318	0.000	96.176	Intermediary
A-3	35.433	14.486	2.850	22.694	0.016	0.351	8.193	0.028	0.143	9.602	1.718	0.311	0.000	95.825	Core
A-4	35.948	14.533	2.927	22.779	0.000	0.354	8.254	0.027	0.083	9.750	1.645	0.289	0.000	96.589	Intermediary
A-5	35.405	14.796	2.687	23.225	0.000	0.314	8.732	0.033	0.087	9.142	1.435	0.279	0.000	96.135	Rim
A-16	35.603	15.309	2.176	22.680	0.048	0.405	8.544	0.178	0.084	9.589	1.590	0.273	0.000	96.479	Rim
A-17	36.247	15.704	2.227	22.389	0.000	0.373	8.306	0.101	0.077	9.322	1.872	0.386	0.000	97.004	Rim
A-18	35.756	14.813	2.691	22.096	0.014	0.306	8.317	0.000	0.095	9.731	1.789	0.278	0.000	95.886	Rim
A-19	35.796	14.423	3.088	22.446	0.000	0.346	8.262	0.013	0.052	9.650	1.790	0.254	0.000	96.120	Core
A-20	35.585	14.284	3.058	22.811	0.000	0.377	8.190	0.000	0.032	9.667	1.643	0.274	0.000	95.921	Core
A-21	36.539	14.315	3.132	21.979	0.000	0.342	8.203	0.032	0.074	9.661	1.644	0.271	0.000	96.192	Intermediary
A-22	35.924	14.805	2.838	21.700	0.000	0.348	8.395	0.025	0.078	9.760	1.741	0.258	0.000	95.872	Rim
A-35	36.826	14.861	2.718	21.457	0.005	0.329	8.073	0.033	0.118	9.512	1.682	0.269	0.000	95.883	Core
A-36	36.602	15.607	2.912	21.466	0.001	0.315	8.080	0.000	0.065	9.504	1.752	0.277	0.000	96.581	Rim
A-37	35.486	15.105	2.715	21.950	0.047	0.357	8.427	0.041	0.111	9.471	1.692	0.257	0.000	95.659	Core
A-38	35.743	15.565	3.234	21.363	0.000	0.329	8.528	0.045	0.102	9.575	1.511	0.264	0.000	96.259	Rim
A-48	36.048	15.132	2.607	21.879	0.015	0.361	8.028	0.014	0.111	9.465	1.675	0.263	0.000	95.598	Rim
A-49	36.066	15.378	2.671	21.239	0.000	0.297	8.217	0.016	0.076	9.376	1.728	0.249	0.000	95.313	Core
A-50	36.238	15.292	2.639	21.385	0.000	0.392	8.649	0.061	0.064	9.224	1.677	0.264	0.000	95.885	Rim
A-51	36.110	15.042	2.902	21.572	0.000	0.343	8.889	0.032	0.145	9.270	1.734	0.273	0.000	96.312	Rim
A-52	36.203	15.295	2.893	21.614	0.000	0.355	8.022	0.019	0.111	9.272	1.774	0.253	0.000	95.811	Core
A-53	35.684	14.710	2.774	22.165	0.023	0.363	8.139	0.011	0.045	9.275	1.420	0.251	0.000	94.860	Core
A-54	36.066	15.424	2.748	21.123	0.000	0.232	8.862	0.045	0.089	9.336	1.606	0.279	0.000	95.810	Rim
B-8	36.443	15.825	2.441	21.795	0.064	0.239	8.381	0.006	0.093	9.478	1.688	0.275	0.000	96.728	Rim
B-9	36.766	15.474	2.342	21.586	0.014	0.265	8.194	0.053	0.139	9.477	1.669	0.411	0.000	96.390	Intermediary
B-10	36.382	15.372	2.485	21.318	0.024	0.354	8.398	0.013	0.090	9.397	1.811	0.275	0.000	95.919	Core
B-11	37.050	15.451	2.356	21.368	0.000	0.345	8.213	0.056	0.115	9.059	1.525	0.253	0.000	95.791	Intermediary
B-12	36.549	15.205	2.316	21.768	0.016	0.271	8.415	0.042	0.083	9.383	1.609	0.265	0.000	95.922	Rim
B-27	36.757	15.318	2.585	21.676	0.002	0.305	8.240	0.005	0.078	9.385	1.794	0.273	0.000	96.418	Rim
B-28	36.761	15.242	2.716	21.448	0.000	0.309	8.334	0.023	0.106	9.339	1.649	0.254	0.000	96.181	Core

Spot	SiO_2	Al_2O_3	TiO_2	FeO	Cr_2O_3	MnO	MgO	CaO	Na_2O	K_2O	F	Cl	ZrO_2	Total	Position
Electron-microprobe analyses of biotite from Sample CA-02															
Major element compositions (wt%)															
B-29	36.434	15.199	2.309	21.356	0.005	0.329	8.454	0.178	0.008	9.100	1.235	0.247	0.000	94.854	Core
B-30	36.515	15.274	2.636	20.860	0.012	0.402	8.229	0.006	0.074	9.199	1.755	0.255	0.000	95.217	Rim
B-31	36.651	15.318	2.651	20.952	0.003	0.297	8.952	0.033	0.086	8.972	1.627	0.216	0.000	95.758	Rim
B-32	36.539	15.545	2.600	21.654	0.046	0.255	8.268	0.017	0.085	9.259	1.753	0.240	0.000	96.261	Rim
B-33	37.590	14.422	2.408	21.672	0.006	0.321	8.335	0.009	0.103	9.207	1.724	0.233	0.000	96.030	Rim
B-34	37.481	15.368	2.570	20.375	0.004	0.331	9.846	0.031	0.109	9.102	1.611	0.244	0.000	97.072	Core
B-35	37.242	14.258	2.579	21.254	0.007	0.361	9.036	0.004	0.102	9.087	1.697	0.258	0.000	95.885	Core
B-37	36.120	15.136	2.264	21.317	0.019	0.331	9.470	0.041	0.201	9.112	2.085	0.246	0.000	96.342	Core
B-39	35.944	15.669	1.897	20.549	0.012	0.291	9.332	0.036	0.122	9.037	1.791	0.213	0.004	94.897	Rim
B-70	36.485	15.007	2.136	21.413	0.000	0.342	9.259	0.000	0.080	9.041	1.428	0.264	0.036	95.491	Rim
B-71	36.541	15.099	2.083	21.963	0.010	0.329	8.626	0.017	0.094	9.030	1.787	0.246	0.000	95.825	Core
B-72	36.061	15.024	2.154	21.194	0.000	0.345	9.407	0.000	0.078	8.995	1.590	0.257	0.000	95.105	Core
B-73	37.041	15.249	2.232	20.817	0.000	0.285	9.570	0.000	0.038	9.012	1.718	0.255	0.000	96.217	Rim

Spot	Si	^{IV}Al	^{VI}Al	Ti	Fe	Cr	Mn	Mg	Ca	Na	K	F	Cl	Zr	Fe#	Mg#
	Electron-microprobe analyses of biotite from Sample CA-02														**Fe/(Fe+Mg)**	**Mg/(Mg+Fe)**
	Numbers of ions on the basis of 22 oxygen															
A-1	5.6158	2.3842	0.3700	0.3240	2.9982	0.0010	0.0415	1.9431	0.0089	0.0304	1.9614	0.8361	0.0849	0.0000	0.61	0.39
A-2	5.6343	2.3657	0.3699	0.3222	2.9903	0.0000	0.0449	1.9509	0.0042	0.0380	1.9484	0.9061	0.0852	0.0000	0.61	0.39
A-3	5.6258	2.3742	0.3363	0.3404	3.0133	0.0020	0.0472	1.9393	0.0048	0.0440	1.9447	0.8625	0.0837	0.0000	0.61	0.39
A-4	5.6501	2.3499	0.3420	0.3461	2.9942	0.0000	0.0471	1.9340	0.0045	0.0253	1.9547	0.8176	0.0770	0.0000	0.61	0.39
A-5	5.5770	2.4230	0.3237	0.3184	3.0595	0.0000	0.0419	2.0506	0.0056	0.0266	1.8369	0.7148	0.0745	0.0000	0.60	0.40
A-16	5.5934	2.4066	0.4278	0.2572	2.9798	0.0060	0.0539	2.0011	0.0300	0.0256	1.9216	0.7899	0.0727	0.0000	0.60	0.40
A-17	5.6493	2.3507	0.5338	0.2611	2.9182	0.0000	0.0492	1.9299	0.0169	0.0233	1.8533	0.9226	0.1020	0.0000	0.60	0.40
A-18	5.6512	2.3488	0.4102	0.3199	2.9206	0.0017	0.0410	1.9597	0.0000	0.0291	1.9618	0.8941	0.0745	0.0000	0.60	0.40
A-19	5.6519	2.3481	0.3357	0.3668	2.9639	0.0000	0.0463	1.9448	0.0022	0.0159	1.9436	0.8937	0.0680	0.0000	0.60	0.40
A-20	5.6393	2.3607	0.3070	0.3645	3.0232	0.0000	0.0506	1.9349	0.0000	0.0098	1.9542	0.8233	0.0736	0.0000	0.61	0.39
A-21	5.7311	2.2689	0.3771	0.3695	2.8830	0.0000	0.0454	1.9181	0.0054	0.0225	1.9329	0.8154	0.0720	0.0000	0.60	0.40

Spot	Si	^{IV}Al	^{VI}Al	Ti	Fe	Cr	Mn	Mg	Ca	Na	K	F	Cl	Zr	Fe#	Mg#
	Electron-microprobe analyses of biotite from Sample CA-02														Fe/(Fe+Mg)	Mg/(Mg+Fe)
	Numbers of ions on the basis of 22 oxygen															
A-22	5.6624	2.3376	0.4126	0.3365	2.8605	0.0000	0.0465	1.9727	0.0042	0.0238	1.9623	0.8677	0.0689	0.0000	0.59	0.41
A-35	5.7667	2.2333	0.5092	0.3202	2.8100	0.0006	0.0436	1.8846	0.0055	0.0358	1.9000	0.8329	0.0714	0.0000	0.60	0.40
A-36	5.6882	2.3118	0.5465	0.3404	2.7899	0.0001	0.0415	1.8720	0.0000	0.0196	1.8840	0.8610	0.0730	0.0000	0.60	0.40
A-37	5.6073	2.3927	0.4201	0.3227	2.9006	0.0059	0.0478	1.9851	0.0069	0.0340	1.9090	0.8454	0.0688	0.0000	0.59	0.41
A-38	5.5778	2.4222	0.4403	0.3796	2.7880	0.0000	0.0435	1.9840	0.0075	0.0309	1.9060	0.7456	0.0698	0.0000	0.58	0.42
A-48	5.6843	2.3157	0.4964	0.3092	2.8853	0.0019	0.0482	1.8873	0.0024	0.0339	1.9038	0.8352	0.0703	0.0000	0.60	0.40
A-49	5.6809	2.3191	0.5356	0.3165	2.7978	0.0000	0.0396	1.9296	0.0027	0.0232	1.8839	0.8607	0.0665	0.0000	0.59	0.41
A-50	5.6703	2.3297	0.4902	0.3106	2.7984	0.0000	0.0519	2.0176	0.0102	0.0194	1.8411	0.8298	0.0700	0.0000	0.58	0.42
A-51	5.6403	2.3597	0.4092	0.3410	2.8179	0.0000	0.0454	2.0699	0.0054	0.0439	1.8470	0.8564	0.0723	0.0000	0.58	0.42
A-52	5.6820	2.3180	0.5110	0.3415	2.8370	0.0000	0.0472	1.8770	0.0032	0.0338	1.8563	0.8804	0.0673	0.0000	0.60	0.40
A-53	5.6674	2.3326	0.4206	0.3314	2.9440	0.0029	0.0488	1.9271	0.0019	0.0139	1.8790	0.7131	0.0676	0.0000	0.60	0.40
A-54	5.6395	2.3605	0.4819	0.3232	2.7623	0.0000	0.0307	2.0659	0.0075	0.0270	1.8622	0.7941	0.0739	0.0000	0.57	0.43
B-8	5.6591	2.3409	0.5551	0.2851	2.8304	0.0079	0.0314	1.9402	0.0010	0.0280	1.8774	0.8289	0.0724	0.0000	0.59	0.41
B-9	5.7303	2.2697	0.5725	0.2746	2.8136	0.0017	0.0350	1.9039	0.0088	0.0420	1.8841	0.8225	0.1086	0.0000	0.60	0.40
B-10	5.6990	2.3010	0.5367	0.2928	2.7927	0.0030	0.0470	1.9611	0.0022	0.0273	1.8776	0.8970	0.0730	0.0000	0.59	0.41
B-11	5.7680	2.2320	0.6028	0.2759	2.7821	0.0000	0.0455	1.9062	0.0093	0.0347	1.7990	0.7507	0.0668	0.0000	0.59	0.41
B-12	5.7202	2.2798	0.5246	0.2727	2.8491	0.0020	0.0359	1.9634	0.0070	0.0252	1.8732	0.7963	0.0703	0.0000	0.59	0.41
B-27	5.7262	2.2738	0.5384	0.3029	2.8240	0.0002	0.0402	1.9137	0.0008	0.0236	1.8650	0.8837	0.0721	0.0000	0.60	0.40
B-28	5.7252	2.2748	0.5228	0.3182	2.7936	0.0000	0.0408	1.9350	0.0038	0.0320	1.8553	0.8121	0.0670	0.0000	0.59	0.41
B-29	5.7270	2.2730	0.5425	0.2730	2.8074	0.0006	0.0438	1.9811	0.0300	0.0024	1.8246	0.6138	0.0658	0.0000	0.59	0.41
B-30	5.7377	2.2623	0.5661	0.3116	2.7412	0.0015	0.0535	1.9277	0.0010	0.0225	1.8438	0.8720	0.0679	0.0000	0.59	0.41
B-31	5.7051	2.2949	0.5152	0.3104	2.7275	0.0004	0.0392	2.0774	0.0055	0.0260	1.7815	0.8008	0.0570	0.0000	0.57	0.43
B-32	5.6938	2.3062	0.5486	0.3048	2.8219	0.0057	0.0337	1.9208	0.0028	0.0257	1.8404	0.8638	0.0634	0.0000	0.60	0.40
B-33	5.8606	2.1394	0.5105	0.2824	2.8257	0.0007	0.0424	1.9373	0.0015	0.0311	1.8310	0.8499	0.0616	0.0000	0.59	0.41
B-34	5.7285	2.2715	0.4966	0.2955	2.6043	0.0005	0.0428	2.2435	0.0051	0.0323	1.7745	0.7786	0.0632	0.0000	0.54	0.46
B-35	5.8097	2.1903	0.4309	0.3026	2.7728	0.0009	0.0477	2.1015	0.0007	0.0308	1.8082	0.8371	0.0682	0.0000	0.57	0.43
B-37	5.6477	2.3523	0.4368	0.2663	2.7875	0.0023	0.0438	2.2075	0.0069	0.0609	1.8174	1.0309	0.0652	0.0000	0.56	0.44
B-39	5.6595	2.3405	0.5671	0.2247	2.7059	0.0015	0.0388	2.1905	0.0061	0.0372	1.8150	0.8917	0.0568	0.0003	0.55	0.45
B-70	5.7092	2.2908	0.4767	0.2514	2.8022	0.0000	0.0453	2.1600	0.0000	0.0243	1.8046	0.7066	0.0700	0.0027	0.56	0.44
B-71	5.7301	2.2699	0.5205	0.2457	2.8803	0.0012	0.0437	2.0166	0.0029	0.0286	1.8063	0.8861	0.0654	0.0000	0.59	0.41

Spot	Si	^{IV}Al	^{VI}Al	Ti	Fe	Cr	Mn	Mg	Ca	Na	K	F	Cl	Zr	Fe#	Mg#
	Electron-microprobe analyses of biotite from Sample CA-02														Fe/(Fe+Mg)	Mg/(Mg+Fe)
	Numbers of ions on the basis of 22 oxygen															
B-72	5.6759	2.3241	0.4627	0.2550	2.7898	0.0000	0.0460	2.2073	0.0000	0.0238	1.8059	0.7913	0.0686	0.0000	0.56	0.44
B-73	5.7348	2.2652	0.5171	0.2599	2.6953	0.0000	0.0374	2.2089	0.0000	0.0114	1.7798	0.8411	0.0669	0.0000	0.55	0.45

Spot	SiO_2	Al_2O_3	TiO_2	FeO	Cr_2O_3	MnO	MgO	CaO	Na_2O	K_2O	F	Cl	ZrO_2	Total	Position
Electron-microprobe analyses of biotite from Sample CA-04															
Major element compositions (wt%)															
6	35.923	14.632	3.520	18.095	0.004	0.038	11.797	0.004	0.167	9.537	1.812	0.554	0.000	96.083	Core
7	35.646	15.111	2.220	24.172	0.020	0.071	11.512	0.050	0.170	5.653	1.220	0.345	0.000	96.190	Rim (altered)
19	37.125	14.368	3.639	16.510	0.023	0.077	12.902	0.044	0.148	9.521	1.791	0.605	0.000	96.753	Rim
20	36.404	13.818	3.669	16.883	0.001	0.058	13.346	0.045	0.154	9.545	1.930	0.525	0.000	96.378	Core
21	36.401	13.558	3.337	18.416	0.008	0.065	11.859	0.055	0.122	9.488	1.645	0.764	0.000	95.718	Rim
22	36.613	13.625	3.379	17.586	0.000	0.077	12.333	0.049	0.072	9.580	1.857	0.758	0.000	95.929	Rim
23	36.247	13.655	3.534	16.187	0.006	0.201	13.235	0.021	0.145	9.466	1.954	0.504	0.000	95.155	Core
24	36.714	13.699	3.455	16.744	0.000	0.085	12.951	0.013	0.097	9.524	2.066	0.605	0.000	95.953	Core
26	36.391	13.935	3.514	18.377	0.000	0.027	12.029	0.011	0.146	9.535	1.983	0.547	0.000	96.495	Rim
52	36.380	13.806	3.705	16.770	0.046	0.051	12.511	0.010	0.123	9.438	1.839	0.597	0.000	95.276	Rim
53	36.329	13.787	3.782	17.026	0.047	0.080	12.271	0.046	0.098	9.646	1.925	0.537	0.000	95.574	Rim
54	36.580	13.976	3.752	16.760	0.006	0.115	12.549	0.022	0.128	9.479	1.889	0.571	0.000	95.827	Rim
96	35.991	13.487	3.886	16.946	0.024	0.116	12.484	0.011	0.124	9.563	1.956	0.516	0.000	95.104	Rim
97	36.312	14.328	3.128	19.818	0.000	0.098	12.795	0.008	0.118	7.994	1.341	0.457	0.000	96.397	Core
98	36.418	13.869	3.679	16.967	0.000	0.079	12.812	0.010	0.116	9.716	1.839	0.566	0.000	96.071	Core
99	36.151	13.593	3.511	18.223	0.000	0.027	12.280	0.000	0.093	9.595	1.778	0.854	0.000	96.105	Core
100	36.751	14.196	2.976	19.742	0.009	0.042	12.784	0.016	0.095	8.157	1.477	0.462	0.000	96.707	Rim
101	36.084	13.380	3.401	18.514	0.000	0.080	11.809	0.021	0.151	9.527	1.585	0.809	0.011	95.372	Rim
102	35.899	14.771	3.797	19.673	0.000	0.051	11.108	0.003	0.111	8.394	1.418	0.490	0.000	95.715	Rim
119	36.305	13.475	4.187	17.747	0.047	0.024	12.679	0.020	0.119	9.683	1.567	0.551	0.000	96.404	Rim

Spot	SiO_2	Al_2O_3	TiO_2	FeO	Cr_2O_3	MnO	MgO	CaO	Na_2O	K_2O	F	Cl	ZrO_2	Total	Position
Electron-microprobe analyses of biotite from Sample CA-04															
Major element compositions (wt%)															
120	36.237	13.581	4.190	17.762	0.049	0.083	12.322	0.013	0.147	9.637	1.946	0.502	0.000	96.469	Core
121	36.187	13.423	4.143	16.796	0.002	0.108	12.293	0.000	0.103	9.754	1.917	0.498	0.000	95.224	Core
122	36.871	13.847	4.285	16.330	0.015	0.163	12.696	0.017	0.152	9.567	2.048	0.486	0.021	96.498	Rim

Spot	Si	^{IV}Al	^{VI}Al	Ti	Fe	Cr	Mn	Mg	Ca	Na	K	F	Cl	Zr	Fe#	Mg#
	Electron-microprobe analyses of biotite from Sample CA-04															
	Numbers of ions on the basis of 22 oxygen															
6	5.5650	2.4350	0.2363	0.4102	2.3443	0.0005	0.0050	2.7245	0.0007	0.0502	1.8846	0.8876	0.1455	0.0000	0.46	0.54
7	5.4982	2.5018	0.2451	0.2576	3.1181	0.0024	0.0093	2.6472	0.0083	0.0508	1.1122	0.5950	0.0902	0.0000	0.54	0.46
19	5.6514	2.3486	0.2290	0.4167	2.1019	0.0028	0.0099	2.9280	0.0072	0.0437	1.8488	0.8621	0.1561	0.0000	0.42	0.58
20	5.5965	2.4035	0.0999	0.4243	2.1706	0.0001	0.0076	3.0587	0.0074	0.0459	1.8718	0.9382	0.1368	0.0000	0.42	0.58
21	5.6730	2.3270	0.1632	0.3912	2.4003	0.0010	0.0086	2.7553	0.0092	0.0369	1.8862	0.8107	0.2018	0.0000	0.47	0.53
22	5.6810	2.3190	0.1725	0.3944	2.2820	0.0000	0.0101	2.8529	0.0081	0.0217	1.8961	0.9111	0.1993	0.0000	0.44	0.56
23	5.6318	2.3682	0.1321	0.4130	2.1033	0.0007	0.0264	3.0657	0.0035	0.0437	1.8761	0.9600	0.1327	0.0000	0.41	0.59
24	5.6718	2.3282	0.1659	0.4015	2.1633	0.0000	0.0111	2.9828	0.0022	0.0291	1.8768	1.0092	0.1584	0.0000	0.42	0.58
26	5.6277	2.3723	0.1673	0.4088	2.3767	0.0000	0.0035	2.7733	0.0018	0.0438	1.8809	0.9697	0.1434	0.0000	0.46	0.54
52	5.6497	2.3503	0.1765	0.4328	2.1780	0.0056	0.0067	2.8966	0.0017	0.0370	1.8696	0.9031	0.1571	0.0000	0.43	0.57
53	5.6414	2.3586	0.1646	0.4418	2.2111	0.0058	0.0105	2.8408	0.0077	0.0295	1.9107	0.9452	0.1413	0.0000	0.44	0.56
54	5.6461	2.3539	0.1884	0.4356	2.1634	0.0007	0.0150	2.8876	0.0036	0.0383	1.8663	0.9220	0.1494	0.0000	0.43	0.57
96	5.6231	2.3769	0.1065	0.4567	2.2142	0.0030	0.0153	2.9078	0.0018	0.0376	1.9058	0.9663	0.1366	0.0000	0.43	0.57

Spot	Si	^{IV}Al	^{VI}Al	Ti	Fe	Cr	Mn	Mg	Ca	Na	K	F	Cl	Zr	Fe#	Mg#
	Electron-microprobe analyses of biotite from Sample CA-04															
	Numbers of ions on the basis of 22 oxygen															
97	5.5627	2.4373	0.1494	0.3605	2.5390	0.0000	0.0127	2.9221	0.0013	0.0350	1.5621	0.6496	0.1186	0.0000	0.46	0.54
98	5.6199	2.3801	0.1421	0.4271	2.1897	0.0000	0.0103	2.9475	0.0017	0.0347	1.9125	0.8974	0.1480	0.0000	0.43	0.57
99	5.6249	2.3751	0.1174	0.4109	2.3713	0.0000	0.0036	2.8485	0.0000	0.0281	1.9044	0.8748	0.2252	0.0000	0.45	0.55
100	5.6147	2.3853	0.1706	0.3420	2.5224	0.0011	0.0054	2.9117	0.0026	0.0281	1.5896	0.7135	0.1196	0.0000	0.46	0.54
101	5.6562	2.3438	0.1280	0.4010	2.4270	0.0000	0.0106	2.7596	0.0035	0.0459	1.9049	0.7856	0.2149	0.0008	0.47	0.53
102	5.5563	2.4437	0.2505	0.4421	2.5464	0.0000	0.0067	2.5631	0.0005	0.0333	1.6572	0.6940	0.1285	0.0000	0.50	0.50
119	5.5908	2.4092	0.0363	0.4850	2.2856	0.0057	0.0031	2.9108	0.0033	0.0355	1.9021	0.7630	0.1438	0.0000	0.44	0.56
120	5.5968	2.4032	0.0688	0.4868	2.2943	0.0060	0.0109	2.8372	0.0022	0.0440	1.8986	0.9504	0.1314	0.0000	0.45	0.55
121	5.6413	2.3587	0.1073	0.4858	2.1897	0.0002	0.0143	2.8570	0.0000	0.0311	1.9396	0.9450	0.1316	0.0000	0.43	0.57
122	5.6450	2.3550	0.1435	0.4935	2.0909	0.0018	0.0211	2.8978	0.0028	0.0451	1.8684	0.9915	0.1261	0.0016	0.42	0.58

Spot	SiO_2	Al_2O_3	TiO_2	FeO	Cr_2O_3	MnO	MgO	CaO	Na_2O	K_2O	F	Cl	ZrO_2	Total	Position
	Electron-microprobe analyses of biotite from Sample CA-05														
	Major element compositions (wt%)														
1	35.017	13.759	4.742	19.568	0.056	0.172	10.317	0.027	0.048	9.965	1.004	0.458	0.000	95.133	Rim
3	34.960	13.996	4.866	19.208	0.023	0.172	10.355	0.006	0.081	9.894	0.822	0.469	0.000	94.852	Core
4	35.735	14.149	4.864	19.313	0.000	0.200	10.297	0.006	0.057	9.960	0.803	0.481	0.000	95.865	Core
5	35.801	14.124	4.911	19.522	0.049	0.268	10.317	0.007	0.062	9.927	0.820	0.471	0.000	96.279	Rim
10	35.462	14.066	4.809	19.631	0.000	0.214	10.246	0.037	0.063	9.827	0.791	0.447	0.000	95.593	Rim
11	35.009	13.997	4.780	20.242	0.026	0.264	10.371	0.000	0.102	9.864	0.787	0.480	0.000	95.922	Intermediary
12	35.313	14.119	5.006	20.037	0.000	0.254	10.283	0.022	0.065	9.936	0.596	0.461	0.000	96.092	Core
13	35.318	13.865	4.863	19.679	0.002	0.228	10.224	0.008	0.069	9.850	0.786	0.466	0.000	95.358	Core
14	35.384	14.236	5.049	20.022	0.046	0.047	9.809	0.032	0.108	9.787	0.952	0.563	0.000	96.035	Rim
25	36.161	13.627	4.706	19.912	0.025	0.204	10.663	0.046	0.069	9.674	0.888	0.436	0.000	96.411	Rim
26	36.423	13.407	4.712	19.728	0.037	0.233	9.792	0.041	0.090	9.673	0.898	0.424	0.000	95.458	Rim
27	35.595	13.637	4.641	20.315	0.000	0.125	10.283	0.057	0.069	9.806	0.794	0.428	0.000	95.750	Rim
40	36.716	14.800	5.136	18.031	0.000	0.253	10.032	0.020	0.130	9.721	0.644	0.390	0.021	95.894	Rim
41	36.578	13.724	5.145	18.442	0.000	0.297	10.181	0.042	0.157	9.560	0.735	0.409	0.000	95.270	Core

Spot	SiO_2	Al_2O_3	TiO_2	FeO	Cr_2O_3	MnO	MgO	CaO	Na_2O	K_2O	F	Cl	ZrO_2	Total	Position
Electron-microprobe analyses of biotite from Sample CA-05															
Major element compositions (wt%)															
42	36.403	13.740	4.934	18.876	0.030	0.307	10.174	0.072	0.178	9.473	0.625	0.416	0.092	95.320	Core
43	35.355	13.966	4.925	18.972	0.003	0.299	10.443	0.059	0.072	9.542	0.765	0.375	0.000	94.776	Core
44	36.996	13.557	4.664	18.874	0.000	0.290	10.565	0.044	0.101	9.501	0.837	0.400	0.000	95.829	Rim
73	36.503	14.994	4.690	19.477	0.000	0.213	10.214	0.005	0.063	9.509	0.724	0.455	0.013	96.860	Rim
74	36.581	14.947	4.657	19.540	0.000	0.244	10.086	0.025	0.072	9.383	0.745	0.470	0.000	96.750	Core
75	36.291	14.213	4.810	19.361	0.000	0.143	10.146	0.031	0.070	9.522	0.752	0.452	0.000	95.791	Core
76	36.634	14.049	4.849	19.638	0.000	0.227	10.165	0.000	0.067	9.362	0.890	0.482	0.000	96.363	Rim

Spot	Si	^{IV}Al	^{VI}Al	Ti	Fe	Cr	Mn	Mg	Ca	Na	K	F	Cl	Zr	Fe#	Mg#
	Electron-microprobe analyses of biotite from Sample CA-05															
	Numbers of ions on the basis of 22 oxygen															
1	5.5074	2.4926	0.0577	0.5610	2.5738	0.0070	0.0229	2.4191	0.0045	0.0146	1.9992	0.4993	0.1221	0.0000	0.52	0.48
3	5.4917	2.5083	0.0827	0.5750	2.5234	0.0029	0.0229	2.4250	0.0010	0.0247	1.9825	0.4083	0.1249	0.0000	0.51	0.49
4	5.5409	2.4591	0.1264	0.5673	2.5044	0.0000	0.0263	2.3802	0.0010	0.0171	1.9699	0.3937	0.1264	0.0000	0.51	0.49
5	5.5330	2.4670	0.1055	0.5709	2.5232	0.0060	0.0351	2.3771	0.0012	0.0186	1.9570	0.4007	0.1234	0.0000	0.51	0.49
10	5.5227	2.4773	0.1042	0.5634	2.5568	0.0000	0.0282	2.3788	0.0062	0.0190	1.9522	0.3895	0.1180	0.0000	0.52	0.48
11	5.4629	2.5371	0.0369	0.5611	2.6416	0.0032	0.0349	2.4126	0.0000	0.0309	1.9634	0.3883	0.1269	0.0000	0.52	0.48
12	5.4771	2.5229	0.0579	0.5841	2.5990	0.0000	0.0334	2.3777	0.0037	0.0195	1.9658	0.2923	0.1212	0.0000	0.52	0.48
13	5.5218	2.4782	0.0764	0.5719	2.5731	0.0002	0.0302	2.3830	0.0013	0.0209	1.9644	0.3886	0.1235	0.0000	0.52	0.48
14	5.5063	2.4937	0.1171	0.5910	2.6057	0.0057	0.0062	2.2757	0.0053	0.0326	1.9427	0.4685	0.1485	0.0000	0.53	0.47
25	5.5816	2.4184	0.0605	0.5464	2.5704	0.0031	0.0267	2.4537	0.0076	0.0206	1.9047	0.4334	0.1141	0.0000	0.51	0.49
26	5.6720	2.3280	0.1325	0.5520	2.5693	0.0046	0.0307	2.2733	0.0068	0.0272	1.9215	0.4422	0.1119	0.0000	0.53	0.47
27	5.5504	2.4496	0.0565	0.5444	2.6492	0.0000	0.0165	2.3905	0.0095	0.0209	1.9505	0.3915	0.1131	0.0000	0.53	0.47
40	5.6118	2.3882	0.2776	0.5905	2.3048	0.0000	0.0327	2.2859	0.0033	0.0385	1.8952	0.3112	0.1010	0.0016	0.50	0.50
41	5.6549	2.3451	0.1553	0.5983	2.3844	0.0000	0.0389	2.3465	0.0070	0.0471	1.8853	0.3593	0.1072	0.0000	0.50	0.50
42	5.6340	2.3660	0.1401	0.5744	2.4432	0.0037	0.0402	2.3475	0.0119	0.0534	1.8702	0.3059	0.1091	0.0069	0.51	0.49
43	5.5274	2.4726	0.1006	0.5792	2.4806	0.0004	0.0396	2.4340	0.0099	0.0218	1.9029	0.3782	0.0994	0.0000	0.50	0.50
44	5.6933	2.3067	0.1520	0.5399	2.4291	0.0000	0.0378	2.4238	0.0073	0.0301	1.8650	0.4073	0.1043	0.0000	0.50	0.50

Spot	Si	^{IV}Al	^{VI}Al	Ti	Fe	Cr	Mn	Mg	Ca	Na	K	F	Cl	Zr	Fe#	Mg#
	Electron-microprobe analyses of biotite from Sample CA-05															
	Numbers of ions on the basis of 22 oxygen															
73	5.5611	2.4389	0.2531	0.5375	2.4815	0.0000	0.0275	2.3198	0.0008	0.0186	1.8479	0.3488	0.1175	0.0010	0.52	0.48
74	5.5788	2.4212	0.2653	0.5342	2.4922	0.0000	0.0315	2.2931	0.0041	0.0213	1.8253	0.3593	0.1215	0.0000	0.52	0.48
75	5.6006	2.3994	0.1856	0.5584	2.4988	0.0000	0.0187	2.3343	0.0051	0.0209	1.8744	0.3670	0.1182	0.0000	0.52	0.48
76	5.6280	2.3720	0.1715	0.5604	2.5231	0.0000	0.0295	2.3281	0.0000	0.0200	1.8346	0.4323	0.1255	0.0000	0.52	0.48

Spot	SiO_2	Al_2O_3	TiO_2	FeO	Cr_2O_3	MnO	MgO	CaO	Na_2O	K_2O	F	Cl	ZrO_2	BaO	P2O5	SrO	Total	Position
	Electron-microprobe analyses of feldspar from Sample CA-02																	
	Major element compositions (wt%)																	
A-27	64.667	19.162	0.000	0.015	0.015	0.007	0.000	0.052	0.817	14.379	0.000	0.020	0.000	0.515	0.029	0.000	99.678	Rim
A-28	64.057	19.158	0.000	0.013	0.047	0.004	0.000	0.078	0.966	14.469	0.000	0.000	0.000	0.444	0.008	0.000	99.244	Core
A-29	64.088	19.398	0.000	0.021	0.000	0.012	0.000	0.072	0.762	14.053	0.000	0.011	0.000	0.430	0.000	0.000	98.847	Core
A-30	64.777	19.004	0.000	0.049	0.027	0.000	0.001	0.162	1.030	13.487	0.082	0.012	0.000	0.539	0.000	0.000	99.170	Rim
A-31	60.283	23.843	0.026	0.043	0.014	0.000	0.000	5.965	7.993	0.261	0.000	0.011	0.000	0.005	0.026	0.000	98.470	Rim
A-32	60.179	24.223	0.013	0.081	0.007	0.027	0.000	5.889	7.756	0.269	0.000	0.000	0.068	0.011	0.000	0.000	98.523	Core
A-33	60.142	23.861	0.004	0.053	0.015	0.015	0.023	5.967	8.083	0.202	0.052	0.000	0.000	0.025	0.000	0.000	98.442	Core
A-34	59.983	24.450	0.000	0.052	0.023	0.017	0.000	6.426	7.870	0.220	0.023	0.006	0.000	0.000	0.000	0.000	99.070	Rim
B-53	64.641	18.066	0.000	0.000	0.000	0.025	0.022	0.080	0.830	15.579	0.000	0.001	0.000	0.405	0.000	0.000	99.649	Rim
B-54	63.954	18.100	0.000	0.006	0.010	0.000	0.000	0.028	0.787	15.588	0.016	0.006	0.000	0.532	0.000	0.000	99.027	Intermediary
B-55	64.662	18.842	0.000	0.000	0.024	0.027	0.000	0.052	0.932	14.541	0.030	0.034	0.018	0.515	0.011	0.000	99.688	Core
B-56	64.067	17.950	0.000	0.036	0.000	0.037	0.000	0.029	0.781	15.657	0.025	0.000	0.018	0.472	0.000	0.000	99.072	Core
B-16	60.444	24.802	0.009	0.105	0.003	0.004	0.000	5.822	7.948	0.146	0.000	0.006	0.000	0.058	0.000	0.000	99.347	Rim
B-17	60.943	24.470	0.017	0.254	0.010	0.009	0.025	2.775	7.580	2.176	0.000	0.001	0.000	0.000	0.000	0.000	98.260	Core
B-18	60.216	24.963	0.000	0.058	0.012	0.000	0.005	6.262	7.859	0.200	0.053	0.006	0.000	0.024	0.000	0.000	99.658	Core
B-19	60.309	24.945	0.000	0.071	0.000	0.005	0.000	5.052	8.491	0.219	0.000	0.002	0.000	0.022	0.000	0.000	99.116	Rim
B-57	61.337	24.160	0.003	0.022	0.000	0.000	0.000	5.343	8.315	0.218	0.000	0.007	0.000	0.001	0.000	0.000	99.406	Core
B-58	61.581	23.433	0.009	0.080	0.000	0.000	0.000	5.692	8.143	0.170	0.000	0.005	0.000	0.000	0.026	0.000	99.139	Intermediary
B-59	63.578	23.074	0.000	0.028	0.019	0.031	0.000	1.405	9.100	1.284	0.000	0.026	0.000	0.045	0.018	0.000	98.608	Intermediary
B-60	61.825	23.519	0.003	0.074	0.002	0.020	0.000	5.838	8.021	0.181	0.105	0.005	0.000	0.015	0.028	0.000	99.636	Rim

Spot	SiO_2	Al_2O_3	TiO_2	FeO	Cr_2O_3	MnO	MgO	CaO	Na_2O	K_2O	F	Cl	ZrO_2	BaO	P2O5	SrO	Total	Position
Electron-microprobe analyses of feldspar from Sample CA-02																		
Major element compositions (wt%)																		
B-61	61.319	24.114	0.000	0.060	0.000	0.009	0.000	5.218	8.431	0.233	0.000	0.000	0.000	0.001	0.000	0.000	99.385	Rim
B-62	61.687	24.097	0.002	0.026	0.000	0.000	0.000	4.987	8.588	0.166	0.000	0.009	0.017	0.004	0.000	0.000	99.583	Core
B-63	61.776	23.982	0.000	0.038	0.000	0.023	0.000	5.244	8.568	0.186	0.000	0.000	0.000	0.034	0.015	0.000	99.866	Rim
B-64	61.655	23.439	0.009	0.000	0.000	0.048	0.000	5.890	8.100	0.177	0.000	0.005	0.000	0.005	0.000	0.000	99.328	Rim
B-65	61.797	23.593	0.000	0.027	0.000	0.000	0.000	4.660	8.308	0.819	0.000	0.002	0.000	0.040	0.000	0.000	99.246	Rim
B-66	61.144	23.802	0.000	0.054	0.000	0.014	0.000	6.128	7.805	0.179	0.077	0.004	0.000	0.000	0.000	0.000	99.207	Core
B-67	60.187	24.291	0.001	0.105	0.001	0.005	0.000	6.523	7.816	0.156	0.052	0.008	0.000	0.005	0.000	0.000	99.150	Core
B-68	61.742	23.540	0.013	0.081	0.017	0.000	0.000	5.742	8.156	0.256	0.000	0.002	0.003	0.025	0.003	0.000	99.580	Intermediary
B-69	63.385	22.206	0.000	0.059	0.003	0.000	0.000	2.755	9.693	0.135	0.000	0.000	0.000	0.000	0.049	0.000	98.285	Rim

Spot	Si	Al	Ti	Fe	Cr	Mn	Mg	Ca	Na	K	F	Cl	Zr	Ba	P	Sr	An	Or	Ab
	Electron-microprobe analyses of feldspar from Sample CA-02																		
	Numbers of ions on the basis of 32 oxygen																		
A-27	11.9253	4.1644	0.0000	0.0023	0.0022	0.0011	0.0000	0.0103	0.2921	3.3824	0.0000	0.0063	0.0000	0.0372	0.0045	0.0000	0.28	91.79	7.93
A-28	11.8838	4.1886	0.0000	0.0020	0.0069	0.0006	0.0000	0.0155	0.3474	3.4240	0.0000	0.0000	0.0000	0.0323	0.0013	0.0000	0.41	90.42	9.17
A-29	11.8928	4.2422	0.0000	0.0033	0.0000	0.0019	0.0000	0.0143	0.2741	3.3265	0.0000	0.0035	0.0000	0.0313	0.0000	0.0000	0.40	92.02	7.58
A-30	11.9675	4.1377	0.0000	0.0076	0.0039	0.0000	0.0003	0.0321	0.3689	3.1784	0.0479	0.0038	0.0000	0.0390	0.0000	0.0000	0.90	88.80	10.31
A-31	10.8883	5.0752	0.0035	0.0065	0.0020	0.0000	0.0000	1.1542	2.7989	0.0601	0.0000	0.0034	0.0000	0.0004	0.0040	0.0000	28.76	1.50	69.74
A-32	10.8574	5.1504	0.0018	0.0122	0.0010	0.0041	0.0000	1.1383	2.7128	0.0619	0.0000	0.0000	0.0060	0.0008	0.0000	0.0000	29.09	1.58	69.33
A-33	10.8765	5.0854	0.0005	0.0080	0.0021	0.0023	0.0062	1.1561	2.8339	0.0466	0.0297	0.0000	0.0000	0.0018	0.0000	0.0000	28.64	1.15	70.21
A-34	10.7879	5.1823	0.0000	0.0078	0.0033	0.0026	0.0000	1.2381	2.7441	0.0505	0.0131	0.0018	0.0000	0.0000	0.0000	0.0000	30.70	1.25	68.05
B-53	12.0083	3.9552	0.0000	0.0000	0.0000	0.0039	0.0061	0.0159	0.2989	3.6917	0.0000	0.0003	0.0000	0.0295	0.0000	0.0000	0.40	92.14	7.46
B-54	11.9775	3.9949	0.0000	0.0009	0.0015	0.0000	0.0000	0.0056	0.2857	3.7239	0.0095	0.0019	0.0000	0.0390	0.0000	0.0000	0.14	92.74	7.12
B-55	11.9496	4.1036	0.0000	0.0000	0.0035	0.0042	0.0000	0.0103	0.3339	3.4277	0.0175	0.0106	0.0016	0.0373	0.0017	0.0000	0.27	90.87	8.85
B-56	11.9959	3.9609	0.0000	0.0056	0.0000	0.0059	0.0000	0.0058	0.2835	3.7395	0.0148	0.0000	0.0016	0.0346	0.0000	0.0000	0.14	92.82	7.04
B-16	10.8118	5.2283	0.0012	0.0157	0.0004	0.0006	0.0000	1.1157	2.7562	0.0333	0.0000	0.0018	0.0000	0.0041	0.0000	0.0000	28.57	0.85	70.58

Spot	Si	Al	Ti	Fe	Cr	Mn	Mg	Ca	Na	K	F	Cl	Zr	Ba	P	Sr	An	Or	Ab
	Electron-microprobe analyses of feldspar from Sample CA-02																		
	Numbers of ions on the basis of 32 oxygen																		
B-17	11.0089	5.2093	0.0023	0.0384	0.0014	0.0014	0.0067	0.5370	2.6546	0.5014	0.0000	0.0003	0.0000	0.0000	0.0000	0.0000	14.54	13.58	71.88
B-18	10.7592	5.2565	0.0000	0.0087	0.0017	0.0000	0.0013	1.1987	2.7223	0.0456	0.0299	0.0018	0.0000	0.0017	0.0000	0.0000	30.22	1.15	68.63
B-19	10.8075	5.2681	0.0000	0.0106	0.0000	0.0008	0.0000	0.9699	2.9499	0.0501	0.0000	0.0006	0.0000	0.0015	0.0000	0.0000	24.43	1.26	74.31
B-57	10.9451	5.0807	0.0004	0.0033	0.0000	0.0000	0.0000	1.0214	2.8765	0.0496	0.0000	0.0021	0.0000	0.0001	0.0000	0.0000	25.87	1.26	72.87
B-58	11.0199	4.9418	0.0012	0.0120	0.0000	0.0000	0.0000	1.0912	2.8250	0.0388	0.0000	0.0015	0.0000	0.0000	0.0039	0.0000	27.59	0.98	71.43
B-59	11.3521	4.8554	0.0000	0.0042	0.0027	0.0047	0.0000	0.2688	3.1501	0.2924	0.0000	0.0079	0.0000	0.0031	0.0027	0.0000	7.24	7.88	84.88
B-60	11.0204	4.9406	0.0004	0.0110	0.0003	0.0030	0.0000	1.1149	2.7719	0.0412	0.0592	0.0015	0.0000	0.0010	0.0042	0.0000	28.38	1.05	70.57
B-61	10.9477	5.0737	0.0000	0.0090	0.0000	0.0014	0.0000	0.9981	2.9182	0.0531	0.0000	0.0000	0.0000	0.0001	0.0000	0.0000	25.14	1.34	73.52
B-62	10.9795	5.0546	0.0003	0.0039	0.0000	0.0000	0.0000	0.9509	2.9634	0.0377	0.0000	0.0027	0.0015	0.0003	0.0000	0.0000	24.06	0.95	74.98
B-63	10.9772	5.0221	0.0000	0.0056	0.0000	0.0035	0.0000	0.9983	2.9516	0.0422	0.0000	0.0000	0.0000	0.0024	0.0023	0.0000	25.01	1.06	73.94
B-64	11.0175	4.9361	0.0012	0.0000	0.0000	0.0073	0.0000	1.1276	2.8061	0.0403	0.0000	0.0015	0.0000	0.0004	0.0000	0.0000	28.37	1.02	70.61
B-65	11.0533	4.9732	0.0000	0.0040	0.0000	0.0000	0.0000	0.8930	2.8809	0.1869	0.0000	0.0006	0.0000	0.0028	0.0000	0.0000	22.55	4.72	72.74
B-66	10.9512	5.0240	0.0000	0.0081	0.0000	0.0021	0.0000	1.1758	2.7101	0.0409	0.0436	0.0012	0.0000	0.0000	0.0000	0.0000	29.94	1.04	69.02
B-67	10.8156	5.1442	0.0001	0.0158	0.0001	0.0008	0.0000	1.2558	2.7229	0.0358	0.0295	0.0024	0.0000	0.0004	0.0000	0.0000	31.28	0.89	67.83
B-68	11.0104	4.9472	0.0017	0.0121	0.0024	0.0000	0.0000	1.0970	2.8197	0.0582	0.0000	0.0006	0.0003	0.0017	0.0005	0.0000	27.60	1.47	70.94
B-69	11.3558	4.6885	0.0000	0.0088	0.0004	0.0000	0.0000	0.5288	3.3667	0.0309	0.0000	0.0000	0.0000	0.0000	0.0074	0.0000	13.47	0.79	85.75

Spot	SiO_2	Al_2O_3	TiO_2	FeO	Cr_2O_3	MnO	MgO	CaO	Na_2O	K_2O	F	Cl	ZrO_2	BaO	P2O5	SrO	Total	Position
	Electron-microprobe analyses of feldspar from Sample CA-04																	
	Major element compositions (wt%)																	
14	64.992	18.692	0.000	0.007	0.027	0.016	0.001	0.113	1.831	13.420	0.109	0.005	0.000	0.277	0.012	0.000	99.502	Rim
15	64.019	19.554	0.000	0.041	0.000	0.000	0.002	0.115	1.520	14.181	0.070	0.011	0.026	0.274	0.022	0.000	99.835	Core
16	63.848	18.502	0.000	0.016	0.016	0.005	0.006	0.098	1.419	15.327	0.000	0.000	0.000	0.333	0.055	0.000	99.625	Core
17	64.523	19.325	0.000	0.070	0.011	0.014	0.000	0.158	1.479	14.073	0.011	0.003	0.000	0.338	0.000	0.000	100.005	Core
18	64.457	18.239	0.000	0.000	0.000	0.000	0.000	0.100	1.077	14.912	0.000	0.000	0.000	0.304	0.000	0.000	99.089	Rim
47	64.883	18.399	0.000	0.093	0.002	0.047	0.004	0.054	1.010	14.890	0.018	0.000	0.000	0.332	0.024	0.000	99.756	Rim
48	64.101	18.588	0.000	0.015	0.024	0.000	0.017	0.077	1.793	14.903	0.035	0.006	0.000	0.344	0.029	0.000	99.932	Core
49	64.121	18.248	0.000	0.016	0.019	0.000	0.008	0.043	0.903	15.176	0.070	0.005	0.000	0.245	0.000	0.000	98.854	Rim

Spot	SiO_2	Al_2O_3	TiO_2	FeO	Cr_2O_3	MnO	MgO	CaO	Na_2O	K_2O	F	Cl	ZrO_2	BaO	P2O5	SrO	Total	Position
Electron-microprobe analyses of feldspar from Sample CA-04																		
Major element compositions (wt%)																		
81	64.734	18.409	0.000	0.026	0.000	0.017	0.000	0.116	1.167	14.784	0.000	0.002	0.000	0.276	0.053	0.000	99.584	Rim
82	64.713	18.481	0.000	0.040	0.015	0.013	0.043	0.153	0.987	14.700	0.000	0.009	0.000	0.369	0.000	0.000	99.523	Rim
83	64.633	18.606	0.000	0.053	0.000	0.017	0.007	0.124	1.282	14.454	0.097	0.000	0.014	0.310	0.000	0.000	99.597	Core
114	64.637	18.460	0.000	0.033	0.000	0.008	0.000	0.118	1.301	14.602	0.000	0.001	0.000	0.362	0.045	0.000	99.567	Rim
115	64.416	18.477	0.000	0.000	0.040	0.000	0.000	0.112	1.148	14.993	0.104	0.001	0.000	0.267	0.066	0.000	99.624	Core
116	63.677	18.390	0.000	0.053	0.008	0.000	0.021	0.106	1.307	14.804	0.107	0.000	0.000	0.294	0.000	0.000	98.767	Rim
38	60.347	24.752	0.002	0.076	0.005	0.000	0.000	6.850	7.486	0.197	0.000	0.000	0.000	0.004	0.023	0.000	99.742	Rim
39	59.674	24.716	0.018	0.053	0.024	0.006	0.000	7.225	7.423	0.243	0.000	0.000	0.000	0.011	0.000	0.000	99.393	Core
40	59.967	24.721	0.000	0.041	0.011	0.000	0.000	7.281	7.294	0.230	0.000	0.008	0.000	0.002	0.000	0.000	99.555	Core
41	58.910	24.635	0.016	0.108	0.027	0.010	0.000	7.185	7.510	0.221	0.000	0.000	0.000	0.017	0.000	0.000	98.639	Rim
42	59.889	24.235	0.000	0.191	0.000	0.000	0.000	6.886	7.616	0.181	0.021	0.000	0.000	0.027	0.000	0.000	99.046	Rim
43	60.262	24.424	0.010	0.119	0.000	0.003	0.000	6.542	7.909	0.147	0.023	0.000	0.000	0.000	0.000	0.000	99.439	Rim
44	59.433	25.153	0.008	0.092	0.042	0.014	0.000	7.070	7.452	0.227	0.000	0.005	0.000	0.000	0.067	0.000	99.563	Core
45	60.073	24.860	0.004	0.115	0.000	0.000	0.000	7.017	7.497	0.215	0.074	0.002	0.000	0.004	0.005	0.000	99.866	Core
46	58.880	24.412	0.012	0.070	0.008	0.000	0.000	6.834	7.521	0.224	0.079	0.001	0.000	0.000	0.001	0.000	98.042	Rim
71	60.749	24.319	0.020	0.045	0.000	0.005	0.000	6.776	7.817	0.141	0.003	0.003	0.000	0.001	0.054	0.000	99.933	Rim
72	59.777	24.674	0.000	0.107	0.000	0.000	0.000	7.339	7.429	0.221	0.000	0.004	0.000	0.000	0.025	0.000	99.576	Core
73	59.490	24.642	0.000	0.033	0.003	0.013	0.000	7.246	7.345	0.245	0.000	0.006	0.000	0.001	0.021	0.000	99.045	Core
74	59.330	24.602	0.006	0.079	0.027	0.005	0.000	6.748	7.638	0.263	0.001	0.014	0.000	0.026	0.028	0.000	98.767	Core
75	60.395	24.285	0.014	0.053	0.000	0.014	0.000	6.463	7.964	0.143	0.000	0.020	0.000	0.020	0.000	0.000	99.371	Rim
76	59.746	24.874	0.004	0.058	0.000	0.000	0.000	7.329	7.318	0.218	0.000	0.003	0.000	0.002	0.000	0.000	99.552	Rim
77	59.379	25.199	0.010	0.087	0.061	0.005	0.000	7.972	6.971	0.246	0.000	0.006	0.000	0.000	0.012	0.000	99.948	Core
78	59.474	25.030	0.010	0.103	0.000	0.000	0.000	7.814	7.120	0.240	0.044	0.000	0.000	0.048	0.000	0.000	99.883	Core
79	58.794	24.943	0.000	0.089	0.058	0.015	0.000	7.450	7.153	0.225	0.000	0.000	0.075	0.012	0.051	0.000	98.865	Core
80	60.221	24.385	0.023	0.072	0.000	0.000	0.000	6.585	7.928	0.145	0.026	0.055	0.000	0.045	0.010	0.000	99.495	Rim
106	60.029	24.082	0.005	0.160	0.000	0.003	0.000	6.320	7.889	0.117	0.002	0.101	0.000	0.000	0.028	0.000	98.736	Core
107	60.398	24.595	0.007	0.051	0.013	0.000	0.000	6.791	7.623	0.238	0.000	0.061	0.000	0.006	0.043	0.000	99.826	Core
108	59.427	24.749	0.009	0.059	0.000	0.000	0.002	6.833	7.720	0.199	0.000	0.002	0.000	0.000	0.001	0.000	99.001	Rim
109	59.014	25.102	0.008	0.068	0.021	0.003	0.000	7.471	7.530	0.207	0.000	0.000	0.000	0.000	0.006	0.000	99.430	Rim
110	59.546	24.944	0.011	0.063	0.020	0.003	0.000	7.305	7.266	0.224	0.000	0.000	0.000	0.000	0.000	0.000	99.382	Core

Spot	SiO_2	Al_2O_3	TiO_2	FeO	Cr_2O_3	MnO	MgO	CaO	Na_2O	K_2O	F	Cl	ZrO_2	BaO	P2O5	SrO	Total	Position
Electron-microprobe analyses of feldspar from Sample CA-04																		
Major element compositions (wt%)																		
111	59.335	25.048	0.008	0.060	0.026	0.003	0.000	7.465	7.428	0.266	0.054	0.000	0.000	0.017	0.000	0.000	99.710	Core
112	59.749	24.890	0.026	0.094	0.000	0.000	0.000	7.297	7.313	0.266	0.000	0.000	0.000	0.000	0.013	0.000	99.648	Core
113	59.438	24.566	0.007	0.069	0.025	0.000	0.000	7.109	7.494	0.191	0.000	0.000	0.000	0.010	0.000	0.000	98.909	Rim

Spot	Si	Al	Ti	Fe	Cr	Mn	Mg	Ca	Na	K	F	Cl	Zr	Ba	P	Sr	An	Or	Ab
	Electron-microprobe analyses of feldspar from Sample CA-04																		
	Numbers of ions on the basis of 32 oxygen																		
14	11.9753	4.0590	0.0000	0.0011	0.0039	0.0025	0.0003	0.0223	0.6541	3.1542	0.0635	0.0016	0.0000	0.0200	0.0019	0.0000	0.58	82.34	17.07
15	11.8101	4.2512	0.0000	0.0063	0.0000	0.0000	0.0006	0.0227	0.5436	3.3370	0.0408	0.0034	0.0023	0.0198	0.0034	0.0000	0.58	85.49	13.93
16	11.8821	4.0578	0.0000	0.0025	0.0024	0.0008	0.0017	0.0195	0.5120	3.6384	0.0000	0.0000	0.0000	0.0243	0.0087	0.0000	0.47	87.25	12.28
17	11.8661	4.1884	0.0000	0.0108	0.0016	0.0022	0.0000	0.0311	0.5273	3.3013	0.0064	0.0009	0.0000	0.0244	0.0000	0.0000	0.81	85.53	13.66
18	11.9964	4.0005	0.0000	0.0000	0.0000	0.0000	0.0000	0.0199	0.3886	3.5402	0.0000	0.0000	0.0000	0.0222	0.0000	0.0000	0.50	89.65	9.84
47	11.9924	4.0077	0.0000	0.0144	0.0003	0.0074	0.0011	0.0107	0.3619	3.5106	0.0105	0.0000	0.0000	0.0240	0.0038	0.0000	0.28	90.40	9.32
48	11.8809	4.0602	0.0000	0.0023	0.0035	0.0000	0.0047	0.0153	0.6443	3.5235	0.0205	0.0019	0.0000	0.0250	0.0046	0.0000	0.37	84.23	15.40
49	11.9821	4.0186	0.0000	0.0025	0.0028	0.0000	0.0022	0.0086	0.3271	3.6174	0.0414	0.0016	0.0000	0.0179	0.0000	0.0000	0.22	91.51	8.28
81	11.9773	4.0141	0.0000	0.0040	0.0000	0.0027	0.0000	0.0230	0.4186	3.4892	0.0000	0.0006	0.0000	0.0200	0.0083	0.0000	0.58	88.77	10.65
82	11.9795	4.0318	0.0000	0.0062	0.0022	0.0020	0.0119	0.0303	0.3542	3.4712	0.0000	0.0028	0.0000	0.0268	0.0000	0.0000	0.79	90.03	9.19
83	11.9583	4.0569	0.0000	0.0082	0.0000	0.0027	0.0019	0.0246	0.4598	3.4112	0.0567	0.0000	0.0013	0.0225	0.0000	0.0000	0.63	87.57	11.80
114	11.9644	4.0269	0.0000	0.0051	0.0000	0.0013	0.0000	0.0234	0.4669	3.4477	0.0000	0.0003	0.0000	0.0263	0.0071	0.0000	0.59	87.55	11.86
115	11.9440	4.0375	0.0000	0.0000	0.0059	0.0000	0.0000	0.0222	0.4127	3.5461	0.0610	0.0003	0.0000	0.0194	0.0104	0.0000	0.56	89.08	10.37
116	11.9241	4.0584	0.0000	0.0083	0.0012	0.0000	0.0059	0.0213	0.4745	3.5362	0.0634	0.0000	0.0000	0.0216	0.0000	0.0000	0.53	87.70	11.77
38	10.7707	5.2063	0.0003	0.0113	0.0007	0.0000	0.0000	1.3098	2.5903	0.0448	0.0000	0.0000	0.0000	0.0003	0.0035	0.0000	33.20	1.14	65.66
39	10.7135	5.2294	0.0024	0.0080	0.0034	0.0009	0.0000	1.3896	2.5836	0.0556	0.0000	0.0000	0.0000	0.0008	0.0000	0.0000	34.49	1.38	64.13
40	10.7383	5.2170	0.0000	0.0061	0.0016	0.0000	0.0000	1.3968	2.5322	0.0525	0.0000	0.0024	0.0000	0.0001	0.0000	0.0000	35.08	1.32	63.60
41	10.6716	5.2592	0.0022	0.0164	0.0039	0.0015	0.0000	1.3944	2.6375	0.0511	0.0000	0.0000	0.0000	0.0012	0.0000	0.0000	34.15	1.25	64.60
42	10.7869	5.1442	0.0000	0.0288	0.0000	0.0000	0.0000	1.3287	2.6594	0.0416	0.0120	0.0000	0.0000	0.0019	0.0000	0.0000	32.97	1.03	65.99
43	10.7981	5.1576	0.0013	0.0178	0.0000	0.0005	0.0000	1.2558	2.7475	0.0336	0.0130	0.0000	0.0000	0.0000	0.0000	0.0000	31.11	0.83	68.06
44	10.6508	5.3122	0.0011	0.0138	0.0060	0.0021	0.0000	1.3574	2.5890	0.0519	0.0000	0.0015	0.0000	0.0000	0.0102	0.0000	33.95	1.30	64.75

Spot	Si	Al	Ti	Fe	Cr	Mn	Mg	Ca	Na	K	F	Cl	Zr	Ba	P	Sr	An	Or	Ab
	Electron-microprobe analyses of feldspar from Sample CA-04																		
	Numbers of ions on the basis of 32 oxygen																		
45	10.7316	5.2338	0.0005	0.0172	0.0000	0.0000	0.0000	1.3429	2.5965	0.0490	0.0418	0.0006	0.0000	0.0003	0.0008	0.0000	33.67	1.23	65.10
46	10.7202	5.2381	0.0016	0.0107	0.0012	0.0000	0.0000	1.3330	2.6547	0.0520	0.0455	0.0003	0.0000	0.0000	0.0002	0.0000	33.00	1.29	65.72
71	10.8238	5.1064	0.0027	0.0067	0.0000	0.0008	0.0000	1.2934	2.7002	0.0320	0.0017	0.0009	0.0000	0.0001	0.0081	0.0000	32.13	0.80	67.07
72	10.7152	5.2124	0.0000	0.0160	0.0000	0.0000	0.0000	1.4094	2.5817	0.0505	0.0000	0.0012	0.0000	0.0000	0.0038	0.0000	34.87	1.25	63.88
73	10.7149	5.2306	0.0000	0.0050	0.0004	0.0020	0.0000	1.3982	2.5647	0.0563	0.0000	0.0018	0.0000	0.0001	0.0032	0.0000	34.79	1.40	63.81
74	10.7183	5.2379	0.0008	0.0119	0.0039	0.0008	0.0000	1.3060	2.6751	0.0606	0.0006	0.0043	0.0000	0.0018	0.0043	0.0000	32.31	1.50	66.19
75	10.8247	5.1296	0.0019	0.0079	0.0000	0.0021	0.0000	1.2410	2.7673	0.0327	0.0000	0.0061	0.0000	0.0014	0.0000	0.0000	30.71	0.81	68.48
76	10.7046	5.2522	0.0005	0.0087	0.0000	0.0000	0.0000	1.4068	2.5419	0.0498	0.0000	0.0009	0.0000	0.0001	0.0000	0.0000	35.18	1.25	63.57
77	10.6183	5.3105	0.0013	0.0130	0.0086	0.0008	0.0000	1.5273	2.4167	0.0561	0.0000	0.0018	0.0000	0.0000	0.0018	0.0000	38.18	1.40	60.42
78	10.6476	5.2810	0.0013	0.0154	0.0000	0.0000	0.0000	1.4987	2.4712	0.0548	0.0249	0.0000	0.0000	0.0034	0.0000	0.0000	37.24	1.36	61.40
79	10.6245	5.3120	0.0000	0.0135	0.0083	0.0023	0.0000	1.4423	2.5060	0.0519	0.0000	0.0000	0.0066	0.0008	0.0078	0.0000	36.06	1.30	62.65
80	10.7951	5.1515	0.0031	0.0108	0.0000	0.0000	0.0000	1.2646	2.7552	0.0332	0.0147	0.0167	0.0000	0.0032	0.0015	0.0000	31.20	0.82	67.98
106	10.8328	5.1216	0.0007	0.0241	0.0000	0.0005	0.0000	1.2219	2.7600	0.0269	0.0011	0.0309	0.0000	0.0000	0.0043	0.0000	30.48	0.67	68.85
107	10.7822	5.1744	0.0009	0.0076	0.0018	0.0000	0.0000	1.2988	2.6383	0.0542	0.0000	0.0185	0.0000	0.0004	0.0065	0.0000	32.54	1.36	66.10
108	10.7074	5.2552	0.0012	0.0089	0.0000	0.0000	0.0005	1.3190	2.6967	0.0457	0.0000	0.0006	0.0000	0.0000	0.0002	0.0000	32.48	1.13	66.40
109	10.6125	5.3199	0.0011	0.0102	0.0030	0.0005	0.0000	1.4393	2.6252	0.0475	0.0000	0.0000	0.0000	0.0000	0.0009	0.0000	35.00	1.15	63.84
110	10.6872	5.2760	0.0015	0.0095	0.0028	0.0005	0.0000	1.4046	2.5282	0.0513	0.0000	0.0000	0.0000	0.0000	0.0000	0.0000	35.26	1.29	63.46
111	10.6420	5.2944	0.0011	0.0090	0.0037	0.0005	0.0000	1.4344	2.5828	0.0609	0.0306	0.0000	0.0000	0.0012	0.0000	0.0000	35.17	1.49	63.33
112	10.6982	5.2521	0.0035	0.0141	0.0000	0.0000	0.0000	1.3997	2.5385	0.0608	0.0000	0.0000	0.0000	0.0000	0.0020	0.0000	35.00	1.52	63.48
113	10.7212	5.2221	0.0009	0.0104	0.0036	0.0000	0.0000	1.3738	2.6206	0.0439	0.0000	0.0000	0.0000	0.0007	0.0000	0.0000	34.02	1.09	64.89

spot	SiO_2	Al_2O_3	TiO_2	FeO	Cr_2O_3	MnO	MgO	CaO	Na_2O	K_2O	F	Cl	ZrO_2	BaO	P2O5	SrO	Total	Position
	Electron-microprobe analyses of feldspar from Sample CA-05																	
	Major element compositions (wt%)																	
47	64.551	18.268	0.000	0.000	0.021	0.005	0.008	0.068	0.720	15.548	0.050	0.000	0.000	0.160	0.058	0.000	99.457	Rim
48	64.236	18.185	0.000	0.042	0.000	0.057	0.008	0.035	0.712	15.555	0.000	0.001	0.000	0.082	0.000	0.000	98.913	Core
49	64.913	18.225	0.000	0.065	0.007	0.000	0.012	0.089	0.707	15.717	0.044	0.000	0.000	0.155	0.000	0.000	99.934	Rim
50	64.173	18.262	0.000	0.029	0.011	0.000	0.000	0.065	0.727	15.832	0.029	0.000	0.000	0.146	0.028	0.000	99.302	Rim

spot	SiO_2	Al_2O_3	TiO_2	FeO	Cr_2O_3	MnO	MgO	CaO	Na_2O	K_2O	F	Cl	ZrO_2	BaO	P2O5	SrO	Total	Position
Electron-microprobe analyses of feldspar from Sample CA-05																		
Major element compositions (wt%)																		
61	64.475	18.025	0.000	0.013	0.026	0.000	0.007	0.063	0.586	15.665	0.004	0.003	0.000	0.196	0.053	0.000	99.116	Core
62	64.877	18.238	0.000	0.036	0.000	0.005	0.000	0.088	0.588	15.620	0.000	0.003	0.000	0.194	0.000	0.000	99.649	Rim
63	64.717	18.215	0.000	0.022	0.039	0.000	0.003	0.052	0.550	15.618	0.135	0.000	0.000	0.159	0.043	0.000	99.553	Rim
64	63.980	18.176	0.000	0.032	0.015	0.000	0.001	0.084	0.664	15.551	0.000	0.002	0.000	0.172	0.027	0.000	98.704	Rim
21	57.813	26.103	0.007	0.078	0.059	0.000	0.008	8.847	6.347	0.437	0.000	0.004	0.000	0.000	0.000	0.000	99.703	Rim
22	57.409	26.244	0.008	0.104	0.007	0.042	0.004	9.053	6.259	0.488	0.000	0.004	0.000	0.009	0.011	0.000	99.642	Core
23	57.135	26.191	0.012	0.135	0.008	0.000	0.002	9.476	6.068	0.468	0.000	0.003	0.000	0.004	0.000	0.000	99.502	Core
24	57.564	25.980	0.010	0.079	0.000	0.018	0.000	8.488	6.422	0.446	0.028	0.007	0.000	0.020	0.007	0.000	99.069	Rim
51	58.135	25.953	0.001	0.052	0.000	0.000	0.000	8.590	6.639	0.378	0.000	0.001	0.000	0.030	0.019	0.000	99.798	Rim
52	57.703	25.817	0.000	0.144	0.030	0.018	0.000	8.702	6.502	0.444	0.094	0.000	0.000	0.000	0.009	0.000	99.463	Core
53	54.763	27.495	0.000	0.081	0.000	0.007	0.000	11.032	5.364	0.240	0.000	0.000	0.000	0.000	0.000	0.000	98.982	Core
54	54.871	27.488	0.019	0.136	0.000	0.007	0.000	10.711	5.458	0.243	0.019	0.002	0.000	0.000	0.000	0.000	98.954	Core
55	57.716	26.017	0.000	0.077	0.008	0.000	0.000	8.724	6.724	0.328	0.000	0.000	0.000	0.014	0.000	0.000	99.608	Rim
56	58.959	25.007	0.013	0.313	0.000	0.000	0.096	6.331	7.053	0.742	0.065	0.005	0.000	0.034	0.000	0.000	98.618	Rim
57	59.186	26.241	0.008	0.115	0.037	0.022	0.000	7.238	6.300	0.755	0.038	0.026	0.000	0.000	0.000	0.000	99.966	Intermediary
58	58.043	25.467	0.000	0.167	0.052	0.060	0.000	8.945	6.235	0.526	0.017	0.002	0.000	0.000	0.000	0.000	99.514	Core
59	58.637	25.717	0.018	0.145	0.000	0.004	0.000	8.290	6.591	0.477	0.000	0.005	0.000	0.017	0.000	0.000	99.901	Core
60	58.353	25.616	0.000	0.111	0.000	0.006	0.000	8.313	6.531	0.524	0.001	0.000	0.000	0.000	0.023	0.000	99.478	Core

Spot	Si	Al	Ti	Fe	Cr	Mn	Mg	Ca	Na	K	F	Cl	Zr	Ba	P	Sr	An	Or	Ab
	Electron-microprobe analyses of feldspar from Sample CA-05																		
	Numbers of ions on the basis of 32 oxygen																		
47	11.9880	3.9982	0.0000	0.0000	0.0031	0.0008	0.0022	0.0135	0.2592	3.6832	0.0294	0.0000	0.0000	0.0116	0.0091	0.0000	0.34	93.11	6.55
48	11.9931	4.0013	0.0000	0.0066	0.0000	0.0090	0.0022	0.0070	0.2577	3.7045	0.0000	0.0003	0.0000	0.0060	0.0000	0.0000	0.18	93.33	6.49
49	12.0078	3.9731	0.0000	0.0101	0.0010	0.0000	0.0033	0.0176	0.2535	3.7086	0.0257	0.0000	0.0000	0.0112	0.0000	0.0000	0.44	93.19	6.37
50	11.9632	4.0121	0.0000	0.0045	0.0016	0.0000	0.0000	0.0130	0.2627	3.7648	0.0171	0.0000	0.0000	0.0107	0.0044	0.0000	0.32	93.18	6.50
61	12.0176	3.9594	0.0000	0.0020	0.0038	0.0000	0.0019	0.0126	0.2118	3.7245	0.0024	0.0009	0.0000	0.0143	0.0084	0.0000	0.32	94.32	5.36
62	12.0190	3.9819	0.0000	0.0056	0.0000	0.0008	0.0000	0.0175	0.2112	3.6912	0.0000	0.0009	0.0000	0.0141	0.0000	0.0000	0.45	94.17	5.39

Spot	Si	Al	Ti	Fe	Cr	Mn	Mg	Ca	Na	K	F	Cl	Zr	Ba	P	Sr	An	Or	Ab
	Electron-microprobe analyses of feldspar from Sample CA-05																		
	Numbers of ions on the basis of 32 oxygen																		
63	12.0120	3.9843	0.0000	0.0034	0.0057	0.0000	0.0008	0.0103	0.1979	3.6977	0.0792	0.0000	0.0000	0.0116	0.0068	0.0000	0.26	94.67	5.07
64	11.9789	4.0105	0.0000	0.0050	0.0022	0.0000	0.0003	0.0168	0.2410	3.7140	0.0000	0.0006	0.0000	0.0126	0.0043	0.0000	0.42	93.51	6.07
21	10.4029	5.5354	0.0009	0.0117	0.0084	0.0000	0.0021	1.7055	2.2141	0.1003	0.0000	0.0012	0.0000	0.0000	0.0000	0.0000	42.43	2.50	55.08
22	10.3519	5.5770	0.0011	0.0157	0.0010	0.0064	0.0011	1.7489	2.1880	0.1122	0.0000	0.0012	0.0000	0.0006	0.0017	0.0000	43.19	2.77	54.04
23	10.3268	5.5789	0.0016	0.0204	0.0011	0.0000	0.0005	1.8349	2.1263	0.1079	0.0000	0.0009	0.0000	0.0003	0.0000	0.0000	45.09	2.65	52.25
24	10.4202	5.5424	0.0014	0.0120	0.0000	0.0028	0.0000	1.6461	2.2537	0.1030	0.0160	0.0021	0.0000	0.0014	0.0011	0.0000	41.12	2.57	56.30
51	10.4439	5.4947	0.0001	0.0078	0.0000	0.0000	0.0000	1.6533	2.3123	0.0866	0.0000	0.0003	0.0000	0.0021	0.0029	0.0000	40.80	2.14	57.06
52	10.4238	5.4962	0.0000	0.0218	0.0043	0.0028	0.0000	1.6841	2.2771	0.1023	0.0537	0.0000	0.0000	0.0000	0.0014	0.0000	41.44	2.52	56.04
53	9.9924	5.9124	0.0000	0.0124	0.0000	0.0011	0.0000	2.1565	1.8975	0.0559	0.0000	0.0000	0.0000	0.0000	0.0000	0.0000	52.47	1.36	46.17
54	10.0105	5.9100	0.0026	0.0207	0.0000	0.0011	0.0000	2.0935	1.9304	0.0565	0.0110	0.0006	0.0000	0.0000	0.0000	0.0000	51.30	1.39	47.31
55	10.4007	5.5253	0.0000	0.0116	0.0011	0.0000	0.0000	1.6842	2.3491	0.0754	0.0000	0.0000	0.0000	0.0010	0.0000	0.0000	40.99	1.84	57.17
56	10.6801	5.3385	0.0018	0.0474	0.0000	0.0000	0.0259	1.2286	2.4769	0.1715	0.0372	0.0015	0.0000	0.0024	0.0000	0.0000	31.69	4.42	63.89
57	10.5646	5.5201	0.0011	0.0172	0.0052	0.0033	0.0000	1.3841	2.1801	0.1719	0.0214	0.0079	0.0000	0.0000	0.0000	0.0000	37.05	4.60	58.35
58	10.4747	5.4163	0.0000	0.0252	0.0074	0.0092	0.0000	1.7294	2.1814	0.1211	0.0097	0.0006	0.0000	0.0000	0.0000	0.0000	42.89	3.00	54.10
59	10.5138	5.4343	0.0024	0.0217	0.0000	0.0006	0.0000	1.5924	2.2911	0.1091	0.0000	0.0015	0.0000	0.0012	0.0000	0.0000	39.88	2.73	57.38
60	10.5078	5.4361	0.0000	0.0167	0.0000	0.0009	0.0000	1.6037	2.2800	0.1204	0.0006	0.0000	0.0000	0.0000	0.0035	0.0000	40.05	3.01	56.94

Spot	SiO_2	Al_2O_3	TiO_2	FeO	Cr_2O_3	MnO	MgO	CaO	Na_2O	K_2O	F	Cl	ZrO_2	BaO	P2O5	SrO	Total	Position
	Electron-microprobe analyses of titanite from Sample CA-02																	
	Major element compositions (wt%)																	
A-6	30.899	3.972	32.481	1.879	0.000	0.188	0.000	28.867	0.057	0.018	1.284	0.005	0.000	0.000	0.006	0.000	99.656	Rim
A-7	30.600	3.649	32.586	1.944	0.000	0.163	0.023	29.110	0.041	0.001	1.364	0.000	0.000	0.000	0.053	0.000	99.534	Core
A-8	30.300	3.439	32.034	1.931	0.000	0.245	0.007	29.487	0.069	0.003	0.985	0.000	0.000	0.000	0.029	0.000	98.529	Core
A-9	30.751	3.620	32.387	2.134	0.000	0.172	0.003	28.302	0.024	0.005	1.086	0.000	0.000	0.000	0.000	0.000	98.484	Rim
A-13	29.621	3.499	32.736	2.002	0.019	0.142	0.000	29.958	0.048	0.000	0.952	0.007	0.000	0.000	0.035	0.000	99.019	Core
A-14	30.604	3.396	32.957	2.081	0.000	0.158	0.051	29.171	0.069	0.014	1.109	0.007	0.000	0.000	0.000	0.000	99.617	Core
A-15	30.436	3.686	32.035	2.983	0.005	0.126	0.005	29.883	0.069	0.016	1.136	0.001	0.000	0.000	0.039	0.000	100.420	Core
A-23	30.551	3.639	31.971	2.155	0.000	0.220	0.053	29.525	0.103	0.014	1.083	0.000	0.000	0.000	0.007	0.000	99.321	Rim

A-24	30.585	3.544	32.222	2.934	0.000	0.196	0.000	29.076	0.088	0.006	1.110	0.004	0.000	0.000	0.000	0.000	99.765	Core
A-25	30.778	3.699	31.969	1.997	0.031	0.222	0.025	29.656	0.069	0.005	1.316	0.000	0.000	0.000	0.000	0.000	99.767	Core
A-26	30.889	4.030	32.630	1.846	0.037	0.154	0.000	29.108	0.072	0.012	1.217	0.000	0.000	0.000	0.000	0.000	99.995	Rim
B-74	30.973	3.504	32.203	1.981	0.000	0.169	0.012	29.989	0.052	0.006	1.393	0.010	0.000	0.000	0.007	0.000	100.299	Rim
B-75	30.956	3.708	32.817	2.041	0.000	0.178	0.000	29.314	0.085	0.011	1.407	0.007	0.000	0.000	0.010	0.000	100.534	Core
B-76	31.061	3.578	31.790	1.980	0.006	0.218	0.011	28.961	0.100	0.013	0.977	0.010	0.024	0.000	0.000	0.000	98.729	Core
B-77	31.133	3.796	31.371	2.007	0.000	0.188	0.000	28.765	0.078	0.005	1.196	0.002	0.000	0.000	0.000	0.000	98.541	Rim

Spot	**Si**	**Al**	**Ti**	**Fe**	**Cr**	**Mn**	**Mg**	**Ca**	**Na**	**K**	**F**	**Cl**	**Zr**	**Ba**	**P**	**Sr**
	Electron-microprobe analyses of titanite from Sample CA-02															
	Numbers of ions on the basis of 4 silicon															
A-6	4.0000	0.6060	3.1629	0.2034	0.0000	0.0206	0.0000	4.0035	0.0143	0.0030	0.5256	0.0011	0.0000	0.0000	0.0007	0.0000
A-7	4.0000	0.5621	3.2042	0.2125	0.0000	0.0180	0.0045	4.0766	0.0104	0.0002	0.5638	0.0000	0.0000	0.0000	0.0059	0.0000
A-8	4.0000	0.5350	3.1811	0.2132	0.0000	0.0274	0.0014	4.1703	0.0177	0.0005	0.4112	0.0000	0.0000	0.0000	0.0032	0.0000
A-9	4.0000	0.5549	3.1690	0.2321	0.0000	0.0189	0.0006	3.9440	0.0061	0.0008	0.4467	0.0000	0.0000	0.0000	0.0000	0.0000
A-13	4.0000	0.5568	3.3253	0.2261	0.0020	0.0162	0.0000	4.3341	0.0126	0.0000	0.4065	0.0016	0.0000	0.0000	0.0040	0.0000
A-14	4.0000	0.5231	3.2402	0.2275	0.0000	0.0175	0.0099	4.0847	0.0175	0.0023	0.4583	0.0016	0.0000	0.0000	0.0000	0.0000
A-15	4.0000	0.5709	3.1670	0.3279	0.0005	0.0140	0.0010	4.2074	0.0176	0.0027	0.4721	0.0002	0.0000	0.0000	0.0043	0.0000
A-23	4.0000	0.5615	3.1487	0.2360	0.0000	0.0244	0.0103	4.1414	0.0261	0.0023	0.4484	0.0000	0.0000	0.0000	0.0008	0.0000
A-24	4.0000	0.5462	3.1699	0.3209	0.0000	0.0217	0.0000	4.0739	0.0223	0.0010	0.4590	0.0009	0.0000	0.0000	0.0000	0.0000
A-25	4.0000	0.5665	3.1253	0.2171	0.0032	0.0244	0.0048	4.1291	0.0174	0.0008	0.5408	0.0000	0.0000	0.0000	0.0000	0.0000
A-26	4.0000	0.6150	3.1785	0.1999	0.0038	0.0169	0.0000	4.0382	0.0181	0.0020	0.4983	0.0000	0.0000	0.0000	0.0000	0.0000
B-74	4.0000	0.5333	3.1284	0.2140	0.0000	0.0185	0.0023	4.1492	0.0130	0.0010	0.5689	0.0022	0.0000	0.0000	0.0008	0.0000
B-75	4.0000	0.5647	3.1898	0.2206	0.0000	0.0195	0.0000	4.0580	0.0213	0.0018	0.5749	0.0015	0.0000	0.0000	0.0011	0.0000
B-76	4.0000	0.5430	3.0795	0.2132	0.0006	0.0238	0.0021	3.9956	0.0250	0.0021	0.3978	0.0022	0.0015	0.0000	0.0000	0.0000
B-77	4.0000	0.5748	3.0319	0.2157	0.0000	0.0205	0.0000	3.9594	0.0194	0.0008	0.4859	0.0004	0.0000	0.0000	0.0000	0.0000

Spot	SiO_2	Al_2O_3	TiO_2	FeO	Cr_2O_3	MnO	MgO	CaO	Na_2O	K_2O	F	Cl	ZrO_2	BaO	P2O5	SrO	Total	Position
Electron-microprobe analyses of rutile from Sample CA-04																		
Major element compositions (wt%)																		
1	0.108	0.000	99.117	0.593	0.027	0.000	0.015	0.023	0.005	0.044	0.000	0.000	0.000	0.000	0.000	0.000	99.932	Core
2	0.090	0.000	99.304	0.419	0.002	0.000	0.008	0.024	0.000	0.007	0.000	0.000	0.000	0.000	0.037	0.028	99.919	Core
3	0.576	0.000	94.435	4.064	0.000	0.161	0.116	0.197	0.093	0.042	0.000	0.007	0.010	0.000	0.034	0.000	99.735	Core
4	0.059	0.000	99.031	0.465	0.007	0.000	0.000	0.015	0.027	0.015	0.082	0.000	0.000	0.000	0.000	0.000	99.701	Core
5	0.070	0.000	98.991	0.574	0.000	0.020	0.000	0.041	0.086	0.017	0.013	0.006	0.000	0.000	0.000	0.000	99.818	Core
27	0.044	0.000	99.243	0.386	0.000	0.000	0.000	0.026	0.000	0.017	0.198	0.001	0.000	0.000	0.003	0.000	99.918	Core
28	0.072	0.000	98.384	0.364	0.000	0.000	0.000	0.053	0.013	0.012	0.000	0.001	0.000	0.000	0.047	0.000	98.946	Core
29	0.044	0.000	98.530	0.416	0.014	0.000	0.000	0.024	0.035	0.015	0.082	0.000	0.000	0.000	0.059	0.000	99.219	Core
30	0.033	0.000	98.290	0.406	0.003	0.026	0.030	0.022	0.023	0.092	0.000	0.004	0.000	0.000	0.000	0.000	98.929	Rim
31	0.105	0.000	98.986	0.366	0.074	0.000	0.000	0.038	0.031	0.077	0.000	0.000	0.000	0.000	0.024	0.011	99.712	Core
65	0.038	0.000	97.888	0.339	0.039	0.000	0.000	0.039	0.015	0.005	0.017	0.006	0.000	0.000	0.022	0.000	98.408	Rim
66	0.051	0.000	98.026	0.282	0.000	0.006	0.000	0.066	0.000	0.007	0.000	0.000	0.000	0.000	0.038	0.012	98.488	Core
67	0.031	0.000	98.562	0.280	0.000	0.011	0.016	0.166	0.014	0.003	0.000	0.000	0.000	0.000	0.019	0.025	99.127	Rim
92	0.183	0.000	98.667	0.474	0.000	0.028	0.012	0.025	0.014	0.046	0.070	0.000	0.000	0.000	0.000	0.000	99.519	Core
93	0.080	0.000	98.309	0.457	0.012	0.000	0.013	0.062	0.045	0.022	0.000	0.007	0.000	0.000	0.000	0.000	99.007	Core
94	0.079	0.000	99.033	0.408	0.035	0.000	0.000	0.059	0.000	0.018	0.117	0.008	0.076	0.000	0.033	0.000	99.866	Core
123	0.114	0.000	97.597	0.808	0.021	0.000	0.000	0.027	0.008	0.179	0.000	0.000	0.000	0.000	0.000	0.096	98.850	Core
124	0.096	0.000	97.913	0.642	0.013	0.029	0.000	0.050	0.016	0.200	0.000	0.001	0.000	0.000	0.000	0.057	99.017	Core
125	0.085	0.000	98.383	0.396	0.000	0.000	0.000	0.073	0.006	0.203	0.012	0.000	0.040	0.000	0.000	0.066	99.264	Core

Spot	Si	Al	Ti	Fe	Cr	Mn	Mg	Ca	Na	K	F	Cl	Zr	Ba	P	Sr
	Electron-microprobe analyses of rutile from Sample CA-04															
	Numbers of ions on the basis of 2 oxygen															
1	0.0014	0.0000	0.9945	0.0066	0.0003	0.0000	0.0003	0.0003	0.0001	0.0007	0.0000	0.0000	0.0000	0.0000	0.0000	0.0000
2	0.0012	0.0000	0.9955	0.0047	0.0000	0.0000	0.0002	0.0003	0.0000	0.0001	0.0000	0.0000	0.0000	0.0000	0.0004	0.0002
3	0.0078	0.0000	0.9642	0.0461	0.0000	0.0019	0.0023	0.0029	0.0024	0.0007	0.0000	0.0002	0.0001	0.0000	0.0004	0.0000
4	0.0008	0.0000	0.9962	0.0052	0.0001	0.0000	0.0000	0.0002	0.0007	0.0003	0.0035	0.0000	0.0000	0.0000	0.0000	0.0000
5	0.0009	0.0000	0.9948	0.0064	0.0000	0.0002	0.0000	0.0006	0.0022	0.0003	0.0005	0.0001	0.0000	0.0000	0.0000	0.0000

Spot	Si	Al	Ti	Fe	Cr	Mn	Mg	Ca	Na	K	F	Cl	Zr	Ba	P	Sr
	Electron-microprobe analyses of rutile from Sample CA-04															
	Numbers of ions on the basis of 2 oxygen															
27	0.0006	0.0000	0.9970	0.0043	0.0000	0.0000	0.0000	0.0004	0.0000	0.0003	0.0084	0.0000	0.0000	0.0000	0.0000	0.0000
28	0.0010	0.0000	0.9958	0.0041	0.0000	0.0000	0.0000	0.0008	0.0003	0.0002	0.0000	0.0000	0.0000	0.0000	0.0005	0.0000
29	0.0006	0.0000	0.9957	0.0047	0.0001	0.0000	0.0000	0.0003	0.0009	0.0003	0.0035	0.0000	0.0000	0.0000	0.0007	0.0000
30	0.0004	0.0000	0.9961	0.0046	0.0000	0.0003	0.0006	0.0003	0.0006	0.0016	0.0000	0.0001	0.0000	0.0000	0.0000	0.0000
31	0.0014	0.0000	0.9948	0.0041	0.0008	0.0000	0.0000	0.0005	0.0008	0.0013	0.0000	0.0000	0.0000	0.0000	0.0003	0.0001
65	0.0005	0.0000	0.9965	0.0038	0.0004	0.0000	0.0000	0.0006	0.0004	0.0001	0.0007	0.0001	0.0000	0.0000	0.0003	0.0000
66	0.0007	0.0000	0.9966	0.0032	0.0000	0.0001	0.0000	0.0010	0.0000	0.0001	0.0000	0.0000	0.0000	0.0000	0.0004	0.0001
67	0.0004	0.0000	0.9961	0.0031	0.0000	0.0001	0.0003	0.0024	0.0004	0.0001	0.0000	0.0000	0.0000	0.0000	0.0002	0.0002
92	0.0025	0.0000	0.9941	0.0053	0.0000	0.0003	0.0002	0.0004	0.0004	0.0008	0.0030	0.0000	0.0000	0.0000	0.0000	0.0000
93	0.0011	0.0000	0.9953	0.0051	0.0001	0.0000	0.0003	0.0009	0.0012	0.0004	0.0000	0.0002	0.0000	0.0000	0.0000	0.0000
94	0.0011	0.0000	0.9949	0.0046	0.0004	0.0000	0.0000	0.0008	0.0000	0.0003	0.0049	0.0002	0.0005	0.0000	0.0004	0.0000
123	0.0015	0.0000	0.9923	0.0091	0.0002	0.0000	0.0000	0.0004	0.0002	0.0031	0.0000	0.0000	0.0000	0.0000	0.0000	0.0008
124	0.0013	0.0000	0.9933	0.0072	0.0001	0.0003	0.0000	0.0007	0.0004	0.0034	0.0000	0.0000	0.0000	0.0000	0.0000	0.0004
125	0.0011	0.0000	0.9947	0.0045	0.0000	0.0000	0.0000	0.0011	0.0002	0.0035	0.0005	0.0000	0.0003	0.0000	0.0000	0.0005

Spot	SiO_2	Al_2O_3	TiO_2	FeO	Cr_2O_3	MnO	MgO	CaO	Na_2O	K_2O	F	Cl	ZrO_2	BaO	P2O5	SrO	Total	Position
	Electron-microprobe analyses of zircon from Sample CA-02																	
	Major element compositions (wt%)																	
A-39	32.051	0.000	0.020	0.360	0.000	0.000	0.001	0.000	0.000	0.034	0.000	0.009	65.707	0.032	0.000	0.000	98.214	Rim
A-40	32.343	0.007	0.004	0.282	0.000	0.012	0.031	0.000	0.000	0.026	0.091	0.000	65.966	0.032	0.057	0.000	98.851	Core
A-41	32.018	0.007	0.021	0.294	0.000	0.000	0.000	0.031	0.000	0.024	0.036	0.003	65.598	0.002	0.000	0.000	98.034	Rim
A-42	32.956	0.028	0.003	0.129	0.000	0.027	0.008	0.021	0.000	0.019	0.154	0.000	65.430	0.000	0.072	0.000	98.847	Core
A-43	33.334	0.002	0.022	0.277	0.028	0.035	0.000	0.000	0.000	0.006	0.135	0.000	65.159	0.000	0.026	0.000	99.024	Rim
B-20	32.967	0.000	0.036	0.325	0.000	0.045	0.001	0.029	0.000	0.022	0.062	0.000	65.177	0.003	0.035	0.000	98.702	Core
B-21	32.225	0.002	0.083	0.222	0.032	0.000	0.028	0.000	0.000	0.001	0.133	0.003	65.745	0.000	0.060	0.000	98.534	Core
B-22	32.669	0.000	0.276	0.568	0.000	0.033	0.015	0.027	0.000	0.004	0.000	0.000	65.432	0.000	0.000	0.000	99.024	Rim
B-23	32.545	0.003	0.000	0.185	0.000	0.000	0.000	0.060	0.000	0.001	0.016	0.009	65.654	0.012	0.013	0.000	98.498	Rim
B-24	33.879	0.000	0.021	0.154	0.029	0.000	0.027	0.038	0.000	0.013	0.142	0.007	65.027	0.000	0.127	0.000	99.464	Core

Spot	SiO_2	Al_2O_3	TiO_2	FeO	Cr_2O_3	MnO	MgO	CaO	Na_2O	K_2O	F	Cl	ZrO_2	BaO	P2O5	SrO	Total	Position
Electron-microprobe analyses of zircon from Sample CA-02																		
Major element compositions (wt%)																		
B-25	32.603	0.000	0.006	0.172	0.015	0.051	0.000	0.056	0.000	0.011	0.104	0.004	65.581	0.038	0.030	0.000	98.671	Core
B-26	33.779	0.031	0.000	0.561	0.001	0.000	0.000	0.077	0.000	0.010	0.037	0.008	65.387	0.034	0.036	0.000	99.961	Rim
B-46	32.467	0.007	0.012	0.203	0.008	0.000	0.005	0.047	0.000	0.007	0.000	0.012	65.524	0.028	0.062	0.000	98.382	Rim
B-47	32.829	0.026	0.024	0.167	0.009	0.000	0.023	0.051	0.000	0.010	0.148	0.008	65.690	0.000	0.059	0.000	99.044	Core
B-48	32.147	0.018	0.000	0.182	0.000	0.000	0.000	0.037	0.000	0.019	0.000	0.012	65.766	0.024	0.029	0.000	98.234	Core
B-49	33.360	0.000	0.019	0.168	0.000	0.036	0.023	0.007	0.000	0.013	0.167	0.007	65.148	0.000	0.097	0.000	99.045	Rim
B-50	33.161	0.000	0.000	0.170	0.005	0.020	0.000	0.066	0.000	0.010	0.097	0.005	65.463	0.000	0.054	0.000	99.051	Core

Spot	Si	Al	Ti	Fe	Cr	Mn	Mg	Ca	Na	K	F	Cl	Zr	Ba	P	Sr
	Electron-microprobe analyses of zircon from Sample CA-02															
	Numbers of ions on the basis of 16 oxygen															
A-39	3.9894	0.0000	0.0019	0.0375	0.0000	0.0000	0.0002	0.0000	0.0000	0.0054	0.0000	0.0019	3.9878	0.0016	0.0000	0.0000
A-40	3.9968	0.0010	0.0004	0.0291	0.0000	0.0013	0.0057	0.0000	0.0000	0.0041	0.0356	0.0000	3.9747	0.0015	0.0060	0.0000
A-41	3.9915	0.0010	0.0020	0.0307	0.0000	0.0000	0.0000	0.0041	0.0000	0.0038	0.0142	0.0006	3.9873	0.0001	0.0000	0.0000
A-42	4.0530	0.0041	0.0003	0.0133	0.0000	0.0028	0.0015	0.0028	0.0000	0.0030	0.0599	0.0000	3.9234	0.0000	0.0075	0.0000
A-43	4.0838	0.0003	0.0020	0.0284	0.0027	0.0036	0.0000	0.0000	0.0000	0.0009	0.0523	0.0000	3.8923	0.0000	0.0027	0.0000
B-20	4.0582	0.0000	0.0033	0.0335	0.0000	0.0047	0.0002	0.0038	0.0000	0.0035	0.0241	0.0000	3.9119	0.0001	0.0036	0.0000
B-21	3.9943	0.0003	0.0077	0.0230	0.0031	0.0000	0.0052	0.0000	0.0000	0.0002	0.0521	0.0006	3.9734	0.0000	0.0063	0.0000
B-22	4.0172	0.0000	0.0255	0.0584	0.0000	0.0034	0.0027	0.0036	0.0000	0.0006	0.0000	0.0000	3.9231	0.0000	0.0000	0.0000
B-23	4.0250	0.0004	0.0000	0.0191	0.0000	0.0000	0.0000	0.0079	0.0000	0.0002	0.0063	0.0019	3.9591	0.0006	0.0014	0.0000
B-24	4.1152	0.0000	0.0019	0.0156	0.0028	0.0000	0.0049	0.0049	0.0000	0.0020	0.0545	0.0014	3.8512	0.0000	0.0131	0.0000
B-25	4.0276	0.0000	0.0006	0.0178	0.0015	0.0053	0.0000	0.0074	0.0000	0.0017	0.0406	0.0008	3.9502	0.0018	0.0031	0.0000
B-26	4.0937	0.0044	0.0000	0.0569	0.0001	0.0000	0.0000	0.0100	0.0000	0.0015	0.0142	0.0016	3.8637	0.0016	0.0037	0.0000
B-46	4.0193	0.0010	0.0011	0.0210	0.0008	0.0000	0.0009	0.0062	0.0000	0.0011	0.0000	0.0025	3.9551	0.0014	0.0065	0.0000
B-47	4.0352	0.0038	0.0022	0.0172	0.0009	0.0000	0.0042	0.0067	0.0000	0.0016	0.0575	0.0017	3.9369	0.0000	0.0061	0.0000

B-48	3.9955	0.0026	0.0000	0.0189	0.0000	0.0000	0.0000	0.0049	0.0000	0.0030	0.0000	0.0025	3.9855	0.0012	0.0031	0.0000
B-49	4.0837	0.0000	0.0017	0.0172	0.0000	0.0037	0.0042	0.0009	0.0000	0.0020	0.0646	0.0015	3.8885	0.0000	0.0101	0.0000
B-50	4.0652	0.0000	0.0000	0.0174	0.0005	0.0021	0.0000	0.0087	0.0000	0.0016	0.0376	0.0010	3.9129	0.0000	0.0056	0.0000

Spot	SiO_2	Al_2O_3	TiO_2	FeO	Cr_2O_3	MnO	MgO	CaO	Na_2O	K_2O	F	Cl	ZrO_2	BaO	P2O5	SrO	Total	Position
Electron-microprobe analyses of zircon from Sample CA-04																		
Major element compositions (wt%)																		
12	32.296	0.037	0.352	0.252	0.001	0.000	0.010	0.032	0.000	0.003	0.081	0.003	66.126	0.000	0.068	0.000	99.261	Core
13	31.901	0.011	0.583	0.585	0.015	0.006	0.000	0.018	0.000	0.019	0.002	0.000	65.099	0.000	0.157	0.000	98.396	Core
50	32.382	0.000	0.100	0.221	0.000	0.000	0.000	0.036	0.000	0.013	0.103	0.002	66.254	0.000	0.000	0.000	99.111	Rim
51	31.829	0.035	0.198	0.028	0.019	0.000	0.000	0.019	0.000	0.011	0.167	0.009	65.900	0.000	0.086	0.000	98.301	Rim
68	31.857	0.011	0.049	0.000	0.004	0.037	0.000	0.019	0.000	0.010	0.026	0.009	66.064	0.000	0.025	0.000	98.111	Core
69	32.016	0.021	0.013	0.011	0.039	0.000	0.026	0.042	0.000	0.000	0.081	0.000	65.872	0.018	0.172	0.000	98.311	Core
70	32.189	0.000	0.020	0.073	0.000	0.030	0.036	0.054	0.000	0.004	0.007	0.000	65.939	0.000	0.035	0.000	98.387	Rim
117	32.331	0.000	0.011	0.255	0.000	0.008	0.000	0.044	0.000	0.019	0.122	0.001	65.909	0.000	0.053	0.000	98.753	Core
118	32.238	0.009	0.067	0.248	0.021	0.000	0.015	0.046	0.000	0.017	0.035	0.001	66.239	0.000	0.007	0.000	98.943	Rim

Spot	Si	Al	Ti	Fe	Cr	Mn	Mg	Ca	Na	K	F	Cl	Zr	Ba	P	Sr
	Electron-microprobe analyses of zircon from Sample CA-04															
	Numbers of ions on the basis of 16 oxygen															
12	3.9725	0.0054	0.0326	0.0259	0.0001	0.0000	0.0018	0.0042	0.0000	0.0005	0.0315	0.0006	3.9659	0.0000	0.0071	0.0000
13	3.9550	0.0016	0.0544	0.0607	0.0015	0.0006	0.0000	0.0024	0.0000	0.0030	0.0008	0.0000	3.9352	0.0000	0.0165	0.0000
50	3.9930	0.0000	0.0093	0.0228	0.0000	0.0000	0.0000	0.0048	0.0000	0.0020	0.0402	0.0004	3.9834	0.0000	0.0000	0.0000
51	3.9620	0.0051	0.0185	0.0029	0.0019	0.0000	0.0000	0.0025	0.0000	0.0017	0.0657	0.0019	3.9997	0.0000	0.0091	0.0000
68	3.9714	0.0016	0.0046	0.0000	0.0004	0.0039	0.0000	0.0025	0.0000	0.0016	0.0102	0.0019	4.0156	0.0000	0.0026	0.0000
69	3.9761	0.0031	0.0012	0.0011	0.0038	0.0000	0.0048	0.0056	0.0000	0.0000	0.0318	0.0000	3.9887	0.0009	0.0181	0.0000
70	3.9929	0.0000	0.0019	0.0076	0.0000	0.0032	0.0067	0.0072	0.0000	0.0006	0.0027	0.0000	3.9882	0.0000	0.0037	0.0000
117	3.9994	0.0000	0.0010	0.0264	0.0000	0.0008	0.0000	0.0058	0.0000	0.0030	0.0477	0.0002	3.9753	0.0000	0.0056	0.0000
118	3.9826	0.0013	0.0062	0.0256	0.0021	0.0000	0.0028	0.0061	0.0000	0.0027	0.0137	0.0002	3.9899	0.0000	0.0007	0.0000

Spot	SiO_2	Al_2O_3	TiO_2	FeO	Cr_2O_3	MnO	MgO	CaO	Na_2O	K_2O	F	Cl	ZrO_2	BaO	P2O5	SrO	Total	Position
Electron-microprobe analyses of zircon from Sample CA-05																		
Major element compositions (wt%)																		
6	32.458	0.000	0.011	0.115	0.005	0.000	0.004	0.008	0.000	0.015	0.108	0.000	66.715	0.000	0.034	0.000	99.473	Core
7	32.603	0.000	0.046	0.300	0.000	0.000	0.000	0.000	0.000	0.013	0.091	0.000	66.630	0.001	0.117	0.000	99.801	Rim
8	32.035	0.000	0.000	0.056	0.021	0.020	0.000	0.011	0.000	0.003	0.100	0.007	66.713	0.017	0.041	0.000	99.024	Core
9	32.134	0.012	0.000	0.268	0.023	0.020	0.024	0.004	0.000	0.006	0.000	0.000	65.589	0.000	0.064	0.000	98.144	Rim
15	32.094	0.000	0.030	0.043	0.050	0.000	0.029	0.002	0.000	0.016	0.000	0.000	65.899	0.022	0.132	0.000	98.317	Core
16	32.125	0.017	0.000	0.114	0.000	0.000	0.000	0.003	0.000	0.003	0.000	0.002	65.738	0.053	0.107	0.000	98.162	Rim
17	32.388	0.000	0.000	0.044	0.000	0.000	0.008	0.000	0.000	0.013	0.002	0.002	65.934	0.013	0.084	0.000	98.488	Rim
18	32.706	0.000	0.000	0.039	0.022	0.000	0.012	0.014	0.000	0.015	0.027	0.004	66.445	0.000	0.076	0.000	99.360	Rim
45	32.371	0.000	0.016	0.245	0.011	0.028	0.033	0.047	0.000	0.026	0.104	0.006	66.056	0.000	0.000	0.000	98.943	Rim
46	32.710	0.006	0.024	0.269	0.000	0.000	0.000	0.009	0.000	0.014	0.074	0.000	66.631	0.030	0.144	0.000	99.911	Rim

Spot	Si	Al	Ti	Fe	Cr	Mn	Mg	Ca	Na	K	F	Cl	Zr	Ba	P	Sr
	Electron-microprobe analyses of zircon from Sample CA-05															
	Numbers of ions on the basis of 16 oxygen															
6	3.9890	0.0000	0.0010	0.0118	0.0005	0.0000	0.0007	0.0011	0.0000	0.0024	0.0420	0.0000	3.9978	0.0000	0.0035	0.0000
7	3.9894	0.0000	0.0042	0.0307	0.0000	0.0000	0.0000	0.0000	0.0000	0.0020	0.0352	0.0000	3.9753	0.0000	0.0121	0.0000
8	3.9634	0.0000	0.0000	0.0058	0.0021	0.0021	0.0000	0.0015	0.0000	0.0005	0.0391	0.0015	4.0244	0.0008	0.0043	0.0000
9	3.9950	0.0018	0.0000	0.0279	0.0023	0.0021	0.0044	0.0005	0.0000	0.0010	0.0000	0.0000	3.9759	0.0000	0.0067	0.0000
15	3.9827	0.0000	0.0028	0.0045	0.0049	0.0000	0.0054	0.0003	0.0000	0.0025	0.0000	0.0000	3.9873	0.0011	0.0139	0.0000
16	3.9928	0.0025	0.0000	0.0118	0.0000	0.0000	0.0000	0.0004	0.0000	0.0005	0.0000	0.0004	3.9838	0.0026	0.0113	0.0000
17	4.0074	0.0000	0.0000	0.0046	0.0000	0.0000	0.0015	0.0000	0.0000	0.0021	0.0008	0.0004	3.9778	0.0006	0.0088	0.0000
18	4.0109	0.0000	0.0000	0.0040	0.0021	0.0000	0.0022	0.0018	0.0000	0.0023	0.0105	0.0008	3.9730	0.0000	0.0079	0.0000
45	3.9983	0.0000	0.0015	0.0253	0.0011	0.0029	0.0061	0.0062	0.0000	0.0041	0.0406	0.0013	3.9781	0.0000	0.0000	0.0000
46	3.9950	0.0009	0.0022	0.0275	0.0000	0.0000	0.0000	0.0012	0.0000	0.0022	0.0286	0.0000	3.9679	0.0014	0.0149	0.0000

Spot	Al_2O_3	TiO_2	FeO	Cr_2O_3	MnO	MgO	CaO	Na_2O	K_2O	F	Cl	ZrO_2	BaO	P2O5	SrO	Total	Position
Electron-microprobe analyses of apatite from Sample CA-02																	

Major element compositions (wt%)																
A-45	0.032	0.006	0.253	0.000	0.095	0.000	54.854	0.014	0.048	3.947	0.013	0.000	0.000	42.476	0.010	101.748	Rim
B-13	0.004	0.004	0.119	0.010	0.075	0.000	55.578	0.038	0.007	5.279	0.011	0.000	0.009	39.069	0.004	100.207	Rim
B-14	0.031	0.013	0.108	0.000	0.074	0.000	54.919	0.000	0.000	5.282	0.011	0.000	0.000	40.264	0.000	100.702	Core
B-15	0.012	0.043	0.068	0.000	0.063	0.000	55.286	0.000	0.007	5.103	0.006	0.000	0.000	40.345	0.010	100.943	Rim
B-51	0.000	0.004	0.162	0.035	0.070	0.000	55.002	0.000	0.027	5.085	0.002	0.000	0.007	39.542	0.000	99.936	Core
B-52	0.005	0.000	0.229	0.000	0.063	0.000	55.911	0.000	0.024	4.964	0.006	0.000	0.000	39.866	0.000	101.068	Core

Spot	**Al**	**Ti**	**Fe**	**Cr**	**Mn**	**Mg**	**Ca**	**Na**	**K**	**F**	**Cl**	**Zr**	**Ba**	**P**	**Sr**
	Electron-microprobe analyses of apatite from Sample CA-02														
	Numbers of ions on the basis of 26 (O, F, Cl)														
A-45	0.0061	0.0007	0.0340	0.0000	0.0129	0.0000	9.4566	0.0044	0.0099	2.0084	0.0035	0.0000	0.0000	5.7863	0.0009
B-13	0.0008	0.0005	0.0163	0.0013	0.0104	0.0000	9.7258	0.0120	0.0015	2.7267	0.0030	0.0000	0.0006	5.4024	0.0004
B-14	0.0059	0.0016	0.0146	0.0000	0.0101	0.0000	9.5016	0.0000	0.0000	2.6973	0.0030	0.0000	0.0000	5.5046	0.0000
B-15	0.0023	0.0052	0.0092	0.0000	0.0086	0.0000	9.5669	0.0000	0.0014	2.6064	0.0016	0.0000	0.0000	5.5167	0.0009
B-51	0.0000	0.0005	0.0222	0.0045	0.0097	0.0000	9.6382	0.0000	0.0056	2.6300	0.0006	0.0000	0.0004	5.4753	0.0000
B-52	0.0010	0.0000	0.0311	0.0000	0.0087	0.0000	9.7186	0.0000	0.0050	2.5468	0.0016	0.0000	0.0000	5.4757	0.0000

Spot	**Al_2O_3**	**TiO_2**	**FeO**	**Cr_2O_3**	**MnO**	**MgO**	**CaO**	**Na_2O**	**K_2O**	**F**	**Cl**	**ZrO_2**	**BaO**	**P2O5**	**SrO**	**Total**	**Position**
Electron-microprobe analyses of apatite from Sample CA-04																	
Major element compositions (wt%)																	
32	0.012	0.022	0.332	0.000	0.701	0.000	55.494	0.066	0.008	4.590	0.306	0.000	0.015	40.282	0.009	101.837	Rim
34	0.002	0.079	0.059	0.017	0.083	0.000	55.543	0.022	0.013	4.656	0.102	0.000	0.000	41.005	0.000	101.581	Core
35	0.014	0.000	0.273	0.000	0.717	0.000	55.246	0.082	0.000	4.024	0.878	0.000	0.010	40.481	0.014	101.739	Core
36	0.000	0.033	0.340	0.000	0.622	0.000	55.592	0.062	0.006	4.527	0.642	0.000	0.000	40.508	0.081	102.413	Rim
37	0.010	0.000	0.187	0.014	0.466	0.000	55.040	0.062	0.001	4.062	0.533	0.000	0.000	40.638	0.086	101.099	Rim
61	0.020	0.000	0.299	0.000	0.359	0.000	55.272	0.060	0.001	4.331	0.534	0.000	0.015	41.239	0.034	102.164	Core
62	0.000	0.000	0.254	0.020	0.363	0.000	55.048	0.075	0.006	4.345	0.524	0.000	0.000	41.229	0.091	101.955	Rim
64	0.002	0.000	0.179	0.014	0.276	0.000	55.410	0.201	0.000	4.703	0.641	0.000	0.000	39.893	0.031	101.350	Core

Spot	Al	Ti	Fe	Cr	Mn	Mg	Ca	Na	K	F	Cl	Zr	Ba	P	Sr
	Electron-microprobe analyses of apatite from Sample CA-04														
	Numbers of ions on the basis of 26 (O, F, Cl)														
32	0.0023	0.0027	0.0449	0.0000	0.0960	0.0000	9.6163	0.0207	0.0017	2.3476	0.0839	0.0000	0.0010	5.5158	0.0008
34	0.0004	0.0096	0.0079	0.0022	0.0113	0.0000	9.5812	0.0069	0.0027	2.3706	0.0278	0.0000	0.0000	5.5893	0.0000
35	0.0027	0.0000	0.0371	0.0000	0.0987	0.0000	9.6164	0.0258	0.0000	2.0674	0.2418	0.0000	0.0006	5.5679	0.0013
36	0.0000	0.0040	0.0457	0.0000	0.0847	0.0000	9.5785	0.0193	0.0012	2.3022	0.1750	0.0000	0.0000	5.5152	0.0076
37	0.0019	0.0000	0.0255	0.0018	0.0644	0.0000	9.6171	0.0196	0.0002	2.0949	0.1473	0.0000	0.0000	5.6109	0.0081
61	0.0038	0.0000	0.0402	0.0000	0.0489	0.0000	9.5173	0.0187	0.0002	2.2012	0.1455	0.0000	0.0009	5.6111	0.0032
62	0.0000	0.0000	0.0342	0.0025	0.0495	0.0000	9.4925	0.0234	0.0012	2.2115	0.1429	0.0000	0.0000	5.6179	0.0085
64	0.0004	0.0000	0.0243	0.0018	0.0379	0.0000	9.6244	0.0632	0.0000	2.4111	0.1761	0.0000	0.0000	5.4754	0.0029

Spot	Al_2O_3	TiO_2	FeO	Cr_2O_3	MnO	MgO	CaO	Na_2O	K_2O	F	Cl	ZrO_2	BaO	P2O5	SrO	Total	Position
	Electron-microprobe analyses of apatite from Sample CA-05																
	Major element compositions (wt%)																
65	0.000	0.000	0.240	0.000	0.285	0.000	56.822	0.101	0.000	4.237	0.595	0.000	0.000	39.103	0.009	101.392	Rim
66	0.000	0.000	0.212	0.000	0.250	0.000	56.870	0.104	0.000	4.278	0.554	0.000	0.005	38.889	0.011	101.173	Rim
68	0.004	0.000	0.223	0.000	0.328	0.000	56.341	0.100	0.000	4.188	0.527	0.000	0.003	40.258	0.059	102.031	Core
70	0.010	0.017	0.173	0.024	0.236	0.000	56.561	0.102	0.000	4.368	0.666	0.000	0.029	39.762	0.036	101.984	Core

Spot	Al	Ti	Fe	Cr	Mn	Mg	Ca	Na	K	F	Cl	Zr	Ba	P	Sr
	Electron-microprobe analyses of apatite from Sample CA-05														
	Numbers of ions on the basis of 26 (O, F, Cl)														
65	0.0000	0.0000	0.0329	0.0000	0.0396	0.0000	9.9805	0.0321	0.0000	2.1966	0.1653	0.0000	0.0000	5.4273	0.0009
66	0.0000	0.0000	0.0291	0.0000	0.0348	0.0000	10.0135	0.0331	0.0000	2.2233	0.1543	0.0000	0.0003	5.4108	0.0010
68	0.0008	0.0000	0.0302	0.0000	0.0451	0.0000	9.7900	0.0314	0.0000	2.1479	0.1449	0.0000	0.0002	5.5277	0.0055
70	0.0019	0.0021	0.0235	0.0031	0.0324	0.0000	9.8323	0.0321	0.0000	2.2412	0.1831	0.0000	0.0018	5.4618	0.0034

Spot	SiO_2	Al_2O_3	TiO_2	FeO	MnO	MgO	CaO	P_2O_5	UO_2	ThO_2	PbO	Y_2O_3	Gd_2O_3	Sm_2O_3	Nd_2O_3	Pr_2O_3	Ce_2O_3	La_2O_3	Total	Position
Electron-microprobe analyses of allanite from Sample CA-02																				
Major element compositions (wt%)																				
1	35.308	16.192	1.203	14.200	0.445	0.479	10.905	0.019	0.048	0.944	0.045	0.111	0.135	0.349	3.018	1.006	9.708	4.697	98.812	Rim
2	39.966	15.705	2.802	11.032	0.486	0.322	9.279	0.001	0.059	1.947	0.030	0.080	0.155	0.285	2.398	0.890	9.186	4.407	99.030	Core
3	39.069	14.507	2.830	9.414	0.501	0.219	7.637	0.000	0.096	2.594	0.027	0.204	0.156	0.254	2.264	0.770	8.070	3.604	92.216	Core
4	34.076	15.910	1.164	14.142	0.611	0.430	10.871	0.000	0.026	1.070	0.066	0.035	0.140	0.299	2.982	0.981	10.503	5.249	98.555	Rim
5	34.581	15.970	1.192	15.019	0.698	0.338	10.745	0.000	0.017	0.994	0.113	0.000	0.072	0.164	2.678	0.904	10.680	5.575	99.740	Rim
6	37.941	14.683	2.731	12.016	0.477	0.362	8.318	0.015	0.066	1.656	0.042	0.073	0.130	0.250	2.292	0.895	9.490	4.801	96.238	Core
7	34.987	17.489	1.295	12.436	0.720	0.187	10.926	0.000	0.027	1.239	0.043	0.051	0.179	0.319	3.158	1.110	10.502	5.276	99.944	Rim
8	38.563	15.089	2.886	12.848	0.471	0.417	8.877	0.032	0.078	1.512	0.055	0.045	0.079	0.218	2.359	0.922	9.811	4.954	99.216	Core
9	44.877	13.884	2.792	5.779	0.282	0.174	6.165	0.017	0.340	3.205	0.023	0.167	0.108	0.360	2.544	0.882	8.360	3.418	93.377	Rim
10	32.235	14.177	1.874	17.250	0.398	1.118	10.361	0.001	0.006	0.739	0.006	0.010	0.123	0.351	3.213	1.042	11.884	6.035	100.823	Core
11	32.333	14.247	1.908	17.386	0.400	1.138	10.281	0.000	0.001	0.736	0.008	0.029	0.137	0.299	3.150	1.105	11.893	6.085	101.136	Core
12	45.255	15.410	1.970	7.272	0.333	0.264	8.229	0.021	0.379	2.235	0.035	0.116	0.121	0.316	2.634	0.873	8.998	3.941	98.402	Rim
13	44.439	14.737	2.200	7.176	0.329	0.281	8.250	0.002	0.286	2.137	0.023	0.000	0.106	0.267	2.408	0.855	8.925	4.306	96.727	Core
14	32.904	18.168	0.712	11.969	0.851	0.202	11.086	0.000	0.036	1.238	0.069	0.000	0.115	0.344	3.002	1.021	10.085	4.947	96.749	Rim
15	38.477	16.509	1.896	11.150	0.468	0.249	10.304	0.000	0.036	2.427	0.051	0.031	0.082	0.249	2.465	0.848	8.909	4.269	98.420	Core
16	37.843	15.795	1.983	10.550	0.479	0.226	9.872	0.000	0.036	2.682	0.054	0.030	0.116	0.325	2.402	0.850	8.481	3.903	95.627	Core
17	32.988	17.133	0.572	13.440	0.652	0.214	12.229	0.002	0.030	1.237	0.056	0.000	0.129	0.277	2.555	0.914	9.139	4.737	96.304	Rim
18	32.098	16.502	0.553	12.823	0.674	0.124	11.589	0.000	0.016	1.188	0.037	0.000	0.087	0.243	3.074	1.080	10.255	5.075	95.418	Rim

Spot	Si	Al	Ti	Fe	Mn	Mg	Ca	P	U	Th	Pb	Y	Gd	Sm	Nd	Pr	Ce	La
	Electron-microprobe analyses of allanite from Sample CA-02																	
	Numbers of ions on the basis of 12.5 oxygen																	
1	3.2285	1.7448	0.0827	1.0859	0.0345	0.0653	1.0682	0.0015	0.0010	0.0196	0.0011	0.0054	0.0041	0.0154	0.0985	0.0335	0.3250	0.1584
2	3.5060	1.6236	0.1849	0.8094	0.0361	0.0421	0.8721	0.0001	0.0012	0.0389	0.0007	0.0037	0.0045	0.0121	0.0751	0.0284	0.2950	0.1426
3	3.6293	1.5882	0.1978	0.7314	0.0394	0.0303	0.7600	0.0000	0.0020	0.0548	0.0007	0.0101	0.0048	0.0114	0.0751	0.0261	0.2744	0.1235
4	3.1717	1.7452	0.0815	1.1008	0.0482	0.0597	1.0840	0.0000	0.0005	0.0227	0.0017	0.0017	0.0043	0.0134	0.0991	0.0333	0.3579	0.1802
5	3.1813	1.7314	0.0825	1.1555	0.0544	0.0464	1.0590	0.0000	0.0003	0.0208	0.0028	0.0000	0.0022	0.0073	0.0880	0.0303	0.3597	0.1891
6	3.4728	1.5839	0.1880	0.9198	0.0370	0.0494	0.8157	0.0012	0.0013	0.0345	0.0010	0.0036	0.0039	0.0111	0.0749	0.0298	0.3180	0.1621
7	3.1745	1.8701	0.0884	0.9437	0.0553	0.0253	1.0621	0.0000	0.0005	0.0256	0.0011	0.0025	0.0054	0.0140	0.1023	0.0367	0.3488	0.1765
8	3.4345	1.5837	0.1933	0.9570	0.0355	0.0554	0.8470	0.0024	0.0015	0.0306	0.0013	0.0021	0.0023	0.0094	0.0750	0.0299	0.3199	0.1627
9	3.9824	1.4520	0.1864	0.4289	0.0212	0.0230	0.5861	0.0013	0.0067	0.0647	0.0005	0.0079	0.0032	0.0154	0.0806	0.0285	0.2716	0.1119
10	3.0364	1.5738	0.1328	1.3589	0.0318	0.1570	1.0456	0.0001	0.0001	0.0158	0.0002	0.0005	0.0038	0.0160	0.1081	0.0358	0.4098	0.2096
11	3.0355	1.5763	0.1347	1.3651	0.0318	0.1593	1.0341	0.0000	0.0000	0.0157	0.0002	0.0014	0.0043	0.0136	0.1056	0.0378	0.4087	0.2107
12	3.8504	1.5451	0.1261	0.5174	0.0240	0.0335	0.7501	0.0015	0.0072	0.0433	0.0008	0.0053	0.0034	0.0130	0.0800	0.0271	0.2803	0.1237
13	3.8529	1.5058	0.1435	0.5203	0.0242	0.0363	0.7663	0.0001	0.0055	0.0422	0.0005	0.0000	0.0030	0.0112	0.0746	0.0270	0.2833	0.1377
14	3.0867	2.0086	0.0502	0.9390	0.0676	0.0283	1.1141	0.0000	0.0008	0.0264	0.0017	0.0000	0.0036	0.0156	0.1006	0.0349	0.3463	0.1711
15	3.4223	1.7305	0.1269	0.8294	0.0353	0.0330	0.9818	0.0000	0.0007	0.0491	0.0012	0.0015	0.0024	0.0107	0.0783	0.0275	0.2901	0.1400
16	3.4562	1.7000	0.1362	0.8058	0.0370	0.0308	0.9659	0.0000	0.0007	0.0557	0.0013	0.0015	0.0035	0.0143	0.0783	0.0283	0.2835	0.1315
17	3.1073	1.9019	0.0405	1.0587	0.0520	0.0301	1.2341	0.0002	0.0006	0.0265	0.0014	0.0000	0.0040	0.0126	0.0859	0.0314	0.3151	0.1646
18	3.0971	1.8765	0.0401	1.0348	0.0551	0.0178	1.1980	0.0000	0.0003	0.0261	0.0010	0.0000	0.0028	0.0113	0.1059	0.0380	0.3622	0.1806

APPENDIX G - Supplementary File 4.D - Geochemistry Data

Data Source	G5 local name	Rock-type	Sample	SiO_2	TiO_2	Al_2O_3	FeO	Fe_2O_3	MnO	MgO	CaO	Na_2O	K_2O	P_2O_5
This work	Aracê	Titanite-allanite-biotite granite	CA-02	68.50	0.67	14.30	-	3.85	0.05	0.70	1.97	2.67	6.04	0.19
This work	Vitória	Biotite granite	CA-04	68.40	0.71	13.90	-	5.72	0.05	0.79	1.63	2.53	5.58	0.28
This work	Mestre Álvaro	Biotite tonalite	CA-05	65.40	1.08	14.60	-	6.77	0.07	2.05	4.00	2.78	2.19	0.08
Mendes et al., 2005	Várzea Alegre	Charnockitic rock	VA42	64.90	0.94	15.10	-	5.57	0.11	0.99	3.60	3.50	3.60	0.42
Mendes et al., 2005	Várzea Alegre	Charnockitic rock	VA164	64.00	0.78	16.10	-	5.45	0.08	1.00	4.80	3.50	3.40	0.39
Mendes et al., 2005	Várzea Alegre	Charnockitic rock	HR29	62.40	1.40	15.30	-	7.38	0.17	1.60	3.80	3.00	3.70	0.49
Mendes et al., 2005	Várzea Alegre	Charnockitic rock	VA262	62.39	0.89	16.14	-	6.45	0.15	1.02	3.64	3.21	4.14	0.39
Mendes et al., 2005	Várzea Alegre	Charnockitic rock	VA244	61.82	1.37	14.84	-	7.93	0.13	1.98	3.58	3.01	3.72	0.50
Mendes et al., 2005	Várzea Alegre	Charnockitic rock	VA125	61.00	1.10	16.10	-	6.75	0.10	2.60	3.90	3.20	3.60	0.53
Mendes et al., 2005	Várzea Alegre	Charnockitic rock	VA16	61.00	1.30	16.10	-	7.08	0.12	1.70	4.50	3.50	3.10	0.44
Mendes et al., 2005	Várzea Alegre	Charnockitic rock	MP161	60.70	1.10	17.50	-	6.46	0.11	0.99	4.60	3.50	3.90	0.42
Mendes et al., 2005	Várzea Alegre	Charnockitic rock	MP128	59.90	1.00	17.20	-	7.81	0.11	1.00	4.40	3.50	4.10	0.41
Mendes et al., 2005	Várzea Alegre	Charnockitic rock	VA90	59.00	1.50	15.10	-	9.30	0.14	1.80	5.00	3.50	3.40	0.66
Mendes et al., 2005	Várzea Alegre	Charnockitic rock	VA264	57.43	1.58	15.89	-	9.52	0.16	2.29	4.99	3.39	2.84	0.73
Mendes et al., 2005	Várzea Alegre	Charnockitic rock	VA261	53.99	1.97	16.58	-	11.28	0.18	2.76	6.22	3.28	2.02	0.95
Mendes et al., 2005	Várzea Alegre	Charnockitic rock	MP718	54.40	1.90	17.10	-	11.20	0.18	1.80	6.60	3.00	2.40	0.86
Mendes et al., 2005	Várzea Alegre	Charnockitic rock	MP173	53.10	1.90	16.20	-	9.60	0.15	3.70	7.90	3.20	2.30	0.77
Mendes et al., 2002	Venda Nova	Norite	VN5	42.17	2.46	18.69	-	15.68	0.21	5.42	12.61	1.34	0.28	0.81
Mendes et al., 2002	Venda Nova	Norite	VN22	42.41	1.99	18.64	-	15.38	0.24	5.95	12.41	1.21	0.29	0.70
Mendes et al., 2002	Venda Nova	Norite	VN10	43.29	1.65	18.81	-	13.97	0.19	6.49	13.38	0.72	0.11	0.35
Mendes et al., 2002	Venda Nova	Norite	VN9	43.38	2.31	18.25	-	14.91	0.21	5.75	12.75	0.74	0.14	0.64
Mendes et al., 2002	Venda Nova	Norite	VN7	43.84	1.53	18.29	-	13.66	0.21	6.80	13.36	0.67	0.11	0.39
Mendes et al., 2002	Venda Nova	Norite	VN3	43.88	2.15	18.19	-	14.53	0.21	5.67	11.98	1.67	0.27	0.76
Mendes et al., 2002	Venda Nova	Norite	VN26	44.95	1.42	19.04	-	12.21	0.19	7.11	12.76	1.04	0.22	0.27
Mendes et al., 2002	Venda Nova	Norite	VN8	45.27	1.47	18.21	-	13.04	0.19	6.46	12.72	1.19	0.18	0.30
Mendes et al., 2002	Venda Nova	Norite	VN6	46.45	1.69	19.16	-	13.37	0.21	4.86	10.80	2.25	0.28	0.48
Mendes et al., 2002	Venda Nova	Norite	VN14	46.57	0.99	18.44	-	10.91	0.18	7.79	13.28	0.66	0.13	0.16
Mendes et al., 2002	Venda Nova	Norite	VN11	48.88	1.19	17.69	-	12.97	0.22	5.85	10.20	1.56	0.43	0.32
Mendes et al., 2002	Venda Nova	Charnoenderbite	VN38	54.46	0.89	18.03	-	8.57	0.21	4.27	8.01	3.67	1.00	0.22

Data Source	G5 local name	Rock-type	Sample	SiO_2	TiO_2	Al_2O_3	FeO	Fe_2O_3	MnO	MgO	CaO	Na_2O	K_2O	P_2O_5
Mendes et al., 2002	Venda Nova	Charnoenderbite	VN35	54.96	0.87	17.49	-	9.19	0.17	4.23	7.75	3.28	1.23	0.21
Mendes et al., 2002	Venda Nova	Charnoenderbite	VN17	55.24	0.88	17.79	-	8.79	0.16	4.08	7.92	3.36	0.66	0.22
Mendes et al., 2002	Venda Nova	Charnoenderbite	VN36	56.31	0.87	17.45	-	8.41	0.16	3.96	7.39	3.38	0.91	0.21
Mendes et al., 2002	Venda Nova	Charnoenderbite	VN20	56.37	0.84	17.41	-	8.28	0.15	3.98	7.67	3.61	0.87	0.21
Mendes et al., 2002	Venda Nova	Charnoenderbite	VN23	56.77	0.89	16.28	-	8.84	0.15	4.21	7.53	3.02	0.96	0.23
Mendes et al., 2002	Venda Nova	Charnoenderbite	VN15	57.40	0.84	17.72	-	8.23	0.14	3.23	7.35	3.43	0.71	0.22
Mendes et al., 2002	Venda Nova	Charnoenderbite	VN19	57.43	0.81	17.23	-	8.15	0.14	3.94	6.99	3.29	0.96	0.20
Mendes et al., 2002	Venda Nova	Charnoenderbite	VN18	57.47	0.80	17.12	-	8.16	0.14	3.75	7.09	3.39	1.14	0.20
Mendes et al., 2002	Venda Nova	Charnoenderbite	VN1	58.41	0.79	16.74	-	7.83	0.12	3.64	6.95	3.12	1.52	0.19
Mendes et al., 2002	Venda Nova	Charnoenderbite	VN16	59.06	0.77	16.59	-	7.50	0.13	3.34	6.80	3.06	1.59	0.19
Mendes et al., 2002	Venda Nova	Charnoenderbite	VN13	61.13	0.90	16.92	-	7.15	0.14	2.44	5.26	3.72	1.43	0.27
Mendes et al., 2002	Venda Nova	Charnoenderbite	VN24	62.45	0.76	16.18	-	6.87	0.14	2.47	5.35	3.64	1.17	0.23
Mendes et al., 2002	Venda Nova	Charnoenderbite	VN2	65.17	0.71	15.67	-	6.77	0.13	1.34	5.80	2.73	0.76	0.22
Mendes et al., 2002	Venda Nova	Charnoenderbite	VN27	66.24	0.53	15.64	-	5.21	0.12	1.28	4.47	3.96	1.35	0.21
Mendes et al., 2002	Venda Nova	Charnoenderbite	VN31	67.12	0.50	15.49	-	4.81	0.12	1.22	3.79	3.88	1.85	0.20
Mendes et al., 1997	Várzea Alegre	Charnockitic rock	VA 260	63.14	0.88	16.29	-	5.75	0.10	0.94	4.10	3.45	3.70	0.30
Mendes et al., 1997	Várzea Alegre	Charnockitic rock	VA 252	62.73	0.92	15.89	-	6.27	0.14	0.99	4.05	3.33	3.58	0.36
Mendes et al., 1997	Várzea Alegre	Charnockitic rock	VA 250	63.35	0.76	16.28	-	5.03	0.09	0.84	3.63	3.20	4.73	0.26
Mendes et al., 1997	Várzea Alegre	Charnockitic rock	VA 241	60.01	1.49	14.84	-	8.64	0.14	2.14	4.16	2.99	3.41	0.62
Mendes et al., 1997	Várzea Alegre	Charnockitic rock	VA 249	59.51	1.16	16.78	-	7.38	0.15	1.55	4.92	3.45	3.23	0.46
Mendes et al., 1997	Várzea Alegre	Charnockitic rock	VA 242	58.71	1.70	14.86	-	10.09	0.16	2.58	4.41	2.95	2.94	0.72
Mendes et al., 1997	Várzea Alegre	Charnockitic rock	VA 263	60.17	0.99	17.21	-	6.42	0.11	1.26	4.41	3.58	4.01	0.35
Mendes et al., 1997	Várzea Alegre	Charnockitic rock	VA 253	57.34	1.65	15.71	-	9.76	0.15	2.36	5.19	3.09	2.78	0.76
Mendes et al., 1997	Várzea Alegre	Charnockitic rock	VA 56	56.46	1.40	16.37	-	8.43	0.14	1.90	5.28	3.41	3.49	0.60
Mendes et al., 1997	Várzea Alegre	Charnockitic rock	VA 237	56.81	1.78	14.68	-	11.14	0.18	2.57	5.00	3.09	2.46	0.90
Mendes et al., 1997	Várzea Alegre	Charnockitic rock	VA 257	56.22	1.74	15.37	-	10.43	0.17	2.47	5.39	3.32	2.62	0.84
Mendes et al., 1997	Várzea Alegre	Charnockitic rock	VA 182	55.23	1.95	15.55	-	11.61	0.18	2.83	5.39	3.18	2.39	0.96
De Campos, 2015	Santa Angélica	Diorite	1	54.48	2.11	15.73	8.71	-	0.13	4.45	7.14	3.30	2.78	1.17
De Campos, 2015	Santa Angélica	Diorite	2	52.79	2.80	14.93	9.53	-	0.13	4.89	7.74	3.06	2.48	1.65
De Campos, 2015	Santa Angélica	Diorite	3	54.24	2.05	16.02	8.29	-	0.13	4.78	7.49	3.23	2.65	1.13

Data Source	G5 local name	Rock-type	Sample	SiO_2	TiO_2	Al_2O_3	FeO	Fe_2O_3	MnO	MgO	CaO	Na_2O	K_2O	P_2O_5
De Campos, 2015	Santa Angélica	Diorite	4a	53.31	2.63	15.04	9.79	-	0.14	4.36	7.33	3.30	2.70	1.40
De Campos, 2015	Santa Angélica	Gabbro	4b	51.48	2.94	14.82	10.58	-	0.16	4.56	7.83	3.25	2.67	1.72
De Campos, 2015	Santa Angélica	Diorite	5b	52.45	3.23	14.77	9.71	-	0.13	4.40	7.59	3.07	2.83	1.82
De Campos, 2015	Santa Angélica	Diorite	6	59.38	1.85	16.09	7.47	-	0.14	2.19	4.15	3.50	4.62	0.61
De Campos, 2015	Santa Angélica	Diorite	8	53.33	2.11	15.45	9.16	-	0.14	5.76	7.97	3.15	1.93	1.02
De Campos, 2015	Santa Angélica	Diorite	9	62.21	1.55	16.15	6.11	-	0.10	1.70	3.10	3.67	5.01	0.42
De Campos, 2015	Santa Angélica	Granite	10	68.88	0.50	16.54	2.94	-	0.07	0.85	3.26	3.89	2.95	0.13
De Campos, 2015	Santa Angélica	Diorite	12	54.62	2.43	15.14	8.94	-	0.14	4.20	7.02	3.34	2.97	1.20
De Campos, 2015	Santa Angélica	Granite	13	74.78	0.36	13.15	1.62	-	0.05	0.20	1.00	3.09	5.71	0.06
De Campos, 2015	Santa Angélica	Gabbro	14a	52.08	1.94	16.16	8.27	-	0.11	6.44	8.52	3.23	2.28	0.96
De Campos, 2015	Santa Angélica	Diorite	14b	55.27	2.21	16.34	8.98	-	0.15	2.92	5.43	3.69	4.17	0.84
De Campos, 2015	Santa Angélica	Gabbro	15	51.31	2.63	16.73	10.22	-	0.15	4.54	6.45	3.67	3.06	1.25
De Campos, 2015	Santa Angélica	Granite	17	75.83	0.22	13.38	1.28	-	0.03	0.20	1.07	3.19	4.77	0.04
De Campos, 2015	Santa Angélica	Granite	20	73.66	0.31	14.06	1.98	-	0.06	0.45	1.85	3.49	4.06	0.08
De Campos, 2015	Santa Angélica	Granite	21a	75.29	0.21	13.60	1.37	-	0.05	0.25	1.40	3.23	4.56	0.05
De Campos, 2015	Santa Angélica	Diorite	21b	54.59	2.25	16.42	8.45	-	0.12	3.79	6.47	3.74	3.14	1.02
De Campos, 2015	Santa Angélica	Granite	22	74.67	0.23	13.76	1.52	-	0.04	0.29	1.58	3.44	4.43	0.05
De Campos, 2015	Santa Angélica	Granite	23a	72.85	0.34	14.64	1.88	-	0.06	0.41	1.99	3.68	4.08	0.07
De Campos, 2015	Santa Angélica	Diorite	23b	54.29	2.64	15.05	10.26	-	0.14	3.40	6.66	3.34	3.07	1.17
De Campos, 2015	Santa Angélica	Diorite	25	53.25	2.63	16.04	9.48	-	0.14	3.87	6.52	3.47	3.28	1.33
De Campos, 2015	Santa Angélica	Diorite	27	62.24	1.46	15.68	6.44	-	0.09	2.16	3.79	3.73	3.81	0.60
De Campos, 2015	Santa Angélica	Diorite	28	58.22	1.67	17.45	6.95	-	0.12	2.15	4.13	4.38	4.29	0.64
De Campos, 2015	Santa Angélica	Diorite	31	57.68	2.10	16.06	8.64	-	0.15	2.29	4.99	3.63	3.83	0.63
De Campos, 2015	Santa Angélica	Granite	32	75.69	0.13	13.86	1.01	-	0.04	0.14	1.19	3.58	4.33	0.03
De Campos, 2015	Santa Angélica	Gabbro	33	50.37	3.86	14.90	11.12	-	0.15	3.93	7.36	3.17	3.05	2.10
De Campos, 2015	Santa Angélica	Diorite	34	52.65	1.76	18.11	8.05	-	0.14	4.98	7.67	3.56	2.25	0.84
De Campos, 2015	Santa Angélica	Gabbro	35	50.15	2.59	16.12	10.70	-	0.16	4.78	8.10	3.68	2.49	1.24
De Campos, 2015	Santa Angélica	Diorite	36	60.22	0.86	19.23	5.55	-	0.16	1.61	5.22	4.30	2.64	0.22
De Campos, 2015	Santa Angélica	Diorite	37	60.77	0.86	19.41	5.09	-	0.15	1.51	5.42	4.12	2.46	0.21
De Campos, 2015	Santa Angélica	Granite	38a	69.31	0.40	15.77	3.01	-	0.06	0.62	2.28	4.41	4.03	0.11

Data Source	G5 local name	Rock-type	Sample	SiO_2	TiO_2	Al_2O_3	FeO	Fe_2O_3	MnO	MgO	CaO	Na_2O	K_2O	P_2O_5
De Campos, 2015	Santa Angélica	Gabbro	39a	48.56	1.51	15.89	9.79	-	0.15	10.74	8.11	2.83	1.78	0.65
De Campos, 2015	Santa Angélica	Gabbro	39b	47.95	2.92	17.31	12.53	-	0.17	3.74	6.84	3.54	3.37	1.63
De Campos, 2015	Santa Angélica	Diorite	40	54.91	2.16	16.78	8.92	-	0.15	3.11	5.34	4.53	3.02	1.09
De Campos, 2015	Santa Angélica	Gabbro	41	48.63	2.29	14.89	10.80	-	0.17	7.76	8.91	2.82	2.71	1.03
De Campos, 2015	Santa Angélica	Gabbro	42a	50.88	1.77	14.32	10.40	-	0.19	8.39	7.86	2.91	1.61	1.67
De Campos, 2015	Santa Angélica	Gabbro	42b	49.82	2.40	16.37	10.16	-	0.16	6.13	8.41	3.20	2.20	1.17
De Campos, 2015	Santa Angélica	Diorite	43	59.15	1.50	17.46	6.06	-	0.12	2.03	4.09	4.29	4.73	0.57
De Campos, 2015	Santa Angélica	Diorite	44	53.18	1.96	15.67	9.20	-	0.20	5.38	6.81	3.87	2.85	0.88
De Campos, 2015	Santa Angélica	Gabbro	45	50.10	2.98	15.52	10.59	-	0.16	4.91	8.51	3.20	2.44	1.59
De Campos, 2015	Santa Angélica	Gabbro	46	50.58	2.56	15.97	11.41	-	0.16	5.57	6.93	3.41	2.43	0.99
De Campos, 2015	Santa Angélica	Gabbro	47	51.66	2.15	16.26	10.54	-	0.15	5.86	6.73	3.47	2.31	0.87
De Campos, 2015	Santa Angélica	Diorite	48	55.82	2.30	16.37	8.86	-	0.13	2.70	5.30	3.79	3.82	0.93
De Campos, 2015	Santa Angélica	Diorite	49	55.34	2.40	15.57	9.69	-	0.13	3.12	5.98	3.37	3.42	0.98
De Campos, 2015	Santa Angélica	Granite	50	68.22	0.73	15.43	2.96	-	0.06	0.70	1.77	3.74	6.23	0.18
Bayer et al., 1987	Santa Angélica	Fine-grained gabbro	P438B	48.45	2.58	16.53	5.46	3.64	0.10	5.83	6.98	4.53	2.42	1.52
Bayer et al., 1987	Santa Angélica	Fine-grained gabbro	P191	49.24	1.84	16.26	4.53	3.02	0.08	6.81	10.30	3.60	1.99	0.80
Bayer et al., 1987	Santa Angélica	Fine-grained gabbro	P007B	42.35	3.39	15.00	8.41	5.60	0.20	6.23	8.07	3.79	2.74	2.01
Bayer et al., 1987	Santa Angélica	Fine-grained gabbro	P297B	49.32	2.39	16.07	6.08	4.05	0.13	6.23	7.10	2.91	3.10	1.70
Bayer et al., 1987	Santa Angélica	Coarse-grained gabbro	R412C	51.46	2.85	15.59	5.96	3.98	0.13	4.98	6.74	1.90	3.33	1.85
Bayer et al., 1987	Santa Angélica	Coarse-grained gabbro	P050	50.07	2.98	15.71	5.31	3.54	0.11	5.72	8.45	2.93	1.99	1.94
Bayer et al., 1987	Santa Angélica	Coarse-grained gabbro	P180A	51.88	2.39	15.58	5.32	3.55	0.14	4.49	6.42	4.13	3.04	1.39
Bayer et al., 1987	Santa Angélica	Coarse-grained gabbro	R410S	50.65	2.68	14.40	6.22	4.15	0.18	5.36	7.24	2.98	2.78	1.49
Bayer et al., 1987	Santa Angélica	Hybrid rock	P491A	59.24	1.89	15.01	4.78	3.19	0.09	2.78	4.69	2.29	4.25	0.89
Bayer et al., 1987	Santa Angélica	Hybrid rock	R410A	57.10	1.29	17.73	3.76	2.51	0.59	3.22	4.51	3.47	4.16	0.64
Bayer et al., 1987	Santa Angélica	Hybrid rock	R410B	53.19	2.80	14.56	5.87	3.91	0.13	4.23	5.72	4.32	3.48	1.74
Bayer et al., 1987	Santa Angélica	Hybrid rock	R410E	58.63	2.19	14.41	4.78	3.19	0.13	2.88	4.65	2.48	4.07	1.19

Data Source	G5 local name	Rock-type	Sample	SiO_2	TiO_2	Al_2O_3	FeO	Fe_2O_3	MnO	MgO	CaO	Na_2O	K_2O	P_2O_5
Bayer et al., 1987	Santa Angélica	Hybrid rock	R410G	56.76	2.28	14.54	4.88	3.26	0.14	3.57	4.96	3.67	3.47	1.19
Bayer et al., 1987	Santa Angélica	Hybrid rock	P485A	61.26	1.69	13.78	4.51	3.00	0.11	2.60	4.58	2.79	4.18	0.75
Bayer et al., 1987	Santa Angélica	Granite	P485B	75.61	0.13	12.67	0.77	0.51	0.03	0.50	1.02	3.08	4.53	0.01
Bayer et al., 1987	Santa Angélica	Granite	P495	74.75	0.13	12.98	0.66	0.44	0.05	0.12	1.33	3.55	4.62	0.01
Bayer et al., 1987	Santa Angélica	Granite	P354E	71.66	0.26	14.12	1.05	0.70	0.06	0.45	1.25	3.25	5.78	0.05
Bayer et al., 1987	Santa Angélica	Granite	P187B	69.48	0.44	15.03	1.68	1.12	0.05	0.90	2.69	3.78	3.53	0.12
Mello, 2000	Aimorés	Qtz monzodiorite	FAM32	50.05	3.39	15.29	-	13.76	0.19	3.05	7.35	3.14	1.77	1.29
Mello, 2000	Aimorés	Monzodiorite	FAM28	50.73	2.92	15.19	-	13.65	0.20	3.46	7.37	3.27	2.20	1.38
Mello, 2000	Aimorés	Monzodiorite	FAM52	51.00	2.94	15.35	-	13.70	0.20	3.51	7.41	3.22	2.19	1.40
Mello, 2000	Aimorés	Monzodiorite	FAM85	51.62	2.66	16.05	-	12.71	0.19	2.88	7.29	3.23	2.43	1.24
Mello, 2000	Aimorés	Tonalite to granodiorite	FAM21G	62.94	0.78	16.22	-	6.06	0.10	1.76	4.47	3.35	2.04	0.22
Mello, 2000	Aimorés	Tonalite to granodiorite	FAM21	63.66	0.83	16.58	-	6.63	0.12	1.92	4.62	3.36	1.82	0.24
Mello, 2000	Aimorés	Tonalite to granodiorite	FAM21D	64.73	0.76	16.25	-	5.98	0.10	1.80	4.49	3.32	1.96	0.21
Mello, 2000	Aimorés	Qtz monzodiorite titanite-bearing	FAM71	55.41	2.15	16.77	-	9.14	0.13	2.94	5.79	3.46	3.24	0.80
Mello, 2000	Aimorés	Qtz monzodiorite titanite-bearing	FAM47	55.78	2.33	16.41	-	9.68	0.14	2.30	5.50	2.96	2.84	0.95
Mello, 2000	Aimorés	Qtzo monzonite	FAM10	57.34	1.65	15.25	-	10.77	0.18	1.69	4.56	3.43	3.74	0.67
Mello, 2000	Aimorés	Qtzo monzonite	FAM84D	60.69	1.40	15.39	-	9.73	0.16	1.39	3.93	3.43	3.88	0.57
Mello, 2000	Aimorés	Qtzo monzonite	FAM84E	62.57	1.14	15.62	-	7.74	0.13	1.14	3.32	3.34	4.89	0.42
Mello, 2000	Aimorés	Qtzo monzonite	FAM4L	62.60	1.10	15.50	-	7.34	0.12	1.09	3.23	3.40	4.86	0.42
Mello, 2000	Aimorés	Qtzo monzonite	FAM84F	62.71	1.03	15.98	-	7.14	0.11	1.00	3.32	3.56	4.98	0.40
Mello, 2000	Aimorés	Qtzo monzonite	FAM4	62.84	0.76	16.75	-	5.33	0.09	0.83	2.86	3.48	5.79	0.30
Mello, 2000	Aimorés	Qtzo monzonite	FAM4I	62.96	0.83	16.35	-	6.11	0.09	1.63	3.31	3.21	5.24	0.32
Mello, 2000	Aimorés	Qtzo monzonite	FAM4J	63.35	0.90	15.37	-	6.00	0.10	0.93	2.71	3.20	4.98	0.34
Mello, 2000	Aimorés	Qtzo monzonite	FAM4K	63.78	0.94	15.89	-	6.24	0.10	0.88	3.33	3.35	4.98	0.38
Mello, 2000	Aimorés	Qtzo monzonite	FAM4H	63.80	0.96	15.64	-	6.27	0.10	0.95	2.95	3.23	5.24	0.38
Mello, 2000	Aimorés	Qtzo monzonite	FAM4G	64.55	0.87	15.62	-	5.83	0.09	0.85	2.64	3.19	5.90	0.37
Mello, 2000	Aimorés	Granite	FAM84C	67.43	0.67	15.42	-	4.67	0.08	0.71	2.70	3.32	5.13	0.31

Data Source	G5 local name	Rock-type	Sample	SiO_2	TiO_2	Al_2O_3	FeO	Fe_2O_3	MnO	MgO	CaO	Na_2O	K_2O	P_2O_5
Mello, 2000	Aimorés	Qtz monzodiorite	FAM25	62.59	1.22	14.82	-	8.55	0.14	1.24	3.47	3.02	4.32	0.47
Mello, 2000	Aimorés	Granite	FAM24A	64.27	0.84	15.27	-	5.68	0.09	0.96	2.60	3.10	5.12	0.34
Mello, 2000	Aimorés	Granite	FAM5A	65.11	0.89	15.43	-	5.91	0.09	0.98	2.64	3.12	5.09	0.34
Mello, 2000	Aimorés	Granite	FAM9B	72.76	0.24	14.81	-	1.76	0.03	0.50	1.32	2.74	5.90	0.08
Mello, 2000	Aimorés	Granite	FAM1	73.08	0.21	14.11	-	1.81	0.02	0.47	1.09	2.52	5.60	0.13
Mello, 2000	Aimorés	Granite	FAM9A	74.65	0.28	13.36	-	2.44	0.04	0.53	1.17	2.45	5.34	0.09
Mello, 2000	Lagoa Preta	Leucogabbro	MLP1	43.01	0.05	24.26	-	7.41	0.09	13.08	12.60	0.33	0.04	0.00
Mello, 2000	Lagoa Preta	Diorite	MLP4	47.64	2.93	14.43	-	18.17	0.32	3.47	8.44	3.24	0.52	1.45
Mello, 2000	Ibituba	Qtzo monzonite	I4	57.02	1.93	15.98	-	9.31	0.15	2.40	5.51	3.35	3.96	0.82
Ludka and Wiedemann-Leonardos, 2000	Amparo	Coronitic rock	A2	41.46	0.17	15.98	10.29	2.29	0.15	20.73	8.16	1.11	0.08	0.04
Ludka and Wiedemann-Leonardos, 2000	Amparo	Coronitic rock	A6.2	42.06	0.12	19.09	8.54	2.45	0.13	16.07	9.69	0.99	0.06	0.03
Ludka and Wiedemann-Leonardos, 2000	Amparo	Coronitic rock	A8.1	43.40	0.24	18.01	8.09	2.49	0.14	14.73	10.66	1.06	0.09	0.04
Ludka and Wiedemann-Leonardos, 2000	Jacutinga	Gabbro-norite	J470	46.46	1.27	17.57	8.32	3.60	0.18	8.60	11.25	1.17	0.23	0.10
Ludka and Wiedemann-Leonardos, 2000	Jacutinga	Gabbro-norite	J471	45.72	2.08	18.34	8.89	3.84	0.18	7.24	11.11	1.29	0.21	0.39
Ludka and Wiedemann-Leonardos, 2000	Jacutinga	Gabbro-norite	J472	44.70	1.83	18.20	9.56	4.12	0.21	6.87	11.04	1.72	0.31	0.36
Ludka and Wiedemann-Leonardos, 2000	Jacutinga	Gabbro-norite	J475	41.90	2.50	15.00	10.70	7.80	0.24	7.40	11.90	1.10	0.07	0.06
Ludka and Wiedemann-Leonardos, 2000	Itaoca	Gabbro-norite	Ita25	46.82	0.75	22.63	5.15	2.39	0.15	5.64	15.13	0.64	0.22	0.01

Data Source	G5 local name	Rock-type	Sample	SiO_2	TiO_2	Al_2O_3	FeO	Fe_2O_3	MnO	MgO	CaO	Na_2O	K_2O	P_2O_5
Ludka and Wiedemann-Leonardos, 2000	Itaoca	Coronitic rock	Ita31	45.88	0.96	21.02	7.66	2.29	0.12	6.94	12.55	1.93	0.11	0.33
Ludka and Wiedemann-Leonardos, 2000	Itaoca	Piroxineto	Ita34	48.39	0.57	6.47	6.27	4.20	0.34	15.93	14.41	1.34	0.26	0.38
Ludka and Wiedemann-Leonardos, 2000	Itaoca	Piroxineto	Ita95	48.54	0.59	8.78	6.93	3.72	0.14	13.52	15.65	1.49	0.49	0.40
De Campos et al., 2004	Santa Angélica	Gabbro	SA1.1	45.24	2.83	16.66	8.03	5.35	0.19	5.87	7.71	2.83	2.64	1.34
De Campos et al., 2004	Santa Angélica	Gabbro	SA1.2	42.35	3.39	15.00	8.41	5.60	0.20	6.23	8.07	3.79	2.74	2.01
De Campos et al., 2004	Santa Angélica	Gabbro	SA1.3	48.41	2.08	15.49	5.18	3.45	0.13	7.42	7.52	4.08	3.50	1.39
De Campos et al., 2004	Santa Angélica	Gabbro	SA1.4	48.95	2.45	16.34	5.94	3.96	0.12	5.80	6.91	3.21	3.04	2.12
De Campos et al., 2004	Castelo	Gabbro	CA1.1	50.19	2.96	13.31	6.49	4.33	0.14	5.50	6.35	3.96	3.09	2.12
De Campos et al., 2004	Castelo	Diorite	CA1.2	53.34	2.64	14.33	5.52	3.68	0.11	5.11	5.70	2.04	4.14	1.78
De Campos et al., 2004	Venda Nova	Gabbro	VN1.1	47.47	2.29	18.00	5.54	3.69	0.16	5.26	6.59	4.54	4.20	1.32
De Campos et al., 2004	Venda Nova	Gabbro	VN1.2	43.07	2.49	15.12	6.71	4.48	0.26	8.31	11.44	3.28	1.99	1.19
De Campos et al., 2004	Venda Nova	Gabbro	VN1.3	48.97	2.47	15.63	5.85	3.90	0.20	5.77	7.37	4.38	2.59	1.44
De Campos et al., 2004	Santa Angélica	Diorite	SA2.1	54.74	2.11	16.95	5.13	3.42	0.10	3.36	5.28	2.54	3.86	1.24

Data Source	G5 local name	Rock-type	Sample	SiO_2	TiO_2	Al_2O_3	FeO	Fe_2O_3	MnO	MgO	CaO	Na_2O	K_2O	P_2O_5
De Campos et al., 2004	Santa Angélica	Diorite	SA2.2	52.38	3.07	14.37	5.85	3.90	0.13	4.26	5.75	3.57	3.22	1.85
De Campos et al., 2004	Santa Angélica	Diorite	SA2.3	53.23	3.03	14.67	5.96	3.97	0.13	4.33	5.72	2.79	3.23	1.74
De Campos et al., 2004	Santa Angélica	Diorite	SA2.4	52.69	2.44	14.84	5.56	3.71	0.12	5.63	6.69	2.63	3.37	1.60
De Campos et al., 2004	Castelo	Diorite	CA2.1	57.25	1.87	13.42	5.93	3.95	0.14	4.21	5.57	1.57	3.48	1.69
De Campos et al., 2004	Castelo	Diorite	CA2.2	58.17	2.18	13.63	5.71	381.00	0.14	3.86	5.35	0.99	3.27	1.29
De Campos et al., 2004	Castelo	Diorite	CA2.3	57.58	2.18	13.65	5.91	3.94	0.14	3.66	5.43	0.99	3.82	1.24
De Campos et al., 2004	Venda Nova	Gabbro	VN2.1	50.88	1.30	15.26	5.22	3.48	0.13	8.63	10.76	1.80	1.06	0.65
De Campos et al., 2004	Venda Nova	Diorite	VN2.2	56.30	1.69	19.33	3.25	2.17	0.09	1.95	4.14	4.39	5.45	0.52
De Campos et al., 2004	Venda Nova	Diorite	VN2.3	52.49	1.91	19.61	3.30	2.20	0.06	3.28	3.53	4.69	4.70	1.13
De Campos et al., 2004	Santa Angélica	Diorite	SA3.1	56.76	2.28	14.54	4.88	3.26	0.14	3.57	4.96	3.67	3.47	1.19
De Campos et al., 2004	Santa Angélica	Diorite	SA3.2	56.09	2.11	14.51	5.26	3.51	0.14	4.19	5.69	2.67	3.07	1.09
De Campos et al., 2004	Santa Angélica	Diorite	SA3.3	57.10	1.29	17.73	3.76	2.51	0.59	3.22	4.51	3.47	4.16	0.64
De Campos et al., 2004	Santa Angélica	Diorite	SA3.4	57.56	1.69	17.24	4.12	2.75	0.06	2.05	3.68	3.07	5.50	0.70
De Campos et al., 2004	Castelo	Diorite	CA3.1	61.89	1.74	14.86	5.76	1.02	0.09	2.26	2.40	1.29	5.03	1.08
De Campos et al., 2004	Castelo	Granite	CA3.2	66.97	0.74	15.28	3.68	0.65	0.07	1.45	2.40	2.13	4.89	0.31

Data Source	G5 local name	Rock-type	Sample	SiO_2	TiO_2	Al_2O_3	FeO	Fe_2O_3	MnO	MgO	CaO	Na_2O	K_2O	P_2O_5
De Campos et al., 2004	Venda Nova	Diorite	VN3.1	58.57	0.93	22.62	2.36	1.57	0.06	0.95	2.20	1.89	6.53	0.32
De Campos et al., 2004	Venda Nova	Diorite	VN3.2	59.07	1.30	19.03	2.80	1.86	0.07	1.30	3.19	3.49	6.38	0.40
De Campos et al., 2004	Venda Nova	Diorite	VN3.3	62.54	0.82	17.51	3.31	2.21	0.06	1.61	5.13	3.50	1.18	0.15
De Campos et al., 2004	Santa Angélica	Granite	SA4.1	71.81	0.42	13.86	1.36	0.90	0.04	0.69	2.68	3.34	3.47	0.10
De Campos et al., 2004	Santa Angélica	Granite	SA4.2	76.20	0.15	12.44	0.71	0.47	0.04	0.36	1.00	3.93	4.33	0.02
De Campos et al., 2004	Castelo	Granite	CA4.1	68.15	0.80	14.23	2.49	1.66	0.11	0.85	2.73	2.33	5.38	0.36
De Campos et al., 2004	Castelo	Granite	CA4.3	70.78	0.53	14.47	1.68	1.12	0.06	0.52	1.55	2.18	6.02	0.09
De Campos et al., 2004	Castelo	Granite	CA4.4	72.44	0.35	13.30	1.45	0.97	0.03	0.42	1.49	1.94	5.90	0.12
De Campos et al., 2004	Venda Nova	Granite	VN4.1	70.06	0.55	16.57	0.83	0.55	0.05	0.71	1.21	2.16	6.23	0.12
De Campos et al., 2004	Venda Nova	Granite	VN4.2	74.01	0.20	14.77	0.68	0.45	0.02	0.31	0.57	1.64	5.92	0.13
De Campos et al., 2004	Venda Nova	Granite	VN4.3	74.63	0.18	14.09	0.65	0.43	0.01	0.29	0.34	1.58	5.45	0.06
De Campos et al., 2004	Santa Angélica	Granite	SA5.2	68.14	0.70	14.82	4.16	0.73	0.08	0.99	4.38	2.79	1.99	0.19
De Campos et al., 2004	Santa Angélica	Granite	SA5.3	68.72	0.70	14.74	2.90	0.51	0.09	0.41	2.79	2.00	5.58	0.14
De Campos et al., 2004	Santa Angélica	Granite	SA5.4	72.45	0.66	11.87	2.62	0.46	0.05	0.84	1.84	2.83	4.94	0.18
De Campos et al., 2004	Castelo	Granite	CA5.1	71.99	0.36	14.04	2.09	0.37	0.06	0.55	1.44	2.29	5.92	0.18

Data Source	G5 local name	Rock-type	Sample	SiO_2	TiO_2	Al_2O_3	FeO	Fe_2O_3	MnO	MgO	CaO	Na_2O	K_2O	P_2O_5
De Campos et al., 2004	Castelo	Granite	CA5.2	72.12	0.47	13.81	2.31	0.41	0.06	0.78	1.46	1.49	5.83	0.17
De Campos et al., 2004	Castelo	Granite	CA5.3	74.17	0.18	13.54	1.35	0.24	0.03	0.35	1.29	3.09	4.93	0.06
Ludka et al., 1998	G5 - Venda Nova	Syeno-monzonite	-	57.60	1.04	18.96	2.45	1.76	0.09	1.57	4.11	4.40	6.02	0.27
Ludka et al., 1998	Venda Nova	Syeno-monzonite	-	56.67	1.21	18.64	2.13	2.86	0.10	1.78	4.38	4.40	5.74	0.33
Ludka et al., 1998	Venda Nova	Monzodiorite	-	53.03	2.74	14.94	3.82	6.76	0.15	3.24	6.15	3.34	3.41	1.41
Ludka et al., 1998	Venda Nova	Monzodiorite	-	52.75	2.43	15.24	5.08	4.92	0.15	3.94	6.66	3.52	3.15	1.21
Ludka et al., 1998	Venda Nova	Gabbro-norite	-	46.10	2.30	15.50	6.80	5.10	0.17	6.40	10.30	2.50	1.50	1.07
Ludka et al., 1998	Venda Nova	Gabbro-norite	-	48.44	3.00	15.56	5.91	3.95	0.14	6.67	10.03	2.55	1.41	1.56
Ludka et al., 1998	Venda Nova	Gabbro-norite	-	50.38	1.44	15.28	6.23	2.37	0.17	7.24	10.33	2.90	1.19	0.65
Ludka et al., 1998	Venda Nova	Gabbro-norite	-	49.75	1.77	15.10	6.15	2.97	0.16	7.71	10.64	2.70	1.16	0.98
Offman, 1990 in Ludka et al., 1998	Venda Nova	Allanite granite	-	71.40	0.53	13.63	1.79	1.49	0.02	0.49	1.42	2.59	6.37	0.22
Offman, 1990 in Ludka et al., 1998	Venda Nova	Allanite granite	-	70.14	0.62	13.58	2.05	1.45	0.05	0.63	1.76	2.67	6.42	0.18
Offman, 1990 in Ludka et al., 1998	Venda Nova	Allanite granite	-	-	-	-	-	-	-	-	-	-	-	-
Offman, 1990 in Ludka et al., 1998	Venda Nova	Granite	-	72.67	0.46	13.11	0.79	1.37	0.07	0.50	0.95	3.32	5.45	0.10
Offman, 1990 in Ludka et al., 1998	Venda Nova	Leucogranite	-	74.52	0.18	13.34	0.58	1.43	0.06	0.37	2.34	3.08	3.30	0.04
Wiedemann et al., 2002	Várzea Alegre	Basic rock	VA-1	47.57	2.95	19.14	-	11.16	0.15	3.94	10.06	3.17	0.77	1.38
Wiedemann et al., 2002	Várzea Alegre	Basic rock	VA-2	50.84	1.51	17.95	-	9.06	0.13	6.30	8.36	2.88	1.30	0.70
Wiedemann et al., 2002	Várzea Alegre	Basic rock	VA-3	51.27	3.72	13.87	-	12.51	0.18	3.81	7.53	2.30	2.42	2.00
Wiedemann et al., 2002	Várzea Alegre	Intermediate rock	VA-4	53.70	2.51	15.29	-	10.50	0.15	3.57	6.45	2.82	2.75	1.01

Data Source	G5 local name	Rock-type	Sample	SiO_2	TiO_2	Al_2O_3	FeO	Fe_2O_3	MnO	MgO	CaO	Na_2O	K_2O	P_2O_5
Wiedemann et al., 2002	Várzea Alegre	Intermediate rock	VA-5	52.64	2.30	15.66	-	10.13	0.14	4.20	7.24	3.10	2.37	1.01
Wiedemann et al., 2002	Várzea Alegre	Intermediate rock	VA-6	52.83	2.57	14.83	-	10.77	0.15	3.85	7.06	2.91	2.35	1.13
Wiedemann et al., 2002	Várzea Alegre	Intermediate rock	VA-7	64.52	1.05	15.46	-	4.54	0.50	1.32	2.78	2.77	5.55	0.40
Wiedemann et al., 2002	Várzea Alegre	Acid rock	VA-8	68.48	0.67	14.71	-	4.04	0.07	0.76	1.88	3.19	4.74	0.40
Wiedemann et al., 2002	Várzea Alegre	Acid rock	VA-9	71.49	0.30	14.69	-	2.35	0.03	0.32	1.40	3.16	6.05	0.15
Wiedemann et al., 2002	Várzea Alegre	Intermediate rock	VAc-1	53.99	1.97	16.58	-	11.28	0.18	2.76	6.22	3.28	2.02	0.95
Wiedemann et al., 2002	Várzea Alegre	Intermediate rock	Vac-2	56.98	1.66	15.82	-	9.74	0.16	2.39	4.87	3.16	3.33	0.77
Wiedemann et al., 2002	Várzea Alegre	Intermediate rock	VAc-3	59.00	1.50	15.10	-	9.30	0.14	1.80	5.00	3.50	3.40	0.66
Wiedemann et al., 2002	Várzea Alegre	Intermediate rock	Vac-4	62.39	0.89	16.14	-	6.45	0.15	1.02	3.64	3.21	4.14	0.39
Wiedemann et al., 2002	Várzea Alegre	Intermediate rock	Vac-5	64.90	0.94	15.10	-	5.57	0.11	0.99	3.60	3.50	3.60	0.42
Wiedemann et al., 2002	Santa Angélica	Basic rock	SA-1	42.35	3.39	15.00	8.41	5.60	0.20	6.23	8.07	3.79	2.74	2.01
Wiedemann et al., 2002	Santa Angélica	Basic rock	SA-2	48.95	2.45	16.34	5.94	3.96	0.12	5.80	6.91	3.21	3.04	2.12
Wiedemann et al., 2002	Santa Angélica	Intermediate rock	SA-3	54.74	2.11	16.95	5.13	3.42	0.10	3.36	5.28	2.54	3.86	1.24
Wiedemann et al., 2002	Santa Angélica	Intermediate rock	SA-4	52.69	2.44	14.84	5.56	3.71	0.12	5.63	6.69	2.63	3.37	1.60
Wiedemann et al., 2002	Santa Angélica	Intermediate rock	SA-5	56.09	2.11	14.51	5.26	3.51	0.14	4.19	5.69	2.67	3.07	1.09

Data Source	G5 local name	Rock-type	Sample	SiO_2	TiO_2	Al_2O_3	FeO	Fe_2O_3	MnO	MgO	CaO	Na_2O	K_2O	P_2O_5
Wiedemann et al., 2002	Santa Angélica	Intermediate rock	SA-6	57.10	1.29	17.73	3.76	2.51	0.59	3.22	4.51	3.47	4.16	0.64
Wiedemann et al., 2002	Castelo	Basic rock	CA-1	50.19	2.96	13.31	6.49	4.33	0.14	5.50	6.35	3.96	3.09	2.12
Wiedemann et al., 2002	Castelo	Intermediate rock	CA-2	53.34	2.64	14.33	5.52	3.68	0.11	5.11	5.70	2.04	4.14	1.78
Wiedemann et al., 2002	Castelo	Intermediate rock	CA-3	58.17	2.18	13.63	5.71	3.81	0.14	3.86	5.35	0.99	3.27	1.29
Wiedemann et al., 2002	Castelo	Intermediate rock	CA-4	57.58	2.18	13.65	5.91	3.94	0.14	3.66	5.43	0.99	3.82	1.24
Wiedemann et al., 2002	Castelo	Intermediate rock	CA-5	61.89	1.74	14.86	5.76	1.02	0.09	2.26	2.40	1.29	5.03	1.08
Wiedemann et al., 2002	Castelo	Acid rock	CA-6	66.97	0.74	15.28	3.68	0.65	0.07	1.45	2.40	2.13	4.89	0.31
Wiedemann et al., 2002	Castelo	Acid rock	CA-7	72.12	0.47	13.81	2.31	0.41	0.06	0.78	1.46	1.49	5.83	0.17
Wiedemann et al., 2002	Castelo	Acid rock	CA-8	72.44	0.35	13.30	1.45	0.97	0.03	0.42	1.49	1.94	5.90	0.12
Wiedemann et al., 2002	Santa Angélica	Acid rock	SA-7	71.81	0.42	13.86	1.36	0.90	0.04	0.69	2.68	3.34	3.47	0.10
Wiedemann et al., 2002	Santa Angélica	Acid rock	SA-8	76.20	0.15	12.44	0.71	0.47	0.04	0.36	1.00	3.93	4.33	0.02
Wiedemann et al., 2002	Santa Angélica	Acid rock	SA-9	72.45	0.66	11.87	2.62	0.46	0.05	0.84	1.84	2.83	4.94	0.18
Wiedemann et al., 2002	Mimoso do Sul	High-calk-alkaline/alkaline rocks	MI-1	64.81	0.43	17.39	1.51	0.55	0.28	0.42	2.32	2.83	8.31	0.22
Wiedemann et al., 2002	Mimoso do Sul	High-calk-alkaline/alkaline rocks	MI-2	56.55	1.13	17.29	4.30	2.35	0.14	3.70	5.37	1.81	5.27	0.72

Data Source	G5 local name	Rock-type	Sample	SiO_2	TiO_2	Al_2O_3	FeO	Fe_2O_3	MnO	MgO	CaO	Na_2O	K_2O	P_2O_5
Wiedemann et al., 2002	Mimoso do Sul	High-calk-alkaline/alkaline rocks	MI-3	46.66	2.22	12.35	5.66	4.62	0.28	7.30	7.42	4.59	5.14	2.04
Wiedemann et al., 2002	Mimoso do Sul	High-calk-alkaline/alkaline rocks	MI-4	38.11	2.27	9.02	10.31	4.93	0.21	10.28	14.78	1.69	3.09	2.37
Wiedemann et al., 2002	Conceição do Muqui	High-calk-alkaline/alkaline rocks	CM-1	71.34	0.41	13.36	1.41	1.04	0.05	0.18	1.75	2.83	5.29	0.17
Wiedemann et al., 2002	Conceição do Muqui	High-calk-alkaline/alkaline rocks	CM-2	66.05	0.67	14.33	2.36	0.69	0.08	1.02	3.22	4.23	5.59	0.14
Wiedemann et al., 2002	Conceição do Muqui	High-calk-alkaline/alkaline rocks	CM-3	52.27	1.33	15.69	3.41	2.67	0.09	2.98	3.20	4.03	4.84	0.84
Wiedemann et al., 2002	Conceição do Muqui	High-calk-alkaline/alkaline rocks	CM-4	45.83	2.60	15.72	5.99	5.10	0.09	6.01	7.41	2.57	4.92	2.81
Zanon et al., 2015	Santa Angélica	Diorite	D5MIX23A	56.39	2.08	15.62	10.09	-	0.11	2.22	4.85	3.52	4.22	0.65
Zanon et al., 2015	Santa Angélica	Diorite	M5G9	52.31	2.55	15.74	10.64	-	0.14	3.95	6.13	3.04	3.50	1.38
Zanon et al., 2015	Santa Angélica	Gabbro	M5G17	51.80	2.96	14.93	11.24	-	0.15	4.12	7.00	3.21	3.54	1.72
Zanon et al., 2015	Santa Angélica	Diorite	F5G38	61.28	1.29	16.41	6.34	-	0.09	1.45	3.38	3.48	6.03	0.42
Zanon et al., 2015	Santa Angélica	Diorite	H18	59.37	1.65	14.73	7.54	-	0.11	1.81	3.80	3.20	4.87	0.59
Zanon et al., 2015	Santa Angélica	Diorite	H517	58.32	1.96	16.53	8.63	-	0.09	1.85	4.00	3.71	5.17	0.58
Zanon et al., 2015	Santa Angélica	Diorite	H16A	55.77	2.50	15.63	9.86	-	0.13	2.58	4.98	3.23	4.43	1.11
Zanon et al., 2015	Santa Angélica	Diorite	M5G16	52.43	1.89	16.33	10.28	-	0.12	5.06	7.41	3.05	2.88	0.86
Zanon et al., 2015	Santa Angélica	Granite	F5G15	65.10	0.74	16.24	4.32	-	0.08	0.77	1.95	4.11	7.01	0.21
Zanon et al., 2015	Santa Angélica	Gabbro	MP19	51.96	2.00	14.64	9.84	-	0.15	5.23	6.32	3.16	2.73	0.90
Paes et al., 2010	Medina		CP-334	71.20	0.60	14.40	2.10	-	0.00	0.60	1.20	2.70	6.00	0.20
Paes et al., 2010	Medina		PJ-404	70.40	0.60	13.90	3.20	-	0.00	0.50	1.30	2.40	6.00	0.30

Data Source	G5 local name	Rock-type	Sample	SiO_2	TiO_2	Al_2O_3	FeO	Fe_2O_3	MnO	MgO	CaO	Na_2O	K_2O	P_2O_5
Paes et al., 2010	Medina		CP-12	71.10	0.50	14.20	3.00	-	0.10	0.50	1.40	2.90	5.70	0.30
Paes et al., 2010	Medina		CP-005B	72.30	0.40	13.60	2.80	-	0.00	0.30	1.50	2.40	5.60	0.20
Paes et al., 2010	Medina		CP-358	72.80	0.40	13.60	3.00	-	0.00	0.30	1.40	2.60	5.30	0.20
Paes et al., 2010	Medina		CP-005A	73.40	0.30	13.40	2.60	-	0.00	0.20	1.30	2.40	6.00	0.20
Paes et al., 2010	Medina		CP-119A	74.80	0.30	12.60	2.60	-	0.00	0.30	1.20	2.60	5.20	0.10
Paes et al., 2010	Medina		CP-019	75.00	0.30	12.50	2.60	-	0.00	0.20	1.20	1.60	5.20	0.10
Paes et al., 2010	Medina		CP-361	73.50	0.50	13.00	3.00	-	0.00	0.50	1.60	3.00	4.40	0.30
Paes et al., 2010	Medina		CH-530	71.10	0.40	14.10	2.70	-	0.00	0.30	1.40	2.50	6.30	0.20
Paes et al., 2010	Medina		CP-353	70.70	0.60	13.80	3.90	-	0.10	0.50	1.50	2.60	5.70	0.30
Paes et al., 2010	Medina		CP-009A	73.20	0.30	13.50	2.50	-	0.00	0.30	1.10	2.60	5.90	0.10
Paes et al., 2010	Medina		CP-009B	74.30	0.20	13.60	1.60	-	0.00	0.20	1.00	2.80	6.00	0.10
Paes et al., 2010	Medina		CP-015A	72.10	0.70	12.90	3.60	-	0.10	0.70	1.90	2.80	4.40	0.30
Paes et al., 2010	Medina		CP-051	73.00	0.30	14.80	1.40	-	0.00	0.30	0.90	3.70	5.60	0.10
Paes et al., 2010	Medina		CP-003	67.50	0.90	14.40	4.80	-	0.10	0.80	2.40	2.70	5.20	0.60
Paes et al., 2010	Medina		CP-023	66.20	1.00	14.30	5.00	-	0.10	1.00	2.30	2.40	6.10	0.80
Paes et al., 2010	Medina		CP-118	64.40	1.50	14.30	6.50	-	0.10	1.30	3.00	2.60	4.90	0.70
Paes et al., 2010	Medina		CP-001	67.00	1.10	14.00	5.50	-	0.10	1.00	2.70	2.50	4.70	0.70
Serrano et al., 2018	Medina	Granite	M61B	72.90	0.40	13.30	2.30	-	0.00	0.30	0.80	2.40	6.10	0.10
Serrano et al., 2018	Medina	Granite	R13A	68.30	0.80	14.40	4.20	-	0.10	0.60	1.90	2.70	5.40	0.40
Paes et al., 2010	Caladão		PJ-302B	70.20	0.60	14.40	5.30	-	0.00	0.60	1.20	2.60	6.00	0.30
Paes et al., 2010	Caladão		PJ-389	70.90	0.40	14.80	3.20	-	0.00	0.50	1.20	3.30	5.70	0.20
Paes et al., 2010	Córrego do Calção		CH-89	70.10	0.50	14.60	4.60	-	0.00	0.50	1.00	2.80	6.20	0.30
Paes et al., 2010	Córrego do Calção		CH-90	69.20	0.60	14.40	5.20	-	0.00	0.60	1.40	2.80	6.10	0.30
Paes et al., 2010	Córrego do Calção		CH-91	71.44	0.27	15.50	0.93	1.82	0.02	0.40	1.33	4.45	4.19	0.12
Paes et al., 2010	Emparedado		CP-170	72.30	0.40	13.10	3.70	-	0.10	0.60	1.70	3.60	4.60	0.30
Paes et al., 2010	Emparedado		CP-175A	71.23	0.23	15.06	0.61	1.46	0.04	0.40	1.12	3.62	6.11	0.18
Paes et al., 2010	Emparedado		CP-251	69.17	0.50	14.79	0.85	2.75	0.04	0.85	1.82	3.33	5.27	0.31
Paes et al., 2010	Fazenda Liberdade		PJ-185	70.40	0.50	14.60	3.90	-	0.00	0.60	1.20	2.70	6.30	0.20
Paes et al., 2010	Fazenda Liberdade		PJ-192	70.60	0.50	14.80	4.50	-	0.00	0.60	1.20	2.50	6.30	0.30
Paes et al., 2010	Fazenda Liberdade		PJ-196	67.90	0.70	14.90	8.00	-	0.10	1.50	1.30	2.40	5.00	0.20

Data Source	G5 local name	Rock-type	Sample	SiO_2	TiO_2	Al_2O_3	FeO	Fe_2O_3	MnO	MgO	CaO	Na_2O	K_2O	P_2O_5
Paes et al., 2010	Fazenda Liberdade		PJ-250	68.10	0.80	14.90	6.00	-	0.10	1.00	1.60	2.80	5.70	0.40
Paes et al., 2010	Fazenda Liberdade		PJ-272	72.20	0.40	14.00	4.10	-	0.00	0.60	0.90	2.80	5.40	0.20
Paes et al., 2010	Fazenda Liberdade		PJ-280	70.02	0.61	14.17	2.40	3.58	0.03	0.59	1.19	2.61	6.03	0.27
Paes et al., 2010	Fazenda Liberdade		PJ-306	69.18	0.68	14.18	2.60	4.01	0.04	0.67	1.31	2.65	5.76	0.31
Paes et al., 2010	General Dutra		CH-021	69.30	0.50	15.10	4.50	-	0.00	0.70	1.20	3.10	5.90	0.20
Paes et al., 2010	General Dutra		CH-290	64.90	1.20	14.90	8.10	-	0.10	1.50	2.80	3.40	3.50	0.60
Paes et al., 2010	General Dutra		CH-574	74.10	0.50	12.50	5.10	-	0.10	0.50	1.20	2.50	4.90	0.20
Paes et al., 2010	General Dutra		CH-600	67.26	0.75	15.24	2.90	3.98	0.04	0.88	1.83	2.71	5.74	0.33
Paes et al., 2010	Landim		CH-010	71.40	0.40	14.10	3.50	-	0.00	0.60	1.90	3.70	3.90	0.20
Paes et al., 2010	Landim		CH-511	71.55	0.27	14.46	0.54	1.22	0.01	0.31	0.23	2.68	7.74	0.17
Paes et al., 2010	Landim		CH-514	67.80	0.60	15.00	4.30	-	0.00	0.90	1.90	3.50	5.00	1.30
Paes et al., 2010	Pau de Canoa		CH-310	68.92	0.70	15.10	2.40	3.30	0.04	0.82	1.58	2.73	5.52	0.12
Paes et al., 2010	Pau de Canoa		CH-389	67.60	0.80	15.30	6.50	-	0.00	1.10	1.50	3.00	5.40	0.40
Paes et al., 2010	Pedra Azul		CP-167	68.80	0.80	14.50	4.80	-	0.10	0.80	2.10	3.10	5.80	0.40
Paes et al., 2010	Pedra Azul		CP-215A	65.80	1.00	15.30	6.00	-	0.10	1.40	2.80	3.60	4.50	0.60
Paes et al., 2010	Pedra Azul		CP-228A	70.28	0.30	15.68	0.57	1.26	0.01	0.33	2.01	3.36	5.44	0.12
Paes et al., 2010	Pedra Grande		PJ-007	68.10	0.80	14.40	6.40	-	0.10	0.90	2.20	2.40	5.10	0.30
Paes et al., 2010	Pedra Grande		PJ-008	67.70	0.90	14.80	5.80	-	0.10	1.10	1.90	2.50	4.90	0.40
Paes et al., 2010	Pedra Grande		PJ-017	67.50	0.90	14.80	6.10	-	0.00	0.90	1.70	2.70	5.80	0.40
Paes et al., 2010	Santa Cruz de Salinas		CH-102	71.40	0.40	14.00	3.80	-	0.00	0.40	1.40	3.20	5.70	0.10
Paes et al., 2010	Santa Cruz de Salinas		CH-108	71.30	0.40	14.20	3.90	-	0.00	0.40	1.20	3.20	5.50	0.10
Paes et al., 2010	Santa Cruz de Salinas		CH-171	72.96	0.16	14.33	0.86	1.47	<0,01	0.18	0.43	2.86	7.01	0.06
Paes et al., 2010	Santa Cruz de Salinas		CH-237	71.70	0.30	14.20	3.20	-	0.00	0.30	1.10	3.20	5.90	0.10
Aranda, 2018	Cláudio Afonso	Monzogranite	P 246-A	49.40	2.60	15.33	-	11.59	0.17	6.30	8.46	3.16	1.98	1.15
Aranda, 2018	Cláudio Afonso	Monzogranite	P 276-A	50.42	2.97	15.31	-	12.42	0.19	3.71	7.33	3.21	2.47	1.36
Aranda, 2018	Cláudio Afonso	Monzodiorite	P 292-B	51.17	2.71	16.80	-	11.92	0.18	3.38	6.49	3.85	3.95	1.18

Data Source	G5 local name	Rock-type	Sample	SiO_2	TiO_2	Al_2O_3	FeO	Fe_2O_3	MnO	MgO	CaO	Na_2O	K_2O	P_2O_5
Aranda, 2018	Cláudio Afonso	Monzogranite	P 292-A	51.36	2.97	14.51	-	11.22	0.17	4.68	7.76	3.14	2.37	1.32
Aranda, 2018	Cláudio Afonso	Monzodiorite	P 277-A	52.35	2.34	16.13	-	10.06	0.15	3.05	6.34	3.40	3.12	1.07
Aranda, 2018	Cláudio Afonso	Jotunite	P 193-B	53.29	2.43	13.79	-	10.89	0.20	2.66	5.78	2.90	3.43	1.12
Aranda, 2018	Cláudio Afonso	Monzodiorite	P 156-A	54.99	2.53	14.96	-	10.73	0.15	3.93	6.59	2.94	2.95	1.11
Aranda, 2018	Cláudio Afonso	Qtz mangerite	P 197-C	55.70	1.67	15.92	-	9.09	0.08	2.04	4.91	3.76	3.52	0.71
Aranda, 2018	Cláudio Afonso	Qtz monzonite	P 288	59.68	1.18	15.76	-	7.07	0.12	1.41	4.11	3.43	3.90	0.49
Aranda, 2018	Cláudio Afonso	Qtz monzonite	P 295-B	62.28	1.55	14.32	-	7.96	0.12	1.73	4.05	3.45	3.57	0.52
Aranda, 2018	Cláudio Afonso	Qtz monzonite	P 285-B	62.37	1.15	15.09	-	6.62	0.12	1.40	3.69	3.17	4.57	0.47
Aranda, 2018	Cláudio Afonso	Qtz monzonite	P 206-D	62.81	0.90	15.80	-	5.21	0.10	1.02	4.07	3.37	4.12	0.35
Aranda, 2018	Cláudio Afonso	Qtz monzonite	P 98	63.65	1.07	14.96	-	5.24	0.08	1.33	3.36	3.21	5.15	0.41
Aranda, 2018	Cláudio Afonso	Qtz monzonite	P 297	65.27	0.86	16.06	-	4.13	0.06	1.00	2.67	3.43	6.01	0.31
Aranda, 2018	Cláudio Afonso	Qtz monzonite	P 296	65.43	1.33	14.58	-	6.86	0.11	1.53	3.60	3.05	4.69	0.49
Aranda, 2018	Cláudio Afonso	Qtz monzonite	P 146-B	66.65	0.94	14.39	-	5.36	0.09	1.17	2.98	3.11	5.00	0.37
Aranda, 2018	Cláudio Afonso	Qtz monzonite	P 291	66.71	1.07	14.50	-	5.35	0.09	1.22	3.07	3.25	4.98	0.39
Aranda, 2018	Cláudio Afonso	Qtz monzonite	P 298	66.77	0.60	16.29	-	4.05	0.07	0.72	2.87	3.78	4.62	0.21
Aranda, 2018	Cláudio Afonso	Qtz monzonite	P 90-A	66.86	0.69	14.44	-	3.97	0.08	0.77	2.17	3.19	5.69	0.26
Aranda, 2018	Cláudio Afonso	Qtz monzonite	P 102	69.08	1.01	13.79	-	5.30	0.09	1.20	2.67	3.13	4.87	0.34
Baltazar et al., 2010	Aimorés	Charnockite	OF174A	72.48	0.27	13.32	-	3.39	0.05	0.18	1.51	2.57	5.51	0.08
Baltazar et al., 2010	Aimorés	Charnockite	OF172A	70.51	0.33	13.76	-	3.28	0.05	0.16	1.53	2.68	6.10	0.10
Baltazar et al., 2010	Aimorés	Charnockite	OF198	62.94	1.31	15.18	-	7.84	0.13	1.48	3.62	2.83	3.49	0.53
Baltazar et al., 2010	Aimorés	Charnockite	SS058	65.12	0.97	15.93	-	5.40	0.08	1.33	3.98	2.93	3.24	0.35
Baltazar et al., 2010	Aimorés	Charnockite	SS023	65.04	0.54	17.09	-	5.32	0.10	1.59	4.80	2.99	1.86	0.21
Baltazar et al., 2010	Aimorés	Charnockite	OF245C	57.97	2.03	14.13	-	11.50	0.17	1.52	4.55	2.67	2.38	1.12
Baltazar et al., 2010	Aimorés	Granite	OF156	63.94	1.51	14.55	-	5.47	0.06	1.29	3.34	2.50	4.89	0.56
Baltazar et al., 2010	Aimorés	Granite	OF166B	66.15	0.69	14.97	-	5.37	0.08	0.63	2.30	3.14	5.53	0.28
Baltazar et al., 2010	Aimorés	Granite	SS094	68.40	0.76	14.78	-	4.04	0.03	0.65	1.62	2.42	5.70	0.21
Baltazar et al., 2010	Aimorés	Mangerite	LC168	59.10	1.48	16.21	-	8.47	0.13	1.55	4.74	3.36	3.77	0.55
Baltazar et al., 2010	Aimorés	Mangerite	OF144	59.80	0.79	17.47	-	7.70	0.14	3.36	5.76	2.50	1.82	0.22
Baltazar et al., 2010	Aimorés	Mangerite	SS027A	59.83	1.46	16.14	-	8.04	0.12	1.54	4.61	3.28	4.17	0.56
Baltazar et al., 2010	Aimorés	Mangerite	OF051	57.99	2.62	13.85	-	10.17	0.14	1.74	4.71	2.50	3.58	1.10

Data Source	G5 local name	Rock-type	Sample	SiO_2	TiO_2	Al_2O_3	FeO	Fe_2O_3	MnO	MgO	CaO	Na_2O	K_2O	P_2O_5
Baltazar et al., 2010	Aimorés	Diorite	OF022	54.97	2.45	14.54	-	9.89	0.13	2.69	6.20	2.72	3.39	0.99
Baltazar et al., 2010	Aimorés	Mangerite	OF074B	67.28	0.75	14.56	-	5.06	0.05	0.56	1.65	2.26	6.08	0.33
Baltazar et al., 2010	Aimorés	Mangerite	OF117	62.51	1.25	14.50	-	8.66	0.14	0.97	3.28	2.76	4.59	0.53
Baltazar et al., 2010	Aimorés	Charnockite	OF23	67.56	0.49	17.36	-	6.29	0.13	1.56	4.50	3.10	2.36	0.12
Baltazar et al., 2010	Aimorés	Charnockite	OF24	64.38	0.53	16.27	-	6.38	0.09	1.45	3.64	2.60	4.12	0.22
Baltazar et al., 2010	Aimorés	Charnockite	OF93	60.89	1.07	16.17	-	9.06	0.08	2.71	4.27	2.91	2.56	0.30
Baltazar et al., 2010	Aimorés	Charnockite	OF98A	68.28	0.34	15.80	-	4.59	0.09	0.99	3.48	3.20	3.05	0.11
Baltazar et al., 2010	Aimorés	Charnockite	OF101	66.09	0.50	16.56	-	5.85	0.12	1.22	4.18	3.14	2.24	0.12
Baltazar et al., 2010	Aimorés	Gabbro	SA16	48.61	4.00	14.06	-	15.22	0.18	3.43	7.84	2.41	2.09	1.75
Pedrosa-Soares et al., 2006	Aimorés	Granite	SC-01A	67.80	0.63	15.35	-	4.66	0.06	0.60	2.46	2.98	5.21	0.23
Pedrosa-Soares et al., 2006	Aimorés	Granite	SC-13	65.17	1.13	15.62	-	5.37	0.07	1.24	3.03	2.97	5.09	0.35
Pedrosa-Soares, et al. 2006	Aimorés	Granite	MQ-03A	69.00	0.89	14.40	-	3.95	0.08	0.64	2.70	2.60	4.69	0.33
Pedrosa-Soares, et al. 2006	Aimorés	Charnockite	MQ-03B	69.10	0.89	14.20	-	3.77	0.08	0.64	2.90	2.55	4.34	0.34
Pedrosa-Soares, et al. 2006	Aimorés	Granite	MQ-04	70.10	0.69	14.60	-	3.11	0.07	1.70	3.63	3.02	2.07	0.07
Pedrosa-Soares, et al. 2006	Aimorés	Charnockite	MQ-81	70.40	0.93	14.20	-	2.35	0.02	0.71	2.01	2.27	5.47	0.32
Pedrosa-Soares, et al. 2006	Aimorés	Charnockite	MQ-123	67.90	0.83	14.50	-	4.61	0.08	0.57	2.32	2.64	5.74	0.39
Pedrosa-Soares, et al. 2006	Aimorés	Charnockite	EC-92	73.50	0.81	14.60	-	4.67	0.01	0.37	0.05	0.13	4.59	0.04
Pedrosa-Soares, et al. 2006	Aimorés	Charnockite	EC-90	73.20	0.32	14.10	-	1.98	0.05	0.16	1.47	2.65	4.97	0.13
Pedrosa-Soares, et al. 2006	Aimorés	Sienogranite	EC-01	70.90	0.75	14.20	-	1.98	0.01	0.54	1.27	2.15	5.80	0.29

Data Source	G5 local name	Rock-type	Sample	SiO_2	TiO_2	Al_2O_3	FeO	Fe_2O_3	MnO	MgO	CaO	Na_2O	K_2O	P_2O_5
Pedrosa-Soares, et al. 2006	Aimorés	Charnockite	EB-89A	69.60	0.60	14.40	-	2.43	0.04	0.75	2.25	2.60	4.64	0.27
Pedrosa-Soares, et al. 2006	Aimorés	Norite	EP-15	53.60	1.50	15.20	-	10.50	0.11	6.12	8.11	2.97	0.42	0.05
Wiedemann et al., 2002	Pedra Azul	Basic rock	PA-I	51.91	3.10	14.95	-	12.56	0.18	3.32	6.25	2.81	2.78	1.59
Wiedemann et al., 2002	Pedra Azul	Basic rock	PA-2	51.41	3.11	14.83	-	12.54	0.18	3.27	6.27	2.62	2.76	1.60
Wiedemann et al., 2002	Pedra Azul	Intermediate rock	PA-3	53.46	2.73	13.95	-	11.13	0.14	2.95	6.32	2.81	2.95	1.54
Wiedemann et al., 2002	Pedra Azul	Intermediate rock	PA-4	59.24	2.15	14.51	-	9.02	0.13	2.25	4.54	2.88	3.74	0.96
Wiedemann et al., 2002	Pedra Azul	Intermediate rock	PA-5	61.81	1.62	14.56	-	7.84	0.11	1.83	3.74	2.83	4.00	0.70
Wiedemann et al., 2002	Pedra Azul	Acid rock	PA-6	67.02	1.02	14.26	-	4.97	0.07	0.87	2.54	2.89	5.27	0.31
Wiedemann et al., 2002	Pedra Azul	Acid rock	PA-7	71.57	0.38	13.71	-	2.98	0.08	0.44	1.14	2.57	5.93	0.11

Data Source	G5 local name	Rock-type	Sample	Ba	Rb	Sr	Zn	Zr	V	Ce	Co	Cs	Cu	Dy	Er	Eu	Ga	Gd	Hf	Ho	La
This work	Aracê	Titanite-allanite-biotite granite	CA-02	1645	203.8	275	94	556	40	492	75.10	1.27	8	16.38	10.03	2.59	18.3	17.80	13.51	3.44	267.90
This work	Vitória	Biotite granite	CA-04	1278	171.9	420	86	784	55	473	148.90	0.33	18	4.07	1.36	1.90	21.5	10.18	20.74	0.56	240.10
This work	Mestre Álvaro	Biotite tonalite	CA-05	268	108.4	231	103	447	115	63	51.60	0.89	8	1.59	0.81	0.92	20.3	2.07	11.68	0.27	36.10

Data Source	G5 local name	Rock-type	Sample	Ba	Rb	Sr	Zn	Zr	V	Ce	Co	Cs	Cu	Dy	Er	Eu	Ga	Gd	Hf	Ho	La
Mendes et al., 2005	Várzea Alegre	Charnockitic rock	VA42	2246	79.0	428	101	819	35	-	-	-	-	-	-	-	20.0	-	22.30	-	-
Mendes et al., 2005	Várzea Alegre	Charnockitic rock	VA164	2593	82.0	458	98	642	31	-	-	-	-	-	-	-	23.0	-	17.10	-	-
Mendes et al., 2005	Várzea Alegre	Charnockitic rock	HR29	2060	110.0	510	105	50	178	89	-	-	-	-	1.57	8.43	30.0	4.23	1000.00	0.78	190.70
Mendes et al., 2005	Várzea Alegre	Charnockitic rock	VA262	2588	84.0	475	102	840	43	127	-	-	-	-	0.94	3.54	19.0	7.21	22.00	5.04	56.18
Mendes et al., 2005	Várzea Alegre	Charnockitic rock	VA244	2101	87.0	437	117	767	88	213	-	-	-	-	1.06	3.26	19.0	9.69	22.00	5.91	100.90
Mendes et al., 2005	Várzea Alegre	Charnockitic rock	VA125	3043	91.0	518	126	915	67	-	-	-	-	-	-	-	23.0	-	22.90	-	-
Mendes et al., 2005	Várzea Alegre	Charnockitic rock	VA16	2594	72.0	534	130	860	57	-	-	-	-	-	-	-	22.0	-	21.80	-	-
Mendes et al., 2005	Várzea Alegre	Charnockitic rock	MP161	3010	79.0	650	65	0	122	8	-	-	-	-	1.38	3.80	30.0	0.66	18.00	1.60	48.98
Mendes et al., 2005	Várzea Alegre	Charnockitic rock	MP128	3400	110.0	531	31	0	182	11	-	-	-	-	1.91	4.95	40.0	0.93	25.00	2.52	58.44
Mendes et al., 2005	Várzea Alegre	Charnockitic rock	VA90	2727	64.0	579	134	724	125	-	-	-	-	-	-	-	21.0	-	18.30	-	-
Mendes et al., 2005	Várzea Alegre	Charnockitic rock	VA264	2154	62.0	581	135	828	106	153	-	-	-	-	1.32	3.73	21.0	9.75	20.50	6.95	67.15
Mendes et al., 2005	Várzea Alegre	Charnockitic rock	VA261	1746	36.0	677	169	1084	121	160	-	-	-	-	1.27	3.46	21.0	9.67	23.00	6.77	70.38
Mendes et al., 2005	Várzea Alegre	Charnockitic rock	MP718	2030	38.0	760	58	70	160	85	-	-	-	-	2.74	10.19	30.0	6.16	1760.00	1.15	140.10
Mendes et al., 2005	Várzea Alegre	Charnockitic rock	MP173	1070	67.0	890	85	54	216	-	-	-	-	-	-	-	28.0	-	600.00	-	-
Mendes et al., 2002	Venda Nova	Norite	VN5	88	-	479	-	106	323	-	-	-	-	-	-	-	24.0	-	-	-	-

Data Source	G5 local name	Rock-type	Sample	Ba	Rb	Sr	Zn	Zr	V	Ce	Co	Cs	Cu	Dy	Er	Eu	Ga	Gd	Hf	Ho	La
Mendes et al., 2002	Venda Nova	Norite	VN22	64	-	475	-	57	290	50	-	-	-	2.91	1.31	1.54	21.0	3.91	-	0.55	18.15
Mendes et al., 2002	Venda Nova	Norite	VN10	53	-	454	-	46	447	-	-	-	-	-	-	-	21.0	-	-	-	-
Mendes et al., 2002	Venda Nova	Norite	VN9	29	-	435	-	76	452	-	-	-	-	-	-	-	22.0	-	-	-	-
Mendes et al., 2002	Venda Nova	Norite	VN7	35	-	439	-	39	377	22	-	-	-	2.22	1.05	0.89	21.0	2.39	-	0.43	8.71
Mendes et al., 2002	Venda Nova	Norite	VN3	130	-	481	-	154	297	-	-	-	-	-	-	-	22.0	-	-	-	-
Mendes et al., 2002	Venda Nova	Norite	VN26	53	-	419	-	71	330	29	-	-	-	2.59	1.08	1.02	19.0	3.03	-	0.48	11.18
Mendes et al., 2002	Venda Nova	Norite	VN8	89	-	418	-	97	381	-	-	-	-	-	-	-	20.0	-	-	-	-
Mendes et al., 2002	Venda Nova	Norite	VN6	159	-	554	-	149	278	23	-	-	-	2.70	1.06	1.06	21.0	3.06	-	0.49	8.44
Mendes et al., 2002	Venda Nova	Norite	VN14	62	-	391	-	38	292	-	-	-	-	-	-	-	17.0	-	-	-	-
Mendes et al., 2002	Venda Nova	Norite	VN11	284	10.0	453	-	139	240	-	-	-	-	-	-	-	23.0	-	-	-	-
Mendes et al., 2002	Venda Nova	Charnoenderbite	VN38	436	19.0	561	-	144	202	41	-	-	-	2.41	1.13	0.88	21.0	2.80	-	0.46	18.98
Mendes et al., 2002	Venda Nova	Charnoenderbite	VN35	382	29.0	459	-	99	198	-	-	-	-	-	-	-	21.0	-	-	-	-
Mendes et al., 2002	Venda Nova	Charnoenderbite	VN17	338	17.0	557	-	113	188	39	-	-	-	2.78	1.48	0.94	20.0	2.71	-	0.55	16.44
Mendes et al., 2002	Venda Nova	Charnoenderbite	VN36	356	19.0	464	-	94	182	-	-	-	-	-	-	-	20.0	-	-	-	-
Mendes et al., 2002	Venda Nova	Charnoenderbite	VN20	417	22.0	506	-	114	183	-	-	-	-	-	-	-	21.0	-	-	-	-

Data Source	G5 local name	Rock-type	Sample	Ba	Rb	Sr	Zn	Zr	V	Ce	Co	Cs	Cu	Dy	Er	Eu	Ga	Gd	Hf	Ho	La
Mendes et al., 2002	Venda Nova	Charnoenderbite	VN23	428	26.0	495	-	125	189	70	-	-	-	3.95	2.21	1.13	19.0	3.77	-	0.80	29.09
Mendes et al., 2002	Venda Nova	Charnoenderbite	VN15	429	21.0	489	-	154	162	-	-	-	-	-	-	-	19.0	-	-	-	-
Mendes et al., 2002	Venda Nova	Charnoenderbite	VN19	554	26.0	513	-	126	165	8	-	-	-	0.54	0.24	0.17	20.0	0.47	-	0.10	3.68
Mendes et al., 2002	Venda Nova	Charnoenderbite	VN18	282	36.0	467	-	111	176	-	-	-	-	-	-	-	20.0	-	-	-	-
Mendes et al., 2002	Venda Nova	Charnoenderbite	VN1	458	53.0	454	-	124	157	-	-	-	-	-	-	-	19.0	-	-	-	-
Mendes et al., 2002	Venda Nova	Charnoenderbite	VN16	445	62.0	436	-	121	154	45	-	-	-	3.65	2.19	0.93	19.0	3.36	-	0.76	19.21
Mendes et al., 2002	Venda Nova	Charnoenderbite	VN13	883	37.0	371	-	210	113	35	-	-	-	2.16	0.93	0.99	20.0	2.65	-	0.40	16.06
Mendes et al., 2002	Venda Nova	Charnoenderbite	VN24	581	25.0	380	-	178	110	-	-	-	-	-	-	-	17.0	-	-	-	-
Mendes et al., 2002	Venda Nova	Charnoenderbite	VN2	196	20.0	533	-	377	46	-	-	-	-	-	-	-	20.0	-	-	-	-
Mendes et al., 2002	Venda Nova	Charnoenderbite	VN27	849	34.0	358	-	196	55	39	-	-	-	2.84	1.57	0.88	18.0	2.73	-	0.57	18.47
Mendes et al., 2002	Venda Nova	Charnoenderbite	VN31	679	50.0	315	-	158	46	-	-	-	-	-	-	-	17.0	-	-	-	-
Mendes et al., 1997	Várzea Alegre	Charnockitic rock	VA 260	2356	82.0	487	-	910	43	-	23.00	-	-	-	-	-	19.0	-	-	-	-
Mendes et al., 1997	Várzea Alegre	Charnockitic rock	VA 252	2479	68.0	501	-	937	42	-	36.00	-	-	-	-	-	20.0	-	-	-	-
Mendes et al., 1997	Várzea Alegre	Charnockitic rock	VA 250	3250	85.0	551	-	800	35	-	35.00	-	-	-	-	-	17.0	-	-	-	-
Mendes et al., 1997	Várzea Alegre	Charnockitic rock	VA 241	2317	74.0	498	-	819	93	-	24.00	-	-	-	-	-	20.0	-	-	-	-

Data Source	G5 local name	Rock-type	Sample	Ba	Rb	Sr	Zn	Zr	V	Ce	Co	Cs	Cu	Dy	Er	Eu	Ga	Gd	Hf	Ho	La
Mendes et al., 1997	Várzea Alegre	Charnockitic rock	VA 249	2526	61.0	621	-	980	69	-	29.00	-	-	-	-	-	21.0	-	-	-	-
Mendes et al., 1997	Várzea Alegre	Charnockitic rock	VA 242	2160	60.0	505	-	929	111	-	40.00	-	-	-	-	-	19.0	-	-	-	-
Mendes et al., 1997	Várzea Alegre	Charnockitic rock	VA 263	2708	83.0	564	-	945	55	-	25.00	-	-	-	-	-	20.0	-	-	-	-
Mendes et al., 1997	Várzea Alegre	Charnockitic rock	VA 253	2136	56.0	614	-	894	108	-	48.00	-	-	-	-	-	21.0	-	-	-	-
Mendes et al., 1997	Várzea Alegre	Charnockitic rock	VA 56	3389	50.0	702	-	1049	85	126	24.00	-	-	5.07	2.18	4.30	20.0	7.16	-	0.94	58.44
Mendes et al., 1997	Várzea Alegre	Charnockitic rock	VA 237	1744	60.0	515	-	917	117	-	35.00	-	-	-	-	-	22.0	-	-	-	-
Mendes et al., 1997	Várzea Alegre	Charnockitic rock	VA 257	2063	46.0	594	-	913	112	-	47.00	-	-	-	-	-	21.0	-	-	-	-
Mendes et al., 1997	Várzea Alegre	Charnockitic rock	VA 182	1982	47.0	577	-	932	122	-	31.00	-	-	-	-	-	21.0	-	-	-	-
De Campos, 2015	Santa Angélica	Diorite	1	-	-	-	-	-	-	-	-	-	-	-	-	-	-	-	-	-	-
De Campos, 2015	Santa Angélica	Diorite	2	-	-	-	-	-	-	-	-	-	-	-	-	-	-	-	-	-	-
De Campos, 2015	Santa Angélica	Diorite	3	-	-	-	-	-	-	-	-	-	-	-	-	-	-	-	-	-	-
De Campos, 2015	Santa Angélica	Diorite	4a	-	-	-	-	-	-	-	-	-	-	-	-	-	-	-	-	-	-
De Campos, 2015	Santa Angélica	Gabbro	4b	-	-	-	-	-	-	-	-	-	-	-	-	-	-	-	-	-	-
De Campos, 2015	Santa Angélica	Diorite	5b	-	-	-	-	-	-	-	-	-	-	-	-	-	-	-	-	-	-
De Campos, 2015	Santa Angélica	Diorite	6	-	-	-	-	-	-	-	-	-	-	-	-	-	-	-	-	-	-
De Campos, 2015	Santa Angélica	Diorite	8	-	-	-	-	-	-	-	-	-	-	-	-	-	-	-	-	-	-
De Campos, 2015	Santa Angélica	Diorite	9	-	-	-	-	-	-	-	-	-	-	-	-	-	-	-	-	-	-

Data Source	G5 local name	Rock-type	Sample	Ba	Rb	Sr	Zn	Zr	V	Ce	Co	Cs	Cu	Dy	Er	Eu	Ga	Gd	Hf	Ho	La
De Campos, 2015	Santa Angélica	Granite	10	-	-	-	-	-	-	-	-	-	-	-	-	-	-	-	-	-	-
De Campos, 2015	Santa Angélica	Diorite	12	-	-	-	-	-	-	-	-	-	-	-	-	-	-	-	-	-	-
De Campos, 2015	Santa Angélica	Granite	13	-	-	-	-	-	-	-	-	-	-	-	-	-	-	-	-	-	-
De Campos, 2015	Santa Angélica	Gabbro	14a	-	-	-	-	-	-	-	-	-	-	-	-	-	-	-	-	-	-
De Campos, 2015	Santa Angélica	Diorite	14b	-	-	-	-	-	-	-	-	-	-	-	-	-	-	-	-	-	-
De Campos, 2015	Santa Angélica	Gabbro	15	-	-	-	-	-	-	-	-	-	-	-	-	-	-	-	-	-	-
De Campos, 2015	Santa Angélica	Granite	17	-	-	-	-	-	-	-	-	-	-	-	-	-	-	-	-	-	-
De Campos, 2015	Santa Angélica	Granite	20	-	-	-	-	-	-	-	-	-	-	-	-	-	-	-	-	-	-
De Campos, 2015	Santa Angélica	Granite	21a	-	-	-	-	-	-	-	-	-	-	-	-	-	-	-	-	-	-
De Campos, 2015	Santa Angélica	Diorite	21b	-	-	-	-	-	-	-	-	-	-	-	-	-	-	-	-	-	-
De Campos, 2015	Santa Angélica	Granite	22	-	-	-	-	-	-	-	-	-	-	-	-	-	-	-	-	-	-
De Campos, 2015	Santa Angélica	Granite	23a	-	-	-	-	-	-	-	-	-	-	-	-	-	-	-	-	-	-
De Campos, 2015	Santa Angélica	Diorite	23b	-	-	-	-	-	-	-	-	-	-	-	-	-	-	-	-	-	-
De Campos, 2015	Santa Angélica	Diorite	25	-	-	-	-	-	-	-	-	-	-	-	-	-	-	-	-	-	-
De Campos, 2015	Santa Angélica	Diorite	27	-	-	-	-	-	-	-	-	-	-	-	-	-	-	-	-	-	-
De Campos, 2015	Santa Angélica	Diorite	28	-	-	-	-	-	-	-	-	-	-	-	-	-	-	-	-	-	-
De Campos, 2015	Santa Angélica	Diorite	31	-	-	-	-	-	-	-	-	-	-	-	-	-	-	-	-	-	-
De Campos, 2015	Santa Angélica	Granite	32	-	-	-	-	-	-	-	-	-	-	-	-	-	-	-	-	-	-
De Campos, 2015	Santa Angélica	Gabbro	33	-	-	-	-	-	-	-	-	-	-	-	-	-	-	-	-	-	-
De Campos, 2015	Santa Angélica	Diorite	34	-	-	-	-	-	-	-	-	-	-	-	-	-	-	-	-	-	-

Data Source	G5 local name	Rock-type	Sample	Ba	Rb	Sr	Zn	Zr	V	Ce	Co	Cs	Cu	Dy	Er	Eu	Ga	Gd	Hf	Ho	La
De Campos, 2015	Santa Angélica	Gabbro	35	-	-	-	-	-	-	-	-	-	-	-	-	-	-	-	-	-	-
De Campos, 2015	Santa Angélica	Diorite	36	-	-	-	-	-	-	-	-	-	-	-	-	-	-	-	-	-	-
De Campos, 2015	Santa Angélica	Diorite	37	-	-	-	-	-	-	-	-	-	-	-	-	-	-	-	-	-	-
De Campos, 2015	Santa Angélica	Granite	38a	-	-	-	-	-	-	-	-	-	-	-	-	-	-	-	-	-	-
De Campos, 2015	Santa Angélica	Gabbro	39a	-	-	-	-	-	-	-	-	-	-	-	-	-	-	-	-	-	-
De Campos, 2015	Santa Angélica	Gabbro	39b	-	-	-	-	-	-	-	-	-	-	-	-	-	-	-	-	-	-
De Campos, 2015	Santa Angélica	Diorite	40	-	-	-	-	-	-	-	-	-	-	-	-	-	-	-	-	-	-
De Campos, 2015	Santa Angélica	Gabbro	41	-	-	-	-	-	-	-	-	-	-	-	-	-	-	-	-	-	-
De Campos, 2015	Santa Angélica	Gabbro	42a	-	-	-	-	-	-	-	-	-	-	-	-	-	-	-	-	-	-
De Campos, 2015	Santa Angélica	Gabbro	42b	-	-	-	-	-	-	-	-	-	-	-	-	-	-	-	-	-	-
De Campos, 2015	Santa Angélica	Diorite	43	-	-	-	-	-	-	-	-	-	-	-	-	-	-	-	-	-	-
De Campos, 2015	Santa Angélica	Diorite	44	-	-	-	-	-	-	-	-	-	-	-	-	-	-	-	-	-	-
De Campos, 2015	Santa Angélica	Gabbro	45	-	-	-	-	-	-	-	-	-	-	-	-	-	-	-	-	-	-
De Campos, 2015	Santa Angélica	Gabbro	46	-	-	-	-	-	-	-	-	-	-	-	-	-	-	-	-	-	-
De Campos, 2015	Santa Angélica	Gabbro	47	-	-	-	-	-	-	-	-	-	-	-	-	-	-	-	-	-	-
De Campos, 2015	Santa Angélica	Diorite	48	-	-	-	-	-	-	-	-	-	-	-	-	-	-	-	-	-	-
De Campos, 2015	Santa Angélica	Diorite	49	-	-	-	-	-	-	-	-	-	-	-	-	-	-	-	-	-	-
De Campos, 2015	Santa Angélica	Granite	50	-	-	-	-	-	-	-	-	-	-	-	-	-	-	-	-	-	-
Bayer et al., 1987	Santa Angélica	Fine-grained gabbro	P438B	2264	57.0	1389	126	206	307	-	35.00	-	38	-	-	-	24.0	-	-	-	-
Bayer et al., 1987	Santa Angélica	Fine-grained gabbro	P191	1942	35.0	1545	79	81	189	-	51.00	-	35	-	-	-	18.0	-	-	-	-

Data Source	G5 local name	Rock-type	Sample	Ba	Rb	Sr	Zn	Zr	V	Ce	Co	Cs	Cu	Dy	Er	Eu	Ga	Gd	Hf	Ho	La
Bayer et al., 1987	Santa Angélica	Fine-grained gabbro	P007B	2232	59.0	1299	163	361	654	-	36.00	-	29	-	-	-	30.0	-	-	-	-
Bayer et al., 1987	Santa Angélica	Fine-grained gabbro	P297B	1522	70.0	1121	105	414	373	-	47.00	-	26	-	-	-	25.0	-	-	-	-
Bayer et al., 1987	Santa Angélica	Coarse-grained gabbro	R412C	1588	79.0	1045	137	440	315	-	25.00	-	45	-	-	-	25.0	-	-	-	-
Bayer et al., 1987	Santa Angélica	Coarse-grained gabbro	P050	2083	75.0	767	132	344	208	-	12.00	-	31	-	-	-	24.0	-	-	-	-
Bayer et al., 1987	Santa Angélica	Coarse-grained gabbro	P180A	2515	56.0	1115	130	246	239	-	18.00	-	55	-	-	-	24.0	-	-	-	-
Bayer et al., 1987	Santa Angélica	Coarse-grained gabbro	R410S	1607	87.0	1003	173	342	228	-	15.00	-	28	-	-	-	26.0	-	-	-	-
Bayer et al., 1987	Santa Angélica	Hybrid rock	P491A	1777	96.0	948	134	630	198	-	14.00	-	34	-	-	-	24.0	-	-	-	-
Bayer et al., 1987	Santa Angélica	Hybrid rock	R410A	833	122.0	348	157	59	160	-	30.00	-	21	-	-	-	26.0	-	-	-	-
Bayer et al., 1987	Santa Angélica	Hybrid rock	R410B	2440	74.0	1085	172	376	223	-	9.00	-	56	-	-	-	24.0	-	-	-	-
Bayer et al., 1987	Santa Angélica	Hybrid rock	R410E	1423	105.0	837	138	476	221	-	19.00	-	34	-	-	-	25.0	-	-	-	-
Bayer et al., 1987	Santa Angélica	Hybrid rock	R410G	2053	97.0	971	177	289	173	-	7.00	-	47	-	-	-	21.0	-	-	-	-
Bayer et al., 1987	Santa Angélica	Hybrid rock	P485A	1731	89.0	845	172	431	208	-	12.00	-	33	-	-	-	22.0	-	-	-	-
Bayer et al., 1987	Santa Angélica	Granite	P485B	1086	110.0	245	192	54	34	-	5.00	-	18	-	-	-	19.0	-	-	-	-
Bayer et al., 1987	Santa Angélica	Granite	P495	910	108.0	148	184	141	20	-	1.00	-	24	-	-	-	22.0	-	-	-	-
Bayer et al., 1987	Santa Angélica	Granite	P354E	801	151.0	209	172	349	19	-	3.00	-	17	-	-	-	26.0	-	-	-	-
Bayer et al., 1987	Santa Angélica	Granite	P187B	1233	120.0	324	220	180	82	-	6.00	-	26	-	-	-	28.0	-	-	-	-
Mello, 2000	Aimorés	Qtz monzodiorite	FAM32	1345	35.3	643	137	371	183	156	-	5.00	-	7.16	3.09	3.07	24.6	9.84	13.00	-	67.70
Mello, 2000	Aimorés	Monzodiorite	FAM28	1817	42.7	530	128	557	166	196	-	5.00	-	9.62	4.52	4.17	25.0	13.40	13.50	-	86.00
Mello, 2000	Aimorés	Monzodiorite	FAM52	1580	32.4	579	136	497	171	172	-	5.00	-	9.52	4.77	3.99	25.4	12.90	11.00	-	75.60

Data Source	G5 local name	Rock-type	Sample	Ba	Rb	Sr	Zn	Zr	V	Ce	Co	Cs	Cu	Dy	Er	Eu	Ga	Gd	Hf	Ho	La
Mello, 2000	Aimorés	Monzodiorite	FAM85	1660	37.1	651	125	469	142	154	-	5.00	-	9.47	4.41	4.05	26.6	12.40	12.70	-	72.10
Mello, 2000	Aimorés	Tonalite to granodiorite	FAM21G	721	61.1	213	69	198	90	55	-	5.00	-	4.03	1.78	1.33	20.2	4.21	4.50	-	26.80
Mello, 2000	Aimorés	Tonalite to granodiorite	FAM21	535	66.2	204	79	206	98	77	-	5.00	-	-	-	1.68	19.8	-	5.50	-	38.30
Mello, 2000	Aimorés	Tonalite to granodiorite	FAM21D	608	63.7	209	70	189	91	56	-	5.00	-	3.67	1.64	1.30	19.5	4.20	6.10	-	27.80
Mello, 2000	Aimorés	Qtz monzodiorite titanite-bearing	FAM71	1367	82.2	524	116	414	128	223	-	5.00	-	-	-	3.20	23.3	-	12.50	-	101.00
Mello, 2000	Aimorés	Qtz monzodiorite titanite-bearing	FAM47	1509	80.5	488	123	432	136	196	-	5.00	-	7.96	3.60	3.18	22.7	11.40	11.20	-	86.40
Mello, 2000	Aimorés	Qtzo monzonite	FAM10	1852	81.8	400	137	728	59	159	-	5.00	-	9.27	4.40	3.21	23.9	11.40	15.10	-	70.50
Mello, 2000	Aimorés	Qtzo monzonite	FAM84D	1325	120.5	292	135	614	55	161	-	5.00	-	-	-	3.15	24.3	-	12.80	-	66.10
Mello, 2000	Aimorés	Qtzo monzonite	FAM84E	1726	146.6	307	110	560	39	169	-	5.00	-	-	-	3.29	23.3	-	14.90	-	68.80
Mello, 2000	Aimorés	Qtzo monzonite	FAM4L	1645	124.5	303	107	567	39	143	-	5.00	-	6.82	3.08	2.71	23.8	9.67	13.60	-	62.80
Mello, 2000	Aimorés	Qtzo monzonite	FAM84F	1756	130.1	322	93	521	32	111	-	5.00	-	5.70	2.57	2.38	24.1	8.22	13.10	-	54.80
Mello, 2000	Aimorés	Qtzo monzonite	FAM4	1842	138.6	318	83	436	30	136	-	5.00	-	-	-	3.21	24.1	-	10.60	-	64.20
Mello, 2000	Aimorés	Qtzo monzonite	FAM4I	1767	129.1	306	88	427	30	108	-	5.00	-	4.90	2.41	2.68	22.0	6.99	12.20	-	51.30
Mello, 2000	Aimorés	Qtzo monzonite	FAM4J	1746	137.3	292	99	481	32	139	-	7.80	-	-	-	3.16	22.5	-	15.50	-	65.80
Mello, 2000	Aimorés	Qtzo monzonite	FAM4K	1689	125.4	299	93	469	29	111	-	5.00	-	-	-	2.80	23.2	-	14.00	-	51.40
Mello, 2000	Aimorés	Qtzo monzonite	FAM4H	1741	129.5	296	95	514	33	114	-	5.80	-	-	-	3.24	22.1	-	13.40	-	50.30
Mello, 2000	Aimorés	Qtzo monzonite	FAM4G	1973	142.3	304	91	441	30	149	-	5.00	-	-	-	3.31	22.0	-	11.90	-	62.00
Mello, 2000	Aimorés	Granite	FAM84C	1784	134.2	304	69	353	22	112	-	8.20	-	-	-	2.59	21.1	-	10.80	-	48.80
Mello, 2000	Aimorés	Qtz monzodiorite	FAM25	1753	124.5	315	130	593	43	118	-	5.90	-	9.34	4.61	3.37	22.4	12.10	10.70	-	47.80
Mello, 2000	Aimorés	Granite	FAM24A	1413	160.5	249	96	451	31	119	-	8.70	-	6.11	2.85	2.17	22.8	8.71	10.60	-	82.70
Mello, 2000	Aimorés	Granite	FAM5A	1489	227.1	251	100	481	35	137	-	8.10	-	7.44	3.35	2.54	24.8	9.64	8.40	-	95.30
Mello, 2000	Aimorés	Granite	FAM9B	560	152.9	109	43	136	12	118	-	6.80	-	5.11	3.09	0.76	17.1	8.32	3.60	-	55.20
Mello, 2000	Aimorés	Granite	FAM1	371	144.6	75	33	108	6	41	-	5.00	-	2.11	0.65	0.49	15.2	3.81	3.00	-	20.10
Mello, 2000	Aimorés	Granite	FAM9A	380	138.7	78	43	115	10	90	-	5.00	-	-	-	0.65	16.2	-	3.00	-	42.70
Mello, 2000	Lagoa Preta	Leucogabbro	MLP1	28	2.0	445	34	23	23	2	-	5.00	-	-	-	0.20	12.6	-	3.00	-	0.95

Data Source	G5 local name	Rock-type	Sample	Ba	Rb	Sr	Zn	Zr	V	Ce	Co	Cs	Cu	Dy	Er	Eu	Ga	Gd	Hf	Ho	La
Mello, 2000	Lagoa Preta	Diorite	MLP4	245	3.2	491	147	246	0	42	-	5.00	-	-	-	3.45	23.9	-	3.90	-	20.00
Mello, 2000	Ibituba	Qtzo monzonite	I4	2484	57.0	639	116	402	3	217	-	5.00	-	-	-	4.29	23.9	-	11.70	-	98.10
Ludka and Wiedemann-Leonardos, 2000	Amparo	Coronitic rock	A2	29	0.9	186	-	23	-	7	-	-	-	0.61	0.33	0.34	-	0.81	-	0.12	2.91
Ludka and Wiedemann-Leonardos, 2000	Amparo	Coronitic rock	A6.2	49	0.2	228	-	14	-	7	-	-	-	0.34	0.14	0.24	-	0.48	-	0.06	3.17
Ludka and Wiedemann-Leonardos, 2000	Amparo	Coronitic rock	A8.1	16	0.3	246	-	22	-	15	-	-	-	0.50	0.25	0.29	-	0.69	-	0.10	6.62
Ludka and Wiedemann-Leonardos, 2000	Jacutinga	Gabbro-norite	J470	74	3.9	420	-	62	-	25	-	-	-	2.08	1.19	0.87	-	2.21	-	0.43	10.53
Ludka and Wiedemann-Leonardos, 2000	Jacutinga	Gabbro-norite	J471	58	2.1	516	-	51	-	38	-	-	-	2.59	1.36	1.18	-	3.03	-	0.51	15.49
Ludka and Wiedemann-Leonardos, 2000	Jacutinga	Gabbro-norite	J472	69	0.9	485	-	93	-	53	-	-	-	3.86	1.85	1.65	-	4.81	-	0.74	18.80
Ludka and Wiedemann-Leonardos, 2000	Jacutinga	Gabbro-norite	J475	37	7.0	319	-	45	-	18	-	-	-	1.61	0.66	0.80	-	1.97	-	0.29	7.11
Ludka and Wiedemann-Leonardos, 2000	Itaoca	Gabbro-norite	Ita25	200	8.0	519	-	47	-	43	-	-	-	3.71	2.07	1.38	-	4.75	-	0.90	18.70
Ludka and Wiedemann-Leonardos, 2000	Itaoca	Coronitic rock	Ita31	313	3.0	362	-	18	-	18	-	-	-	1.87	1.12	0.83	-	1.88	-	0.39	7.84

Data Source	G5 local name	Rock-type	Sample	Ba	Rb	Sr	Zn	Zr	V	Ce	Co	Cs	Cu	Dy	Er	Eu	Ga	Gd	Hf	Ho	La
Ludka and Wiedemann-Leonardos, 2000	Itaoca	Piroxineto	Ita34	97	3.0	95	-	-	-	18	-	-	-	1.73	0.87	0.54	-	2.19	-	0.56	6.99
Ludka and Wiedemann-Leonardos, 2000	Itaoca	Piroxineto	Ita95	-	-	-	-	-	-	18	-	-	-	2.36	1.25	0.60	-	2.26	-	0.34	7.50
De Campos et al., 2004	Santa Angélica	Gabbro	SA1.1	1032	132.0	327	156	1290	103	-	10.00	-	23	-	-	-	28.0	-	-	-	-
De Campos et al., 2004	Santa Angélica	Gabbro	SA1.2	2232	59.0	1299	163	361	654	-	36.00	-	29	-	-	-	30.0	-	-	-	-
De Campos et al., 2004	Santa Angélica	Gabbro	SA1.3	2714	65.0	1711	85	140	267	-	35.00	-	66	-	-	-	18.0	-	-	-	-
De Campos et al., 2004	Santa Angélica	Gabbro	SA1.4	1485	59.0	1271	130	401	333	-	34.00	-	51	-	-	-	26.0	-	-	-	-
De Campos et al., 2004	Castelo	Gabbro	CA1.1	2316	63.0	1395	137	147	349	-	24.00	-	86	-	-	-	21.0	-	-	-	-
De Campos et al., 2004	Castelo	Diorite	CA1.2	3358	105.0	1120	192	178	178	-	4.00	-	69	-	-	-	22.0	-	-	-	-
De Campos et al., 2004	Venda Nova	Gabbro	VN1.1	2878	40.0	1466	103	123	252	-	18.00	-	51	-	-	-	23.0	-	-	-	-
De Campos et al., 2004	Venda Nova	Gabbro	VN1.2	1778	34.0	1370	93	241	401	-	590.00	-	52	-	-	-	19.0	-	-	-	-
De Campos et al., 2004	Venda Nova	Gabbro	VN1.3	3108	33.0	1970	103	105	319	-	30.00	-	45	-	-	-	25.0	-	-	-	-
De Campos et al., 2004	Santa Angélica	Diorite	SA2.1	1337	86.0	1150	109	622	286	-	35.00	-	28	-	-	-	22.0	-	-	-	-
De Campos et al., 2004	Santa Angélica	Diorite	SA2.2	1870	80.0	1076	136	709	432	-	24.00	-	50	-	-	-	24.0	-	-	-	-
De Campos et al., 2004	Santa Angélica	Diorite	SA2.3	1461	74.0	1084	131	449	370	-	32.00	-	38	-	-	-	26.0	-	-	-	-

Data Source	G5 local name	Rock-type	Sample	Ba	Rb	Sr	Zn	Zr	V	Ce	Co	Cs	Cu	Dy	Er	Eu	Ga	Gd	Hf	Ho	La
De Campos et al., 2004	Santa Angélica	Diorite	SA2.4	2621	214.0	1371	119	317	243	-	20.00	-	27	-	-	-	32.0	-	-	-	-
De Campos et al., 2004	Castelo	Diorite	CA2.1	1460	97.0	825	154	446	311	-	36.00	-	38	-	-	-	25.0	-	-	-	-
De Campos et al., 2004	Castelo	Diorite	CA2.2	992	184.0	758	175	623	281	-	25.00	-	28	-	-	-	28.0	-	-	-	-
De Campos et al., 2004	Castelo	Diorite	CA2.3	1815	93.0	884	143	423	279	-	24.00	-	53	-	-	-	22.0	-	-	-	-
De Campos et al., 2004	Venda Nova	Gabbro	VN2.1	1358	19.0	1614	76	324	170	-	58.00	-	31	-	-	-	17.0	-	-	-	-
De Campos et al., 2004	Venda Nova	Diorite	VN2.2	4297	70.0	1440	118	543	132	-	4.00	-	38	-	-	-	30.0	-	-	-	-
De Campos et al., 2004	Venda Nova	Diorite	VN2.3	4048	74.0	1439	148	704	179	-	5.00	-	44	-	-	-	28.0	-	-	-	-
De Campos et al., 2004	Santa Angélica	Diorite	SA3.1	2053	97.0	971	177	289	173	-	7.00	-	47	-	-	-	21.0	-	-	-	-
De Campos et al., 2004	Santa Angélica	Diorite	SA3.2	2287	83.0	1178	171	304	162	-	9.00	-	31	-	-	-	27.0	-	-	-	-
De Campos et al., 2004	Santa Angélica	Diorite	SA3.3	833	122.0	348	157	59	160	-	30.00	-	21	-	-	-	26.0	-	-	-	-
De Campos et al., 2004	Santa Angélica	Diorite	SA3.4	2719	104.0	1079	100	868	212	-	14.00	-	26	-	-	-	27.0	-	-	-	-
De Campos et al., 2004	Castelo	Diorite	CA3.1	751	222.0	507	130	550	49	-	28.00	-	26	-	-	-	27.0	-	-	-	-
De Campos et al., 2004	Castelo	Granite	CA3.2	1446	200.0	509	127	395	137	-	12.00	-	22	-	-	-	22.0	-	-	-	-
De Campos et al., 2004	Venda Nova	Diorite	VN3.1	4073	94.0	1262	95	423	82	-	5.00	-	38	-	-	-	32.0	-	-	-	-
De Campos et al., 2004	Venda Nova	Diorite	VN3.2	3258	69.0	1076	92	930	99	-	5.00	-	35	-	-	-	27.0	-	-	-	-

Data Source	G5 local name	Rock-type	Sample	Ba	Rb	Sr	Zn	Zr	V	Ce	Co	Cs	Cu	Dy	Er	Eu	Ga	Gd	Hf	Ho	La
De Campos et al., 2004	Venda Nova	Diorite	VN3.3	862	45.0	363	126	161	132	-	29.00	-	24	-	-	-	23.0	-	-	-	-
De Campos et al., 2004	Santa Angélica	Granite	SA4.1	1547	68.0	1041	114	309	344	-	40.00	-	36	-	-	-	24.0	-	-	-	-
De Campos et al., 2004	Santa Angélica	Granite	SA4.2	530	107.0	143	275	149	17	-	1.00	-	32	-	-	-	21.0	-	-	-	-
De Campos et al., 2004	Castelo	Granite	CA4.1	1308	211.0	475	134	448	81	-	6.00	-	27	-	-	-	30.0	-	-	-	-
De Campos et al., 2004	Castelo	Granite	CA4.3	598	265.0	263	121	459	59	-	8.00	-	18	-	-	-	24.0	-	-	-	-
De Campos et al., 2004	Castelo	Granite	CA4.4	1483	185.0	585	101	321	35	-	5.00	-	22	-	-	-	23.0	-	-	-	-
De Campos et al., 2004	Venda Nova	Granite	VN4.1	889	99.0	199	93	1070	42	-	6.00	-	13	-	-	-	23.0	-	-	-	-
De Campos et al., 2004	Venda Nova	Granite	VN4.2	1310	134.0	193	98	150	25	-	6.00	-	29	-	-	-	17.0	-	-	-	-
De Campos et al., 2004	Venda Nova	Granite	VN4.3	1058	124.0	183	158	164	36	-	5.00	-	23	-	-	-	20.0	-	-	-	-
De Campos et al., 2004	Santa Angélica	Granite	SA5.2	1528	273.0	936	126	398	255	-	23.00	-	24	-	-	-	24.0	-	-	-	-
De Campos et al., 2004	Santa Angélica	Granite	SA5.3	529	234.0	297	96	651	81	-	11.00	-	10	-	-	-	22.0	-	-	-	-
De Campos et al., 2004	Santa Angélica	Granite	SA5.4	1230	130.0	345	99	446	99	-	12.00	-	26	-	-	-	19.0	-	-	-	-
De Campos et al., 2004	Castelo	Granite	CA5.1	909	265.0	228	195	330	55	-	5.00	-	28	-	-	-	21.0	-	-	-	-
De Campos et al., 2004	Castelo	Granite	CA5.2	1039	219.0	3335	143	438	50	-	4.00	-	25	-	-	-	24.0	-	-	-	-
De Campos et al., 2004	Castelo	Granite	CA5.3	804	236.0	157	129	140	36	-	6.00	-	16	-	-	-	21.0	-	-	-	-

Data Source	G5 local name	Rock-type	Sample	Ba	Rb	Sr	Zn	Zr	V	Ce	Co	Cs	Cu	Dy	Er	Eu	Ga	Gd	Hf	Ho	La
Ludka et al., 1998	G5 - Venda Nova	Syeno-monzonite	-	5028	86.0	1338	46	158	59	489	13.00	-	-	12.34	3.82	6.09	-	21.68	-	0.72	218.40
Ludka et al., 1998	Venda Nova	Syeno-monzonite	-	6043	81.0	1332	62	1186	69	348	12.00	-	-	9.42	2.88	7.23	-	19.72	-	0.74	160.30
Ludka et al., 1998	Venda Nova	Monzodiorite	-	4588	69.0	1441	104	610	216	213	20.00	-	-	6.18	2.59	3.77	-	10.48	-	1.14	89.37
Ludka et al., 1998	Venda Nova	Monzodiorite	-	3634	58.0	1326	104	580	190	254	20.00	-	-	4.16	1.51	4.02	-	9.12	-	0.74	117.70
Ludka et al., 1998	Venda Nova	Gabbro-norite	-	3185	26.0	1324	-	121	-	-	-	-	-	-	-	-	-	-	-	-	-
Ludka et al., 1998	Venda Nova	Gabbro-norite	-	1517	28.0	1350	88	258	199	-	30.00	-	-	-	-	-	-	-	-	-	-
Ludka et al., 1998	Venda Nova	Gabbro-norite	-	1779	24.0	1915	77	-	173	-	49.00	-	-	-	-	-	-	-	-	-	-
Ludka et al., 1998	Venda Nova	Gabbro-norite	-	1499	23.0	1528	84	185	183	-	37.00	-	-	-	-	-	-	-	-	-	-
Offman, 1990 in Ludka et al., 1998	Venda Nova	Allanite granite	-	1010	218.0	299	134	442	44	82	3.00	-	-	1.74	0.65	0.92	-	3.72	-	0.61	36.73
Offman, 1990 in Ludka et al., 1998	Venda Nova	Allanite granite	-	1135	210.0	360	222	482	55	97	4.00	-	-	2.40	0.95	1.15	-	4.77	-	0.27	48.99
Offman, 1990 in Ludka et al., 1998	Venda Nova	Allanite granite	-	-	-	-	-	-	-	91	-	-	-	-	1.08	1.68	-	6.23	-	0.70	38.91
Offman, 1990 in Ludka et al., 1998	Venda Nova	Granite	-	1628	217.0	289	49	343	23	66	21.00	-	-	3.60	2.14	0.85	-	3.77	-	0.77	25.37
Offman, 1990 in Ludka et al., 1998	Venda Nova	Leucogranite	-	797	54.0	238	39	122	22	15	19.00	-	-	1.07	0.52	0.68	-	1.19	-	0.10	8.18
Wiedemann et al., 2002	Várzea Alegre	Basic rock	VA-1	720	6.0	1188	115	96	284	-	93.00	-	31	-	-	-	23.0	-	-	-	-
Wiedemann et al., 2002	Várzea Alegre	Basic rock	VA-2	1091	27.0	1393	102	109	157	-	63.00	-	23	-	-	-	21.0	-	-	-	-

Data Source	G5 local name	Rock-type	Sample	Ba	Rb	Sr	Zn	Zr	V	Ce	Co	Cs	Cu	Dy	Er	Eu	Ga	Gd	Hf	Ho	La
Wiedemann et al., 2002	Várzea Alegre	Basic rock	VA-3	1300	67.0	684	155	364	320	-	65.00	-	29	-	-	-	-	-	-	-	-
Wiedemann et al., 2002	Várzea Alegre	Intermediate rock	VA-4	1660	90.0	714	138	435	-	-	51.00	-	25	-	-	-	-	-	-	-	-
Wiedemann et al., 2002	Várzea Alegre	Intermediate rock	VA-5	1841	49.0	1040	127	340	195	-	60.00	-	28	-	-	-	22.0	-	-	-	-
Wiedemann et al., 2002	Várzea Alegre	Intermediate rock	VA-6	1826	52.0	891	142	368	232	-	72.00	-	30	-	-	-	21.0	-	-	-	-
Wiedemann et al., 2002	Várzea Alegre	Intermediate rock	VA-7	1836	184.0	341	93	651	69	-	48.00	-	13	-	-	-	19.0	-	-	-	-
Wiedemann et al., 2002	Várzea Alegre	Acid rock	VA-8	1613	212.0	280	86	359	8	-	69.00	-	32	-	-	-	22.0	-	-	-	-
Wiedemann et al., 2002	Várzea Alegre	Acid rock	VA-9	771	229.0	147	-	224	15	-	42.00	-	43	-	-	-	22.0	-	-	-	-
Wiedemann et al., 2002	Várzea Alegre	Intermediate rock	VAc-1	1746	36.0	677	169	1084	121	-	31.00	-	-	-	-	-	21.0	-	-	-	-
Wiedemann et al., 2002	Várzea Alegre	Intermediate rock	Vac-2	2779	58.0	614	128	841	107	-	38.00	-	-	-	-	-	20.0	-	-	-	-
Wiedemann et al., 2002	Várzea Alegre	Intermediate rock	VAc-3	2727	64.0	579	134	724	125	-	61.00	-	-	-	-	-	21.0	-	-	-	-
Wiedemann et al., 2002	Várzea Alegre	Intermediate rock	Vac-4	2588	84.0	475	102	840	43	-	22.00	-	-	-	-	-	19.0	-	-	-	-
Wiedemann et al., 2002	Várzea Alegre	Intermediate rock	Vac-5	2246	79.0	428	101	819	35	-	56.00	-	-	-	-	-	20.0	-	-	-	-
Wiedemann et al., 2002	Santa Angélica	Basic rock	SA-1	2232	59.0	1299	163	361	654	-	36.00	-	29	-	-	-	30.0	-	-	-	-
Wiedemann et al., 2002	Santa Angélica	Basic rock	SA-2	1485	59.0	1271	130	401	333	-	34.00	-	51	-	-	-	26.0	-	-	-	-
Wiedemann et al., 2002	Santa Angélica	Intermediate rock	SA-3	1337	86.0	1150	109	622	286	-	35.00	-	28	-	-	-	22.0	-	-	-	-

Data Source	G5 local name	Rock-type	Sample	Ba	Rb	Sr	Zn	Zr	V	Ce	Co	Cs	Cu	Dy	Er	Eu	Ga	Gd	Hf	Ho	La
Wiedemann et al., 2002	Santa Angélica	Intermediate rock	SA-4	2621	214.0	1371	119	317	243	-	20.00	-	27	-	-	-	32.0	-	-	-	-
Wiedemann et al., 2002	Santa Angélica	Intermediate rock	SA-5	2287	83.0	1178	171	304	162	-	9.00	-	31	-	-	-	27.0	-	-	-	-
Wiedemann et al., 2002	Santa Angélica	Intermediate rock	SA-6	833	122.0	348	157	59	160	-	30.00	-	21	-	-	-	26.0	-	-	-	-
Wiedemann et al., 2002	Castelo	Basic rock	CA-1	2316	63.0	1395	137	147	349	-	24.00	-	86	-	-	-	21.0	-	-	-	-
Wiedemann et al., 2002	Castelo	Intermediate rock	CA-2	3358	105.0	1120	192	178	178	-	4.00	-	69	-	-	-	22.0	-	-	-	-
Wiedemann et al., 2002	Castelo	Intermediate rock	CA-3	992	184.0	758	175	623	281	-	25.00	-	28	-	-	-	28.0	-	-	-	-
Wiedemann et al., 2002	Castelo	Intermediate rock	CA-4	1815	93.0	884	143	423	279	-	24.00	-	53	-	-	-	22.0	-	-	-	-
Wiedemann et al., 2002	Castelo	Intermediate rock	CA-5	751	222.0	507	130	550	49	-	28.00	-	26	-	-	-	27.0	-	-	-	-
Wiedemann et al., 2002	Castelo	Acid rock	CA-6	1446	200.0	509	127	395	137	-	12.00	-	22	-	-	-	22.0	-	-	-	-
Wiedemann et al., 2002	Castelo	Acid rock	CA-7	1039	219.0	3335	143	438	50	-	4.00	-	25	-	-	-	24.0	-	-	-	-
Wiedemann et al., 2002	Castelo	Acid rock	CA-8	1483	185.0	585	101	321	35	-	5.00	-	22	-	-	-	23.0	-	-	-	-
Wiedemann et al., 2002	Santa Angélica	Acid rock	SA-7	1547	68.0	1041	114	309	344	-	40.00	-	36	-	-	-	24.0	-	-	-	-
Wiedemann et al., 2002	Santa Angélica	Acid rock	SA-8	530	107.0	143	275	149	17	-	1.00	-	32	-	-	-	21.0	-	-	-	-
Wiedemann et al., 2002	Santa Angélica	Acid rock	SA-9	1230	130.0	345	99	446	99	-	12.00	-	26	-	-	-	19.0	-	-	-	-

Data Source	G5 local name	Rock-type	Sample	Ba	Rb	Sr	Zn	Zr	V	Ce	Co	Cs	Cu	Dy	Er	Eu	Ga	Gd	Hf	Ho	La
Wiedemann et al., 2002	Mimoso do Sul	High-calk-alkaline/alkaline rocks	MI-1	-	201.0	3001	124	369	9	-	2.00	-	6	-	-	-	23.0	-	-	-	-
Wiedemann et al., 2002	Mimoso do Sul	High-calk-alkaline/alkaline rocks	MI-2	-	145.0	2532	94	758	173	-	14.00	-	37	-	-	-	78.0	-	-	-	-
Wiedemann et al., 2002	Mimoso do Sul	High-calk-alkaline/alkaline rocks	MI-3	-	102.0	5001	67	478	291	-	42.00	-	66	-	-	-	21.0	-	-	-	-
Wiedemann et al., 2002	Mimoso do Sul	High-calk-alkaline/alkaline rocks	MI-4	-	6673.0	2322	106	323	457	-	93.00	-	55	-	-	-	65.0	-	-	-	-
Wiedemann et al., 2002	Conceição do Muqui	High-calk-alkaline/alkaline rocks	CM-1	1640	195.0	305	128	325	24	-	4.00	-	3	-	-	-	27.0	-	-	-	-
Wiedemann et al., 2002	Conceição do Muqui	High-calk-alkaline/alkaline rocks	CM-2	-	425.0	2070	80	385	14	-	2.00	-	28	-	-	-	21.0	-	-	-	-
Wiedemann et al., 2002	Conceição do Muqui	High-calk-alkaline/alkaline rocks	CM-3	2471	160.0	1187	162	612	130	-	7.00	-	31	-	-	-	26.0	-	-	-	-
Wiedemann et al., 2002	Conceição do Muqui	High-calk-alkaline/alkaline rocks	CM-4	6757	70.0	3215	127	272	28	-	15.00	-	72	-	-	-	24.0	-	-	-	-
Zanon et al., 2015	Santa Angélica	Diorite	D5MIX23A	2961	93.5	992	155	855	166	320	21.40	0.49	22	10.15	5.21	3.52	26.1	15.86	14.67	1.90	179.10
Zanon et al., 2015	Santa Angélica	Diorite	M5G9	2364	74.7	1328	140	491	186	179	31.30	0.75	33	5.12	2.11	2.85	20.7	8.66	6.48	0.93	108.50
Zanon et al., 2015	Santa Angélica	Gabbro	M5G17	2410	67.3	1145	145	568	178	204	34.90	0.58	22	5.80	2.38	3.15	21.9	10.82	7.91	1.05	110.60
Zanon et al., 2015	Santa Angélica	Diorite	F5G38	3342	144.8	834	107	807	94	292	11.30	0.65	14	6.24	2.97	3.29	26.7	11.05	13.43	1.08	174.30

Data Source	G5 local name	Rock-type	Sample	Ba	Rb	Sr	Zn	Zr	V	Ce	Co	Cs	Cu	Dy	Er	Eu	Ga	Gd	Hf	Ho	La
Zanon et al., 2015	Santa Angélica	Diorite	H18	2756	135.3	889	110	663	102	285	16.40	0.62	17	6.98	3.12	3.43	27.2	12.72	12.23	1.23	171.20
Zanon et al., 2015	Santa Angélica	Diorite	H517	3721	97.2	1135	108	679	132	142	18.40	0.88	13	4.36	2.11	2.44	25.9	7.56	8.72	0.85	86.50
Zanon et al., 2015	Santa Angélica	Diorite	H16A	2718	116.2	1017	153	677	122	258	23.50	0.71	19	6.94	2.96	3.46	24.0	12.15	8.88	1.15	147.10
Zanon et al., 2015	Santa Angélica	Diorite	M5G16	2476	49.6	1270	99	684	126	125	40.00	0.37	24	4.28	2.13	2.58	19.9	7.24	8.97	0.79	73.90
Zanon et al., 2015	Santa Angélica	Granite	F5G15	2254	164.5	479	76	1100	29	377	5.20	0.46	6	6.86	3.40	3.25	21.9	11.64	12.24	1.24	227.40
Zanon et al., 2015	Santa Angélica	Gabbro	MP19	1935	66.4	1026	108	306	168	190	44.10	0.30	26	5.41	2.69	3.03	23.5	10.41	5.98	1.09	112.10
Paes et al., 2010	Medina		CP-334	666	278.6	101	-	347	-	291	2.40	3.00	-	9.00	2.80	1.10	22.4	13.60	10.40	1.20	126.20
Paes et al., 2010	Medina		PJ-404	621	272.7	136	-	441	-	415	3.40	1.20	-	13.20	4.90	1.10	25.0	18.80	13.40	1.90	181.80
Paes et al., 2010	Medina		CP-12	1075	277.9	244	-	353	-	234	3.00	3.20	-	7.50	4.10	1.40	23.1	10.90	10.90	1.50	114.90
Paes et al., 2010	Medina		CP-005B	1353	214.5	342	-	265	-	299	2.10	1.00	-	6.20	2.00	1.90	21.7	9.90	7.80	0.80	149.60
Paes et al., 2010	Medina		CP-358	1040	236.4	253	-	312	-	417	2.50	0.90	-	8.60	2.70	1.90	23.1	14.50	10.60	1.30	197.00
Paes et al., 2010	Medina		CP-005A	1052	236.5	322	-	220	-	220	2.00	1.10	-	5.30	2.00	1.70	21.8	7.50	7.00	0.80	112.10
Paes et al., 2010	Medina		CP-119A	410	214.6	169	-	202	-	199	1.60	0.90	-	4.30	1.10	1.00	20.5	7.30	7.10	0.60	92.50
Paes et al., 2010	Medina		CP-019	592	250.9	153	-	228	-	271	1.50	1.40	-	8.60	2.90	1.10	21.8	13.10	8.00	1.20	129.70
Paes et al., 2010	Medina		CP-361	630	230.2	201	-	281	-	254	3.20	2.60	-	7.40	2.80	1.40	22.4	10.90	8.50	1.20	121.50
Paes et al., 2010	Medina		CH-530	1294	247.8	338	-	196	-	299	1.30	1.20	-	6.30	1.90	1.70	18.4	7.30	5.80	0.80	155.00
Paes et al., 2010	Medina		CP-353	1091	266.4	276	-	452	-	438	3.80	1.40	-	10.90	3.90	1.80	24.6	15.80	13.50	1.60	209.00
Paes et al., 2010	Medina		CP-009A	803	255.1	202	-	229	-	267	1.90	1.20	-	6.20	2.10	1.40	22.0	9.50	7.60	1.00	132.20
Paes et al., 2010	Medina		CP-009B	389	243.3	173	-	139	-	100	1.50	0.90	-	2.40	0.80	1.20	21.9	3.90	4.50	0.30	50.60
Paes et al., 2010	Medina		CP-015A	750	213.1	227	-	284	-	299	3.80	2.10	-	8.00	2.70	1.50	21.8	11.30	8.80	1.10	143.00

Data Source	G5 local name	Rock-type	Sample	Ba	Rb	Sr	Zn	Zr	V	Ce	Co	Cs	Cu	Dy	Er	Eu	Ga	Gd	Hf	Ho	La
Paes et al., 2010	Medina		CP-051	701	198.3	182	-	164	-	100	1.30	3.50	-	2.50	0.80	0.80	22.9	4.20	5.10	0.40	53.60
Paes et al., 2010	Medina		CP-003	1892	261.7	522	-	544	-	440	5.60	1.70	-	10.30	4.50	2.90	25.6	13.90	16.20	1.70	228.00
Paes et al., 2010	Medina		CP-023	1542	310.3	347	-	591	-	269	5.70	3.50	-	9.90	4.50	2.10	24.5	13.20	17.30	1.70	126.50
Paes et al., 2010	Medina		CP-118	2290	194.1	626	-	696	-	500	9.30	1.00	-	10.70	4.70	3.90	25.2	15.40	16.50	1.70	255.40
Paes et al., 2010	Medina		CP-001	2054	212.8	621	-	554	-	467	6.40	1.30	-	10.80	4.60	3.60	24.9	13.60	15.40	1.70	248.00
Serrano et al., 2018	Medina	Granite	M61B	541	277.6	107	-	213	-	158	81.20	0.60	-	3.80	1.10	0.70	21.4	8.20	7.00	0.50	71.50
Serrano et al., 2018	Medina	Granite	R13A	1548	268.0	336	-	473	-	371	49.00	1.30	-	9.70	4.30	2.20	26.6	16.20	12.10	1.60	179.80
Paes et al., 2010	Caladão		PJ-302B	676	270.0	97	-	515	-	456	3.30	1.40	-	13.20	3.70	1.30	23.7	18.80	14.70	1.90	196.90
Paes et al., 2010	Caladão		PJ-389	838	251.0	118	-	346	-	344	2.50	1.60	-	5.50	0.80	1.00	25.3	11.60	10.90	0.50	163.50
Paes et al., 2010	Córrego do Calção		CH-89	1203	250.0	271	-	353	-	312	3.40	4.20	-	6.90	2.60	2.00	22.1	8.90	11.10	1.00	168.50
Paes et al., 2010	Córrego do Calção		CH-90	1098	232.0	291	-	394	-	332	3.40	1.90	-	6.50	2.30	1.80	21.0	8.20	11.60	1.00	174.50
Paes et al., 2010	Córrego do Calção		CH-91	942	177.8	407	56	148	25	88	1.10	4.80	2	1.30	0.38	0.90	24.8	1.98	4.40	0.19	48.50
Paes et al., 2010	Emparedado		CP-170	1325	234.0	881	-	247	-	224	2.70	6.20	-	4.70	2.10	1.80	27.0	7.60	7.50	0.80	121.20
Paes et al., 2010	Emparedado		CP-175A	2027	304.9	972	39	148	17	110	2.10	3.70	1	2.64	1.62	1.76	27.0	3.75	4.10	0.51	61.10
Paes et al., 2010	Emparedado		CP-251	2863	131.9	1315	59	290	37	265	4.50	0.80	6	3.40	1.50	2.95	22.6	7.00	7.40	0.56	150.00
Paes et al., 2010	Fazenda Liberdade		PJ-185	474	330.0	120	-	291	-	257	3.20	3.00	-	3.70	1.00	0.80	25.3	8.80	7.80	0.60	105.60
Paes et al., 2010	Fazenda Liberdade		PJ-192	396	347.0	99	-	349	-	319	3.40	1.80	-	5.80	1.80	0.80	25.1	10.20	10.20	0.80	126.40

Data Source	G5 local name	Rock-type	Sample	Ba	Rb	Sr	Zn	Zr	V	Ce	Co	Cs	Cu	Dy	Er	Eu	Ga	Gd	Hf	Ho	La
Paes et al., 2010	Fazenda Liberdade		PJ-196	532	301.0	123	-	304	-	199	9.00	5.00	-	5.10	1.80	1.10	27.6	8.20	8.60	0.90	83.50
Paes et al., 2010	Fazenda Liberdade		PJ-250	1212	288.0	762	-	429	-	477	7.60	6.20	-	5.10	2.50	3.20	25.6	9.70	11.40	1.00	221.00
Paes et al., 2010	Fazenda Liberdade		PJ-272	368	254.0	89	-	256	-	203	3.70	1.40	-	8.20	3.50	1.20	22.7	11.10	8.40	1.50	85.30
Paes et al., 2010	Fazenda Liberdade		PJ-280	660	273.7	108	118	533	20	506	3.70	0.60	5	13.83	5.88	1.52	25.0	18.90	14.90	2.50	214.50
Paes et al., 2010	Fazenda Liberdade		PJ-306	745	257.7	108	121	566	24	540	4.00	2.80	10	19.07	8.35	1.65	24.8	21.28	16.80	3.19	233.90
Paes et al., 2010	General Dutra		CH-021	640	245.0	172	-	235	-	183	3.80	1.90	-	4.90	2.10	1.10	23.8	6.70	8.80	0.80	91.80
Paes et al., 2010	General Dutra		CH-290	864	199.0	449	-	529	-	297	7.70	6.10	-	6.70	2.60	2.30	26.3	10.00	14.10	1.10	155.00
Paes et al., 2010	General Dutra		CH-574	560	224.0	186	-	286	-	201	2.60	2.30	-	6.00	2.50	1.10	21.3	8.40	9.60	0.90	97.70
Paes et al., 2010	General Dutra		CH-600	2871	223.3	530	83	434	39	367	5.70	2.40	5	16.51	7.83	4.72	23.5	18.96	12.80	3.08	195.20
Paes et al., 2010	Landim		CH-010	1552	183.0	1131	-	265	-	250	3.60	2.60	-	4.40	1.80	2.20	24.0	5.30	8.70	0.60	146.10
Paes et al., 2010	Landim		CH-511	972	262.1	531	25	123	<8	84	1.30	2.30	1	2.24	0.53	0.89	18.7	5.16	4.20	0.28	38.70
Paes et al., 2010	Landim		CH-514	2245	194.0	1233	-	368	-	350	6.90	3.40	-	5.30	1.90	2.80	24.6	6.40	10.70	0.80	204.00
Paes et al., 2010	Pau de Canoa		CH-310	1097	262.2	210	69	396	32	295	5.10	7.30	10	11.67	6.56	1.81	24.8	13.07	10.90	2.19	136.50
Paes et al., 2010	Pau de Canoa		CH-389	899	289.0	204	-	428	-	304	7.60	7.30	-	8.10	3.60	1.90	26.6	11.40	11.30	1.40	139.70
Paes et al., 2010	Pedra Azul		CP-167	1290	203.0	489	-	474	-	452	4.40	1.00	-	5.10	1.60	2.50	24.8	9.80	12.70	0.80	236.00
Paes et al., 2010	Pedra Azul		CP-215A	1370	211.0	628	-	523	-	248	7.10	2.60	-	3.00	1.30	2.70	28.1	5.70	12.70	0.50	132.70
Paes et al., 2010	Pedra Azul		CP-228A	5592	119.6	1794	18	202	20	73	1.70	0.30	1	1.52	0.67	2.35	22.2	2.59	5.60	0.24	46.70
Paes et al., 2010	Pedra Grande		PJ-007	1654	227.0	330	-	395	-	265	7.00	5.50	-	8.60	3.60	2.40	24.9	10.50	11.10	1.30	123.70
Paes et al., 2010	Pedra Grande		PJ-008	876	289.0	250	-	410	-	266	7.90	4.60	-	9.70	3.40	1.70	28.6	11.80	11.10	1.10	120.40

Data Source	G5 local name	Rock-type	Sample	Ba	Rb	Sr	Zn	Zr	V	Ce	Co	Cs	Cu	Dy	Er	Eu	Ga	Gd	Hf	Ho	La
Paes et al., 2010	Pedra Grande		PJ-017	902	287.0	172	-	627	-	486	6.30	1.40	-	10.70	4.00	1.70	26.4	16.10	17.40	1.50	206.30
Paes et al., 2010	Santa Cruz de Salinas		CH-102	1305	229.0	284	-	276	-	244	2.50	1.90	-	5.80	2.50	1.50	25.2	8.40	8.50	1.00	135.90
Paes et al., 2010	Santa Cruz de Salinas		CH-108	762	246.0	164	-	245	-	171	2.40	2.00	-	8.00	4.20	1.20	20.2	6.50	8.10	1.60	92.20
Paes et al., 2010	Santa Cruz de Salinas		CH-171	899	321.1	177	30	89	<8	100	1.30	4.30	0	5.23	2.76	1.25	23.3	4.85	3.10	1.03	61.90
Paes et al., 2010	Santa Cruz de Salinas		CH-237	1150	212.0	179	-	252	-	218	2.50	1.60	-	7.10	3.40	1.20	21.8	9.20	8.00	1.30	117.20
Aranda, 2018	Cláudio Afonso	Monzogranite	P 246-A	1980	39.6	1238	130	352	229	191	36.30	0.52	33	6.94	3.16	3.52	18.5	11.53	7.48	1.20	93.30
Aranda, 2018	Cláudio Afonso	Monzogranite	P 276-A	2482	36.5	818	174	556	227	250	30.30	0.39	19	10.58	4.62	4.52	21.3	16.93	11.81	1.80	113.40
Aranda, 2018	Cláudio Afonso	Monzodiorite	P 292-B	4081	77.5	1171	168	701	191	297	24.40	0.60	20	9.82	4.31	5.08	24.0	16.05	13.94	1.69	145.30
Aranda, 2018	Cláudio Afonso	Monzogranite	P 292-A	2435	52.5	1156	148	595	224	265	70.70	0.34	29	8.22	3.67	4.51	21.5	13.98	15.20	1.39	130.10
Aranda, 2018	Cláudio Afonso	Monzodiorite	P 277-A	2960	77.2	1150	138	628	160	229	21.40	1.69	21	7.05	3.24	4.02	21.0	12.24	13.21	1.21	109.20
Aranda, 2018	Cláudio Afonso	Jotunite	P 193-B	2609	78.8	824	149	489	205	230	23.90	0.43	18	8.73	3.88	4.33	21.2	13.72	11.59	1.43	110.30
Aranda, 2018	Cláudio Afonso	Monzodiorite	P 156-A	1964	78.0	879	131	446	235	179	22.00	1.37	17	7.22	3.30	3.53	20.9	11.66	9.94	1.24	86.70
Aranda, 2018	Cláudio Afonso	Qtz mangerite	P 197-C	2875	81.0	993	139	1019	135	242	16.40	0.91	17	5.90	2.59	3.88	25.0	10.51	21.91	0.97	121.80
Aranda, 2018	Cláudio Afonso	Qtz monzonite	P 288	4492	80.3	1003	156	837	80	299	9.50	0.69	16	7.16	3.09	4.95	22.8	13.01	18.41	1.18	150.20
Aranda, 2018	Cláudio Afonso	Qtz monzonite	P 295-B	1966	103.2	627	142	832	109	416	13.10	0.49	13	19.14	8.21	5.38	24.4	26.73	20.36	3.23	184.50
Aranda, 2018	Cláudio Afonso	Qtz monzonite	P 285-B	4735	89.2	898	115	854	75	268	9.90	0.44	8	7.98	3.81	4.73	22.4	13.53	18.13	1.38	129.70
Aranda, 2018	Cláudio Afonso	Qtz monzonite	P 206-D	4307	82.6	935	102	806	61	264	7.20	0.42	8	7.20	3.31	5.16	24.1	12.69	18.97	1.21	132.10
Aranda, 2018	Cláudio Afonso	Qtz monzonite	P 98	3059	134.7	741	82	458	83	225	10.50	2.20	9	5.48	2.46	2.91	21.7	9.41	11.95	0.97	113.70
Aranda, 2018	Cláudio Afonso	Qtz monzonite	P 297	3635	144.0	809	68	413	78	157	8.00	2.22	7	5.11	2.45	2.74	23.1	7.92	8.29	0.92	79.80
Aranda, 2018	Cláudio Afonso	Qtz monzonite	P 296	2798	116.7	685	106	647	98	263	12.80	0.69	18	8.51	3.67	3.65	22.2	13.74	14.62	1.37	128.80
Aranda, 2018	Cláudio Afonso	Qtz monzonite	P 146-B	2999	117.0	705	104	555	60	316	7.90	0.59	5	8.48	3.64	3.81	21.8	14.16	13.41	1.47	152.90
Aranda, 2018	Cláudio Afonso	Qtz monzonite	P 291	2772	131.1	635	98	586	63	275	9.70	1.14	16	8.15	3.52	3.50	22.8	12.71	12.67	1.36	135.20
Aranda, 2018	Cláudio Afonso	Qtz monzonite	P 298	3327	113.9	764	84	529	45	457	5.30	1.88	6	7.42	3.16	4.31	20.8	13.43	11.64	1.24	221.40
Aranda, 2018	Cláudio Afonso	Qtz monzonite	P 90-A	2926	138.8	641	79	412	50	303	5.50	1.25	11	6.22	2.58	4.73	20.5	12.87	9.96	1.06	302.60
Aranda, 2018	Cláudio Afonso	Qtz monzonite	P 102	2545	130.4	586	98	533	72	281	8.70	1.13	11	7.87	3.69	3.38	21.5	12.89	13.14	1.37	141.50

Data Source	G5 local name	Rock-type	Sample	Ba	Rb	Sr	Zn	Zr	V	Ce	Co	Cs	Cu	Dy	Er	Eu	Ga	Gd	Hf	Ho	La
Baltazar et al., 2010	Aimorés	Charnockite	OF174A	1537	165.1	159	56	348	5	311	1.50	1.00	6	6.88	2.26	2.32	20.8	11.99	9.30	1.07	153.50
Baltazar et al., 2010	Aimorés	Charnockite	OF172A	2096	165.3	188	47	486	5	118	1.70	0.50	3	4.44	1.92	2.68	20.0	6.38	12.00	0.76	57.40
Baltazar et al., 2010	Aimorés	Charnockite	OF198	981	78.7	180	55	895	69	349	12.80	1.10	18	18.62	9.84	2.84	22.3	25.38	22.80	3.63	161.30
Baltazar et al., 2010	Aimorés	Charnockite	SS058	938	70.3	182	48	528	66	270	10.60	0.90	15	12.86	5.96	2.43	21.9	19.48	13.70	2.28	124.30
Baltazar et al., 2010	Aimorés	Charnockite	SS023	537	64.2	342	48	114	54	43	8.40	0.70	6	2.66	1.36	1.21	18.3	3.16	3.30	0.49	21.10
Baltazar et al., 2010	Aimorés	Charnockite	OF245C	1019	88.8	402	118	683	72	153	13.70	2.80	22	11.22	4.91	3.75	24.4	11.78	15.70	1.85	59.00
Baltazar et al., 2010	Aimorés	Granite	OF156	2320	195.0	448	146	1086	62	673	8.90	0.60	9	5.62	1.78	3.56	26.6	11.68	28.70	0.75	318.40
Baltazar et al., 2010	Aimorés	Granite	OF166B	1540	204.4	226	86	593	22	176	5.50	2.00	4	8.39	4.03	2.61	24.1	11.80	15.00	1.45	80.20
Baltazar et al., 2010	Aimorés	Granite	SS094	2379	194.8	242	83	737	28	488	4.40	0.40	7	3.08	0.97	2.67	22.6	6.73	18.10	0.45	250.30
Baltazar et al., 2010	Aimorés	Mangerite	LC168	2385	68.7	537	43	958	78	208	12.20	0.20	8	7.61	3.79	4.17	25.2	11.22	23.00	1.23	96.10
Baltazar et al., 2010	Aimorés	Mangerite	OF144	381	85.7	200	48	118	157	62	18.30	1.40	38	4.48	2.57	1.20	21.2	4.44	3.30	0.83	31.50
Baltazar et al., 2010	Aimorés	Mangerite	SS027A	2527	74.8	564	35	838	76	194	12.20	0.40	7	7.42	3.70	4.31	22.7	11.24	19.80	1.38	88.00
Baltazar et al., 2010	Aimorés	Mangerite	OF051	1554	133.6	409	123	721	103	248	17.60	1.00	14	10.65	4.65	4.14	27.4	15.03	19.30	1.79	111.00
Baltazar et al., 2010	Aimorés	Diorite	OF022	2204	89.3	811	116	635	170	315	19.80	0.30	17	10.46	4.69	4.43	24.8	15.53	15.50	1.73	142.20
Baltazar et al., 2010	Aimorés	Mangerite	OF074B	1902	225.8	289	100	575	26	283	5.70	1.70	7	4.60	1.84	3.21	25.0	8.88	15.40	0.71	134.60

Data Source	G5 local name	Rock-type	Sample	Ba	Rb	Sr	Zn	Zr	V	Ce	Co	Cs	Cu	Dy	Er	Eu	Ga	Gd	Hf	Ho	La
Baltazar et al., 2010	Aimorés	Mangerite	OF117	1806	153.5	343	94	746	49	225	12.70	0.90	12	9.97	4.44	4.03	26.9	13.98	17.30	1.67	105.30
Baltazar et al., 2010	Aimorés	Charnockite	OF23	511	79.4	318	44	178	100	28	10.50	0.90	11	5.22	4.85	1.28	19.2	3.14	4.90	1.30	16.30
Baltazar et al., 2010	Aimorés	Charnockite	OF24	797	166.8	286	55	168	68	62	10.30	1.60	13	3.30	1.77	1.23	16.8	3.75	4.40	0.59	33.60
Baltazar et al., 2010	Aimorés	Charnockite	OF93	742	114.4	286	57	313	125	102	17.80	1.10	20	2.29	0.52	1.83	20.6	5.62	8.30	0.29	55.50
Baltazar et al., 2010	Aimorés	Charnockite	OF98A	559	81.7	269	32	109	35	35	6.00	0.70	2	4.70	2.74	0.97	15.7	3.51	3.70	1.01	21.10
Baltazar et al., 2010	Aimorés	Charnockite	OF101	590	65.6	350	28	136	49	41	7.50	0.30	3	4.83	2.41	1.16	16.2	3.48	4.10	0.92	25.10
Baltazar et al., 2010	Aimorés	Gabbro	SA16	1375	47.9	883	134	545	256	239	27.20	0.40	23	8.66	3.43	4.46	22.5	15.10	12.30	1.48	105.20
Pedrosa-Soares et al., 2006	Aimorés	Granite	SC-01A	649	130.0	190	60	189	77	145	44.00	-	-	6.36	2.61	3.10	9.0	8.62	13.30	1.08	83.10
Pedrosa-Soares et al., 2006	Aimorés	Granite	SC-13	555	116.0	210	59	196	107	143	41.00	-	-	5.01	2.05	2.43	9.0	7.33	13.40	0.80	77.50
Pedrosa-Soares, et al. 2006	Aimorés	Granite	MQ-03A	-	-	-	-	-	-	-	-	-	-	-	-	-	-	-	-	-	-
Pedrosa-Soares, et al. 2006	Aimorés	Charnockite	MQ-03B	-	-	-	-	-	-	-	-	-	-	-	-	-	-	-	-	-	-
Pedrosa-Soares, et al. 2006	Aimorés	Granite	MQ-04	-	-	-	-	-	-	-	-	-	-	-	-	-	-	-	-	-	-
Pedrosa-Soares, et al. 2006	Aimorés	Charnockite	MQ-81	-	-	-	-	-	-	-	-	-	-	-	-	-	-	-	-	-	-
Pedrosa-Soares, et al. 2006	Aimorés	Charnockite	MQ-123	-	-	-	-	-	-	-	-	-	-	-	-	-	-	-	-	-	-

Data Source	G5 local name	Rock-type	Sample	Ba	Rb	Sr	Zn	Zr	V	Ce	Co	Cs	Cu	Dy	Er	Eu	Ga	Gd	Hf	Ho	La
Pedrosa-Soares, et al. 2006	Aimorés	Charnockite	EC-92	-	-	-	-	-	-	-	-	-	-	-	-	-	-	-	-	-	-
Pedrosa-Soares, et al. 2006	Aimorés	Charnockite	EC-90	-	-	-	-	-	-	-	-	-	-	-	-	-	-	-	-	-	-
Pedrosa-Soares, et al. 2006	Aimorés	Sienogranite	EC-01	-	-	-	-	-	-	-	-	-	-	-	-	-	-	-	-	-	-
Pedrosa-Soares, et al. 2006	Aimorés	Charnockite	EB-89A	-	-	-	-	-	-	-	-	-	-	-	-	-	-	-	-	-	-
Pedrosa-Soares, et al. 2006	Aimorés	Norite	EP-15	-	-	-	-	-	-	-	-	-	-	-	-	-	-	-	-	-	-
Wiedemann et al., 2002	Pedra Azul	Basic rock	PA-I	2842	78.0	1176	223	385	166	-	37.00	-	24	-	-	-	-	-	-	-	-
Wiedemann et al., 2002	Pedra Azul	Basic rock	PA-2	2836	78.0	1168	221	388	166	-	38.00	-	25	-	-	-	-	-	-	-	-
Wiedemann et al., 2002	Pedra Azul	Intermediate rock	PA-3	2277	-	-	149	50	167	-	49.00	-	21	-	-	-	-	-	-	-	-
Wiedemann et al., 2002	Pedra Azul	Intermediate rock	PA-4	2016	171.0	594	152	722	108	-	27.00	-	12	-	-	-	-	-	-	-	-
Wiedemann et al., 2002	Pedra Azul	Intermediate rock	PA-5	1882	191.0	466	124	746	90	-	35.00	-	14	-	-	-	-	-	-	-	-
Wiedemann et al., 2002	Pedra Azul	Acid rock	PA-6	1354	291.0	229	91	749	36	-	23.00	-	7	-	-	-	-	-	-	-	-
Wiedemann et al., 2002	Pedra Azul	Acid rock	PA-7	927	260.0	179	64	323	13	-	29.00	-	2	-	-	-	-	-	-	-	-

Data Source	G5 local name	Rock-type	Sample	Lu	Mo	Nb	Nd	Ni	Pr	Sm	Sn	Ta	Tb	Th	Tl	Tm	U	Y	Yb	Eu/Eu*[a]	La_N/Yb_N[a]
This work	Aracê	Titanite-allanite-biotite granite	CA-02	0.93	4.0	46.7	166.8	7	51.05	25.80	4.80	6.16	2.61	55.90	0.60	1.45	2.74	97.22	8.10	0.37	22.30
This work	Vitória	Biotite granite	CA-04	0.16	3.0	8.4	170.8	16	51.43	20.00	1.80	0.75	0.94	110.90	0.70	0.15	1.33	14.92	0.80	0.41	202.34
This work	Mestre Álvaro	Biotite tonalite	CA-05	0.12	5.0	16.9	22.7	14	6.38	2.90	2.50	0.64	0.24	8.40	<0,5	0.14	0.62	7.36	0.80	1.15	30.42
Mendes et al., 2005	Várzea Alegre	Charnockitic rock	VA42	-	-	36.2	-	-	-	-	-	-	-	-	-	-	-	29.00	-	-	-
Mendes et al., 2005	Várzea Alegre	Charnockitic rock	VA164	-	-	28.0	-	-	-	-	-	-	-	-	-	-	-	26.00	-	-	-
Mendes et al., 2005	Várzea Alegre	Charnockitic rock	HR29	0.13	-	50.0	12.1	-	-	3.19	-	-	-	-	-	-	-	0.30	1.03	7.02	124.82
Mendes et al., 2005	Várzea Alegre	Charnockitic rock	VA262	1.48	-	29.5	57.7	-	-	10.50	-	-	-	-	-	-	-	34.00	2.21	1.24	17.14
Mendes et al., 2005	Várzea Alegre	Charnockitic rock	VA244	1.33	-	33.8	93.9	-	-	15.28	-	-	-	-	-	-	-	32.00	2.24	0.82	30.37
Mendes et al., 2005	Várzea Alegre	Charnockitic rock	VA125	-	-	33.2	-	-	-	-	-	-	-	-	-	-	-	32.00	-	-	-
Mendes et al., 2005	Várzea Alegre	Charnockitic rock	VA16	-	-	33.4	-	-	-	-	-	-	-	-	-	-	-	32.00	-	-	-
Mendes et al., 2005	Várzea Alegre	Charnockitic rock	MP161	-	-	940.0	3.8	-	-	6.15	-	-	-	-	-	-	-	409.60	0.18	5.77	183.46
Mendes et al., 2005	Várzea Alegre	Charnockitic rock	MP128	-	-	1000.0	4.1	-	-	8.02	-	-	-	-	-	-	-	309.30	0.26	5.54	151.54
Mendes et al., 2005	Várzea Alegre	Charnockitic rock	VA90	-	-	35.2	-	-	-	-	-	-	-	-	-	-	-	36.00	-	-	-
Mendes et al., 2005	Várzea Alegre	Charnockitic rock	VA264	2.28	-	38.6	14.1	-	-	79.22	-	-	-	-	-	-	-	36.00	3.20	0.41	14.15
Mendes et al., 2005	Várzea Alegre	Charnockitic rock	VA261	2.14	-	46.0	82.6	-	-	14.08	-	-	-	-	-	-	-	36.00	3.03	0.91	15.66
Mendes et al., 2005	Várzea Alegre	Charnockitic rock	MP718	0.28	-	64.0	13.6	-	-	4.32	-	-	-	-	-	-	-	0.24	2.19	6.04	43.13

Data Source	G5 local name	Rock-type	Sample	Lu	Mo	Nb	Nd	Ni	Pr	Sm	Sn	Ta	Tb	Th	Tl	Tm	U	Y	Yb	Eu/Eu*[a]	La_N/Yb_N[a]
Mendes et al., 2005	Várzea Alegre	Charnockitic rock	MP173	-	-	26.0	-	-	-	-	-	-	-	-	-	-	-	0.43	-	-	-
Mendes et al., 2002	Venda Nova	Norite	VN5	-	-	15.0	-	20	-	-	-	-	-	-	-	-	-	-	-	-	-
Mendes et al., 2002	Venda Nova	Norite	VN22	0.12	-	9.0	29.0	14	-	5.51	-	-	-	-	-	-	-	-	-	1.01	-
Mendes et al., 2002	Venda Nova	Norite	VN10	-	-	5.4	-	11	-	-	-	-	-	-	-	-	-	-	-	-	-
Mendes et al., 2002	Venda Nova	Norite	VN9	-	-	8.6	-	18	-	-	-	-	-	-	-	-	-	-	-	-	-
Mendes et al., 2002	Venda Nova	Norite	VN7	0.10	-	6.0	13.3	29	-	2.94	-	-	-	-	-	-	-	-	-	1.03	-
Mendes et al., 2002	Venda Nova	Norite	VN3	-	-	13.7	-	26	-	-	-	-	-	-	-	-	-	-	-	-	-
Mendes et al., 2002	Venda Nova	Norite	VN26	0.09	-	8.1	18.1	21	-	4.05	-	-	-	-	-	-	-	-	-	0.89	-
Mendes et al., 2002	Venda Nova	Norite	VN8	-	-	8.2	-	19	-	-	-	-	-	-	-	-	-	-	-	-	-
Mendes et al., 2002	Venda Nova	Norite	VN6	0.09	-	12.2	15.4	18	-	3.64	-	-	-	-	-	-	-	-	-	0.97	-
Mendes et al., 2002	Venda Nova	Norite	VN14	-	-	6.0	-	22	-	-	-	-	-	-	-	-	-	-	-	-	-
Mendes et al., 2002	Venda Nova	Norite	VN11	-	-	9.4	-	23	-	-	-	-	-	-	-	-	-	-	-	-	-
Mendes et al., 2002	Venda Nova	Charnoenderbite	VN38	0.12	-	16.4	18.9	41	-	3.60	-	-	-	-	-	-	-	-	-	0.85	-
Mendes et al., 2002	Venda Nova	Charnoenderbite	VN35	-	-	14.8	-	27	-	-	-	-	-	-	-	-	-	-	-	-	-
Mendes et al., 2002	Venda Nova	Charnoenderbite	VN17	0.18	-	9.5	19.4	33	-	3.62	-	-	-	-	-	-	-	-	-	0.92	-

Data Source	G5 local name	Rock-type	Sample	Lu	Mo	Nb	Nd	Ni	Pr	Sm	Sn	Ta	Tb	Th	Tl	Tm	U	Y	Yb	Eu/Eu*[a]	La_N/Yb_N[a]
Mendes et al., 2002	Venda Nova	Charnoenderbite	VN36	-	-	9.1	-	31	-	-	-	-	-	-	-	-	-	-	-	-	-
Mendes et al., 2002	Venda Nova	Charnoenderbite	VN20	-	-	9.2	-	32	-	-	-	-	-	-	-	-	-	-	-	-	-
Mendes et al., 2002	Venda Nova	Charnoenderbite	VN23	0.25	-	9.0	30.1	34	-	5.24	-	-	-	-	-	-	-	-	-	0.78	-
Mendes et al., 2002	Venda Nova	Charnoenderbite	VN15	-	-	8.5	-	23	-	-	-	-	-	-	-	-	-	-	-	-	-
Mendes et al., 2002	Venda Nova	Charnoenderbite	VN19	0.04	-	9.9	3.2	31	-	0.64	-	-	-	-	-	-	-	-	-	0.95	-
Mendes et al., 2002	Venda Nova	Charnoenderbite	VN18	-	-	11.7	-	45	-	-	-	-	-	-	-	-	-	-	-	-	-
Mendes et al., 2002	Venda Nova	Charnoenderbite	VN1	-	-	9.3	-	27	-	-	-	-	-	-	-	-	-	-	-	-	-
Mendes et al., 2002	Venda Nova	Charnoenderbite	VN16	0.25	-	9.4	21.2	28	-	4.26	-	-	-	-	-	-	-	-	-	0.75	-
Mendes et al., 2002	Venda Nova	Charnoenderbite	VN13	0.11	-	11.0	16.6	20	-	3.37	-	-	-	-	-	-	-	-	-	1.01	-
Mendes et al., 2002	Venda Nova	Charnoenderbite	VN24	-	-	9.9	-	21	-	-	-	-	-	-	-	-	-	-	-	-	-
Mendes et al., 2002	Venda Nova	Charnoenderbite	VN2	-	-	10.7	-	18	-	-	-	-	-	-	-	-	-	-	-	-	-
Mendes et al., 2002	Venda Nova	Charnoenderbite	VN27	0.19	-	14.0	17.0	41	-	3.19	-	-	-	-	-	-	-	-	-	0.91	-
Mendes et al., 2002	Venda Nova	Charnoenderbite	VN31	-	-	10.5	-	31	-	-	-	-	-	-	-	-	-	-	-	-	-
Mendes et al., 1997	Várzea Alegre	Charnockitic rock	VA 260	-	-	29.3	-	-	-	-	-	-	-	-	-	-	-	23.00	-	-	-
Mendes et al., 1997	Várzea Alegre	Charnockitic rock	VA 252	-	-	31.0	-	-	-	-	-	-	-	-	-	-	-	26.00	-	-	-

Data Source	G5 local name	Rock-type	Sample	Lu	Mo	Nb	Nd	Ni	Pr	Sm	Sn	Ta	Tb	Th	Tl	Tm	U	Y	Yb	Eu/Eu*[a]	La_N/Yb_N[a]
Mendes et al., 1997	Várzea Alegre	Charnockitic rock	VA 250	-	-	22.4	-	-	-	-	-	-	-	-	-	-	-	19.00	-	-	-
Mendes et al., 1997	Várzea Alegre	Charnockitic rock	VA 241	-	-	33.8	-	-	-	-	-	-	-	-	-	-	-	32.00	-	-	-
Mendes et al., 1997	Várzea Alegre	Charnockitic rock	VA 249	-	-	32.2	-	-	-	-	-	-	-	-	-	-	-	31.00	-	-	-
Mendes et al., 1997	Várzea Alegre	Charnockitic rock	VA 242	-	-	39.5	-	-	-	-	-	-	-	-	-	-	-	37.00	-	-	-
Mendes et al., 1997	Várzea Alegre	Charnockitic rock	VA 263	-	-	30.6	-	-	-	-	-	-	-	-	-	-	-	29.00	-	-	-
Mendes et al., 1997	Várzea Alegre	Charnockitic rock	VA 253	-	-	36.8	-	-	-	-	-	-	-	-	-	-	-	37.00	-	-	-
Mendes et al., 1997	Várzea Alegre	Charnockitic rock	VA 56	0.20	-	30.3	64.6	-	-	10.73	-	-	-	-	-	-	-	25.00	1.54	1.50	25.58
Mendes et al., 1997	Várzea Alegre	Charnockitic rock	VA 237	-	-	43.5	-	-	-	-	-	-	-	-	-	-	-	41.00	-	-	-
Mendes et al., 1997	Várzea Alegre	Charnockitic rock	VA 257	-	-	41.5	-	-	-	-	-	-	-	-	-	-	-	35.00	-	-	-
Mendes et al., 1997	Várzea Alegre	Charnockitic rock	VA 182	-	-	45.0	-	-	-	-	-	-	-	-	-	-	-	40.00	-	-	-
De Campos, 2015	Santa Angélica	Diorite	1	-	-	-	-	-	-	-	-	-	-	-	-	-	-	-	-	-	-
De Campos, 2015	Santa Angélica	Diorite	2	-	-	-	-	-	-	-	-	-	-	-	-	-	-	-	-	-	-
De Campos, 2015	Santa Angélica	Diorite	3	-	-	-	-	-	-	-	-	-	-	-	-	-	-	-	-	-	-
De Campos, 2015	Santa Angélica	Diorite	4a	-	-	-	-	-	-	-	-	-	-	-	-	-	-	-	-	-	-
De Campos, 2015	Santa Angélica	Gabbro	4b	-	-	-	-	-	-	-	-	-	-	-	-	-	-	-	-	-	-
De Campos, 2015	Santa Angélica	Diorite	5b	-	-	-	-	-	-	-	-	-	-	-	-	-	-	-	-	-	-
De Campos, 2015	Santa Angélica	Diorite	6	-	-	-	-	-	-	-	-	-	-	-	-	-	-	-	-	-	-

Data Source	G5 local name	Rock-type	Sample	Lu	Mo	Nb	Nd	Ni	Pr	Sm	Sn	Ta	Tb	Th	Tl	Tm	U	Y	Yb	Eu/Eu*[a]	La_N/Yb_N[a]
De Campos, 2015	Santa Angélica	Diorite	8	-	-	-	-	-	-	-	-	-	-	-	-	-	-	-	-	-	-
De Campos, 2015	Santa Angélica	Diorite	9	-	-	-	-	-	-	-	-	-	-	-	-	-	-	-	-	-	-
De Campos, 2015	Santa Angélica	Granite	10	-	-	-	-	-	-	-	-	-	-	-	-	-	-	-	-	-	-
De Campos, 2015	Santa Angélica	Diorite	12	-	-	-	-	-	-	-	-	-	-	-	-	-	-	-	-	-	-
De Campos, 2015	Santa Angélica	Granite	13	-	-	-	-	-	-	-	-	-	-	-	-	-	-	-	-	-	-
De Campos, 2015	Santa Angélica	Gabbro	14a	-	-	-	-	-	-	-	-	-	-	-	-	-	-	-	-	-	-
De Campos, 2015	Santa Angélica	Diorite	14b	-	-	-	-	-	-	-	-	-	-	-	-	-	-	-	-	-	-
De Campos, 2015	Santa Angélica	Gabbro	15	-	-	-	-	-	-	-	-	-	-	-	-	-	-	-	-	-	-
De Campos, 2015	Santa Angélica	Granite	17	-	-	-	-	-	-	-	-	-	-	-	-	-	-	-	-	-	-
De Campos, 2015	Santa Angélica	Granite	20	-	-	-	-	-	-	-	-	-	-	-	-	-	-	-	-	-	-
De Campos, 2015	Santa Angélica	Granite	21a	-	-	-	-	-	-	-	-	-	-	-	-	-	-	-	-	-	-
De Campos, 2015	Santa Angélica	Diorite	21b	-	-	-	-	-	-	-	-	-	-	-	-	-	-	-	-	-	-
De Campos, 2015	Santa Angélica	Granite	22	-	-	-	-	-	-	-	-	-	-	-	-	-	-	-	-	-	-
De Campos, 2015	Santa Angélica	Granite	23a	-	-	-	-	-	-	-	-	-	-	-	-	-	-	-	-	-	-
De Campos, 2015	Santa Angélica	Diorite	23b	-	-	-	-	-	-	-	-	-	-	-	-	-	-	-	-	-	-
De Campos, 2015	Santa Angélica	Diorite	25	-	-	-	-	-	-	-	-	-	-	-	-	-	-	-	-	-	-
De Campos, 2015	Santa Angélica	Diorite	27	-	-	-	-	-	-	-	-	-	-	-	-	-	-	-	-	-	-
De Campos, 2015	Santa Angélica	Diorite	28	-	-	-	-	-	-	-	-	-	-	-	-	-	-	-	-	-	-
De Campos, 2015	Santa Angélica	Diorite	31	-	-	-	-	-	-	-	-	-	-	-	-	-	-	-	-	-	-
De Campos, 2015	Santa Angélica	Granite	32	-	-	-	-	-	-	-	-	-	-	-	-	-	-	-	-	-	-

Data Source	G5 local name	Rock-type	Sample	Lu	Mo	Nb	Nd	Ni	Pr	Sm	Sn	Ta	Tb	Th	Tl	Tm	U	Y	Yb	Eu/Eu*[a]	La_N/Yb_N[a]
De Campos, 2015	Santa Angélica	Gabbro	33	-	-	-	-	-	-	-	-	-	-	-	-	-	-	-	-	-	-
De Campos, 2015	Santa Angélica	Diorite	34	-	-	-	-	-	-	-	-	-	-	-	-	-	-	-	-	-	-
De Campos, 2015	Santa Angélica	Gabbro	35	-	-	-	-	-	-	-	-	-	-	-	-	-	-	-	-	-	-
De Campos, 2015	Santa Angélica	Diorite	36	-	-	-	-	-	-	-	-	-	-	-	-	-	-	-	-	-	-
De Campos, 2015	Santa Angélica	Diorite	37	-	-	-	-	-	-	-	-	-	-	-	-	-	-	-	-	-	-
De Campos, 2015	Santa Angélica	Granite	38a	-	-	-	-	-	-	-	-	-	-	-	-	-	-	-	-	-	-
De Campos, 2015	Santa Angélica	Gabbro	39a	-	-	-	-	-	-	-	-	-	-	-	-	-	-	-	-	-	-
De Campos, 2015	Santa Angélica	Gabbro	39b	-	-	-	-	-	-	-	-	-	-	-	-	-	-	-	-	-	-
De Campos, 2015	Santa Angélica	Diorite	40	-	-	-	-	-	-	-	-	-	-	-	-	-	-	-	-	-	-
De Campos, 2015	Santa Angélica	Gabbro	41	-	-	-	-	-	-	-	-	-	-	-	-	-	-	-	-	-	-
De Campos, 2015	Santa Angélica	Gabbro	42a	-	-	-	-	-	-	-	-	-	-	-	-	-	-	-	-	-	-
De Campos, 2015	Santa Angélica	Gabbro	42b	-	-	-	-	-	-	-	-	-	-	-	-	-	-	-	-	-	-
De Campos, 2015	Santa Angélica	Diorite	43	-	-	-	-	-	-	-	-	-	-	-	-	-	-	-	-	-	-
De Campos, 2015	Santa Angélica	Diorite	44	-	-	-	-	-	-	-	-	-	-	-	-	-	-	-	-	-	-
De Campos, 2015	Santa Angélica	Gabbro	45	-	-	-	-	-	-	-	-	-	-	-	-	-	-	-	-	-	-
De Campos, 2015	Santa Angélica	Gabbro	46	-	-	-	-	-	-	-	-	-	-	-	-	-	-	-	-	-	-
De Campos, 2015	Santa Angélica	Gabbro	47	-	-	-	-	-	-	-	-	-	-	-	-	-	-	-	-	-	-
De Campos, 2015	Santa Angélica	Diorite	48	-	-	-	-	-	-	-	-	-	-	-	-	-	-	-	-	-	-
De Campos, 2015	Santa Angélica	Diorite	49	-	-	-	-	-	-	-	-	-	-	-	-	-	-	-	-	-	-
De Campos, 2015	Santa Angélica	Granite	50	-	-	-	-	-	-	-	-	-	-	-	-	-	-	-	-	-	-

Data Source	G5 local name	Rock-type	Sample	Lu	Mo	Nb	Nd	Ni	Pr	Sm	Sn	Ta	Tb	Th	Tl	Tm	U	Y	Yb	Eu/Eu*[a]	La_N/Yb_N[a]
Bayer et al., 1987	Santa Angélica	Fine-grained gabbro	P438B	-	-	24.0	-	46	-	-	-	-	-	-	-	-	-	36.00	-	-	-
Bayer et al., 1987	Santa Angélica	Fine-grained gabbro	P191	-	-	17.0	-	45	-	-	-	-	-	-	-	-	-	33.00	-	-	-
Bayer et al., 1987	Santa Angélica	Fine-grained gabbro	P007B	-	-	27.0	-	23	-	-	-	-	-	-	-	-	-	53.00	-	-	-
Bayer et al., 1987	Santa Angélica	Fine-grained gabbro	P297B	-	-	23.0	-	57	-	-	-	-	-	-	-	-	-	41.00	-	-	-
Bayer et al., 1987	Santa Angélica	Coarse-grained gabbro	R412C	-	-	25.0	-	33	-	-	-	-	-	-	-	-	-	49.00	-	-	-
Bayer et al., 1987	Santa Angélica	Coarse-grained gabbro	P050	-	-	18.0	-	39	-	-	-	-	-	-	-	-	-	54.00	-	-	-
Bayer et al., 1987	Santa Angélica	Coarse-grained gabbro	P180A	-	-	25.0	-	44	-	-	-	-	-	-	-	-	-	53.00	-	-	-
Bayer et al., 1987	Santa Angélica	Coarse-grained gabbro	R410S	-	-	25.0	-	37	-	-	-	-	-	-	-	-	-	52.00	-	-	-
Bayer et al., 1987	Santa Angélica	Hybrid rock	P491A	-	-	21.0	-	41	-	-	-	-	-	-	-	-	-	50.00	-	-	-
Bayer et al., 1987	Santa Angélica	Hybrid rock	R410A	-	-	18.0	-	21	-	-	-	-	-	-	-	-	-	12.00	-	-	-
Bayer et al., 1987	Santa Angélica	Hybrid rock	R410B	-	-	25.0	-	63	-	-	-	-	-	-	-	-	-	44.00	-	-	-
Bayer et al., 1987	Santa Angélica	Hybrid rock	R410E	-	-	24.0	-	26	-	-	-	-	-	-	-	-	-	52.00	-	-	-
Bayer et al., 1987	Santa Angélica	Hybrid rock	R410G	-	-	22.0	-	47	-	-	-	-	-	-	-	-	-	43.00	-	-	-
Bayer et al., 1987	Santa Angélica	Hybrid rock	P485A	-	-	21.0	-	47	-	-	-	-	-	-	-	-	-	60.00	-	-	-
Bayer et al., 1987	Santa Angélica	Granite	P485B	-	-	5.0	-	26	-	-	-	-	-	-	-	-	-	6.00	-	-	-
Bayer et al., 1987	Santa Angélica	Granite	P495	-	-	1.0	-	60	-	-	-	-	-	-	-	-	-	27.00	-	-	-
Bayer et al., 1987	Santa Angélica	Granite	P354E	-	-	16.0	-	12	-	-	-	-	-	-	-	-	-	27.00	-	-	-

Data Source	G5 local name	Rock-type	Sample	Lu	Mo	Nb	Nd	Ni	Pr	Sm	Sn	Ta	Tb	Th	Tl	Tm	U	Y	Yb	Eu/Eu*[a]	La_N/Yb_N[a]
Bayer et al., 1987	Santa Angélica	Granite	P187B	-	-	12.0	-	58	-	-	-	-	-	-	-	-	-	27.00	-	-	-
Mello, 2000	Aimorés	Qtz monzodiorite	FAM32	-	-	38.6	78.3	22	-	15.40	-	-	-	2.20	-	-	-	32.30	2.41	0.76	18.94
Mello, 2000	Aimorés	Monzodiorite	FAM28	-	-	51.8	98.4	4	-	20.50	-	-	-	2.20	-	-	-	50.80	3.53	0.77	16.43
Mello, 2000	Aimorés	Monzodiorite	FAM52	-	-	44.9	108.0	4	-	19.50	-	-	-	2.90	-	-	-	46.80	3.30	0.77	15.45
Mello, 2000	Aimorés	Monzodiorite	FAM85	-	-	43.6	98.4	5	-	16.40	-	-	-	6.40	-	-	-	47.80	3.43	0.87	14.17
Mello, 2000	Aimorés	Tonalite to granodiorite	FAM21G	-	-	14.8	25.0	11	-	5.72	-	-	-	5.00	-	-	-	22.50	1.22	0.83	14.81
Mello, 2000	Aimorés	Tonalite to granodiorite	FAM21	-	-	27.7	-	12	-	-	-	-	-	6.90	-	-	-	22.00	1.49	-	17.33
Mello, 2000	Aimorés	Tonalite to granodiorite	FAM21D	-	-	21.0	25.7	12	-	6.09	-	-	-	4.90	-	-	-	18.50	0.95	0.79	19.73
Mello, 2000	Aimorés	Qtz monzodiorite titanite-bearing	FAM71	-	-	34.0	-	8	-	-	-	-	-	9.10	-	-	-	30.90	2.57	-	26.50
Mello, 2000	Aimorés	Qtz monzodiorite titanite-bearing	FAM47	-	-	36.3	100.0	5	-	19.70	-	-	-	3.70	-	-	-	40.80	2.58	0.65	22.58
Mello, 2000	Aimorés	Qtzo monzonite	FAM10	-	-	49.5	86.7	4	-	17.80	-	-	-	3.10	-	-	-	45.20	3.11	0.69	15.28
Mello, 2000	Aimorés	Qtzo monzonite	FAM84D	-	-	45.4	-	3	-	-	-	-	-	6.50	-	-	-	44.40	4.17	-	10.69
Mello, 2000	Aimorés	Qtzo monzonite	FAM84E	-	-	47.0	-	3	-	-	-	-	-	12.00	-	-	-	37.40	3.27	-	14.18
Mello, 2000	Aimorés	Qtzo monzonite	FAM4L	-	-	29.8	72.4	2	-	15.90	-	-	-	5.50	-	-	-	33.50	2.34	0.67	18.09
Mello, 2000	Aimorés	Qtzo monzonite	FAM84F	-	-	37.3	61.3	2	-	13.60	-	-	-	7.70	-	-	-	28.70	1.91	0.69	19.34
Mello, 2000	Aimorés	Qtzo monzonite	FAM4	-	-	44.9	-	2	-	-	-	-	-	8.20	-	-	-	22.80	2.06	-	21.01
Mello, 2000	Aimorés	Qtzo monzonite	FAM4I	-	-	33.6	57.8	15	-	12.40	-	-	-	6.50	-	-	-	26.70	2.04	0.88	16.95
Mello, 2000	Aimorés	Qtzo monzonite	FAM4J	-	-	33.8	-	2	-	-	-	-	-	9.50	-	-	-	27.80	2.49	-	17.82
Mello, 2000	Aimorés	Qtzo monzonite	FAM4K	-	-	29.0	-	2	-	-	-	-	-	8.50	-	-	-	21.70	-	-	-
Mello, 2000	Aimorés	Qtzo monzonite	FAM4H	-	-	33.7	-	2	-	-	-	-	-	4.40	-	-	-	26.60	-	-	-
Mello, 2000	Aimorés	Qtzo monzonite	FAM4G	-	-	32.3	-	2	-	-	-	-	-	8.20	-	-	-	26.10	-	-	-
Mello, 2000	Aimorés	Granite	FAM84C	-	-	23.6	-	2	-	-	-	-	-	5.20	-	-	-	20.20	-	-	-
Mello, 2000	Aimorés	Qtz monzodiorite	FAM25	-	-	52.2	82.2	2	-	16.20	-	-	-	10.00	-	-	-	49.70	3.39	0.74	9.51
Mello, 2000	Aimorés	Granite	FAM24A	-	-	32.8	80.5	1	-	13.30	-	-	-	12.30	-	-	-	31.30	2.15	0.62	25.93

Data Source	G5 local name	Rock-type	Sample	Lu	Mo	Nb	Nd	Ni	Pr	Sm	Sn	Ta	Tb	Th	Tl	Tm	U	Y	Yb	Eu/Eu*[a]	La_N/Yb_N[a]
Mello, 2000	Aimorés	Granite	FAM5A	-	-	36.3	91.1	2	-	15.70	-	-	-	12.40	-	-	-	34.20	2.32	0.63	27.69
Mello, 2000	Aimorés	Granite	FAM9B	-	-	10.2	63.5	2	-	12.80	-	-	-	27.60	-	-	-	29.00	2.69	0.23	13.83
Mello, 2000	Aimorés	Granite	FAM1	-	-	8.0	21.5	1	-	4.49	-	-	-	14.00	-	-	-	8.69	0.42	0.36	32.26
Mello, 2000	Aimorés	Granite	FAM9A	-	-	12.9	-	2	-	-	-	-	-	24.30	-	-	-	23.20	2.15	-	13.39
Mello, 2000	Lagoa Preta	Leucogabbro	MLP1	-	-	17.6	-	164	-	-	-	-	-	1.30	-	-	-	0.44	0.35	-	1.83
Mello, 2000	Lagoa Preta	Diorite	MLP4	-	-	25.0	-	1	-	-	-	-	-	4.90	-	-	-	41.70	1.58	-	8.53
Mello, 2000	Ibituba	Qtzo monzonite	I4	-	-	32.9	-	6	-	-	-	-	-	3.90	-	-	-	42.90	1.75	-	37.79
Ludka and Wiedemann-Leonardos, 2000	Amparo	Coronitic rock	A2	-	-	-	4.5	-	-	1.10	-	-	-	-	-	-	-	4.00	0.22	1.10	8.92
Ludka and Wiedemann-Leonardos, 2000	Amparo	Coronitic rock	A6.2	-	-	-	3.2	-	-	0.80	-	-	-	-	-	-	-	3.00	0.12	1.18	17.81
Ludka and Wiedemann-Leonardos, 2000	Amparo	Coronitic rock	A8.1	0.05	-	-	6.0	-	-	1.12	-	-	-	-	-	-	-	4.00	0.20	1.01	22.32
Ludka and Wiedemann-Leonardos, 2000	Jacutinga	Gabbro-norite	J470	0.15	-	-	14.8	-	-	3.24	-	-	-	-	-	-	-	1.30	0.82	0.99	8.66
Ludka and Wiedemann-Leonardos, 2000	Jacutinga	Gabbro-norite	J471	0.13	-	-	21.5	-	-	4.43	-	-	-	-	-	-	-	15.00	0.87	0.98	12.00
Ludka and Wiedemann-Leonardos, 2000	Jacutinga	Gabbro-norite	J472	0.16	-	-	32.9	-	-	6.97	-	-	-	-	-	-	-	30.00	1.21	0.87	10.48
Ludka and Wiedemann-Leonardos, 2000	Jacutinga	Gabbro-norite	J475	0.09	-	-	11.3	-	-	2.81	-	-	-	-	-	-	-	-	0.53	1.04	9.04

Data Source	G5 local name	Rock-type	Sample	Lu	Mo	Nb	Nd	Ni	Pr	Sm	Sn	Ta	Tb	Th	Tl	Tm	U	Y	Yb	Eu/Eu*[a]	La_N/Yb_N[a]
Ludka and Wiedemann-Leonardos, 2000	Itaoca	Gabbro-norite	Ita25	0.25	-	-	18.6	-	-	3.91	-	-	-	-	-	-	-	5.00	2.19	0.98	5.76
Ludka and Wiedemann-Leonardos, 2000	Itaoca	Coronitic rock	Ita31	0.11	-	-	10.3	-	-	2.66	-	-	-	-	-	-	-	7.00	0.74	1.13	7.14
Ludka and Wiedemann-Leonardos, 2000	Itaoca	Piroxineto	Ita34	0.20	-	-	4.6	-	-	1.05	-	-	-	-	-	-	-	3.00	0.91	1.09	5.18
Ludka and Wiedemann-Leonardos, 2000	Itaoca	Piroxineto	Ita95	0.16	-	-	9.0	-	-	1.21	-	-	-	-	-	-	-	-	1.33	1.11	3.80
De Campos et al., 2004	Santa Angélica	Gabbro	SA1.1	-	-	25.0	-	18	-	-	-	-	-	-	-	-	-	141.00	-	-	-
De Campos et al., 2004	Santa Angélica	Gabbro	SA1.2	-	-	27.0	-	23	-	-	-	-	-	-	-	-	-	53.00	-	-	-
De Campos et al., 2004	Santa Angélica	Gabbro	SA1.3	-	-	23.0	-	41	-	-	-	-	-	-	-	-	-	51.00	-	-	-
De Campos et al., 2004	Santa Angélica	Gabbro	SA1.4	-	-	24.0	-	42	-	-	-	-	-	-	-	-	-	37.00	-	-	-
De Campos et al., 2004	Castelo	Gabbro	CA1.1	-	-	25.0	-	66	-	-	-	-	-	-	-	-	-	60.00	-	-	-
De Campos et al., 2004	Castelo	Diorite	CA1.2	-	-	26.0	-	115	-	-	-	-	-	-	-	-	-	34.00	-	-	-
De Campos et al., 2004	Venda Nova	Gabbro	VN1.1	-	-	21.0	-	35	-	-	-	-	-	-	-	-	-	60.00	-	-	-
De Campos et al., 2004	Venda Nova	Gabbro	VN1.2	-	-	19.0	-	55	-	-	-	-	-	-	-	-	-	39.00	-	-	-
De Campos et al., 2004	Venda Nova	Gabbro	VN1.3	-	-	23.0	-	36	-	-	-	-	-	-	-	-	-	63.00	-	-	-

Data Source	G5 local name	Rock-type	Sample	Lu	Mo	Nb	Nd	Ni	Pr	Sm	Sn	Ta	Tb	Th	Tl	Tm	U	Y	Yb	Eu/Eu*[a]	La_N/Yb_N[a]
De Campos et al., 2004	Santa Angélica	Diorite	SA2.1	-	-	23.0	-	21	-	-	-	-	-	-	-	-	-	50.00	-	-	-
De Campos et al., 2004	Santa Angélica	Diorite	SA2.2	-	-	25.0	-	51	-	-	-	-	-	-	-	-	-	51.00	-	-	-
De Campos et al., 2004	Santa Angélica	Diorite	SA2.3	-	-	24.0	-	41	-	-	-	-	-	-	-	-	-	47.00	-	-	-
De Campos et al., 2004	Santa Angélica	Diorite	SA2.4	-	-	31.0	-	55	-	-	-	-	-	-	-	-	-	11.00	-	-	-
De Campos et al., 2004	Castelo	Diorite	CA2.1	-	-	25.0	-	36	-	-	-	-	-	-	-	-	-	71.00	-	-	-
De Campos et al., 2004	Castelo	Diorite	CA2.2	-	-	29.0	-	37	-	-	-	-	-	-	-	-	-	61.00	-	-	-
De Campos et al., 2004	Castelo	Diorite	CA2.3	-	-	25.0	-	34	-	-	-	-	-	-	-	-	-	69.00	-	-	-
De Campos et al., 2004	Venda Nova	Gabbro	VN2.1	-	-	18.0	-	72	-	-	-	-	-	-	-	-	-	30.00	-	-	-
De Campos et al., 2004	Venda Nova	Diorite	VN2.2	-	-	25.0	-	27	-	-	-	-	-	-	-	-	-	72.00	-	-	-
De Campos et al., 2004	Venda Nova	Diorite	VN2.3	-	-	26.0	-	25	-	-	-	-	-	-	-	-	-	95.00	-	-	-
De Campos et al., 2004	Santa Angélica	Diorite	SA3.1	-	-	22.0	-	47	-	-	-	-	-	-	-	-	-	43.00	-	-	-
De Campos et al., 2004	Santa Angélica	Diorite	SA3.2	-	-	22.0	-	35	-	-	-	-	-	-	-	-	-	36.00	-	-	-
De Campos et al., 2004	Santa Angélica	Diorite	SA3.3	-	-	18.0	-	21	-	-	-	-	-	-	-	-	-	12.00	-	-	-
De Campos et al., 2004	Santa Angélica	Diorite	SA3.4	-	-	23.0	-	20	-	-	-	-	-	-	-	-	-	41.00	-	-	-
De Campos et al., 2004	Castelo	Diorite	CA3.1	-	-	26.0	-	22	-	-	-	-	-	-	-	-	-	54.00	-	-	-

Data Source	G5 local name	Rock-type	Sample	Lu	Mo	Nb	Nd	Ni	Pr	Sm	Sn	Ta	Tb	Th	Tl	Tm	U	Y	Yb	Eu/Eu*[a]	La_N/Yb_N[a]
De Campos et al., 2004	Castelo	Granite	CA3.2	-	-	21.0	-	18	-	-	-	-	-	-	-	-	-	24.00	-	-	-
De Campos et al., 2004	Venda Nova	Diorite	VN3.1	-	-	25.0	-	40	-	-	-	-	-	-	-	-	-	57.00	-	-	-
De Campos et al., 2004	Venda Nova	Diorite	VN3.2	-	-	25.0	-	19	-	-	-	-	-	-	-	-	-	41.00	-	-	-
De Campos et al., 2004	Venda Nova	Diorite	VN3.3	-	-	13.0	-	23	-	-	-	-	-	-	-	-	-	36.00	-	-	-
De Campos et al., 2004	Santa Angélica	Granite	SA4.1	-	-	24.0	-	20	-	-	-	-	-	-	-	-	-	50.00	-	-	-
De Campos et al., 2004	Santa Angélica	Granite	SA4.2	-	-	2.0	-	71	-	-	-	-	-	-	-	-	-	16.00	-	-	-
De Campos et al., 2004	Castelo	Granite	CA4.1	-	-	24.0	-	44	-	-	-	-	-	-	-	-	-	45.00	-	-	-
De Campos et al., 2004	Castelo	Granite	CA4.3	-	-	22.0	-	18	-	-	-	-	-	-	-	-	-	34.00	-	-	-
De Campos et al., 2004	Castelo	Granite	CA4.4	-	-	16.0	-	34	-	-	-	-	-	-	-	-	-	30.00	-	-	-
De Campos et al., 2004	Venda Nova	Granite	VN4.1	-	-	12.0	-	18	-	-	-	-	-	-	-	-	-	101.00	-	-	-
De Campos et al., 2004	Venda Nova	Granite	VN4.2	-	-	12.0	-	20	-	-	-	-	-	-	-	-	-	2.00	-	-	-
De Campos et al., 2004	Venda Nova	Granite	VN4.3	-	-	7.0	-	33	-	-	-	-	-	-	-	-	-	5.00	-	-	-
De Campos et al., 2004	Santa Angélica	Granite	SA5.2	-	-	30.0	-	23	-	-	-	-	-	-	-	-	-	14.00	-	-	-
De Campos et al., 2004	Santa Angélica	Granite	SA5.3	-	-	23.0	-	3	-	-	-	-	-	-	-	-	-	20.00	-	-	-
De Campos et al., 2004	Santa Angélica	Granite	SA5.4	-	-	17.0	-	17	-	-	-	-	-	-	-	-	-	44.00	-	-	-

Data Source	G5 local name	Rock-type	Sample	Lu	Mo	Nb	Nd	Ni	Pr	Sm	Sn	Ta	Tb	Th	Tl	Tm	U	Y	Yb	Eu/Eu*[a]	La_N/Yb_N[a]
De Campos et al., 2004	Castelo	Granite	CA5.1	-	-	22.0	-	28	-	-	-	-	-	-	-	-	-	54.00	-	-	-
De Campos et al., 2004	Castelo	Granite	CA5.2	-	-	18.0	-	36	-	-	-	-	-	-	-	-	-	34.00	-	-	-
De Campos et al., 2004	Castelo	Granite	CA5.3	-	-	15.0	-	25	-	-	-	-	-	-	-	-	-	18.00	-	-	-
Ludka et al., 1998	G5 - Venda Nova	Syeno-monzonite	-	0.75	-	2.0	189.9	10	55.62	30.77	-	-	-	-	-	-	-	28.00	4.19	0.72	35.14
Ludka et al., 1998	Venda Nova	Syeno-monzonite	-	0.31	-	2.1	164.8	15	42.77	27.48	-	-	-	-	-	-	-	34.00	3.10	0.95	34.86
Ludka et al., 1998	Venda Nova	Monzodiorite	-	0.18	-	29.0	114.2	29	-	17.97	-	-	-	-	-	-	-	37.00	1.38	0.84	43.66
Ludka et al., 1998	Venda Nova	Monzodiorite	-	0.09	-	30.0	117.9	40	-	17.84	-	-	-	-	-	-	-	3835.00	0.57	0.96	139.22
Ludka et al., 1998	Venda Nova	Gabbro-norite	-	-	-	14.0	-	-	-	-	-	-	-	-	-	-	-	26.00	-	-	-
Ludka et al., 1998	Venda Nova	Gabbro-norite	-	-	-	20.0	-	95	-	-	-	-	-	-	-	-	-	24.00	-	-	-
Ludka et al., 1998	Venda Nova	Gabbro-norite	-	-	-	-	-	87	-	-	-	-	-	-	-	-	-	-	-	-	-
Ludka et al., 1998	Venda Nova	Gabbro-norite	-	-	-	17.0	-	140	-	-	-	-	-	-	-	-	-	22.00	-	-	-
Offman, 1990 in Ludka et al., 1998	Venda Nova	Allanite granite	-	0.14	-	-	30.1	-	10.42	6.00	-	-	-	-	-	-	-	27.00	0.66	0.60	37.52
Offman, 1990 in Ludka et al., 1998	Venda Nova	Allanite granite	-	0.15	-	-	37.3	-	13.18	6.36	-	-	-	-	-	-	-	39.00	1.10	0.64	30.03
Offman, 1990 in Ludka et al., 1998	Venda Nova	Allanite granite	-	0.10	-	-	38.8	-	10.81	7.17	-	-	-	-	-	-	-	-	1.07	0.77	24.52
Offman, 1990 in Ludka et al., 1998	Venda Nova	Granite	-	0.23	-	35.0	25.2	9	9.09	5.23	-	-	-	-	-	-	-	114.00	2.20	0.59	7.77

Data Source	G5 local name	Rock-type	Sample	Lu	Mo	Nb	Nd	Ni	Pr	Sm	Sn	Ta	Tb	Th	Tl	Tm	U	Y	Yb	Eu/Eu*[a]	La_N/Yb_N[a]
Offman, 1990 in Ludka et al., 1998	Venda Nova	Leucogranite	-	0.12	-	9.0	4.7	10	-	1.79	-	-	-	-	-	-	-	8.00	0.56	-	-
Wiedemann et al., 2002	Várzea Alegre	Basic rock	VA-1	-	-	19.8	-	14	-	-	-	-	-	-	-	-	-	26.00	-	-	-
Wiedemann et al., 2002	Várzea Alegre	Basic rock	VA-2	-	-	10.4	-	46	-	-	-	-	-	-	-	-	-	18.00	-	-	-
Wiedemann et al., 2002	Várzea Alegre	Basic rock	VA-3	-	-	35.7	-	12	-	-	-	-	-	-	-	-	-	54.00	-	-	-
Wiedemann et al., 2002	Várzea Alegre	Intermediate rock	VA-4	-	-	27.6	-	16	-	-	-	-	-	-	-	-	-	42.00	-	-	-
Wiedemann et al., 2002	Várzea Alegre	Intermediate rock	VA-5	-	-	24.1	-	25	-	-	-	-	-	-	-	-	-	33.00	-	-	-
Wiedemann et al., 2002	Várzea Alegre	Intermediate rock	VA-6	-	-	27.5	-	25	-	-	-	-	-	-	-	-	-	36.00	-	-	-
Wiedemann et al., 2002	Várzea Alegre	Intermediate rock	VA-7	-	-	-	-	10	-	-	-	-	-	-	-	-	-	15.00	-	-	-
Wiedemann et al., 2002	Várzea Alegre	Acid rock	VA-8	-	-	33.0	-	10	-	-	-	-	-	-	-	-	-	48.00	-	-	-
Wiedemann et al., 2002	Várzea Alegre	Acid rock	VA-9	-	-	25.0	-	10	-	-	-	-	-	-	-	-	-	39.00	-	-	-
Wiedemann et al., 2002	Várzea Alegre	Intermediate rock	VAc-1	-	-	46.0	-	17	-	-	-	-	-	-	-	-	-	36.00	-	-	-
Wiedemann et al., 2002	Várzea Alegre	Intermediate rock	Vac-2	-	-	36.0	-	15	-	-	-	-	-	-	-	-	-	35.00	-	-	-
Wiedemann et al., 2002	Várzea Alegre	Intermediate rock	VAc-3	-	-	35.0	-	14	-	-	-	-	-	-	-	-	-	36.00	-	-	-
Wiedemann et al., 2002	Várzea Alegre	Intermediate rock	Vac-4	-	-	29.0	-	-	-	-	-	-	-	-	-	-	-	34.00	-	-	-

Data Source	G5 local name	Rock-type	Sample	Lu	Mo	Nb	Nd	Ni	Pr	Sm	Sn	Ta	Tb	Th	Tl	Tm	U	Y	Yb	Eu/Eu*[a]	La_N/Yb_N[a]
Wiedemann et al., 2002	Várzea Alegre	Intermediate rock	Vac-5	-	-	36.0	-	11	-	-	-	-	-	-	-	-	-	29.00	-	-	-
Wiedemann et al., 2002	Santa Angélica	Basic rock	SA-1	-	-	27.0	-	23	-	-	-	-	-	-	-	-	-	53.00	-	-	-
Wiedemann et al., 2002	Santa Angélica	Basic rock	SA-2	-	-	24.0	-	42	-	-	-	-	-	-	-	-	-	37.00	-	-	-
Wiedemann et al., 2002	Santa Angélica	Intermediate rock	SA-3	-	-	23.0	-	21	-	-	-	-	-	-	-	-	-	50.00	-	-	-
Wiedemann et al., 2002	Santa Angélica	Intermediate rock	SA-4	-	-	31.0	-	55	-	-	-	-	-	-	-	-	-	11.00	-	-	-
Wiedemann et al., 2002	Santa Angélica	Intermediate rock	SA-5	-	-	22.0	-	35	-	-	-	-	-	-	-	-	-	36.00	-	-	-
Wiedemann et al., 2002	Santa Angélica	Intermediate rock	SA-6	-	-	18.0	-	21	-	-	-	-	-	-	-	-	-	12.00	-	-	-
Wiedemann et al., 2002	Castelo	Basic rock	CA-1	-	-	25.0	-	66	-	-	-	-	-	-	-	-	-	60.00	-	-	-
Wiedemann et al., 2002	Castelo	Intermediate rock	CA-2	-	-	26.0	-	115	-	-	-	-	-	-	-	-	-	34.00	-	-	-
Wiedemann et al., 2002	Castelo	Intermediate rock	CA-3	-	-	29.0	-	37	-	-	-	-	-	-	-	-	-	61.00	-	-	-
Wiedemann et al., 2002	Castelo	Intermediate rock	CA-4	-	-	25.0	-	34	-	-	-	-	-	-	-	-	-	69.00	-	-	-
Wiedemann et al., 2002	Castelo	Intermediate rock	CA-5	-	-	26.0	-	22	-	-	-	-	-	-	-	-	-	54.00	-	-	-
Wiedemann et al., 2002	Castelo	Acid rock	CA-6	-	-	21.0	-	18	-	-	-	-	-	-	-	-	-	24.00	-	-	-
Wiedemann et al., 2002	Castelo	Acid rock	CA-7	-	-	18.0	-	36	-	-	-	-	-	-	-	-	-	34.00	-	-	-
Wiedemann et al., 2002	Castelo	Acid rock	CA-8	-	-	16.0	-	34	-	-	-	-	-	-	-	-	-	30.00	-	-	-

Data Source	G5 local name	Rock-type	Sample	Lu	Mo	Nb	Nd	Ni	Pr	Sm	Sn	Ta	Tb	Th	Tl	Tm	U	Y	Yb	Eu/Eu*[a]	La_N/Yb_N[a]
Wiedemann et al., 2002	Santa Angélica	Acid rock	SA-7	-	-	24.0	-	20	-	-	-	-	-	-	-	-	-	50.00	-	-	-
Wiedemann et al., 2002	Santa Angélica	Acid rock	SA-8	-	-	2.0	-	71	-	-	-	-	-	-	-	-	-	16.00	-	-	-
Wiedemann et al., 2002	Santa Angélica	Acid rock	SA-9	-	-	17.0	-	17	-	-	-	-	-	-	-	-	-	44.00	-	-	-
Wiedemann et al., 2002	Mimoso do Sul	High-calk-alkaline/alkaline rocks	MI-1	-	-	-	-	-	-	-	-	-	-	-	-	-	-	-	-	-	-
Wiedemann et al., 2002	Mimoso do Sul	High-calk-alkaline/alkaline rocks	MI-2	-	-	-	-	-	-	-	-	-	-	-	-	-	-	52.00	-	-	-
Wiedemann et al., 2002	Mimoso do Sul	High-calk-alkaline/alkaline rocks	MI-3	-	-	-	-	-	-	-	-	-	-	-	-	-	-	79.00	-	-	-
Wiedemann et al., 2002	Mimoso do Sul	High-calk-alkaline/alkaline rocks	MI-4	-	-	-	-	-	-	-	-	-	-	-	-	-	-	73.00	-	-	-
Wiedemann et al., 2002	Conceição do Muqui	High-calk-alkaline/alkaline rocks	CM-1	-	-	-	-	-	-	-	-	-	-	-	-	-	-	25.00	-	-	-
Wiedemann et al., 2002	Conceição do Muqui	High-calk-alkaline/alkaline rocks	CM-2	-	-	-	-	-	-	-	-	-	-	-	-	-	-	2.00	-	-	-
Wiedemann et al., 2002	Conceição do Muqui	High-calk-alkaline/alkaline rocks	CM-3	-	-	-	-	-	-	-	-	-	-	-	-	-	-	56.00	-	-	-
Wiedemann et al., 2002	Conceição do Muqui	High-calk-alkaline/alkaline rocks	CM-4	-	-	-	-	-	-	-	-	-	-	-	-	-	-	41.00	-	-	-

Data Source	G5 local name	Rock-type	Sample	Lu	Mo	Nb	Nd	Ni	Pr	Sm	Sn	Ta	Tb	Th	Tl	Tm	U	Y	Yb	Eu/Eu*[a]	La_N/Yb_N[a]
Zanon et al., 2015	Santa Angélica	Diorite	D5MIX23A	0.84	-	62.0	152.3	23	38.96	22.50	-	1.62	2.14	12.30	-	0.76	1.09	32.00	5.40	0.57	22.36
Zanon et al., 2015	Santa Angélica	Diorite	M5G9	0.24	-	55.0	86.1	34	22.47	13.50	-	0.15	0.95	8.10	-	0.24	1.86	29.00	1.80	0.81	40.64
Zanon et al., 2015	Santa Angélica	Gabbro	M5G17	0.30	-	49.0	98.3	39	24.64	14.20	-	0.43	1.26	6.10	-	0.32	1.78	31.00	1.80	0.78	41.43
Zanon et al., 2015	Santa Angélica	Diorite	F5G38	0.33	-	61.0	121.6	7	33.59	16.50	-	0.37	1.43	17.50	-	0.37	2.49	29.00	2.30	0.74	51.09
Zanon et al., 2015	Santa Angélica	Diorite	H18	0.40	-	56.0	119.9	9	32.56	18.60	-	1.59	1.59	17.60	-	0.42	2.30	32.00	2.50	0.68	46.17
Zanon et al., 2015	Santa Angélica	Diorite	H517	0.28	-	39.0	70.0	5	17.75	10.70	-	1.76	0.92	8.80	-	0.26	1.65	20.00	1.40	0.83	41.66
Zanon et al., 2015	Santa Angélica	Diorite	H16A	0.32	-	57.0	114.4	14	30.01	17.20	-	3.46	1.51	15.40	-	0.39	2.20	36.00	2.50	0.73	39.67
Zanon et al., 2015	Santa Angélica	Diorite	M5G16	0.31	-	25.0	62.1	41	14.98	9.70	-	0.60	0.89	3.90	-	0.23	0.91	22.00	1.70	0.94	29.31
Zanon et al., 2015	Santa Angélica	Granite	F5G15	0.29	-	71.0	134.3	3	39.71	19.60	-	3.04	1.55	21.20	-	0.50	2.42	27.00	2.80	0.66	54.75
Zanon et al., 2015	Santa Angélica	Gabbro	MP19	0.45	-	51.0	88.8	44	22.96	13.50	-	1.82	1.17	9.00	-	0.36	1.35	27.00	2.30	0.78	32.86
Paes et al., 2010	Medina		CP-334	0.30	-	26.4	116.3	6	33.60	22.90	-	0.90	2.00	-	-	0.40	-	35.80	1.90	0.19	44.78
Paes et al., 2010	Medina		PJ-404	0.60	-	54.1	173.3	1	47.60	27.50	-	1.70	3.10	-	-	0.70	-	56.50	4.30	0.15	28.50
Paes et al., 2010	Medina		CP-12	0.60	-	39.2	94.0	6	26.10	15.70	-	2.70	1.50	-	-	0.70	-	41.60	3.60	0.33	21.52
Paes et al., 2010	Medina		CP-005B	0.20	-	29.3	104.5	5	31.10	17.10	-	1.30	1.50	-	-	0.30	-	26.20	1.50	0.45	67.24
Paes et al., 2010	Medina		CP-358	0.20	-	31.3	147.5	7	45.30	24.20	-	1.10	2.10	-	-	0.30	-	35.30	1.80	0.31	73.79
Paes et al., 2010	Medina		CP-005A	0.20	-	27.6	77.8	5	23.30	13.50	-	1.50	1.10	-	-	0.20	-	24.30	1.30	0.52	58.14
Paes et al., 2010	Medina		CP-119A	0.10	-	30.7	69.9	5	21.60	13.70	-	1.20	1.20	-	-	0.20	-	18.60	1.00	0.31	62.36
Paes et al., 2010	Medina		CP-019	0.20	-	36.9	105.8	5	29.40	19.70	-	1.10	1.80	-	-	0.30	-	35.60	1.80	0.21	48.58
Paes et al., 2010	Medina		CP-361	0.30	-	28.9	92.1	5	27.70	16.70	-	1.50	1.60	-	-	0.40	-	33.10	2.00	0.32	40.96
Paes et al., 2010	Medina		CH-530	0.20	-	25.8	121.6	0	34.60	16.40	-	1.00	1.30	-	-	0.30	-	24.60	1.70	0.48	61.47

Data Source	G5 local name	Rock-type	Sample	Lu	Mo	Nb	Nd	Ni	Pr	Sm	Sn	Ta	Tb	Th	Tl	Tm	U	Y	Yb	Eu/Eu*[a]	La_N/Yb_N[a]
Paes et al., 2010	Medina		CP-353	0.40	-	38.6	156.2	5	48.20	27.40	-	1.60	2.30	-	-	0.50	-	46.40	3.00	0.26	46.97
Paes et al., 2010	Medina		CP-009A	0.20	-	28.4	100.5	5	28.90	16.60	-	1.10	1.50	-	-	0.20	-	26.40	1.70	0.34	52.43
Paes et al., 2010	Medina		CP-009B	0.10	-	18.4	36.3	5	10.80	6.70	-	0.70	0.50	-	-	0.10	-	9.20	0.50	0.72	68.23
Paes et al., 2010	Medina		CP-015A	0.30	-	34.6	124.4	5	33.80	20.80	-	1.80	1.70	-	-	0.40	-	31.20	2.20	0.30	43.82
Paes et al., 2010	Medina		CP-051	0.10	-	18.7	33.6	5	10.20	6.20	-	1.30	0.60	-	-	0.10	-	11.70	0.80	0.48	45.17
Paes et al., 2010	Medina		CP-003	0.50	-	53.8	160.5	5	46.30	25.30	-	3.70	2.10	-	-	0.80	-	49.90	4.20	0.47	36.60
Paes et al., 2010	Medina		CP-023	0.50	-	49.7	117.3	5	30.50	19.90	-	3.10	2.00	-	-	0.60	-	48.80	3.80	0.40	22.44
Paes et al., 2010	Medina		CP-118	0.40	-	54.0	187.1	5	53.70	28.50	-	2.80	2.30	-	-	0.60	-	51.50	3.20	0.57	53.81
Paes et al., 2010	Medina		CP-001	0.40	-	45.1	175.3	5	48.90	26.50	-	2.70	2.10	-	-	0.60	-	53.00	2.80	0.58	59.71
Serrano et al., 2018	Medina	Granite	M61B	0.10	-	12.9	61.6		18.00	11.90	-	0.10	1.00	-	-	0.10	-	12.90	0.70	0.22	68.86
Serrano et al., 2018	Medina	Granite	R13A	0.50	-	40.3	135.9		39.00	23.30	-	1.50	2.10	-	-	0.60	-	44.40	3.70	0.35	32.76
Paes et al., 2010	Caladão		PJ-302B	0.30	-	38.0	180.5	3	48.10	31.10	-	1.40	3.00	-	-	0.50	-	55.70	2.40	0.16	55.31
Paes et al., 2010	Caladão		PJ-389	0.10	-	26.8	126.0	2	37.20	18.60	-	1.30	1.60	-	-	0.10	-	15.00	0.50	0.21	220.46
Paes et al., 2010	Córrego do Calção		CH-89	0.30	-	28.2	125.3	1	35.40	18.40	-	1.20	1.70	-	-	0.40	-	32.90	1.80	0.48	63.11
Paes et al., 2010	Córrego do Calção		CH-90	0.30	-	28.2	123.5	2	37.50	19.10	-	1.10	1.60	-	-	0.30	-	27.50	1.80	0.44	65.36
Paes et al., 2010	Córrego do Calção		CH-91	0.06	0.3	12.5	33.8	2	9.36	5.00	6.00	1.00	0.39	23.30	-	0.07	6.20	6.00	0.36	0.27	90.83
Paes et al., 2010	Emparedado		CP-170	0.20	-	30.8	77.8	2	23.30	13.40	-	2.30	1.10	-	-	0.30	-	24.40	1.70	0.55	48.07
Paes et al., 2010	Emparedado		CP-175A	0.20	0.1	22.0	39.3	2	11.00	6.40	4.00	1.40	0.64	19.70	-	0.25	5.10	18.10	1.31	0.78	31.45
Paes et al., 2010	Emparedado		CP-251	0.14	0.1	11.7	87.9	3	26.15	12.60	3.00	0.30	0.76	25.80	-	0.18	1.80	19.90	0.84	1.23	120.39

Data Source	G5 local name	Rock-type	Sample	Lu	Mo	Nb	Nd	Ni	Pr	Sm	Sn	Ta	Tb	Th	Tl	Tm	U	Y	Yb	Eu/Eu*[a]	La_N/Yb_N[a]
Paes et al., 2010	Fazenda Liberdade		PJ-185	0.10	-	18.4	105.0	3	28.80	18.80	-	1.10	1.10	-	-	0.10	-	16.40	0.80	0.19	88.99
Paes et al., 2010	Fazenda Liberdade		PJ-192	0.20	-	22.3	129.2	8	35.00	21.30	-	0.90	1.20	-	-	0.20	-	24.90	1.40	0.17	60.87
Paes et al., 2010	Fazenda Liberdade		PJ-196	0.20	-	27.9	75.6	18	21.20	13.80	-	1.60	1.20	-	-	0.30	-	25.70	1.60	0.32	35.18
Paes et al., 2010	Fazenda Liberdade		PJ-250	0.30	-	19.6	173.3	7	48.20	23.50	-	1.50	1.40	-	-	0.40	-	33.10	2.10	0.65	70.95
Paes et al., 2010	Fazenda Liberdade		PJ-272	0.40	-	23.9	80.1	6	21.70	15.10	-	0.90	1.70	-	-	0.50	-	48.60	2.90	0.28	19.83
Paes et al., 2010	Fazenda Liberdade		PJ-280	0.57	2.9	44.5	192.7	3	53.42	33.30	<1	1.50	2.92	136.30	-	0.82	5.60	70.50	4.56	0.65	31.71
Paes et al., 2010	Fazenda Liberdade		PJ-306	0.88	2.1	50.7	206.9	4	56.32	35.10	1.00	1.80	3.53	136.50	-	1.21	5.10	98.50	5.03	0.75	31.35
Paes et al., 2010	General Dutra		CH-021	0.30	-	20.0	82.9	6	21.30	13.10	-	0.70	1.20	-	-	0.40	-	22.80	2.00	0.36	30.95
Paes et al., 2010	General Dutra		CH-290	0.30	-	43.4	126.4	5	35.80	17.60	-	2.10	1.30	-	-	0.40	-	27.00	2.20	0.53	47.50
Paes et al., 2010	General Dutra		CH-574	0.30	-	24.4	84.7	2	24.30	13.90	-	1.10	1.20	-	-	0.40	-	27.60	2.20	0.31	29.94
Paes et al., 2010	General Dutra		CH-600	0.65	1.1	30.6	166.4	4	45.36	25.00	3.00	1.40	3.13	85.60	-	1.03	4.00	113.00	4.99	2.70	26.37
Paes et al., 2010	Landim		CH-010	0.20	-	30.3	86.1	2	26.40	12.70	-	2.40	1.10	-	-	0.20	-	19.50	1.30	0.82	75.77
Paes et al., 2010	Landim		CH-511	0.05	0.5	15.7	36.8	1	10.16	7.76	7.00	0.90	0.54	29.20	-	0.08	5.70	7.10	0.42	0.45	62.12
Paes et al., 2010	Landim		CH-514	0.20	-	31.3	133.2	4	37.70	16.90	-	2.70	1.10	-	-	0.30	-	21.50	1.60	0.82	85.96
Paes et al., 2010	Pau de Canoa		CH-310	0.99	0.9	25.9	111.3	5	30.97	20.10	4.00	1.80	2.11	71.40	-	1.06	9.50	67.30	6.52	0.89	14.11
Paes et al., 2010	Pau de Canoa		CH-389	0.40	-	29.7	116.4	9	32.10	19.50	-	1.60	1.80	-	-	0.50	-	45.80	2.80	0.39	33.64
Paes et al., 2010	Pedra Azul		CP-167	0.20	-	41.3	160.8	2	47.20	22.00	-	1.60	1.20	-	-	0.20	-	22.90	1.50	0.52	106.07
Paes et al., 2010	Pedra Azul		CP-215A	0.20	-	36.7	93.1	5	26.10	12.60	-	2.40	0.80	-	-	0.20	-	15.30	1.40	0.97	63.90

Data Source	G5 local name	Rock-type	Sample	Lu	Mo	Nb	Nd	Ni	Pr	Sm	Sn	Ta	Tb	Th	Tl	Tm	U	Y	Yb	Eu/Eu*[a]	La_N/Yb_N[a]
Paes et al., 2010	Pedra Azul		CP-228A	0.08	0.1	9.2	23.2	1	7.13	3.90	1.00	0.40	0.31	6.90	-	0.10	0.80	7.40	0.50	1.18	62.97
Paes et al., 2010	Pedra Grande		PJ-007	0.40	-	35.5	111.3	7	30.60	16.00	-	1.90	1.80	-	-	0.50	-	40.20	2.80	0.57	29.78
Paes et al., 2010	Pedra Grande		PJ-008	0.30	-	49.1	110.4	7	30.20	16.80	-	2.80	2.00	-	-	0.40	-	41.20	2.30	0.37	35.29
Paes et al., 2010	Pedra Grande		PJ-017	0.40	-	41.8	211.3	3	57.30	28.60	-	1.70	2.40	-	-	0.60	-	46.30	2.90	0.24	47.96
Paes et al., 2010	Santa Cruz de Salinas		CH-102	0.30	-	38.3	537.0	1	27.10	13.50	-	1.80	1.10	-	-	0.30	-	23.50	1.90	0.43	48.22
Paes et al., 2010	Santa Cruz de Salinas		CH-108	0.60	-	31.1	63.5	1	18.40	10.80	-	2.80	1.60	-	-	0.60	-	47.90	3.20	0.44	19.43
Paes et al., 2010	Santa Cruz de Salinas		CH-171	0.22	0.4	18.6	42.4	0	11.78	6.41	6.00	1.30	0.95	44.00	-	0.31	12.50	37.90	1.70	0.71	24.55
Paes et al., 2010	Santa Cruz de Salinas		CH-237	0.40	-	20.8	79.0	1	24.20	13.00	-	1.20	1.30	-	-	0.50	-	33.00	2.90	0.34	27.25
Aranda, 2018	Cláudio Afonso	Monzogranite	P 246-A	0.36	<2	21.5	87.3	88	22.59	15.20	<0.3	0.60	1.36	4.20	<0.5	0.40	0.77	30.76	2.50	0.81	25.16
Aranda, 2018	Cláudio Afonso	Monzogranite	P 276-A	0.50	<2	33.2	128.0	36	31.22	22.80	<0.3	0.88	2.02	2.20	<0.5	0.56	0.33	45.24	3.50	0.70	21.84
Aranda, 2018	Cláudio Afonso	Monzodiorite	P 292-B	0.48	<2	34.6	135.7	12	35.66	21.90	<0.3	0.92	1.88	4.70	<0.5	0.55	0.80	42.86	3.30	0.83	29.68
Aranda, 2018	Cláudio Afonso	Monzogranite	P 292-A	0.42	2	29.1	120.6	50	30.87	19.70	<0.3	1.02	1.66	5.70	<0.5	0.46	0.92	36.55	3.00	0.83	29.24
Aranda, 2018	Cláudio Afonso	Monzodiorite	P 277-A	0.35	<2	27.0	102.3	21	27.05	17.40	<0.3	0.81	1.44	7.80	<0.5	0.40	1.48	31.52	2.50	0.84	29.45
Aranda, 2018	Cláudio Afonso	Jotunite	P 193-B	0.44	<2	31.3	110.7	10	27.76	18.60	<0.3	0.91	1.71	5.40	<0.5	0.52	0.60	37.94	3.10	0.83	23.99
Aranda, 2018	Cláudio Afonso	Monzodiorite	P 156-A	0.36	<2	23.7	86.5	30	21.71	15.30	<0.3	0.64	1.41	9.90	<0.5	0.41	1.32	31.74	2.50	0.81	23.38
Aranda, 2018	Cláudio Afonso	Qtz mangerite	P 197-C	0.31	<2	14.7	100.3	11	27.11	15.50	<0.3	<0.05	1.21	5.00	<0.5	0.33	0.99	26.23	2.10	0.93	39.10
Aranda, 2018	Cláudio Afonso	Qtz monzonite	P 288	0.34	<2	20.5	128.2	10	34.48	19.80	<0.3	0.18	1.45	9.30	<0.5	0.38	0.76	30.48	2.30	0.94	44.03
Aranda, 2018	Cláudio Afonso	Qtz monzonite	P 295-B	0.77	<2	43.5	212.4	12	52.64	39.00	<0.3	2.23	3.55	17.30	<0.5	0.98	1.29	85.34	5.80	0.51	21.45
Aranda, 2018	Cláudio Afonso	Qtz monzonite	P 285-B	0.39	<2	17.3	122.1	9	31.54	19.50	<0.3	0.20	1.58	6.60	<0.5	0.44	0.60	38.03	2.70	0.89	32.39
Aranda, 2018	Cláudio Afonso	Qtz monzonite	P 206-D	0.35	<2	20.6	116.6	10	30.59	18.50	<0.3	0.16	1.47	7.50	<0.5	0.40	0.62	30.45	2.50	1.03	35.62
Aranda, 2018	Cláudio Afonso	Qtz monzonite	P 98	0.34	<2	19.8	88.8	13	25.00	13.60	<0.3	1.39	1.09	16.40	1.00	0.34	2.11	24.61	2.10	0.79	36.50
Aranda, 2018	Cláudio Afonso	Qtz monzonite	P 297	0.31	<2	18.7	66.7	10	18.71	11.20	<0.3	0.42	0.99	9.00	<0.5	0.33	1.92	26.22	2.10	0.89	25.62
Aranda, 2018	Cláudio Afonso	Qtz monzonite	P 296	0.41	<2	28.0	116.4	12	30.96	18.70	<0.3	0.64	1.63	10.40	<0.5	0.49	1.02	38.64	2.90	0.70	29.94
Aranda, 2018	Cláudio Afonso	Qtz monzonite	P 146-B	0.44	<2	22.5	130.4	12	36.40	20.50	<0.3	1.17	1.64	15.70	0.70	0.48	1.10	38.90	3.10	0.68	33.25

Data Source	G5 local name	Rock-type	Sample	Lu	Mo	Nb	Nd	Ni	Pr	Sm	Sn	Ta	Tb	Th	Tl	Tm	U	Y	Yb	Eu/Eu*[a]	La_N/Yb_N[a]
Aranda, 2018	Cláudio Afonso	Qtz monzonite	P 291	0.40	<2	26.8	113.2	10	30.95	19.10	<0.3	0.50	1.57	12.90	<0.5	0.47	1.20	36.99	2.90	0.69	31.43
Aranda, 2018	Cláudio Afonso	Qtz monzonite	P 298	0.38	<2	15.9	159.9	11	46.61	22.00	<0.3	0.34	1.51	19.80	<0.5	0.41	1.26	30.65	2.50	0.77	59.71
Aranda, 2018	Cláudio Afonso	Qtz monzonite	P 90-A	0.33	<2	16.8	166.0	8	50.32	20.60	<0.3	0.26	1.38	16.90	<0.5	0.35	1.86	30.38	2.20	0.89	92.73
Aranda, 2018	Cláudio Afonso	Qtz monzonite	P 102	0.40	<2	27.3	113.8	10	31.62	18.70	1.50	0.67	1.57	14.60	<0.5	0.47	1.45	37.16	3.00	0.67	31.80
Baltazar et al., 2010	Aimorés	Charnockite	OF174A	0.21	0.7	16.4	127.4	11	35.22	19.60	-	0.60	1.62	19.70	-	0.28	0.90	27.30	1.46	70.88	4.93
Baltazar et al., 2010	Aimorés	Charnockite	OF172A	0.21	0.8	23.5	52.6	5	13.72	8.50	-	0.80	0.94	4.90	-	0.26	0.70	21.30	1.68	23.03	4.25
Baltazar et al., 2010	Aimorés	Charnockite	OF198	1.33	0.9	40.8	159.3	9	41.89	29.60	-	2.50	3.57	68.40	-	1.36	1.80	101.20	8.68	12.53	3.43
Baltazar et al., 2010	Aimorés	Charnockite	SS058	0.78	0.6	22.4	124.8	14	32.23	23.10	-	1.60	2.57	62.60	-	0.80	1.40	66.10	5.42	15.46	3.38
Baltazar et al., 2010	Aimorés	Charnockite	SS023	0.16	0.1	5.9	20.3	5	5.17	3.90	-	0.30	0.52	1.50	-	0.19	0.20	17.00	0.95	14.97	3.40
Baltazar et al., 2010	Aimorés	Charnockite	OF245C	0.48	0.9	44.5	85.8	9	21.04	16.10	-	3.60	2.00	2.20	-	0.59	2.80	57.40	3.48	11.43	2.31
Baltazar et al., 2010	Aimorés	Granite	OF156	0.18	0.7	29.1	256.0	5	75.21	29.90	-	1.20	1.31	108.90	-	0.25	2.10	24.70	1.53	140.30	6.70
Baltazar et al., 2010	Aimorés	Granite	OF166B	0.46	2.7	34.6	88.4	5	22.57	16.60	-	1.60	1.77	6.30	-	0.54	1.50	42.80	3.34	16.19	3.04
Baltazar et al., 2010	Aimorés	Granite	SS094	0.12	0.9	24.0	174.6	7	51.18	18.80	-	1.00	0.92	17.70	-	0.11	0.40	12.50	0.85	198.53	8.37
Baltazar et al., 2010	Aimorés	Mangerite	LC168	0.44	1.1	34.3	107.3	11	25.88	16.70	-	1.80	1.56	3.50	-	0.50	0.90	39.70	3.32	19.52	3.62
Baltazar et al., 2010	Aimorés	Mangerite	OF144	0.32	0.2	9.0	26.7	16	7.12	4.60	-	0.70	0.79	4.40	-	0.37	0.40	25.80	2.26	9.40	4.31
Baltazar et al., 2010	Aimorés	Mangerite	SS027A	0.43	0.7	31.2	94.9	10	24.04	16.00	-	1.70	1.53	1.90	-	0.50	0.80	38.00	2.80	21.19	3.46
Baltazar et al., 2010	Aimorés	Mangerite	OF051	0.59	1.1	36.9	122.8	10	31.00	21.10	-	2.40	2.16	14.50	-	0.59	1.10	55.00	3.95	18.95	3.31

Data Source	G5 local name	Rock-type	Sample	Lu	Mo	Nb	Nd	Ni	Pr	Sm	Sn	Ta	Tb	Th	Tl	Tm	U	Y	Yb	Eu/Eu*[a]	La_N/Yb_N[a]
Baltazar et al., 2010	Aimorés	Diorite	OF022	0.53	0.8	34.3	153.7	18	38.78	23.90	-	1.70	2.22	4.60	-	0.62	0.60	53.90	4.11	23.33	3.74
Baltazar et al., 2010	Aimorés	Mangerite	OF074B	0.24	1.3	20.0	119.9	7	32.89	16.20	-	0.90	1.05	35.10	-	0.25	1.80	22.30	1.71	53.07	5.23
Baltazar et al., 2010	Aimorés	Mangerite	OF117	0.54	0.9	35.7	106.2	9	27.49	18.80	-	1.90	2.00	13.80	-	0.54	0.60	47.60	3.42	20.76	3.52
Baltazar et al., 2010	Aimorés	Charnockite	OF23	1.12	0.2	9.7	12.6	9	3.22	2.83	-	0.30	0.77	0.80	-	0.93	0.40	35.20	6.89	1.59	3.62
Baltazar et al., 2010	Aimorés	Charnockite	OF24	0.33	0.3	10.4	26.0	7	7.06	4.69	-	0.50	0.57	8.50	-	0.32	0.70	19.10	1.98	11.44	4.51
Baltazar et al., 2010	Aimorés	Charnockite	OF93	0.10	0.1	15.2	49.8	21	13.02	7.77	-	0.50	0.66	13.30	-	0.08	0.40	8.60	0.51	73.37	4.49
Baltazar et al., 2010	Aimorés	Charnockite	OF98A	0.38	3.8	6.9	17.1	5	4.49	3.18	-	0.30	0.73	2.30	-	0.44	0.40	31.40	2.56	5.56	4.17
Baltazar et al., 2010	Aimorés	Charnockite	OF101	0.31	0.1	11.2	20.1	6	5.21	3.15	-	0.30	0.75	1.20	-	0.34	0.30	27.60	2.17	7.80	5.01
Baltazar et al., 2010	Aimorés	Gabbro	SA16	0.41	0.9	38.8	122.6	10	30.06	20.17	-	1.60	1.80	9.30	-	0.52	1.20	41.20	3.00	23.64	3.28
Pedrosa-Soares et al., 2006	Aimorés	Granite	SC-01A	0.31	-	17.0	75.7	30	18.03	12.30	-	1.20	1.21	16.30	-	0.35	-	36.00	2.07	27.07	4.25
Pedrosa-Soares et al., 2006	Aimorés	Granite	SC-13	0.29	-	14.0	78.2	31	18.58	12.10	-	1.40	0.04	16.70	-	0.29	-	31.00	2.00	0.79	26.12
Pedrosa-Soares, et al. 2006	Aimorés	Granite	MQ-03A	-	-	-	-	-	-	-	-	-	-	-	-	-	-	-	-	-	-
Pedrosa-Soares, et al. 2006	Aimorés	Charnockite	MQ-03B	-	-	-	-	-	-	-	-	-	-	-	-	-	-	-	-	-	-
Pedrosa-Soares, et al. 2006	Aimorés	Granite	MQ-04	-	-	-	-	-	-	-	-	-	-	-	-	-	-	-	-	-	-

Data Source	G5 local name	Rock-type	Sample	Lu	Mo	Nb	Nd	Ni	Pr	Sm	Sn	Ta	Tb	Th	Tl	Tm	U	Y	Yb	Eu/Eu*[a]	La_N/Yb_N[a]
Pedrosa-Soares, et al. 2006	Aimorés	Charnockite	MQ-81	-	-	-	-	-	-	-	-	-	-	-	-	-	-	-	-	-	-
Pedrosa-Soares, et al. 2006	Aimorés	Charnockite	MQ-123	-	-	-	-	-	-	-	-	-	-	-	-	-	-	-	-	-	-
Pedrosa-Soares, et al. 2006	Aimorés	Charnockite	EC-92	-	-	-	-	-	-	-	-	-	-	-	-	-	-	-	-	-	-
Pedrosa-Soares, et al. 2006	Aimorés	Charnockite	EC-90	-	-	-	-	-	-	-	-	-	-	-	-	-	-	-	-	-	-
Pedrosa-Soares, et al. 2006	Aimorés	Sienogranite	EC-01	-	-	-	-	-	-	-	-	-	-	-	-	-	-	-	-	-	-
Pedrosa-Soares, et al. 2006	Aimorés	Charnockite	EB-89A	-	-	-	-	-	-	-	-	-	-	-	-	-	-	-	-	-	-
Pedrosa-Soares, et al. 2006	Aimorés	Norite	EP-15	-	-	-	-	-	-	-	-	-	-	-	-	-	-	-	-	-	-
Wiedemann et al., 2002	Pedra Azul	Basic rock	PA-I	-	-	55.0	-	26	-	-	-	-	-	-	-	-	-	50.00	-	-	-
Wiedemann et al., 2002	Pedra Azul	Basic rock	PA-2	-	-	57.0	-	27	-	-	-	-	-	-	-	-	-	37.00	-	-	-
Wiedemann et al., 2002	Pedra Azul	Intermediate rock	PA-3	-	-	-	-	25	-	-	-	-	-	-	-	-	-	48.00	-	-	-
Wiedemann et al., 2002	Pedra Azul	Intermediate rock	PA-4	-	-	51.0	-	17	-	-	-	-	-	-	-	-	-	55.00	-	-	-
Wiedemann et al., 2002	Pedra Azul	Intermediate rock	PA-5	-	-	59.0	-	16	-	-	-	-	-	-	-	-	-	65.00	-	-	-
Wiedemann et al., 2002	Pedra Azul	Acid rock	PA-6	-	-	52.0	-	8	-	-	-	-	-	-	-	-	-	75.00	-	-	-
Wiedemann et al., 2002	Pedra Azul	Acid rock	PA-7	-	-	34.0	-	5	-	-	-	-	-	-	-	-	-	37.00	-	-	-

Data Source	G5 local name	Rock-type	Sample	Lu	Mo	Nb	Nd	Ni	Pr	Sm	Sn	Ta	Tb	Th	Tl	Tm	U	Y	Yb	Eu/Eu*[a]	La_N/Yb_N[a]

[a] Normalized elements for chondrite (Boynton, 1984).

$Eu/Eu^* = Eu_N / [(Sm_N) + (Gd_N)]^{1/2}$

References

Aranda, R., 2018. Petrology of the Afonso Cláudio Intrusive Complex (Espírito Santo State, Araçuaí Orogen): Insights from Petrography, Lithogeochemistry, U-Pb Geochronology and Lu-Hf Isotopes. Instituto de Geociências, Universidade Federal de Minas Gerais, Belo Horizonte (MS Dissertation, 64pp.).

Baltazar, O.F., Zucchetti, M., Oliveira, S.A.M., Scandolara, J., Silva, L.C., 2010. Geologia das Folhas São Gabriel Da Palha e Linhares. Programa Geologia do Brasil, CPRM–Serviço Geológico do Brasil, Belo Horizonte.

Bayer, P., Schmidt-Thomé, R., Weber-Diefenbach, K., Horn, H.A., 1987. Complex concentric granitoid intrusions in the Coastal Mobile Belt, Espírito Santo, Brazil: the Santa Angélica pluton - an example. Geologische Rundschau 76, 357-371.

Boynton, W.V., 1984. Cosmochemistry of the rare earth elements: meteorites studies. In: Henderson, P. (Ed.), Rare Earth Element Geochemistry. Elsevier, pp. 63–114.

De Campos, C.P., Mendes, J.C., Ludka, I.P., Medeiros, S.R., Moura, J.C., Wallfass, C., 2004. A review of the Brasilian magmatism in southern Espírito Santo, Brazil, with emphasis on post-collisional magmatism. Journal of the Virtual Explorer 17, 1-35.

De Campos, C.P., 2015. Chaotic flow patterns from a deep plutonic environment: a case study on natural magma mixing. Pure and Applied Geophysics 172, 1815–1833.

Ludka, I.P., Wiedemann, C.M., Töpfner, C., 1998. On the origin of incompatible element enrichment in the Venda Nova pluton, State of Espírito Santo, southeast Brazil. Journal of South America Earth Sciences 11, 473-486.

Ludka, I.P., Wiedemann-Leonardos, C.M., 2000. Further signs of an enriched mantle source under the Neoproterozoic Araçuaí-Ribeira Mobile Belt. Revista Brasileira de Geociências 30, 95-98.

Mello, F.M., 2000. Litogeoquímica e Química Mineral do Maciço Charnockítico Aimorés-MG. Universidade de São Paulo, São Paulo (Ph.D. Thesis, 167 pp.).

Mendes, J.C., McReath, I., Wiedemann, C.M., Figueiredo M.C.H., 1997. Charnockitóides do Maciço de Várzea Alegre: um novo exemplo do magmatismo cálcio-alcalino de alto-K no arco magmático do Espírito Santo. Revista Brasileira de Geociências 27, 13-24.

Mendes, J.C., Wiedemann, C.M., McReath, I., 2002. Norito e Charnoenderbitos da Borda do Maciço Intrusivo de Venda Nova, Espírito Santo. Anuário do Instituto de Geociências - UFRJ 25, 99-124.

Mendes, J.C., Medeiros, S.R., McReath, I., De Campos, C.M.P., 2005. Cambro-Ordovician magmatism in SE Brazil: U-Pb and Rb-Sr ages, combined with Sr and Nd isotopic data of Charnockitic rocks from the Várzea Alegre complex. Gondwana Research 8, 337-345.

Paes, V.J.C., Raposo, F.O., Pinto, C.P., Oliveira, F.A.R. (Orgs.), 2010. Projeto Jequitinhonha, Estados de Minas Gerais e Bahia: texto explicativo. Geologia e Recursos Minerais das Folhas Comercinho, Jequitinhonha, Almenara, Itaobim, Joaíma e Rio do Prado. Programa Geologia do Brasil. CPRM – Serviço Geológico do Brasil, Belo Horizonte.

Pedrosa-Soares, A.C., Queiroga, G.N., Gradim, C.T., Roncato, J.G., Novo, T.A., Jacobsohn, T., Silva, K.L., 2006. Nota Explicativa da Folha Mantena, 1:100.000. Programa Geologia do Brasil, CPRM–UFMG.

Serrano, P., Pedrosa-Soares, A., Medeiros-Junior, E., Fonte-Boa, T., Araujo, C., Dussin, I., Queiroga, G., Lana, C., 2018. A-type Medina batholith and post-collisional anatexis in the Araçuaí orogen (SE Brazil). Lithos 320-321, 515-536.

Wiedemann, C.M., Medeiros, S.R., Ludka, I.P., Mendes, J.C., Costa-de-Moura, J., 2002. Architecture of late orogenic plutons in the Araçuaí-Ribeira fold belt, Southeast Brazil. Gondwana Research 5, 381-399.

Zanon, M.L., Chaves, A.O., Rangel, C.V.G.T., Gaburo, L., Pires, C.R., 2015. Os aspectos geológicos do Maciço anta Angélica (ES): uma nova abordagem. Brazilian Journal of Geology 45, 609-633.

APPENDIX H - Supplementary File 4.E - U-Pb and Lu-Hf Data

LA(SF)-ICP-MS U-Pb zircon results data from Sample CA-02 (Aracê - Pedra Azul pluton)

Identifier	Lu-Hf identifier	f206[a]	^{207}Pb	^{206}Pb	U	Th[b]/U	^{206}Pb/^{204}Pb	Ratios[c]									Ages (Ma)[c]								% conc[e]
								^{207}Pb/^{206}Pb	2s (%)	^{207}Pb/^{235}U	2s (%)	^{206}Pb/^{238}U	2s (%)	Rho[d]	^{208}Pb/^{232}Th	2s (%)	^{207}Pb/^{206}Pb	2s	^{206}Pb/^{238}U	2s	^{207}Pb/^{235}U	2s	^{208}Pb/^{232}Th	2s	
								Data for Wetherill plot										abs		abs		abs		abs	
		(%)	CPS	CPS	(ppm)																				
5.sSMPABC090	seq0166.dat	0.00	14658	845	40	2.54	0	0.058	1.647	0.659	2.394	0.083	1.738	0.726	0.025	2.314	518	36	513	9	514	10	500	11	100
5.sSMPABC055	seq0137.dat	0.00	12639	728	34	3.02	0	0.058	2.343	0.660	3.292	0.083	2.312	0.702	0.025	3.238	515	51	514	11	514	13	493	16	100
5.sSMPABC087	-	0.00	14966	863	40	2.51	0	0.058	1.630	0.661	2.379	0.083	1.733	0.728	0.024	2.317	518	36	515	9	515	10	483	11	100
5.sSMPABC062	seq0149.dat	0.00	23001	1322	62	3.84	0	0.057	2.106	0.661	2.931	0.083	2.038	0.696	0.023	2.791	509	46	516	10	515	12	458	13	100
5.sSMPABC092	-	0.00	13856	798	37	2.86	0	0.058	1.961	0.663	2.742	0.083	1.916	0.699	0.024	2.733	515	43	517	10	517	11	482	13	100
5.sSMPABC016	seq0133.dat	0.00	14164	818	38	2.51	0	0.058	2.148	0.666	3.007	0.084	2.104	0.700	0.026	2.886	519	47	518	10	518	12	512	15	100
5.sSMPABC073	seq0168.dat	0.00	16677	961	45	2.16	0	0.058	1.458	0.666	2.164	0.084	1.598	0.739	0.026	2.074	515	32	519	8	518	9	520	11	100
5.sSMPABC026	-	0.00	18205	1065	49	2.84	0	0.058	1.795	0.676	2.603	0.084	1.884	0.724	0.025	2.470	548	39	519	9	524	11	501	12	99
5.sSMPABC069	-	0.00	32097	1880	86	2.70	0	0.059	1.417	0.678	2.135	0.084	1.597	0.748	0.024	2.165	552	31	519	8	525	9	480	10	99
5.sSMPABC070	seq0169.dat	0.00	20973	1225	56	2.58	0	0.058	1.763	0.677	2.544	0.084	1.834	0.721	0.025	2.724	546	39	520	9	525	10	498	13	99
5.sSMPABC010	seq0143.dat	0.26	41214	2401	110	1.91	1050	0.058	1.439	0.676	2.102	0.084	1.532	0.729	0.025	1.604	540	31	520	8	524	9	498	8	99
5.sSMPABC046	seq0160.dat	0.00	27696	1612	74	2.91	0	0.058	1.392	0.675	2.080	0.084	1.546	0.743	0.024	1.962	537	30	521	8	524	9	489	9	99
5.sSMPABC041	seq0139.dat	0.00	58481	3407	156	1.46	0	0.058	1.253	0.676	2.044	0.084	1.615	0.790	0.023	2.135	540	27	521	8	525	8	468	10	99
5.sSMPABC014	-	0.83	34740	2001	92	1.92	326	0.058	3.160	0.669	4.034	0.084	2.508	0.622	0.023	1.878	515	69	522	13	520	17	468	9	100
5.sSMPABC079	seq0163.dat	0.00	15879	924	42	2.35	0	0.058	1.650	0.677	2.409	0.084	1.754	0.728	0.026	2.481	536	36	522	9	525	10	515	13	99
5.sSMPABC012	-	0.82	28399	1629	75	2.53	332	0.057	3.141	0.668	3.979	0.084	2.443	0.614	0.026	1.784	506	69	523	12	520	16	515	9	101
5.sSMPABC048	-	0.00	20496	1193	54	2.09	0	0.058	1.546	0.679	2.282	0.085	1.679	0.736	0.027	2.279	538	34	523	8	526	9	543	12	99
5.sSMPABC089	seq0167.dat	0.00	23059	1343	61	2.58	0	0.058	1.666	0.679	2.433	0.085	1.773	0.729	0.025	2.596	538	36	523	9	526	10	508	13	99
5.sSMPABC094	seq0165.dat	0.00	30145	1766	80	1.71	0	0.059	1.605	0.683	2.427	0.085	1.821	0.750	0.025	2.923	552	35	523	9	529	10	506	14	99
5.sSMPABC029	seq0145.dat	0.00	68543	3966	181	1.41	0	0.058	1.106	0.676	1.815	0.085	1.439	0.793	0.025	1.681	524	24	524	7	524	7	499	8	100

LA(SF)-ICP-MS U-Pb zircon results data from Sample CA-02 (Aracê - Pedra Azul pluton)

Identifier	Lu-Hf identifier	f206[a]	^{207}Pb	^{206}Pb	U	Th[b]/U	$^{206}Pb/^{204}Pb$	Ratios[c]									Ages (Ma)[c]									% conc[e]
								$^{207}Pb/^{206}Pb$	2s (%)	$^{207}Pb/^{235}U$	2s (%)	$^{206}Pb/^{238}U$	2s (%)	Rho[d]	$^{208}Pb/^{232}Th$	2s (%)	$^{207}Pb/^{206}Pb$	2s	$^{206}Pb/^{238}U$	2s	$^{207}Pb/^{235}U$	2s	$^{208}Pb/^{232}Th$	2s		
		(%)	CPS	CPS	(ppm)			Data for Wetherill plot									abs		abs		abs		abs		
5.sSMPABC007	-	0.00	22642	1310	60	2.41	0	0.058	1.400	0.676	2.111	0.085	1.581	0.749	0.025	1.925	525	31	525	8	525	9	498	10	100
5.sSMPABC078	seq0164.dat	0.00	56287	3289	149	1.35	0	0.058	1.095	0.684	1.789	0.085	1.414	0.791	0.027	1.725	546	24	525	7	529	7	532	9	99
5.sSMPABC047	-	0.00	19227	1111	51	2.91	0	0.058	1.489	0.677	2.238	0.085	1.671	0.747	0.024	1.964	521	33	526	8	525	9	488	9	100
5.sSMPABC006	seq0141.dat	0.00	28480	1647	75	3.07	0	0.058	1.521	0.678	2.242	0.085	1.647	0.735	0.026	2.013	524	33	526	8	526	9	515	10	100
5.sSMPABC030	seq0146.dat	0.00	37998	2197	100	1.49	0	0.058	1.245	0.678	1.990	0.085	1.552	0.780	0.027	1.962	523	27	526	8	526	8	529	10	100
5.sSMPABC027	-	0.43	55210	3213	145	1.36	625	0.058	1.846	0.683	2.524	0.085	1.721	0.682	0.025	1.573	537	40	527	9	529	10	508	8	100
5.sSMPABC011	seq0162.dat	0.00	28517	1648	75	2.37	0	0.058	1.367	0.679	2.120	0.085	1.620	0.764	0.024	1.994	522	30	527	8	526	9	481	9	100
5.sSMPABC071	-	0.00	23642	1372	62	1.96	0	0.058	1.706	0.683	2.517	0.085	1.851	0.735	0.027	2.765	531	37	528	9	529	10	548	15	100
5.sSMPABC043	seq0138.dat	0.00	18376	1078	49	2.95	0	0.059	1.704	0.692	2.496	0.086	1.823	0.731	0.024	2.389	555	37	529	9	534	10	485	12	99
5.sSMPABC045	seq0150.dat	0.00	15604	913	42	2.76	0	0.059	1.726	0.691	2.509	0.086	1.821	0.726	0.026	2.366	549	38	530	9	533	10	523	12	99
5.sSMPABC037	**seq0140.dat**	**0.00**	**21108**	**1235**	**55**	**1.68**	**0**	**0.059**	**1.778**	**0.695**	**2.621**	**0.086**	**1.926**	**0.735**	**0.028**	**2.956**	**549**	**39**	**533**	**10**	**536**	**11**	**567**	**16**	**99**
5.sSMPABC032	**seq0134.dat**	**0.00**	**20486**	**1203**	**53**	**1.61**	**0**	**0.059**	**1.805**	**0.701**	**2.599**	**0.087**	**1.871**	**0.720**	**0.027**	**3.093**	**557**	**39**	**535**	**10**	**540**	**11**	**529**	**16**	**99**
5.sSMPABC058	**-**	**0.00**	**22454**	**1312**	**58**	**2.64**	**0**	**0.058**	**1.387**	**0.702**	**2.088**	**0.087**	**1.561**	**0.748**	**0.025**	**1.989**	**545**	**30**	**539**	**8**	**540**	**9**	**502**	**10**	**100**
5.sSMPABC008	**seq0144.dat**	**0.00**	**12823**	**748**	**33**	**1.86**	**0**	**0.058**	**1.972**	**0.701**	**2.822**	**0.087**	**2.018**	**0.715**	**0.026**	**3.042**	**542**	**43**	**539**	**10**	**540**	**12**	**512**	**16**	**100**
5.sSMPABC054	**-**	**0.00**	**21234**	**1241**	**56**	**2.61**	**0**	**0.058**	**1.642**	**0.703**	**2.412**	**0.087**	**1.766**	**0.732**	**0.026**	**2.407**	**547**	**36**	**539**	**9**	**541**	**10**	**514**	**12**	**100**
5.sSMPABC004	**seq0142.dat**	**0.00**	**11067**	**652**	**29**	**2.65**	**0**	**0.059**	**2.411**	**0.722**	**3.390**	**0.089**	**2.383**	**0.703**	**0.027**	**3.335**	**563**	**53**	**549**	**13**	**552**	**15**	**538**	**18**	**100**
5.sSMPABC040	**-**	**0.00**	**15484**	**914**	**38**	**1.80**	**0**	**0.059**	**1.439**	**0.744**	**2.183**	**0.091**	**1.641**	**0.752**	**0.028**	**2.236**	**569**	**31**	**564**	**9**	**565**	**10**	**553**	**12**	**100**
5.sSMPABC059	**seq0147.dat**	**0.00**	**72683**	**4280**	**178**	**1.67**	**0**	**0.059**	**1.172**	**0.743**	**1.927**	**0.092**	**1.530**	**0.794**	**0.028**	**1.890**	**563**	**26**	**565**	**8**	**564**	**8**	**549**	**10**	**100**
5.sSMPABC057	**seq0136.dat**	**0.00**	**39682**	**2370**	**93**	**1.05**	**0**	**0.060**	**1.222**	**0.788**	**1.988**	**0.096**	**1.567**	**0.789**	**0.027**	**2.291**	**593**	**26**	**589**	**9**	**590**	**9**	**540**	**12**	**100**
5.sSMPABC053	**seq0161.dat**	**0.00**	**126232**	**7566**	**289**	**1.17**	**0**	**0.060**	**1.068**	**0.807**	**1.837**	**0.098**	**1.495**	**0.814**	**0.030**	**1.822**	**601**	**23**	**601**	**9**	**601**	**8**	**590**	**11**	**100**

LA(SF)-ICP-MS U-Pb zircon results data from Sample CA-02 (Aracê - Pedra Azul pluton)

Identifier	Lu-Hf identifier	f206[a]	^{207}Pb	^{206}Pb	U	Th[b]/U	^{206}Pb/^{204}Pb	Ratios[c]									Ages (Ma)[c]								% conc[e]
								^{207}Pb/^{206}Pb	2s (%)	^{207}Pb/^{235}U	2s (%)	^{206}Pb/^{238}U	2s (%)	Rho[d]	^{208}Pb/^{232}Th	2s (%)	^{207}Pb/^{206}Pb	2s	^{206}Pb/^{238}U	2s	^{207}Pb/^{235}U	2s	^{208}Pb/^{232}Th	2s	
		(%)	CPS	CPS	(ppm)			Data for Wetherill plot									abs		abs		abs		abs	

LA(SF)-ICP-MS U-Pb zircon results data from Sample CA-04 (Vitória pluton)

Identifier	Lu-Hf identifier	f206[a]	^{207}Pb	^{206}Pb	U	Th[b]/U	^{206}Pb/^{204}Pb	Ratios[c]									Ages (Ma)[c]								% conc[e]
								^{207}Pb/^{206}Pb	2s (%)	^{207}Pb/^{235}U	2s (%)	^{206}Pb/^{238}U	2s (%)	Rho[d]	^{208}Pb/^{232}Th	*2s (%)*	^{207}Pb/^{206}Pb	2s	^{206}Pb/^{238}U	2s	^{207}Pb/^{235}U	2s	^{208}Pb/^{232}Th	2s	
		(%)	CPS	CPS	(ppm)			Data for Wetherill plot									abs		abs		abs		abs	
5.sSMPABC114	seq0181.dat	0.00	26907	1535	41	2.14	24	0.057	1.595	0.622	2.450	0.079	1.860	0.759	0.025	2.123	493	35	490	9	491	9	508	10	100
5.sSMPABC017	seq0170.dat	0.00	33589	1920	50	1.86	1920	0.057	1.382	0.631	2.218	0.080	1.734	0.782	0.025	1.820	497	30	496	8	496	9	505	9	100
5.sSMPABC016	-	0.00	29190	1671	44	1.84	1671	0.057	2.656	0.632	3.493	0.080	2.269	0.649	0.023	3.269	500	58	497	11	497	14	465	15	100
5.sSMPABC027	seq0192.dat	0.00	31337	1781	47	2.21	1781	0.057	1.601	0.630	2.431	0.080	1.829	0.752	0.024	2.042	485	35	498	9	496	9	489	10	100
5.sSMPABC049	seq0185.dat	0.00	43066	2441	64	1.69	41	0.057	1.711	0.631	2.536	0.081	1.871	0.738	0.025	2.386	479	38	500	9	497	10	502	12	100
5.sSMPABC014	-	0.00	22967	1302	34	2.32	17	0.057	1.765	0.631	2.535	0.081	1.819	0.718	0.023	1.958	479	39	501	9	497	10	469	9	100
5.sSMPABC116	-	0.00	120051	6826	178	1.51	6826	0.057	1.143	0.633	2.086	0.081	1.745	0.836	0.025	1.928	486	25	500	8	498	8	497	9	100
5.sSMPABC032	-	0.00	56607	3230	84	2.42	3230	0.057	1.349	0.637	2.202	0.081	1.740	0.790	0.023	1.751	494	30	502	8	500	9	457	8	100
5.sSMPABC059	seq0197.dat	0.00	34249	1947	51	2.31	1947	0.057	1.442	0.635	2.260	0.081	1.740	0.770	0.026	1.872	486	32	502	8	499	9	512	9	100
5.sSMPABC067	seq0179.dat	0.00	30201	1726	45	1.98	1726	0.057	1.400	0.638	2.232	0.081	1.739	0.779	0.024	1.825	497	31	502	8	501	9	482	9	100

LA(SF)-ICP-MS U-Pb zircon results data from Sample CA-04 (Vitória pluton)

Identifier	Lu-Hf identifier	f206[a]	^{207}Pb	^{206}Pb	U	Th[b]/U	^{206}Pb/^{204}Pb	Ratios[c]									Ages (Ma)[c]								% conc[e]
								^{207}Pb/^{206}Pb	2s (%)	^{207}Pb/^{235}U	2s (%)	^{206}Pb/^{238}U	2s (%)	Rho[d]	^{208}Pb/^{232}Th	*2s (%)*	^{207}Pb/^{206}Pb	2s	^{206}Pb/^{238}U	2s	^{207}Pb/^{235}U	2s	^{208}Pb/^{232}Th	2s	
								Data for Wetherill plot										abs		abs		abs		abs	
5.sSMPABC030	-	0.00	59061	3360	87	1.74	1680	0.057	1.195	0.636	2.046	0.081	1.661	0.812	0.023	1.717	487	26	503	8	500	8	466	8	100
5.sSMPABC115	-	0.00	30878	1780	45	2.40	12	0.058	1.474	0.647	2.331	0.081	1.805	0.775	0.024	1.934	517	32	505	9	507	9	475	9	99
5.sSMPABC009	-	0.00	24831	1416	37	2.39	1416	0.057	1.490	0.640	2.321	0.081	1.779	0.767	0.024	1.808	493	33	505	8	503	9	486	9	100
5.sSMPABC069	-	0.00	26435	1512	39	2.24	1512	0.057	1.399	0.642	2.243	0.081	1.753	0.782	0.026	1.787	498	31	505	8	504	9	514	9	100
5.sSMPABC095	-	0.00	111881	6424	164	2.66	6424	0.057	1.184	0.645	2.095	0.082	1.728	0.825	0.022	1.797	508	26	505	8	506	8	445	8	100
5.sSMPABC054	seq0184.dat	0.00	45735	2628	67	2.38	2628	0.057	1.218	0.646	2.093	0.082	1.702	0.813	0.026	1.646	510	27	505	8	506	8	509	8	99
5.sSMPABC068	seq0180.dat	0.00	96396	5540	142	0.94	504	0.057	1.061	0.647	1.962	0.082	1.650	0.841	0.025	1.669	510	23	506	8	506	8	502	8	100
5.sSMPABC047	seq0198.dat	0.00	44064	2539	65	2.15	2539	0.058	1.319	0.649	2.190	0.082	1.748	0.798	0.025	1.776	515	29	506	8	508	9	495	9	99
5.sSMPABC099	-	0.00	33243	1904	49	2.24	112	0.057	1.344	0.646	2.205	0.082	1.748	0.793	0.024	1.803	502	30	506	8	506	9	487	9	100
5.sSMPABC090	seq0177.dat	0.00	37132	2122	54	2.29	2122	0.057	1.330	0.644	2.196	0.082	1.747	0.796	0.025	1.782	497	29	507	8	505	9	493	9	100
5.sSMPABC019	-	0.00	51400	2939	75	2.82	2939	0.057	1.242	0.645	2.103	0.082	1.697	0.807	0.025	1.612	498	27	507	8	505	8	496	8	100
5.sSMPABC075	-	0.00	20060	1151	29	2.08	1151	0.057	1.604	0.647	2.427	0.082	1.822	0.751	0.027	1.952	505	35	507	9	507	10	531	10	100
5.sSMPABC013	-	0.00	27873	1591	41	2.14	35	0.057	1.647	0.644	2.474	0.082	1.846	0.746	0.026	1.999	494	36	507	9	505	10	519	10	100
5.sSMPABC051	seq0187.dat	0.00	52132	2979	76	1.48	186	0.057	1.295	0.645	2.173	0.082	1.745	0.803	0.025	1.900	497	29	507	8	505	9	504	9	100
5.sSMPABC055	seq0183.dat	0.00	36255	2080	53	2.75	149	0.057	1.307	0.648	2.181	0.082	1.745	0.800	0.026	1.692	506	29	507	8	507	9	519	9	100
5.sSMPABC057	seq0196.dat	0.00	56295	3213	82	2.09	3213	0.057	1.192	0.644	2.051	0.082	1.670	0.814	0.025	1.629	494	26	507	8	505	8	491	8	100
5.sSMPABC109	seq0195.dat	0.00	60695	3472	89	1.30	3472	0.057	1.189	0.646	2.070	0.082	1.695	0.819	0.024	1.845	499	26	507	8	506	8	477	9	100
5.sSMPABC078	-	0.00	36312	2076	53	2.04	2076	0.057	1.312	0.646	2.162	0.082	1.719	0.795	0.023	1.810	498	29	508	8	506	9	464	8	100
5.sSMPABC091	-	0.00	22402	1279	33	1.94	1279	0.057	1.559	0.645	2.376	0.082	1.793	0.755	0.025	2.033	495	34	508	9	506	9	491	10	100
5.sSMPABC056	-	0.00	21669	1239	32	1.98	1239	0.057	1.626	0.647	2.438	0.082	1.816	0.745	0.026	2.027	499	36	508	9	507	10	512	10	100

LA(SF)-ICP-MS U-Pb zircon results data from Sample CA-04 (Vitória pluton)

Identifier	Lu-Hf identifier	f206[a]	^{207}Pb	^{206}Pb	U	Th[b]/U	^{206}Pb/^{204}Pb	Ratios[c]									Ages (Ma)[c]								% conc[e]
								^{207}Pb/^{206}Pb	2s (%)	^{207}Pb/^{235}U	2s (%)	^{206}Pb/^{238}U	2s (%)	Rho[d]	^{208}Pb/^{232}Th	*2s (%)*	^{207}Pb/^{206}Pb	2s abs	^{206}Pb/^{238}U	2s abs	^{207}Pb/^{235}U	2s abs	^{208}Pb/^{232}Th	2s abs	
		(%)	CPS	CPS	(ppm)			Data for Wetherill plot																	
5.sSMPABC011	seq0172.dat	0.09	74111	4241	108	2.27	70	0.057	1.294	0.648	2.101	0.082	1.655	0.788	0.024	1.722	500	28	509	8	507	8	487	8	100
5.sSMPABC031	-	0.00	22403	1280	33	1.50	1280	0.057	1.558	0.647	2.392	0.082	1.815	0.759	0.025	2.184	497	34	509	9	506	9	494	11	100
5.sSMPABC072	-	0.00	69487	3980	101	1.22	3980	0.057	1.135	0.648	2.016	0.082	1.666	0.826	0.025	1.730	502	25	509	8	507	8	508	9	100
5.sSMPABC080	-	0.00	27932	1599	41	2.54	400	0.057	1.468	0.648	2.334	0.082	1.815	0.778	0.026	1.877	501	32	509	9	507	9	510	9	100
5.sSMPABC008	-	0.00	137977	7877	201	1.89	7877	0.057	1.104	0.647	1.997	0.082	1.665	0.834	0.023	1.665	495	24	509	8	506	8	456	7	100
5.sSMPABC060	-	0.00	29244	1669	43	1.62	334	0.057	1.437	0.646	2.256	0.082	1.739	0.771	0.027	1.947	494	32	509	8	506	9	533	10	100
5.sSMPABC035	seq0191.dat	0.00	23184	1319	34	1.85	120	0.057	2.180	0.645	3.034	0.082	2.110	0.696	0.024	2.735	487	48	509	10	505	12	482	13	100
5.sSMPABC028	-	0.15	45767	2606	67	1.99	84	0.057	1.366	0.646	2.201	0.082	1.726	0.784	0.022	1.695	489	30	509	8	506	9	448	8	100
5.sSMPABC058	-	0.00	38364	2179	56	2.07	16	0.057	1.831	0.644	2.701	0.082	1.985	0.735	0.025	2.334	483	40	510	10	505	11	496	12	101
5.sSMPABC079	-	0.00	19884	1135	29	2.13	1135	0.057	1.699	0.648	2.501	0.082	1.836	0.734	0.026	2.130	495	37	510	9	507	10	525	11	100
5.sSMPABC092	-	0.00	38274	2175	56	2.01	57	0.057	1.302	0.645	2.151	0.082	1.712	0.796	0.025	1.850	485	29	510	8	505	8	497	9	101
5.sSMPABC107	seq0173.dat	0.00	166780	9490	243	1.57	316	0.057	1.002	0.645	1.919	0.082	1.637	0.853	0.025	1.590	488	22	510	8	506	8	502	8	100
5.sSMPABC113	seq0189.dat	0.00	88132	4987	128	0.72	4987	0.057	1.290	0.643	2.221	0.082	1.807	0.814	0.026	2.431	475	29	511	9	504	9	525	13	101
5.sSMPABC010	-	0.00	85550	4863	124	1.20	540	0.057	1.126	0.646	1.984	0.082	1.634	0.823	0.026	1.725	485	25	511	8	506	8	509	8	101
5.sSMPABC087	seq0178.dat	0.00	86701	4922	126	1.97	41	0.057	1.180	0.646	2.096	0.082	1.732	0.826	0.025	1.769	483	26	511	8	506	8	497	9	101
5.sSMPABC108	**-**	**0.00**	**38694**	**2216**	**56**	**1.72**	**2216**	**0.057**	**1.362**	**0.659**	**2.225**	**0.084**	**1.760**	**0.791**	**0.025**	**1.994**	**502**	**30**	**517**	**9**	**514**	**9**	**500**	**10**	**100**
5.sSMPABC040	**-**	**0.00**	**57871**	**3327**	**83**	**1.62**	**35**	**0.057**	**1.635**	**0.663**	**2.528**	**0.084**	**1.928**	**0.763**	**0.025**	**2.358**	**510**	**36**	**518**	**9**	**516**	**10**	**491**	**12**	**100**
5.sSMPABC038	**seq0190.dat**	**0.00**	**43458**	**2492**	**62**	**2.66**	**2492**	**0.057**	**1.360**	**0.663**	**2.180**	**0.084**	**1.704**	**0.782**	**0.024**	**1.733**	**505**	**30**	**519**	**8**	**516**	**9**	**484**	**8**	**100**
5.sSMPABC070	**-**	**0.20**	**34169**	**1957**	**49**	**1.77**	**67**	**0.057**	**1.579**	**0.663**	**2.389**	**0.084**	**1.793**	**0.751**	**0.025**	**1.888**	**503**	**35**	**520**	**9**	**517**	**10**	**507**	**9**	**100**
5.sSMPABC074	**seq0182.dat**	**0.12**	**87290**	**5041**	**122**	**1.91**	**60**	**0.058**	**1.286**	**0.683**	**2.200**	**0.086**	**1.785**	**0.811**	**0.027**	**1.840**	**520**	**28**	**530**	**9**	**529**	**9**	**542**	**10**	**100**

LA(SF)-ICP-MS U-Pb zircon results data from Sample CA-04 (Vitória pluton)

Identifier	Lu-Hf identifier	f206[a] (%)	^{207}Pb CPS	^{206}Pb CPS	U (ppm)	Th[b]/U	^{206}Pb/^{204}Pb	Ratios[c] ^{207}Pb/^{206}Pb	2s (%)	^{207}Pb/^{235}U	2s (%)	^{206}Pb/^{238}U	2s (%)	Rho[d]	^{208}Pb/^{232}Th	*2s (%)*	Ages (Ma)[c] ^{207}Pb/^{206}Pb	2s abs	^{206}Pb/^{238}U	2s abs	^{207}Pb/^{235}U	2s abs	^{208}Pb/^{232}Th	2s abs	% conc[e]
										Data for Wetherill plot															
5.sSMPABC015	**seq0171.dat**	**0.00**	**42431**	**2462**	**58**	**1.78**	**2462**	**0.058**	**1.258**	**0.700**	**2.117**	**0.087**	**1.703**	**0.804**	**0.027**	**1.727**	**531**	**28**	**541**	**9**	**539**	**9**	**531**	**9**	**100**
5.sSMPABC100	seq0174.dat	0.00	60304	3447	91	0.75	3447	0.057	1.330	0.623	2.203	0.079	1.756	0.797	0.024	2.407	498	29	490	8	492	9	481	12	99
5.sSMPABC018	seq0175.dat	0.00	43607	2503	66	1.01	2503	0.057	1.307	0.628	2.162	0.079	1.723	0.797	0.026	2.027	507	29	492	8	495	8	512	10	99
5.sSMPABC089	-	0.00	32822	1874	50	2.19	55	0.057	1.366	0.625	2.198	0.079	1.722	0.783	0.025	1.833	495	30	493	8	493	9	501	9	100
5.sSMPABC097	seq0176.dat	0.31	92352	5207	138	1.19	36	0.056	1.704	0.622	2.507	0.080	1.839	0.733	0.024	2.161	467	38	496	9	491	10	481	10	101
5.sSMPABC029	seq0193.dat	0.00	80835	4616	121	0.73	4616	0.057	1.173	0.633	2.046	0.080	1.676	0.819	0.025	1.989	495	26	498	8	498	8	502	10	100
5.sSMPABC117	seq0194.dat	0.06	98900	5629	147	0.61	245	0.057	1.228	0.634	2.158	0.081	1.774	0.822	0.025	2.326	488	27	501	8	499	8	498	12	100
5.sSMPABC039	-	0.00	36666	2093	54	1.34	16	0.057	1.524	0.640	2.384	0.081	1.833	0.769	0.025	2.279	495	34	504	9	502	9	491	11	100
5.sSMPABC077	-	0.57	41933	2396	62	0.83	23	0.057	2.434	0.643	3.335	0.082	2.280	0.684	0.026	2.377	497	54	506	11	504	13	520	12	100

LA(SF)-ICP-MS U-Pb zircon results data from Sample CA-05 (Mestre Álvaro pluton)

Identifier	Lu-Hf identifier	f206[a] (%)	^{207}Pb CPS	^{206}Pb CPS	U (ppm)	Th[b]/U	^{206}Pb/^{204}Pb	Ratios[c] ^{207}Pb/^{206}Pb	2s (%)	^{207}Pb/^{235}U	2s (%)	^{206}Pb/^{238}U	2s (%)	Rho[d]	^{208}Pb/^{232}Th	*2s (%)*	Ages (Ma)[c] ^{207}Pb/^{206}Pb	2s abs	^{206}Pb/^{238}U	2s abs	^{207}Pb/^{235}U	2s abs	^{208}Pb/^{232}Th	2s abs	% conc[e]
										Data for Wetherill plot															
5.sSMPABC010	seq0255.dat	0.31	29931	1725	58	1.63	869	0.058	1.831	0.660	2.538	0.083	1.759	0.693	0.026	2.317	515	40	514	9	514	10	517	12	100
5.sSMPABC046	-	0.00	42862	2472	83	0.98	0	0.058	1.092	0.661	1.735	0.083	1.348	0.777	0.026	1.779	518	24	515	7	515	7	516	9	100
5.sSMPABC067	-	0.00	35204	2039	74	1.79	0	0.058	1.623	0.674	2.389	0.084	1.754	0.734	0.027	2.625	527	36	522	9	523	10	547	14	100
5.sSMPABC038	seq0247.dat	0.01	124859	7262	238	0.70	27518	0.058	1.015	0.678	1.632	0.085	1.278	0.783	0.025	1.619	536	22	523	6	526	7	493	8	100
5.sSMPABC041	seq0249.dat	0.20	30099	1747	57	1.35	1369	0.058	1.416	0.677	2.092	0.085	1.540	0.736	0.025	2.048	531	31	523	8	525	9	507	10	100

LA(SF)-ICP-MS U-Pb zircon results data from Sample CA-05 (Mestre Álvaro pluton)

Identifier	Lu-Hf identifier	f206[a]	^{207}Pb	^{206}Pb	U	Th[b]/U	^{206}Pb/^{204}Pb	Ratios[c]								Ages (Ma)[c]								% conc[e]
								^{207}Pb/^{206}Pb	2s (%)	^{207}Pb/^{235}U	2s (%)	^{206}Pb/^{238}U	2s (%)	Rho[d]	^{208}Pb/^{232}Th	*2s (%)*	^{207}Pb/^{206}Pb	2s abs	^{206}Pb/^{238}U	2s abs	^{207}Pb/^{235}U	2s abs	^{208}Pb/^{232}Th	2s abs	
								Data for Wetherill plot																
5.sSMPABC028-2	seq0261.dat	0.00	31010	1810	60	1.60	0	0.058	1.662	0.683	2.461	0.085	1.815	0.737	0.025	3.239	543	36	525	9	528	10	505	16	99
5.sSMPABC030	seq0268.dat	0.00	1775647	103804	3363	0.24	0	0.058	0.924	0.685	1.688	0.085	1.413	0.837	0.031	1.655	547	20	526	7	530	7	625	10	99
5.sSMPABC037-2	seq0282.dat	0.40	45755	2667	88	2.59	673	0.058	2.165	0.683	2.909	0.085	1.943	0.668	0.025	3.236	540	47	526	10	528	12	494	16	99
5.sSMPABC029-2	seq0278.dat	0.00	48177	2796	91	0.89	0	0.058	1.241	0.680	1.952	0.085	1.506	0.772	0.026	2.503	531	27	526	8	527	8	510	12	100
5.sSMPABC015	seq0258.dat	0.00	355210	20549	670	0.39	0	0.058	0.933	0.679	1.538	0.085	1.222	0.795	0.026	1.320	524	20	526	6	526	6	514	7	100
5.sSMPABC007-2	seq0262.dat	0.00	36056	2089	68	1.70	0	0.058	1.553	0.681	2.313	0.085	1.714	0.741	0.026	2.572	528	34	527	9	527	10	527	13	100
5.sSMPABC017	seq0256.dat	0.00	306532	17678	578	0.49	0	0.058	0.971	0.678	1.672	0.085	1.361	0.814	0.026	1.705	517	21	527	7	525	7	515	9	100
5.sSMPABC011-2	seq0272.dat	0.21	32053	1854	60	2.46	1309	0.058	1.558	0.681	2.281	0.085	1.666	0.730	0.025	1.967	524	34	528	8	527	9	508	10	100
5.sSMPABC074	-	0.00	30704	1783	64	0.99	0	0.058	1.361	0.684	2.077	0.085	1.569	0.755	0.026	2.607	532	30	528	8	529	9	520	13	100
5.sSMPABC088	seq0260.dat	0.00	30213	1758	63	1.28	0	0.058	1.289	0.686	1.976	0.085	1.498	0.758	0.026	2.226	537	28	529	8	530	8	520	11	100
5.sSMPABC026-2	seq0263.dat	0.00	67534	3901	127	0.70	0	0.058	1.454	0.681	2.226	0.085	1.685	0.757	0.024	3.620	521	32	529	9	527	9	475	17	100
5.sSMPABC054	-	0.00	180703	10488	340	0.40	0	0.058	1.017	0.684	1.622	0.085	1.263	0.779	0.027	1.993	531	22	529	6	529	7	540	11	100
5.sSMPABC044	seq0250.dat	0.00	274615	15900	516	0.64	0	0.058	0.950	0.683	1.580	0.086	1.262	0.799	0.027	1.354	526	21	529	6	529	7	530	7	100
5.sSMPABC040	seq0246.dat	0.21	592535	34285	1114	0.31	1321	0.058	1.173	0.683	1.890	0.086	1.482	0.784	0.029	1.821	524	26	529	8	528	8	569	10	100
5.sSMPABC014-2	seq0276.dat	0.00	298007	17267	559	0.62	0	0.058	1.053	0.684	1.734	0.086	1.378	0.795	0.026	1.860	527	23	530	7	529	7	515	9	100
5.sSMPABC015-2	-	0.19	256103	14770	479	0.53	1454	0.058	1.270	0.683	1.972	0.086	1.509	0.765	0.026	2.112	517	28	531	8	528	8	510	11	100
5.sSMPABC028	seq0271.dat	0.00	194550	11204	365	0.74	0	0.058	0.972	0.682	1.572	0.086	1.235	0.786	0.025	1.417	514	21	531	6	528	6	507	7	101
5.sSMPABC070	-	0.12	54715	3178	113	0.57	2272	0.058	1.388	0.692	2.048	0.086	1.506	0.735	0.029	3.107	533	30	535	8	534	9	577	18	100
5.sSMPABC020-2	**seq0269.dat**	**0.00**	**404575**	**23914**	**699**	**0.23**	**0**	**0.059**	**1.066**	**0.758**	**1.774**	**0.093**	**1.418**	**0.799**	**0.030**	**2.280**	**571**	**23**	**574**	**8**	**573**	**8**	**594**	**13**	**100**
5.sSMPABC047	-	0.17	636361	38117	1064	0.39	1600	0.060	1.081	0.794	1.735	0.096	1.357	0.782	0.031	1.364	600	23	592	8	594	8	613	8	100

LA(SF)-ICP-MS U-Pb zircon results data from Sample CA-05 (Mestre Álvaro pluton)

Identifier	Lu-Hf identifier	f206[a]	^{207}Pb	^{206}Pb	U	Th[b]/U	^{206}Pb/^{204}Pb	Ratios[c]								Ages (Ma)[c]								% conc[e]
								^{207}Pb/^{206}Pb	2s (%)	^{207}Pb/^{235}U	2s (%)	^{206}Pb/^{238}U	2s (%)	Rho[d]	^{208}Pb/^{232}Th	*2s (%)*	^{207}Pb/^{206}Pb	2s abs	^{206}Pb/^{238}U	2s abs	^{207}Pb/^{235}U	2s abs	^{208}Pb/^{232}Th	2s abs	
								Data for Wetherill plot																	
		(%)	CPS	CPS	(ppm)																				
5.sSMPABC016-2	seq0265.dat	0.00	230467	13759	384	0.47	0	0.060	1.072	0.794	1.755	0.096	1.390	0.792	0.028	2.057	593	23	593	8	593	8	562	11	100
5.sSMPABC012	seq0254.dat	0.00	770221	45998	1285	0.49	0	0.060	0.938	0.794	1.525	0.096	1.203	0.789	0.030	1.350	593	20	594	7	593	7	590	8	100
5.sSMPABC087	-	0.00	195538	11687	361	0.43	0	0.060	1.021	0.795	1.674	0.096	1.327	0.793	0.030	1.923	595	22	594	8	594	8	601	11	100
5.sSMPABC094	-	0.00	129098	7750	238	0.40	0	0.060	1.083	0.799	1.712	0.097	1.326	0.775	0.031	2.314	605	23	594	8	596	8	619	14	100
5.sSMPABC068	seq0257.dat	0.00	158791	9415	292	0.36	0	0.059	1.029	0.791	1.644	0.097	1.282	0.780	0.030	2.011	578	22	595	7	592	7	594	12	101
5.sSMPABC045	-	0.00	114706	6878	191	1.27	0	0.060	1.051	0.800	1.722	0.097	1.364	0.792	0.030	1.609	602	23	596	8	597	8	594	9	100
5.sSMPABC033-2	seq0280.dat	0.30	71235	4249	118	0.96	922	0.060	1.737	0.796	2.407	0.097	1.666	0.692	0.028	3.179	591	38	596	9	595	11	552	17	100
5.sSMPABC057	seq0252.dat	0.00	155800	9317	258	1.08	0	0.060	1.020	0.799	1.636	0.097	1.279	0.782	0.030	1.602	596	22	597	7	597	7	597	9	100
5.sSMPABC083	-	0.00	99026	5920	182	0.94	0	0.060	1.020	0.800	1.652	0.097	1.299	0.786	0.029	1.583	596	22	597	7	597	7	579	9	100
5.sSMPABC073	-	0.00	141259	8488	259	0.75	0	0.060	0.982	0.805	1.626	0.097	1.297	0.797	0.029	1.498	607	21	598	7	600	7	585	9	100
5.sSMPABC099	-	0.00	182884	10962	335	0.47	0	0.060	1.018	0.803	1.665	0.097	1.317	0.791	0.030	1.851	601	22	598	8	599	8	602	11	100
5.sSMPABC025	seq0264.dat	0.00	117963	7057	195	0.83	0	0.060	0.986	0.802	1.596	0.097	1.255	0.786	0.032	1.452	597	21	598	7	598	7	630	9	100
5.sSMPABC086	-	0.00	235966	14026	432	0.28	0	0.059	1.026	0.797	1.636	0.097	1.274	0.779	0.030	2.237	583	22	599	7	595	7	605	13	101
5.sSMPABC027-2	-	0.13	883926	52810	1459	0.37	2162	0.060	1.230	0.802	1.926	0.097	1.482	0.770	0.031	2.473	594	27	599	8	598	9	612	15	100
5.sSMPABC066	-	0.00	123298	7373	226	0.91	0	0.060	1.020	0.803	1.648	0.097	1.294	0.785	0.029	1.582	596	22	599	7	598	7	579	9	100
5.sSMPABC080	-	0.00	259836	15546	476	0.39	0	0.060	1.003	0.803	1.637	0.097	1.294	0.790	0.029	1.870	597	22	599	7	599	7	575	11	100
5.sSMPABC102	seq0274.dat	0.11	374458	22322	685	0.43	2379	0.060	1.125	0.801	1.808	0.097	1.416	0.783	0.031	2.089	590	24	599	8	597	8	610	13	100
5.sSMPABC075	-	0.14	172897	10349	316	0.26	1950	0.060	1.152	0.804	1.756	0.097	1.325	0.755	0.031	2.476	598	25	599	8	599	8	611	15	100
5.sSMPABC055	-	0.00	190957	11446	315	0.60	0	0.060	1.001	0.806	1.602	0.098	1.251	0.781	0.030	1.731	601	22	600	7	600	7	598	10	100
5.sSMPABC084	-	0.00	267439	15889	488	0.71	0	0.059	1.044	0.799	1.676	0.098	1.312	0.783	0.029	1.853	582	23	600	8	596	8	581	11	101

LA(SF)-ICP-MS U-Pb zircon results data from Sample CA-05 (Mestre Álvaro pluton)

Identifier	Lu-Hf identifier	f206[a] (%)	^{207}Pb CPS	^{206}Pb CPS	U (ppm)	Th[b]/U	^{206}Pb/^{204}Pb	Ratios[c] ^{207}Pb/^{206}Pb	2s (%)	^{207}Pb/^{235}U	2s (%)	^{206}Pb/^{238}U	2s (%)	Rho[d]	^{208}Pb/^{232}Th	*2s (%)*	Ages (Ma)[c] ^{207}Pb/^{206}Pb	2s abs	^{206}Pb/^{238}U	2s abs	^{207}Pb/^{235}U	2s abs	^{208}Pb/^{232}Th	2s abs	% conc[e]
										Data for Wetherill plot															
5.sSMPABC013-2	seq0275.dat	0.00	208632	12451	343	0.43	0	0.060	1.005	0.803	1.652	0.098	1.311	0.794	0.030	1.596	592	22	601	8	599	8	599	10	100
5.sSMPABC082	-	0.00	404501	24197	738	0.26	0	0.060	1.020	0.805	1.710	0.098	1.372	0.803	0.031	2.132	597	22	601	8	600	8	616	13	100
5.sSMPABC085	seq0259.dat	0.02	278057	16547	507	0.51	17330	0.060	0.959	0.801	1.592	0.098	1.270	0.798	0.030	1.451	586	21	601	7	598	7	604	9	101
5.sSMPABC089	-	0.00	102947	6167	188	0.41	0	0.060	1.185	0.807	1.892	0.098	1.474	0.779	0.032	2.841	600	26	601	8	601	9	631	18	100
5.sSMPABC096	-	0.00	139741	8341	255	0.28	0	0.060	1.039	0.805	1.671	0.098	1.309	0.783	0.033	2.248	592	23	602	8	600	8	655	15	100
5.sSMPABC100	seq0277.dat	0.00	513673	30562	936	0.28	73096	0.059	1.009	0.802	1.685	0.098	1.349	0.801	0.029	1.907	585	22	602	8	598	8	585	11	101
5.sSMPABC095	-	0.00	397492	23722	724	0.27	0	0.060	0.955	0.805	1.587	0.098	1.267	0.799	0.031	1.533	592	21	602	7	600	7	623	9	100
5.sSMPABC018-2	seq0266.dat	0.00	218482	13052	359	0.29	0	0.060	1.021	0.806	1.675	0.098	1.328	0.793	0.030	1.775	594	22	602	8	600	8	606	11	100
5.sSMPABC036-2	-	0.00	231324	13875	379	0.88	0	0.060	1.267	0.811	2.002	0.098	1.550	0.774	0.028	2.857	603	27	603	9	603	9	558	16	100
5.sSMPABC032	seq0270.dat	0.00	155594	9239	255	0.32	0	0.059	1.027	0.803	1.614	0.098	1.244	0.771	0.032	2.116	581	22	603	7	598	7	640	13	101
5.sSMPABC033	seq0248.dat	0.00	349041	20974	568	0.34	0	0.060	0.949	0.818	1.590	0.099	1.276	0.802	0.030	1.575	607	21	607	7	607	7	607	9	100
5.sSMPABC010-2	**seq0273.dat**	**0.00**	**108300**	**6535**	**175**	**0.30**	**0**	**0.060**	**1.028**	**0.829**	**1.692**	**0.100**	**1.344**	**0.795**	**0.032**	**2.026**	**616**	**22**	**612**	**8**	**613**	**8**	**629**	**13**	**100**
5.sSMPABC101	**-**	**0.11**	**766518**	**46407**	**1369**	**0.30**	**2436**	**0.061**	**1.074**	**0.833**	**1.673**	**0.100**	**1.283**	**0.767**	**0.031**	**1.864**	**623**	**23**	**613**	**8**	**615**	**8**	**619**	**11**	**100**
5.sSMPABC031-2	**-**	**0.00**	**209850**	**12675**	**338**	**0.49**	**0**	**0.060**	**1.109**	**0.831**	**1.805**	**0.100**	**1.424**	**0.789**	**0.028**	**2.333**	**618**	**24**	**613**	**8**	**614**	**8**	**564**	**13**	**100**
5.sSMPABC019	**-**	**0.00**	**289492**	**17465**	**467**	**0.66**	**0**	**0.060**	**0.945**	**0.830**	**1.545**	**0.100**	**1.222**	**0.791**	**0.031**	**1.306**	**615**	**20**	**613**	**7**	**614**	**7**	**610**	**8**	**100**
5.sSMPABC018	**seq0253.dat**	**0.00**	**149626**	**9027**	**241**	**0.50**	**0**	**0.060**	**1.028**	**0.831**	**1.738**	**0.100**	**1.402**	**0.806**	**0.033**	**2.005**	**615**	**22**	**614**	**8**	**614**	**8**	**655**	**13**	**100**
5.sSMPABC059	**-**	**0.00**	**69493**	**4190**	**112**	**0.61**	**0**	**0.060**	**1.028**	**0.831**	**1.674**	**0.100**	**1.321**	**0.789**	**0.032**	**1.752**	**614**	**22**	**614**	**8**	**614**	**8**	**636**	**11**	**100**
5.sSMPABC017-2	**-**	**0.00**	**365561**	**22054**	**587**	**0.38**	**0**	**0.060**	**1.028**	**0.832**	**1.720**	**0.100**	**1.379**	**0.802**	**0.032**	**1.809**	**615**	**22**	**615**	**8**	**615**	**8**	**638**	**12**	**100**
5.sSMPABC056	**seq0251.dat**	**0.00**	**105902**	**6402**	**170**	**0.33**	**0**	**0.060**	**1.042**	**0.834**	**1.649**	**0.100**	**1.278**	**0.775**	**0.032**	**2.249**	**620**	**22**	**615**	**8**	**616**	**8**	**637**	**14**	**100**
5.sSMPABC019-2	**seq0267.dat**	**0.07**	**660422**	**39603**	**1060**	**0.31**	**3734**	**0.060**	**1.030**	**0.828**	**1.664**	**0.100**	**1.306**	**0.785**	**0.030**	**1.552**	**602**	**22**	**615**	**8**	**612**	**8**	**590**	**9**	**100**

LA(SF)-ICP-MS U-Pb zircon results data from Sample CA-05 (Mestre Álvaro pluton)

Identifier	Lu-Hf identifier	f206[a] (%)	^{207}Pb CPS	^{206}Pb CPS	U (ppm)	Th[b]/U	$^{206}Pb/^{204}Pb$	Ratios[c] $^{207}Pb/^{206}Pb$	2s (%)	$^{207}Pb/^{235}U$	2s (%)	$^{206}Pb/^{238}U$	2s (%)	Rho[d]	$^{208}Pb/^{232}Th$	2s (%)	Ages (Ma)[c] $^{207}Pb/^{206}Pb$	2s abs	$^{206}Pb/^{238}U$	2s abs	$^{207}Pb/^{235}U$	2s abs	$^{208}Pb/^{232}Th$	2s abs	% conc[e]
										Data for Wetherill plot															
5.sSMPABC035-2	**seq0281.dat**	**0.08**	**444622**	**27032**	**692**	**0.36**	**3239**	**0.061**	**1.105**	**0.865**	**1.742**	**0.103**	**1.347**	**0.773**	**0.030**	**1.908**	**632**	**24**	**633**	**8**	**633**	**8**	**605**	**11**	**100**

[a] *percentage of the common Pb on the ^{206}Pb*

[b] *Th/U ratios are calculated relative to BB reference zircon*

[c] *data corrected for background, within-run Pb/U fractionation (in case of $^{206}Pb/^{238}U$) and common Pb using Stacey and Kramers (1975) model Pb composition*

[d] *Rho is the error correlation defined as the quotient of the propagated errors of the $^{206}Pb/^{238}U$ and the $^{207}Pb/^{235}U$ ratio*

[e] *Concordance calculated as (^{206}Pb-^{238}U age/^{207}Pb-^{206}Pb age)*100*

CPS = count per second Spots in domains of dissolution–recrystallization or overgrowth rims are in red letter

Zircon grains not used for concordia age are in bold letter

LA(SF)-ICP-MS U-Pb zircon results data from Sample CA-06 (Nova Venécia complex)

Identifier	Lu-Hf identifier	f206[a] (%)	^{207}Pb CPS	^{206}Pb CPS	U (ppm)	Th[b]/U	$^{206}Pb/^{204}Pb$	Ratios[c] $^{207}Pb/^{206}Pb$	2s (%)	$^{207}Pb/^{235}U$	2s (%)	$^{206}Pb/^{238}U$	2s (%)	Rho[d]	$^{208}Pb/^{232}Th$	2s (%)	Ages (Ma)[c] $^{207}Pb/^{206}Pb$	2s abs	$^{206}Pb/^{238}U$	2s abs	$^{207}Pb/^{235}U$	2s abs	$^{208}Pb/^{232}Th$	2s abs	% conc[e]
										Data for Wetherill plot															
5.sSMPABC123	-	0.00	142520	8044	466	0.04	0	0.056	1.081	0.599	1.630	0.077	1.220	0.749	0.029	4.447	470	24	478	6	477	6	582	26	100
5.sSMPABC073	seq0207.dat	0.00	113448	6452	370	0.08	0	0.057	1.073	0.605	1.642	0.077	1.244	0.757	0.026	3.176	486	24	479	6	481	6	528	17	100
5.sSMPABC048	-	0.33	157460	9010	483	0.03	823	0.057	1.535	0.648	2.160	0.082	1.520	0.704	0.043	3.875	500	34	509	7	507	9	848	32	100
5.sSMPABC075	-	0.24	163827	9363	502	0.08	1137	0.057	1.328	0.648	1.939	0.082	1.413	0.729	0.028	2.893	497	29	510	7	508	8	551	16	100
5.sSMPABC013	-	0.00	145855	8395	444	0.01	0	0.058	1.025	0.656	1.660	0.083	1.306	0.787	0.051	6.476	513	23	512	6	512	7	999	63	100
5.sSMPABC121	-	0.00	154051	8898	468	0.14	0	0.058	1.004	0.661	1.606	0.083	1.253	0.780	0.028	1.994	521	22	514	6	515	7	560	11	100

LA(SF)-ICP-MS U-Pb zircon results data from Sample CA-06 (Nova Venécia complex)

Identifier	Lu-Hf identifier	f206[a]	^{207}Pb	^{206}Pb	U	Th[b]/U	$^{206}Pb/^{204}Pb$	Ratios[c]									Ages (Ma)[c]								% conc[e]
								$^{207}Pb/^{206}Pb$	2s (%)	$^{207}Pb/^{235}U$	2s (%)	$^{206}Pb/^{238}U$	2s (%)	Rho[d]	$^{208}Pb/^{232}Th$	2s (%)	$^{207}Pb/^{206}Pb$	2s abs	$^{206}Pb/^{238}U$	2s abs	$^{207}Pb/^{235}U$	2s abs	$^{208}Pb/^{232}Th$	2s abs	
		(%)	CPS	CPS	(ppm)			Data for Wetherill plot																	
5.sSMPABC082	-	0.00	189133	10890	574	0.49	0	0.058	0.990	0.659	1.597	0.083	1.253	0.785	0.025	1.352	514	22	514	6	514	6	502	7	100
5.sSMPABC049	seq0198.dat	0.07	204291	11798	613	0.15	3793	0.058	1.034	0.668	1.679	0.084	1.322	0.787	0.030	2.022	520	23	519	7	520	7	591	12	100
5.sSMPABC032	-	0.00	218244	12737	640	0.17	0	0.058	0.994	0.691	1.585	0.086	1.235	0.779	0.030	1.656	543	22	531	6	533	7	601	10	100
5.sSMPABC091	seq0206.dat	0.04	192528	11211	563	0.26	7205	0.058	1.004	0.692	1.609	0.086	1.257	0.781	0.027	1.568	538	22	533	6	534	7	534	8	100
5.sSMPABC105	-	0.00	117928	6885	341	0.09	0	0.058	1.045	0.701	1.639	0.087	1.263	0.770	0.034	2.638	544	23	538	7	540	7	678	18	100
5.sSMPABC104	-	0.12	169773	9877	490	0.01	2270	0.058	1.175	0.701	1.727	0.087	1.266	0.733	0.040	9.428	537	26	540	7	539	7	790	73	100
5.sSMPABC012	-	0.16	169683	9868	489	0.22	1665	0.058	1.160	0.701	1.735	0.087	1.291	0.744	0.031	1.696	536	25	540	7	539	7	610	10	100
5.sSMPABC145	-	0.00	149892	8725	430	0.29	0	0.058	1.048	0.704	1.669	0.088	1.299	0.778	0.029	1.892	538	23	542	7	541	7	569	11	100
5.sSMPABC026	-	0.00	177127	10385	505	0.60	0	0.059	1.006	0.714	1.601	0.088	1.245	0.778	0.027	1.325	553	22	546	7	547	7	542	7	100
5.sSMPABC066	-	0.00	197655	11594	563	0.28	0	0.059	1.006	0.716	1.599	0.088	1.243	0.777	0.028	1.555	555	22	546	7	548	7	564	9	100
5.sSMPABC076	-	0.12	181225	10602	515	0.39	2342	0.059	1.068	0.715	1.658	0.089	1.268	0.765	0.027	1.405	549	23	548	7	548	7	539	8	100
5.sSMPABC132	-	0.00	194932	11368	553	0.46	0	0.058	1.012	0.715	1.616	0.089	1.260	0.780	0.028	1.477	542	22	549	7	548	7	567	8	100
5.sSMPABC143	-	0.12	145669	8530	412	0.22	2180	0.059	1.205	0.719	1.879	0.089	1.442	0.767	0.030	2.753	551	26	550	8	550	8	593	16	100
5.sSMPABC131	seq0205.dat	0.00	112448	6603	317	1.55	0	0.059	1.056	0.723	1.691	0.089	1.321	0.781	0.025	1.459	557	23	551	7	552	7	493	7	100
5.sSMPABC047	-	0.00	229900	13557	647	0.37	0	0.059	1.051	0.727	1.601	0.089	1.207	0.754	0.028	1.787	566	23	552	6	555	7	558	10	100
5.sSMPABC084	-	0.06	187543	10994	528	0.34	4211	0.059	1.014	0.724	1.617	0.090	1.259	0.779	0.028	1.506	553	22	553	7	553	7	556	8	100
5.sSMPABC147	-	0.00	196653	11555	551	1.12	0	0.059	0.987	0.729	1.606	0.090	1.267	0.789	0.026	1.365	558	22	555	7	556	7	526	7	100
5.sSMPABC106	-	0.00	155320	9089	434	0.24	0	0.059	1.042	0.728	1.604	0.090	1.219	0.760	0.031	1.931	549	23	557	7	555	7	619	12	100
5.sSMPABC067	-	0.01	190525	11177	529	0.55	37206	0.059	1.006	0.733	1.645	0.091	1.302	0.791	0.027	1.434	555	22	559	7	559	7	529	8	100
5.sSMPABC014	-	0.00	207775	12244	574	0.32	0	0.059	1.035	0.741	1.658	0.091	1.295	0.781	0.030	1.669	565	23	562	7	563	7	597	10	100

LA(SF)-ICP-MS U-Pb zircon results data from Sample CA-06 (Nova Venécia complex)

Identifier	Lu-Hf identifier	f206[a]	^{207}Pb	^{206}Pb	U	Th[b]/U	$^{206}Pb/^{204}Pb$	Ratios[c]									Ages (Ma)[c]									% conc[e]
								$^{207}Pb/^{206}Pb$	2s (%)	$^{207}Pb/^{235}U$	2s (%)	$^{206}Pb/^{238}U$	2s (%)	Rho[d]	$^{208}Pb/^{232}Th$	2s (%)	$^{207}Pb/^{206}Pb$	2s	$^{206}Pb/^{238}U$	2s	$^{207}Pb/^{235}U$	2s	$^{208}Pb/^{232}Th$	2s	
		(%)	CPS	CPS	(ppm)			Data for Wetherill plot									abs		abs		abs		abs		
5.sSMPABC044	-	0.19	273811	16078	753	0.30	1438	0.059	1.208	0.742	1.814	0.092	1.353	0.746	0.032	1.620	557	26	565	7	563	8	639	10	100
5.sSMPABC054	seq0183.dat	0.00	296933	17489	816	0.35	0	0.059	1.002	0.744	1.580	0.092	1.222	0.773	0.030	1.378	563	22	565	7	565	7	607	8	100
5.sSMPABC130	-	0.00	105822	6253	291	0.76	0	0.059	1.049	0.747	1.661	0.092	1.288	0.775	0.027	1.498	570	23	565	7	566	7	533	8	100
5.sSMPABC009	-	0.05	149904	8840	412	0.46	5091	0.059	1.017	0.746	1.627	0.092	1.270	0.780	0.029	1.456	566	22	566	7	566	7	575	8	100
5.sSMPABC125	-	0.00	149586	8802	410	1.16	0	0.059	1.020	0.745	1.623	0.092	1.263	0.778	0.027	1.327	561	22	567	7	566	7	541	7	100
5.sSMPABC103	-	0.16	162096	9540	444	0.17	1681	0.059	1.189	0.746	1.739	0.092	1.269	0.730	0.030	2.197	562	26	567	7	566	8	598	13	100
5.sSMPABC064	-	0.00	353207	20769	960	0.03	0	0.059	1.020	0.752	1.565	0.093	1.187	0.758	0.041	3.241	560	22	571	6	569	7	807	25	100
5.sSMPABC139	-	0.00	128565	7660	347	0.66	0	0.060	1.041	0.767	1.637	0.093	1.264	0.772	0.029	1.528	588	23	576	7	578	7	574	9	100
5.sSMPABC052	-	0.06	210080	12493	565	0.89	4738	0.059	1.110	0.768	1.732	0.094	1.329	0.768	0.027	1.708	584	24	577	7	579	8	537	9	100
5.sSMPABC039	seq0185.dat	0.08	236669	14049	635	0.64	3423	0.059	1.029	0.768	1.617	0.094	1.247	0.771	0.030	1.279	580	22	578	7	579	7	592	7	100
5.sSMPABC142	seq0180.dat	0.00	308133	18288	826	0.57	0	0.059	0.994	0.769	1.585	0.094	1.235	0.779	0.028	1.378	580	22	579	7	579	7	550	8	100
5.sSMPABC046	-	0.00	343211	20397	919	0.45	0	0.059	1.010	0.771	1.577	0.094	1.211	0.768	0.028	1.348	583	22	580	7	581	7	562	7	100
5.sSMPABC031	seq0189.dat	0.00	259535	15411	693	0.14	0	0.059	1.010	0.773	1.607	0.094	1.250	0.778	0.031	1.828	581	22	581	7	581	7	610	11	100
5.sSMPABC086	-	0.00	135919	8135	360	0.72	0	0.060	1.036	0.785	1.617	0.095	1.241	0.768	0.028	1.428	598	22	585	7	588	7	558	8	100
5.sSMPABC113	seq0215.dat	0.00	70444	4220	186	1.10	0	0.060	1.068	0.786	1.685	0.095	1.302	0.773	0.027	1.478	600	23	586	7	589	8	540	8	100
5.sSMPABC150	seq0204.dat	0.00	61370	3653	162	0.82	0	0.060	1.142	0.784	1.809	0.096	1.402	0.775	0.027	1.948	587	25	588	8	588	8	533	10	100
5.sSMPABC035	-	0.00	129673	7727	342	0.64	0	0.060	1.040	0.785	1.663	0.096	1.297	0.780	0.028	1.500	589	23	589	7	589	7	558	8	100
5.sSMPABC019	-	0.00	210262	12538	553	1.94	0	0.060	1.006	0.787	1.591	0.096	1.233	0.775	0.029	1.180	590	22	589	7	589	7	574	7	100
5.sSMPABC077	-	0.05	180155	10730	474	0.17	5466	0.060	1.021	0.786	1.620	0.096	1.258	0.776	0.029	1.844	588	22	589	7	589	7	584	10	100
5.sSMPABC007	-	0.00	160573	9556	423	0.97	0	0.060	1.008	0.785	1.609	0.096	1.254	0.779	0.028	1.208	586	22	589	7	589	7	561	7	100

LA(SF)-ICP-MS U-Pb zircon results data from Sample CA-06 (Nova Venécia complex)

Identifier	Lu-Hf identifier	f206[a]	^{207}Pb	^{206}Pb	U	Th[b]/U	$^{206}Pb/^{204}Pb$	Ratios[c]									Ages (Ma)[c]								% conc[e]
								$^{207}Pb/^{206}Pb$	2s (%)	$^{207}Pb/^{235}U$	2s (%)	$^{206}Pb/^{238}U$	2s (%)	Rho[d]	$^{208}Pb/^{232}Th$	2s (%)	$^{207}Pb/^{206}Pb$	2s	$^{206}Pb/^{238}U$	2s	$^{207}Pb/^{235}U$	2s	$^{208}Pb/^{232}Th$	2s	
		(%)	CPS	CPS	(ppm)			Data for Wetherill plot									abs		abs		abs		abs	
5.sSMPABC114	-	0.00	81847	4903	215	1.49	0	0.060	1.068	0.791	1.711	0.096	1.337	0.781	0.023	1.472	600	23	589	8	592	8	462	7	100
5.sSMPABC053	-	0.15	120910	7215	318	0.90	1816	0.060	1.125	0.789	1.712	0.096	1.290	0.754	0.028	1.287	592	24	590	7	591	8	558	7	100
5.sSMPABC065	-	0.00	76043	4561	200	0.81	0	0.060	1.050	0.793	1.666	0.096	1.293	0.776	0.029	1.460	603	23	590	7	593	8	573	8	100
5.sSMPABC085	-	0.00	125916	7501	331	0.68	0	0.060	1.007	0.788	1.606	0.096	1.251	0.779	0.027	1.401	588	22	591	7	590	7	541	7	100
5.sSMPABC094	-	0.00	184617	11012	485	0.52	0	0.060	1.006	0.789	1.605	0.096	1.251	0.779	0.029	1.451	591	22	591	7	591	7	577	8	100
5.sSMPABC083	-	0.01	83559	5000	219	0.36	24994	0.060	1.154	0.792	1.843	0.096	1.437	0.780	0.032	2.465	598	25	591	8	592	8	630	15	100
5.sSMPABC152	seq0202.dat	0.00	173067	10284	454	0.63	0	0.059	1.094	0.787	1.773	0.096	1.395	0.787	0.027	2.013	583	24	591	8	589	8	535	11	100
5.sSMPABC030	-	0.17	176083	10501	462	1.72	1592	0.060	1.159	0.790	1.756	0.096	1.319	0.751	0.028	1.205	590	25	591	7	591	8	563	7	100
5.sSMPABC087	seq0221.dat	0.00	106132	6337	278	0.45	0	0.060	1.089	0.792	1.752	0.096	1.373	0.784	0.028	2.044	593	24	592	8	592	8	566	11	100
5.sSMPABC110	seq0212.dat	0.00	76770	4584	201	0.42	0	0.060	1.072	0.792	1.676	0.096	1.288	0.769	0.029	1.858	593	23	592	7	592	8	579	11	100
5.sSMPABC070	seq0190.dat	0.05	137399	8237	359	0.65	5809	0.060	1.029	0.796	1.635	0.096	1.270	0.777	0.028	1.446	602	22	593	7	595	7	552	8	100
5.sSMPABC133	-	0.08	153712	9152	401	0.78	3232	0.060	1.047	0.792	1.651	0.096	1.277	0.773	0.028	1.375	587	23	594	7	592	7	551	8	100
5.sSMPABC027	-	0.00	78192	4668	204	1.49	0	0.060	1.089	0.794	1.765	0.096	1.389	0.787	0.026	1.480	593	24	594	8	594	8	512	7	100
5.sSMPABC148	seq0179.dat	0.00	184669	11128	478	0.39	0	0.060	1.012	0.809	1.610	0.097	1.252	0.778	0.029	1.571	613	22	599	7	602	7	583	9	100
5.sSMPABC037	-	0.00	266298	15986	688	0.12	0	0.060	1.000	0.807	1.586	0.097	1.231	0.776	0.036	1.683	605	22	600	7	601	7	708	12	100
5.sSMPABC034	seq0199.dat	0.00	170669	10228	441	0.34	0	0.060	1.035	0.806	1.655	0.098	1.292	0.781	0.030	1.759	601	22	600	7	600	8	589	10	100
5.sSMPABC071	-	0.00	106709	6415	275	1.11	0	0.060	1.031	0.811	1.634	0.098	1.268	0.776	0.029	1.325	608	22	602	7	603	7	572	8	100
5.sSMPABC126	-	0.00	128909	7745	331	0.88	0	0.060	1.015	0.812	1.621	0.098	1.264	0.780	0.029	1.397	606	22	603	7	604	7	571	8	100
5.sSMPABC008	seq0195.dat	0.00	197115	11831	505	0.61	0	0.060	1.000	0.813	1.594	0.098	1.241	0.779	0.030	1.324	604	22	604	7	604	7	602	8	100
5.sSMPABC093	-	0.00	128470	7729	329	0.84	0	0.060	1.047	0.817	1.622	0.098	1.239	0.764	0.028	1.484	609	23	605	7	606	7	564	8	100

LA(SF)-ICP-MS U-Pb zircon results data from Sample CA-06 (Nova Venécia complex)

Identifier	Lu-Hf identifier	f206[a]	^{207}Pb	^{206}Pb	U	Th[b]/U	^{206}Pb/^{204}Pb	Ratios[c]									Ages (Ma)[c]								% conc[e]
								^{207}Pb/^{206}Pb	2s (%)	^{207}Pb/^{235}U	2s (%)	^{206}Pb/^{238}U	2s (%)	Rho[d]	^{208}Pb/^{232}Th	2s (%)	^{207}Pb/^{206}Pb	2s	^{206}Pb/^{238}U	2s	^{207}Pb/^{235}U	2s	^{208}Pb/^{232}Th	2s	
								Data for Wetherill plot										abs		abs		abs		abs	
5.sSMPABC011	-	0.00	168383	10123	430	0.41	0	0.060	1.015	0.818	1.615	0.099	1.257	0.778	0.033	1.413	608	22	606	7	607	7	648	9	100
5.sSMPABC095	seq0219.dat	0.00	167375	10041	427	0.65	0	0.060	1.050	0.816	1.607	0.099	1.216	0.757	0.029	1.502	603	23	607	7	606	7	584	9	100
5.sSMPABC051	seq0201.dat	0.00	58461	3512	149	0.79	0	0.060	1.182	0.817	1.831	0.099	1.398	0.764	0.030	1.878	606	26	607	8	607	8	594	11	100
5.sSMPABC050	seq0200.dat	0.10	278486	16739	710	1.27	2641	0.060	1.056	0.819	1.638	0.099	1.252	0.764	0.030	1.195	607	23	607	7	607	8	600	7	100
5.sSMPABC090	seq0208.dat	0.00	78679	4725	200	0.83	0	0.060	1.049	0.819	1.682	0.099	1.315	0.782	0.027	1.540	606	23	608	8	607	8	544	8	100
5.sSMPABC089	seq0209.dat	0.00	246278	14777	627	0.61	0	0.060	1.000	0.818	1.588	0.099	1.234	0.777	0.028	1.343	604	22	608	7	607	7	564	7	100
5.sSMPABC127	-	0.22	167212	10034	425	0.70	1227	0.060	1.300	0.819	1.943	0.099	1.445	0.744	0.027	1.776	604	28	609	8	608	9	539	9	100
5.sSMPABC128	-	0.00	178303	10716	454	0.80	0	0.060	0.998	0.821	1.601	0.099	1.252	0.782	0.029	1.394	607	22	609	7	608	7	572	8	100
5.sSMPABC058	seq0186.dat	0.00	342489	20512	871	0.38	0	0.060	1.002	0.818	1.572	0.099	1.212	0.771	0.031	1.342	600	22	609	7	607	7	623	8	100
5.sSMPABC096	seq0220.dat	0.00	312198	18747	793	0.61	0	0.060	1.016	0.821	1.595	0.099	1.230	0.771	0.030	1.353	605	22	610	7	609	7	589	8	100
5.sSMPABC144	-	0.00	416629	24860	1056	0.44	0	0.060	1.006	0.818	1.587	0.099	1.227	0.774	0.030	1.418	592	22	611	7	607	7	590	8	101
5.sSMPABC153	seq0181.dat	0.00	179275	10774	454	0.47	0	0.060	1.015	0.824	1.623	0.099	1.267	0.780	0.029	1.500	607	22	611	7	610	7	585	9	100
5.sSMPABC036	-	0.00	412872	24929	1039	0.30	0	0.060	0.994	0.833	1.572	0.100	1.219	0.775	0.033	1.331	617	21	615	7	616	7	657	8	100
5.sSMPABC149	seq0203.dat	0.00	104021	6292	261	1.02	0	0.060	1.041	0.837	1.647	0.100	1.276	0.775	0.029	1.503	621	22	616	8	617	8	583	8	100
5.sSMPABC074	-	0.00	424436	25568	1062	0.36	0	0.060	0.996	0.836	1.554	0.101	1.192	0.767	0.029	1.371	612	22	618	7	617	7	581	8	100
5.sSMPABC102	seq0191.dat	0.00	169204	10173	423	0.86	0	0.060	1.065	0.836	1.657	0.101	1.270	0.766	0.029	1.577	608	23	619	8	617	8	581	9	100
5.sSMPABC140	-	0.08	268132	16236	668	0.33	3476	0.061	1.024	0.845	1.620	0.101	1.255	0.775	0.033	1.457	623	22	621	7	622	8	655	9	100
5.sSMPABC072	seq0188.dat	0.00	255897	15436	636	1.30	0	0.060	1.011	0.842	1.588	0.101	1.224	0.771	0.030	1.220	615	22	622	7	620	7	588	7	100
5.sSMPABC010	seq0197.dat	0.02	74837	4521	185	0.01	12303	0.060	1.062	0.847	1.662	0.102	1.279	0.769	0.029	62.381	619	23	624	8	623	8	586	360	100
5.sSMPABC124	seq0218.dat	0.00	58701	3533	145	1.76	0	0.060	1.113	0.848	1.720	0.102	1.311	0.762	0.029	1.498	610	24	627	8	624	8	585	9	101

LA(SF)-ICP-MS U-Pb zircon results data from Sample CA-06 (Nova Venécia complex)

Identifier	Lu-Hf identifier	f206[a]	^{207}Pb	^{206}Pb	U	Th[b]/U	$^{206}Pb/^{204}Pb$	Ratios[c]									Ages (Ma)[c]								% conc[e]
								$^{207}Pb/^{206}Pb$	2s (%)	$^{207}Pb/^{235}U$	2s (%)	$^{206}Pb/^{238}U$	2s (%)	Rho[d]	$^{208}Pb/^{232}Th$	2s (%)	$^{207}Pb/^{206}Pb$	2s abs	$^{206}Pb/^{238}U$	2s abs	$^{207}Pb/^{235}U$	2s abs	$^{208}Pb/^{232}Th$	2s abs	
		(%)	CPS	CPS	(ppm)			Data for Wetherill plot																	
5.sSMPABC107	seq0211.dat	0.00	81124	4953	200	0.88	0	0.061	1.048	0.862	1.661	0.102	1.289	0.776	0.029	1.504	641	23	628	8	631	8	583	9	100
5.sSMPABC018	seq0194.dat	0.00	239599	14548	587	1.20	0	0.061	1.005	0.861	1.584	0.103	1.225	0.773	0.031	1.214	629	22	631	7	631	7	623	7	100
5.sSMPABC016	seq0192.dat	0.00	131428	7970	321	0.73	0	0.061	1.072	0.863	1.806	0.103	1.454	0.805	0.027	1.800	626	23	633	9	632	9	532	10	100
5.sSMPABC006	seq0196.dat	0.00	306809	18623	749	1.01	0	0.061	1.005	0.864	1.566	0.103	1.201	0.767	0.030	1.195	629	22	633	7	632	7	600	7	100
5.sSMPABC038	seq0184.dat	1.00	818910	49907	1998	0.18	0	0.061	3.431	0.868	4.119	0.103	2.279	0.553	0.034	1.402	637	74	633	14	634	20	680	9	100
5.sSMPABC056	-	0.00	151500	9217	369	1.73	0	0.061	1.003	0.867	1.640	0.103	1.297	0.791	0.029	1.262	634	22	634	8	634	8	568	7	100
5.sSMPABC112	seq0214.dat	0.00	1150354	69988	2805	0.58	0	0.061	1.003	0.867	1.549	0.103	1.181	0.762	0.030	1.343	634	22	634	7	634	7	593	8	100
5.sSMPABC055	seq0182.dat	0.00	166266	10224	393	0.84	0	0.061	0.992	0.904	1.586	0.107	1.238	0.780	0.032	1.265	656	21	653	8	654	8	629	8	100
5.sSMPABC092	seq0210.dat	0.14	182568	11177	430	1.25	1932	0.061	1.129	0.903	1.694	0.107	1.263	0.746	0.030	1.389	647	24	655	8	653	8	602	8	100
5.sSMPABC063	seq0187.dat	0.01	902524	55265	2123	0.23	25369	0.061	0.997	0.904	1.571	0.107	1.214	0.773	0.036	1.342	647	21	656	8	654	8	710	10	100
5.sSMPABC122	seq0216.dat	0.00	154817	9498	364	0.79	0	0.061	1.043	0.907	1.657	0.107	1.288	0.777	0.030	1.515	652	22	656	8	655	8	605	9	100
5.sSMPABC146	seq0178.dat	0.15	430589	27004	918	0.54	1807	0.063	1.174	1.021	1.724	0.118	1.263	0.732	0.036	1.929	699	25	720	9	715	9	720	14	101
5.sSMPABC115	seq0217.dat	0.00	153087	9795	314	0.40	0	0.064	1.032	1.083	1.624	0.123	1.254	0.772	0.036	1.687	741	22	747	9	745	9	706	12	100
5.sSMPABC017	seq0193.dat	0.00	1723344	110932	3459	0.22	0	0.064	0.994	1.114	1.617	0.126	1.275	0.788	0.039	1.395	754	21	762	9	760	9	768	11	100
5.sSMPABC069	seq0213.dat	0.30	188641	12520	347	0.55	913	0.066	1.365	1.254	1.946	0.137	1.387	0.713	0.042	1.522	818	29	828	11	825	11	833	12	100
5.sSMPABC015	-	0.00	26682	1725	72	1.09	0	0.065	1.238	0.834	1.877	0.094	1.411	0.752	0.031	1.831	763	26	577	8	616	9	609	11	94
5.sSMPABC020	-	0.00	127174	7955	333	0.87	0	0.063	1.039	0.830	1.624	0.096	1.248	0.768	0.030	1.336	693	22	592	7	613	8	596	8	97
5.sSMPABC025	-	0.00	118227	7243	328	1.09	0	0.061	1.045	0.766	1.617	0.091	1.234	0.763	0.028	1.309	648	22	560	7	578	7	549	7	97
5.sSMPABC029	-	0.00	141363	8534	418	0.58	0	0.060	1.044	0.709	1.606	0.085	1.221	0.760	0.028	1.434	617	23	527	6	544	7	556	8	97
5.sSMPABC045	-	0.38	135457	8196	427	0.03	714	0.061	1.640	0.667	2.257	0.080	1.550	0.687	0.058	3.360	622	35	496	7	519	9	1146	37	96

LA(SF)-ICP-MS U-Pb zircon results data from Sample CA-06 (Nova Venécia complex)

Identifier	Lu-Hf identifier	f206[a]	^{207}Pb	^{206}Pb	U	Th[b]/U	$^{206}Pb/^{204}Pb$	Ratios[c]									Ages (Ma)[c]								% conc[e]
								$^{207}Pb/^{206}Pb$	2s (%)	$^{207}Pb/^{235}U$	2s (%)	$^{206}Pb/^{238}U$	2s (%)	Rho[d]	$^{208}Pb/^{232}Th$	2s (%)	$^{207}Pb/^{206}Pb$	2s abs	$^{206}Pb/^{238}U$	2s abs	$^{207}Pb/^{235}U$	2s abs	$^{208}Pb/^{232}Th$	2s abs	
		(%)	CPS	CPS	(ppm)			Data for Wetherill plot																	
5.sSMPABC057	-	0.00	136254	8403	375	0.42	0	0.062	1.038	0.778	1.621	0.092	1.245	0.768	0.030	1.534	663	22	565	7	585	7	597	9	97
5.sSMPABC068	-	0.00	160236	10225	407	0.15	0	0.064	1.019	0.873	1.612	0.099	1.249	0.775	0.040	1.862	735	22	610	7	637	8	788	14	96
5.sSMPABC101	-	0.00	193696	11893	565	0.49	0	0.061	1.026	0.731	1.582	0.086	1.204	0.761	0.026	1.531	653	22	534	6	557	7	521	8	96
5.sSMPABC129	-	0.00	131272	7844	404	0.19	0	0.060	1.054	0.675	1.631	0.082	1.245	0.763	0.032	2.020	595	23	508	6	524	7	630	13	97
5.sSMPABC141	-	0.00	94662	5802	265	0.44	0	0.061	1.044	0.760	1.660	0.090	1.290	0.777	0.028	1.703	649	22	555	7	574	7	562	9	97

LA(SF)-ICP-MS U-Pb zircon results data from Sample CA-07 (Ataléia suite)

Identifier	Lu-Hf identifier	f206[a]	^{207}Pb	^{206}Pb	U	Th[b]/U	$^{206}Pb/^{204}Pb$	Ratios[c]									Ages (Ma)[c]								% conc[e]
								$^{207}Pb/^{206}Pb$	2s (%)	$^{207}Pb/^{235}U$	2s (%)	$^{206}Pb/^{238}U$	2s (%)	Rho[d]	$^{208}Pb/^{232}Th$	2s (%)	$^{207}Pb/^{206}Pb$	2s abs	$^{206}Pb/^{238}U$	2s abs	$^{207}Pb/^{235}U$	2s abs	$^{208}Pb/^{232}Th$	2s abs	
		(%)	CPS	CPS	(ppm)			Data for Wetherill plot																	
5.sSMPABC203	**-**	**0.00**	**158789**	**9126**	**524**	**0.00**	**0**	**0.057**	**1.027**	**0.633**	**1.638**	**0.080**	**1.276**	**0.779**	**0.105**	**10.365**	**510**	**23**	**496**	**6**	**498**	**6**	**2021**	**199**	**99**
5.sSMPABC183	**-**	**0.00**	**213048**	**12167**	**697**	**0.15**	**0**	**0.057**	**1.016**	**0.635**	**1.623**	**0.081**	**1.266**	**0.780**	**0.024**	**2.053**	**496**	**22**	**500**	**6**	**499**	**6**	**487**	**10**	**100**
5.sSMPABC028	**-**	**0.03**	**194721**	**11230**	**759**	**0.08**	**9622**	**0.058**	**0.993**	**0.664**	**1.632**	**0.084**	**1.295**	**0.793**	**0.033**	**2.198**	**517**	**22**	**517**	**6**	**517**	**7**	**652**	**14**	**100**
5.sSMPABC197	**-**	**0.18**	**146643**	**8457**	**460**	**0.23**	**1531**	**0.058**	**1.224**	**0.668**	**1.807**	**0.084**	**1.330**	**0.736**	**0.026**	**2.062**	**517**	**27**	**520**	**7**	**520**	**7**	**523**	**11**	**100**
5.sSMPABC061	**-**	**0.00**	**155203**	**8955**	**597**	**0.16**	**0**	**0.058**	**1.127**	**0.673**	**1.738**	**0.085**	**1.324**	**0.762**	**0.028**	**2.934**	**518**	**25**	**524**	**7**	**523**	**7**	**557**	**16**	**100**
5.sSMPABC030	**-**	**0.00**	**85979**	**4964**	**331**	**0.15**	**0**	**0.058**	**1.074**	**0.674**	**1.704**	**0.085**	**1.324**	**0.777**	**0.028**	**2.748**	**520**	**24**	**524**	**7**	**523**	**7**	**552**	**15**	**100**
5.sSMPABC072	**seq0125.dat**	**0.00**	**118628**	**6853**	**454**	**0.14**	**0**	**0.058**	**1.056**	**0.678**	**1.706**	**0.085**	**1.340**	**0.785**	**0.027**	**2.581**	**521**	**23**	**526**	**7**	**525**	**7**	**541**	**14**	**100**
5.sSMPABC071	**-**	**0.00**	**125287**	**7272**	**478**	**0.18**	**0**	**0.058**	**1.051**	**0.683**	**1.699**	**0.085**	**1.335**	**0.786**	**0.027**	**2.314**	**531**	**23**	**528**	**7**	**529**	**7**	**534**	**12**	**100**
5.sSMPABC167	**seq0090.dat**	**0.00**	**204287**	**11855**	**626**	**0.41**	**0**	**0.058**	**1.051**	**0.688**	**1.620**	**0.086**	**1.233**	**0.761**	**0.026**	**1.760**	**531**	**23**	**532**	**6**	**532**	**7**	**521**	**9**	**100**

LA(SF)-ICP-MS U-Pb zircon results data from Sample CA-07 (Ataléia suite)

Identifier	Lu-Hf identifier	f206[a]	^{207}Pb	^{206}Pb	U	Th[b]/U	$^{206}Pb/^{204}Pb$	Ratios[c]									Ages (Ma)[c]								
								$^{207}Pb/^{206}Pb$	2s (%)	$^{207}Pb/^{235}U$	2s (%)	$^{206}Pb/^{238}U$	2s (%)	Rho[d]	$^{208}Pb/^{232}Th$	2s (%)	$^{207}Pb/^{206}Pb$	2s	$^{206}Pb/^{238}U$	2s	$^{207}Pb/^{235}U$	2s	$^{208}Pb/^{232}Th$	2s	% conc[e]
		(%)	CPS	CPS	(ppm)			Data for Wetherill plot										abs		abs		abs		abs	
5.sSMPABC073	-	**0.00**	**176539**	**10255**	**668**	**0.19**	**0**	**0.058**	**1.050**	**0.689**	**1.673**	**0.086**	**1.302**	**0.778**	**0.026**	**2.176**	**533**	**23**	**532**	**7**	**532**	**7**	**513**	**11**	**100**
5.sSMPABC009	-	**0.27**	**137971**	**7984**	**522**	**0.31**	**1022**	**0.058**	**1.373**	**0.687**	**1.990**	**0.086**	**1.441**	**0.724**	**0.027**	**1.702**	**525**	**30**	**532**	**7**	**531**	**8**	**539**	**9**	**100**
5.sSMPABC031	-	**0.07**	**322129**	**18705**	**1215**	**0.06**	**3658**	**0.058**	**1.031**	**0.691**	**1.649**	**0.086**	**1.287**	**0.780**	**0.036**	**2.048**	**532**	**23**	**533**	**7**	**533**	**7**	**717**	**14**	**100**
5.sSMPABC033	-	**0.00**	**252506**	**14693**	**947**	**0.22**	**0**	**0.058**	**0.997**	**0.696**	**1.631**	**0.087**	**1.291**	**0.792**	**0.028**	**1.703**	**537**	**22**	**536**	**7**	**536**	**7**	**562**	**9**	**100**
5.sSMPABC169	-	**0.00**	**92284**	**5392**	**279**	**0.63**	**0**	**0.058**	**1.095**	**0.702**	**1.671**	**0.087**	**1.262**	**0.755**	**0.027**	**1.773**	**546**	**24**	**539**	**7**	**540**	**7**	**540**	**10**	**100**
5.sSMPABC190	**seq0116.dat**	**0.00**	**272785**	**15920**	**825**	**0.11**	**0**	**0.058**	**1.045**	**0.701**	**1.747**	**0.087**	**1.400**	**0.801**	**0.032**	**2.773**	**543**	**23**	**539**	**7**	**540**	**7**	**646**	**17**	**100**
5.sSMPABC184	-	**0.17**	**166561**	**9664**	**504**	**0.35**	**1555**	**0.058**	**1.212**	**0.697**	**1.779**	**0.087**	**1.302**	**0.732**	**0.027**	**1.805**	**530**	**27**	**539**	**7**	**537**	**7**	**531**	**9**	**100**
5.sSMPABC182	-	**0.00**	**113340**	**6608**	**343**	**0.43**	**0**	**0.058**	**1.046**	**0.701**	**1.657**	**0.087**	**1.284**	**0.775**	**0.026**	**1.752**	**541**	**23**	**539**	**7**	**539**	**7**	**524**	**9**	**100**
5.sSMPABC026	**seq0099.dat**	**0.00**	**176631**	**10301**	**658**	**0.07**	**0**	**0.058**	**1.029**	**0.703**	**1.644**	**0.087**	**1.282**	**0.780**	**0.029**	**2.718**	**542**	**22**	**540**	**7**	**540**	**7**	**586**	**16**	**100**
5.sSMPABC210	-	**0.16**	**279657**	**16323**	**843**	**0.19**	**1701**	**0.058**	**1.135**	**0.704**	**1.733**	**0.087**	**1.309**	**0.756**	**0.028**	**1.741**	**544**	**25**	**541**	**7**	**541**	**7**	**550**	**9**	**100**
5.sSMPABC177	-	**0.00**	**66109**	**3861**	**199**	**0.53**	**0**	**0.058**	**1.147**	**0.707**	**1.802**	**0.088**	**1.390**	**0.771**	**0.025**	**2.222**	**545**	**25**	**542**	**7**	**543**	**8**	**503**	**11**	**100**
5.sSMPABC179	-	**0.00**	**314043**	**18334**	**939**	**0.28**	**0**	**0.058**	**1.011**	**0.710**	**1.606**	**0.088**	**1.248**	**0.777**	**0.026**	**1.611**	**544**	**22**	**545**	**7**	**545**	**7**	**520**	**8**	**100**
5.sSMPABC006	-	**0.00**	**263060**	**15326**	**970**	**0.22**	**0**	**0.058**	**1.013**	**0.709**	**1.623**	**0.088**	**1.269**	**0.782**	**0.029**	**1.648**	**540**	**22**	**545**	**7**	**544**	**7**	**580**	**9**	**100**
5.sSMPABC060	**seq0129.dat**	**0.00**	**109798**	**6423**	**405**	**0.32**	**0**	**0.059**	**1.026**	**0.712**	**1.684**	**0.088**	**1.336**	**0.793**	**0.027**	**1.905**	**549**	**22**	**546**	**7**	**546**	**7**	**544**	**10**	**100**
5.sSMPABC165	-	**0.23**	**131281**	**7689**	**391**	**0.68**	**1208**	**0.059**	**1.378**	**0.715**	**1.954**	**0.089**	**1.385**	**0.709**	**0.028**	**2.090**	**551**	**30**	**547**	**7**	**548**	**8**	**553**	**11**	**100**
5.sSMPABC180	-	**0.01**	**239742**	**14000**	**714**	**0.37**	**34284**	**0.058**	**1.028**	**0.713**	**1.613**	**0.089**	**1.243**	**0.771**	**0.027**	**1.644**	**545**	**22**	**547**	**7**	**546**	**7**	**534**	**9**	**100**
5.sSMPABC196	**seq0132.dat**	**0.00**	**206304**	**12075**	**614**	**0.40**	**0**	**0.059**	**1.042**	**0.715**	**1.621**	**0.089**	**1.241**	**0.766**	**0.026**	**1.816**	**550**	**23**	**547**	**7**	**548**	**7**	**527**	**9**	**100**
5.sSMPABC070	-	**0.00**	**119721**	**7011**	**437**	**0.34**	**0**	**0.059**	**1.042**	**0.719**	**1.685**	**0.089**	**1.325**	**0.786**	**0.026**	**1.998**	**551**	**23**	**550**	**7**	**550**	**7**	**519**	**10**	**100**
5.sSMPABC202	-	**0.00**	**239382**	**14011**	**707**	**0.17**	**0**	**0.059**	**1.008**	**0.720**	**1.610**	**0.089**	**1.255**	**0.780**	**0.028**	**1.885**	**550**	**22**	**551**	**7**	**551**	**7**	**550**	**10**	**100**
5.sSMPABC208	seq0118.dat	0.00	111298	6570	329	0.42	0	0.059	1.152	0.726	1.875	0.089	1.479	0.789	0.024	2.648	568	25	551	8	554	8	483	13	99

LA(SF)-ICP-MS U-Pb zircon results data from Sample CA-07 (Ataléia suite)

Identifier	Lu-Hf identifier	f206[a]	207Pb	206Pb	U	Th[b]/U	206Pb/204Pb	Ratios[c]									Ages (Ma)[c]								% conc[e]
								207Pb/206Pb	2s (%)	207Pb/235U	2s (%)	206Pb/238U	2s (%)	Rho[d]	208Pb/232Th	2s (%)	207Pb/206Pb	2s abs	206Pb/238U	2s abs	207Pb/235U	2s abs	208Pb/232Th	2s abs	
		(%)	CPS	CPS	(ppm)			Data for Wetherill plot																	
5.sSMPABC010	**-**	**0.00**	**80023**	**4681**	**291**	**0.44**	**0**	**0.058**	**1.043**	**0.721**	**1.682**	**0.089**	**1.320**	**0.785**	**0.027**	**1.727**	**548**	**23**	**552**	**7**	**551**	**7**	**531**	**9**	**100**
5.sSMPABC032	seq0102.dat	0.02	160733	9422	585	0.26	11827	0.059	1.010	0.723	1.645	0.089	1.298	0.789	0.028	1.713	553	22	552	7	552	7	559	10	100
5.sSMPABC181	-	0.00	183947	10785	542	0.52	0	0.059	1.006	0.723	1.607	0.089	1.252	0.780	0.026	1.547	553	22	552	7	552	7	516	8	100
5.sSMPABC206	-	0.00	159011	9309	469	0.15	0	0.059	1.042	0.722	1.629	0.089	1.252	0.769	0.028	2.316	550	23	552	7	552	7	551	13	100
5.sSMPABC185	-	0.00	213170	12509	628	0.29	0	0.059	1.040	0.725	1.609	0.090	1.228	0.763	0.027	1.769	555	23	553	7	553	7	541	10	100
5.sSMPABC091	seq0131.dat	0.00	184070	10726	668	0.10	0	0.058	1.167	0.720	1.844	0.090	1.428	0.774	0.027	3.795	540	26	553	8	551	8	536	20	100
5.sSMPABC043	**-**	**0.00**	**198204**	**11621**	**719**	**0.49**	**0**	**0.059**	**1.023**	**0.725**	**1.649**	**0.090**	**1.293**	**0.784**	**0.027**	**1.621**	**553**	**22**	**554**	**7**	**554**	**7**	**541**	**9**	**100**
5.sSMPABC200	-	0.00	153690	9003	451	0.37	0	0.059	1.024	0.727	1.629	0.090	1.267	0.778	0.025	1.746	552	22	555	7	555	7	503	9	100
5.sSMPABC205	-	0.05	217979	12762	639	0.29	5181	0.059	1.057	0.727	1.654	0.090	1.272	0.769	0.027	1.871	550	23	556	7	555	7	533	10	100
5.sSMPABC191	-	0.00	163966	9603	480	0.74	0	0.059	1.024	0.728	1.628	0.090	1.265	0.777	0.026	1.550	551	22	556	7	555	7	515	8	100
5.sSMPABC187	-	0.21	82261	4813	241	0.51	1275	0.059	1.287	0.727	1.880	0.090	1.371	0.729	0.025	1.854	549	28	556	7	555	8	495	9	100
5.sSMPABC075	-	0.00	72146	4236	260	0.57	0	0.059	1.090	0.730	1.772	0.090	1.397	0.788	0.026	2.073	556	24	557	7	557	8	520	11	100
5.sSMPABC164	**-**	**0.00**	**91728**	**5634**	**268**	**0.52**	**0**	**0.061**	**1.058**	**0.765**	**1.664**	**0.090**	**1.285**	**0.772**	**0.027**	**1.760**	**654**	**23**	**557**	**7**	**577**	**7**	**544**	**10**	**97**
5.sSMPABC094	-	0.03	336948	19735	1213	0.20	7796	0.059	1.099	0.730	1.708	0.090	1.308	0.766	0.029	2.458	551	24	558	7	556	7	584	14	100
5.sSMPABC199	seq0130.dat	0.00	132607	7784	387	0.54	0	0.059	1.039	0.732	1.651	0.090	1.283	0.777	0.026	1.683	556	23	558	7	558	7	522	9	100
5.sSMPABC008	seq0093.dat	0.00	288961	17089	1040	0.18	0	0.059	1.116	0.737	1.684	0.090	1.261	0.749	0.031	2.665	572	24	558	7	561	7	613	16	99
5.sSMPABC189	-	0.00	167315	9818	488	0.22	0	0.059	1.176	0.732	1.757	0.090	1.305	0.743	0.026	3.029	555	26	558	7	558	8	527	16	100
5.sSMPABC048	-	0.17	137826	8085	496	0.36	1619	0.059	1.202	0.731	1.813	0.090	1.357	0.748	0.028	1.881	555	26	558	7	557	8	551	10	100
5.sSMPABC074	seq0119.dat	0.06	287308	16764	1034	0.15	4905	0.058	1.147	0.728	1.742	0.090	1.310	0.752	0.028	3.008	543	25	558	7	555	7	557	16	101
5.sSMPABC207	-	0.00	141775	8355	413	0.52	0	0.059	1.035	0.735	1.648	0.090	1.282	0.778	0.026	1.683	565	23	558	7	560	7	522	9	100

LA(SF)-ICP-MS U-Pb zircon results data from Sample CA-07 (Ataléia suite)

Identifier	Lu-Hf identifier	f206[a]	207Pb	206Pb	U	Th[b]/U	206Pb/204Pb	Ratios[c]									Ages (Ma)[c]								% conc[e]
								207Pb/206Pb	2s (%)	207Pb/235U	2s (%)	206Pb/238U	2s (%)	Rho[d]	208Pb/232Th	2s (%)	207Pb/206Pb	2s	206Pb/238U	2s	207Pb/235U	2s	208Pb/232Th	2s	
		(%)	CPS	CPS	(ppm)			Data for Wetherill plot									abs		abs		abs		abs	
5.sSMPABC053	-	0.00	118415	6964	425	0.22	0	0.059	1.037	0.735	1.682	0.091	1.324	0.787	0.028	2.084	560	23	559	7	559	7	555	12	100
5.sSMPABC020	-	0.00	148650	8748	533	0.34	0	0.059	1.037	0.736	1.664	0.091	1.301	0.782	0.028	1.737	562	23	560	7	560	7	551	9	100
5.sSMPABC076	-	0.00	301288	17704	1080	0.27	0	0.059	1.021	0.736	1.653	0.091	1.300	0.786	0.027	1.871	558	22	560	7	560	7	533	10	100
5.sSMPABC092	**seq0101.dat**	**0.00**	**60256**	**3545**	**216**	**0.58**	**0**	**0.059**	**1.122**	**0.737**	**1.783**	**0.091**	**1.386**	**0.777**	**0.026**	**2.199**	**561**	**24**	**561**	**7**	**561**	**8**	**526**	**11**	**100**
5.sSMPABC025	-	0.35	96943	5675	347	0.37	779	0.059	1.585	0.735	2.200	0.091	1.526	0.694	0.027	1.762	550	35	562	8	559	10	543	10	100
5.sSMPABC068	-	0.11	154981	9111	554	0.29	2498	0.059	1.118	0.738	1.744	0.091	1.339	0.768	0.027	2.053	559	24	562	7	561	8	544	11	100
5.sSMPABC188	**seq0115.dat**	**0.00**	**194742**	**11488**	**564**	**0.20**	**0**	**0.059**	**1.017**	**0.741**	**1.612**	**0.091**	**1.251**	**0.776**	**0.028**	**1.895**	**567**	**22**	**562**	**7**	**563**	**7**	**568**	**11**	**100**
5.sSMPABC011	**seq0092.dat**	**0.00**	**98980**	**5832**	**353**	**0.53**	**0**	**0.059**	**1.035**	**0.740**	**1.675**	**0.091**	**1.317**	**0.786**	**0.026**	**1.637**	**564**	**23**	**562**	**7**	**563**	**7**	**512**	**8**	**100**
5.sSMPABC057	-	0.00	165039	9708	589	0.25	0	0.059	1.054	0.740	1.686	0.091	1.316	0.780	0.026	2.039	560	23	563	7	562	7	528	11	100
5.sSMPABC041	-	0.08	291339	17123	1040	0.17	3541	0.059	1.005	0.739	1.647	0.091	1.305	0.792	0.031	1.623	559	22	563	7	562	7	613	10	100
5.sSMPABC040	-	0.00	79599	4690	284	0.26	0	0.059	1.426	0.741	2.079	0.091	1.513	0.728	0.027	4.327	564	31	563	8	563	9	535	23	100
5.sSMPABC029	**seq0098.dat**	**0.00**	**275826**	**16224**	**982**	**0.24**	**0**	**0.059**	**1.020**	**0.741**	**1.663**	**0.091**	**1.313**	**0.790**	**0.028**	**1.783**	**560**	**22**	**564**	**7**	**563**	**7**	**559**	**10**	**100**
5.sSMPABC054	-	0.00	73529	4346	261	0.52	0	0.059	1.167	0.748	1.904	0.092	1.505	0.790	0.024	2.483	571	25	566	8	567	8	483	12	100
5.sSMPABC186	**-**	**0.13**	**200934**	**11847**	**578**	**0.25**	**2033**	**0.059**	**1.115**	**0.746**	**1.711**	**0.092**	**1.298**	**0.759**	**0.028**	**1.771**	**566**	**24**	**566**	**7**	**566**	**7**	**563**	**10**	**100**
5.sSMPABC170	**seq0096.dat**	**0.00**	**172946**	**10197**	**497**	**0.38**	**0**	**0.059**	**1.035**	**0.746**	**1.616**	**0.092**	**1.242**	**0.768**	**0.028**	**1.739**	**566**	**23**	**566**	**7**	**566**	**7**	**550**	**9**	**100**
5.sSMPABC059	**-**	**0.09**	**148259**	**8741**	**525**	**0.20**	**3070**	**0.059**	**1.094**	**0.747**	**1.715**	**0.092**	**1.321**	**0.770**	**0.028**	**2.192**	**566**	**24**	**566**	**7**	**566**	**7**	**564**	**12**	**100**
5.sSMPABC201	seq0128.dat	0.04	77508	4583	222	0.52	7008	0.059	1.074	0.752	1.706	0.092	1.325	0.777	0.025	1.999	572	23	569	7	569	7	499	10	100
5.sSMPABC017	seq0097.dat	0.00	184909	10821	652	0.37	0	0.059	1.025	0.744	1.639	0.092	1.279	0.780	0.027	1.687	549	22	569	7	565	7	544	9	101
5.sSMPABC013	-	0.20	93545	5541	327	0.23	1331	0.059	1.254	0.760	1.868	0.093	1.384	0.741	0.027	2.207	576	27	573	8	574	8	542	12	100
5.sSMPABC047	seq0094.dat	0.00	145284	8607	507	0.50	0	0.059	1.165	0.761	1.850	0.093	1.438	0.777	0.031	2.341	576	25	574	8	575	8	612	14	100

LA(SF)-ICP-MS U-Pb zircon results data from Sample CA-07 (Ataléia suite)

Identifier	Lu-Hf identifier	f206[a]	207Pb	206Pb	U	Th[b]/U	206Pb/204Pb	Ratios[c]									Ages (Ma)[c]								% conc[e]
								207Pb/206Pb	2s (%)	207Pb/235U	2s (%)	206Pb/238U	2s (%)	Rho[d]	208Pb/232Th	2s (%)	207Pb/206Pb	2s abs	206Pb/238U	2s abs	207Pb/235U	2s abs	208Pb/232Th	2s abs	
		(%)	CPS	CPS	(ppm)			Data for Wetherill plot																	
5.sSMPABC015	-	0.49	88555	5220	309	0.54	556	0.059	1.958	0.758	2.590	0.093	1.694	0.654	0.027	1.630	565	43	575	9	573	11	538	9	100
5.sSMPABC039	seq0104.dat	0.00	232574	13740	811	0.97	0	0.059	1.032	0.761	1.665	0.093	1.306	0.785	0.027	1.553	570	22	575	7	574	7	539	8	100
5.sSMPABC014	seq0127.dat	0.19	105248	6223	366	0.47	1399	0.059	1.224	0.763	1.837	0.094	1.369	0.745	0.026	1.686	572	27	576	8	575	8	521	9	100
5.sSMPABC083	**-**	**0.00**	**77198**	**4252**	**268**	**0.27**	**0**	**0.055**	**1.071**	**0.713**	**1.734**	**0.094**	**1.363**	**0.786**	**0.027**	**2.324**	**415**	**24**	**578**	**8**	**547**	**7**	**532**	**12**	**106**
5.sSMPABC086	seq0124.dat	0.00	133047	7892	461	0.30	0	0.059	1.247	0.768	1.977	0.094	1.533	0.776	0.028	3.341	579	27	579	8	579	9	549	18	100
5.sSMPABC178	-	0.00	83517	4955	234	0.57	0	0.059	1.264	0.768	2.003	0.094	1.554	0.776	0.026	2.824	579	27	579	9	579	9	523	15	100
5.sSMPABC042	-	0.00	62100	3687	215	0.61	0	0.059	1.145	0.771	1.859	0.094	1.465	0.788	0.026	2.250	581	25	580	8	580	8	515	11	100
5.sSMPABC046	**-**	**0.11**	**154019**	**8705**	**532**	**0.10**	**2488**	**0.057**	**1.064**	**0.735**	**1.692**	**0.094**	**1.315**	**0.777**	**0.029**	**2.395**	**473**	**24**	**581**	**7**	**559**	**7**	**582**	**14**	**104**
5.sSMPABC088	seq0126.dat	0.00	124817	7424	430	0.16	0	0.059	1.160	0.775	1.783	0.095	1.354	0.759	0.030	3.313	585	25	582	8	583	8	601	20	100
5.sSMPABC027	seq0100.dat	0.00	256275	15169	880	0.34	0	0.059	1.081	0.774	1.763	0.095	1.393	0.790	0.027	2.149	574	24	584	8	582	8	538	11	100
5.sSMPABC019	-	0.00	370022	21998	1270	0.10	0	0.059	1.009	0.777	1.635	0.095	1.286	0.787	0.036	1.934	584	22	584	7	584	7	719	13	100
5.sSMPABC082	seq0120.dat	0.00	66040	3933	225	0.45	0	0.060	1.092	0.783	1.747	0.095	1.363	0.781	0.027	2.160	587	24	587	8	587	8	536	12	100
5.sSMPABC044	-	0.00	104931	6245	356	0.38	0	0.060	1.075	0.786	1.699	0.096	1.315	0.774	0.029	1.996	586	23	590	7	589	8	579	11	100
5.sSMPABC166	seq0089.dat	0.00	124242	7412	340	0.44	0	0.060	1.106	0.793	1.680	0.096	1.265	0.753	0.030	2.158	591	24	594	7	593	8	591	13	100
5.sSMPABC069	-	0.00	93880	5575	315	0.48	0	0.059	1.246	0.795	1.921	0.097	1.462	0.761	0.028	2.930	581	27	597	8	594	9	558	16	101
5.sSMPABC163	seq0091.dat	0.00	121465	7262	330	0.40	0	0.060	1.037	0.801	1.644	0.097	1.276	0.776	0.032	1.702	596	22	598	7	598	7	632	11	100
5.sSMPABC084	seq0122.dat	0.00	128271	7628	428	0.60	0	0.059	1.143	0.799	1.757	0.097	1.334	0.759	0.027	2.455	584	25	600	8	596	8	536	13	101
5.sSMPABC090	seq0117.dat	0.00	50104	3000	167	0.47	0	0.060	1.353	0.808	2.014	0.098	1.492	0.741	0.029	3.343	599	29	602	9	601	9	572	19	100
5.sSMPABC089	-	0.46	86305	5142	287	0.45	596	0.060	1.967	0.804	2.583	0.098	1.675	0.648	0.028	2.879	588	43	602	10	599	12	568	16	100
5.sSMPABC012	**seq0105.dat**	**0.00**	**114766**	**6752**	**379**	**0.17**	**0**	**0.059**	**1.054**	**0.798**	**1.674**	**0.098**	**1.300**	**0.777**	**0.033**	**2.247**	**561**	**23**	**605**	**8**	**596**	**8**	**655**	**14**	**102**

LA(SF)-ICP-MS U-Pb zircon results data from Sample CA-07 (Ataléia suite)

Identifier	Lu-Hf identifier	f206[a]	207Pb	206Pb	U	Th[b]/U	206Pb/204Pb	Ratios[c]									Ages (Ma)[c]								% conc[e]
								207Pb/206Pb	2s (%)	207Pb/235U	2s (%)	206Pb/238U	2s (%)	Rho[d]	208Pb/232Th	2s (%)	207Pb/206Pb	2s abs	206Pb/238U	2s abs	207Pb/235U	2s abs	208Pb/232Th	2s abs	
		(%)	CPS	CPS	(ppm)			Data for Wetherill plot																	
5.sSMPABC085	**seq0123.dat**	**0.00**	**87488**	**5244**	**287**	**0.39**	**0**	**0.060**	**1.385**	**0.819**	**2.052**	**0.099**	**1.514**	**0.738**	**0.027**	**3.898**	**601**	**30**	**609**	**9**	**607**	**9**	**542**	**21**	**100**
5.sSMPABC055	**seq0095.dat**	**0.00**	**85350**	**5094**	**280**	**0.54**	**0**	**0.060**	**1.156**	**0.815**	**1.841**	**0.099**	**1.433**	**0.778**	**0.028**	**2.320**	**592**	**25**	**609**	**8**	**605**	**8**	**567**	**13**	**101**
5.sSMPABC045	**-**	**0.00**	**136934**	**7790**	**441**	**0.33**	**0**	**0.057**	**1.002**	**0.792**	**1.647**	**0.101**	**1.307**	**0.794**	**0.028**	**1.799**	**487**	**22**	**620**	**8**	**592**	**7**	**554**	**10**	**105**
5.sSMPABC081	**seq0121.dat**	**0.00**	**125072**	**7587**	**399**	**0.51**	**0**	**0.061**	**1.022**	**0.853**	**1.680**	**0.102**	**1.333**	**0.794**	**0.028**	**1.854**	**627**	**22**	**626**	**8**	**626**	**8**	**559**	**10**	**100**
5.sSMPABC162	**seq0088.dat**	**0.45**	**43233**	**2610**	**111**	**0.21**	**605**	**0.060**	**2.067**	**0.851**	**2.706**	**0.102**	**1.747**	**0.645**	**0.054**	**4.032**	**617**	**45**	**628**	**10**	**625**	**13**	**1064**	**42**	**100**
5.sSMPABC158	**seq0084.dat**	**0.11**	**82253**	**5063**	**202**	**0.45**	**2448**	**0.062**	**1.163**	**0.913**	**1.772**	**0.108**	**1.337**	**0.754**	**0.039**	**2.028**	**659**	**25**	**658**	**8**	**658**	**9**	**782**	**16**	**100**
5.sSMPABC095	**-**	**0.30**	**114626**	**7027**	**345**	**0.19**	**910**	**0.061**	**1.435**	**0.914**	**2.035**	**0.108**	**1.444**	**0.709**	**0.045**	**2.198**	**650**	**31**	**662**	**9**	**659**	**10**	**899**	**19**	**100**
5.sSMPABC161	**seq0087.dat**	**0.29**	**38477**	**2387**	**91**	**0.86**	**955**	**0.062**	**1.512**	**0.954**	**2.100**	**0.112**	**1.458**	**0.694**	**0.037**	**1.987**	**675**	**32**	**681**	**9**	**680**	**10**	**739**	**14**	**100**
5.sSMPABC159	**seq0085.dat**	**0.00**	**88723**	**5674**	**194**	**0.39**	**0**	**0.064**	**1.142**	**1.063**	**1.776**	**0.121**	**1.360**	**0.766**	**0.045**	**2.326**	**740**	**24**	**734**	**9**	**735**	**9**	**884**	**20**	**100**
5.sSMPABC160	**seq0086.dat**	**0.00**	**54749**	**3493**	**120**	**0.32**	**0**	**0.064**	**1.238**	**1.062**	**1.888**	**0.121**	**1.425**	**0.755**	**0.050**	**2.850**	**735**	**26**	**735**	**10**	**735**	**10**	**983**	**28**	**100**
5.sSMPABC034	**seq0103.dat**	**0.00**	**130626**	**8735**	**311**	**0.79**	**0**	**0.067**	**1.032**	**1.262**	**1.753**	**0.137**	**1.417**	**0.808**	**0.036**	**1.763**	**834**	**22**	**827**	**11**	**829**	**10**	**721**	**12**	**100**
5.sSMPABC087	**-**	**0.00**	**497846**	**39609**	**803**	**0.70**	**0**	**0.080**	**1.043**	**2.213**	**1.666**	**0.202**	**1.299**	**0.780**	**0.056**	**2.041**	**1186**	**21**	**1184**	**14**	**1185**	**12**	**1099**	**22**	**100**

LA(SF)-ICP-MS U-Pb zircon results data from Sample CA-09 (Nova Venécia complex)

Identifier	Lu-Hf identifier	f206[a]	207Pb	206Pb	U	Th[b]/U	206Pb/204Pb	Ratios[c]									Ages (Ma)[c]								% conc[e]
								207Pb/206Pb	2s (%)	207Pb/235U	2s (%)	206Pb/238U	2s (%)	Rho[d]	208Pb/232Th	2s (%)	207Pb/206Pb	2s abs	206Pb/238U	2s abs	207Pb/235U	2s abs	208Pb/232Th	2s abs	
		(%)	CPS	CPS	(ppm)			Data for Wetherill plot																	
5.sSMPABC038	-	0.00	172728	9885	522	0.06	0	0.057	1.013	0.614	1.558	0.078	1.183	0.759	0.027	2.780	500	22	483	6	486	6	545	15	99
5.sSMPABC082	-	0.15	240391	14099	746	0.04	1777	0.059	1.148	0.687	1.700	0.085	1.253	0.737	0.040	2.872	554	25	526	6	531	7	800	23	99

LA(SF)-ICP-MS U-Pb zircon results data from Sample CA-09 (Nova Venécia complex)

Identifier	Lu-Hf identifier	f206[a]	^{207}Pb	^{206}Pb	U	Th[b]/U	$^{206}Pb/^{204}Pb$	Ratios[c]									Ages (Ma)[c]									% conc[e]
								$^{207}Pb/^{206}Pb$	2s (%)	$^{207}Pb/^{235}U$	2s (%)	$^{206}Pb/^{238}U$	2s (%)	Rho[d]	$^{208}Pb/^{232}Th$	2s (%)	$^{207}Pb/^{206}Pb$	2s abs	$^{206}Pb/^{238}U$	2s abs	$^{207}Pb/^{235}U$	2s abs	$^{208}Pb/^{232}Th$	2s abs			
		(%)	CPS	CPS	(ppm)			Data for Wetherill plot																		
5.sSMPABC027	-	0.00	241903	14149	668	0.11	0	0.058	1.009	0.686	1.549	0.085	1.175	0.759	0.032	1.774	548	22	526	6	531	6	628	11	99
5.sSMPABC089	-	0.00	334960	19408	1027	0.18	0	0.058	1.036	0.687	1.610	0.086	1.232	0.766	0.031	1.769	527	23	532	6	531	7	608	11	100
5.sSMPABC148	-	0.00	71609	4233	213	0.45	0	0.059	1.100	0.723	1.692	0.089	1.286	0.760	0.031	1.901	571	24	548	7	552	7	607	11	99
5.sSMPABC039	-	0.00	141060	8287	374	0.29	0	0.059	1.055	0.719	1.646	0.089	1.263	0.767	0.028	1.958	558	23	548	7	550	7	550	10	100
5.sSMPABC152	seq0151.dat	0.00	266236	15655	791	0.34	0	0.059	1.020	0.720	1.588	0.089	1.216	0.766	0.029	1.568	560	22	548	6	551	7	585	9	100
5.sSMPABC074	-	0.00	345135	20301	1022	1.20	0	0.059	0.986	0.722	1.563	0.089	1.213	0.776	0.023	1.222	560	21	550	6	552	7	458	5	100
5.sSMPABC144	-	0.00	97475	5677	287	0.36	0	0.058	1.082	0.720	1.652	0.090	1.249	0.756	0.030	1.940	539	24	554	7	551	7	596	11	101
5.sSMPABC013	-	0.00	184871	10833	551	0.01	0	0.059	1.024	0.725	1.564	0.090	1.182	0.756	0.051	6.916	552	22	554	6	553	7	998	67	100
5.sSMPABC140	-	0.00	167499	9789	491	0.06	0	0.058	1.044	0.724	1.608	0.090	1.223	0.761	0.043	2.687	546	23	555	7	553	7	854	23	100
5.sSMPABC184	-	0.00	141431	8291	413	1.50	0	0.059	1.075	0.730	1.640	0.090	1.239	0.756	0.027	1.716	553	23	558	7	557	7	535	9	100
5.sSMPABC178	seq0139.dat	0.00	120061	7024	350	0.59	0	0.059	1.077	0.731	1.640	0.091	1.237	0.754	0.028	1.865	549	24	559	7	557	7	556	10	100
5.sSMPABC181	seq0135.dat	0.00	158202	9307	460	0.96	0	0.059	1.054	0.735	1.624	0.091	1.236	0.761	0.028	1.656	561	23	559	7	560	7	554	9	100
5.sSMPABC104	-	0.00	157751	9463	443	0.85	0	0.060	1.017	0.776	1.584	0.094	1.215	0.767	0.028	1.338	603	22	578	7	583	7	566	7	99
5.sSMPABC177	-	0.26	86357	5114	241	1.43	1044	0.059	1.421	0.770	1.986	0.094	1.387	0.698	0.029	1.709	575	31	581	8	580	9	583	10	100
5.sSMPABC108	seq0160.dat	0.00	286254	17152	799	0.72	0	0.060	1.018	0.781	1.562	0.095	1.185	0.759	0.029	1.389	601	22	582	7	586	7	574	8	99
5.sSMPABC159	-	0.13	240176	14250	669	0.34	2037	0.059	1.138	0.775	1.696	0.095	1.257	0.741	0.030	1.678	579	25	583	7	582	8	594	10	100
5.sSMPABC024	seq0124.dat	0.00	294937	17569	732	1.27	0	0.060	1.007	0.778	1.537	0.095	1.161	0.755	0.028	1.081	588	22	584	6	584	7	553	6	100
5.sSMPABC158	-	0.00	240254	14322	668	1.01	0	0.060	1.023	0.779	1.595	0.095	1.223	0.767	0.028	1.484	589	22	584	7	585	7	564	8	100
5.sSMPABC126	-	0.00	135312	8025	375	1.18	0	0.059	1.045	0.779	1.605	0.095	1.218	0.759	0.028	1.429	578	23	586	7	585	7	558	8	100
5.sSMPABC064	-	0.00	289044	17149	800	0.69	0	0.059	0.994	0.780	1.555	0.095	1.196	0.769	0.027	1.252	579	22	587	7	585	7	541	7	100

LA(SF)-ICP-MS U-Pb zircon results data from Sample CA-09 (Nova Venécia complex)

Identifier	Lu-Hf identifier	f206[a]	^{207}Pb	^{206}Pb	U	Th[b]/U	$^{206}Pb/^{204}Pb$	Ratios[c]									Ages (Ma)[c]									% conc[e]
								$^{207}Pb/^{206}Pb$	2s (%)	$^{207}Pb/^{235}U$	2s (%)	$^{206}Pb/^{238}U$	2s (%)	Rho[d]	$^{208}Pb/^{232}Th$	2s (%)	$^{207}Pb/^{206}Pb$	2s	$^{206}Pb/^{238}U$	2s	$^{207}Pb/^{235}U$	2s	$^{208}Pb/^{232}Th$	2s		
								Data for Wetherill plot										abs		abs		abs		abs		
		(%)	CPS	CPS	(ppm)																					
5.sSMPABC161	-	0.00	61899	3667	171	0.71	0	0.059	1.182	0.779	1.757	0.095	1.301	0.740	0.030	2.096	576	26	587	7	585	8	589	12	100
5.sSMPABC071	-	0.20	240647	14251	665	0.86	1348	0.059	1.208	0.779	1.752	0.095	1.268	0.724	0.027	1.240	575	26	587	7	585	8	547	7	100
5.sSMPABC151	seq0152.dat	0.00	159809	9465	441	0.66	0	0.059	1.013	0.780	1.598	0.096	1.236	0.773	0.028	1.523	576	22	588	7	585	7	550	8	100
5.sSMPABC182	-	0.00	211486	12569	582	1.87	0	0.059	1.010	0.785	1.609	0.096	1.252	0.779	0.028	1.496	583	22	590	7	588	7	560	8	100
5.sSMPABC034	-	0.00	394329	23608	962	0.13	0	0.060	0.985	0.795	1.524	0.096	1.163	0.763	0.033	1.468	599	21	593	7	594	7	650	9	100
5.sSMPABC105	-	0.00	163171	9807	446	1.56	0	0.060	1.015	0.799	1.574	0.096	1.204	0.764	0.028	1.267	607	22	593	7	596	7	567	7	100
5.sSMPABC075	-	0.00	330359	19792	898	0.23	0	0.060	1.018	0.801	1.540	0.097	1.155	0.750	0.031	1.499	600	22	597	7	597	7	611	9	100
5.sSMPABC087	seq0163.dat	0.00	93812	5621	255	0.68	0	0.060	1.051	0.801	1.624	0.097	1.237	0.762	0.028	1.492	601	23	597	7	598	7	561	8	100
5.sSMPABC006	seq0121.dat	0.00	124500	7456	343	1.17	0	0.060	1.102	0.803	1.717	0.097	1.317	0.767	0.029	1.538	600	24	598	8	598	8	570	9	100
5.sSMPABC100	-	0.00	133544	8014	362	0.11	0	0.060	1.033	0.805	1.594	0.097	1.213	0.761	0.042	2.184	604	22	598	7	600	7	834	18	100
5.sSMPABC010	-	0.00	216384	12909	592	0.73	0	0.060	1.022	0.804	1.551	0.098	1.166	0.752	0.031	1.241	591	22	601	7	599	7	610	7	100
5.sSMPABC055	-	0.21	522209	31036	1255	1.18	1281	0.059	1.211	0.801	1.807	0.098	1.341	0.742	0.026	1.250	583	26	602	8	598	8	511	6	101
5.sSMPABC052	-	0.00	213655	12809	505	1.18	0	0.060	1.018	0.822	1.563	0.099	1.186	0.759	0.029	1.174	602	22	611	7	609	7	577	7	100
5.sSMPABC050	-	0.00	857531	51237	2026	0.66	153060	0.060	0.987	0.820	1.574	0.099	1.226	0.779	0.027	1.269	594	21	611	7	608	7	534	7	101
5.sSMPABC076	seq0132.dat	0.00	203471	12208	539	1.10	0	0.060	1.017	0.823	1.562	0.100	1.185	0.759	0.029	1.234	604	22	612	7	610	7	581	7	100
5.sSMPABC085	-	0.00	685152	41212	1814	0.23	0	0.060	1.014	0.826	1.560	0.100	1.185	0.760	0.032	1.560	609	22	612	7	611	7	638	10	100
5.sSMPABC106	-	0.00	613017	36799	1623	0.87	0	0.060	1.016	0.824	1.546	0.100	1.165	0.754	0.030	1.348	605	22	612	7	610	7	591	8	100
5.sSMPABC053	seq0131.dat	0.00	84773	5102	200	0.53	0	0.060	1.097	0.827	1.628	0.100	1.204	0.739	0.030	1.783	610	24	613	7	612	8	603	11	100
5.sSMPABC171	-	0.00	137274	8263	363	0.79	0	0.060	1.063	0.827	1.636	0.100	1.244	0.760	0.031	1.684	610	23	613	7	612	8	615	10	100
5.sSMPABC150	-	0.00	88352	5293	233	0.43	0	0.060	1.052	0.826	1.642	0.100	1.261	0.768	0.030	1.773	600	23	614	7	611	8	606	11	100

LA(SF)-ICP-MS U-Pb zircon results data from Sample CA-09 (Nova Venécia complex)

Identifier	Lu-Hf identifier	f206[a]	^{207}Pb	^{206}Pb	U	Th[b]/U	$^{206}Pb/^{204}Pb$	Ratios[c]									Ages (Ma)[c]								% conc[e]
								$^{207}Pb/^{206}Pb$	2s (%)	$^{207}Pb/^{235}U$	2s (%)	$^{206}Pb/^{238}U$	2s (%)	Rho[d]	$^{208}Pb/^{232}Th$	2s (%)	$^{207}Pb/^{206}Pb$	2s abs	$^{206}Pb/^{238}U$	2s abs	$^{207}Pb/^{235}U$	2s abs	$^{208}Pb/^{232}Th$	2s abs	
		(%)	CPS	CPS	(ppm)			Data for Wetherill plot																	
5.sSMPABC095	-	0.28	115567	6912	305	0.07	961	0.060	1.420	0.825	1.969	0.100	1.364	0.693	0.058	2.877	597	31	614	8	611	9	1147	32	101
5.sSMPABC163	-	0.12	316090	19028	831	0.05	2252	0.060	1.106	0.832	1.662	0.100	1.240	0.746	0.043	2.322	611	24	616	7	615	8	852	20	100
5.sSMPABC129	-	0.00	387277	23008	1018	0.22	0	0.059	1.060	0.822	1.659	0.100	1.276	0.769	0.031	2.154	582	23	616	8	609	8	610	13	101
5.sSMPABC145	seq0155.dat	0.00	144638	8636	379	0.90	0	0.060	1.005	0.829	1.589	0.101	1.231	0.775	0.027	1.401	593	22	619	7	613	7	541	8	101
5.sSMPABC103	-	0.00	278500	16841	727	0.89	0	0.060	1.009	0.842	1.559	0.101	1.188	0.762	0.030	1.321	620	22	620	7	620	7	603	8	100
5.sSMPABC093	seq0161.dat	0.00	68451	4158	178	1.22	0	0.061	1.070	0.847	1.642	0.101	1.246	0.759	0.030	1.422	630	23	621	7	623	8	588	8	100
5.sSMPABC166	seq0142.dat	0.00	149460	8983	387	0.79	0	0.060	1.048	0.845	1.621	0.102	1.236	0.763	0.030	1.609	607	23	626	7	622	8	594	10	101
5.sSMPABC170	seq0140.dat	0.00	305393	18156	783	0.78	0	0.059	1.043	0.843	1.624	0.103	1.245	0.767	0.031	1.685	584	23	631	7	621	8	614	10	102
5.sSMPABC094	-	0.00	108275	6626	278	0.74	0	0.061	1.029	0.868	1.600	0.103	1.225	0.766	0.029	1.466	646	22	631	7	634	8	571	8	99
5.sSMPABC146	-	0.55	131953	8023	337	1.10	499	0.061	2.073	0.867	2.638	0.103	1.631	0.618	0.030	1.418	632	45	634	10	634	13	590	8	100
5.sSMPABC169	-	0.00	233644	14271	595	0.59	0	0.061	1.048	0.873	1.605	0.104	1.216	0.758	0.031	1.748	642	23	636	7	637	8	615	11	100
5.sSMPABC092	-	0.16	220507	13488	561	0.90	1680	0.061	1.131	0.874	1.690	0.104	1.256	0.743	0.029	1.313	645	24	636	8	638	8	577	7	100
5.sSMPABC068	seq0125.dat	0.00	395349	24073	1005	0.03	0	0.061	1.002	0.871	1.650	0.104	1.311	0.795	0.089	2.974	635	22	636	8	636	8	1731	49	100
5.sSMPABC139	-	0.00	134727	8147	340	0.89	0	0.060	1.042	0.871	1.623	0.105	1.244	0.767	0.031	1.537	620	22	641	8	636	8	621	9	101
5.sSMPABC164	seq0141.dat	0.00	302666	18438	764	1.08	0	0.061	1.067	0.878	1.653	0.105	1.263	0.764	0.030	1.840	636	23	641	8	640	8	606	11	100
5.sSMPABC048	seq0128.dat	0.10	91149	5532	205	1.03	2621	0.061	1.235	0.875	1.890	0.105	1.430	0.757	0.028	1.914	628	27	641	9	638	9	562	10	100
5.sSMPABC091	seq0162.dat	0.00	642439	38739	1589	0.43	4188001	0.060	1.012	0.872	1.542	0.105	1.163	0.755	0.031	1.270	614	22	643	7	637	7	627	8	101
5.sSMPABC138	seq0149.dat	0.00	264115	16037	663	0.62	0	0.061	1.087	0.879	1.633	0.105	1.219	0.746	0.032	1.976	629	23	644	7	641	8	644	12	101
5.sSMPABC111	seq0166.dat	0.02	350278	21297	879	0.72	15640	0.061	0.989	0.881	1.554	0.105	1.199	0.772	0.030	1.249	632	21	644	7	642	7	606	8	100
5.sSMPABC101	seq0165.dat	0.00	387728	23543	961	0.67	0	0.061	1.021	0.891	1.549	0.106	1.165	0.752	0.030	1.402	629	22	652	7	647	7	597	8	101

LA(SF)-ICP-MS U-Pb zircon results data from Sample CA-09 (Nova Venécia complex)

Identifier	Lu-Hf identifier	f206[a]	^{207}Pb	^{206}Pb	U	Th[b]/U	$^{206}Pb/^{204}Pb$	Ratios[c]									Ages (Ma)[c]									% conc[e]
								$^{207}Pb/^{206}Pb$	2s (%)	$^{207}Pb/^{235}U$	2s (%)	$^{206}Pb/^{238}U$	2s (%)	Rho[d]	$^{208}Pb/^{232}Th$	2s (%)	$^{207}Pb/^{206}Pb$	2s abs	$^{206}Pb/^{238}U$	2s abs	$^{207}Pb/^{235}U$	2s abs	$^{208}Pb/^{232}Th$	2s abs			
		(%)	CPS	CPS	(ppm)			Data for Wetherill plot																		
5.sSMPABC131	seq0137.dat	0.00	145803	9092	361	0.93	0	0.062	1.106	0.916	1.647	0.107	1.220	0.741	0.032	1.853	686	24	653	8	660	8	644	12	99
5.sSMPABC041	seq0144.dat	0.00	397716	23732	872	0.75	0	0.060	1.039	0.881	1.555	0.107	1.157	0.744	0.032	1.457	592	23	656	7	642	7	628	9	102
5.sSMPABC180	-	0.16	449247	27693	1101	0.50	1731	0.062	1.202	0.915	1.730	0.108	1.243	0.719	0.034	2.128	662	26	659	8	660	8	673	14	100
5.sSMPABC133	seq0156.dat	0.00	210776	13150	515	0.20	0	0.062	0.994	0.929	1.590	0.108	1.241	0.781	0.041	1.692	688	21	661	8	667	8	819	14	99
5.sSMPABC062	-	0.00	1273124	78119	3109	0.17	0	0.061	1.027	0.914	1.540	0.108	1.148	0.745	0.032	1.636	652	22	661	7	659	7	633	10	100
5.sSMPABC007	-	0.00	411121	25095	1016	0.48	0	0.061	0.999	0.911	1.534	0.108	1.164	0.759	0.032	1.139	641	21	662	7	657	7	629	7	101
5.sSMPABC063	-	0.00	432585	26422	1052	0.29	0	0.061	0.999	0.913	1.575	0.108	1.217	0.773	0.032	1.442	642	21	664	8	659	8	635	9	101
5.sSMPABC049	seq0129.dat	0.00	271187	16507	587	0.39	0	0.061	1.019	0.912	1.544	0.109	1.160	0.751	0.032	1.376	635	22	665	7	658	8	636	9	101
5.sSMPABC014	seq0123.dat	0.05	1139997	70840	2770	0.32	5823	0.062	0.993	0.943	1.518	0.110	1.148	0.756	0.034	1.128	679	21	673	7	674	8	670	7	100
5.sSMPABC083	seq0133.dat	0.00	168040	10539	392	0.14	0	0.063	1.100	0.977	1.711	0.113	1.310	0.766	0.039	2.818	699	23	690	9	692	9	774	22	100
5.sSMPABC168	-	0.00	138391	8726	321	0.15	0	0.063	1.094	0.988	1.661	0.114	1.249	0.752	0.043	2.600	710	23	694	8	698	8	852	22	99
5.sSMPABC037	-	0.15	497029	31048	1026	1.48	1874	0.062	1.113	0.981	1.615	0.114	1.170	0.725	0.033	1.136	690	24	695	8	694	8	665	7	100
5.sSMPABC065	-	0.15	1424096	88659	3284	0.01	1830	0.062	1.107	0.982	1.621	0.114	1.184	0.730	0.343	2.023	683	24	698	8	694	8	5961	104	101
5.sSMPABC123	seq0145.dat	1.00	224129	13799	513	0.35	0	0.062	3.411	0.977	4.006	0.115	2.101	0.524	0.035	1.718	659	73	703	14	692	20	694	12	101
5.sSMPABC102	seq0164.dat	0.00	97775	6334	214	1.35	0	0.065	1.096	1.077	1.734	0.121	1.344	0.775	0.037	1.568	767	23	734	9	742	9	734	11	99
5.sSMPABC127	seq0147.dat	0.00	109939	7072	240	0.42	0	0.064	1.073	1.073	1.690	0.121	1.306	0.773	0.045	1.848	752	23	736	9	740	9	898	16	99
5.sSMPABC147	seq0154.dat	0.00	146593	9430	318	0.44	0	0.064	1.010	1.077	1.609	0.121	1.252	0.778	0.036	1.651	752	21	739	9	742	9	721	12	100
5.sSMPABC072	-	0.00	154129	10151	320	0.99	0	0.066	1.017	1.153	1.583	0.127	1.213	0.766	0.036	1.273	802	21	771	9	779	9	717	9	99
5.sSMPABC130	seq0148.dat	0.00	310814	20337	643	0.19	0	0.065	1.039	1.149	1.571	0.127	1.177	0.750	0.039	1.904	788	22	773	9	777	9	771	14	99
5.sSMPABC109	seq0158.dat	0.10	447496	29348	925	0.37	2669	0.066	1.040	1.153	1.674	0.128	1.312	0.783	0.041	1.659	793	22	774	10	779	9	812	13	99

LA(SF)-ICP-MS U-Pb zircon results data from Sample CA-09 (Nova Venécia complex)

Identifier	Lu-Hf identifier	f206[a]	^{207}Pb	^{206}Pb	U	Th[b]/U	$^{206}Pb/^{204}Pb$	Ratios[c]									Ages (Ma)[c]									% conc[e]
								$^{207}Pb/^{206}Pb$	2s (%)	$^{207}Pb/^{235}U$	2s (%)	$^{206}Pb/^{238}U$	2s (%)	Rho[d]	$^{208}Pb/^{232}Th$	2s (%)	$^{207}Pb/^{206}Pb$	2s abs	$^{206}Pb/^{238}U$	2s abs	$^{207}Pb/^{235}U$	2s abs	$^{208}Pb/^{232}Th$	2s abs			
		(%)	CPS	CPS	(ppm)			Data for Wetherill plot																		
5.sSMPABC176	seq0138.dat	0.00	747035	48961	1531	0.67	0	0.066	1.007	1.163	1.576	0.129	1.212	0.769	0.042	1.534	792	21	780	9	783	9	826	13	100
5.sSMPABC022	seq0122.dat	0.18	595354	39971	1029	0.34	1539	0.067	1.121	1.259	1.678	0.136	1.250	0.744	0.040	1.341	842	23	822	10	827	10	798	11	99
5.sSMPABC067	seq0126.dat	0.11	453320	30266	876	2.75	2521	0.067	1.042	1.256	1.621	0.136	1.242	0.766	0.026	1.225	830	22	825	10	826	9	521	6	100
5.sSMPABC056	seq0127.dat	0.00	257690	17250	444	1.93	0	0.067	1.076	1.260	1.591	0.137	1.172	0.737	0.028	1.492	836	22	825	9	828	9	561	8	100
5.sSMPABC128	seq0146.dat	0.00	456419	30502	881	0.16	0	0.067	1.077	1.259	1.725	0.137	1.347	0.781	0.045	2.444	832	22	825	10	827	10	890	21	100
5.sSMPABC011	-	0.15	256236	17022	500	0.31	1879	0.066	1.103	1.255	1.620	0.137	1.188	0.733	0.040	1.396	820	23	828	9	826	9	795	11	100
5.sSMPABC119	-	0.03	279813	18591	537	0.35	9382	0.066	1.027	1.260	1.575	0.138	1.194	0.758	0.044	1.535	820	21	831	9	828	9	876	13	100
5.sSMPABC183	seq0153.dat	0.13	177788	11790	340	1.47	2172	0.066	1.082	1.262	1.682	0.138	1.288	0.766	0.038	1.517	816	23	834	10	829	10	759	11	101
5.sSMPABC179	seq0136.dat	1.00	287314	19863	509	0.70	0	0.069	3.060	1.418	3.569	0.149	1.836	0.514	0.047	1.498	903	63	894	15	897	21	923	14	100
5.sSMPABC110	seq0157.dat	0.00	138608	9425	249	0.58	0	0.068	1.074	1.374	1.673	0.147	1.283	0.767	0.044	1.786	869	22	882	11	878	10	864	15	100
5.sSMPABC073	seq0130.dat	0.16	426780	28830	765	0.50	1754	0.068	1.112	1.370	1.638	0.147	1.203	0.734	0.044	1.318	855	23	885	10	876	10	871	11	101
5.sSMPABC167	seq0143.dat	0.00	308329	20667	548	0.26	0	0.067	1.029	1.371	1.591	0.148	1.214	0.763	0.045	1.746	839	21	891	10	876	9	883	15	102
5.sSMPABC040	-	0.00	237030	16850	351	0.48	0	0.071	1.069	1.556	1.586	0.159	1.171	0.739	0.047	1.779	960	22	950	10	953	10	933	16	100
5.sSMPABC157	seq0134.dat	0.00	161899	11480	269	0.52	0	0.071	1.058	1.554	1.615	0.159	1.221	0.756	0.048	1.761	955	22	951	11	952	10	942	16	100
5.sSMPABC124	-	0.00	142454	10081	236	2.66	0	0.071	1.032	1.552	1.617	0.159	1.245	0.770	0.046	1.346	951	21	951	11	951	10	910	12	100
5.sSMPABC141	seq0150.dat	0.08	435772	30424	711	0.51	3656	0.070	1.181	1.556	1.722	0.162	1.254	0.728	0.045	2.599	923	24	966	11	953	11	882	22	101
5.sSMPABC107	seq0159.dat	0.00	342876	24677	547	0.16	0	0.072	0.987	1.640	1.618	0.165	1.283	0.793	0.050	2.000	985	20	986	12	986	10	986	19	100
5.sSMPABC160	-	0.00	209649	15101	334	0.74	0	0.072	1.027	1.643	1.605	0.165	1.233	0.768	0.048	1.575	987	21	987	11	987	10	952	15	100
5.sSMPABC025	-	0.00	273370	19983	381	0.35	0	0.073	0.999	1.702	1.614	0.169	1.268	0.786	0.049	1.676	1017	20	1006	12	1009	10	966	16	100
5.sSMPABC090	-	1.00	792343	57592	1232	1.08	0	0.073	2.924	1.700	3.367	0.170	1.668	0.495	0.050	1.211	1005	59	1010	16	1008	22	977	12	100

LA(SF)-ICP-MS U-Pb zircon results data from Sample CA-09 (Nova Venécia complex)

Identifier	Lu-Hf identifier	f206[a]	^{207}Pb	^{206}Pb	U	Th[b]/U	$^{206}Pb/^{204}Pb$	Ratios[c]									Ages (Ma)[c]									% conc[e]
								$^{207}Pb/^{206}Pb$	2s (%)	$^{207}Pb/^{235}U$	2s (%)	$^{206}Pb/^{238}U$	2s (%)	Rho[d]	$^{208}Pb/^{232}Th$	2s (%)	$^{207}Pb/^{206}Pb$	2s abs	$^{206}Pb/^{238}U$	2s abs	$^{207}Pb/^{235}U$	2s abs	$^{208}Pb/^{232}Th$	2s abs			
		(%)	CPS	CPS	(ppm)			Data for Wetherill plot																		
5.sSMPABC113	-	0.08	296278	22120	440	0.42	3484	0.075	1.015	1.827	1.604	0.178	1.243	0.775	0.052	1.498	1059	20	1053	12	1055	11	1026	15	100
5.sSMPABC121	-	0.00	238663	17788	353	0.45	0	0.075	1.006	1.831	1.584	0.178	1.224	0.772	0.050	1.479	1056	20	1057	12	1057	10	987	14	100
5.sSMPABC088	-	0.04	514111	56011	427	1.07	7650	0.109	1.003	4.765	1.539	0.317	1.167	0.758	0.089	1.264	1782	18	1776	18	1779	13	1716	21	100
5.sSMPABC086	-	0.00	172482	19306	144	1.42	0	0.112	1.063	4.862	1.690	0.315	1.314	0.777	0.092	1.601	1831	19	1765	20	1796	14	1787	27	98
5.sSMPABC120	-	1.00	156563	17784	124	1.42	0	0.114	2.040	5.209	2.534	0.333	1.503	0.593	0.082	1.702	1858	37	1851	24	1854	22	1598	26	100
5.sSMPABC142	-	0.00	385678	43867	307	1.48	0	0.114	1.020	5.199	1.566	0.331	1.189	0.759	0.094	1.536	1860	18	1846	19	1852	13	1811	27	100
5.sSMPABC143	-	0.09	257251	28607	225	0.62	3373	0.111	1.037	4.630	1.591	0.302	1.207	0.758	0.090	1.619	1819	19	1701	18	1755	13	1745	27	97
5.sSMPABC165	-	0.00	125979	14315	100	0.90	0	0.114	1.100	5.190	1.701	0.331	1.298	0.763	0.096	2.148	1858	20	1845	21	1851	15	1851	38	100
5.sSMPABC054	-	0.00	94883	9299	87	0.68	0	0.098	1.204	3.469	1.860	0.257	1.418	0.762	0.078	2.559	1586	23	1473	19	1520	15	1521	38	97
5.sSMPABC132	-	0.00	350807	34351	364	0.74	0	0.098	1.021	3.436	1.578	0.254	1.202	0.762	0.082	1.584	1585	19	1462	16	1513	12	1594	24	97
5.sSMPABC088	-	0.04	514111	56011	427	1.07	7650	0.109	1.003	4.765	1.539	0.317	1.167	0.758	0.089	1.264	1782	18	1776	18	1779	13	1716	21	100
5.sSMPABC162	-	0.00	112807	11685	108	0.93	0	0.104	1.043	3.933	1.655	0.275	1.285	0.777	0.080	1.681	1689	19	1568	18	1621	13	1550	25	97
5.sSMPABC035	-	0.05	196783	13528	367	0.45	5451	0.069	1.029	1.194	1.564	0.126	1.177	0.753	0.044	1.314	891	21	765	8	798	9	873	11	96
5.sSMPABC008	-	0.00	126158	7798	374	0.18	0	0.062	1.133	0.770	1.780	0.090	1.373	0.771	0.035	2.859	668	24	557	7	580	8	695	20	96
5.sSMPABC020	-	0.00	139403	8459	405	0.27	0	0.061	1.088	0.746	1.644	0.089	1.233	0.750	0.028	2.086	628	23	551	7	566	7	555	11	97
5.sSMPABC023	-	0.14	662422	46515	1508	0.35	1932	0.070	1.115	1.000	1.607	0.103	1.157	0.720	0.041	1.513	935	23	633	7	704	8	812	12	90
5.sSMPABC028	-	0.39	566696	39741	1299	0.09	705	0.070	1.481	0.991	2.057	0.103	1.427	0.694	0.074	1.430	932	30	629	9	699	10	1446	20	90
5.sSMPABC029	-	0.05	1255262	143174	840	0.17	5656	0.114	1.013	5.521	1.504	0.351	1.111	0.739	0.094	1.440	1865	18	1940	19	1904	13	1825	25	102
5.sSMPABC043	-	0.00	142606	8481	382	0.18	0	0.059	1.127	0.719	1.653	0.088	1.209	0.732	0.031	2.746	584	24	542	6	550	7	609	16	99
5.sSMPABC057	-	0.00	204265	22424	178	0.15	0	0.110	1.020	4.078	1.681	0.269	1.336	0.795	0.088	2.795	1796	19	1538	18	1650	14	1705	46	93

LA(SF)-ICP-MS U-Pb zircon results data from Sample CA-09 (Nova Venécia complex)

Identifier	Lu-Hf identifier	f206[a]	^{207}Pb	^{206}Pb	U	Th[b]/U	$^{206}Pb/^{204}Pb$	Ratios[c]								Ages (Ma)[c]								% conc[e]
								$^{207}Pb/^{206}Pb$	2s (%)	$^{207}Pb/^{235}U$	2s (%)	$^{206}Pb/^{238}U$	2s (%)	Rho[d]	$^{208}Pb/^{232}Th$	2s (%)	$^{207}Pb/^{206}Pb$	2s abs	$^{206}Pb/^{238}U$	2s abs	$^{207}Pb/^{235}U$	2s abs	$^{208}Pb/^{232}Th$	2s abs	
		(%)	CPS	CPS	(ppm)			Data for Wetherill plot																
5.sSMPABC066	-	0.00	400898	24703	1182	0.08	0	0.062	1.055	0.760	1.553	0.089	1.140	0.734	0.044	2.318	661	23	552	6	574	7	871	20	96
5.sSMPABC070	-	0.00	125595	14477	91	1.22	0	0.115	1.058	5.812	1.795	0.366	1.449	0.808	0.087	1.831	1884	19	2009	25	1948	16	1694	30	103
5.sSMPABC086	-	0.00	172482	19306	144	1.42	0	0.112	1.063	4.862	1.690	0.315	1.314	0.777	0.092	1.601	1831	19	1765	20	1796	14	1787	27	98
5.sSMPABC112	-	0.00	134663	8276	395	0.59	0	0.061	1.058	0.762	1.601	0.090	1.201	0.751	0.028	1.627	655	23	555	6	575	7	564	9	97
5.sSMPABC114	-	0.00	343021	38003	327	0.19	0	0.111	0.975	4.230	1.602	0.277	1.271	0.794	0.076	1.918	1812	18	1576	18	1680	13	1483	28	94
5.sSMPABC120	-	1.00	156563	17784	124	1.42	0	0.114	2.040	5.209	2.534	0.333	1.503	0.593	0.082	1.702	1858	37	1851	24	1854	22	1598	26	100
5.sSMPABC125	-	0.00	206900	22188	222	0.40	0	0.107	1.007	3.641	1.581	0.246	1.218	0.771	0.080	1.541	1753	18	1419	16	1558	13	1564	23	91
5.sSMPABC142	-	0.00	385678	43867	307	1.48	0	0.114	1.020	5.199	1.566	0.331	1.189	0.759	0.094	1.536	1860	18	1846	19	1852	13	1811	27	100
5.sSMPABC143	-	0.09	257251	28607	225	0.62	3373	0.111	1.037	4.630	1.591	0.302	1.207	0.758	0.090	1.619	1819	19	1701	18	1755	13	1745	27	97
5.sSMPABC165	-	0.00	125979	14315	100	0.90	0	0.114	1.100	5.190	1.701	0.331	1.298	0.763	0.096	2.148	1858	20	1845	21	1851	15	1851	38	100

LA(SF)-ICP-MS U-Pb zircon results data from Sample CA-10 (Nova Venécia complex)

Identifier	Lu-Hf identifier	f206[a]	^{207}Pb	^{206}Pb	U	Th[b]/U	$^{206}Pb/^{204}Pb$	Ratios[c]								Ages (Ma)[c]								% conc[e]
								$^{207}Pb/^{206}Pb$	2s (%)	$^{207}Pb/^{235}U$	2s (%)	$^{206}Pb/^{238}U$	2s (%)	Rho[d]	$^{208}Pb/^{232}Th$	2s (%)	$^{207}Pb/^{206}Pb$	2s abs	$^{206}Pb/^{238}U$	2s abs	$^{207}Pb/^{235}U$	2s abs	$^{208}Pb/^{232}Th$	2s abs	
		(%)	CPS	CPS	(ppm)			Data for Wetherill plot																
5.sSMPABC094	-	0.00	267260	15247	846	0.01	0	0.057	1.034	0.632	1.618	0.080	1.245	0.769	0.025	9.880	493	23	498	6	497	6	501	49	100
5.sSMPABC115	seq0087.dat	0.00	44697	2544	141	1.25	0	0.057	1.581	0.632	2.260	0.080	1.615	0.715	0.022	2.792	488	35	499	8	497	9	444	12	100
5.sSMPABC103	-	0.00	326617	18581	1027	0.02	0	0.057	1.037	0.634	1.711	0.081	1.361	0.795	0.074	4.409	487	23	501	7	499	7	1442	61	100
5.sSMPABC096	seq0110.dat	0.00	276907	15925	851	0.01	0	0.058	1.026	0.656	1.603	0.083	1.232	0.769	0.034	6.259	511	23	513	6	512	6	680	42	100

LA(SF)-ICP-MS U-Pb zircon results data from Sample CA-10 (Nova Venécia complex)

Identifier	Lu-Hf identifier	f206[a]	^{207}Pb	^{206}Pb	U	Th[b]/U	$^{206}Pb/^{204}Pb$	Ratios[c]									Ages (Ma)[c]									% conc[e]
								$^{207}Pb/^{206}Pb$	2s (%)	$^{207}Pb/^{235}U$	2s (%)	$^{206}Pb/^{238}U$	2s (%)	Rho[d]	$^{208}Pb/^{232}Th$	2s (%)	$^{207}Pb/^{206}Pb$	2s	$^{206}Pb/^{238}U$	2s	$^{207}Pb/^{235}U$	2s	$^{208}Pb/^{232}Th$	2s		
								Data for Wetherill plot										abs		abs		abs		abs		
		(%)	CPS	CPS	(ppm)																					
5.sSMPABC146	-	0.00	405290	23373	1241	0.50	0	0.058	1.040	0.660	1.742	0.083	1.397	0.802	0.018	2.185	517	23	514	7	515	7	367	8	100
5.sSMPABC114	-	0.00	167867	9812	509	0.06	0	0.058	1.027	0.676	1.610	0.084	1.240	0.770	0.035	3.273	547	22	519	6	524	7	692	22	99
5.sSMPABC071	-	0.00	429837	25055	1301	0.03	0	0.058	1.012	0.675	1.618	0.084	1.262	0.780	0.046	2.630	541	22	520	6	524	7	916	23	99
5.sSMPABC034	-	0.00	166975	9686	502	0.46	0	0.058	1.017	0.677	1.613	0.085	1.253	0.776	0.023	1.447	530	22	524	6	525	7	469	7	100
5.sSMPABC143	-	0.01	198487	11671	587	0.20	20559	0.059	1.072	0.697	1.651	0.086	1.256	0.760	0.028	2.282	560	23	532	6	537	7	559	13	99
5.sSMPABC076	-	0.00	356587	20807	1049	0.00	0	0.058	1.011	0.695	1.626	0.086	1.273	0.783	0.083	9.954	543	22	534	7	536	7	1611	154	100
5.sSMPABC081	-	0.06	681118	39963	2003	0.24	4288	0.059	1.045	0.700	1.618	0.086	1.234	0.763	0.025	1.704	555	23	535	6	539	7	492	8	99
5.sSMPABC038	seq0072.dat	0.00	160205	9311	468	0.64	0	0.058	1.015	0.697	1.604	0.087	1.242	0.774	0.026	1.387	534	22	538	6	537	7	518	7	100
5.sSMPABC120	-	0.00	401490	23495	1173	0.03	0	0.059	1.042	0.702	1.766	0.087	1.425	0.807	0.065	3.333	549	23	538	7	540	7	1281	41	100
5.sSMPABC111	seq0111.dat	0.00	146634	8480	427	0.36	0	0.058	1.107	0.697	1.659	0.087	1.236	0.745	0.029	2.087	523	24	540	6	537	7	573	12	101
5.sSMPABC090	-	0.04	287427	16817	818	0.22	7014	0.059	1.051	0.721	1.638	0.089	1.256	0.767	0.028	1.871	549	23	552	7	551	7	554	10	100
5.sSMPABC092	-	0.00	205605	12114	571	1.26	0	0.059	1.001	0.744	1.598	0.092	1.245	0.779	0.027	1.350	564	22	565	7	565	7	532	7	100
5.sSMPABC083	-	0.00	407590	23950	1131	0.38	0	0.059	1.004	0.742	1.582	0.092	1.222	0.773	0.027	1.482	558	22	565	7	564	7	538	8	100
5.sSMPABC106	seq0082.dat	0.00	1118572	66387	3097	0.21	0	0.059	1.045	0.751	1.573	0.092	1.176	0.748	0.030	1.801	580	23	566	6	569	7	597	11	100
5.sSMPABC084	-	0.00	185198	10841	513	0.18	0	0.059	1.025	0.741	1.661	0.092	1.307	0.787	0.029	2.239	550	22	566	7	563	7	587	13	101
5.sSMPABC129	-	0.00	274175	16250	756	0.57	0	0.059	1.012	0.754	1.598	0.092	1.236	0.774	0.026	1.679	577	22	569	7	570	7	523	9	100
5.sSMPABC089	-	0.00	642741	37530	1772	0.29	0	0.058	1.028	0.743	1.591	0.092	1.214	0.763	0.028	1.563	544	22	569	7	564	7	561	8	101
5.sSMPABC148	-	0.00	160717	9489	442	0.58	0	0.059	1.050	0.752	1.637	0.092	1.256	0.767	0.028	1.846	569	23	570	7	569	7	562	10	100
5.sSMPABC044	-	0.00	550854	33299	1499	0.04	0	0.060	1.026	0.779	1.561	0.093	1.177	0.754	0.035	2.635	620	22	576	6	585	7	694	18	98
5.sSMPABC057	-	0.06	687530	40765	1863	0.38	4250	0.059	1.035	0.767	1.602	0.094	1.223	0.763	0.029	1.326	578	22	578	7	578	7	571	8	100

LA(SF)-ICP-MS U-Pb zircon results data from Sample CA-10 (Nova Venécia complex)

Identifier	Lu-Hf identifier	f206[a]	^{207}Pb	^{206}Pb	U	Th[b]/U	$^{206}Pb/^{204}Pb$	Ratios[c]									Ages (Ma)[c]								% conc[e]
								$^{207}Pb/^{206}Pb$	2s (%)	$^{207}Pb/^{235}U$	2s (%)	$^{206}Pb/^{238}U$	2s (%)	Rho[d]	$^{208}Pb/^{232}Th$	2s (%)	$^{207}Pb/^{206}Pb$	2s abs	$^{206}Pb/^{238}U$	2s abs	$^{207}Pb/^{235}U$	2s abs	$^{208}Pb/^{232}Th$	2s abs	
		(%)	CPS	CPS	(ppm)			Data for Wetherill plot																	
5.sSMPABC121	-	0.17	557222	33271	1506	0.10	1597	0.060	1.142	0.775	1.781	0.094	1.367	0.768	0.040	2.071	593	25	580	8	582	8	785	16	100
5.sSMPABC087	-	0.00	108333	6440	293	0.86	0	0.059	1.110	0.771	1.675	0.094	1.254	0.749	0.029	1.720	584	24	580	7	581	7	579	10	100
5.sSMPABC035	seq0073.dat	0.00	102868	6121	276	1.57	0	0.060	1.076	0.777	1.662	0.095	1.267	0.762	0.030	1.355	585	23	584	7	584	7	588	8	100
5.sSMPABC063	seq0078.dat	0.00	189080	11258	503	1.22	0	0.060	1.041	0.785	1.614	0.096	1.234	0.764	0.027	1.382	587	23	589	7	589	7	548	7	100
5.sSMPABC093	-	0.09	339576	20269	899	0.72	3128	0.060	1.047	0.790	1.625	0.096	1.243	0.765	0.029	1.380	592	23	591	7	591	7	578	8	100
5.sSMPABC127	-	0.00	270462	16136	716	0.07	0	0.060	1.039	0.791	1.722	0.096	1.373	0.797	0.052	2.943	591	23	592	8	592	8	1018	29	100
5.sSMPABC067	seq0080.dat	0.00	172356	10236	456	1.14	0	0.059	1.061	0.787	1.638	0.096	1.248	0.762	0.028	1.498	581	23	592	7	590	7	559	8	100
5.sSMPABC032	-	0.41	78510	4662	207	1.05	667	0.059	1.760	0.788	2.376	0.096	1.595	0.672	0.026	1.610	581	38	593	9	590	11	521	8	100
5.sSMPABC133	-	0.00	336014	19963	886	1.10	0	0.059	1.044	0.790	1.624	0.096	1.244	0.766	0.029	1.702	582	23	594	7	591	7	585	10	100
5.sSMPABC055	-	0.24	1097114	66186	2870	0.44	1158	0.060	1.214	0.809	1.885	0.097	1.442	0.765	0.022	1.486	615	26	598	8	602	9	431	6	99
5.sSMPABC102	-	0.00	76673	4655	200	0.48	0	0.061	1.120	0.817	1.740	0.098	1.331	0.765	0.030	2.164	629	24	601	8	607	8	589	13	99
5.sSMPABC107	seq0079.dat	0.04	408685	24413	1061	0.06	6886	0.060	1.046	0.807	1.598	0.098	1.207	0.756	0.033	2.552	594	23	603	7	601	7	655	17	100
5.sSMPABC149	-	0.30	224227	13496	582	1.05	907	0.060	1.437	0.813	2.024	0.098	1.426	0.704	0.027	1.782	610	31	603	8	604	9	537	9	100
5.sSMPABC075	seq0083.dat	0.00	132440	7785	343	0.11	0	0.059	1.293	0.795	1.866	0.098	1.345	0.721	0.032	5.188	559	28	603	8	594	8	644	33	102
5.sSMPABC068	seq0081.dat	0.00	157095	9380	404	1.16	0	0.060	1.022	0.814	1.617	0.099	1.254	0.775	0.027	1.387	593	22	608	7	605	7	546	7	101
5.sSMPABC007	seq0104.dat	0.00	236270	14025	607	0.26	0	0.059	1.129	0.810	1.671	0.099	1.233	0.737	0.035	2.314	580	25	608	7	603	8	704	16	101
5.sSMPABC037	-	0.16	217108	13026	558	1.16	1760	0.060	1.126	0.819	1.699	0.099	1.272	0.749	0.029	1.257	603	24	609	7	608	8	571	7	100
5.sSMPABC126	seq0088.dat	0.00	143940	8704	369	1.32	0	0.060	1.075	0.827	1.649	0.099	1.250	0.758	0.032	1.752	620	23	610	7	612	8	636	11	100
5.sSMPABC150	-	0.00	459226	27622	1175	0.47	0	0.060	1.064	0.824	1.655	0.099	1.268	0.766	0.031	1.990	609	23	611	7	610	8	620	12	100
5.sSMPABC065	-	0.00	174175	10395	445	1.08	0	0.060	1.022	0.819	1.611	0.100	1.246	0.773	0.028	1.361	592	22	612	7	607	7	557	7	101

LA(SF)-ICP-MS U-Pb zircon results data from Sample CA-10 (Nova Venécia complex)

Identifier	Lu-Hf identifier	f206[a]	^{207}Pb	^{206}Pb	U	Th[b]/U	$^{206}Pb/^{204}Pb$	Ratios[c]									Ages (Ma)[c]									% conc[e]
								$^{207}Pb/^{206}Pb$	2s (%)	$^{207}Pb/^{235}U$	2s (%)	$^{206}Pb/^{238}U$	2s (%)	Rho[d]	$^{208}Pb/^{232}Th$	2s (%)	$^{207}Pb/^{206}Pb$	2s abs	$^{206}Pb/^{238}U$	2s abs	$^{207}Pb/^{235}U$	2s abs	$^{208}Pb/^{232}Th$	2s abs			
		(%)	CPS	CPS	(ppm)			Data for Wetherill plot																		
5.sSMPABC144	seq0090.dat	0.00	232600	13977	590	0.52	0	0.060	1.015	0.830	1.616	0.100	1.258	0.778	0.029	1.778	607	22	615	7	614	7	583	10	100
5.sSMPABC011	-	0.27	186141	11322	462	0.71	1015	0.061	1.339	0.859	1.893	0.102	1.338	0.707	0.027	1.260	633	29	629	8	630	9	538	7	100
5.sSMPABC048	seq0070.dat	0.00	132501	8098	329	0.88	0	0.061	1.014	0.864	1.608	0.103	1.248	0.776	0.028	1.351	643	22	629	7	632	8	561	8	100
5.sSMPABC039	seq0071.dat	0.00	87315	5353	216	0.41	0	0.061	1.142	0.868	1.839	0.103	1.442	0.784	0.030	2.412	650	25	630	9	634	9	595	14	99
5.sSMPABC056	-	0.00	299191	18212	739	1.40	0	0.061	1.019	0.864	1.593	0.103	1.224	0.769	0.029	1.296	635	22	631	7	632	8	584	7	100
5.sSMPABC082	seq0084.dat	0.03	1249006	76044	3080	0.32	10410	0.061	1.071	0.866	1.597	0.103	1.184	0.742	0.029	1.997	635	23	633	7	633	8	579	11	100
5.sSMPABC123	-	0.00	335223	20251	826	0.19	0	0.060	1.043	0.859	1.621	0.103	1.241	0.766	0.031	2.030	618	23	633	7	630	8	608	12	101
5.sSMPABC122	-	0.00	215261	13159	529	0.30	0	0.061	1.047	0.872	1.621	0.103	1.238	0.764	0.032	1.880	644	23	634	7	636	8	635	12	100
5.sSMPABC008	seq0099.dat	0.00	208460	12722	511	0.31	0	0.061	1.065	0.874	1.734	0.104	1.368	0.789	0.035	2.015	640	23	637	8	637	8	690	14	100
5.sSMPABC073	seq0086.dat	0.00	195839	11895	477	0.52	0	0.061	1.004	0.874	1.600	0.104	1.246	0.778	0.030	1.459	630	22	640	8	638	8	601	9	100
5.sSMPABC112	-	0.03	303938	18604	735	0.58	8114	0.061	1.003	0.887	1.623	0.105	1.277	0.786	0.029	1.651	647	22	644	8	645	8	579	9	100
5.sSMPABC014	-	0.20	54669	3337	132	0.94	1343	0.061	1.413	0.886	2.031	0.105	1.459	0.718	0.029	2.099	641	30	645	9	644	10	570	12	100
5.sSMPABC132	seq0101.dat	0.00	255605	15686	614	0.49	0	0.061	1.059	0.896	1.636	0.106	1.247	0.762	0.033	1.898	652	23	649	8	650	8	650	12	100
5.sSMPABC033	seq0107.dat	0.00	168053	10315	403	0.45	0	0.061	1.026	0.898	1.613	0.106	1.244	0.771	0.033	1.454	653	22	650	8	651	8	657	10	100
5.sSMPABC141	-	0.10	424499	26245	1012	1.06	2678	0.062	1.102	0.909	1.669	0.107	1.253	0.751	0.033	1.819	668	24	653	8	657	8	656	12	99
5.sSMPABC142	-	0.00	469716	29136	1117	0.68	0	0.062	1.080	0.914	1.626	0.107	1.216	0.748	0.035	2.111	675	23	655	8	659	8	697	14	99
5.sSMPABC064	-	0.00	70037	4319	166	1.36	0	0.062	1.200	0.910	1.917	0.107	1.496	0.780	0.026	1.890	663	26	655	9	657	9	528	10	100
5.sSMPABC031	-	0.00	205727	12726	487	0.33	0	0.062	1.035	0.916	1.649	0.107	1.284	0.779	0.038	1.637	669	22	658	8	660	8	752	12	100
5.sSMPABC130	seq0102.dat	0.11	104502	6478	240	0.54	2617	0.062	1.148	0.945	1.773	0.111	1.351	0.762	0.032	2.157	674	25	676	9	676	9	627	13	100
5.sSMPABC113	-	0.00	269594	16825	619	0.24	0	0.062	1.009	0.953	1.603	0.111	1.246	0.777	0.042	1.756	688	22	677	8	680	8	834	14	100

LA(SF)-ICP-MS U-Pb zircon results data from Sample CA-10 (Nova Venécia complex)

Identifier	Lu-Hf identifier	f206[a]	^{207}Pb	^{206}Pb	U	Th[b]/U	$^{206}Pb/^{204}Pb$	Ratios[c]									Ages (Ma)[c]									% conc[e]
								$^{207}Pb/^{206}Pb$	2s (%)	$^{207}Pb/^{235}U$	2s (%)	$^{206}Pb/^{238}U$	2s (%)	Rho[d]	$^{208}Pb/^{232}Th$	2s (%)	$^{207}Pb/^{206}Pb$	2s abs	$^{206}Pb/^{238}U$	2s abs	$^{207}Pb/^{235}U$	2s abs	$^{208}Pb/^{232}Th$	2s abs			
		(%)	CPS	CPS	(ppm)			Data for Wetherill plot																		
5.sSMPABC046	seq0068.dat	0.07	809282	50203	1854	0.99	3669	0.062	1.013	0.949	1.609	0.111	1.250	0.777	0.029	1.225	675	22	679	8	678	8	585	7	100
5.sSMPABC026	seq0091.dat	0.00	104659	6514	239	0.70	0	0.062	1.125	0.955	1.674	0.111	1.239	0.741	0.036	1.704	682	24	681	8	681	8	722	12	100
5.sSMPABC051	seq0075.dat	0.00	207727	12877	471	0.32	0	0.062	1.000	0.958	1.586	0.112	1.231	0.776	0.032	1.541	674	21	685	8	682	8	645	10	100
5.sSMPABC074	-	0.00	520338	32048	1178	0.29	0	0.062	1.023	0.953	1.572	0.112	1.194	0.759	0.034	1.611	660	22	686	8	680	8	666	11	101
5.sSMPABC025	seq0089.dat	0.00	390585	23912	883	0.02	0	0.061	1.045	0.949	1.572	0.112	1.174	0.747	0.072	3.291	647	22	687	8	678	8	1400	45	101
5.sSMPABC006	seq0103.dat	0.02	268382	16768	595	0.40	15618	0.062	1.026	0.987	1.663	0.115	1.309	0.787	0.041	1.526	691	22	699	9	697	8	805	12	100
5.sSMPABC016	seq0094.dat	0.12	147384	9145	326	0.54	2328	0.062	1.176	0.983	1.705	0.115	1.235	0.724	0.039	1.833	676	25	701	8	695	9	779	14	101
5.sSMPABC015	seq0093.dat	0.06	138507	8858	291	1.10	4759	0.064	1.063	1.067	1.713	0.121	1.342	0.784	0.030	1.478	740	22	736	9	737	9	593	9	100
5.sSMPABC012	seq0105.dat	0.00	70112	4543	147	0.63	0	0.065	1.173	1.083	1.741	0.121	1.287	0.739	0.049	1.833	768	25	738	9	745	9	969	17	99
5.sSMPABC125	-	0.00	424326	27492	888	0.14	0	0.065	1.034	1.085	1.610	0.122	1.234	0.767	0.040	1.993	768	22	739	9	746	9	796	16	99
5.sSMPABC029	seq0092.dat	0.00	174502	11257	364	3.47	0	0.065	1.054	1.083	1.685	0.122	1.314	0.780	0.031	1.303	758	22	741	9	745	9	611	8	99
5.sSMPABC091	seq0109.dat	0.07	208861	13426	434	0.22	3807	0.064	1.097	1.085	1.748	0.122	1.361	0.779	0.040	2.402	751	23	744	10	746	9	792	19	100
5.sSMPABC018	seq0095.dat	0.00	103434	6644	215	0.26	0	0.064	1.074	1.085	1.641	0.122	1.241	0.756	0.046	1.981	749	23	745	9	746	9	918	18	100
5.sSMPABC047	seq0069.dat	0.10	111042	7377	205	0.60	2909	0.066	1.136	1.261	1.705	0.138	1.271	0.746	0.041	1.804	820	24	832	10	829	10	812	14	100
5.sSMPABC147	-	0.00	240830	16323	437	0.43	0	0.068	1.048	1.309	1.680	0.140	1.314	0.782	0.043	2.069	862	22	845	10	850	10	842	17	99
5.sSMPABC128	-	0.00	439001	29580	794	0.16	0	0.067	1.024	1.306	1.617	0.141	1.252	0.774	0.045	1.927	850	21	848	10	848	9	883	17	100
5.sSMPABC085	seq0100.dat	0.00	97422	6661	172	0.40	0	0.068	1.068	1.358	1.676	0.144	1.291	0.771	0.045	2.003	880	22	867	10	871	10	888	17	100
5.sSMPABC139	seq0096.dat	0.00	304935	20870	538	0.20	0	0.068	1.023	1.360	1.615	0.144	1.249	0.774	0.042	1.997	882	21	868	10	872	9	833	16	100
5.sSMPABC049	seq0074.dat	0.00	82576	5616	145	0.69	0	0.068	1.103	1.360	1.777	0.145	1.393	0.784	0.042	1.889	869	23	873	11	872	10	838	15	100
5.sSMPABC019	-	0.23	97786	6624	171	0.55	1210	0.068	1.312	1.355	1.843	0.145	1.294	0.702	0.046	1.907	861	27	873	11	870	11	912	17	100

LA(SF)-ICP-MS U-Pb zircon results data from Sample CA-10 (Nova Venécia complex)

Identifier	Lu-Hf identifier	f206[a]	^{207}Pb	^{206}Pb	U	Th[b]/U	$^{206}Pb/^{204}Pb$	Ratios[c]									Ages (Ma)[c]									% conc[e]
								$^{207}Pb/^{206}Pb$	2s (%)	$^{207}Pb/^{235}U$	2s (%)	$^{206}Pb/^{238}U$	2s (%)	Rho[d]	$^{208}Pb/^{232}Th$	2s (%)	$^{207}Pb/^{206}Pb$	2s abs	$^{206}Pb/^{238}U$	2s abs	$^{207}Pb/^{235}U$	2s abs	$^{208}Pb/^{232}Th$	2s abs		
		(%)	CPS	CPS	(ppm)			Data for Wetherill plot																		
5.sSMPABC053	seq0077.dat	0.00	362299	25274	603	0.22	0	0.070	1.046	1.468	1.616	0.153	1.231	0.762	0.046	1.922	921	22	916	11	917	10	905	17	100
5.sSMPABC030	seq0106.dat	0.00	239048	16657	397	0.19	0	0.070	1.005	1.471	1.596	0.153	1.241	0.777	0.053	1.632	919	21	918	11	919	10	1038	17	100
5.sSMPABC028	-	0.00	194718	13556	322	0.23	0	0.070	1.034	1.475	1.612	0.154	1.236	0.767	0.060	1.640	917	21	922	11	920	10	1173	19	100
5.sSMPABC036	-	0.02	290966	20246	481	0.87	11446	0.070	0.994	1.477	1.585	0.154	1.235	0.779	0.042	1.225	916	20	923	11	921	10	841	10	100
5.sSMPABC134	seq0098.dat	0.00	359657	25345	583	1.10	0	0.070	1.064	1.523	1.701	0.157	1.327	0.780	0.045	1.966	942	22	939	12	940	10	885	17	100
5.sSMPABC110	-	0.00	166993	11756	270	0.79	0	0.070	1.037	1.528	1.630	0.157	1.258	0.772	0.049	1.646	940	21	942	11	942	10	959	15	100
5.sSMPABC009	seq0097.dat	0.00	161700	11356	261	0.12	0	0.070	1.153	1.524	1.707	0.157	1.258	0.737	0.059	3.550	935	24	942	11	940	11	1151	40	100
5.sSMPABC109	-	0.00	576939	41128	923	0.85	65579	0.071	1.052	1.562	1.602	0.159	1.208	0.754	0.049	1.819	966	21	951	11	955	10	976	17	100
5.sSMPABC088	-	0.15	171650	12181	274	1.05	1923	0.071	1.095	1.557	1.668	0.159	1.258	0.754	0.045	1.452	956	22	952	11	953	10	899	13	100
5.sSMPABC105	seq0085.dat	0.00	436424	30999	697	1.71	0	0.071	1.000	1.558	1.586	0.159	1.232	0.776	0.047	1.447	958	20	952	11	954	10	928	13	100
5.sSMPABC131	-	0.00	305313	21766	488	1.14	0	0.071	1.066	1.564	1.638	0.159	1.244	0.759	0.048	1.932	966	22	952	11	956	10	941	18	100
5.sSMPABC066	-	0.00	114654	8374	175	1.13	0	0.073	1.054	1.678	1.689	0.167	1.320	0.781	0.047	1.563	1015	21	994	12	1000	11	935	14	99
5.sSMPABC058	-	0.00	224458	16350	328	0.98	0	0.073	1.043	1.747	1.622	0.174	1.242	0.766	0.051	1.490	1010	21	1034	12	1026	11	1006	15	101
5.sSMPABC020	-	0.00	111270	8074	162	0.52	0	0.073	1.213	1.750	1.805	0.175	1.337	0.741	0.062	2.416	1002	25	1039	13	1027	12	1217	29	101
5.sSMPABC045	-	0.09	554713	62381	423	1.62	3253	0.112	1.071	5.171	1.600	0.334	1.189	0.743	0.092	1.694	1839	19	1855	19	1848	14	1780	29	100
5.sSMPABC013	-	0.00	204042	23619	152	0.64	67680	0.116	1.071	5.457	1.639	0.342	1.240	0.757	0.113	1.836	1892	19	1896	20	1894	14	2170	38	100
5.sSMPABC070	-	0.00	251672	29003	187	0.77	0	0.115	1.050	5.439	1.606	0.342	1.215	0.757	0.097	1.703	1884	19	1898	20	1891	14	1880	31	100
5.sSMPABC017	-	0.12	218993	13266	463	0.44	2260	0.061	1.100	1.005	1.662	0.120	1.246	0.750	0.040	1.338	624	24	733	9	706	8	800	11	104
5.sSMPABC027	-	0.00	136725	8299	289	0.08	0	0.061	1.186	1.006	1.734	0.120	1.264	0.729	0.046	4.464	629	26	732	9	707	9	912	40	104
5.sSMPABC050	-	0.00	163374	19794	110	1.37	0	0.121	0.999	6.288	1.607	0.376	1.259	0.784	0.096	1.313	1973	18	2059	22	2017	14	1852	23	102

LA(SF)-ICP-MS U-Pb zircon results data from Sample CA-10 (Nova Venécia complex)

Identifier	Lu-Hf identifier	f206[a]	^{207}Pb	^{206}Pb	U	Th[b]/U	$^{206}Pb/^{204}Pb$	Ratios[c]								Ages (Ma)[c]								% conc[e]
								$^{207}Pb/^{206}Pb$	2s (%)	$^{207}Pb/^{235}U$	2s (%)	$^{206}Pb/^{238}U$	2s (%)	Rho[d]	$^{208}Pb/^{232}Th$	2s (%)	$^{207}Pb/^{206}Pb$	2s abs	$^{206}Pb/^{238}U$	2s abs	$^{207}Pb/^{235}U$	2s abs	$^{208}Pb/^{232}Th$	2s abs	
		(%)	CPS	CPS	(ppm)			Data for Wetherill plot																
5.sSMPABC095	-	0.00	1082579	124464	880	0.10	1077837	0.115	0.983	4.959	1.573	0.313	1.228	0.781	0.092	1.592	1879	18	1755	19	1812	13	1773	27	97
5.sSMPABC108	-	0.21	273558	31494	219	0.88	1426	0.115	1.080	5.039	1.655	0.317	1.255	0.758	0.089	1.575	1882	19	1777	20	1826	14	1721	26	97
5.sSMPABC013	-	0.00	204042	23619	152	0.64	67680	0.116	1.071	5.457	1.639	0.342	1.240	0.757	0.113	1.836	1892	19	1896	20	1894	14	2170	38	100
5.sSMPABC070	-	0.00	251672	29003	187	0.77	0	0.115	1.050	5.439	1.606	0.342	1.215	0.757	0.097	1.703	1884	19	1898	20	1891	14	1880	31	100
5.sSMPABC052	-	0.02	122145	22288	70	2.27	16877	0.182	1.009	11.138	1.636	0.443	1.288	0.787	0.134	1.301	2676	17	2363	26	2535	15	2538	31	93

[a] percentage of the common Pb on the ^{206}Pb

[b] Th/U ratios are calculated relative to BB reference zircon

[c] data corrected for background, within-run Pb/U fractionation (in case of $^{206}Pb/^{238}U$) and common Pb using Stacey and Kramers (1975) model Pb composition

[d] Rho is the error correlation defined as the quotient of the propagated errors of the $^{206}Pb/^{238}U$ and the $^{207}Pb/^{235}U$ ratio

*[e] Concordance calculated as (^{206}Pb-^{238}U age/^{207}Pb-^{206}Pb age)*100*

CPS = count per second

Zircon grains not used for concordia age are in bold letter

PRIMARY REFERENCE STANDARD

LA(SF)-ICP-MS U-Pb zircon results data from BB-09 primary standard of the Sample CA-02 (Aracê - Pedra Azul pluton)

Identifier	f206[a]	^{207}Pb	^{206}Pb	U	Th[b]/U	$^{206}Pb/^{204}Pb$	Ratios[c]									Ages (Ma)[c]								% conc[e]
							$^{207}Pb/^{206}Pb$	2s (%)	$^{207}Pb/^{235}U$	2s (%)	$^{206}Pb/^{238}U$	2s (%)	Rho[d]	$^{208}Pb/^{232}Th$	2s (%)	$^{207}Pb/^{206}Pb$	2s abs	$^{206}Pb/^{238}U$	2s abs	$^{207}Pb/^{235}U$	2s abs	$^{208}Pb/^{232}Th$	2s abs	
	(%)	CPS	CPS	(ppm)			Data for Wetherill plot																	
5.sSMPABC017	0.00	178275	10426	434	0.45	0	0.058	0.975	0.742	1.627	0.092	1.303	0.801	0.029	1.579	548	21	568	7	564	7	581	9	101
5.sSMPABC033	0.00	162483	9442	401	0.45	0	0.058	0.981	0.728	1.646	0.091	1.321	0.803	0.028	1.666	534	21	560	7	555	7	551	9	101
5.sSMPABC034	0.00	163882	9533	400	0.44	0	0.058	0.980	0.737	1.651	0.092	1.328	0.805	0.028	1.649	536	21	566	7	560	7	556	9	101
5.sSMPABC049	0.00	160859	9571	398	0.46	0	0.060	0.992	0.743	1.655	0.091	1.326	0.801	0.028	1.687	585	22	559	7	564	7	567	9	99
5.sSMPABC050	0.00	153921	9072	381	0.46	0	0.059	1.001	0.735	1.662	0.090	1.326	0.798	0.028	1.672	565	22	558	7	560	7	549	9	100
5.sSMPABC065	0.00	160640	9383	396	0.46	0	0.058	1.010	0.732	1.680	0.091	1.343	0.799	0.028	1.716	545	22	561	7	558	7	558	10	101
5.sSMPABC080	0.12	165707	9772	407	0.47	2305	0.059	1.094	0.742	1.746	0.091	1.362	0.780	0.028	1.788	566	24	563	7	564	8	558	10	100
5.sSMPABC081	0.00	169057	9959	412	0.46	0	0.059	0.985	0.747	1.669	0.092	1.348	0.808	0.028	1.704	564	21	567	7	566	7	562	9	100

LA(SF)-ICP-MS U-Pb zircon results data from BB-09 primary standard of the Sample CA-04 (Vitória pluton)

Identifier	f206[a]	^{207}Pb	^{206}Pb	U	Th[b]/U	$^{206}Pb/^{204}Pb$	Ratios[c]									Ages (Ma)[c]								% conc[e]
							$^{207}Pb/^{206}Pb$	2s (%)	$^{207}Pb/^{235}U$	2s (%)	$^{206}Pb/^{238}U$	2s (%)	Rho[d]	$^{208}Pb/^{232}Th$	2s (%)	$^{207}Pb/^{206}Pb$	2s abs	$^{206}Pb/^{238}U$	2s abs	$^{207}Pb/^{235}U$	2s abs	$^{208}Pb/^{232}Th$	2s abs	
	(%)	CPS	CPS	(ppm)			Data for Wetherill plot																	
5.sSMPABC001	0.07	348404	20659	443	0.45	169	0.058	0.962	0.755	1.892	0.092	1.610	0.851	0.029	1.724	578	22	570	9	571	8	578	10	100
5.sSMPABC002	0.00	343528	20361	439	0.44	20361	0.058	1.048	0.751	1.876	0.092	1.610	0.859	0.028	1.773	577	21	567	9	569	8	562	10	100
5.sSMPABC021	0.00	319846	18612	413	0.43	18612	0.059	0.965	0.730	1.871	0.091	1.605	0.858	0.028	1.772	537	21	561	9	556	8	563	10	101
5.sSMPABC022	0.12	325286	18909	415	0.44	94	0.059	0.976	0.738	1.937	0.092	1.629	0.841	0.028	1.769	535	23	568	9	561	8	563	10	101

LA(SF)-ICP-MS U-Pb zircon results data from BB-09 primary standard of the Sample CA-04 (Vitória pluton)

Identifier	f206[a]	^{207}Pb	^{206}Pb	U	Th[b]/U	$^{206}Pb/^{204}Pb$	Ratios[c]									Ages (Ma)[c]								% conc[e]
							$^{207}Pb/^{206}Pb$	2s (%)	$^{207}Pb/^{235}U$	2s (%)	$^{206}Pb/^{238}U$	2s (%)	Rho[d]	$^{208}Pb/^{232}Th$	2s (%)	$^{207}Pb/^{206}Pb$	2s	$^{206}Pb/^{238}U$	2s	$^{207}Pb/^{235}U$	2s	$^{208}Pb/^{232}Th$	2s	
	(%)	CPS	CPS	(ppm)			Data for Wetherill plot										abs		abs		abs		abs	
5.sSMPABC041	0.00	311729	18417	404	0.44	212	0.059	0.985	0.738	1.878	0.091	1.611	0.858	0.028	1.801	570	21	559	9	561	8	553	10	100
5.sSMPABC042	0.00	314249	18676	404	0.45	134	0.059	0.970	0.749	1.891	0.091	1.620	0.857	0.028	1.833	583	21	564	9	567	8	565	10	99
5.sSMPABC061	0.05	313497	18369	407	0.45	328	0.059	0.975	0.731	1.894	0.090	1.617	0.854	0.028	1.813	552	22	558	9	557	8	550	10	100
5.sSMPABC062	0.00	313325	18408	400	0.45	3682	0.059	0.963	0.744	1.881	0.092	1.611	0.857	0.028	1.854	558	21	567	9	565	8	559	10	100
5.sSMPABC081	0.03	347431	20396	451	0.44	291	0.059	0.974	0.732	1.887	0.090	1.615	0.856	0.028	1.795	556	21	558	9	558	8	555	10	100
5.sSMPABC082	0.00	355652	21051	459	0.44	21051	0.059	0.968	0.742	1.891	0.091	1.627	0.861	0.028	1.782	574	21	561	9	564	8	559	10	100
5.sSMPABC101	0.01	347486	20363	450	0.44	279	0.059	0.967	0.732	1.901	0.091	1.633	0.859	0.028	1.851	552	21	559	9	558	8	560	10	100
5.sSMPABC102	0.00	348391	20506	446	0.45	20506	0.059	0.965	0.745	1.881	0.092	1.613	0.857	0.028	1.851	562	21	566	9	565	8	560	10	100

LA(SF)-ICP-MS U-Pb zircon results data from BB-09 primary standard of the Sample CA-05 (Mestre Álvaro pluton)

Identifier	f206[a]	^{207}Pb	^{206}Pb	U	Th[b]/U	$^{206}Pb/^{204}Pb$	Ratios[c]									Ages (Ma)[c]								% conc[e]
							$^{207}Pb/^{206}Pb$	2s (%)	$^{207}Pb/^{235}U$	2s (%)	$^{206}Pb/^{238}U$	2s (%)	Rho[d]	$^{208}Pb/^{232}Th$	2s (%)	$^{207}Pb/^{206}Pb$	2s	$^{206}Pb/^{238}U$	2s	$^{207}Pb/^{235}U$	2s	$^{208}Pb/^{232}Th$	2s	
	(%)	CPS	CPS	(ppm)			Data for Wetherill plot										abs		abs		abs		abs	
5.sSMPABC001	0.00	235584	14008	416	0.45	0	0.059	0.992	0.745	1.634	0.091	1.298	0.794	0.028	1.559	584	22	561	7	566	7	563	9	99
5.sSMPABC006	0.00	226489	13125	398	0.46	0	0.058	1.001	0.730	1.652	0.091	1.314	0.796	0.028	1.629	528	22	563	7	556	7	563	9	101
5.sSMPABC022	0.00	240862	14177	423	0.45	0	0.059	1.036	0.742	1.672	0.091	1.312	0.785	0.028	1.691	562	23	564	7	564	7	566	10	100
5.sSMPABC023	0.00	238707	14108	420	0.45	0	0.059	1.032	0.744	1.671	0.091	1.314	0.786	0.028	1.783	571	22	563	7	565	7	559	10	100
5.sSMPABC001	0.00	178394	10504	319	0.48	0	0.059	0.951	0.730	1.567	0.090	1.245	0.795	0.026	1.442	563	21	555	7	557	7	526	8	100
5.sSMPABC004	0.00	241625	14222	423	0.45	0	0.059	0.951	0.745	1.547	0.092	1.220	0.788	0.028	1.414	562	21	566	7	566	7	564	8	100
5.sSMPABC006	0.00	119925	7168	210	0.28	0	0.060	1.004	0.757	1.596	0.092	1.241	0.777	0.030	2.080	595	22	567	7	572	7	594	12	99

LA(SF)-ICP-MS U-Pb zircon results data from BB-09 primary standard of the Sample CA-05 (Mestre Álvaro pluton)

Identifier	f206 [a]	^{207}Pb	^{206}Pb	U	Th[b]/U	$^{206}Pb/^{204}Pb$	Ratios[c]									Ages (Ma)[c]								% conc[e]
							$^{207}Pb/^{206}Pb$	2s (%)	$^{207}Pb/^{235}U$	2s (%)	$^{206}Pb/^{238}U$	2s (%)	Rho[d]	$^{208}Pb/^{232}Th$	2s (%)	$^{207}Pb/^{206}Pb$	2s abs	$^{206}Pb/^{238}U$	2s abs	$^{207}Pb/^{235}U$	2s abs	$^{208}Pb/^{232}Th$	2s abs	
	(%)	CPS	CPS	(ppm)			Data for Wetherill plot																	
5.sSMPABC007	0.26	122887	7257	215	0.29	1059	0.059	1.313	0.748	1.906	0.092	1.381	0.725	0.030	1.867	569	29	567	7	567	8	598	11	100
5.sSMPABC008	0.00	122162	7291	214	0.29	0	0.060	1.005	0.756	1.631	0.092	1.284	0.787	0.030	2.163	592	22	567	7	572	7	589	12	99
5.sSMPABC020	0.00	244625	14274	434	0.45	0	0.058	0.943	0.729	1.554	0.091	1.235	0.795	0.028	1.430	543	21	559	7	556	7	558	8	101
5.sSMPABC021	0.00	244505	14392	433	0.45	0	0.059	0.951	0.737	1.558	0.091	1.234	0.792	0.028	1.410	562	21	560	7	560	7	565	8	100
5.sSMPABC034	0.05	240060	14048	417	0.45	5138	0.059	0.974	0.747	1.574	0.093	1.237	0.786	0.029	1.404	549	21	571	7	566	7	568	8	101
5.sSMPABC048	0.00	232528	13668	408	0.46	0	0.059	0.953	0.743	1.566	0.092	1.243	0.794	0.028	1.447	559	21	566	7	564	7	551	8	100
5.sSMPABC049	0.06	215859	12685	384	0.47	4536	0.059	0.975	0.732	1.600	0.090	1.268	0.793	0.028	1.510	558	21	558	7	558	7	555	8	100
5.sSMPABC076	0.00	221837	13075	435	0.44	0	0.059	0.967	0.738	1.585	0.091	1.256	0.792	0.028	1.556	565	21	560	7	561	7	563	9	100
5.sSMPABC077	0.00	218392	12872	426	0.45	0	0.059	0.967	0.743	1.596	0.091	1.269	0.795	0.028	1.561	565	21	564	7	564	7	562	9	100
5.sSMPABC090	0.00	198092	11689	394	0.46	0	0.059	0.983	0.728	1.627	0.089	1.297	0.797	0.028	1.588	567	21	552	7	555	7	552	9	99
5.sSMPABC091	0.00	203213	12042	394	0.46	0	0.059	0.979	0.750	1.616	0.092	1.285	0.796	0.028	1.565	577	21	566	7	568	7	561	9	100
5.sSMPABC104	0.00	215872	12723	419	0.45	0	0.059	0.984	0.746	1.619	0.092	1.286	0.794	0.028	1.617	565	21	566	7	566	7	567	9	100
5.sSMPABC121	0.00	351712	20740	451	0.44	190	0.059	0.977	0.744	1.884	0.092	1.617	0.858	0.028	1.933	566	21	564	9	565	8	557	10	100

LA(SF)-ICP-MS U-Pb zircon results data from BB-09 primary standard of the Sample CA-06 (Nova Venécia complex)

Identifier	f206 [a]	^{207}Pb	^{206}Pb	U	Th[b]/U	$^{206}Pb/^{204}Pb$	Ratios[c]									Ages (Ma)[c]								% conc[e]
							$^{207}Pb/^{206}Pb$	2s (%)	$^{207}Pb/^{235}U$	2s (%)	$^{206}Pb/^{238}U$	2s (%)	Rho[d]	$^{208}Pb/^{232}Th$	2s (%)	$^{207}Pb/^{206}Pb$	2s abs	$^{206}Pb/^{238}U$	2s abs	$^{207}Pb/^{235}U$	2s abs	$^{208}Pb/^{232}Th$	2s abs	
	(%)	CPS	CPS	(ppm)			Data for Wetherill plot																	
5.sSMPABC001	0.00	155039	9150	424	0.45	0	0.059	1.050	0.750	1.607	0.092	1.216	0.757	0.028	1.982	568	23	568	7	568	7	563	11	100
5.sSMPABC021	0.00	155782	9277	431	0.45	0	0.060	1.058	0.747	1.606	0.091	1.209	0.753	0.028	2.004	587	23	561	7	567	7	557	11	99
5.sSMPABC022	0.00	157878	9440	435	0.45	0	0.060	1.054	0.753	1.600	0.091	1.204	0.752	0.028	1.970	596	23	564	7	570	7	567	11	99

LA(SF)-ICP-MS U-Pb zircon results data from BB-09 primary standard of the Sample CA-05 (Mestre Álvaro pluton)

Identifier	f206[a]	^{207}Pb	^{206}Pb	U	Th[b]/U	^{206}Pb/^{204}Pb	Ratios[c]									Ages (Ma)[c]								% conc[e]
							^{207}Pb/^{206}Pb	2s (%)	^{207}Pb/^{235}U	2s (%)	^{206}Pb/^{238}U	2s (%)	Rho[d]	^{208}Pb/^{232}Th	2s (%)	^{207}Pb/^{206}Pb	2s	^{206}Pb/^{238}U	2s	^{207}Pb/^{235}U	2s	^{208}Pb/^{232}Th	2s	
	(%)	CPS	CPS	(ppm)			Data for Wetherill plot										abs		abs		abs		abs	
5.sSMPABC040	0.00	151925	8964	416	0.45	0	0.059	1.051	0.748	1.608	0.092	1.217	0.757	0.028	2.007	567	23	567	7	567	7	556	11	100
5.sSMPABC041	0.00	157453	9268	433	0.45	0	0.059	1.053	0.743	1.598	0.092	1.201	0.752	0.028	1.997	562	23	565	6	564	7	559	11	100
5.sSMPABC060	0.36	148986	8847	415	0.45	749	0.059	1.620	0.741	2.179	0.091	1.456	0.669	0.028	2.062	581	35	559	8	563	9	561	11	99
5.sSMPABC078	0.00	154118	8999	426	0.45	0	0.058	1.062	0.734	1.608	0.091	1.207	0.751	0.028	2.016	544	23	562	7	559	7	554	11	101
5.sSMPABC079	0.00	147741	8686	408	0.45	0	0.059	1.055	0.739	1.619	0.091	1.228	0.759	0.028	2.088	559	23	562	7	562	7	554	11	100
5.sSMPABC097	0.00	151812	8998	418	0.45	0	0.059	1.063	0.747	1.622	0.091	1.225	0.755	0.029	2.037	577	23	564	7	567	7	587	12	100
5.sSMPABC098	0.00	146946	8640	406	0.45	0	0.059	1.054	0.740	1.618	0.091	1.227	0.758	0.027	2.094	560	23	563	7	562	7	533	11	100
5.sSMPABC116	0.00	147916	8686	406	0.45	0	0.059	1.056	0.743	1.614	0.092	1.221	0.756	0.029	2.077	557	23	566	7	564	7	576	12	100
5.sSMPABC117	0.02	134373	7882	376	0.45	14466	0.059	1.076	0.729	1.627	0.090	1.221	0.750	0.028	2.143	554	23	556	7	556	7	558	12	100
5.sSMPABC136	0.00	139908	8246	384	0.42	0	0.059	1.069	0.746	1.623	0.092	1.221	0.752	0.028	2.230	565	23	566	7	566	7	554	12	100
5.sSMPABC154	0.00	143752	8440	394	0.45	0	0.059	1.073	0.743	1.641	0.092	1.241	0.757	0.028	2.181	556	23	566	7	564	7	567	12	100

LA(SF)-ICP-MS U-Pb zircon results data from BB-09 primary standard of the Sample CA-07 (Ataléia suite)

Identifier	f206[a]	^{207}Pb	^{206}Pb	U	Th[b]/U	^{206}Pb/^{204}Pb	Ratios[c]									Ages (Ma)[c]								% conc[e]
							^{207}Pb/^{206}Pb	2s (%)	^{207}Pb/^{235}U	2s (%)	^{206}Pb/^{238}U	2s (%)	Rho[d]	^{208}Pb/^{232}Th	2s (%)	^{207}Pb/^{206}Pb	2s	^{206}Pb/^{238}U	2s	^{207}Pb/^{235}U	2s	^{208}Pb/^{232}Th	2s	
	(%)	CPS	CPS	(ppm)			Data for Wetherill plot										abs		abs		abs		abs	
5.sSMPABC001	0.00	139583	8212	494	0.45	0	0.059	1.054	0.745	1.661	0.092	1.284	0.773	0.028	2.086	561	23	567	7	566	7	554	11	100
5.sSMPABC005	0.04	127036	7514	455	0.46	6484	0.059	1.041	0.741	1.667	0.091	1.302	0.781	0.028	1.957	572	23	561	7	563	7	550	11	100
5.sSMPABC021	0.00	122156	7134	436	0.45	0	0.058	1.045	0.735	1.662	0.091	1.293	0.778	0.028	2.052	545	23	563	7	559	7	564	12	101
5.sSMPABC022	0.00	119227	6988	425	0.46	0	0.059	1.041	0.739	1.676	0.091	1.313	0.784	0.028	2.039	553	23	564	7	562	7	567	11	100

LA(SF)-ICP-MS U-Pb zircon results data from BB-09 primary standard of the Sample CA-07 (Ataléia suite)

Identifier	f206[a]	^{207}Pb	^{206}Pb	U	Th[b]/U	$^{206}Pb/^{204}Pb$	Ratios[c]									Ages (Ma)[c]								% conc[e]
							$^{207}Pb/^{206}Pb$	2s (%)	$^{207}Pb/^{235}U$	2s (%)	$^{206}Pb/^{238}U$	2s (%)	Rho[d]	$^{208}Pb/^{232}Th$	2s (%)	$^{207}Pb/^{206}Pb$	2s	$^{206}Pb/^{238}U$	2s	$^{207}Pb/^{235}U$	2s	$^{208}Pb/^{232}Th$	2s	
	(%)	CPS	CPS	(ppm)			Data for Wetherill plot									abs		abs		abs		abs		
5.sSMPABC036	0.00	112733	6684	403	0.45	0	0.059	1.063	0.744	1.676	0.091	1.296	0.773	0.029	2.246	578	23	562	7	565	7	585	13	99
5.sSMPABC049	0.00	110782	6506	398	0.46	0	0.059	1.073	0.733	1.705	0.091	1.325	0.777	0.028	2.209	557	23	559	7	559	7	560	12	100
5.sSMPABC050	0.00	119022	6998	421	0.47	0	0.059	1.088	0.745	1.716	0.092	1.327	0.773	0.028	2.301	560	24	567	7	565	7	555	13	100
5.sSMPABC063	0.00	110599	6580	393	0.46	0	0.059	1.059	0.752	1.700	0.092	1.330	0.782	0.028	2.211	585	23	566	7	569	7	559	12	99
5.sSMPABC064	0.00	115844	6777	408	0.46	0	0.059	1.077	0.744	1.705	0.092	1.322	0.775	0.028	2.258	549	24	569	7	565	7	565	13	101
5.sSMPABC077	0.00	107259	6345	387	0.46	0	0.059	1.082	0.735	1.716	0.090	1.332	0.776	0.027	2.384	573	24	556	7	560	7	536	13	99
5.sSMPABC078	0.00	106899	6354	383	0.45	0	0.059	1.094	0.744	1.716	0.091	1.322	0.771	0.029	2.489	583	24	560	7	565	7	577	14	99
5.sSMPABC096	0.00	115918	6813	412	0.46	0	0.059	1.089	0.741	1.722	0.091	1.334	0.775	0.029	2.452	559	24	564	7	563	7	569	14	100
5.sSMPABC097	0.00	115557	6758	407	0.46	0	0.058	1.094	0.744	1.733	0.092	1.344	0.775	0.028	2.483	548	24	569	7	565	8	562	14	101
5.sSMPABC154	0.00	143752	8440	413	0.47	0	0.059	1.073	0.743	1.641	0.092	1.241	0.757	0.028	2.181	556	23	566	7	564	7	567	12	100
5.sSMPABC192	0.00	148557	8694	429	0.44	0	0.059	1.077	0.737	1.648	0.091	1.248	0.757	0.027	2.355	549	24	563	7	561	7	542	12	100

LA(SF)-ICP-MS U-Pb zircon results data from BB-09 primary standard of the Sample CA-09 (Nova Venécia complex)

Identifier	f206[a]	^{207}Pb	^{206}Pb	U	Th[b]/U	$^{206}Pb/^{204}Pb$	Ratios[c]									Ages (Ma)[c]								% conc[e]
							$^{207}Pb/^{206}Pb$	2s (%)	$^{207}Pb/^{235}U$	2s (%)	$^{206}Pb/^{238}U$	2s (%)	Rho[d]	$^{208}Pb/^{232}Th$	2s (%)	$^{207}Pb/^{206}Pb$	2s	$^{206}Pb/^{238}U$	2s	$^{207}Pb/^{235}U$	2s	$^{208}Pb/^{232}Th$	2s	
	(%)	CPS	CPS	(ppm)			Data for Wetherill plot									abs		abs		abs		abs		
5.sSMPABC001	0.00	125001	7420	373	0.44	0	0.059	1.061	0.733	1.573	0.090	1.161	0.738	0.029	1.920	580	23	553	6	558	7	581	11	99
5.sSMPABC005	0.00	144177	8495	428	0.44	0	0.059	1.052	0.732	1.562	0.090	1.155	0.739	0.027	1.896	564	23	556	6	557	7	547	10	100

LA(SF)-ICP-MS U-Pb zircon results data from BB-09 primary standard of the Sample CA-09 (Nova Venécia complex)

Identifier	f206 [a]	^{207}Pb	^{206}Pb	U	Th[b]/U	$^{206}Pb/^{204}Pb$	Ratios[c]									Ages (Ma)[c]								% conc[e]
							$^{207}Pb/^{206}Pb$	2s (%)	$^{207}Pb/^{235}U$	2s (%)	$^{206}Pb/^{238}U$	2s (%)	Rho[d]	$^{208}Pb/^{232}Th$	2s (%)	$^{207}Pb/^{206}Pb$	2s	$^{206}Pb/^{238}U$	2s	$^{207}Pb/^{235}U$	2s	$^{208}Pb/^{232}Th$	2s	
	(%)	CPS	CPS	(ppm)			Data for Wetherill plot										abs		abs		abs		abs	
5.sSMPABC016	0.00	135834	8022	396	0.46	0	0.059	1.050	0.747	1.577	0.092	1.177	0.746	0.028	1.903	569	23	566	6	567	7	566	10	100
5.sSMPABC017	0.00	156321	9343	400	0.45	0	0.060	1.054	0.757	1.563	0.092	1.154	0.738	0.029	1.804	595	23	566	6	572	7	574	10	99
5.sSMPABC031	0.05	160194	9405	408	0.46	5679	0.059	1.052	0.747	1.578	0.092	1.176	0.745	0.028	1.809	556	23	569	6	566	7	551	10	100
5.sSMPABC044	0.00	159555	9390	412	0.45	0	0.059	1.054	0.739	1.570	0.091	1.164	0.741	0.028	1.947	562	23	562	6	562	7	553	11	100
5.sSMPABC045	0.00	164444	9584	421	0.45	0	0.058	1.047	0.737	1.575	0.092	1.177	0.747	0.029	1.750	540	23	566	6	561	7	570	10	101
5.sSMPABC058	0.32	156029	9187	401	0.46	860	0.059	1.505	0.743	2.034	0.091	1.369	0.673	0.026	1.890	563	33	564	7	564	9	528	10	100
5.sSMPABC059	0.00	139184	8204	401	0.45	0	0.059	1.052	0.744	1.581	0.092	1.180	0.746	0.029	1.893	565	23	565	6	565	7	569	11	100
5.sSMPABC077	0.00	139023	8233	401	0.45	0	0.059	1.047	0.747	1.595	0.091	1.203	0.754	0.028	1.866	575	23	564	7	566	7	555	10	100
5.sSMPABC078	0.26	142759	8295	410	0.44	1029	0.058	1.390	0.736	1.923	0.092	1.328	0.691	0.027	1.896	534	30	567	7	560	8	547	10	101
5.sSMPABC097	0.00	136406	8037	397	0.45	0	0.059	1.052	0.737	1.589	0.091	1.191	0.749	0.028	1.975	564	23	559	6	560	7	565	11	100
5.sSMPABC134	0.00	169664	9959	493	0.44	0	0.059	1.056	0.735	1.607	0.091	1.212	0.754	0.028	1.921	556	23	560	7	559	7	560	11	100
5.sSMPABC135	0.00	165759	9650	475	0.45	0	0.058	1.048	0.739	1.605	0.092	1.216	0.758	0.028	1.920	538	23	568	7	562	7	561	11	101
5.sSMPABC153	0.16	139967	8346	403	0.45	1660	0.060	1.206	0.752	1.756	0.092	1.276	0.727	0.028	2.095	590	26	564	7	570	8	552	12	99
5.sSMPABC172	0.00	149490	8796	434	0.45	0	0.059	1.071	0.736	1.634	0.091	1.234	0.755	0.028	2.143	561	23	560	7	560	7	558	12	100
5.sSMPABC173	0.00	150739	8868	433	0.45	0	0.059	1.071	0.744	1.640	0.092	1.242	0.757	0.028	2.185	561	23	566	7	565	7	565	12	100

LA(SF)-ICP-MS U-Pb zircon results data from BB-09 primary standard of the Sample CA-10 (Nova Venécia complex)

Identifier	f206 [a]	^{207}Pb	^{206}Pb	U	Th[b]/U	$^{206}Pb/^{204}Pb$	Ratios[c]									Ages (Ma)[c]								% conc[e]
							$^{207}Pb/^{206}Pb$	2s (%)	$^{207}Pb/^{235}U$	2s (%)	$^{206}Pb/^{238}U$	2s (%)	Rho[d]	$^{208}Pb/^{232}Th$	2s (%)	$^{207}Pb/^{206}Pb$	2s abs	$^{206}Pb/^{238}U$	2s abs	$^{207}Pb/^{235}U$	2s abs	$^{208}Pb/^{232}Th$	2s abs	
	(%)	CPS	CPS	(ppm)			Data for Wetherill plot																	
5.sSMPABC001	0.00	146858	8648	407	0.45	0	0.059	1.053	0.745	1.611	0.092	1.220	0.757	0.027	1.902	563	23	566	7	566	7	545	10	100
5.sSMPABC003	0.00	143157	8502	400	0.44	0	0.059	1.044	0.745	1.615	0.091	1.232	0.763	0.029	1.906	581	23	561	7	565	7	585	11	99
5.sSMPABC004	0.11	146540	8697	406	0.45	2546	0.059	1.105	0.750	1.664	0.092	1.243	0.747	0.029	1.889	580	24	566	7	568	7	570	11	100
5.sSMPABC021	0.00	137419	8084	383	0.43	0	0.059	1.054	0.739	1.619	0.091	1.229	0.759	0.029	1.938	561	23	562	7	562	7	576	11	100
5.sSMPABC022	0.00	149923	8738	416	0.46	0	0.058	1.047	0.736	1.610	0.092	1.223	0.760	0.028	1.869	540	23	565	7	560	7	555	10	101
5.sSMPABC040	0.06	147127	8702	412	0.45	4608	0.059	1.067	0.741	1.635	0.091	1.239	0.758	0.027	1.971	572	23	561	7	563	7	546	11	100
5.sSMPABC041	0.00	143009	8505	402	0.45	0	0.059	1.059	0.743	1.628	0.091	1.237	0.759	0.028	1.973	584	23	559	7	564	7	566	11	99
5.sSMPABC078	0.23	144361	8551	399	0.45	1192	0.059	1.314	0.751	1.874	0.092	1.337	0.713	0.029	2.150	576	29	567	7	569	8	575	12	100
5.sSMPABC098	0.17	148651	8806	410	0.45	1610	0.059	1.222	0.753	1.777	0.092	1.291	0.726	0.029	2.173	576	27	568	7	570	8	569	12	100
5.sSMPABC116	0.00	138089	8198	390	0.45	0	0.059	1.095	0.737	1.657	0.090	1.244	0.751	0.028	2.674	581	24	556	7	561	7	552	15	99
5.sSMPABC135	0.33	154487	9068	433	0.43	821	0.059	1.582	0.734	2.149	0.091	1.455	0.677	0.028	2.545	556	35	559	8	559	9	564	14	100
5.sSMPABC136	0.00	154689	9128	431	0.43	0	0.059	1.085	0.742	1.655	0.091	1.251	0.755	0.028	2.538	567	24	562	7	563	7	550	14	100

[a] percentage of the common Pb on the ^{206}Pb

[b] Th/U ratios are calculated relative to BB reference zircon

[c] data corrected for background, within-run Pb/U fractionation (in case of $^{206}Pb/^{238}U$) and common Pb using Stacey and Kramers (1975) model Pb composition

[d] Rho is the error correlation defined as the quotient of the propagated errors of the $^{206}Pb/^{238}U$ and the $^{207}Pb/^{235}U$ ratio

*[e]Concordance calculated as (^{206}Pb-^{238}U age/^{207}Pb-^{206}Pb age)*100*

CPS = count per second

SECONDARY REFERENCE STANDARD

LA(SF)-ICP-MS U-Pb zircon results data from Plesovice secondary standard of the Sample CA-02 (Aracê - Pedra Azul pluton)

Identifier	f206 [a]	^{207}Pb	^{206}Pb	U	Th[b]/U	$^{206}Pb/^{204}Pb$	Ratios[c]									Ages (Ma)[c]								% conc[e]
							$^{207}Pb/^{206}Pb$	2s (%)	$^{207}Pb/^{235}U$	2s (%)	$^{206}Pb/^{238}U$	2s (%)	Rho[d]	$^{208}Pb/^{232}Th$	2s (%)	$^{207}Pb/^{206}Pb$	2s	$^{206}Pb/^{238}U$	2s	$^{207}Pb/^{235}U$	2s	$^{208}Pb/^{232}Th$	2s	
	(%)	CPS	CPS	(ppm)			Data for Wetherill plot										abs		abs		abs		abs	
5.sSMPABC002	0.00	93718	4976	387	0.12	0	0.053	1.224	0.397	1.888	0.054	1.438	0.761	0.016	5.366	333	28	341	5	340	5	329	18	100
5.sSMPABC003	0.00	185417	9862	765	0.21	0	0.053	1.015	0.398	1.641	0.054	1.289	0.786	0.016	2.427	337	23	341	4	340	5	314	8	100
5.sSMPABC019	0.00	83327	4434	346	0.12	0	0.053	1.071	0.395	1.742	0.054	1.374	0.789	0.019	3.490	338	24	338	5	338	5	379	13	100
5.sSMPABC020	0.07	74507	3990	312	0.12	4035	0.054	1.075	0.395	1.740	0.053	1.369	0.787	0.019	3.178	352	24	336	4	338	5	378	12	99
5.sSMPABC035	0.00	78637	4186	329	0.12	0	0.053	1.052	0.393	1.708	0.053	1.346	0.788	0.019	3.206	339	24	336	4	336	5	387	12	100
5.sSMPABC036	0.00	71615	3811	302	0.11	0	0.053	1.109	0.390	1.751	0.053	1.355	0.774	0.018	4.132	338	25	334	4	334	5	359	15	100
5.sSMPABC051	0.00	76782	4089	323	0.12	0	0.053	1.277	0.391	1.916	0.053	1.429	0.746	0.018	5.159	340	29	334	5	335	5	365	19	100
5.sSMPABC052	0.00	121910	6501	506	0.14	0	0.053	1.106	0.397	1.734	0.054	1.335	0.770	0.018	3.422	343	25	339	4	339	5	363	12	100
5.sSMPABC067	0.00	84076	4469	351	0.12	0	0.053	1.110	0.393	1.799	0.054	1.416	0.787	0.018	3.898	336	25	337	5	337	5	370	14	100
5.sSMPABC082	0.00	71109	3783	293	0.11	0	0.053	1.353	0.398	2.029	0.054	1.511	0.745	0.017	6.092	337	31	341	5	340	6	349	21	100
5.sSMPABC083	0.00	71793	3822	296	0.12	0	0.053	1.127	0.398	1.769	0.054	1.364	0.771	0.017	4.692	339	26	341	5	340	5	342	16	100

LA(SF)-ICP-MS U-Pb zircon results data from Plesovice secondary standard of the Sample CA-04 (Vitória pluton)

Identifier	f206 [a]	^{207}Pb	^{206}Pb	U	Th[b]/U	^{206}Pb/^{204}Pb	Ratios[c]									Ages (Ma)[c]								% conc[e]
							^{207}Pb/^{206}Pb	2s (%)	^{207}Pb/^{235}U	2s (%)	^{206}Pb/^{238}U	2s (%)	Rho[d]	^{208}Pb/^{232}Th	2s (%)	^{207}Pb/^{206}Pb	2s	^{206}Pb/^{238}U	2s	^{207}Pb/^{235}U	2s	^{208}Pb/^{232}Th	2s	
	(%)	CPS	CPS	(ppm)			Data for Wetherill plot										abs		abs		abs		abs	
5.sSMPABC003	0.06	180339	9580	675	0.12	184	0.053	1.039	0.399	1.930	0.054	1.627	0.843	0.016	2.640	334	24	342	5	335	6	319	8	100
5.sSMPABC004	0.00	177887	9462	665	0.12	9462	0.053	1.015	0.399	1.905	0.054	1.612	0.846	0.016	2.609	337	23	342	5	335	5	323	8	100
5.sSMPABC023	0.04	206934	11009	770	0.12	160	0.053	1.063	0.401	1.992	0.055	1.685	0.846	0.018	2.758	337	24	343	6	337	6	363	10	100
5.sSMPABC024	0.00	196515	10421	744	0.12	10421	0.053	1.094	0.393	2.027	0.054	1.707	0.842	0.016	3.262	330	25	338	6	331	6	320	10	100
5.sSMPABC043	0.31	143454	7631	548	0.11	42	0.053	1.755	0.391	2.669	0.053	2.010	0.753	0.016	4.924	337	40	335	6	329	8	318	16	100
5.sSMPABC044	0.00	182241	9672	686	0.12	9672	0.053	1.131	0.396	2.041	0.054	1.699	0.832	0.016	3.681	332	26	339	6	333	6	327	12	100
5.sSMPABC063	0.00	171427	9080	655	0.11	189	0.053	1.019	0.389	1.937	0.053	1.647	0.850	0.016	2.886	328	23	335	5	328	5	320	9	100
5.sSMPABC064	0.05	166741	8836	633	0.11	67	0.053	1.036	0.392	1.946	0.054	1.647	0.846	0.015	2.943	329	24	337	5	330	5	300	9	100
5.sSMPABC083	0.00	192559	10194	742	0.11	537	0.053	1.001	0.386	1.906	0.053	1.622	0.851	0.016	2.508	326	23	332	5	326	5	320	8	100
5.sSMPABC084	0.00	185504	9852	703	0.11	704	0.053	1.017	0.393	1.925	0.054	1.634	0.849	0.015	2.742	333	23	337	5	331	5	307	8	100
5.sSMPABC103	0.01	201083	10641	768	0.11	355	0.053	1.002	0.389	1.927	0.053	1.646	0.854	0.019	2.318	325	23	335	5	328	5	380	9	100
5.sSMPABC104	0.00	194583	10344	744	0.11	10344	0.053	1.016	0.390	1.936	0.053	1.648	0.851	0.016	2.597	336	23	334	5	329	5	324	8	100

LA(SF)-ICP-MS U-Pb zircon results data from Plesovice secondary standard of the Sample CA-05 (Mestre Álvaro pluton)

Identifier	f206 [a]	^{207}Pb	^{206}Pb	U	Th[b]/U	^{206}Pb/^{204}Pb	Ratios[c]									Ages (Ma)[c]								% conc[e]
							^{207}Pb/^{206}Pb	2s (%)	^{207}Pb/^{235}U	2s (%)	^{206}Pb/^{238}U	2s (%)	Rho[d]	^{208}Pb/^{232}Th	2s (%)	^{207}Pb/^{206}Pb	2s	^{206}Pb/^{238}U	2s	^{207}Pb/^{235}U	2s	^{208}Pb/^{232}Th	2s	
	(%)	CPS	CPS	(ppm)			Data for Wetherill plot										abs		abs		abs		abs	
5.sSMPABC002-2	0.00	204735	10886	604	0.13	0	0.053	1.072	0.399	1.790	0.054	1.433	0.801	0.019	3.433	336	24	342	5	341	5	373	13	100
5.sSMPABC004-2	0.12	203018	10809	603	0.16	2154	0.053	1.202	0.397	1.878	0.054	1.443	0.768	0.016	3.157	339	27	340	5	340	5	318	10	100
5.sSMPABC005-2	0.00	122370	6516	364	0.13	0	0.053	1.052	0.396	1.699	0.054	1.334	0.785	0.018	2.776	339	24	339	4	339	5	361	10	100

5.sSMPABC024-2	0.04	173986	9249	520	0.13	7475	0.053	1.081	0.394	1.784	0.054	1.419	0.796	0.018	2.789	336	24	338	5	338	5	359	10	100
5.sSMPABC025-2	0.12	185013	9827	547	0.13	2158	0.053	1.153	0.398	1.869	0.054	1.471	0.787	0.019	2.696	334	26	341	5	340	5	386	10	100

LA(SF)-ICP-MS U-Pb zircon results data from Gj-1 secondary standard of the Sample CA-05 (Mestre Álvaro pluton)

Identifier	f206[a]	^{207}Pb	^{206}Pb	U	Th[b]/U	^{206}Pb/^{204}Pb	Ratios[c]									Ages (Ma)[c]								% conc[e]
							^{207}Pb/^{206}Pb	2s (%)	^{207}Pb/^{235}U	2s (%)	^{206}Pb/^{238}U	2s (%)	Rho[d]	^{208}Pb/^{232}Th	2s (%)	^{207}Pb/^{206}Pb	2s	^{206}Pb/^{238}U	2s	^{207}Pb/^{235}U	2s	^{208}Pb/^{232}Th	2s	
	(%)	CPS	CPS	(ppm)			Data for Wetherill plot										abs		abs		abs		abs	
5.sSMPABC002	1.00	146585	8812	242	0.05	0	0.060	3.474	0.809	4.247	0.098	2.444	0.575	0.040	4.499	608	75	600	14	602	19	784	34	100
5.sSMPABC003	0.00	142505	8550	237	0.05	0	0.060	0.983	0.800	1.583	0.097	1.241	0.784	0.041	4.012	604	21	595	7	597	7	810	32	100
5.sSMPABC022	0.00	144526	8692	241	0.04	0	0.060	0.998	0.799	1.612	0.096	1.266	0.785	0.035	4.950	609	22	593	7	596	7	691	34	99
5.sSMPABC023	0.00	142843	8563	238	0.05	0	0.060	0.951	0.797	1.583	0.096	1.266	0.800	0.045	3.401	602	21	593	7	595	7	895	30	100
5.sSMPABC036	0.00	135204	8093	226	0.04	0	0.060	1.069	0.794	1.674	0.096	1.288	0.770	0.042	5.464	599	23	592	7	594	8	841	45	100
5.sSMPABC051	0.16	142348	8551	238	0.05	1697	0.060	1.207	0.798	1.826	0.096	1.369	0.750	0.043	5.220	606	26	593	8	596	8	842	43	100
5.sSMPABC064	0.00	134513	8067	247	0.05	0	0.060	1.001	0.802	1.623	0.097	1.278	0.787	0.039	4.149	602	22	597	7	598	7	774	31	100
5.sSMPABC065	0.00	134643	8069	246	0.04	0	0.060	0.968	0.806	1.614	0.098	1.292	0.800	0.052	3.536	601	21	600	7	600	7	1026	35	100
5.sSMPABC078	0.00	129010	7746	238	0.05	0	0.060	1.049	0.801	1.673	0.097	1.303	0.779	0.046	4.662	605	23	595	7	597	8	915	42	100
5.sSMPABC079	0.06	133940	8073	245	0.04	4281	0.060	1.034	0.809	1.662	0.097	1.301	0.783	0.044	4.540	613	22	599	7	602	8	863	38	99
5.sSMPABC092	0.00	138430	8309	252	0.05	0	0.060	1.000	0.811	1.661	0.098	1.326	0.799	0.040	4.082	604	22	603	8	603	8	787	32	100

LA(SF)-ICP-MS U-Pb zircon results data from Plesovice secondary standard of the Sample CA-06 (Nova Venécia complex)

Identifier	f206 [a]	^{207}Pb	^{206}Pb	U	Th[b]/U	$^{206}Pb/^{204}Pb$	Ratios[c]									Ages (Ma)[c]								% conc[e]
							$^{207}Pb/^{206}Pb$	2s (%)	$^{207}Pb/^{235}U$	2s (%)	$^{206}Pb/^{238}U$	2s (%)	Rho[d]	$^{208}Pb/^{232}Th$	2s (%)	$^{207}Pb/^{206}Pb$	2s	$^{206}Pb/^{238}U$	2s	$^{207}Pb/^{235}U$	2s	$^{208}Pb/^{232}Th$	2s	
	(%)	CPS	CPS	(ppm)			Data for Wetherill plot										abs		abs		abs		abs	
5.sSMPABC002	0.00	212445	11315	991	0.12	0	0.053	0.995	0.397	1.605	0.054	1.259	0.785	0.018	1.922	340	23	339	4	339	5	354	7	100
5.sSMPABC003	0.00	231715	12320	1074	0.13	0	0.053	1.016	0.399	1.611	0.054	1.251	0.776	0.017	1.871	336	23	341	4	341	5	343	7	100
5.sSMPABC004	0.00	234678	12492	1087	0.12	0	0.053	1.090	0.399	1.743	0.054	1.361	0.781	0.017	2.847	339	25	341	5	341	5	338	9	100
5.sSMPABC023	0.00	253261	13481	1177	0.13	0	0.053	1.052	0.398	1.694	0.054	1.328	0.784	0.016	2.439	339	24	340	4	340	5	329	8	100
5.sSMPABC024	0.00	251822	13387	1168	0.13	0	0.053	1.053	0.398	1.664	0.054	1.289	0.774	0.018	2.286	336	24	341	4	340	5	351	8	100
5.sSMPABC042	0.00	227735	12118	1065	0.13	0	0.053	1.015	0.395	1.591	0.054	1.225	0.770	0.017	1.986	338	23	338	4	338	5	343	7	100
5.sSMPABC061	0.00	182354	9707	841	0.10	0	0.053	1.033	0.401	1.590	0.055	1.208	0.760	0.017	2.536	339	23	343	4	342	5	348	9	100
5.sSMPABC099	0.00	187074	9950	871	0.10	0	0.053	1.034	0.397	1.627	0.054	1.256	0.772	0.018	2.187	337	23	340	4	339	5	366	8	100
5.sSMPABC100	0.00	284588	15126	1323	0.10	0	0.053	1.072	0.397	1.679	0.054	1.292	0.769	0.019	2.677	335	24	340	4	340	5	374	10	100
5.sSMPABC119	0.00	296926	15770	1366	0.12	0	0.053	1.017	0.401	1.577	0.055	1.205	0.764	0.017	1.995	333	23	344	4	342	5	342	7	100
5.sSMPABC156	0.06	324688	17259	1502	0.11	4324	0.053	1.061	0.399	1.654	0.054	1.269	0.767	0.018	2.070	336	24	342	4	341	5	368	8	100
5.sSMPABC157	0.00	259866	13820	1209	0.10	0	0.053	1.034	0.397	1.627	0.054	1.256	0.772	0.017	2.374	336	23	340	4	340	5	338	8	100

LA(SF)-ICP-MS U-Pb zircon results data from Plesovice secondary standard of the Sample CA-07 (Ataléia suite)

Identifier	f206 [a]	^{207}Pb	^{206}Pb	U	Th[b]/U	^{206}Pb/^{204}Pb	Ratios[c]									Ages (Ma)[c]								% conc[e]
							^{207}Pb/^{206}Pb	2s (%)	^{207}Pb/^{235}U	2s (%)	^{206}Pb/^{238}U	2s (%)	Rho[d]	^{208}Pb/^{232}Th	2s (%)	^{207}Pb/^{206}Pb	2s	^{206}Pb/^{238}U	2s	^{207}Pb/^{235}U	2s	^{208}Pb/^{232}Th	2s	
	(%)	CPS	CPS	(ppm)			Data for Wetherill plot										abs		abs		abs		abs	
5.sSMPABC002	0.00	142659	7597	861	0.11	0	0.053	1.108	0.396	1.822	0.054	1.446	0.794	0.020	3.359	339	25	339	5	339	5	393	13	100
5.sSMPABC003	0.00	135434	7206	812	0.11	0	0.053	1.109	0.398	1.786	0.054	1.400	0.784	0.016	3.639	338	25	341	5	340	5	320	11	100
5.sSMPABC023	0.00	157739	8412	956	0.11	0	0.053	1.031	0.395	1.662	0.054	1.304	0.784	0.017	2.403	343	23	337	4	338	5	350	8	100
5.sSMPABC024	0.25	170313	9043	1040	0.11	1086	0.053	1.363	0.390	2.106	0.053	1.606	0.762	0.018	2.157	333	31	335	5	335	6	353	7	100
5.sSMPABC037	0.06	171655	9130	1054	0.11	4170	0.053	1.080	0.389	1.694	0.053	1.305	0.770	0.018	2.352	337	24	333	4	333	5	358	8	100
5.sSMPABC038	0.00	167042	8868	1016	0.11	0	0.053	1.055	0.392	1.680	0.054	1.308	0.778	0.017	2.542	333	24	336	4	336	5	347	9	100
5.sSMPABC051	0.01	158507	8368	963	0.11	19858	0.053	1.062	0.390	1.685	0.054	1.308	0.776	0.017	2.545	320	24	336	4	334	5	347	9	101
5.sSMPABC052	0.00	172119	9140	1063	0.11	0	0.053	1.036	0.386	1.655	0.053	1.291	0.780	0.017	2.401	333	23	331	4	331	5	334	8	100
5.sSMPABC066	0.02	182062	9662	1109	0.11	13364	0.053	1.058	0.391	1.686	0.053	1.313	0.779	0.017	2.471	332	24	335	4	335	5	341	8	100
5.sSMPABC079	0.00	165489	8743	1012	0.13	0	0.053	1.098	0.388	1.713	0.053	1.316	0.768	0.016	2.882	322	25	334	4	333	5	320	9	100
5.sSMPABC080	0.02	166436	8778	1019	0.13	15389	0.053	1.083	0.387	1.706	0.053	1.318	0.773	0.016	2.748	318	25	334	4	332	5	321	9	101
5.sSMPABC098	0.17	159189	8427	973	0.13	1552	0.053	1.243	0.389	1.921	0.053	1.466	0.763	0.018	2.476	326	28	334	5	333	5	356	9	100
5.sSMPABC099	0.00	168697	8998	1047	0.13	0	0.053	1.106	0.386	1.764	0.052	1.374	0.779	0.016	2.855	343	25	329	4	331	5	323	9	99
5.sSMPABC156	0.06	324688	17259	1572	0.11	4324	0.053	1.061	0.399	1.654	0.054	1.269	0.767	0.018	2.070	336	24	342	4	341	5	368	8	100
5.sSMPABC157	0.00	259866	13820	1265	0.11	0	0.053	1.034	0.397	1.627	0.054	1.256	0.772	0.017	2.374	336	23	340	4	340	5	338	8	100
5.sSMPABC175	0.00	208640	11087	1010	0.11	0	0.053	1.073	0.399	1.674	0.054	1.285	0.768	0.016	2.711	335	24	342	4	341	5	325	9	100
5.sSMPABC194	0.14	247245	13133	1198	0.11	1946	0.053	1.209	0.399	1.836	0.054	1.382	0.753	0.016	2.959	334	27	342	5	341	5	325	9	100

LA(SF)-ICP-MS U-Pb zircon results data from Plesovice secondary standard of the Sample CA-09 (Nova Venécia complex)

Identifier	f206 [a]	^{207}Pb	^{206}Pb	U	Th[b]/U	$^{206}Pb/^{204}Pb$	Ratios[c]									Ages (Ma)[c]								% conc[e]
							$^{207}Pb/^{206}Pb$	2s (%)	$^{207}Pb/^{235}U$	2s (%)	$^{206}Pb/^{238}U$	2s (%)	Rho[d]	$^{208}Pb/^{232}Th$	2s (%)	$^{207}Pb/^{206}Pb$	2s	$^{206}Pb/^{238}U$	2s	$^{207}Pb/^{235}U$	2s	$^{208}Pb/^{232}Th$	2s	
	(%)	CPS	CPS	(ppm)			Data for Wetherill plot										abs		abs		abs		abs	
5.sSMPABC004	0.00	113792	6137	572	0.10	0	0.054	1.075	0.395	1.586	0.053	1.166	0.735	0.017	2.656	368	24	334	4	338	5	347	9	99
5.sSMPABC032	0.00	161993	8535	703	0.10	0	0.053	1.063	0.393	1.617	0.054	1.219	0.754	0.020	2.314	315	24	340	4	337	5	398	9	101
5.sSMPABC033	0.13	145132	7680	630	0.10	2014	0.053	1.171	0.395	1.735	0.054	1.280	0.738	0.017	2.582	325	27	340	4	338	5	342	9	101
5.sSMPABC047	0.00	153967	8210	669	0.11	0	0.053	1.050	0.398	1.582	0.054	1.184	0.748	0.017	2.400	342	24	339	4	340	5	334	8	100
5.sSMPABC060	0.00	143066	7623	705	0.10	0	0.053	1.051	0.393	1.592	0.054	1.195	0.751	0.017	2.436	341	24	336	4	337	5	346	9	100
5.sSMPABC061	0.00	151464	8075	742	0.10	0	0.053	1.050	0.396	1.586	0.054	1.188	0.749	0.016	2.733	342	24	338	4	339	5	323	9	100
5.sSMPABC079	0.00	161611	8611	789	0.10	0	0.053	1.051	0.397	1.584	0.054	1.185	0.748	0.015	2.765	341	24	339	4	339	5	305	8	100
5.sSMPABC080	0.00	176522	9402	867	0.10	0	0.053	1.051	0.394	1.589	0.054	1.192	0.750	0.017	2.400	340	24	337	4	338	5	334	8	100
5.sSMPABC098	0.05	180547	9593	891	0.10	5507	0.053	1.051	0.392	1.604	0.053	1.211	0.755	0.017	2.324	335	24	336	4	335	5	345	8	100
5.sSMPABC099	0.00	176162	9400	858	0.10	0	0.053	1.049	0.398	1.581	0.054	1.182	0.748	0.016	2.577	344	24	340	4	340	5	311	8	100
5.sSMPABC117	0.03	186647	9928	913	0.11	7774	0.053	1.042	0.395	1.613	0.054	1.231	0.763	0.017	2.277	337	24	338	4	338	5	335	8	100
5.sSMPABC118	0.00	172704	9165	833	0.11	0	0.053	1.055	0.400	1.631	0.055	1.244	0.763	0.017	2.617	332	24	343	4	342	5	337	9	100
5.sSMPABC136	0.00	189846	10079	931	0.10	0	0.053	1.036	0.393	1.607	0.054	1.228	0.764	0.017	2.299	333	23	338	4	337	5	331	8	100
5.sSMPABC137	0.00	206842	10998	1011	0.11	0	0.053	1.053	0.395	1.614	0.054	1.224	0.758	0.017	2.400	336	24	339	4	338	5	334	8	100
5.sSMPABC156	0.00	131203	6959	643	0.10	0	0.053	1.056	0.394	1.618	0.054	1.227	0.758	0.018	2.694	331	24	338	4	337	5	357	10	100
5.sSMPABC174	0.00	173375	9220	845	0.11	0	0.053	1.166	0.397	1.825	0.054	1.404	0.769	0.017	3.672	336	26	340	5	339	5	349	13	100

LA(SF)-ICP-MS U-Pb zircon results data from Plesovice secondary standard of the Sample CA-10 (Nova Venécia complex)

Identifier	f206[a]	^{207}Pb	^{206}Pb	U	Th[b]/U	^{206}Pb/^{204}Pb	Ratios[c]									Ages (Ma)[c]								% conc[e]
							^{207}Pb/^{206}Pb	2s (%)	^{207}Pb/^{235}U	2s (%)	^{206}Pb/^{238}U	2s (%)	Rho[d]	^{208}Pb/^{232}Th	2s (%)	^{207}Pb/^{206}Pb	2s	^{206}Pb/^{238}U	2s	^{207}Pb/^{235}U	2s	^{208}Pb/^{232}Th	2s	
	(%)	CPS	CPS	(ppm)			Data for Wetherill plot										abs		abs		abs		abs	
5.sSMPABC002	0.00	188706	10039	882	0.11	0	0.053	1.147	0.399	1.779	0.054	1.361	0.765	0.016	3.683	337	26	341	5	341	5	316	12	100
5.sSMPABC005	0.00	165645	8817	780	0.10	0	0.053	1.052	0.396	1.613	0.054	1.222	0.758	0.016	2.682	339	24	339	4	339	5	314	8	100
5.sSMPABC023	0.00	174191	9267	814	0.10	0	0.053	1.053	0.399	1.607	0.054	1.214	0.755	0.017	2.418	337	24	341	4	341	5	332	8	100
5.sSMPABC024	0.00	178486	9453	832	0.10	0	0.053	1.057	0.398	1.607	0.055	1.210	0.753	0.017	2.458	327	24	342	4	340	5	343	8	101
5.sSMPABC042	0.00	167046	8887	785	0.11	0	0.053	1.071	0.397	1.651	0.054	1.256	0.761	0.016	2.936	337	24	340	4	339	5	328	9	100
5.sSMPABC061	0.24	188853	10079	899	0.11	1097	0.053	1.435	0.393	2.171	0.053	1.629	0.750	0.017	3.228	345	32	335	5	336	6	335	11	100
5.sSMPABC062	0.00	193306	10342	917	0.11	0	0.054	1.047	0.395	1.645	0.054	1.268	0.771	0.016	2.694	350	24	337	4	338	5	313	8	99
5.sSMPABC079	0.03	184245	9811	877	0.11	7979	0.053	1.059	0.392	1.632	0.053	1.241	0.761	0.016	2.633	340	24	336	4	336	5	320	8	100
5.sSMPABC080	0.00	190594	10142	907	0.10	0	0.053	1.128	0.392	1.700	0.053	1.273	0.748	0.014	3.968	338	26	336	4	336	5	273	11	100
5.sSMPABC099	0.00	226383	12068	1070	0.11	0	0.053	1.088	0.395	1.725	0.054	1.339	0.776	0.016	3.000	342	25	338	4	338	5	321	10	100
5.sSMPABC100	0.00	196049	10440	920	0.11	0	0.053	1.070	0.398	1.650	0.054	1.256	0.761	0.016	2.866	339	24	340	4	340	5	322	9	100
5.sSMPABC118	0.00	185340	9906	872	0.11	0	0.053	1.048	0.398	1.665	0.054	1.295	0.777	0.018	3.085	348	24	339	4	341	5	364	11	100
5.sSMPABC119	0.00	193203	10263	907	0.11	0	0.053	1.073	0.397	1.679	0.054	1.292	0.769	0.016	3.208	334	24	340	4	339	5	325	10	100
5.sSMPABC137	0.00	164975	8800	779	0.10	0	0.053	1.069	0.396	1.654	0.054	1.263	0.763	0.017	3.125	343	24	338	4	339	5	334	10	100
5.sSMPABC138	0.00	170362	9073	803	0.10	0	0.053	1.108	0.396	1.678	0.054	1.261	0.751	0.017	3.432	340	25	339	4	339	5	339	12	100

[a] *percentage of the common Pb on the ^{206}Pb*

[b] *Th/U ratios are calculated relative to BB reference zircon*

[c] *data corrected for background, within-run Pb/U fractionation (in case of ^{206}Pb/^{238}U) and common Pb using Stacey and Kramers (1975) model Pb composition*

[d] *Rho is the error correlation defined as the quotient of the propagated errors of the ^{206}Pb/^{238}U and the ^{207}/^{235}U ratio*

[e] *Concordance calculated as (^{206}Pb-^{238}U age/^{207}Pb-^{206}Pb age)*100*

CPS = count per second

LA-(MC)ICP-MS Lu-Hf zircon results data from Sample CA-02 (Aracê - Pedra Azul pluton)

Identifier	$^{176}Yb/^{177}Hf$ [a]	±2s	$^{176}Lu/^{177}Hf$ [a]	±2s	$^{178}Hf/^{177}Hf$	$^{180}Hf/^{177}Hf$	Sig_{Hf} [b] (V)	$^{176}Hf/^{177}Hf$	±2s [c]	$^{176}Hf/^{177}Hf_{(t)}$ [d]	eHf(t) [d]	±2s [c]	T_{DM} [e] (Ga)	U-Pb identifier	Age (Ma)[f]	±2σ
seq0133.dat	0.027697	22.4	0.000568	3.4	1.467218	1.886820	11.6	0.281815	16.1	0.281810	-23.0	0.86	2.42	5.sSMPABC016	518	10
seq0134.dat	0.025125	22.8	0.000536	3.6	1.467213	1.886813	11.0	0.281793	15.4	0.281787	-23.4	0.86	2.46	5.sSMPABC032	535	10
seq0136.dat	0.022618	18.3	0.000507	3.0	1.467192	1.886856	14.3	0.281808	17.7	0.281802	-21.6	0.85	2.41	5.sSMPABC057	589	9
seq0137.dat	0.031431	25.3	0.000829	5.0	1.467302	1.886773	8.2	0.281832	17.5	0.281824	-22.5	0.86	2.40	5.sSMPABC055	514	11
seq0138.dat	0.028823	23.7	0.000604	3.9	1.467207	1.886860	11.4	0.281817	20.8	0.281811	-22.7	0.86	2.42	5.sSMPABC043	529	9
seq0139.dat	0.031099	25.2	0.000696	4.2	1.467180	1.886884	13.9	0.281829	16.1	0.281822	-22.4	0.86	2.40	5.sSMPABC041	521	8
seq0140.dat	0.019000	17.3	0.000403	2.7	1.467190	1.886797	12.2	0.281787	15.4	0.281783	-23.6	0.84	2.47	5.sSMPABC037	533	10
seq0141.dat	0.034292	29.9	0.000705	4.8	1.467247	1.887009	11.5	0.281837	20.6	0.281830	-22.1	0.88	2.38	5.sSMPABC006	526	8
seq0142.dat	0.031513	25.4	0.000623	3.7	1.467223	1.886834	9.3	0.281831	17.7	0.281825	-21.7	0.86	2.38	5.sSMPABC004	549	13
seq0143.dat	0.038164	30.8	0.000791	4.7	1.467172	1.886839	12.4	0.281838	17.5	0.281830	-22.2	0.88	2.38	5.sSMPABC010	520	8
seq0144.dat	0.017007	13.7	0.000345	2.1	1.467169	1.886787	13.8	0.281791	19.5	0.281787	-23.3	0.84	2.46	5.sSMPABC008	539	10
seq0145.dat	0.020851	16.8	0.000441	2.6	1.467212	1.886793	13.2	0.281857	20.5	0.281852	-21.3	0.84	2.34	5.sSMPABC029	524	7
seq0146.dat	0.016023	12.9	0.000341	2.0	1.467287	1.886905	12.0	0.281790	20.7	0.281786	-23.6	0.84	2.46	5.sSMPABC030	526	8
seq0147.dat	0.029978	24.1	0.000624	3.7	1.467216	1.886771	12.8	0.281849	18.3	0.281842	-20.8	0.86	2.34	5.sSMPABC059	565	8
seq0149.dat	0.036087	29.0	0.000764	4.6	1.467304	1.886825	12.9	0.281809	17.4	0.281802	-23.3	0.88	2.44	5.sSMPABC062	516	10
seq0150.dat	0.028839	23.1	0.000575	3.5	1.467188	1.886795	14.1	0.281812	14.6	0.281807	-22.8	0.86	2.42	5.sSMPABC045	530	9
seq0160.dat	0.046389	47.6	0.000939	7.1	1.467180	1.886748	9.0	0.281842	17.6	0.281833	-22.1	0.95	2.38	5.sSMPABC046	521	8
seq0161.dat	0.029790	25.4	0.000670	6.7	1.467193	1.886863	9.9	0.281890	20.5	0.281882	-18.6	0.86	2.25	5.sSMPABC053	601	9
seq0162.dat	0.019519	19.2	0.000401	3.2	1.467211	1.886832	14.4	0.281844	19.3	0.281840	-21.7	0.85	2.36	5.sSMPABC011	527	8
seq0163.dat	0.039212	36.9	0.000779	7.0	1.467203	1.886829	11.1	0.281858	27.2	0.281850	-21.4	0.90	2.34	5.sSMPABC079	522	9
seq0164.dat	0.025724	22.0	0.000538	4.0	1.467276	1.886850	13.0	0.281850	39.2	0.281844	-21.6	0.85	2.35	5.sSMPABC078	525	7
seq0165.dat	0.028021	25.3	0.000575	5.0	1.467261	1.886831	13.8	0.281825	25.4	0.281820	-22.5	0.86	2.40	5.sSMPABC094	523	9
seq0166.dat	0.027947	38.1	0.000554	5.8	1.467162	1.886731	12.4	0.281810	16.9	0.281805	-23.2	0.91	2.43	5.sSMPABC090	513	9
seq0167.dat	0.035022	29.7	0.000881	6.7	1.467185	1.886921	12.6	0.281829	14.5	0.281821	-22.5	0.88	2.40	5.sSMPABC089	523	9
seq0168.dat	0.034136	74.9	0.000732	14.9	1.467260	1.886708	11.7	0.281792	38.7	0.281785	-23.8	1.11	2.47	5.sSMPABC073	519	8
seq0169.dat	0.028609	29.1	0.000577	4.4	1.467185	1.886881	12.2	0.281811	24.3	0.281806	-23.1	0.88	2.43	5.sSMPABC070	520	9
								Average		0.281819	-22.3	0.88	2.40			

LA-(MC)ICP-MS Lu-Hf zircon results data from Sample CA-04 (Vitória pluton)

Identifier	$^{176}Yb/^{177}Hf$ [a]	±2s	$^{176}Lu/^{177}Hf$ [a]	±2s	$^{178}Hf/^{177}Hf$	$^{180}Hf/^{177}Hf$	Sig_{Hf} [b] (V)	$^{176}Hf/^{177}Hf$	±2s [c]	$^{176}Hf/^{177}Hf_{(t)}$ [d]	eHf(t) [d]	±2s [c]	T_{DM} [e] (Ga)	U-Pb identifier	Age (Ma)[f]	±2σ
seq0170.dat	0.014642	12.0	0.000303	1.8	1.467200	1.886787	17.7	0.282227	18.7	0.282224	-8.8	0.84	1.63	5.sSMPABC017	496	8
seq0171.dat	0.022399	18.6	0.000436	3.1	1.467226	1.886777	11.0	0.282237	15.0	0.282233	-7.5	0.85	1.60	5.sSMPABC015	541	9
seq0172.dat	0.019901	22.3	0.000400	5.2	1.467237	1.886785	17.4	0.282222	14.8	0.282218	-8.7	0.86	1.64	5.sSMPABC011	509	8
seq0173.dat	0.022483	21.2	0.000438	3.4	1.467197	1.886786	12.1	0.282226	14.4	0.282222	-8.6	0.85	1.63	5.sSMPABC107	510	8
seq0174.dat	0.015054	12.3	0.000430	2.6	1.467250	1.886659	9.1	0.282190	17.4	0.282186	-10.3	0.84	1.71	5.sSMPABC100	490	8
seq0175.dat	0.014198	14.4	0.000291	2.3	1.467237	1.886893	15.0	0.282188	19.1	0.282186	-10.2	0.84	1.71	5.sSMPABC018	492	8
seq0176.dat	0.037325	30.4	0.000722	4.4	1.467222	1.886819	14.5	0.282245	14.1	0.282239	-8.3	0.88	1.61	5.sSMPABC097	496	9
seq0177.dat	0.017419	14.5	0.000452	2.8	1.467246	1.886815	9.9	0.282185	14.5	0.282181	-10.1	0.84	1.71	5.sSMPABC090	507	8
seq0178.dat	0.016682	14.8	0.000347	2.6	1.467195	1.886922	20.0	0.282228	45.8	0.282224	-8.4	0.84	1.63	5.sSMPABC087	511	8
seq0179.dat	0.015683	14.5	0.000303	2.9	1.467220	1.886782	15.8	0.282230	23.4	0.282227	-8.6	0.84	1.63	5.sSMPABC067	502	8
seq0180.dat	0.014629	12.0	0.000361	2.6	1.467213	1.886721	18.6	0.282222	22.7	0.282219	-8.8	0.84	1.64	5.sSMPABC068	506	8
seq0181.dat	0.013994	12.1	0.000275	1.8	1.467272	1.886750	14.9	0.282221	18.3	0.282219	-9.1	0.84	1.65	5.sSMPABC114	490	9
seq0182.dat	0.025906	25.6	0.000507	5.3	1.467277	1.886900	10.6	0.282206	30.4	0.282201	-8.8	0.87	1.67	5.sSMPABC074	530	9
seq0183.dat	0.014178	20.5	0.000284	3.8	1.467246	1.886839	14.0	0.282215	14.6	0.282213	-8.9	0.85	1.65	5.sSMPABC055	507	8
seq0184.dat	0.015567	14.5	0.000319	2.4	1.467213	1.886728	12.5	0.282233	19.5	0.282230	-8.4	0.84	1.62	5.sSMPABC054	505	8
seq0185.dat	0.019004	18.9	0.000372	3.1	1.467208	1.886898	14.5	0.282199	14.5	0.282195	-9.7	0.85	1.69	5.sSMPABC049	500	9
seq0187.dat	0.014439	13.2	0.000294	1.9	1.467227	1.886886	16.4	0.282218	26.7	0.282215	-8.9	0.84	1.65	5.sSMPABC051	507	8
seq0189.dat	0.017326	16.0	0.000356	2.5	1.467205	1.886820	15.8	0.282240	14.4	0.282236	-8.0	0.84	1.61	5.sSMPABC113	511	9
seq0190.dat	0.025863	20.9	0.000585	3.6	1.467235	1.886685	8.5	0.282254	17.7	0.282248	-7.4	0.85	1.58	5.sSMPABC038	519	8
seq0191.dat	0.017741	16.1	0.000355	2.4	1.467202	1.886841	12.6	0.282211	16.4	0.282208	-9.1	0.84	1.66	5.sSMPABC035	509	10
seq0192.dat	0.021433	18.0	0.000441	3.3	1.467268	1.886681	12.8	0.282241	12.9	0.282237	-8.3	0.85	1.61	5.sSMPABC027	498	9
seq0193.dat	0.012804	12.0	0.000283	2.1	1.467217	1.886873	15.5	0.282221	19.5	0.282219	-8.9	0.84	1.64	5.sSMPABC029	498	8
seq0194.dat	0.013188	11.6	0.000293	2.6	1.467170	1.886813	15.7	0.282213	21.8	0.282210	-9.2	0.84	1.66	5.sSMPABC117	501	8
seq0195.dat	0.012132	10.9	0.000257	2.1	1.467226	1.886708	13.8	0.282184	14.4	0.282182	-10.0	0.83	1.71	5.sSMPABC109	507	8
seq0196.dat	0.015904	13.4	0.000330	2.2	1.467227	1.886754	13.6	0.282233	27.8	0.282230	-8.3	0.84	1.62	5.sSMPABC057	507	8
seq0197.dat	0.014560	11.9	0.000289	1.9	1.467227	1.886912	13.8	0.282203	17.9	0.282200	-9.5	0.84	1.68	5.sSMPABC059	502	8

seq0198.dat	0.015246	14.2	0.000305	2.4	1.467211	1.886693	14.2	0.282251	20.3	0.282248	-7.7	0.84	1.59	5.sSMPABC047	506	8
								Average		0.282217	-8.8	0.84	1.65			

LA-(MC)ICP-MS Lu-Hf zircon results data from Sample CA-05 (Mestre Álvaro pluton)

Identifier	$^{176}Yb/^{177}Hf$ [a]	±2s	$^{176}Lu/^{177}Hf$ [a]	±2s	$^{178}Hf/^{177}Hf$	$^{180}Hf/^{177}Hf$	Sig_{Hf} [b] (V)	$^{176}Hf/^{177}Hf$	±2s [c]	$^{176}Hf/^{177}Hf_{(t)}$ [d]	eHf(t) [d]	±2s [c]	T_{DM} [e] (Ga)	U-Pb identifier	Age (Ma)[f]	±2σ
seq0255.dat	0.027070	22.6	0.000548	3.8	1.467213	1.886817	16.4	0.282258	19.2	0.282253	-7.4	0.86	1.57	5.sSMPABC010	514	9
seq0247.dat	0.039603	36.1	0.000843	6.3	1.467200	1.886892	14.7	0.282280	35.7	0.282272	-6.5	0.90	1.53	5.sSMPABC038	523	6
seq0249.dat	0.023601	37.6	0.000609	8.3	1.467251	1.886770	13.0	0.282259	21.1	0.282253	-7.2	0.91	1.57	5.sSMPABC041	523	8
seq0261.dat	0.021626	17.5	0.000444	2.7	1.467207	1.886765	15.2	0.282256	16.8	0.282252	-7.1	0.85	1.57	5.sSMPABC028-2	525	9
seq0268.dat	0.050558	45.9	0.001108	8.1	1.467234	1.886881	10.4	0.282282	21.6	0.282271	-6.5	0.95	1.53	5.sSMPABC030	526	7
seq0282.dat	0.026932	36.2	0.000519	4.9	1.467210	1.886889	14.4	0.282266	25.3	0.282261	-6.8	0.90	1.55	5.sSMPABC037-2	526	10
seq0278.dat	0.035287	29.5	0.000759	4.9	1.467290	1.886855	14.3	0.282261	17.3	0.282253	-7.1	0.88	1.57	5.sSMPABC029-2	526	8
seq0258.dat	0.035555	28.7	0.000745	4.5	1.467270	1.886854	16.6	0.282212	17.0	0.282204	-8.8	0.88	1.66	5.sSMPABC015	526	6
seq0262.dat	0.023153	18.6	0.000474	2.8	1.467160	1.886846	15.0	0.282239	19.7	0.282234	-7.7	0.85	1.60	5.sSMPABC07-2	527	9
seq0256.dat	0.036479	29.3	0.000739	4.4	1.467244	1.886845	18.4	0.282239	20.4	0.282232	-7.8	0.88	1.61	5.sSMPABC017	527	7
seq0272.dat	0.022009	18.2	0.000438	2.8	1.467192	1.886831	13.6	0.282262	22.7	0.282257	-6.9	0.85	1.56	5.sSMPABC011-2	528	8
seq0260.dat	0.020675	16.6	0.000428	2.6	1.467211	1.886858	16.0	0.282235	19.0	0.282231	-7.8	0.84	1.61	5.sSMPABC088	529	8
seq0263.dat	0.055745	44.8	0.001197	7.2	1.467207	1.886969	15.7	0.282293	20.4	0.282281	-6.0	0.94	1.51	5.sSMPABC026-2	529	9
seq0250.dat	0.042683	38.0	0.000845	5.7	1.467220	1.886885	17.4	0.282262	29.5	0.282254	-7.0	0.91	1.56	5.sSMPABC044	529	6
seq0246.dat	0.048059	38.5	0.001105	7.9	1.467241	1.886769	15.5	0.282301	18.4	0.282290	-5.7	0.91	1.49	5.sSMPABC040	529	8
seq0276.dat	0.038183	30.6	0.000821	4.9	1.467210	1.886812	14.9	0.282233	17.4	0.282225	-8.0	0.88	1.62	5.sSMPABC014-2	530	7
seq0271.dat	0.052003	48.4	0.001104	9.4	1.467252	1.886899	14.4	0.282268	26.6	0.282257	-6.8	0.96	1.56	5.sSMPABC028	531	6
seq0269.dat	0.058424	50.2	0.001225	10.5	1.467214	1.886826	16.8	0.282262	18.5	0.282249	-6.2	0.97	1.56	5.sSMPABC020-2	574	8
seq0265.dat	0.070782	90.0	0.001602	17.8	1.467230	1.886877	12.3	0.282307	15.3	0.282290	-4.3	1.22	1.47	5.sSMPABC016-2	593	8
seq0254.dat	0.113393	98.8	0.002344	16.1	1.467183	1.886952	16.4	0.282416	20.6	0.282390	-0.7	1.29	1.27	5.sSMPABC012	594	7
seq0257.dat	0.021636	17.5	0.000430	2.6	1.467240	1.886916	15.7	0.282244	19.5	0.282240	-6.0	0.85	1.57	5.sSMPABC068	595	7
sseq0280.dat	0.047017	39.0	0.000935	6.4	1.467268	1.886909	9.3	0.282260	17.3	0.282250	-5.6	0.91	1.55	5.sSMPABC033-2	596	9
seq0252.dat	0.011703	11.8	0.000215	1.8	1.467243	1.886950	16.1	0.282237	30.9	0.282235	-6.1	0.84	1.57	5.sSMPABC057	597	7
seq0264.dat	0.068811	55.2	0.001486	8.9	1.467194	1.886859	14.5	0.282378	18.7	0.282361	-1.6	0.99	1.33	5.sSMPABC025	598	7

LA-(MC)ICP-MS Lu-Hf zircon results data from Sample CA-05 (Mestre Álvaro pluton)

Identifier	$^{176}Yb/^{177}Hf$ [a]	±2s	$^{176}Lu/^{177}Hf$ [a]	±2s	$^{178}Hf/^{177}Hf$	$^{180}Hf/^{177}Hf$	Sig_{Hf} [b] (V)	$^{176}Hf/^{177}Hf$	±2s [c]	$^{176}Hf/^{177}Hf_{(t)}$ [d]	eHf(t) [d]	±2s [c]	T_{DM} [e] (Ga)	U-Pb identifier	Age (Ma)[f]	±2σ
seq0274.dat	0.046612	38.3	0.001076	6.7	1.467173	1.886886	10.4	0.282276	15.5	0.282264	-5.0	0.91	1.52	5.sSMPABC102	599	8
seq0275.dat	0.057472	62.5	0.001359	12.5	1.467244	1.886850	13.7	0.282306	30.7	0.282290	-4.1	1.04	1.46	5.sSMPABC013-2	601	8
seq0259.dat	0.064220	51.7	0.001379	8.4	1.467244	1.886769	16.0	0.282296	16.1	0.282280	-4.4	0.98	1.48	5.sSMPABC085	601	7
seq0277.dat	0.061276	53.1	0.001276	8.9	1.467224	1.886843	15.7	0.282306	14.3	0.282292	-4.0	0.98	1.46	5.sSMPABC100	602	8
seq0266.dat	0.040657	34.0	0.000916	6.0	1.467160	1.886814	15.2	0.282269	20.9	0.282258	-5.2	0.89	1.53	5.sSMPABC018-2	602	8
seq0270.dat	0.033447	32.6	0.000717	5.4	1.467207	1.886836	15.4	0.282277	18.3	0.282269	-4.8	0.89	1.51	5.sSMPABC032	603	7
seq0248.dat	0.059564	48.9	0.001310	8.2	1.467221	1.886966	17.0	0.282302	16.0	0.282287	-4.1	0.96	1.47	5.sSMPABC033	607	7
seq0273.dat	0.034161	32.7	0.000728	6.0	1.467253	1.886754	12.7	0.282258	22.1	0.282250	-5.3	0.89	1.54	5.sSMPABC010-2	612	8
seq0253.dat	0.059950	50.2	0.001247	8.0	1.467184	1.886924	9.4	0.282249	16.9	0.282235	-5.8	0.97	1.57	5.sSMPABC018	614	8
seq0251.dat	0.032728	26.9	0.000785	5.1	1.467208	1.886758	8.8	0.282243	20.8	0.282234	-5.8	0.87	1.57	5.sSMPABC056	615	8
seq0267.dat	0.068138	55.2	0.001474	10.2	1.467245	1.886927	16.1	0.282322	16.6	0.282305	-3.3	0.99	1.43	5.sSMPABC019-2	615	8
seq0281.dat	0.075211	88.0	0.001673	16.6	1.467257	1.886865	9.1	0.282336	24.2	0.282316	-2.5	1.21	1.40	5.sSMPABC035-2	633	8
								Average younger ages		0.282252	-7.1	0.89	1.57			
								Average older ages		0.282279	-4.5	0.98	1.49			

[a] $^{176}Yb/^{177}Hf = (^{176}Yb/^{173}Yb)_{true} \times (^{173}Yb/^{177}Hf)_{meassured} \times (M_{173(Yb)}/M_{177(Hf)})^{b(Hf)}$, $b(Hf) = \ln(^{179}Hf/^{177}Hf_{true} / {}^{179}Hf/^{177}Hf_{measured}) / \ln(M_{179(Hf)}/M_{177(Hf)})$

M=mass of respective isotope. The $^{176}Lu/^{177}Hf$ were calculated in a similar way by using the $^{175}Lu/^{177}Hf$ and b(Yb)

[b] Mean Hf signal in volt

[c] Uncertainties are quadratic additions of the within-run precision and the daily reproducibility of the zircon standards. Uncertainties for the standard quoted at 2SD (2 standard deviation)

[d] Initial $^{176}Hf/^{177}Hf$ and ƐHf calculated using the apparent Pb-Pb ages of respective zircon domains, and the CHUR parameters: $^{176}Lu/^{177}Hf = 0.0336$, and $^{176}Hf/^{177}Hf = 0.282785$ (Bouvier et al., 2008)

[e] Two stage model age in billion years using the measured $^{176}Lu/^{177}Lu$ of each spot (first stage = age of zircon), a value of 0.0113 for the average continental crust (second stage), and a average MORB (DM) $^{176}Lu/^{177}Hf$ and $^{176}Hf/^{177}Hf$ of 0.0384 and 0.283164

[f] $^{206}Pb/^{238}U$ age determined by LA-ICP-MS

Spots in domains of dissolution–reprecipitation or overgrowth rims are in red letter

LA-(MC)ICP-MS Lu-Hf zircon results data from Sample CA-06 (Nova Venécia complex)

Identifier	$^{176}Yb/^{177}Hf$ [a]	±2s	$^{176}Lu/^{177}Hf$ [a]	±2s	$^{178}Hf/^{177}Hf$	$^{180}Hf/^{177}Hf$	Sig_{Hf} [b] (V)	$^{176}Hf/^{177}Hf$	±2s [c]	$^{176}Hf/^{177}Hf_{(t)}$ [d]	eHf(t) [d]	±2s [c]	T_{DM} [e] (Ga)	U-Pb identifier	Age (Ma)[f]	±2σ	Type
seq0178.dat	0.039421	40.3	0.000825	6.5	1.467218	1.886989	14.5	0.281963	20.0	0.281951	-13.4	0.93	2.07	5.sSMPABC146	720	9	Detrital
seq0179.dat	0.016208	13.1	0.000358	2.3	1.467203	1.886774	13.6	0.282049	17.8	0.282045	-12.8	0.85	1.94	5.sSMPABC148	599	7	Overgrowth
seq0180.dat	0.045137	44.6	0.001005	7.0	1.467236	1.886933	14.9	0.282106	17.6	0.282095	-11.5	0.95	1.85	5.sSMPABC142	579	7	Anatectic
seq0181.dat	0.037070	29.8	0.000748	4.6	1.467225	1.886837	14.7	0.282026	21.0	0.282017	-13.5	0.89	1.99	5.sSMPABC153	611	7	Detrital
seq0182.dat	0.029649	24.4	0.000620	3.9	1.467216	1.886937	14.9	0.282159	20.5	0.282151	-7.8	0.88	1.71	5.sSMPABC055	653	8	Detrital
seq0183.dat	0.056190	57.2	0.001582	12.6	1.467225	1.886773	16.5	0.282067	17.1	0.282051	-13.4	1.02	1.94	5.sSMPABC054	565	7	Dissolution–recrystallization
seq0184.dat	0.069560	61.2	0.001679	10.9	1.467217	1.886915	15.5	0.282059	25.3	0.282039	-12.3	1.04	1.94	5.sSMPABC038	633	14	Detrital
seq0185.dat	0.054030	45.5	0.001228	9.8	1.467248	1.886778	10.9	0.282122	19.1	0.282108	-11.0	0.96	1.83	5.sSMPABC039	578	7	Dissolution–recrystallization
seq0186.dat	0.038591	31.9	0.000792	5.2	1.467244	1.887019	12.7	0.282166	15.0	0.282157	-8.6	0.90	1.72	5.sSMPABC058	609	7	Detrital
seq0187.dat	0.060719	48.8	0.001418	8.5	1.467227	1.886723	11.8	0.282187	16.3	0.282170	-7.1	0.97	1.68	5.sSMPABC063	656	8	Detrital
seq0188.dat	0.055661	44.7	0.001182	7.1	1.467226	1.886795	12.2	0.282038	16.8	0.282024	-13.1	0.95	1.97	5.sSMPABC072	622	7	Detrital
seq0189.dat	0.024151	19.4	0.000506	3.0	1.467167	1.886788	13.1	0.282062	20.1	0.282056	-12.8	0.86	1.93	5.sSMPABC031	581	7	Dissolution–recrystallization
seq0190.dat	0.059652	48.1	0.001167	7.0	1.467196	1.886792	12.8	0.282153	13.9	0.282140	-9.6	0.97	1.76	5.sSMPABC070	593	7	Detrital
seq0191.dat	0.063546	58.6	0.001770	11.8	1.467347	1.886700	7.3	0.282048	15.6	0.282027	-13.0	1.03	1.97	5.sSMPABC102	619	8	Detrital
seq0192.dat	0.024991	20.4	0.000557	3.4	1.467265	1.886933	11.4	0.282090	15.5	0.282083	-10.7	0.87	1.85	5.sSMPABC016	633	9	Detrital
seq0193.dat	0.023137	18.6	0.000505	3.0	1.467223	1.886863	17.2	0.281936	16.7	0.281928	-13.3	0.86	2.10	5.sSMPABC017	762	9	Detrital
seq0194.dat	0.032857	26.5	0.000646	3.9	1.467193	1.886903	12.1	0.282072	20.8	0.282065	-11.4	0.88	1.89	5.sSMPABC018	631	7	Detrital
seq0195.dat	0.045452	36.5	0.000939	5.6	1.467240	1.887043	11.5	0.282016	18.5	0.282005	-14.1	0.92	2.01	5.sSMPABC008	604	7	Detrital
seq0196.dat	0.031374	37.5	0.000639	7.3	1.467184	1.886883	13.4	0.282141	18.1	0.282133	-8.9	0.92	1.76	5.sSMPABC006	633	7	Detrital
seq0197.dat	0.002880	2.7	0.000058	0.5	1.467234	1.886918	15.3	0.282030	14.5	0.282030	-12.8	0.84	1.96	5.sSMPABC010	624	8	Detrital
seq0198.dat	0.037036	34.0	0.000788	6.0	1.467169	1.886796	13.3	0.282102	19.9	0.282095	-12.9	0.91	1.88	5.sSMPABC049	519	7	Dissolution–recrystallization
seq0199.dat	0.056764	58.3	0.001490	11.9	1.467200	1.886794	10.3	0.282023	18.0	0.282006	-14.2	1.02	2.01	5.sSMPABC034	600	7	Detrital
seq0200.dat	0.069698	65.7	0.001516	12.1	1.467241	1.886978	7.6	0.282111	21.4	0.282094	-10.9	1.07	1.84	5.sSMPABC050	607	7	Detrital
seq0201.dat	0.024714	26.4	0.000634	5.4	1.467263	1.886917	5.5	0.282070	15.8	0.282063	-12.0	0.88	1.90	5.sSMPABC051	607	8	Detrital
seq0202.dat	0.027353	26.1	0.000560	4.8	1.467238	1.886979	13.3	0.282051	18.4	0.282045	-13.0	0.88	1.94	5.sSMPABC152	591	8	Detrital
seq0203.dat	0.032575	28.7	0.000662	4.7	1.467223	1.886873	11.0	0.282180	19.1	0.282173	-7.9	0.89	1.69	5.sSMPABC149	616	8	Detrital
seq0204.dat	0.030721	27.3	0.000601	4.0	1.467220	1.886937	11.7	0.282052	25.8	0.282046	-13.0	0.88	1.94	5.sSMPABC150	588	8	Anatectic

LA-(MC)ICP-MS Lu-Hf zircon results data from Sample CA-06 (Nova Venécia complex)

Identifier	$^{176}Yb/^{177}Hf$ [a]	±2s	$^{176}Lu/^{177}Hf$ [a]	±2s	$^{178}Hf/^{177}Hf$	$^{180}Hf/^{177}Hf$	Sig_{Hf} [b] (V)	$^{176}Hf/^{177}Hf$	±2s [c]	$^{176}Hf/^{177}Hf_{(t)}$ [d]	eHf(t) [d]	±2s [c]	T_{DM} [e] (Ga)	U-Pb identifier	Age (Ma)[f]	±2σ	Type
seq0205.dat	0.054367	47.1	0.001389	9.6	1.467234	1.886735	12.1	0.282070	15.1	0.282056	-13.5	0.96	1.94	5.sSMPABC131	551	7	Anatectic
seq0206.dat	0.050911	43.3	0.001327	9.1	1.467223	1.886688	8.8	0.282074	19.9	0.282061	-13.7	0.95	1.94	5.sSMPABC091	533	6	Anatectic
seq0207.dat	0.075484	62.8	0.001622	10.0	1.467225	1.886899	13.8	0.282061	14.8	0.282046	-15.5	1.05	1.99	5.sSMPABC073	479	6	Dissolution–recrystallization
seq0208.dat	0.041891	39.7	0.000857	6.8	1.467227	1.886905	11.2	0.282037	17.3	0.282027	-13.2	0.93	1.97	5.sSMPABC090	608	8	Detrital
seq0209.dat	0.057916	51.9	0.001261	9.2	1.467202	1.886831	14.7	0.282077	18.5	0.282063	-12.0	0.99	1.90	5.sSMPABC089	608	7	Detrital
seq0210.dat	0.027606	22.5	0.000611	3.7	1.467238	1.886991	14.5	0.282097	18.0	0.282090	-10.0	0.87	1.83	5.sSMPABC092	655	8	Detrital
seq0211.dat	0.016984	27.6	0.000349	4.8	1.467243	1.886819	12.2	0.282113	19.6	0.282109	-9.9	0.89	1.81	5.sSMPABC107	628	8	Detrital
seq0212.dat	0.027370	22.9	0.000580	3.6	1.467320	1.886924	7.6	0.282086	20.4	0.282080	-11.7	0.87	1.88	5.sSMPABC110	592	7	Detrital
seq0213.dat	0.056299	47.4	0.001210	7.8	1.467238	1.886882	12.4	0.281867	17.5	0.281848	-14.7	0.97	2.23	5.sSMPABC069	828	11	Detrital
seq0214.dat	0.057104	46.7	0.001201	7.3	1.467204	1.886895	10.8	0.282121	17.6	0.282107	-9.9	0.96	1.81	5.sSMPABC112	634	7	Detrital
seq0215.dat	0.048196	38.7	0.000927	5.6	1.467209	1.886917	10.6	0.282035	20.4	0.282025	-13.8	0.93	1.98	5.sSMPABC113	586	7	Anatectic
seq0216.dat	0.042889	35.5	0.000871	5.9	1.467221	1.886847	13.0	0.282158	21.8	0.282147	-7.9	0.91	1.72	5.sSMPABC122	656	8	Detrital
seq0217.dat	0.058271	46.8	0.001239	7.5	1.467152	1.886812	7.9	0.281907	21.9	0.281889	-15.0	0.96	2.18	5.sSMPABC115	747	9	Detrital
seq0218.dat	0.065932	52.8	0.001564	9.4	1.467252	1.886920	11.4	0.282013	21.3	0.281995	-14.0	0.99	2.03	5.sSMPABC124	627	8	Detrital
seq0219.dat	0.032457	29.8	0.000720	5.1	1.467219	1.886959	13.4	0.282096	22.9	0.282088	-11.1	0.89	1.85	5.sSMPABC095	607	7	Detrital
seq0220.dat	0.047566	38.7	0.001031	6.3	1.467206	1.886977	11.7	0.282117	21.0	0.282105	-10.5	0.93	1.82	5.sSMPABC096	610	7	Detrital
seq0221.dat	0.022127	17.8	0.000487	3.0	1.467183	1.886918	16.3	0.282115	22.9	0.282110	-10.7	0.86	1.82	5.sSMPABC087	592	8	Detrital

LA-(MC)ICP-MS Lu-Hf zircon results data from Sample CA-07 (Ataléia suite)

Identifier	$^{176}Yb/^{177}Hf$ [a]	±2s	$^{176}Lu/^{177}Hf$ [a]	±2s	$^{178}Hf/^{177}Hf$	$^{180}Hf/^{177}Hf$	Sig_{Hf} [b] (V)	$^{176}Hf/^{177}Hf$	±2s [c]	$^{176}Hf/^{177}Hf_{(t)}$ [d]	eHf(t) [d]	±2s [c]	T_{DM} [e] (Ga)	U-Pb identifier	Age (Ma)[f]	±2σ	Type
seq0084.dat	0.047594	38.2	0.001081	6.5	1.467230	1.886859	14.4	0.282253	17.9	0.282240	-4.6	0.91	1.54	5.sSMPABC158	658	8	Inherited
seq0085.dat	0.057712	46.3	0.001308	7.9	1.467225	1.886822	12.3	0.282283	18.6	0.282265	-2.0	0.95	1.46	5.sSMPABC159	734	9	Inherited
seq0086.dat	0.049718	40.9	0.001059	6.4	1.467160	1.886786	16.9	0.282289	13.4	0.282274	-1.7	0.92	1.44	5.sSMPABC160	735	10	Inherited
seq0087.dat	0.045251	37.9	0.001164	7.1	1.467282	1.886674	11.5	0.282291	15.0	0.282276	-2.8	0.91	1.46	5.sSMPABC161	681	9	Inherited
seq0088.dat	0.071490	58.0	0.001552	10.0	1.467244	1.886715	16.4	0.282318	16.8	0.282300	-3.2	1.01	1.43	5.sSMPABC162	628	10	Inherited
seq0089.dat	0.069755	56.3	0.001510	9.1	1.467217	1.886840	17.4	0.282306	21.2	0.282289	-4.3	1.00	1.47	5.sSMPABC166	594	7	Magmatic
seq0090.dat	0.073640	59.4	0.001642	9.9	1.467221	1.886801	13.9	0.282325	20.8	0.282309	-5.0	1.02	1.46	5.sSMPABC167	532	6	Dissolution–recrystallization
seq0091.dat	0.047197	38.0	0.001040	6.2	1.467229	1.886822	12.9	0.282292	20.3	0.282280	-4.5	0.91	1.48	5.sSMPABC163	598	7	Magmatic
seq0092.dat	0.042813	36.9	0.000991	6.9	1.467247	1.886731	13.0	0.282274	15.2	0.282264	-5.9	0.91	1.53	5.sSMPABC011	562	7	Magmatic
seq0093.dat	0.073935	107.0	0.001646	23.9	1.467228	1.886889	16.4	0.282320	15.4	0.282303	-4.6	1.35	1.46	5.sSMPABC008	558	7	Metamorphic recrystallization
seq0094.dat	0.066005	56.4	0.001513	9.9	1.467250	1.886851	13.1	0.282316	17.3	0.282299	-4.4	1.00	1.46	5.sSMPABC047	574	8	Magmatic
seq0095.dat	0.052206	42.8	0.001430	10.4	1.467228	1.886850	10.4	0.282270	21.4	0.282254	-5.2	0.93	1.53	5.sSMPABC055	609	8	Magmatic
seq0096.dat	0.073645	64.2	0.001629	11.2	1.467225	1.886883	13.0	0.282298	13.6	0.282281	-5.2	1.05	1.50	5.sSMPABC170	566	7	Magmatic
seq0097.dat	0.063994	52.1	0.001411	9.4	1.467205	1.886892	15.1	0.282288	18.6	0.282273	-5.4	0.98	1.51	5.sSMPABC017	569	7	Magmatic
seq0098.dat	0.064214	78.3	0.001381	15.3	1.467222	1.886880	14.3	0.282278	15.7	0.282264	-5.9	1.14	1.53	5.sSMPABC029	564	7	Magmatic
seq0099.dat	0.048861	45.1	0.001124	7.7	1.467236	1.886783	13.9	0.282275	22.2	0.282263	-6.4	0.94	1.54	5.sSMPABC026	540	7	Dissolution–recrystallization
seq0100.dat	0.063535	64.2	0.001385	12.7	1.467275	1.886854	15.2	0.282292	18.9	0.282277	-5.0	1.05	1.50	5.sSMPABC027	584	8	Magmatic
seq0101.dat	0.037946	32.9	0.000833	5.7	1.467211	1.886872	14.3	0.282222	13.8	0.282213	-7.7	0.89	1.63	5.sSMPABC092	561	7	Magmatic
seq0102.dat	0.065205	65.2	0.001413	11.4	1.467271	1.886874	15.4	0.282263	14.2	0.282248	-6.7	1.05	1.57	5.sSMPABC032	552	7	Metamorphic recrystallization
seq0103.dat	0.049216	40.5	0.001139	7.0	1.467168	1.886813	13.7	0.282099	13.7	0.282082	-6.4	0.92	1.78	5.sSMPABC034	827	11	Inherited
seq0104.dat	0.052133	45.9	0.001198	8.1	1.467273	1.886780	9.1	0.282285	14.6	0.282272	-5.3	0.95	1.51	5.sSMPABC039	575	7	Magmatic
seq0105.dat	0.083206	78.6	0.001805	14.3	1.467218	1.886802	14.9	0.282335	19.2	0.282314	-3.2	1.14	1.42	5.sSMPABC012	605	8	Magmatic
seq0115.dat	0.031304	29.2	0.000715	5.5	1.467184	1.886772	15.6	0.282236	14.5	0.282229	-7.1	0.88	1.60	5.sSMPABC188	562	7	Magmatic
seq0116.dat	0.061783	55.3	0.001336	10.4	1.467209	1.886827	15.8	0.282305	16.1	0.282292	-5.4	0.99	1.49	5.sSMPABC190	539	7	Dissolution–recrystallization
seq0117.dat	0.050184	58.0	0.001123	11.7	1.467158	1.886829	12.6	0.282260	17.7	0.282247	-5.6	1.01	1.55	5.sSMPABC090	602	9	Magmatic
seq0118.dat	0.047298	39.1	0.001030	6.3	1.467211	1.887016	11.6	0.282252	14.2	0.282241	-7.0	0.91	1.58	5.sSMPABC208	551	8	Metamorphic recrystallization
seq0119.dat	0.069009	57.9	0.001486	9.5	1.467202	1.886762	17.2	0.282292	17.4	0.282277	-5.5	1.01	1.51	5.sSMPABC074	558	7	Metamorphic recrystallization

seq0120.dat	0.038579	31.0	0.000844	5.1	1.467209	1.886870	14.1	0.282262	19.7	0.282253	-5.7	0.88	1.54	5.sSMPABC082	587	8	Magmatic
seq0121.dat	0.040518	35.7	0.000919	6.8	1.467181	1.886798	11.5	0.282087	17.5	0.282077	-11.1	0.90	1.87	5.sSMPABC081	626	8	Inherited
seq0122.dat	0.068967	71.8	0.001530	14.5	1.467209	1.886806	8.6	0.282284	18.0	0.282267	-5.0	1.10	1.51	5.sSMPABC084	600	8	Magmatic
seq0123.dat	0.038708	31.5	0.000854	5.3	1.467239	1.886841	15.8	0.282199	14.7	0.282189	-7.5	0.88	1.66	5.sSMPABC085	609	9	Magmatic
seq0124.dat	0.045711	51.2	0.000985	10.8	1.467216	1.886836	14.4	0.282260	20.1	0.282250	-6.0	0.97	1.55	5.sSMPABC086	579	8	Magmatic
seq0125.dat	0.059627	53.0	0.001325	8.3	1.467192	1.886865	14.7	0.282287	16.0	0.282273	-6.4	0.98	1.53	5.sSMPABC072	526	7	Dissolution–recrystallization
seq0126.dat	0.051256	54.7	0.001096	11.4	1.467209	1.886887	12.7	0.282285	20.7	0.282273	-5.1	0.99	1.51	5.sSMPABC088	582	8	Magmatic
seq0127.dat	0.039711	34.1	0.000904	5.8	1.467185	1.886762	11.1	0.282240	23.9	0.282230	-6.8	0.89	1.59	5.sSMPABC014	576	8	Magmatic
seq0128.dat	0.042023	33.7	0.000965	6.0	1.467263	1.886822	12.7	0.282259	18.3	0.282248	-6.3	0.89	1.56	5.sSMPABC201	569	7	Magmatic
seq0129.dat	0.019568	15.7	0.000425	2.5	1.467257	1.886844	16.0	0.282215	17.2	0.282211	-8.1	0.84	1.64	5.sSMPABC060	546	7	Dissolution–recrystallization
seq0130.dat	0.071093	57.0	0.001549	9.3	1.467288	1.886900	11.6	0.282338	20.7	0.282321	-4.0	1.00	1.42	5.sSMPABC199	558	7	Metamorphic recrystallization
seq0131.dat	0.056490	45.3	0.001270	7.6	1.467179	1.886847	14.4	0.282277	17.4	0.282264	-6.1	0.94	1.53	5.sSMPABC091	555	7	Metamorphic recrystallization
seq0132.dat	0.073611	60.2	0.001650	9.9	1.467215	1.886766	13.3	0.282289	14.3	0.282272	-5.9	1.02	1.52	5.sSMPABC196	547	7	Dissolution–recrystallization

LA-(MC)ICP-MS Lu-Hf zircon results data from Sample CA-09 (Nova Venécia complex)

Identifier	$^{176}Yb/^{177}Hf$ [a]	±2s	$^{176}Lu/^{177}Hf$ [a]	±2s	$^{178}Hf/^{177}Hf$	$^{180}Hf/^{177}Hf$	Sig_{Hf} [b] (V)	$^{176}Hf/^{177}Hf$	±2s [c]	$^{176}Hf/^{177}Hf_{(t)}$ [d]	eHf(t) [d]	±2s [c]	T_{DM} [e] (Ga)	U-Pb identifier	Age (Ma)[f]	±2σ	Type
seq0121.dat	0.029433	23.6	0.000642	3.9	1.467230	1.886858	11.6	0.281968	17.4	0.281960	-15.8	0.87	2.10	5.sSMPABC006	598	8	Detrital
seq0122.dat	0.047682	38.3	0.001030	6.2	1.467274	1.886932	9.8	0.281908	15.8	0.281892	-13.2	0.92	2.15	5.sSMPABC022	822	10	Detrital
seq0123.dat	0.055843	45.1	0.001219	7.3	1.467264	1.886857	13.5	0.282100	14.5	0.282084	-9.8	0.96	1.83	5.sSMPABC014	673	7	Detrital
seq0124.dat	0.064838	52.1	0.001336	8.1	1.467203	1.886907	10.9	0.282138	12.9	0.282123	-10.4	0.99	1.80	5.sSMPABC024	584	6	Detrital
seq0125.dat	0.034729	28.0	0.000831	5.1	1.467216	1.886749	13.2	0.282160	16.6	0.282150	-8.3	0.89	1.72	5.sSMPABC068	636	8	Detrital
seq0126.dat	0.089272	71.8	0.001813	10.9	1.467192	1.886948	12.7	0.282211	20.3	0.282183	-2.9	1.11	1.58	5.sSMPABC067	825	10	Detrital
seq0127.dat	0.024310	19.6	0.000662	4.0	1.467221	1.886808	7.8	0.281740	16.8	0.281730	-18.9	0.86	2.46	5.sSMPABC056	825	9	Detrital
seq0128.dat	0.034790	28.0	0.000719	4.3	1.467261	1.887059	10.4	0.282041	17.3	0.282032	-12.3	0.89	1.95	5.sSMPABC048	641	9	Detrital
seq0129.dat	0.019481	15.7	0.000505	3.0	1.467181	1.886645	8.8	0.282118	16.4	0.282111	-9.0	0.86	1.79	5.sSMPABC049	665	7	Detrital
seq0130.dat	0.027230	21.9	0.000628	3.8	1.467206	1.886931	14.6	0.282027	25.2	0.282016	-7.4	0.87	1.88	5.sSMPABC073	885	10	Detrital
seq0131.dat	0.056813	62.5	0.001180	13.5	1.467225	1.886821	7.9	0.282327	16.9	0.282314	-3.0	1.05	1.41	5.sSMPABC053	613	7	Detrital
seq0132.dat	0.042315	34.4	0.000934	6.0	1.467223	1.886919	12.7	0.282032	16.2	0.282022	-13.4	0.91	1.98	5.sSMPABC076	612	7	Detrital

LA-(MC)ICP-MS Lu-Hf zircon results data from Sample CA-09 (Nova Venécia complex)

Identifier	$^{176}Yb/^{177}Hf$ [a]	±2s	$^{176}Lu/^{177}Hf$ [a]	±2s	$^{178}Hf/^{177}Hf$	$^{180}Hf/^{177}Hf$	Sig_{Hf} [b] (V)	$^{176}Hf/^{177}Hf$	±2s [c]	$^{176}Hf/^{177}Hf_{(t)}$ [d]	eHf(t) [d]	±2s [c]	T_{DM} [e] (Ga)	U-Pb identifier	Age (Ma)[f]	±2σ	Type
seq0133.dat	0.043573	35.5	0.000861	5.2	1.467192	1.886920	14.5	0.281902	13.4	0.281891	-16.2	0.91	2.20	5.sSMPABC083	690	9	Detrital
seq0134.dat	0.023313	20.2	0.000468	3.2	1.467220	1.886837	12.9	0.282068	17.3	0.282060	-4.4	0.87	1.77	5.sSMPABC157	951	11	Detrital
seq0135.dat	0.054100	44.8	0.001125	7.1	1.467165	1.886795	6.9	0.282097	15.9	0.282084	-11.7	0.95	1.87	5.sSMPABC181	559	7	Anatectic
seq0136.dat	0.063083	52.5	0.001360	8.3	1.467251	1.886930	12.4	0.281654	30.9	0.281631	-20.8	0.99	2.62	5.sSMPABC179	894	15	Detrital
seq0137.dat	0.059099	63.1	0.001150	8.9	1.467219	1.886904	8.0	0.282215	25.8	0.282201	-6.1	1.05	1.62	5.sSMPABC131	653	8	Detrital
seq0138.dat	0.030600	24.6	0.000626	3.8	1.467239	1.886862	13.2	0.282046	29.7	0.282036	-9.1	0.88	1.88	5.sSMPABC176	780	9	Detrital
seq0139.dat	0.056942	55.5	0.001279	11.4	1.467200	1.887020	13.2	0.282042	26.6	0.282028	-14.3	1.01	1.99	5.sSMPABC178	559	7	Anatectic
seq0140.dat	0.040123	44.6	0.000829	7.0	1.467238	1.886936	13.7	0.282108	25.7	0.282098	-10.2	0.95	1.83	5.sSMPABC170	631	7	Detrital
seq0141.dat	0.035530	28.7	0.000765	5.0	1.467222	1.886969	13.6	0.282026	21.8	0.282017	-12.9	0.89	1.98	5.sSMPABC164	641	8	Detrital
seq0142.dat	0.041147	35.8	0.000935	5.9	1.467159	1.886807	14.1	0.282068	24.8	0.282057	-11.8	0.91	1.91	5.sSMPABC166	626	7	Detrital
seq0143.dat	0.076980	67.5	0.001721	11.1	1.467190	1.886833	13.8	0.281845	24.9	0.281816	-14.3	1.08	2.26	5.sSMPABC167	891	10	Detrital
seq0144.dat	0.044524	63.3	0.000957	10.4	1.467248	1.886964	13.7	0.281838	32.4	0.281827	-19.3	1.05	2.34	5.sSMPABC041	656	7	Detrital
seq0145.dat	0.052153	43.0	0.001195	7.2	1.467204	1.886821	11.6	0.282157	28.2	0.282141	-7.1	0.95	1.71	5.sSMPABC123	703	14	Detrital
seq0146.dat	0.110959	103.4	0.002249	15.3	1.467256	1.886975	14.1	0.281772	24.2	0.281737	-18.6	1.33	2.44	5.sSMPABC128	825	10	Detrital
seq0147.dat	0.046237	41.1	0.000961	5.9	1.467190	1.886831	13.1	0.281734	18.3	0.281720	-21.2	0.94	2.51	5.sSMPABC127	736	9	Detrital
seq0148.dat	0.041679	33.8	0.000845	5.3	1.467225	1.886898	14.5	0.281958	26.3	0.281946	-12.4	0.91	2.06	5.sSMPABC130	773	9	Detrital
seq0149.dat	0.030716	30.4	0.000740	5.7	1.467251	1.886864	13.5	0.282253	21.0	0.282244	-4.8	0.90	1.54	5.sSMPABC138	644	7	Detrital
seq0150.dat	0.075117	61.8	0.001570	9.6	1.467228	1.886898	14.6	0.281811	29.6	0.281782	-13.9	1.04	2.30	5.sSMPABC141	966	11	Detrital
seq0151.dat	0.062756	51.8	0.001460	9.2	1.467260	1.886850	12.4	0.281973	27.3	0.281958	-17.0	0.99	2.13	5.sSMPABC152	548	6	Dissolution–recrystallization
seq0152.dat	0.071772	57.7	0.001511	9.4	1.467235	1.886799	11.6	0.281978	27.3	0.281961	-16.0	1.02	2.11	5.sSMPABC151	588	7	Detrital
seq0153.dat	0.043030	34.9	0.000958	5.9	1.467218	1.886927	11.4	0.281659	28.3	0.281644	-21.7	0.91	2.62	5.sSMPABC183	834	10	Detrital
seq0154.dat	0.056496	45.4	0.001216	7.6	1.467222	1.886939	13.0	0.281953	27.4	0.281936	-13.5	0.96	2.09	5.sSMPABC147	739	9	Detrital
seq0155.dat	0.090369	75.2	0.001870	11.4	1.467172	1.886908	7.9	0.282036	21.5	0.282014	-13.5	1.13	1.99	5.sSMPABC145	619	7	Detrital
seq0156.dat	0.028122	22.9	0.000581	3.5	1.467252	1.886922	13.6	0.282138	19.9	0.282131	-8.4	0.87	1.75	5.sSMPABC133	661	8	Detrital
seq0157.dat	0.060912	49.1	0.001334	8.1	1.467269	1.886806	11.9	0.281890	22.8	0.281868	-12.7	0.97	2.17	5.sSMPABC110	882	11	Detrital
seq0158.dat	0.061331	49.5	0.001340	8.4	1.467262	1.886877	7.8	0.281870	24.3	0.281851	-15.8	0.98	2.24	5.sSMPABC109	774	10	Detrital
seq0159.dat	0.025032	20.5	0.000494	3.0	1.467199	1.886957	15.6	0.281867	26.0	0.281858	-10.7	0.87	2.15	5.sSMPABC107	986	12	Detrital

LA-(MC)ICP-MS Lu-Hf zircon results data from Sample CA-09 (Nova Venécia complex)

Identifier	$^{176}Yb/^{177}Hf$ [a]	±2s	$^{176}Lu/^{177}Hf$ [a]	±2s	$^{178}Hf/^{177}Hf$	$^{180}Hf/^{177}Hf$	Sig_{Hf} [b] (V)	$^{176}Hf/^{177}Hf$	±2s [c]	$^{176}Hf/^{177}Hf_{(t)}$ [d]	eHf(t) [d]	±2s [c]	T_{DM} [e] (Ga)	U-Pb identifier	Age (Ma)[f]	±2σ	Type
seq0160.dat	0.033118	26.6	0.000750	4.5	1.467217	1.887000	12.2	0.282283	16.2	0.282275	-5.1	0.88	1.50	5.sSMPABC108	582	7	Detrital
seq0161.dat	0.040180	32.3	0.000870	5.2	1.467212	1.886938	10.8	0.282032	18.7	0.282022	-13.2	0.90	1.98	5.sSMPABC093	621	7	Detrital
seq0162.dat	0.029846	24.0	0.000663	4.0	1.467271	1.886762	12.1	0.282092	16.8	0.282084	-10.5	0.88	1.85	5.sSMPABC091	643	7	Detrital
seq0163.dat	0.022031	17.7	0.000428	2.6	1.467178	1.886903	12.1	0.282130	15.1	0.282126	-10.0	0.86	1.79	5.sSMPABC087	597	7	Detrital
seq0164.dat	0.035971	29.1	0.000751	4.5	1.467218	1.887006	8.0	0.281686	14.1	0.281676	-22.9	0.89	2.59	5.sSMPABC102	734	9	Detrital
seq0165.dat	0.072229	60.0	0.001677	10.2	1.467170	1.886821	11.9	0.282204	15.0	0.282184	-6.7	1.03	1.65	5.sSMPABC101	652	7	Detrital
seq0166.dat	0.048061	38.7	0.000990	5.9	1.467228	1.886960	13.5	0.281922	19.9	0.281910	-16.6	0.93	2.18	5.sSMPABC111	644	7	Detrital

LA-(MC)ICP-MS Lu-Hf zircon results data from Sample CA-10 (Nova Venécia complex)

Identifier	$^{176}Yb/^{177}Hf$ [a]	±2s	$^{176}Lu/^{177}Hf$ [a]	±2s	$^{178}Hf/^{177}Hf$	$^{180}Hf/^{177}Hf$	Sig_{Hf} [b] (V)	$^{176}Hf/^{177}Hf$	±2s [c]	$^{176}Hf/^{177}Hf_{(t)}$ [d]	eHf(t) [d]	±2s [c]	T_{DM} [e] (Ga)	U-Pb identifier	Age (Ma)[f]	±2σ	Type
seq0068.dat	0.064511	52.1	0.001242	7.5	1.467218	1.886912	12.1	0.282069	18.7	0.282053	-10.7	0.99	1.89	5.sSMPABC046	679	8	Detrital
seq0069.dat	0.021147	17.1	0.000478	2.9	1.467188	1.886744	12.0	0.282383	18.5	0.282376	4.1	0.86	1.20	5.sSMPABC047	832	10	Detrital
seq0070.dat	0.053513	43.1	0.001094	6.6	1.467237	1.887036	7.9	0.281933	17.5	0.281920	-16.6	0.95	2.17	5.sSMPABC048	629	7	Detrital
seq0071.dat	0.039295	31.7	0.000770	4.6	1.467268	1.886948	10.4	0.282097	16.7	0.282088	-10.6	0.90	1.85	5.sSMPABC039	630	9	Detrital
seq0072.dat	0.068070	58.3	0.001427	10.2	1.467253	1.886913	14.6	0.282069	16.8	0.282055	-13.8	1.02	1.95	5.sSMPABC038	538	6	Dissolution–recrystallization
seq0073.dat	0.033033	27.2	0.000717	4.5	1.467212	1.886849	12.6	0.282021	16.0	0.282013	-14.3	0.88	2.01	5.sSMPABC035	584	7	Detrital
seq0074.dat	0.025591	20.5	0.000572	3.4	1.467207	1.886792	13.4	0.282038	23.7	0.282028	-7.3	0.87	1.86	5.sSMPABC049	873	11	Detrital
seq0075.dat	0.062420	50.1	0.001249	7.5	1.467232	1.886951	8.5	0.282198	21.1	0.282182	-6.0	0.98	1.64	5.sSMPABC051	685	8	Detrital
seq0077.dat	0.064666	52.1	0.001288	7.7	1.467230	1.886929	14.4	0.281873	13.9	0.281851	-12.6	0.99	2.19	5.sSMPABC053	916	11	Detrital
seq0078.dat	0.059963	55.3	0.001216	8.1	1.467167	1.886963	7.8	0.282167	15.6	0.282153	-9.2	1.01	1.74	5.sSMPABC063	589	7	Detrital
seq0079.dat	0.060318	48.5	0.001311	7.9	1.467259	1.886930	13.2	0.282079	20.5	0.282064	-12.1	0.97	1.90	5.sSMPABC107	603	7	Detrital
seq0080.dat	0.048979	39.4	0.001022	6.1	1.467237	1.886816	13.5	0.282236	20.7	0.282224	-6.6	0.93	1.60	5.sSMPABC067	592	7	Detrital
seq0081.dat	0.028251	22.7	0.000593	3.6	1.467231	1.886781	14.3	0.282078	18.3	0.282072	-11.7	0.87	1.89	5.sSMPABC068	608	7	Detrital
seq0082.dat	0.073672	59.3	0.001506	9.0	1.467196	1.886771	15.8	0.282033	15.0	0.282017	-14.6	1.03	2.01	5.sSMPABC106	566	6	Dissolution–recrystallization
seq0083.dat	0.040390	32.5	0.000812	4.9	1.467220	1.886849	14.2	0.281912	17.4	0.281903	-17.7	0.90	2.21	5.sSMPABC075	603	8	Detrital

LA-(MC)ICP-MS Lu-Hf zircon results data from Sample CA-10 (Nova Venécia complex)

Identifier	$^{176}Yb/^{177}Hf$ [a]	±2s	$^{176}Lu/^{177}Hf$ [a]	±2s	$^{178}Hf/^{177}Hf$	$^{180}Hf/^{177}Hf$	Sig_{Hf} [b] (V)	$^{176}Hf/^{177}Hf$	±2s [c]	$^{176}Hf/^{177}Hf_{(t)}$ [d]	eHf(t) [d]	±2s [c]	T_{DM} [e] (Ga)	U-Pb identifier	Age (Ma)[f]	±2σ	Type
seq0084.dat	0.109820	88.0	0.002549	15.4	1.467219	1.886783	21.5	0.281727	14.6	0.281697	-24.4	1.22	2.59	5.sSMPABC082	633	7	Detrital
seq0085.dat	0.071336	57.5	0.001561	9.4	1.467169	1.887036	7.9	0.281558	15.3	0.281530	-23.1	1.02	2.79	5.sSMPABC105	952	11	Detrital
seq0086.dat	0.065709	53.8	0.001671	10.2	1.467248	1.886668	9.6	0.281880	16.4	0.281859	-18.5	1.00	2.28	5.sSMPABC073	640	8	Detrital
seq0087.dat	0.021783	21.5	0.000427	3.6	1.467246	1.886743	13.0	0.282179	17.0	0.282175	-10.5	0.87	1.73	5.sSMPABC115	499	8	Dissolution–recrystallization
seq0088.dat	0.070402	56.4	0.001533	9.3	1.467234	1.886911	12.5	0.281904	14.5	0.281887	-18.2	1.01	2.24	5.sSMPABC126	610	7	Detrital
seq0089.dat	0.037273	30.0	0.000780	4.7	1.467211	1.886751	11.0	0.281996	17.0	0.281986	-12.9	0.89	2.02	5.sSMPABC025	687	8	Detrital
seq0090.dat	0.055935	44.9	0.001219	7.3	1.467214	1.886863	13.3	0.281890	18.0	0.281876	-18.4	0.95	2.26	5.sSMPABC144	615	7	Detrital
seq0091.dat	0.055712	44.7	0.001145	6.9	1.467202	1.886900	12.2	0.282235	17.3	0.282220	-4.8	0.95	1.57	5.sSMPABC026	681	8	Detrital
seq0092.dat	0.050931	41.0	0.001108	6.6	1.467222	1.886873	13.0	0.281680	20.1	0.281665	-23.1	0.93	2.61	5.sSMPABC029	741	9	Detrital
seq0093.dat	0.090873	77.3	0.002031	13.9	1.467188	1.886982	11.0	0.281242	19.9	0.281214	-39.2	1.14	3.47	5.sSMPABC015	736	9	Detrital
seq0094.dat	0.087285	71.8	0.001841	11.3	1.467220	1.886850	11.3	0.281936	25.0	0.281911	-15.3	1.11	2.16	5.sSMPABC016	701	8	Detrital
seq0095.dat	0.016172	14.1	0.000297	2.1	1.467207	1.886915	16.3	0.282018	25.5	0.282014	-10.6	0.85	1.94	5.sSMPABC018	745	9	Detrital
seq0096.dat	0.071179	57.7	0.001453	8.9	1.467204	1.886969	15.9	0.281899	29.7	0.281876	-12.8	1.02	2.16	5.sSMPABC139	868	10	Detrital
seq0097.dat	0.113822	95.6	0.002246	16.3	1.467175	1.886786	13.8	0.281747	24.2	0.281707	-17.1	1.27	2.45	5.sSMPABC009	942	11	Detrital
seq0098.dat	0.033202	27.1	0.000751	4.5	1.467186	1.886857	8.4	0.281675	23.5	0.281662	-18.8	0.88	2.54	5.sSMPABC134	939	12	Detrital
seq0099.dat	0.069101	57.1	0.001440	9.7	1.467230	1.886866	14.4	0.282077	26.8	0.282060	-11.5	1.02	1.90	5.sSMPABC008	637	8	Detrital
seq0100.dat	0.060249	72.7	0.001300	12.8	1.467206	1.886836	11.9	0.281861	25.3	0.281840	-14.0	1.11	2.23	5.sSMPABC085	867	10	Detrital
seq0101.dat	0.025034	20.9	0.000521	3.2	1.467242	1.886925	12.8	0.282135	24.5	0.282129	-8.7	0.87	1.76	5.sSMPABC132	649	8	Detrital
seq0102.dat	0.064302	51.7	0.001403	8.7	1.467211	1.886825	11.9	0.282117	23.8	0.282099	-9.2	0.99	1.80	5.sSMPABC130	676	9	Detrital
seq0103.dat	0.164874	133.4	0.003250	19.5	1.467197	1.886759	12.1	0.281869	24.9	0.281826	-18.3	1.57	2.32	5.sSMPABC006	699	9	Detrital
seq0104.dat	0.072599	58.2	0.001590	9.6	1.467223	1.886920	13.5	0.282033	21.6	0.282015	-13.7	1.02	1.99	5.sSMPABC007	608	7	Detrital
seq0105.dat	0.036023	29.2	0.000769	4.6	1.467156	1.886903	8.2	0.281849	26.9	0.281839	-17.0	0.89	2.28	5.sSMPABC012	738	9	Detrital
seq0106.dat	0.041009	33.3	0.000849	5.1	1.467191	1.886878	12.7	0.281444	24.3	0.281429	-27.4	0.90	2.99	5.sSMPABC030	918	11	Detrital
seq0107.dat	0.028617	23.2	0.000610	3.7	1.467234	1.886931	10.6	0.282095	28.0	0.282087	-10.2	0.87	1.84	5.sSMPABC033	650	8	Detrital
seq0109.dat	0.072536	59.3	0.001543	9.3	1.467199	1.886849	13.5	0.281953	21.7	0.281932	-13.6	1.03	2.10	5.sSMPABC091	744	10	Detrital
seq0110.dat	0.025761	21.2	0.000537	3.3	1.467249	1.886876	12.8	0.282028	25.0	0.282023	-15.5	0.87	2.02	5.sSMPABC096	513	6	Dissolution–recrystallization
seq0111.dat	0.038559	33.6	0.000771	5.5	1.467275	1.886907	13.0	0.281984	25.5	0.281976	-16.6	0.91	2.10	5.sSMPABC111	540	6	Dissolution–recrystallization

(a) $^{176}Yb/^{177}Hf = (^{176}Yb/^{173}Yb)_{true} \times (^{173}Yb/^{177}Hf)_{meassured} \times (M_{173(Yb)}/M_{177(Hf)})^{b(Hf)}$, $b(Hf) = \ln(^{179}Hf/^{177}Hf_{true} / {}^{179}Hf/^{177}Hf_{measured}) / \ln(M_{179(Hf)}/M_{177(Hf)})$

M=mass of respective isotope. The $^{176}Lu/^{177}Hf$ were calculated in a similar way by using the $^{175}Lu/^{177}Hf$ and b(Yb)

(b) Mean Hf signal in volt

(c) Uncertainties are quadratic additions of the within-run precision and the daily reproducibility of the zircon standards. Uncertainties for the standard quoted at 2SD (2 standard deviation)

(d) Initial $^{176}Hf/^{177}Hf$ and ƐHf calculated using the apparent Pb-Pb ages of respective zircon domains, and the CHUR parameters: $^{176}Lu/^{177}Hf = 0.0336$, and $^{176}Hf/^{177}Hf = 0.282785$ (Bouvier et al., 2008)

(e) Two stage model age in billion years using the measured $^{176}Lu/^{177}Lu$ of each spot (first stage = age of zircon), a value of 0.0113 for the average continental crust (second stage), and a average MORB (DM) $^{176}Lu/^{177}Hf$ and $^{176}Hf/^{177}Hf$ of 0.0384 and 0.283164

(f) $^{206}Pb/^{238}U$ age determined by LA-ICP-MS

STANDARDS FOR ANALYSIS OF CA-02, CA-04, AND CA-05 SAMPLES (G5 PLUTONS)

LA-(MC)ICP-MS Lu-Hf zircon results data from BB-09 standard

Identifier	$^{176}Yb/^{177}Hf$ [a]	±2s	$^{176}Lu/^{177}Hf$ [a]	±2s	$^{178}Hf/^{177}Hf$	$^{180}Hf/^{177}Hf$	Sig_{Hf} [b] (V)	$^{176}Hf/^{177}Hf$	±2s [c]	$^{176}Hf/^{177}Hf_{(t)}$ [d]	eHf(t) [d]	±2s [c]	T_{DM} [e] (Ga)	Age (Ma)	±2σ
seq0106.dat	0.007420	6.0	0.000157	0.9	1.467217	1.886836	10.4	0.281672	16.2	0.281671	-26.9	0.83	2.7	560	1
seq0107.dat	0.007386	6.1	0.000156	1.0	1.467255	1.886949	10.5	0.281670	15.7	0.281669	-27.0	0.83	2.7	560	1
seq0108.dat	0.007308	7.0	0.000154	1.3	1.467191	1.886833	10.5	0.281671	15.8	0.281669	-27.0	0.83	2.7	560	1
seq0151.dat	0.007246	5.8	0.000153	0.9	1.467235	1.886901	10.6	0.281669	15.3	0.281668	-27.1	0.83	2.7	560	1
seq0152.dat	0.007194	5.9	0.000153	0.9	1.467224	1.886905	10.6	0.281659	16.4	0.281658	-27.4	0.83	2.7	560	1
seq0153.dat	0.007228	7.1	0.000154	1.3	1.467194	1.886842	10.6	0.281669	17.0	0.281667	-27.1	0.83	2.7	560	1
seq0199.dat	0.007186	7.0	0.000151	1.6	1.467255	1.886915	10.3	0.281668	21.5	0.281666	-27.1	0.83	2.7	560	1
seq0200.dat	0.007175	5.8	0.000151	1.0	1.467196	1.886820	10.2	0.281679	14.4	0.281678	-26.7	0.83	2.7	560	1
seq0201.dat	0.007277	6.3	0.000152	1.0	1.467219	1.886832	10.2	0.281650	16.0	0.281648	-27.7	0.83	2.7	560	1
seq0237.dat	0.007598	6.7	0.000159	1.1	1.467214	1.886817	10.8	0.281650	24.8	0.281649	-27.7	0.83	2.7	560	1

seq0238.dat	0.007514	6.3	0.000158	1.0	1.467194	1.886828	10.6	0.281657	18.0	0.281655	-27.5	0.83	2.7	560	1
seq0239.dat	0.007061	7.6	0.000150	1.4	1.467229	1.886867	10.2	0.281688	15.0	0.281686	-26.4	0.83	2.6	560	1
eq0283.dat	0.007204	6.5	0.000153	1.1	1.467211	1.886890	10.4	0.281667	16.7	0.281665	-27.1	0.83	2.7	560	1
seq0284.dat	0.007180	7.0	0.000153	1.3	1.467226	1.886794	10.4	0.281672	16.1	0.281670	-27.0	0.83	2.7	560	1
seq0285.dat	0.006889	8.8	0.000147	1.7	1.467241	1.886886	10.3	0.281674	13.7	0.281673	-26.9	0.83	2.7	560	1

BB (560Ma): $^{176}Hf/^{177}Hf$=0.2816713±0.0000028 **Average:** 0.281668 16.83

LA-(MC)ICP-MS Lu-Hf zircon results data from Gj-1 standard

Identifier	$^{176}Yb/^{177}Hf$ [a]	±2s	$^{176}Lu/^{177}Hf$ [a]	±2s	$^{178}Hf/^{177}Hf$	$^{180}Hf/^{177}Hf$	Sig_{Hf} [b] (V)	$^{176}Hf/^{177}Hf$	±2s [c]	$^{176}Hf/^{177}Hf_{(t)}$ [d]	eHf(t) [d]	±2s [c]	T_{DM} [e] (Ga)	Age (Ma)	±2σ
seq0112.dat	0.010704	9.3	0.000266	2.0	1.467218	1.886787	9.3	0.281991	13.8	0.281988	-14.8	0.83	2.0	602	1
seq0113.dat	0.010696	8.6	0.000265	1.6	1.467246	1.886957	9.4	0.282039	13.1	0.282036	-13.1	0.83	2.0	602	1
seq0114.dat	0.010667	8.8	0.000265	1.6	1.467163	1.886832	9.3	0.282002	20.0	0.281999	-14.4	0.83	2.0	602	1
seq0157.dat	0.010865	8.7	0.000265	1.6	1.467234	1.886811	9.8	0.282020	17.3	0.282017	-13.7	0.83	2.0	602	1
seq0158.dat	0.010911	8.8	0.000264	1.6	1.467214	1.886892	9.4	0.281982	20.1	0.281979	-15.1	0.83	2.1	602	1
seq0159.dat	0.010956	8.8	0.000264	1.6	1.467202	1.886878	9.3	0.281993	18.1	0.281990	-14.7	0.83	2.0	602	1
seq0205.dat	0.010708	8.6	0.000267	1.6	1.467219	1.886925	9.3	0.281994	20.6	0.281991	-14.7	0.83	2.0	602	1
seq0206.dat	0.010648	8.8	0.000267	1.7	1.467190	1.886852	9.1	0.282017	14.5	0.282014	-13.8	0.83	2.0	602	1
seq0207.dat	0.010605	8.5	0.000265	1.6	1.467184	1.886827	9.2	0.281999	17.9	0.281996	-14.5	0.83	2.0	602	1
seq0243.dat	0.011109	13.7	0.000266	2.9	1.467240	1.886887	9.5	0.282027	17.1	0.282024	-13.5	0.84	2.0	602	1
seq0244.dat	0.011000	9.6	0.000264	1.9	1.467226	1.886900	9.5	0.282003	19.8	0.282000	-14.3	0.83	2.0	602	1
seq0245.dat	0.011115	9.1	0.000265	1.6	1.467190	1.886831	9.8	0.282010	16.2	0.282007	-14.1	0.83	2.0	602	1
seq0289.dat	0.011047	9.4	0.000265	1.8	1.467205	1.886809	10.0	0.281988	21.7	0.281985	-14.9	0.83	2.1	602	1
seq0290.dat	0.011285	9.3	0.000267	1.7	1.467193	1.886855	10.0	0.282009	19.0	0.282006	-14.1	0.83	2.0	602	1
seq0291.dat	0.011042	10.6	0.000267	2.2	1.467143	1.886772	10.1	0.282006	18.5	0.282003	-14.2	0.83	2.0	602	1

GJ-1(602Ma): $^{176}Hf/^{177}Hf$=0.282000±0.000005 **Average:** 0.282005 17.85

LA-(MC)ICP-MS Lu-Hf zircon results data from Plesovice standard

Identifier	$^{176}Yb/^{177}Hf$ [a]	±2s	$^{176}Lu/^{177}Hf$ [a]	±2s	$^{178}Hf/^{177}Hf$	$^{180}Hf/^{177}Hf$	Sig_{Hf} [b] (V)	$^{176}Hf/^{177}Hf$	±2s [c]	$^{176}Hf/^{177}Hf_{(t)}$ [d]	eHf(t) [d]	±2s [c]	T_{DM} [e] (Ga)	Age (Ma)	±2σ
seq0109.dat	0.015499	17.8	0.000234	2.5	1.467190	1.886825	14.2	0.282455	15.5	0.282454	-4.2	0.85	1.3	337	1
seq0110.dat	0.013365	15.2	0.000207	1.9	1.467273	1.886799	14.5	0.282473	18.2	0.282472	-3.6	0.84	1.2	337	1
seq0111.dat	0.009711	12.5	0.000153	1.7	1.467211	1.886875	14.9	0.282461	17.0	0.282460	-4.0	0.84	1.2	337	1
seq0154.dat	0.006358	5.1	0.000097	0.6	1.467248	1.886846	14.8	0.282473	14.5	0.282472	-3.6	0.83	1.2	337	1
seq0155.dat	0.005880	4.7	0.000090	0.5	1.467228	1.886903	14.8	0.282468	17.0	0.282467	-3.7	0.83	1.2	337	1
seq0156.dat	0.005910	4.7	0.000091	0.5	1.467232	1.886782	14.1	0.282471	18.0	0.282470	-3.6	0.83	1.2	337	1
seq0202.dat	0.007035	5.7	0.000109	0.7	1.467214	1.886786	15.4	0.282450	20.4	0.282449	-4.4	0.83	1.3	337	1
seq0203.dat	0.007047	5.7	0.000107	0.6	1.467243	1.886854	15.3	0.282456	16.7	0.282456	-4.1	0.83	1.2	337	1
seq0204.dat	0.007533	6.1	0.000117	0.7	1.467191	1.886877	15.4	0.282461	23.8	0.282460	-4.0	0.83	1.2	337	1
seq0240.dat	0.009856	8.3	0.000148	0.9	1.467257	1.886774	16.3	0.282478	18.9	0.282477	-3.4	0.83	1.2	337	1
seq0241.dat	0.007340	8.4	0.000109	1.2	1.467226	1.886859	16.6	0.282467	24.9	0.282466	-3.8	0.83	1.2	337	1
seq0242.dat	0.008990	12.1	0.000135	1.4	1.467217	1.886773	15.8	0.282474	26.9	0.282474	-3.5	0.84	1.2	337	1
seq0286.dat	0.009985	8.4	0.000154	1.0	1.467246	1.886800	15.4	0.282470	13.0	0.282469	-3.7	0.83	1.2	337	1
seq0287.dat	0.011223	9.4	0.000174	1.2	1.467254	1.886907	15.3	0.282459	17.9	0.282458	-4.1	0.83	1.2	337	1
seq0288.dat	0.004847	4.3	0.000074	0.5	1.467209	1.886878	15.0	0.282452	16.8	0.282452	-4.3	0.83	1.3	337	1
Plesocvice (337Ma): $^{176}Hf/^{177}Hf$=0.282482±0.000013							**Average:**	0.282465	18.62						

STANDARDS FOR ANALYSIS OF CA-06, CA-07, CA-09, AND CA-10 SAMPLES (METASEDIMENTARY ROCKS)

LA-(MC)ICP-MS Lu-Hf zircon results data from BB-09 standard

Identifier	$^{176}Yb/^{177}Hf$ [a]	±2s	$^{176}Lu/^{177}Hf$ [a]	±2s	$^{178}Hf/^{177}Hf$	$^{180}Hf/^{177}Hf$	Sig_{Hf} [b] (V)	$^{176}Hf/^{177}Hf$	±2s [c]	$^{176}Hf/^{177}Hf_{(t)}$ [d]	eHf(t) [d]	±2s [c]	T_{DM} [e] (Ga)	Age (Ma)	±2σ
seq0075.dat	0.007439	11.0	0.000157	2.2	1.467246	1.886837	10.7	0.281691	23.0	0.281690	-26.3	0.83	2.6	560	1
seq0076.dat	0.007034	5.9	0.000148	0.9	1.467239	1.886883	10.8	0.281668	19.4	0.281667	-27.1	0.83	2.7	560	1
seq0077.dat	0.007172	6.4	0.000151	1.1	1.467252	1.886935	10.8	0.281680	17.1	0.281678	-26.7	0.83	2.7	560	1

seq0151.dat	0.007246	5.8	0.000153	0.9	1.467235	1.886901	10.6	0.281669	17.0	0.281667	-27.1	0.83	2.7	560	1
seq0152.dat	0.007194	5.9	0.000153	0.9	1.467224	1.886905	10.6	0.281668	21.5	0.281666	-27.1	0.83	2.7	560	1
seq0153.dat	0.007228	7.1	0.000154	1.3	1.467194	1.886842	10.6	0.281679	14.4	0.281678	-26.7	0.83	2.7	560	1
seq0058.dat	0.007844	7.3	0.000151	1.1	1.467258	1.886979	10.0	0.281682	21.1	0.281680	-26.6	0.84	2.7	560	1
seq0059.dat	0.007838	6.3	0.000151	0.9	1.467224	1.886984	10.0	0.281684	16.6	0.281683	-26.5	0.84	2.6	560	1
seq0061.dat	0.007874	6.6	0.000151	1.0	1.467225	1.886875	10.2	0.281666	18.2	0.281664	-27.2	0.84	2.7	560	1
seq0112.dat	0.007880	6.4	0.000152	0.9	1.467189	1.886890	9.7	0.281659	29.7	0.281658	-27.4	0.84	2.7	560	1
seq0113.dat	0.007927	6.7	0.000153	1.1	1.467178	1.886941	9.7	0.281685	24.2	0.281683	-26.5	0.84	2.6	560	1
seq0114.dat	0.007815	6.4	0.000150	0.9	1.467165	1.886879	9.8	0.281645	23.5	0.281643	-27.9	0.84	2.7	560	1
seq0167.dat	0.007816	6.3	0.000152	0.9	1.467128	1.886826	9.7	0.281672	22.7	0.281671	-27.0	0.84	2.7	560	1
seq0168.dat	0.007866	6.3	0.000152	0.9	1.467206	1.886863	9.6	0.281680	19.4	0.281679	-26.7	0.84	2.7	560	1
seq0169.dat	0.007939	7.3	0.000153	1.1	1.467260	1.886985	9.6	0.281684	21.7	0.281682	-26.6	0.84	2.7	560	1
seq0170.dat	0.007816	6.5	0.000151	1.0	1.467219	1.886828	9.6	0.281680	17.4	0.281678	-26.7	0.84	2.7	560	1
seq0222.dat	0.007890	6.5	0.000151	0.9	1.467291	1.886889	9.5	0.281690	23.2	0.281688	-26.3	0.84	2.6	560	1
seq0223.dat	0.007955	6.4	0.000152	0.9	1.467246	1.886835	9.6	0.281670	23.6	0.281669	-27.0	0.84	2.7	560	1
seq0224.dat	0.007950	6.7	0.000153	1.0	1.467208	1.886854	9.6	0.281673	26.8	0.281671	-26.9	0.84	2.7	560	1
seq0225.dat	0.008098	6.5	0.000155	0.9	1.467254	1.886930	9.5	0.281669	20.7	0.281667	-27.1	0.84	2.7	560	1

BB (560Ma): $^{176}Hf/^{177}Hf$=0.2816713±0.0000028 **Average:** 0.281675 21.05

LA-(MC)ICP-MS Lu-Hf zircon results data from Gj-1 standard

Identifier	$^{176}Yb/^{177}Hf$ [a]	±2s	$^{176}Lu/^{177}Hf$ [a]	±2s	$^{178}Hf/^{177}Hf$	$^{180}Hf/^{177}Hf$	Sig_{Hf} [b] (V)	$^{176}Hf/^{177}Hf$	±2s [c]	$^{176}Hf/^{177}Hf_{(t)}$ [d]	eHf(t) [d]	±2s [c]	T_{DM} [e] (Ga)	Age (Ma)	±2σ
seq0081.dat	0.010847	13.9	0.000264	3.0	1.467217	1.886813	9.7	0.281981	18.7	0.281978	-15.1	0.84	2.1	602	1
seq0082.dat	0.010834	15.9	0.000264	3.6	1.467188	1.886990	9.7	0.281995	15.7	0.281992	-14.6	0.84	2.0	602	1
seq0083.dat	0.010677	8.6	0.000265	1.6	1.467153	1.886710	9.8	0.281985	16.7	0.281982	-15.0	0.83	2.1	602	1
seq0157.dat	0.010865	8.7	0.000265	1.6	1.467234	1.886811	9.8	0.282020	17.3	0.282017	-13.7	0.83	2.0	602	1
seq0158.dat	0.010911	8.8	0.000264	1.6	1.467214	1.886892	9.4	0.281982	20.1	0.281979	-15.1	0.83	2.1	602	1
seq0159.dat	0.010956	8.8	0.000264	1.6	1.467202	1.886878	9.3	0.281993	18.1	0.281990	-14.7	0.83	2.0	602	1
seq0065.dat	0.012121	9.9	0.000271	1.7	1.467195	1.886826	8.9	0.281992	16.6	0.281989	-14.7	0.85	2.0	602	1
seq0118.dat	0.011942	9.6	0.000272	1.6	1.467278	1.886904	8.6	0.282015	14.2	0.282012	-13.9	0.85	2.0	602	1
seq0120.dat	0.012040	9.7	0.000274	1.6	1.467189	1.886924	8.6	0.282001	20.1	0.281998	-14.4	0.85	2.0	602	1
seq0175.dat	0.012097	9.8	0.000273	1.6	1.467212	1.886886	8.6	0.281992	15.7	0.281989	-14.7	0.85	2.0	602	1
seq0176.dat	0.012115	11.1	0.000273	2.0	1.467250	1.886898	8.5	0.281985	15.7	0.281982	-15.0	0.85	2.1	602	1

GJ-1(602Ma): $^{176}Hf/^{177}Hf$=0.282000±0.000005 **Average:** 0.281995 17.17

LA-(MC)ICP-MS Lu-Hf zircon results data from Plesovice standard

Identifier	$^{176}Yb/^{177}Hf$ [a]	±2s	$^{176}Lu/^{177}Hf$ [a]	±2s	$^{178}Hf/^{177}Hf$	$^{180}Hf/^{177}Hf$	Sig_{Hf} [b] (V)	$^{176}Hf/^{177}Hf$	±2s [c]	$^{176}Hf/^{177}Hf_{(t)}$ [d]	eHf(t) [d]	±2s [c]	T_{DM} [e] (Ga)	Age (Ma)	±2σ
seq0078.dat	0.014180	14.4	0.000219	1.7	1.467194	1.886787	14.3	0.282490	16.8	0.282489	-3.0	0.84	1.2	337	1
seq0079.dat	0.005851	9.0	0.000090	1.2	1.467210	1.886931	15.2	0.282465	21.2	0.282465	-3.8	0.83	1.2	337	1
seq0080.dat	0.013917	13.9	0.000221	2.1	1.467227	1.886904	14.0	0.282485	21.6	0.282484	-3.2	0.84	1.2	337	1
seq0154.dat	0.006358	5.1	0.000097	0.6	1.467248	1.886846	14.8	0.282473	14.5	0.282472	-3.6	0.83	1.2	337	1
seq0155.dat	0.005880	4.7	0.000090	0.5	1.467228	1.886903	14.8	0.282468	17.0	0.282467	-3.7	0.83	1.2	337	1
seq0156.dat	0.005910	4.7	0.000091	0.5	1.467232	1.886782	14.1	0.282471	18.0	0.282470	-3.6	0.83	1.2	337	1

LA-(MC)ICP-MS Lu-Hf zircon results data from Plesovice standard

Identifier	$^{176}Yb/^{177}Hf$ [a]	±2s	$^{176}Lu/^{177}Hf$ [a]	±2s	$^{178}Hf/^{177}Hf$	$^{180}Hf/^{177}Hf$	Sig_{Hf} [b] (V)	$^{176}Hf/^{177}Hf$	±2s [c]	$^{176}Hf/^{177}Hf_{(t)}$ [d]	eHf(t) [d]	±2s [c]	T_{DM} [e] (Ga)	Age (Ma)	±2σ
seq0062.dat	0.006481	6.9	0.000093	0.8	1.467194	1.886753	14.6	0.282471	20.1	0.282470	-3.6	0.85	1.2	337	1
seq0063.dat	0.004765	5.2	0.000068	0.7	1.467183	1.886792	14.1	0.282478	25.1	0.282477	-3.4	0.84	1.2	337	1
seq0064.dat	0.007097	6.9	0.000103	1.4	1.467188	1.886884	14.0	0.282477	20.4	0.282476	-3.4	0.85	1.2	337	1
seq0115.dat	0.006538	5.3	0.000093	0.6	1.467263	1.886882	14.1	0.282478	24.0	0.282478	-3.4	0.84	1.2	337	1
seq0116.dat	0.003401	2.7	0.000049	0.3	1.467182	1.886824	14.3	0.282484	20.5	0.282484	-3.2	0.84	1.2	337	1
seq0117.dat	0.006868	5.5	0.000097	0.6	1.467215	1.886914	14.2	0.282457	16.1	0.282456	-4.1	0.84	1.2	337	1
seq0171.dat	0.004144	3.3	0.000059	0.4	1.467223	1.886798	14.3	0.282487	21.5	0.282487	-3.1	0.84	1.2	337	1
seq0172.dat	0.005238	4.4	0.000075	0.5	1.467201	1.886929	14.3	0.282475	22.5	0.282475	-3.5	0.84	1.2	337	1
seq0173.dat	0.008228	6.8	0.000119	0.7	1.467164	1.886870	14.2	0.282454	17.5	0.282453	-4.2	0.85	1.3	337	1
seq0226.dat	0.005397	4.4	0.000079	0.5	1.467247	1.886954	14.4	0.282474	24.8	0.282474	-3.5	0.84	1.2	337	1
seq0227.dat	0.009281	7.5	0.000136	0.9	1.467226	1.886908	13.6	0.282446	20.9	0.282445	-4.5	0.85	1.3	337	1
seq0228.dat	0.007465	6.1	0.000112	0.7	1.467209	1.886781	12.0	0.282478	24.0	0.282477	-3.4	0.84	1.2	337	1
Plesocvice (337Ma): $^{176}Hf/^{177}Hf$=0.282482±0.000013							**Average:**	0.282473	20.36						

[a] $^{176}Yb/^{177}Hf = (^{176}Yb/^{173}Yb)_{true} \times (^{173}Yb/^{177}Hf)_{meassured} \times (M_{173(Yb)}/M_{177(Hf)})^{b(Hf)}$, $b(Hf) = \ln(^{179}Hf/^{177}Hf_{true} / {}^{179}Hf/^{177}Hf_{measured}) / \ln(M_{179(Hf)}/M_{177(Hf)})$
M=mass of respective isotope. The 176Lu/177Hf were calculated in a similar way by using the 175Lu/177Hf and b(Yb)
(b) Mean Hf signal in volt
[c] Uncertainties are quadratic additions of the within-run precision and the daily reproducibility of the zircon standards. Uncertainties for the standard quoted at 2SD (2 standard deviation)
(d) Initial 176Hf/177Hf and εHf calculated using the apparent Pb-Pb ages of respective zircon domains, and the CHUR parameters: 176Lu/177Hf = 0.0336, and 176Hf/177Hf = 0.282785 (Bouvier et al., 2008)

[e] Two stage model age in billion years using the measured $^{176}Lu/^{177}Lu$ of each spot (first stage = age of zircon), a value of 0.0113 for the average continental crust (second stage), and a average MORB (DM) $^{176}Lu/^{177}Hf$ and $^{176}Hf/^{177}Hf$ of 0.0384 and 0.283164

REFERENCES

Stacey, J.S., Kramers, J.D., 1975. Approximation of terrestrial lead isotope evolution by a two-stage model. Earth and Planetary Science Letters 26, 207-221.

Bouvier, A., Vervoort, J.D., Patchett, P.J., 2008. The Lu-Hf and Sm-Nd isotopic composition of CHUR: constraints from unequilibrated chondrites and implications for the bulk composition of terrestrial planets. Earth and Planetary Science Letters 273, 48-57.

APPENDIX I - Petrographic Descriptions

Mineral abbreviations (in accordance to Whitney and Evans, 2010)

Ab	Albite	Opx	Orthopyroxene
Aln	Allanite	Or	Ortoclase
Amp	Amphibole	Pl	Plagioclase
Ap	Apatite	Qz	Quartz
Bt	Biotite	Rt	Rutile
Cb	Carbonate	Scp	Scapolite
Chl	Chorite	Ser	Sericite
Cpx	Clinopyroxene	Sil	Sillimanite
Crd	Cordierite	Ttn	Titanite
Ep	Epidote	Zrn	Zircon
Grt	Garnet		
Hc	Hercynite		
Hgb	Hogbomite		
Ilm	Ilmenite		
Ky	Kyanite		
Kfs	K-feldspar		
Mag	Magnetite		
Mc	Microcline		
Mnz	Monazite		
Ms	Muscovite		
Opq	Opaque minerals		

SHEET OF PETROGRAPHIC DESCRIPTION	
PhD Thesis – Cristina Santos Araujo	
Sample identification: CA-03	**Field identification:** CA-03
Coordinates: -20,41225/-40,85965	**Location:** Marechal Floriano, Espírito Santo state
Local name: Jequitibá suite	**Lithologic unit:** G1 supersuite, pre-collisional plutonism – Rio Doce Magmatic arc
Sample Description	
Foliated biotite granite with milimetric garnet, light gray, fine to coarse-grained, showing about 20% of mafic minerals and local small felsic patches with core of garnet up to 2 cm in diameter (Photographs A and B).	
Lithochemical signature	
Magnesian, calcic, slightly peraluminous, calc-alkaline serie	
Petrography	
Major minerals	Plagioclase (~42%), quartz (~30%), K-feldspar (~15%), biotite (~10%), garnet (~1%)
Accessory minerals	Zircon, apatite, monazite, allanite
Alteration minerals	Sericite, muscovite, opaque minerals, clay minerals, chorite
Thin section description and interpretations	

The sample is relatively poorly deformed and preserves a magmatic appearance (Photograhs C and D). It presents fine to coarse-grained, granoblastic to granolepidoblastic textures, with the contacts between the grains being irregular, interlobate, poligonal, and straight (Photograhs C to H). Foliation is defined by orientation of stretched quartz, feldspars, and biotite (Photograhs C and D).

Plagioclase is subhedral to euhedral and it present light sericitization and saussuritization. Some crystals show irregular twinning, and inclusions of biotite, zircon, apatite, and rounded quartz.

Quartz presents anhedral habit, light undulatory extinction and inclusions of biotite, plagioclase, and orthoclase.

K-feldspar is orthoclase and microcline, with anhedral to euhedral forms, light sericitization, perthitic texture, and biotite, plagioclase, and quartz inclusions.

Biotite shows dark brown to light brown pleochroism, subhedral to euhedral form, moderate chloritization and muscovitization, pleochroic halos, and inclusions of quartz, plagioclase, allanite, monazite, and apatite.

Poikiloblastic garnet presents subhedral habitus, inclusions of rounded quartz and monazite, and elongated biotite and apatite.

Apatite and zircon shows stubby, prismatic and acicular forms, usually included in major minerals.

Allanite is incolor to light beige, with rounded shape.

Monazite shows rounded shape, usually included in major minerals.

Lithology: garnet-biotite metagranodiorite

Photographs

A: Sample in the outcrop; B: Sample CA-03

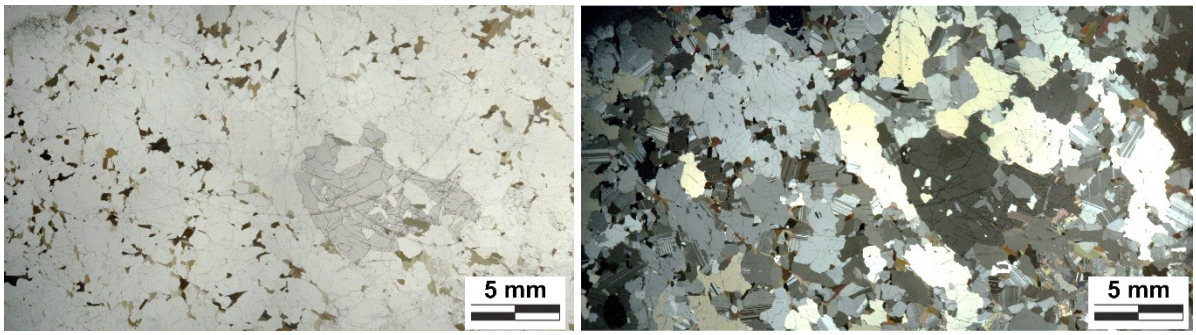

C and D: Photomicrographs showing the main mineralogy and texture.

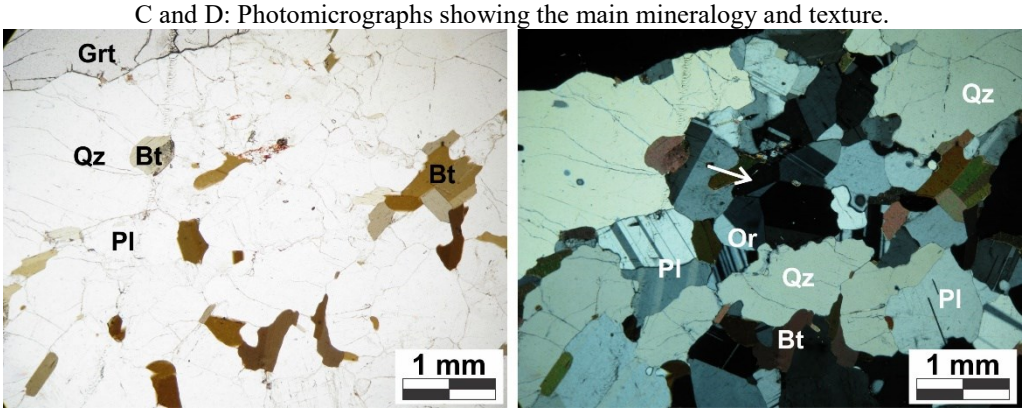

E and F: Photomicrographs showing the main mineralogy and texture. The arrow shows polygonal contact between the grains.

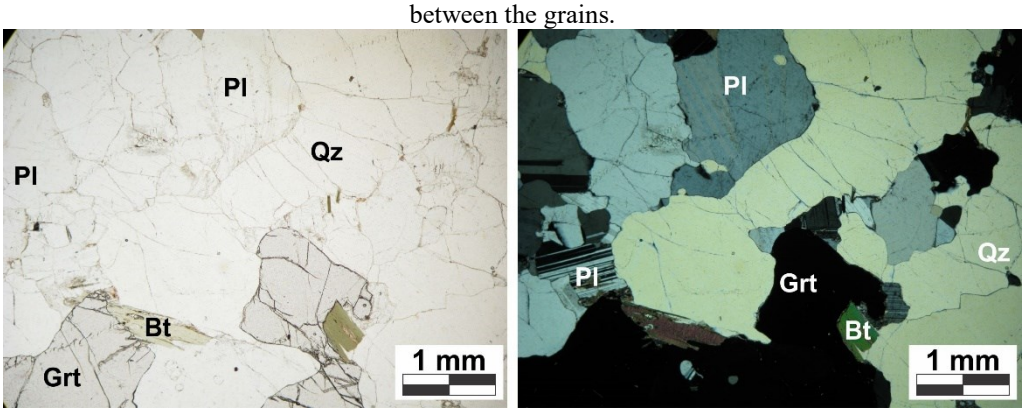

G and H: Photomicrographs showing the main mineralogy and texture.

SHEET OF PETROGRAPHIC DESCRIPTION	
PhD Thesis – Cristina Santos Araujo	
Sample identification: CA-06	**Field identification:** CA-06
Coordinates: -19,798133/-40,36985	**Location:** Ibiraçu, Espírito Santo state
Local name: Nova Venécia complex	**Lithologic unit:** Nova Venécia complex, back-arc basin
Sample Description	
Migmatitic paragneisses (metatexite) stromatic, laminated to banded, with color variations of blue, light brown to greenish being determined by the variation of cordierite, biotite, quartz, feldspar, sillimanite and accessory minerals (Photographs A and B). Granulation ranges from fine to medium in millimeter portions to medium and coarse in centimeter portions.	
Lithochemical signature	
Peraluminous	
Petrography	
Major minerals	K-feldspar (~35%), cordierite (~25%), quartz (20%), biotite (~10%), plagioclase (~5%), opaque minerals (~3%)
Accessory minerals	Hercynite, zircon, apatite, monazite, sillimanite, hogbomite, garnet
Alteration minerals	Sericite, clay minerals, chorite, carbonate
Thin section description and interpretations	

The sample presents foliated, fine to coarse-grained, granoblastic to granonematoblastic textures, with the contacts between the grains being irregular, interlobate, poligonal, and straight. Foliation is defined by ribbonlike deformation bands with flattened and stretched cordierite, quartz, K-feldspar, plagioclase, and sillimanite, and biotite oriented. There are portions free-biotite and bearing-sillimanite-cordierite elongated, and levels with granulation varying (Photographs C to J).

K-feldspar is microcline and triclinized orthoclase, locality in flattened and stretched grains or recrystallized, with anhedral to subhedral forms, light sericitization, perthitic texture, and biotite, zircon, monazite, plagioclase, apatite, opaque minerals, and quartz inclusions. Some crystals show compositional zoning.

Cordierite presents ribbonlike shape, locality recrystallized, with moderate pinitization, abundant inclusions of foliation-oriented sillimanite, pleochroic halos, and inclusions of monazite, quartz, hogbomite, opaques minerals, biotite and K-feldspar. It is frequently associated with opaques minerals and hercynite. The larger crystals are bordered by sillimanite, quartz and feldspar subgrains (Photographs E and F).

Quartz presents anhedral and subhedral habit, locality recrystallized or in flattened and stretched grains, undulatory extinction and inclusions of biotite, K-feldspar, and sillimanite.

Biotite shows reddish brown to light brown pleochroism, subhedral to euhedral form, light chloritization and muscovitization, pleochroic halos, and inclusions of opaque minerals, plagioclase, zircon, quartz, monazite, and apatite.

Plagioclase is subhedral to euhedral, locality in flattened and stretched grains or recrystallized, and it present light sericitization and saussuritization. Some crystals show compositional zoning, and inclusions of biotite, zircon, apatite, sillimanite, microcline, opaque minerals, and hercynite.

Garnet presents anhedral habitus, and inclusions of rounded quartz. It appears as pieces stretched among the essential minerals (Photographs I and J).

Sillimanite has granular, acicular, cubic and prismatic shape, appearing as trails among the essential minerals or included in them.

Hercynite and hogbomite are often associated with opaques minerals, cordierite and sillimanite.

Apatite and zircon shows stubby, prismatic and acicular forms, usually included in major minerals.

Monazite shows rounded shape, usually included in major minerals.

Lithology: Sil-Bt-Crd paragneiss (known as Crd granulite)

Photographs

A: Sil-Bt-Crd paragneiss in the outcrop; B: Sample CA-06

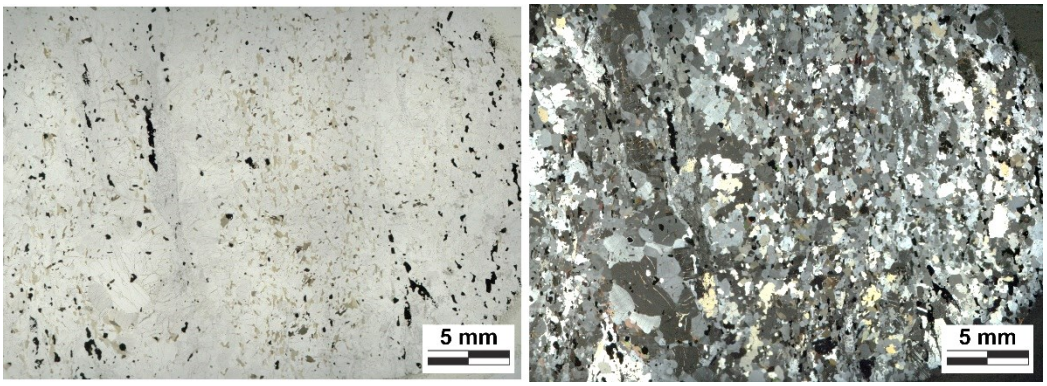

C and D: Photomicrographs showing the main mineralogy and texture.

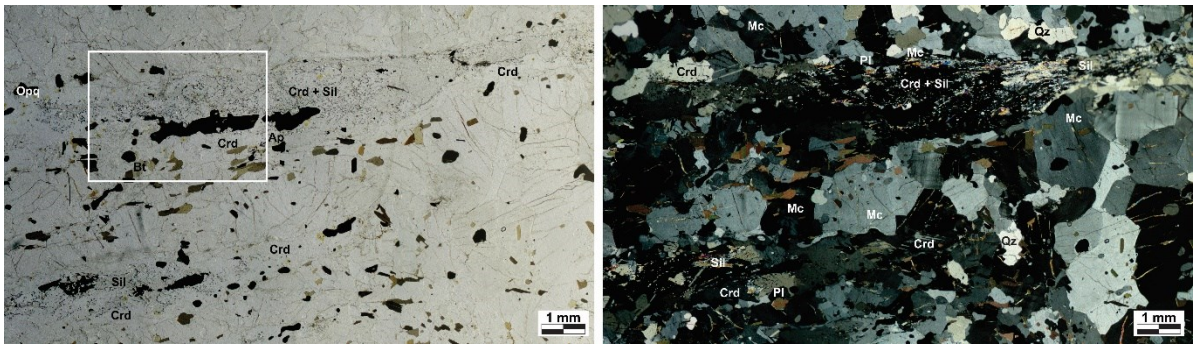

E and F: Photomicrographs showing cordierite with ribbonlike shape, recrystallized, and abundant inclusions of foliation-oriented sillimanite, and bordered by sillimanite, quartz and feldspar subgrains. White rectangle represents photographs G and H.

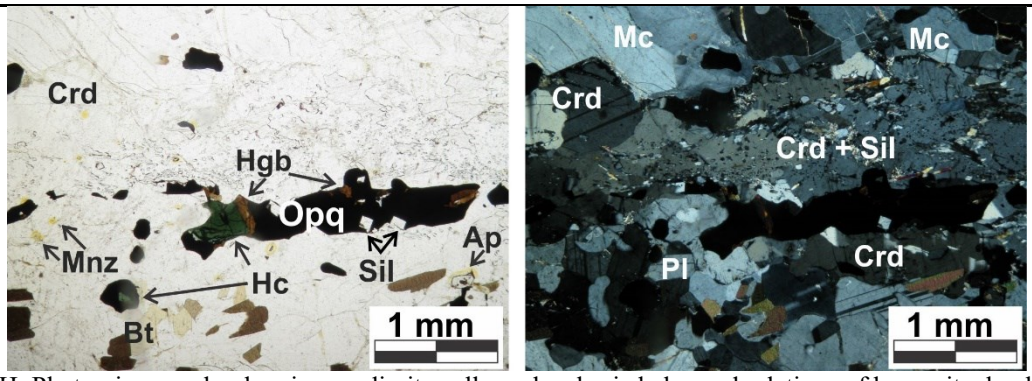

G and H: Photomicrographs showing cordierite yellow pleochroic halos and relations of hercynite, hogbomite, opaque minerals, cordierite and sillimanite.

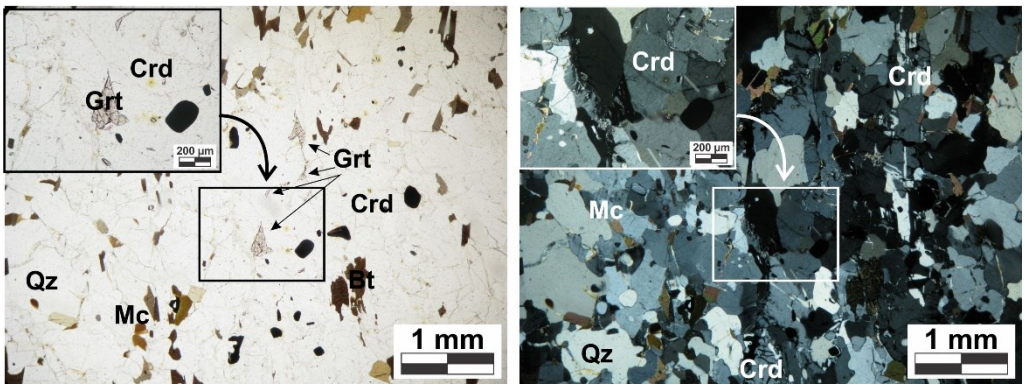

I and J: Photomicrographs showing the main mineralogy and texture. Rectangle shows garnet as pieces stretched among the major minerals.

SHEET OF PETROGRAPHIC DESCRIPTION	
PhD Thesis – Cristina Santos Araujo	
Sample identification: CA-07	**Field identification:** CA-07
Coordinates: -19,932367/-40,40955	**Location:** Fundão, Espírito Santo state
Local name: Ataléia suite	**Lithologic unit:** G2 supersuite, collisional plutonism
Sample Description	
Foliated garnet-biotite granite with centimetric garnet (up until 2 cm in diameter), light gray, medium to coarse-grained, showing about 15% of mafic minerals (Photograph B). In the outcrop, this lithotype occurs in close spatial association with a migmatitic paragneiss of the Nova Venécia complex (Photograph A).	
Lithochemical signature	
Magnesian, calcic-alkalic, peraluminous, calc-alkaline serie	
Petrography	
Major minerals	Plagioclase (~55%), quartz (~25%), biotite (~10%), K-feldspar (~5%), garnet (~2%)
Accessory minerals	Opaque minerals, zircon, apatite, monazite
Alteration minerals	Sericite, muscovite, clay minerals, chorite, carbonate

Thin section description and interpretations

The sample presents foliated, medium to coarse-grained, granoblastic to granolepidoblastic textures, with the contacts between the grains being irregular, poligonal, and straight. Foliation is defined by stretched quartz and feldspars and biotite oriented (Photographs C to H).

Plagioclase is subhedral to euhedral, commonly elongated according to foliation, and it presents moderate sericitization and saussuritization. Some crystals show compositional zoning, deformed and irregular twinning, and inclusions of biotite, zircon, apatite, and opaque minerals.

Quartz presents anhedral and subhedral habits, commonly elongated according to foliation, undulatory extinction, and inclusions of plagioclase, biotite, and K-feldspar.

Biotite shows dark brown to light brown pleochroism, subhedral to euhedral form, light chloritization, pleochroic halos, and inclusions of zircon, quartz, monazite, and apatite.

K-feldspar is essentially microcline, with anhedral to subhedral forms, light sericitization, perthitic texture, and inclusions of biotite, plagioclase, and quartz.

Poikiloblastic garnet presents subhedral habitus, light chloritization, inclusions of opaque minerals, zircon, quartz, monazite, plagioclase, and apatite. Biotite and fine-grained felsic minerals are concentrated around some garnets according to foliation, as pressure shadows.

Apatite and zircon shows stubby, prismatic and acicular forms, usually included in major minerals.

Monazite shows rounded shape, usually included in major minerals.

Lithology: garnet-biotite metatonalite

Photographs

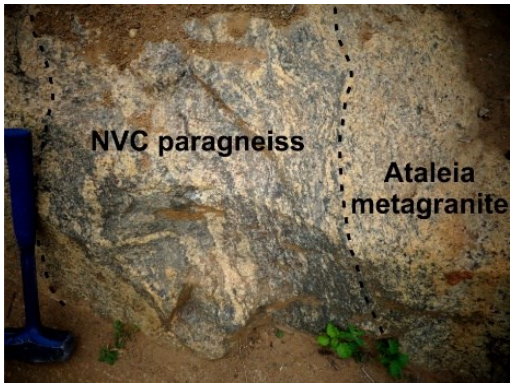

A: The foliated garnet-biotite granite occurs in close spatial association with a migmatitic paragneiss of the Nova Venécia complex (NVC); B: Sample CA-07

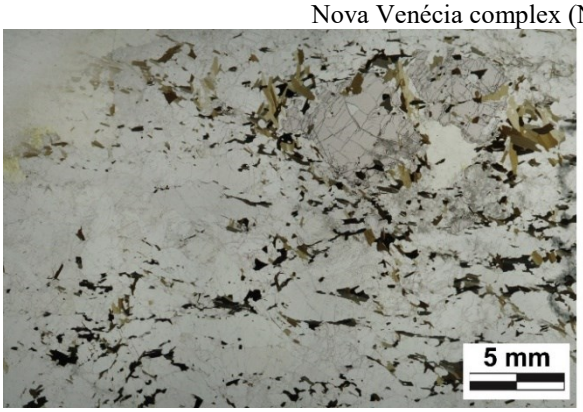

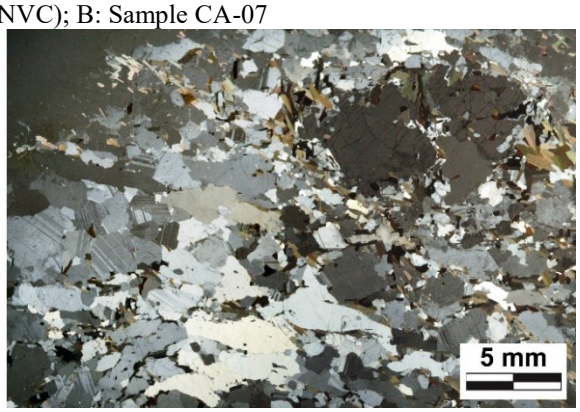

C and D: Photomicrographs showing the main mineralogy and texture.

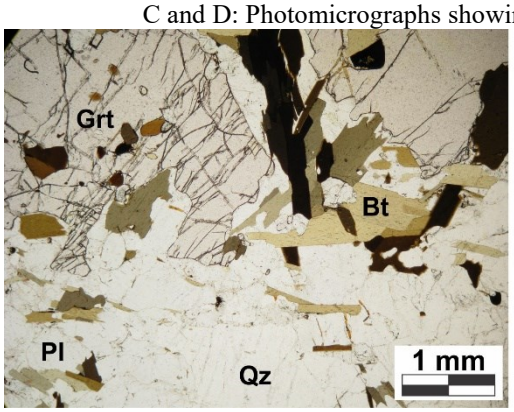

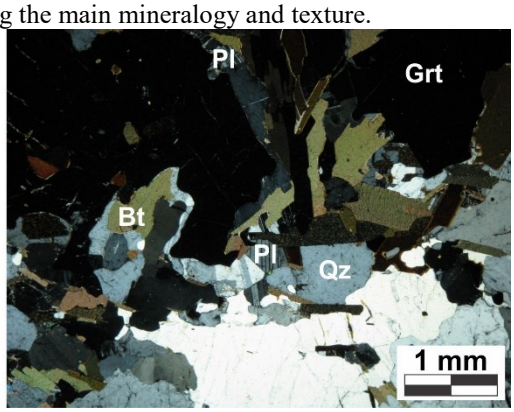

E and F: Photomicrographs showing the main mineralogy and texture.

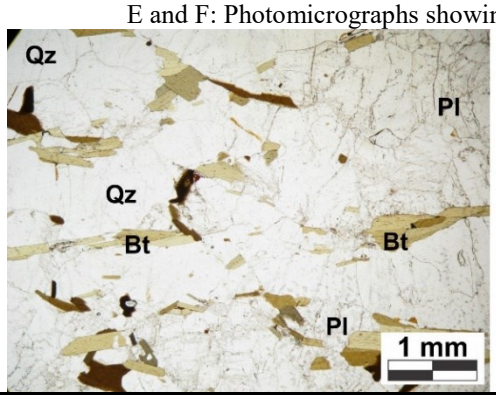

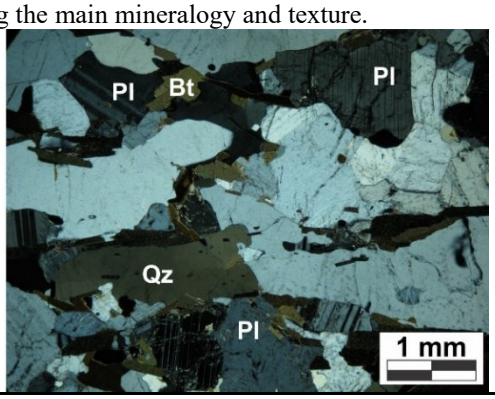

G and H: Photomicrographs showing the main mineralogy and stretched quartz, feldspars and biotite oriented according with foliation.

SHEET OF PETROGRAPHIC DESCRIPTION	
PhD Thesis – Cristina Santos Araujo	
Sample identification: CA-08	**Field identification:** CA-08
Coordinates: -19,935167/-40,498883	**Location:** Santa Tereza, Espírito Santo state
Local name: Santa Tereza suite	**Lithologic unit:** G1 supersuite, pre-collisional plutonism – Rio Doce magmatic arc
Sample Description	
Greenish gray rock, coarse-grained, composed of felsic bands and mafic bands with high concentration of biotite (Photographs A and B).	
Lithochemical signature	
Magnesian, calcic, slightly peraluminous, calc-alkaline serie	
Petrography	
Major minerals	Plagioclase (~50%), quartz (~35%), biotite (~10%), K-feldspar (~6%)
Accessory minerals	Opaque minerals, zircon, apatite, monazite, rutile, allanite
Alteration minerals	Sericite, muscovite, clay minerals, chorite, carbonate, rutile
Thin section description and interpretations	

The sample presents medium to coarse-grained, granoblastic to granolepidoblastic textures, banded, with the contacts between the grains being irregular, poligonal, and interlobate (Photographs C and D). The bands is defined by concentration of felsic minerals (quartz and feldspars, commonly elongated) and mafic minerals (biotite and opaques minerals) (Photographs C to H).

Plagioclase is subhedral to anhedral, commonly elongated according to bands, and it present moderate sericitization and saussuritization. Some crystals show antiperthitic texture, compositional zoning, deformed and irregular twinning, and inclusions of biotite, zircon, quartz, apatite, and monazite (Photographs E and F).

Quartz presents anhedral habit, commonly elongated according to bands, undulatory extinction and inclusions of biotite, plagioclasse, zircon, and biotite (Photographs G and H).

Biotite shows dark brown to light brown pleochroism, subhedral to euhedral form, light chloritization and muscovitization, pleochroic halos, and inclusions of alanite, zircon, quartz, monazite, and apatite.

K-feldspar is essentially microcline, with anhedral to subhedral forms, light sericitization, perthitic texture, and inclusions of biotite, plagioclase, and quartz.

Apatite and zircon shows stubby, and prismatic forms, usually included in major minerals.

Monazite shows rounded shape, usually included in major minerals.

Lithology: biotite metagranodiorite

Photographs

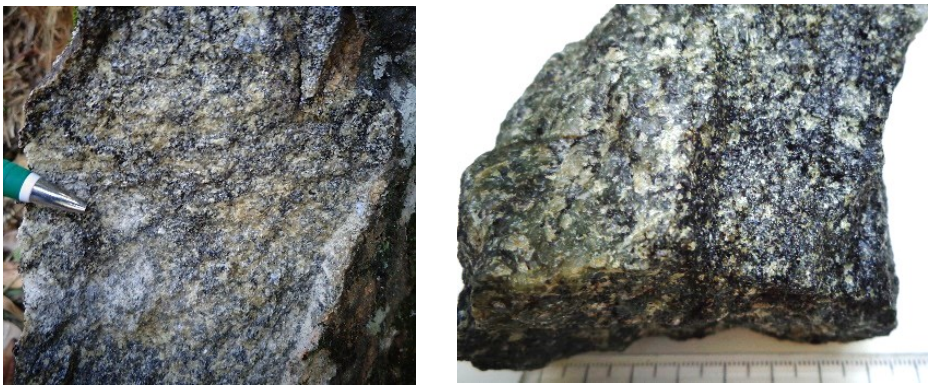

A: Metagranodiorite in outcrop. B: Sample CA-08.

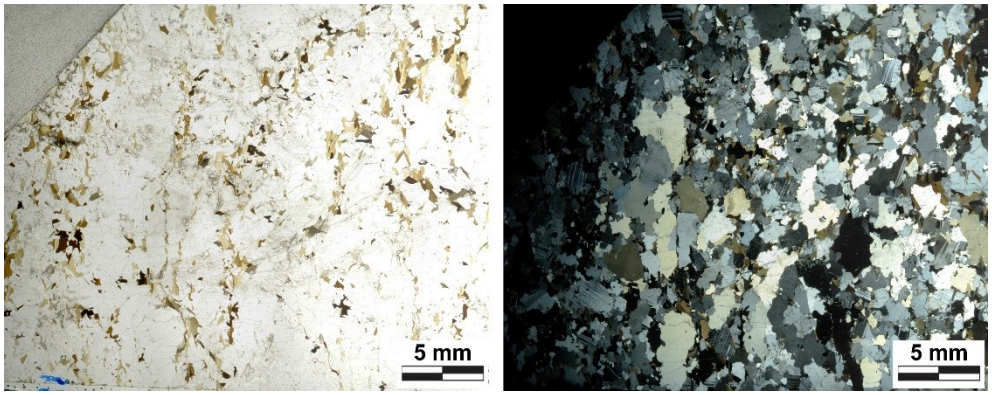

C and D: Photomicrographs showing the main mineralogy and texture.

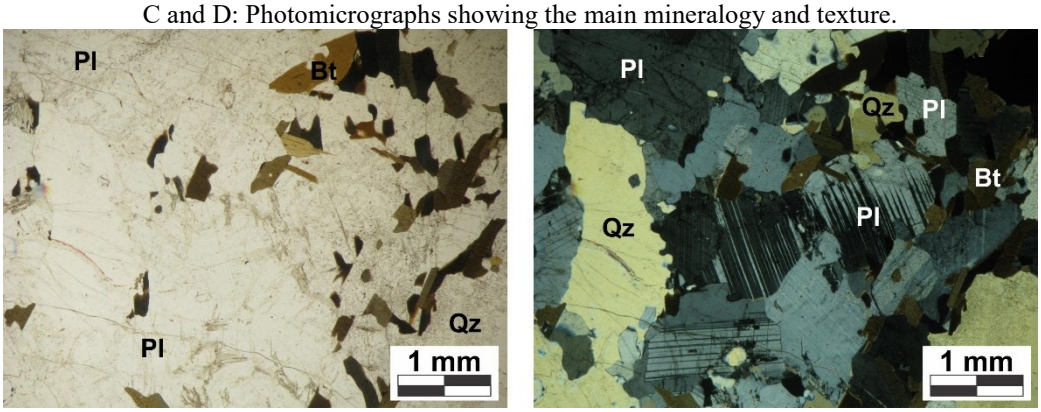

E and F: Photomicrographs showing the main mineralogy, texture, and plagioclase with deformed and irregular twinning.

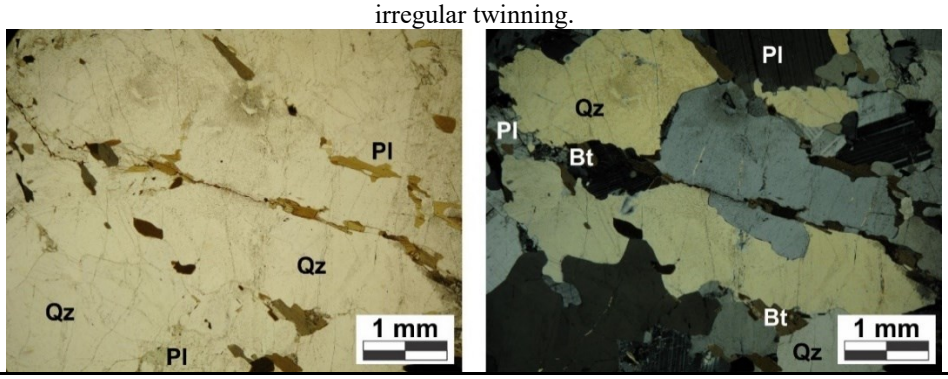

G and H: Photomicrographs showing the main mineralogy and stretched quartz, feldspars and biotite oriented according with foliation.

SHEET OF PETROGRAPHIC DESCRIPTION	
PhD Thesis – Cristina Santos Araujo	
Sample identification: CA-09A	**Field identification:** CA-09
Coordinates: -19,92115/-40,598183	**Location:** Santa Tereza, Espírito Santo state
Local name: Nova Venécia complex	**Lithologic unit:** Nova Venécia complex, back-arc basin
Sample Description	
Migmatitic paragneisses (metatexite) stromatic, laminated to banded, with felsic and mafic variations (Photographs A and B). The compositional levels range from fine to coarse-grained. Euhedral garnet is present in all lithotypes (up until 1 cm in diameter).	
Lithochemical signature	
Peraluminous	
Petrography	
Major minerals	Part A: K-feldspar (~30%), quartz (~25%), biotite (~20%), cordierite (~15%), plagioclase (~5%), garnet (~3%) Part B: Quartz (~32%), K-feldspar (~25%), cordierite (~20%), plagioclase (~15%), sillimanite (~3%), biotite (~2%), garnet (~1%)
Accessory minerals	Part A: Opaque minerals, zircon, apatite, monazite, titanite, rutile, sillimanite, kyanite Part B: Opaque minerals, zircon, apatite, monazite, titanite, rutile
Alteration minerals	Part A: Sericite, muscovite, clay minerals, chorite Part B: Sericite, muscovite, clay minerals, chorite
Thin section description and interpretations	

The sample is banded with one part rich in biotite and garnet (Part A) and another part poor in these minerals (Part B) (Photographs C and D).

Part A (Photographs E and F):

It presents foliated, medium to coarse-grained, granoblastic to granonematoblastic textures, with the contacts between the grains being irregular, interlobate, and straight. Foliation is defined by ribbonlike deformation with flattened and stretched cordierite, quartz, and feldspars, as well sillimanite and biotite oriented.

K-feldspar is microcline and triclinized orthoclase, with anhedral to euhedral forms, locality in flattened and stretched grains, light sericitization, perthitic texture, and biotite, zircon, plagioclase, opaque minerals, and quartz inclusions.

Quartz presents anhedral and subhedral habits, locality recrystallized or in flattened and stretched grains, undulatory extinction and inclusions of biotite, K-feldspar, plagioclase, monazite, and apatite.

Biotite shows reddish brown to light brown pleochroism, subhedral to euhedral form, pleochroic halos, and inclusions of opaque minerals, zircon, quartz, monazite, and apatite. It often shows intergrowth with cordierite, quartz e K-feldspar.

Cordierite is poikiloblastic. It presents ribbonlike shape, with moderate pinitization, pleochroic halos, and inclusions of monazite, zircon, sillimanite, quartz, apatite, opaques minerals, biotite, and K-feldspar. It often shows intergrowth with biotite, quartz e K-feldspar.

Plagioclase is subhedral to euhedral and it present light sericitization and saussuritization. Some crystals show irregular twinning, and inclusions of biotite, zircon, apatite, sillimanite, quartz, monazite, and opaque minerals.

Poikiloblastic garnet presents anhedral form, inclusions of rounded quartz, and biotite, apatite, monazite, sillimanite, and zircon. Biotite are concentrated around some garnets according to foliation.

Sillimanite has granular, acicular and prismatic shape, appearing included in major minerals.

Apatite and zircon shows stubby, and prismatic forms, usually included in major minerals.

Monazite shows rounded shape, usually included in major minerals.

Kyanite is anhedral and subhedral, in paragenesis with plagioclase and cordierite.

Part B (Photographs G and H):

It presents foliated, coarse-grained, granoblastic to granonematoblastic textures, with the contacts between the grains being irregular, interlobate, poligonal, and straight. Foliation is defined by ribbonlike deformation with flattened and stretched cordierite, quartz, garnet, and feldspars, as well sillimanite, acicular opaque, and biotite oriented.

Quartz presents anhedral and subhedral form, locality recrystallized or in flattened and stretched grains, undulatory extinction, subgrains, and inclusions of biotite, zircon, K-feldspar, and sillimanite.

K-feldspar is microcline and triclinized orthoclase, with anhedral to euhedral forms, locality in flattened and stretched grains, light sericitization, perthitic texture, and biotite, opaque minerals, plagioclase, and quartz inclusions.

Cordierite is poikiloblastic. It presents ribbonlike shape, with moderate pinitization, pleochroic halos, abundant inclusions of foliation-oriented (like trails) acicular sillimanite, and inclusions of monazite, zircon, sillimanite, quartz, apatite, opaques minerals, biotite, and K-feldspar. It is frequently associated with opaques minerals.

Plagioclase is subhedral to euhedral and it present light sericitization and saussuritization. Some crystals show antiperthitic texture, irregular twinning, and inclusions of biotite, zircon, apatite, sillimanite, microcline, and opaque minerals.

Poikiloblastic garnet presents anhedral form, light chloritization, inclusions of rounded quartz, and biotite, apatite, monazite, zircon, and abundant foliation-oriented (like trails) acicular sillimanite.

Sillimanite has granular, acicular and prismatic shape, appearing as trails among the essential minerals or included in them.

Biotite shows reddish brown to light brown pleochroism, subhedral to euhedral form, light chloritization, pleochroic halos, and inclusions of opaque minerals, zircon, quartz, monazite, and apatite. Some crystals show intergrowth with cordierite, quartz e K-feldspar.

Apatite and zircon shows stubby, and prismatic forms, usually included in major minerals.

Monazite shows rounded shape, usually included in major minerals.

Opaque minerals present acicular to granular habits. They are oriented according to foliation.

Lithology: Sil-Grt-Crd-Bt paragneiss

Photographs

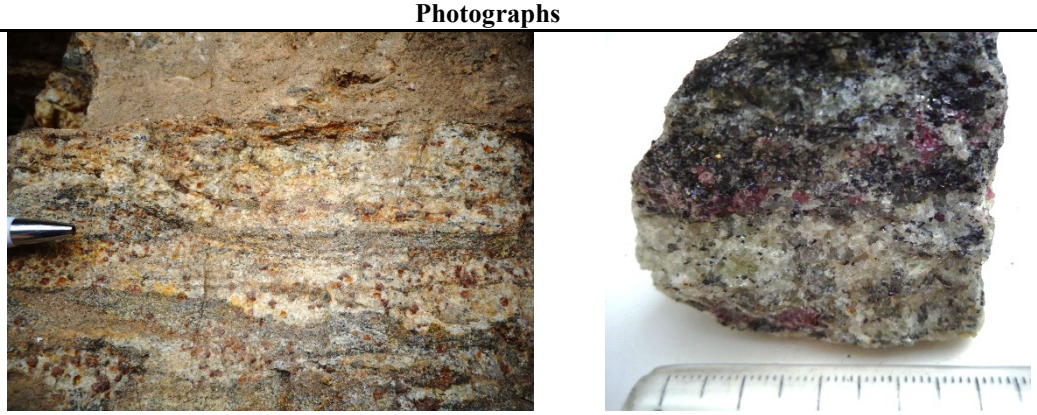

A: Sil-Grt-Crd-Bt paragneiss in the outcrop; B: Sample CA-09A

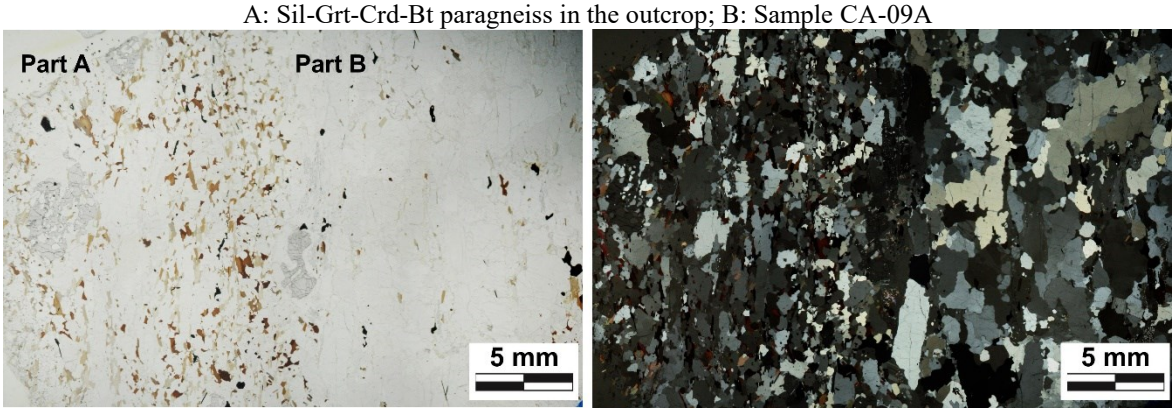

C and D: Photomicrographs showing the main mineralogy and texture.

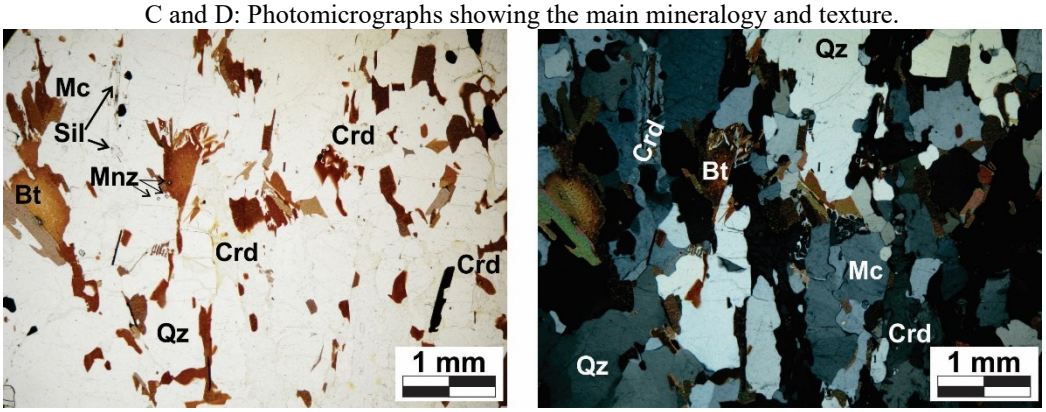

E and F: Photomicrographs showing the main mineralogy and texture of part A.

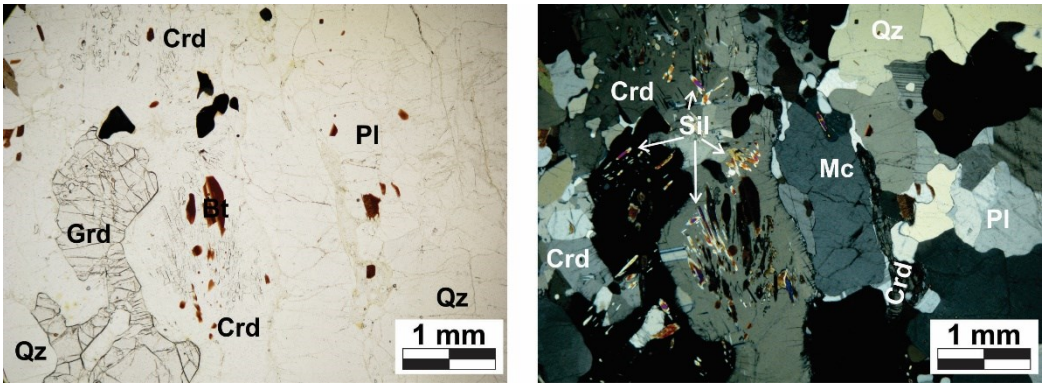

G and H: Photomicrographs showing the main mineralogy and texture of part B.

SHEET OF PETROGRAPHIC DESCRIPTION	
PhD Thesis – Cristina Santos Araujo	
Sample identification: CA-09B	**Field identification:** CA-09
Coordinates: -19,92115/-40,598183	**Location:** Santa Tereza, Espírito Santo state
Local name: Nova Venécia complex	**Lithologic unit:** Nova Venécia complex, back-arc basin
Sample Description	
Migmatitic paragneisses (metatexite) stromatic, laminated to banded, with predominance of felsic minerals (Photographs A and B). The compositional levels range from medium to coarse-grained. Euhedral garnet is present in all levels (up until 1 cm in diameter).	
Lithochemical signature	
-	
Petrography	
Major minerals	Cordierite (~30%), K-feldspar (~25%), quartz (~20%), garnet (~10%), biotite (~8%), plagioclase (~5%)
Accessory minerals	Opaque minerals, zircon, apatite, monazite, sillimanite
Alteration minerals	Sericite, muscovite, clay minerals, chorite
Thin section description and interpretations	

The sample presents foliated, medium to coarse-grained, granoblastic to granolepdoblastic textures, with the contacts between the grains being irregular, poligonal, and straight. Foliation is defined by ribbonlike deformation bands with flattened, stretched, and oriented mineral in felsic and mafic levels (Photographs C to F).

Cordierite is subhedral to anhedral, with some poikiloblastic crystals. It presents ribbonlike shape, with moderate pinitization, pleochroic halos, and inclusions of monazite, zircon, sillimanite, quartz, apatite, opaques minerals, kyanite, and biotite.

K-feldspar is microcline and triclinized orthoclase, with anhedral to subhedral forms, locality in flattened and stretched grains, light sericitization, perthitic texture, and biotite, monazite, zircon, plagioclase, sillimanite, cordierite, garnet, opaque minerals, apatite, and quartz inclusions.

Quartz presents anhedral shapes, in flattened and stretched grains, undulatory extinction and inclusions of biotite, K-feldspar, and zircon, monazite.

Poikiloblastic garnet presents anhedral habitus, inclusions of rounded quartz, and biotite, opaque minerals, apatite, monazite, sillimanite, cordierite, kyanite, microcline, and zircon (Photographs C to H). Biotite are concentrated around some garnets according to foliation.

Biotite shows reddish brown to light brown pleochroism, subhedral to euhedral forms, light chloritization and muscovitization, pleochroic halos, and inclusions of opaque minerals, zircon, quartz, and monazite. It often shows intergrowth with cordierite, K-feldspar, and quartz.

Plagioclase is subhedral to euhedral and it present light sericitization and saussuritization. Some crystals show irregular twinning, and myrmekitic intergrowths, and inclusions of biotite, quartz, and monazite.

Sillimanite has granular, acicular and prismatic shape, appearing included in major minerals as trails according to main foliation.

Apatite and zircon shows stubby, rounded shaped, and prismatic forms, usually included in major minerals.

Monazite shows rounded shape, usually included in major minerals.

Kyanite is anhedral and subhedral included in cordierite and garnet.

Lithology: Bt-Grt-Crd paragneiss

Photographs

A: Paragneiss in the outcrop; B: Sample CA-09B

C and D: Photomicrographs showing the main mineralogy and texture.

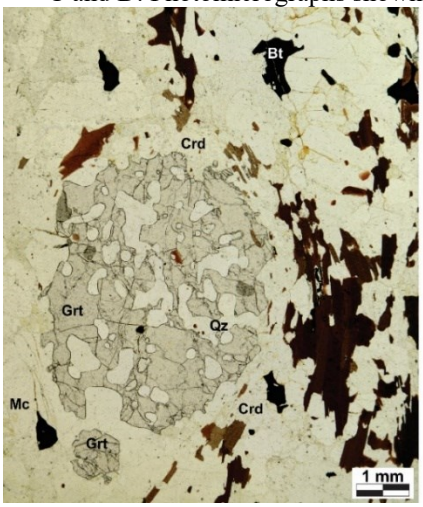

E and F: Photomicrographs showing the main mineralogy and texture.

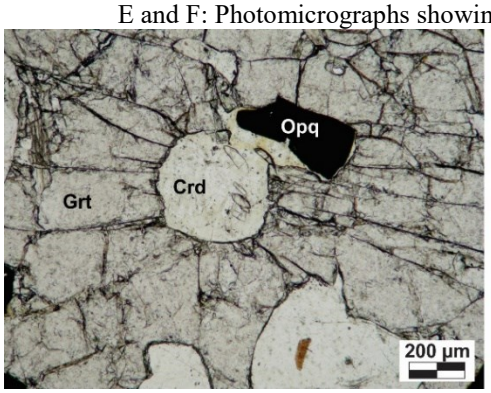

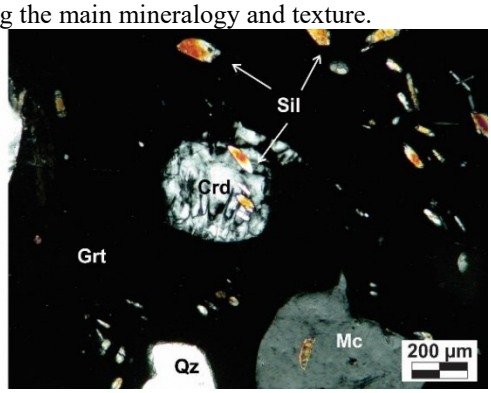

G and H: Photomicrographs showing cordierite inclusion on garnet and sillimanite trails in both.

SHEET OF PETROGRAPHIC DESCRIPTION	
PhD Thesis – Cristina Santos Araujo	
Sample identification: CA-10	**Field identification:** CA-10
Coordinates: -19,814567/-40,67865	**Location:** Santa Tereza, Espírito Santo state
Local name: Nova Venécia complex	**Lithologic unit:** Nova Venécia complex, back-arc basin
Sample Description	
Migmatitic paragneisses (metatexite) stromatic, laminated to banded, with felsic and mafic variations (Photographs A and B). The compositional levels range from fine to coarse-grained. Garnet is larger and more abundant in felsic levels lithotypes.	
Lithochemical signature	
-	
Petrography	
Major minerals	Quartz (~40%), plagioclase (~32%), biotite (~10%), K-feldsdar (~10%), garnet (~5%)
Accessory minerals	Opaque minerals, zircon, apatite, monazite
Alteration minerals	Sericite, muscovite, clay minerals, chorite, carbonate
Thin section description and interpretations	
The sample presents foliated, fine to medium-grained, granoblastic to granolepdoblastic textures, with the contacts between the grains being irregular, poligonal, interlobate, and straight. Foliation is defined by ribbonlike deformation bands with flattened and stretched quartz, garnet, and feldspars, as well biotite and acicular opaques oriented (Photographs C to F). Quartz presents anhedral habits, locality in flattened and stretched grains, undulatory extinction and inclusions of zircon, monazite, and biotite. Plagioclase is subhedral to euhedral and it present light sericitization and saussuritization. Some crystals show antiperthitic texture, compositional zoning, irregular twinning, and inclusions of biotite, quartz, zircon, apatite, and opaque minerals. Biotite shows reddish brown to light brown pleochroism, subhedral to euhedral form, light chloritization and muscovitization, pleochroic halos, and inclusions of opaque minerals, zircon, quartz, monazite, and apatite. K-feldspar is microcline and triclinized orthoclase, with anhedral to subhedral forms, locality in flattened and stretched grains, perthitic texture, and biotite, and quartz inclusions. Poikiloblastic garnet presents anhedral habitus, inclusions of rounded quartz, biotite, K-feldspar, and apatite. Some crystals are stretched according to foliation. Apatite and zircon shows stubby, rounded shaped, and prismatic forms, usually included in major minerals. Monazite shows rounded shape, usually included in major minerals. Opaque minerals are subhedral to euhedral with acicular and prismatic habits.	
Lithology: Grt-Bt gneiss	
Photographs	

A: Grt-Bt gneiss in the outcrop; B: Sample CA-10.

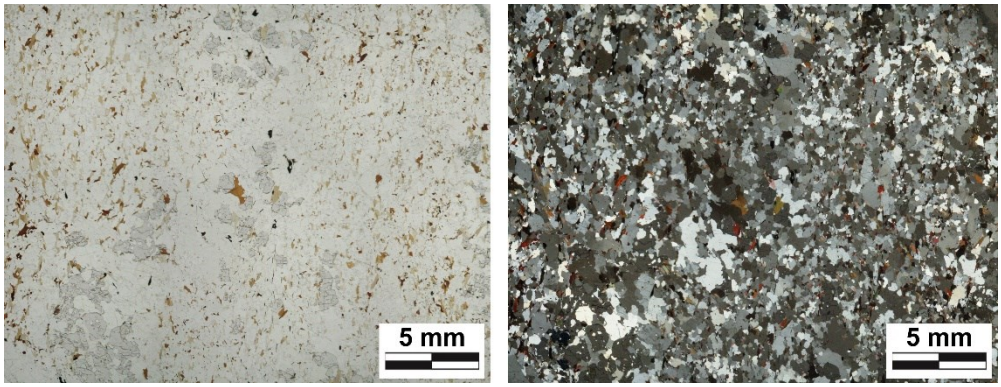

C and D: Photomicrographs showing the main mineralogy and texture.

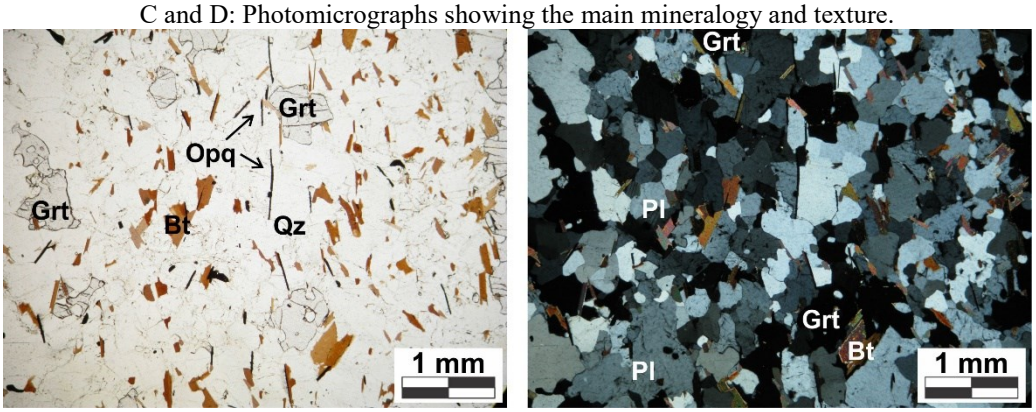

E and F: Photomicrographs showing the main mineralogy and texture.

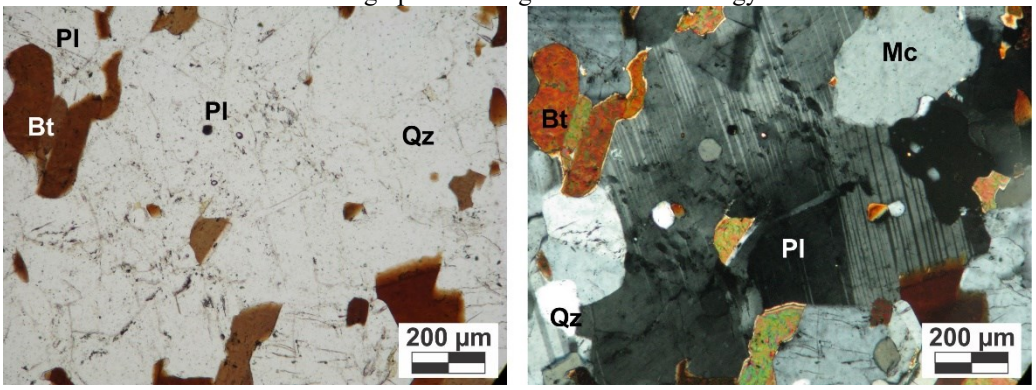

G and H: Photomicrographs showing plagioclase with antiperthitic texture, compositional zoning, and irregular twinning.

SHEET OF PETROGRAPHIC DESCRIPTION	
PhD Thesis – Cristina Santos Araujo	
Sample identification: CA-12A	**Field identification:** CA-12
Coordinates: -19,876179/-40,538724	**Location:** Santa Tereza, Espírito Santo state
Local name: Nova Venécia complex	**Lithologic unit:** Nova Venécia complex, back-arc basin
Sample Description	
Garnet paragneisses greenish, laminated to banded, with felsic and mafic variations (Photographs A and B). The compositional levels range from fine to médium-grained. The garnet porphyroblastic (up until 1 cm in diameter) presents sigmoidal shape and pressure shadows of quartz in the biotitic foliation.	
Lithochemical signature	
-	
Petrography	
Major minerals	Cordierite (~30%), quartz (~20%), biotite (~15%), plagioclase (~15%), K-feldsdar (~10%), garnet (~5%)
Accessory minerals	Opaque minerals, zircon, apatite, monazite, rutile, Kyanite, sillimanite
Alteration minerals	Sericite, muscovite, clay minerals, chorite
Thin section description and interpretations	

The sample presents foliated, fine to medium-grained, granoblastic to granolepdoblastic textures, with the contacts between the grains being irregular, poligonal, and straight. Foliation is defined by ribbonlike deformation bands with flattened and stretched quartz, garnet, feldspars, and cordierite, as well biotite and acicular opaque minerals oriented (Photographs C to H).

Cordierite presents ribbonlike shape oriented according foliation, undulatory extinction, moderate pinitization, pleochroic halos, and inclusions of monazite, zircon, quartz, apatite, opaque minerals, biotite, garnet, Kyanite and K-feldspar. It is frequently associated with opaques minerals and encompassing the garnet (Photographs E to H). Some crystals are bordered by garnet and symplectite texture, with biotite and quartz.

Quartz presents anhedral to subehdral habits, locality recrystallized in flattened and stretched grains, undulatory extinction and inclusions of biotite, K-feldspar, and sillimanite.

Biotite shows reddish brown to light brown pleochroism, subhedral to euhedral form, pleochroic halos, and inclusions of opaque minerals, zircon, quartz, monazite, cordierite, K-feldspar, and apatite. Some crystals show deformated cleavage and borders with cordierite, feldspars, and quartzo intergrowths (Photographs G and H).

Plagioclase is subhedral to anhedral and it present light sericitization and saussuritization. Some crystals show antiperthitic texture, compositional zoning, deformed and irregular twinning, and inclusions of biotite, monazite, zircon, apatite, and quartz.

K-feldspar is microcline, ortoclase, and triclinized orthoclase, with anhedral to euhedral forms, locality recrystallized or in flattened and stretched grains, light sericitization, perthitic texture, and biotite, and quartz inclusions.

Garnet presents anhedral habitus, and some crystals are flattened and stretched according foliation, inclusions of quartz, biotite, cordierite, K-feldspar, apatite, monazite, cordierite, sillimanite, Kyanite, opaques minerals, and zircon. Some crystals are bordered by cordierite + biotite symplectite texture. There are poikiloblastic crystals and cystals without inclusions.

Sillimanite has granular, acicular and prismatic shape, appearing included in major minerals as trails according to main foliation.

Apatite and zircon shows stubby, rounded shaped, and prismatic forms, usually included in major minerals.

Rutile occurs as tiny granular aggregates included in plagioclase, quartz, and biotite.

Monazite shows rounded shape, usually included in major minerals.

Opaque minerals are subhedral to euhedral with acicular and prismatic habits.

Kyanite is anhedral and subhedral included in cordierite and garnet.
Lithology: Grt-Bt-Crd paragneiss
Photographs

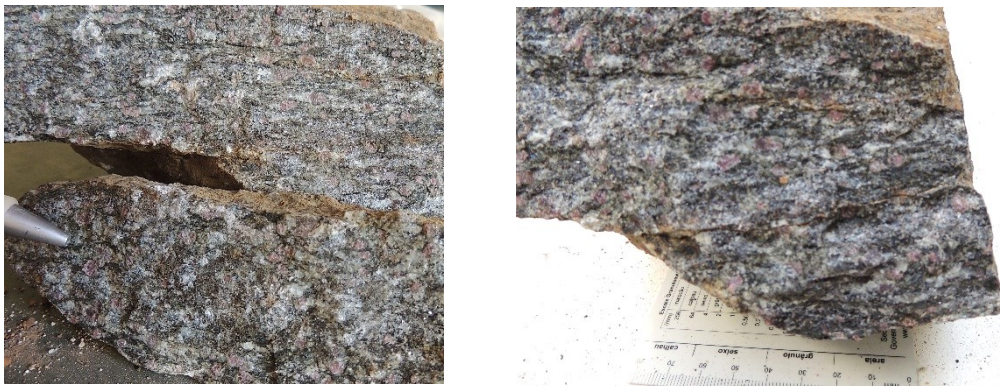

A: Grt-Bt-Crd paragneiss in the outcrop; B: Sample CA-12A

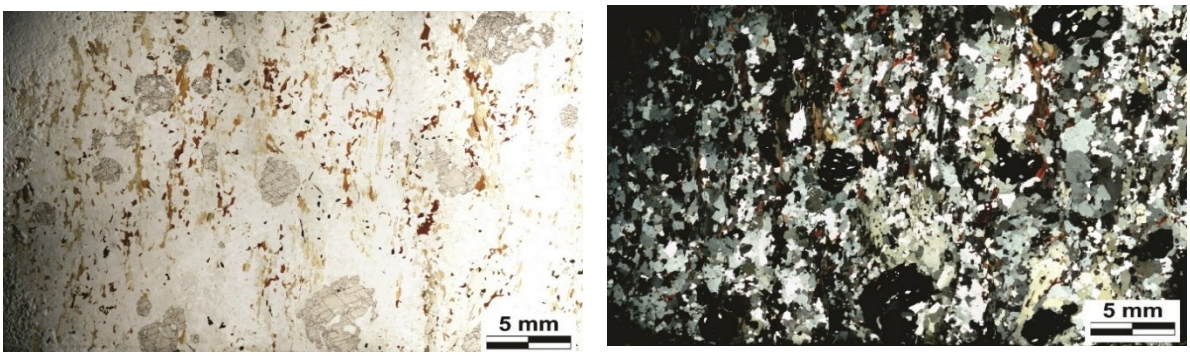

C and D: Photomicrographs showing the main mineralogy and texture.

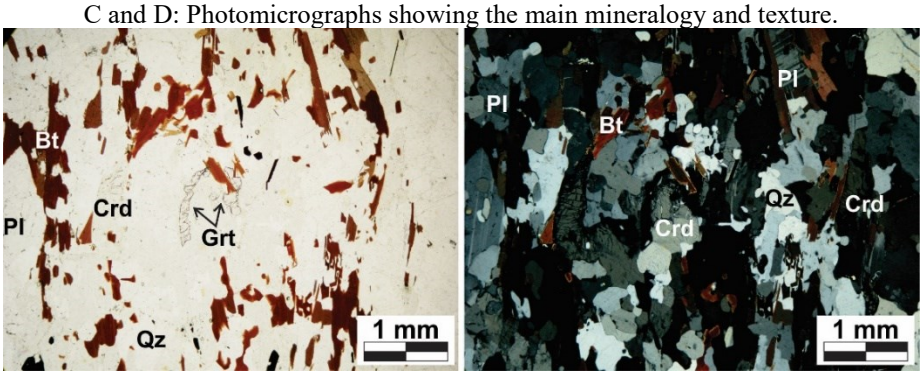

E and F: Photomicrographs showing the main mineralogy and texture.

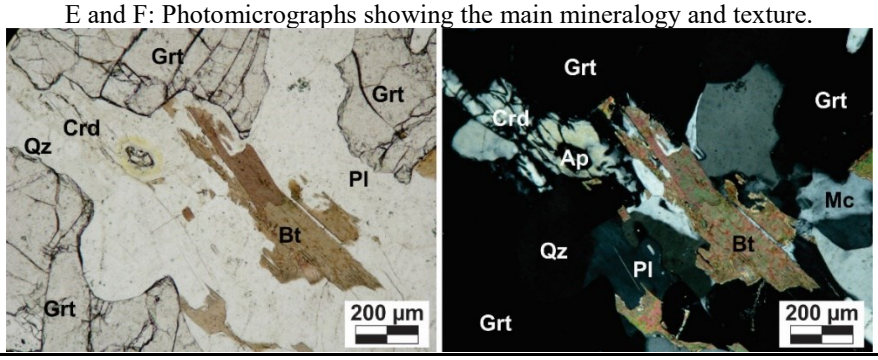

G and H: Photomicrographs showing the main mineralogy and texture. It is possible to note the relatioship between garnet, biotite, cordierite, quartz, and feldspar.

SHEET OF PETROGRAPHIC DESCRIPTION	
PhD Thesis – Cristina Santos Araujo	
Sample identification: CA-12B	**Field identification:** CA-12
Coordinates: -19,876179/-40,538724	**Location:** Santa Tereza, Espírito Santo state
Local name: Nova Venécia complex	**Lithologic unit:** Nova Venécia complex, back-arc basin
Sample Description	
Dark gray rock, fine grained, and isotropic.	
Lithochemical signature	
-	
Petrography	
Major minerals	Quartz (~20%), orthopyroxene (~20%), clinopyroxene (~15%), scapolite (~15%), plagioclase (~10%), amphibole (~10%), titanite (~5%),
Accessory minerals	Zircon, apatite, monazite, epidote
Alteration minerals	Amphibole, sericite, muscovite, clay minerals, chorite, carbonate, opaque minerals
Thin section description and interpretations	

The sample presents fine-grained, granoblastic and equigranular textures, with the contacts between the grains being irregular, poligonal, and straight.

Quartz presents anhedral and euhedral habits, undulatory extinction and inclusions of zircon, monazite, and titanite.

Orthopyroxene is subhedral to euhedral, with incolor to light greenish brown pleochroism and it present light uralitization, and inclusions of titanite, zircon, and apatite.

Clinopyroxene is subhedral to euhedral, with incolor to light greenish brown pleochroism, and it present light uralitization. Some crystals show compositional zoning, and inclusions of of titanite, zircon, and apatite.

Scapolite is incolor, anhedral to subhedral forms, with ligth alteration.

Plagioclase is subhedral to anhedral and it present light saussuritization. Some crystals show irregular twinning, and inclusions zircon, monazite, and titanite.

Amphibole is subhedral to euhedral, with light greenish to light greenish brown pleochroism, and it present light alteration.

Titanite has anhedral to subhedral forms.

Apatite, monazite, and zircon shows stubby, and rounded shaped, usually included in major minerals.

Lithology: Calc-silicate rock

Photographs

A: Sample CA-12B

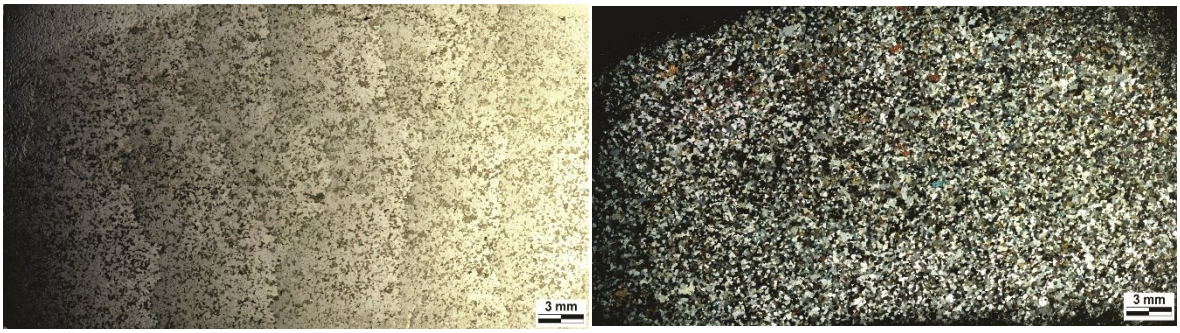

B and C: Photomicrographs showing the main mineralogy and texture.

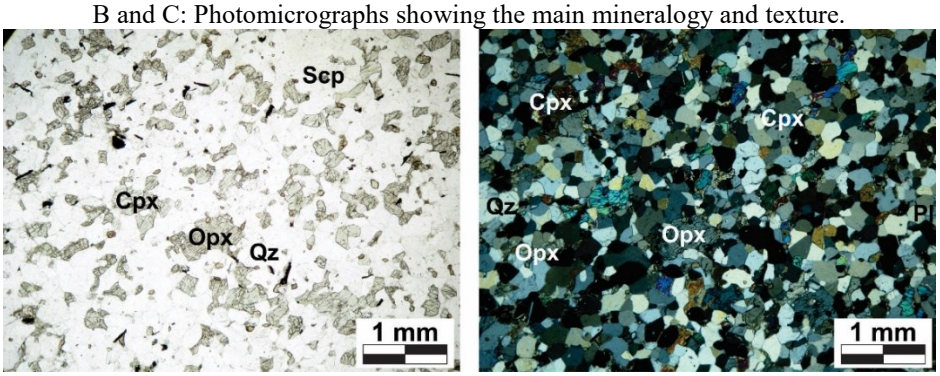

D and E: Photomicrographs showing the main mineralogy and texture.

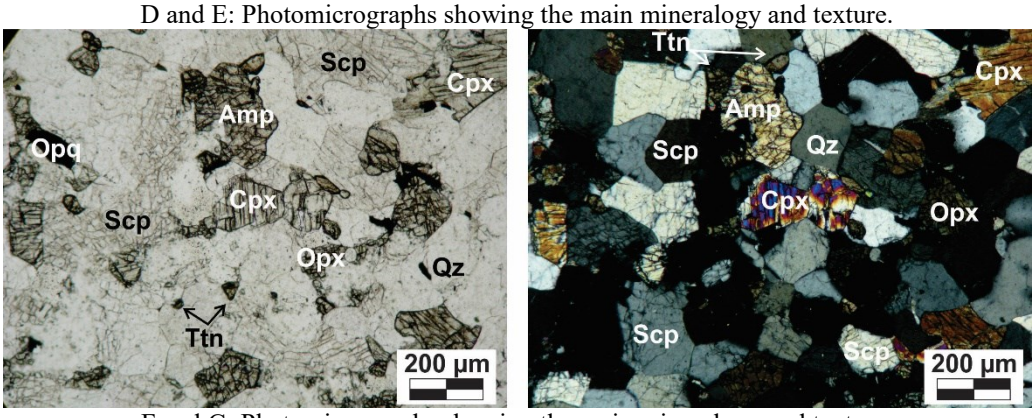

F and G: Photomicrographs showing the main mineralogy and texture.

SHEET OF PETROGRAPHIC DESCRIPTION	
PhD Thesis – Cristina Santos Araujo	
Sample identification: CA-12C	**Field identification:** CA-12
Coordinates: -19,876179/-40,538724	**Location:** Santa Tereza, Espírito Santo state
Local name: Ataléia suite	**Lithologic unit:** G2 supersuite, collisional plutonism
Sample Description	
Foliated garnet-biotite granite, light greenish gray, fine to medium-grained, with milimetric garnet, showing about 10% of mafic minerals (Photograph A). In the outcrop, this lithotype occurs in contact with a migmatitic paragneiss of the Nova Venécia complex (sample CA-12A).	
Lithochemical signature	
-	
Petrography	
Major minerals	Plagioclase (~37%), quartz (~30%), biotite (~20%), garnet (~5%), K-feldspar (~5%)
Accessory minerals	Opaque minerals, zircon, apatite, monazite
Alteration minerals	Sericite, muscovite, clay minerals, carbonate, opaque minerals
Thin section description and interpretations	

The sample presents foliated, medium-grained, granoblastic to granolepidoblastic textures, with the contacts between the grains being irregular, poligonal, and straight. Foliation is defined by biotite oriented (Photographs B to G).

Plagioclase is subhedral to euhedral, and it presents moderate sericitization and saussuritization. Some crystals show antiperthitic texture, compositional zoning, and inclusions of biotite, quartz, monazite, and zircon.

Quartz presents anhedral to subhedral shapes, light undulatory extinction, and inclusions of monazite, apatite, zircon, and biotite.

Biotite shows reddish brown to light brown pleochroism, subhedral to euhedral form, light chloritization and muscovitization, pleochroic halos, and inclusions of opaque minerals, zircon, quartz, monazite, and apatite.

Garnet presents subhedral to anhedral shapes. There are garnet free-inclusions and poikiloblastic with inclusions of quartz, zircon, monazite, opaques minerals, and biotite. Some crystals are bordered by plagioclase. Garnet free-inclusions was not affected by foliation (Photographs D to G).

Apatite, monazite, and zircon shows stubby, prismatic, and rounded shaped, usually included in major minerals.

Opaque minerals are subhedral to euhedral with acicular and granular habits.

Lithology: garnet-biotite metatonalite

Photographs

A: Sample CA-12C

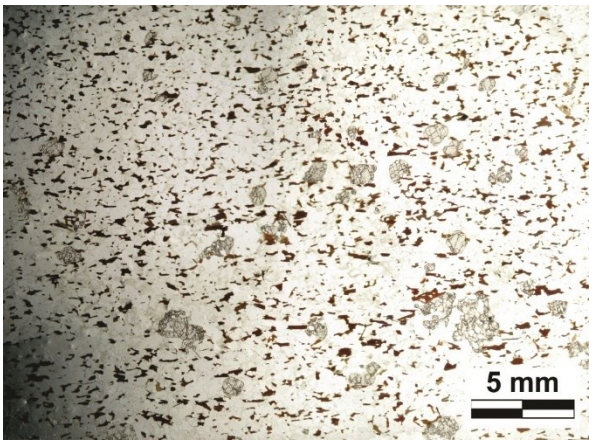

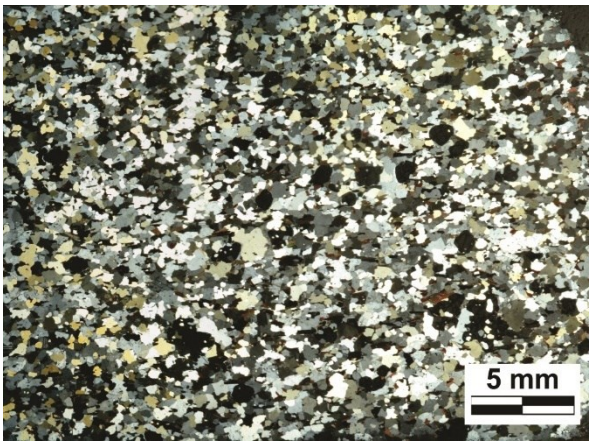

B and C: Photomicrographs showing the main mineralogy and texture.

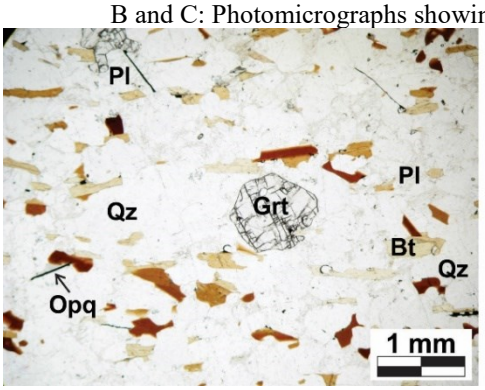

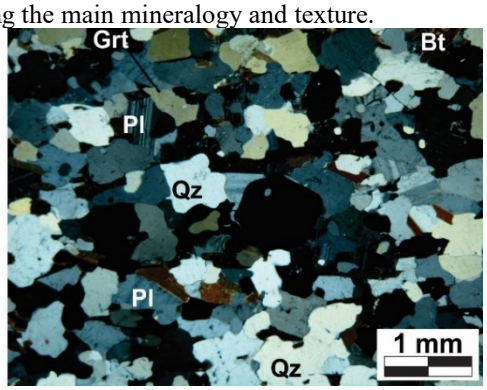

D and E: Photomicrographs showing the main mineralogy and texture.

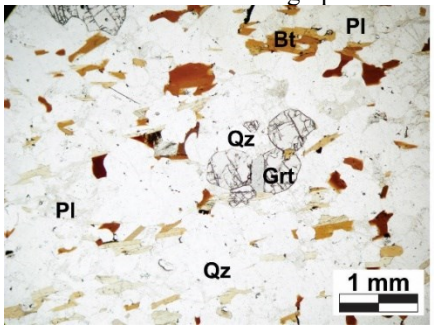

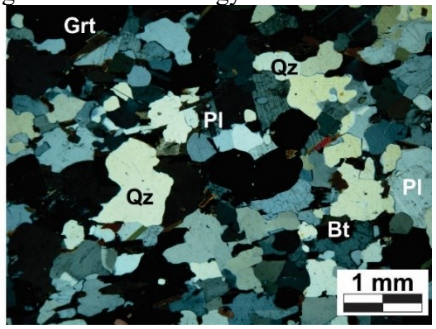

F and G: Photomicrographs showing the main mineralogy and texture.

SHEET OF PETROGRAPHIC DESCRIPTION	
PhD Thesis – Cristina Santos Araujo	
Sample identification: CA-14	**Field identification:** CA-14
Coordinates: -19,857562/-40,516296	**Location:** Santa Tereza, Espírito Santo state
Local name: Santa Tereza suite	**Lithologic unit:** G1 supersuite, pre-collisional plutonism – Rio Doce Magmatic arc
Sample Description	
Greenish gray rock, coarse-grained, with millimetric garnet. Locally, the minerals are oriented (Photograph A).	
Lithochemical signature	
Magnesian, calcic, slightly peraluminous, calc-alkaline serie	
Petrography	
Major minerals	Plagioclase (~40%), quartz (~35%), biotite (~10%), orthopyroxene (~5%), K-feldspar, (~5%), garnet (~4%)
Accessory minerals	Zircon, apatite, monazite, allanite, epidote
Alteration minerals	Amphibole, opaque minerals, sericite, muscovite, biotite, clay minerals, chorite, carbonate
Thin section description and interpretations	

The sample is relatively poorly deformed and preserves a magmatic appearance. It present medium to coarse-grained, granoblastic to granolepidoblastic texture, with the contacts between the grains being irregular, poligonal, interlobate, and straight. Foliation is noted by orientation of orthopyroxne, quartz, feldspars, and biotite, as well by concetration of orthopyroxene and garnet in a levels according the orientation of the other minerals (Photographs B to G).

Quartz presents subhedral to anhedral habits, light undulatory extinction and inclusions of biotite, and plagioclase.

Plagioclase is subhedral to euhedral and it present light sericitization and saussuritization. Some crystals show antiperthitic texture, compositional zoning, deformed and irregular twinning, and inclusions of biotite, zircon, apatite, garnet, and quartz.

Biotite shows dark brown to light brown pleochroism, subhedral to euhedral forms, moderate chloritization, pleochroic halos, and inclusions of zircon, quartz, monazite, allanite, and apatite.

Garnet poikiloblastic presents subhedral to anhedral habitus, light pink color, alteration into chlorite, inclusions of quartz, biotite, zircon, plagioclase, and apatite. There are garnet free-inclusions.

Orthopyroxene is subhedral to anhedral, with incolor to light greenish brown pleochroism and it present moderate uralitization into amphibole and biotite. Some crystals show and inclusions of biotite, plagioclase, zircon, apatite, quartz, and opaque minerals.

Apatite, monazite, and zircon shows stubby, prismatic, and rounded shaped, usually included in major minerals.

Lithology: Grt-Opx-Bt metagranodiorite

Photographs

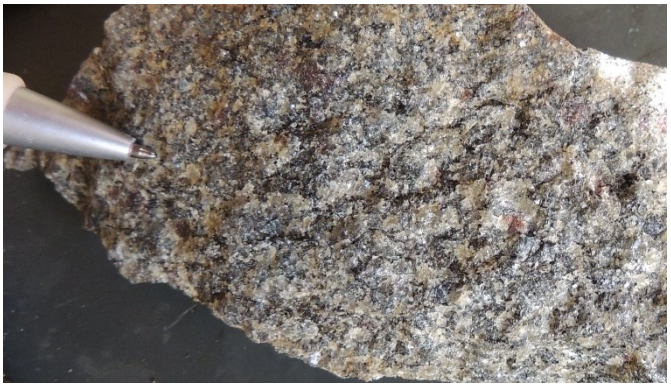

A: Sample CA-14

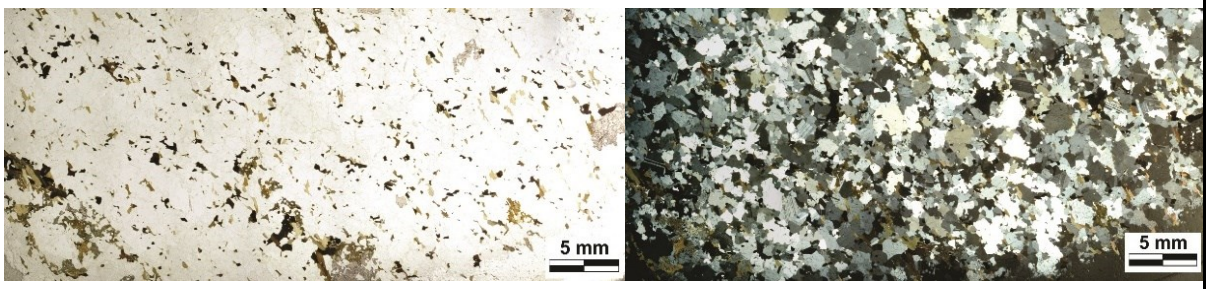

B and C: Photomicrographs showing the main mineralogy and texture.

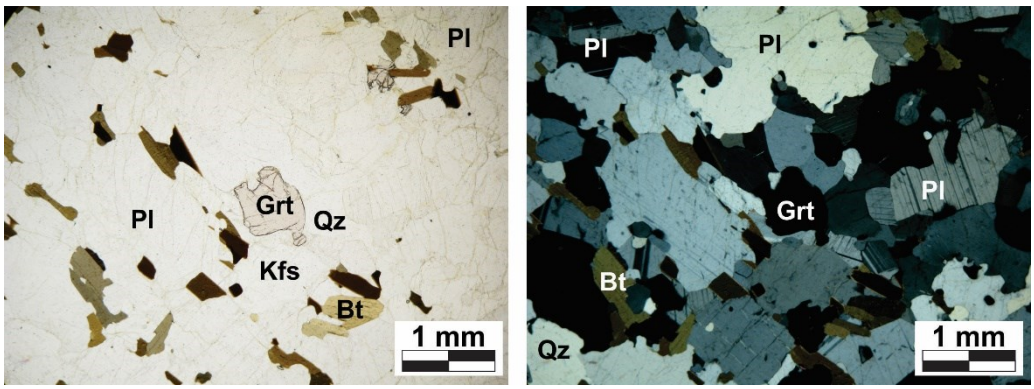

D and E: Photomicrographs showing the main mineralogy and texture.

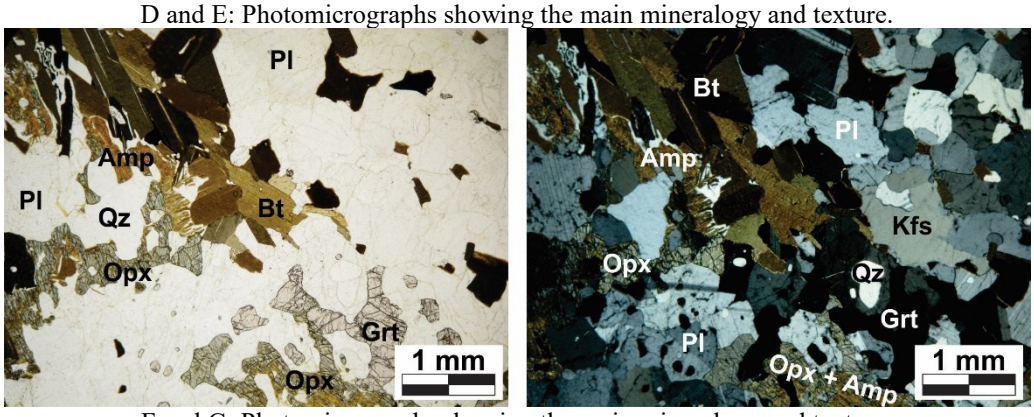

F and G: Photomicrographs showing the main mineralogy and texture.

SHEET OF PETROGRAPHIC DESCRIPTION	
PhD Thesis – Cristina Santos Araujo	
Sample identification: CA-17	**Field identification:** CA-17
Coordinates: -19,933009/-40,465542	**Location:** Fundão, Espírito Santo state
Local name: Santa Tereza suite	**Lithologic unit:** G1 supersuite, pre-collisional plutonism – Rio Doce Magmatic arc
Sample Description	
Greenish gray rock, coarse-grained, with high concentration of biotite. Locally, the minerals are oriented (Photograph A).	
Lithochemical signature	
Magnesian, calc-alkalic, metaluminous, high-K calc-alkaline serie	
Petrography	
Major minerals	Plagioclase (~55%), quartz (~15%), biotite (~15%), orthopyroxene (~5%), K-feldspar (~5%), Amphibole
Accessory minerals	Zircon, apatite, monazite
Alteration minerals	Amphibole, sericite, clay minerals, biotite, opaque minerals, chorite, rutile, carbonate
Thin section description and interpretations	

The sample is relatively poorly deformed and preserves a magmatic appearance. It present medium to coarse-grained, granoblastic to granolepidoblastic texture, with the contacts between the grains being irregular, interlobate, and straight. Foliation is noted by concetration of quartz, feldspar, orthopyroxene and biotite in felsic and mafic levels (Photographs B to G).

Quartz presents subhedral to anhedral habits, light undulatory extinction and inclusions of biotite, and plagioclase.

Plagioclase is subhedral to euhedral and it present moderate sericitization and saussuritization. Some crystals show antiperthitic texture, concentric zoning, deformed and irregular twinning, and inclusions of biotite, zircon, apatite, and quartz (Photographs D to G).

Biotite shows dark brown to light greenish brown pleochroism, subhedral to euhedral form, moderate chloritization, pleochroic halos, and inclusions of zircon, quartz, plagioclase, monazite, and apatite.

Orthopyroxene is subhedral to anhedral, with incolor to light greenish brown pleochroism and it present hight uralitization into amphibole and biotite. Some crystals show inclusions of biotite, zircon, apatite, and quartz.

Apatite, monazite, and zircon shows stubby, prismatic and rounded shaped, usually included in major minerals.

Lithology: Opx-Bt metadiorite

Photographs

A: Sample CA-17

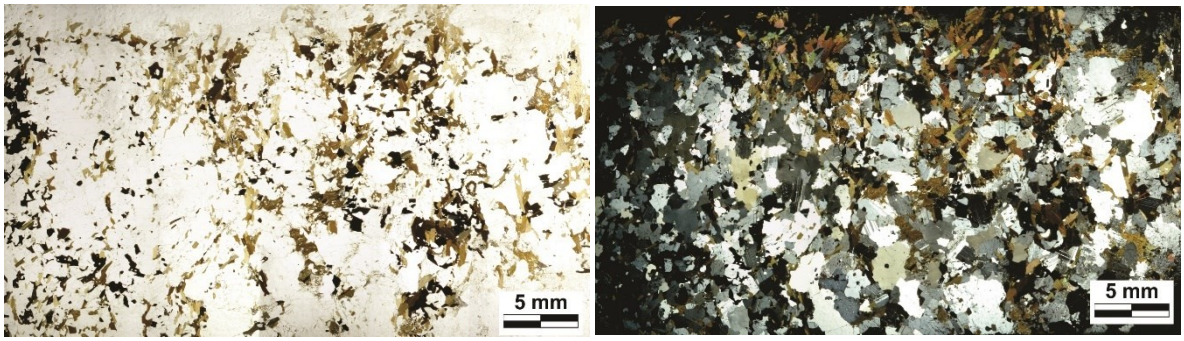

B and C: Photomicrographs showing the main mineralogy and texture.

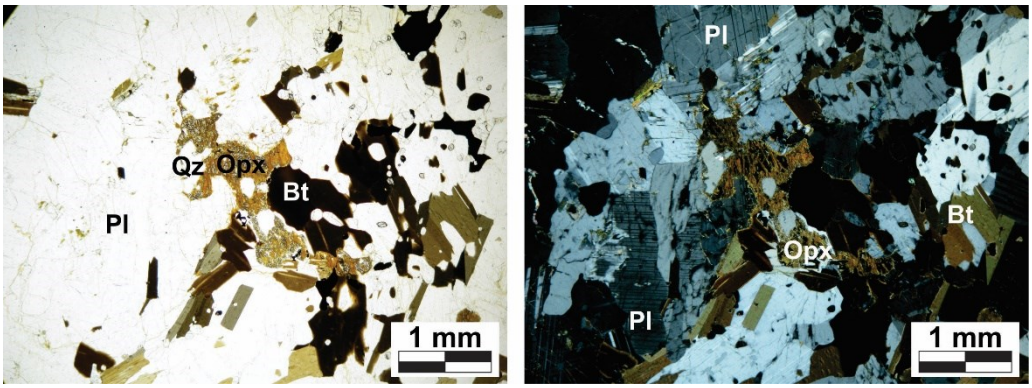

D and E: Photomicrographs showing the main mineralogy and texture.

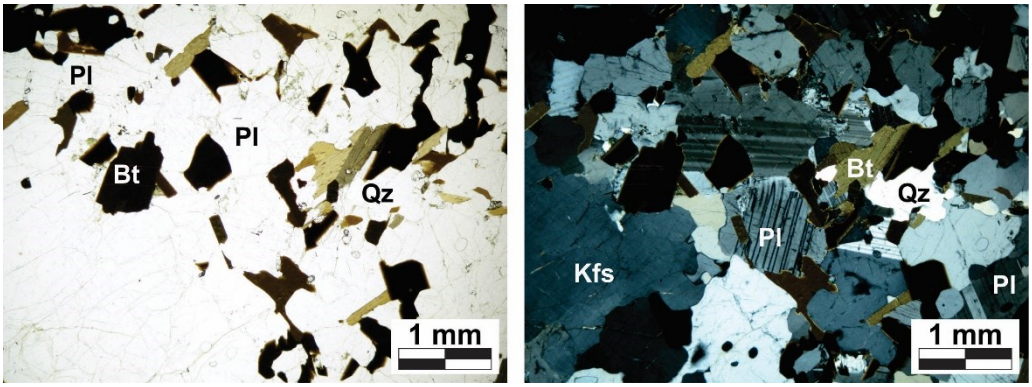

F and G: Photomicrographs showing the main mineralogy and texture.

SHEET OF PETROGRAPHIC DESCRIPTION	
PhD Thesis – Cristina Santos Araujo	
Sample identification: CA-18A	**Field identification:** CA-18
Coordinates: -19,933153/-40,467836	**Location:** Fundão, Espírito Santo state
Local name: Santa Tereza suite	**Lithologic unit:** G1 supersuite, pre-collisional plutonism – Rio Doce Magmatic arc
Sample Description	
Greenish gray rock, coarse-grained, with high concentration of biotite (Photograph A). Locally, the minerals are oriented.	
Lithochemical signature	
Magnesian, alkali-calcic, metaluminous, high-K calc-alkaline serie	
Petrography	
Major minerals	Plagioclase (~47%), biotite (~20%), orthopyroxene (~10%), clinopyroxene (~10%), quartz (~5%), amphibole (~5%)
Accessory minerals	K-feldspar, opaques minerals, zircon, apatite
Alteration minerals	Amphibole, opaque minerals, biotite, clay minerals, chorite, carbonate
Thin section description and interpretations	

The sample is relatively poorly deformed and preserves a magmatic appearance. It present medium to coarse-grained, equigranular texture, with the contacts between the grains being irregular, poligonal, and straight. Minerals are locality oriented (Photographs C to H).

Plagioclase is subhedral to euhedral and it present saussuritization. Some crystals show antiperthitic texture, compositional zoning, deformed and irregular twinning, light undulatory extinction and inclusions of biotite, orthpyrone, zircon, apatite, and quartz.

Biotite shows dark brown to light brown pleochroism, subhedral to euhedral form, locality oriented, moderate chloritization, pleochroic halos, and inclusions of zircon, quartz, monazite, and apatite.

Orthopyroxene is subhedral to anhedral, with incolor to light greenish brown pleochroism and it presents light uralitization into amphibole and biotite. Some crystals show compositional zoning, twinning, and inclusions of amphibole, biotite, zircon, apatite, quartz, and opaque minerals.

Clinopyroxene is subhedral to anhedral, with incolor to light greenish brown pleochroism and it presents light alteration. Some crystals show compositional zoning, and inclusions of amphibole, biotite, zircon, apatite, quartz, and opaque minerals.

Quartz presents subhedral to anhedral habits.

Amphibole presents anhedral to subhedral shapes, with light alteration.

Apatite, monazite, and zircon shows stubby, prismatic and rounded shaped, usually included in major minerals.

Lithology: Opx-Cpx-Bt metagabbro

Photographs

A: Charnockite in the outcrop; B: Sample CA-18A

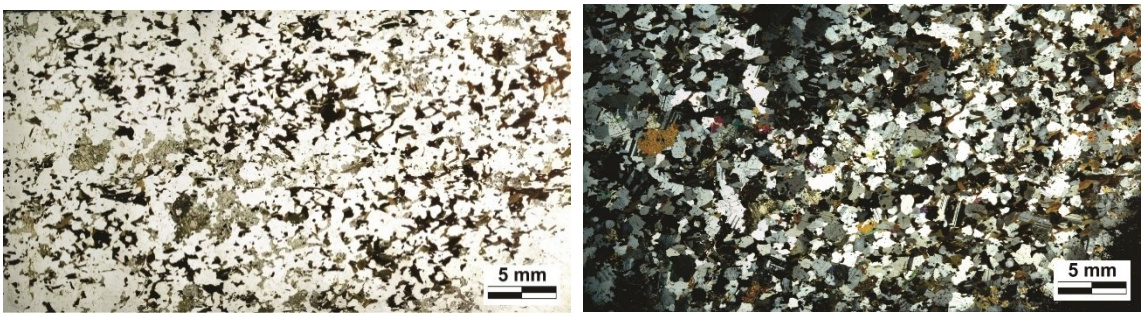

C and D: Photomicrographs showing the main mineralogy and texture.

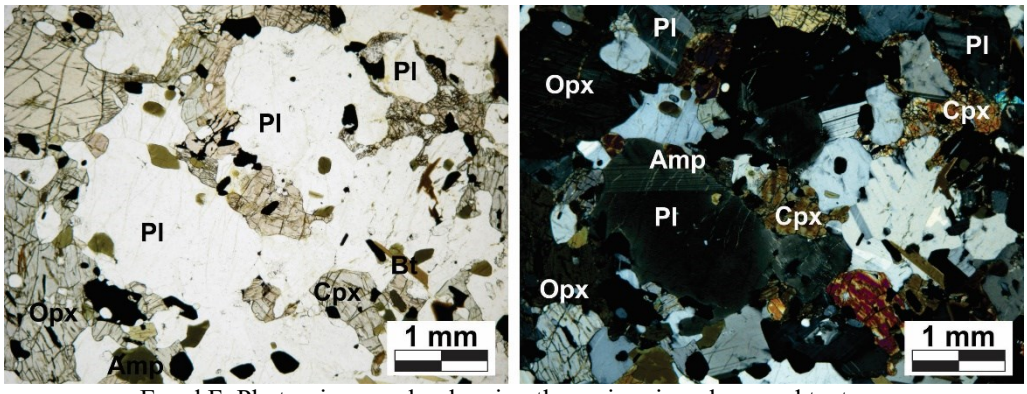

E and F: Photomicrographs showing the main mineralogy and texture.

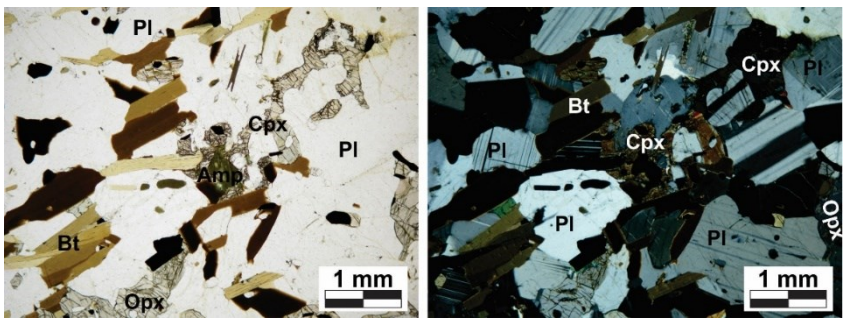

G and H: Photomicrographs showing the main mineralogy and texture.

SHEET OF PETROGRAPHIC DESCRIPTION	
PhD Thesis – Cristina Santos Araujo	
Sample identification: CA-18C	**Field identification:** CA-18
Coordinates: -19,933153/-40,467836	**Location:** Fundão, Espírito Santo state
Local name: Ataléia suite	**Lithologic unit:** G2 supersuite, collisional
Sample Description	
Foliated garnet-biotite granite with milimetric garnet, light gray, fine to medium-grained, showing about 10% of mafic minerals and local small felsic patches with core of garnet (Photograph A and B).	
Lithochemical signature	
Magnesian, alkali-calcic, slightly peraluminous, ultra high-k calc-alkaline serie	
Petrography	
Major minerals	Plagioclase (~47%), quartz (~30%), biotite (~10%), K-feldspar (~10%)
Accessory minerals	Opaque minerals, zircon, apatite, monazite
Alteration minerals	Sericite, clay minerals, chorite, carbonate
Thin section description and interpretations	

The sample preserves a magmatic appearance. It presents medium-grained, inequigranular texture, with the contacts between the grains being irregular, interlobate, and straight. Biotite are oriented locality (Photographs C to H).

Plagioclase is subhedral to anhedral, and it presents moderate sericitization and saussuritization. Some crystals show antiperthitic and myrmekitic intergrowths, compositional zoning, deformed and irregular twinning, and inclusions of biotite, quartz, zircon, apatite, and opaque minerals.

Quartz presents anhedral habit, undulatory extinction, and inclusions of zircon, and biotite.

Biotite shows reddish brown to light brown pleochroism, subhedral to euhedral form, light chloritization, pleochroic halos, and inclusions of opaque minerals, zircon, quartz, monazite, and apatite.

K-feldspar is microcline and triclinized orthoclase, with anhedral to subhedral forms, perthitic texture, and biotite, opaque minerals, and quartz inclusions.

Apatite, monazite, and zircon shows stubby, prismatic, and rounded shaped, usually included in major minerals.

Opaque minerals are subhedral to euhedral with granular habits.

Lithology: Foliated biotite tonalite

Photographs

A: Biotite tonalite in the outcrop; B: Sample CA-18C

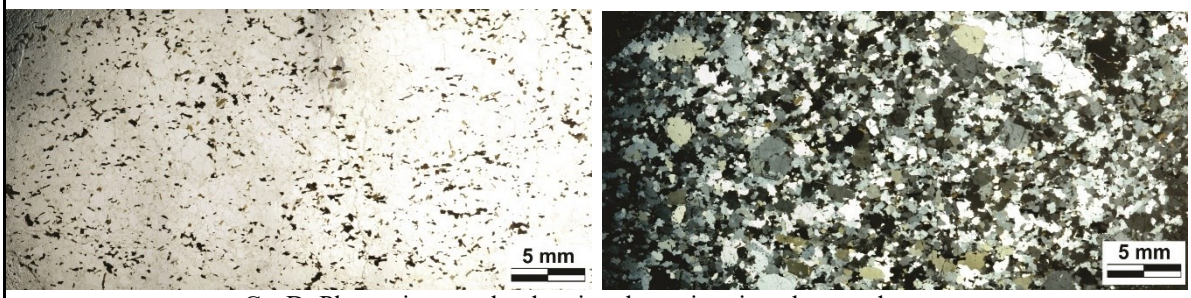

C e D: Photomicrographs showing the main mineralogy and texture.

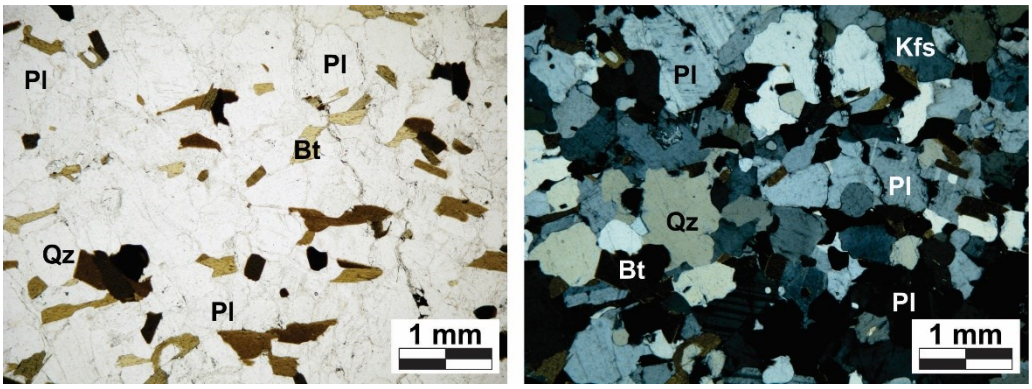

E e F: Photomicrographs showing the main mineralogy and texture.

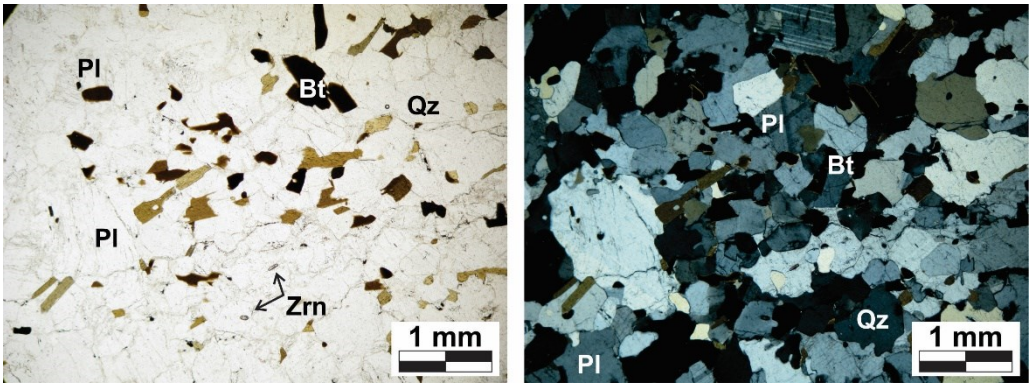

G e H: Photomicrographs showing the main mineralogy and texture.

SHEET OF PETROGRAPHIC DESCRIPTION	
PhD Thesis – Cristina Santos Araujo	
Sample identification: CA-19	**Field identification:** CA-19
Coordinates: -19,936737/-40,483412	**Location:** Santa Tereza, Espírito Santo state
Local name: Santa Tereza suite	**Lithologic unit:** G1 supersuite, pre-collisional plutonism – Rio Doce Magmatic arc
Sample Description	
Foliated biotite granite (Photograph A), light gray, with levels ranging from fine to coarse-grained and concentration of mafic minerals (Photograph B), and local small felsic patches very coarse-grained.	
Lithochemical signature	
Magnesian, calcic, slightly peraluminous, calc-alkaline serie	
Petrography	
Major minerals	Plagioclase (~47%), quartz (~30%), biotite (~15%), K-feldspar (~5%)
Accessory minerals	Zircon, apatite, monazite
Alteration minerals	Sericite, opaque minerals, muscovite, clay minerals, rutile, chorite, carbonate
Thin section description and interpretations	

The sample presents foliated, medium-grained, granoblastic poligonal to granolepidoblastic textures, with the contacts between the grains being irregular, poligonal, and straight. Foliation is defined by biotite oriented (Photographs B to H).

Plagioclase is subhedral to anhedral, and it presents moderate sericitization and saussuritization. Some crystals show antiperthitic intergrowths, compositional zoning, deformed and irregular twinning, and inclusions of biotite, quartz, monazite, zircon, and apatite.

Quartz presents subehdral to anhedral habits, undulatory extinction, and inclusions of biotite, plagioclase, and K-feldspar.

Biotite shows brown to light brown pleochroism, subhedral to euhedral form, light chloritization, pleochroic halos, and inclusions of zircon, quartz, monazite, and apatite.

K-feldspar is microcline and triclinized orthoclase, with anhedral to subhedral forms, perthitic texture, and biotite, and quartz inclusions.

Apatite and zircon shows stubby, rounded shaped, and prismatic forms, usually included in major minerals.

Monazite shows rounded shape, usually included in major minerals.

Lithology: Biotite metagranodiorite

Photographs

A: Biotite metatonalite in the outcrop; B: Sample CA-19

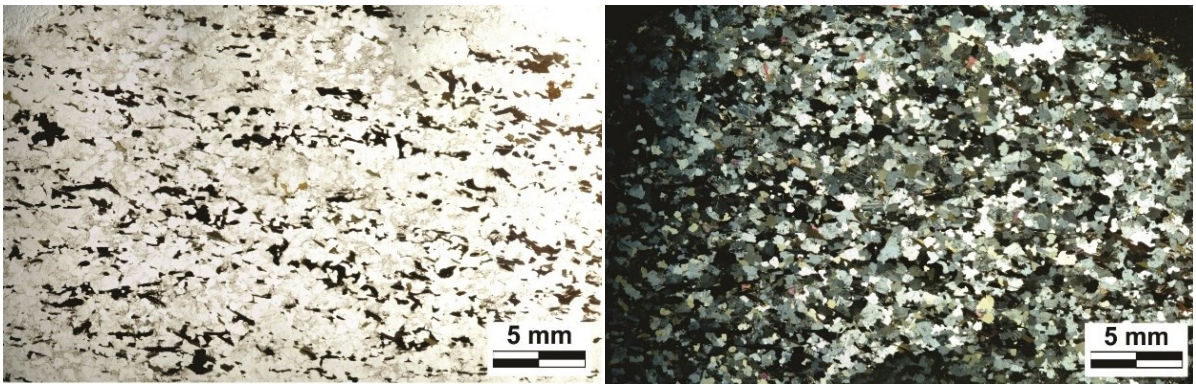

C and D: Photomicrographs showing the main mineralogy and texture.

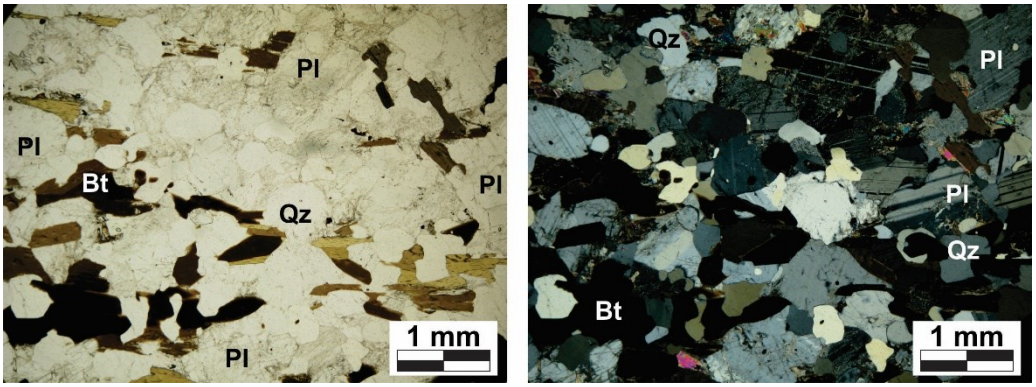

E and F: Photomicrographs showing the main mineralogy and texture.

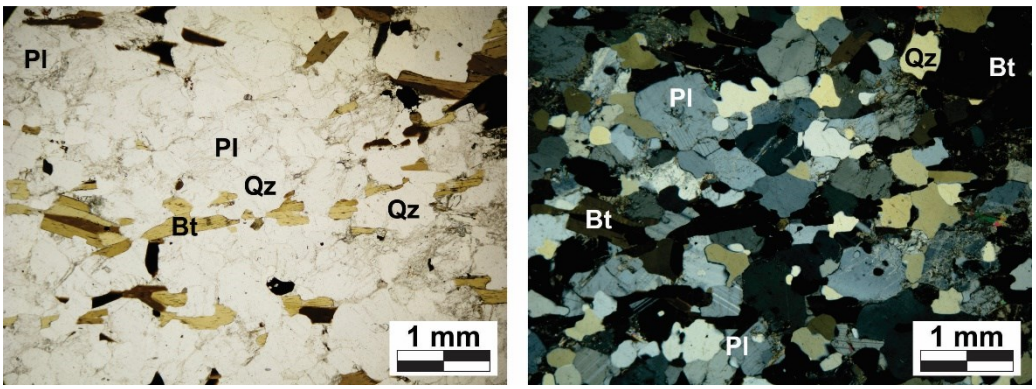

G and H: Photomicrographs showing the main mineralogy and texture.

SHEET OF PETROGRAPHIC DESCRIPTION	
PhD Thesis – Cristina Santos Araujo	
Sample identification: CA-20A	**Field identification:** CA-20
Coordinates: -19,934149/-40,501071	**Location:** Santa Tereza, Espírito Santo state
Local name: Santa Tereza suite	**Lithologic unit:** G1 supersuite, pre-collisional plutonism – Rio Doce Magmatic arc
Sample Description	
Greenish gray rock, coarse-grained, with high concentration of biotite (Photograph B). Locally, the minerals are oriented. In the outcrop there are levels ranging from fine to coarse-grained and variations in concentration of mafic and felsic minerals (Photograph A), and local small felsic patches very coarse-grained.	
Lithochemical signature	
Magnesian, calcic, slightly peraluminous, calc-alkaline serie	
Petrography	
Major minerals	Plagioclase (~52%), quartz (~20%), biotite (~15%), ortopyroxene (5%), garnet (~5%)
Accessory minerals	K-feldspar, opaque minerals, zircon, apatite, monazite, titanite
Alteration minerals	Amphibole, clay minerals, biotite, chorite, opaque minerals
Thin section description and interpretations	

The sample presents foliated, medium to coarse-grained, granoblastic to granolepidoblastic textures, with the contacts between the grains being irregular to straight. Foliation is noted by concetration of quartz, feldspar, orthopyroxene and biotite in felsic and mafic levels (Photographs C to H).

Plagioclase is subhedral to euhedral and it present light saussuritization. Some crystals show antiperthitic texture, compositional zoning, irregular twinning, and inclusions of biotite, zircon, apatite, garnet, and quartz.

Quartz presents subhedral to anhedral habits, light undulatory extinction and inclusions of biotite, plagioclase, apatite, zircon, and monazite.

Biotite shows dark brown to light greenish brown pleochroism, subhedral to euhedral form, pleochroic halos, and inclusions of zircon, quartz, monazite, and apatite.

Orthopyroxene is anhedral, with high uralitization into amphibole and biotite.

Garnet poikiloblastic presents anhedral habitus, light pink color, alteration into chlorite, inclusions of quartz, biotite, plagioclase, and apatite.

K-feldspar is ortoclase pertitic and triclinized. It has subhedral to anedral forms.

Apatite has euhedral to suhedral forms.

Zircon and monazite present prismatic and rounded habits, usually included in major minerals.

Opaque minerals are subhedral to euhedral with granular habits.

Lithology: Grt-Opx-Bt metatonalite

Photographs

A: Sample outcrop; B: Sample CA-20A

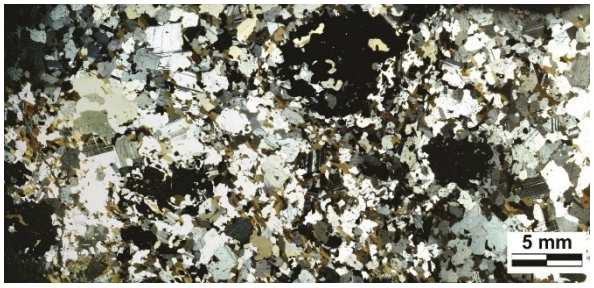

C e D: Photomicrographs showing the main mineralogy and texture.

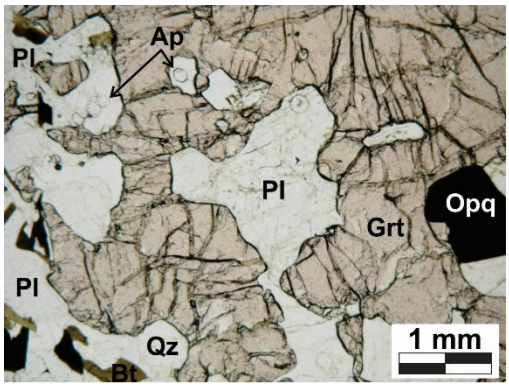

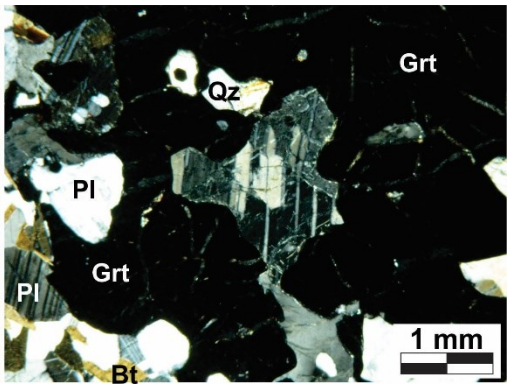

E e F: Photomicrographs showing the main mineralogy and texture.

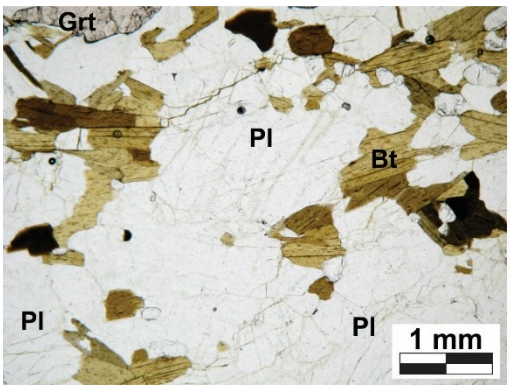

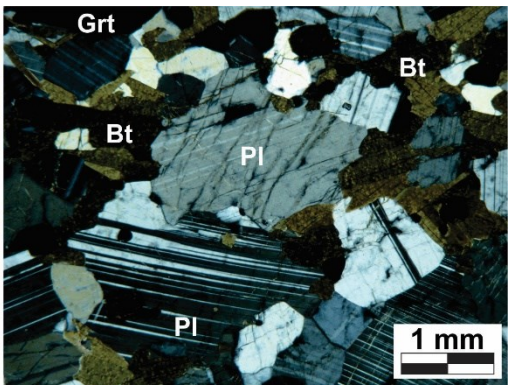

G e H: Photomicrographs showing the main mineralogy and texture.

SHEET OF PETROGRAPHIC DESCRIPTION	
PhD Thesis – Cristina Santos Araujo	
Sample identification: CA-21A	**Field identification:** CA-21
Coordinates: -19,896408/-40,517535	**Location:** Santa Tereza, Espírito Santo state
Local name: Santa Tereza suite	**Lithologic unit:** G1 supersuite, pre-collisional plutonism – Rio Doce Magmatic arc
Sample Description	
Greenish gray rock, coarse-grained, with milimetric garnet (Photographs A and B). Locally, the minerals are oriented. In the outcrop, this lithotype occurs in close spatial association with a fine-grained paragneiss (up contact - 60/15).	
Lithochemical signature	
Ferroan, calcic, slightly peraluminous, calc-alkaline serie	
Petrography	
Major minerals	Plagioclase (~56%), quartz (~15%), K-feldspar (~10%), biotite (~8%), amphibole (~3%), orthopyroxene (~2%), clinopyroxene (~1%), garnet (~1%)
Accessory minerals	Opaque minerals, zircon, apatite, monazite, titanite
Alteration minerals	Sericite, clay minerals, biotite, chorite, carbonate, epidote, opaque minerals
Thin section description and interpretations	

The sample presents foliated, medium to coarse-grained, inequigranular, granoblastic to granolepidoblastic textures, with the contacts between the grains being irregular, interlobate, and straight. Foliation is noted by concetration of quartz, feldspar, orthopyroxene and biotite in felsic and mafic levels (Photographs C to H).

Plagioclase is subhedral to anhedral and it present light sericitization and saussuritization. Some crystals show antiperthitic and myrmekitic intergrowths, compositional zoning, deformed and irregular twinning, and inclusions of biotite, zircon, apatite, and rounded quartz.

Quartz presents subhedral to anhedral habits, slight undulatory extinction and inclusions of biotite, plagioclase, and opaque minerals. Muscovite trails are frequent.

K-feldspar is microcline and triclinized orthoclase, with anhedral to euhedral forms, perthitic texture, and biotite, opaque minerals, and quartz inclusions.

Biotite shows dark brown to light greenish brown pleochroism, subhedral to euhedral forms, pleochroic halos, and inclusions of zircon, opaques minerals, quartz, monazite, and apatite. It is frequently associated with opaques minerals. Some crystals show deformated cleavage and quartz intergrowth.

Amphibole presents greenish brown pleochroism, alteration into chlorite and opaque minerals.

Orthopyroxene is subehdral to anhedral, with light brown to light greenish brown pleochroism and it present high uralitization into amphibole, opaque minerals, and biotite. Some crystals show inclusions of zircon, apatite, quartz, and opaque minerals. It is frequently associated with opaques minerals.

Garnet poikiloblastic presents subhedral habitus, light pink color, light chloritization, inclusions of quartz, and elongated biotite.

Apatite, monazite, and zircon shows stubby, prismatic, and rounded shaped, usually included in major minerals.

Opaque minerals are subhedral to euhedral with granular habits.

Lithology: Grt-Opx-Bt metatonalite

Photographs

A: Charnockite in the outcrop; B: Sample CA-21A.

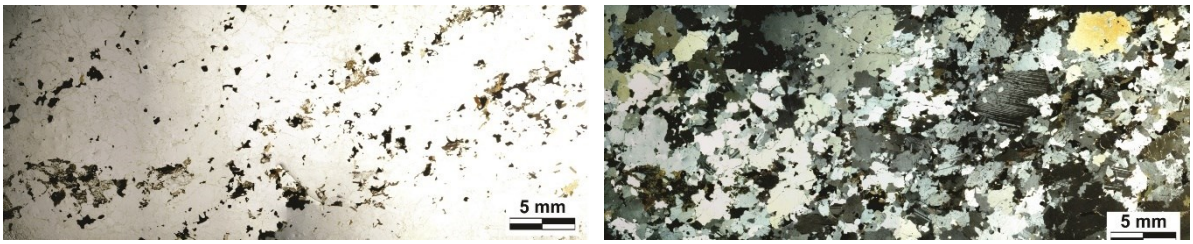

C e D: Photomicrographs showing the main mineralogy and texture.

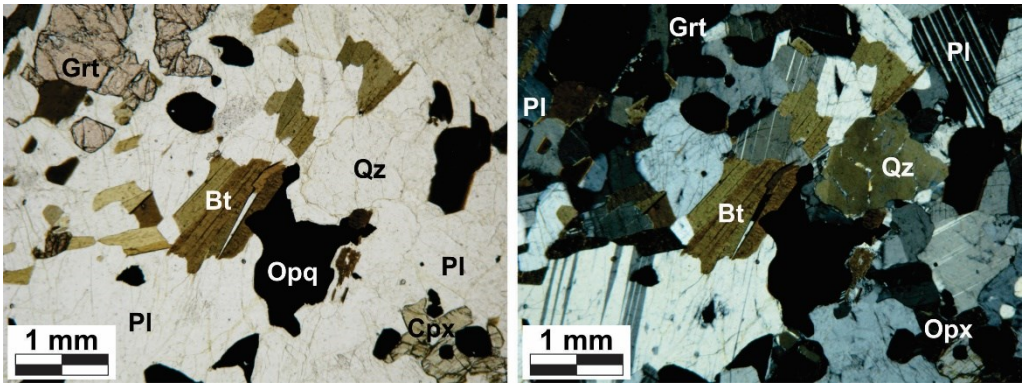

E e F: Photomicrographs showing the main mineralogy and texture.

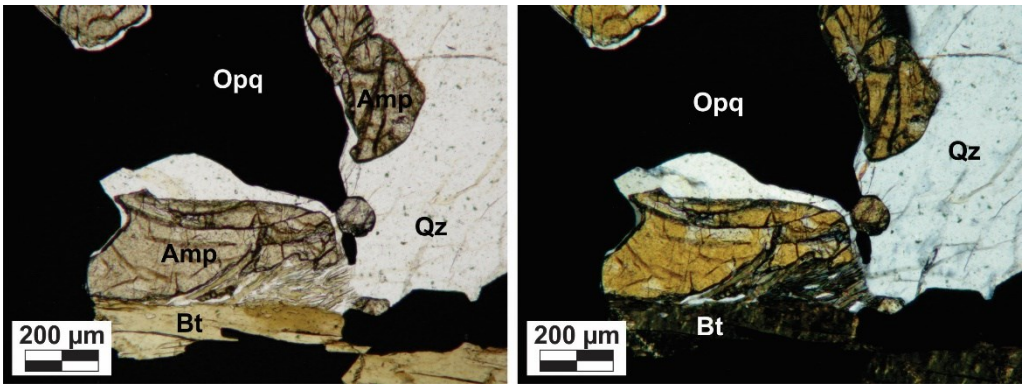

G e H: Photomicrographs showing the main mineralogy and texture.

SHEET OF PETROGRAPHIC DESCRIPTION	
PhD Thesis – Cristina Santos Araujo	
Sample identification: CA-23	**Field identification:** CA-23
Coordinates: -19,957087/-40,517063	**Location:** Santa Tereza, Espírito Santo state
Local name: Ataleia suite	**Lithologic unit:** G2 supersuite, collisional plutonism
Sample Description	
Foliated and banded biotite granite, light gray, with levels ranging from fine to coarse-grained, with milimetric garnet, and concentration of mafic minerals (Photographs A and B), and local small felsic patches very coarse-grained.	
Lithochemical signature	
Magnesian, alkali-calcic, peraluminous, ultra high-K calc-alkaline serie	
Petrography	
Major minerals	K-feldspar (~25%), cordierite (~15%), quartz (~20%), biotite (~15%), plagioclase (~20%), garnet (~2%)
Accessory minerals	Zircon, apatite, monazite, opaque minerals, sillimanite
Alteration minerals	Sericite, muscovite, opaque minerals, clay minerals, chorite, rutile, carbonate

Thin section description and interpretations

The sample presents foliated, fine to coarse-grained, inequigranular, granoblastic poligonal to granolepdoblastic textures, with the contacts between the grains being irregular, interlobate, and straight. Foliation is defined by recrystallized deformation bands with some minerals flattened and stretched, and biotite oriented. There are portions free-biotite, and levels with granulation varying (Photographs C to H).

K-feldspar is microcline with diffuse twinning and triclinized orthoclase, locality recrystallized or in flattened and stretched grains, with anhedral to subhedral forms, perthitic texture, and biotite, zircon, monazite, opaque minerals, and quartz inclusions. Some crystals show compositional zoning.

Cordierite presents anehdral shape, locality in flattened and stretched grains and recrystallized, with moderate pinitization, pleochroic halos, and inclusions of garnet, sillimanite, monazite, quartz, opaques minerals, and biotite. It is frequently associated with biotite and quartz intergrowths or in symplectite texture in garnet (Photographs E to H). Some crystals are bordered by biotite.

Quartz presents anhedral and subhedral habit, locality recrystallized or in flattened and stretched grains, undulatory extinction and inclusions of monazite, biotite, K-feldspar, and sillimanite.

Biotite shows reddish brown to light brown pleochroism, subhedral to euhedral form, light chloritization and muscovitization, pleochroic halos, and inclusions of opaque minerals, plagioclase, zircon, quartz, monazite, and apatite.

Plagioclase is subhedral to euhedral and it present light sericitization and saussuritization. Some crystals show antiperthitic texture, compositional zoning, deformed and irregular twinning, and inclusions of biotite, zircon, apatite, sillimanite, microcline, and opaque minerals.

Garnet presents anhedral habitus, and some crystals appear as pieces stretched among the essential minerals or as cordierite inclusions. They have inclusions of quartz, biotite, K-feldspar, apatite, monazite, cordierite, sillimanite, opaques minerals, and zircon. The larger crystals are bordered by cordierite + biotite symplectite texture (Photographs E to H).

Sillimanite has granular, and prismatic shape, appearing included in essential minerals.

Apatite, monazite, and zircon shows stubby, prismatic, and rounded shaped, usually included in major minerals.

Lithology: Grt-Crd-Bt metatexite

Photographs

A: Grt-Crd-Bt metatexite in the outcrop; B: Sample CA-23

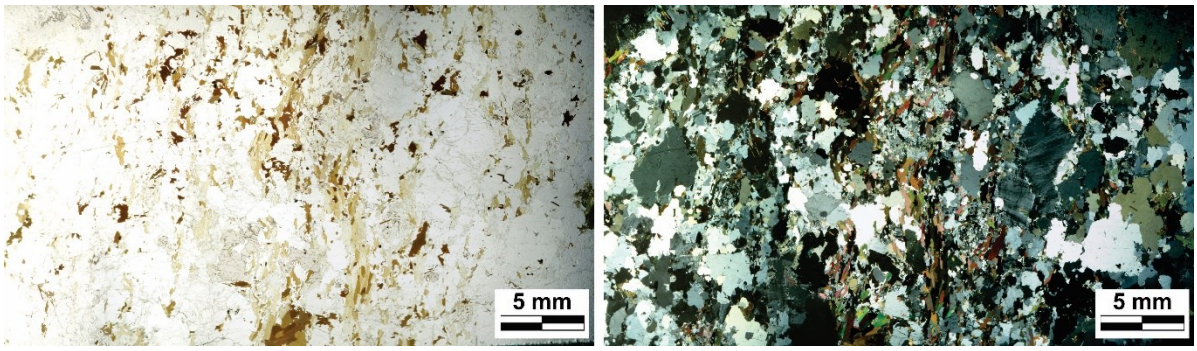

C and D: Photomicrographs showing the main mineralogy and texture.

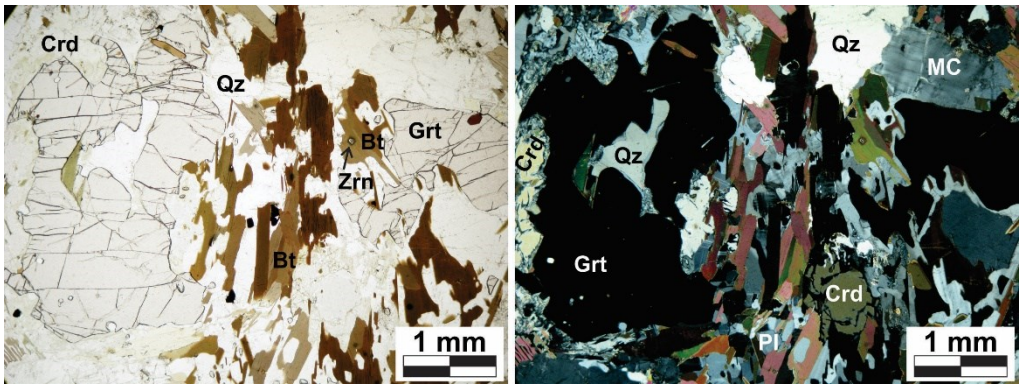

E and F: Photomicrographs showing the main mineralogy and texture. Symplectite texture might be noted in left garnet.

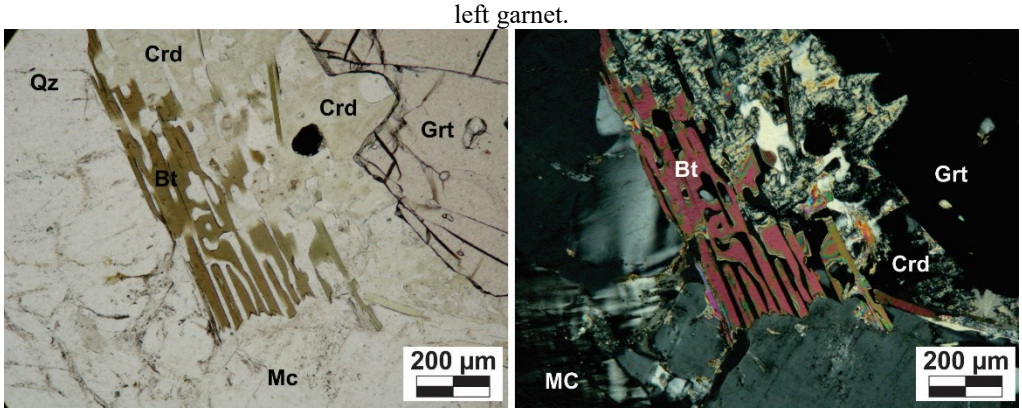

G and H: Photomicrographs showing the detail of symplectite texture and Bt + Crd intergrowth.

SHEET OF PETROGRAPHIC DESCRIPTION	
PhD Thesis – Cristina Santos Araujo	
Sample identification: CA-24	**Field identification:** CA-24
Coordinates: -19,994787/-40,499017	**Location:** Santa Leopoldina, Espírito Santo state
Local name: Santa Tereza suite	**Lithologic unit:** G1 supersuite, pre-collisional plutonism – Rio Doce Magmatic arc
Sample Description	
Greenish gray rock, medium-grained, isotropic	
Lithochemical signature	
Magnesian, calcic, slightly peraluminous, calc-alkaline serie	
Petrography	
Major minerals	Plagioclase (~42%), quartz (~30%), biotite (~15%), orthopyroxene (~8%)
Accessory minerals	K-feldspar, opaque minerals, zircon, apatite, allanite
Alteration minerals	Amphibole, sericite, biotite, clay minerals, chorite, opaque minerals

Thin section description and interpretations

The sample preserves a magmatic appearance. It presents medium-grained, granular texture, with the contacts between the grains being irregular, interlobate, poligonal, and straight. Biotite, quartz, feldspar, and orthopyroxene are concetrated in felsic and mafic levels (Photographs C to H).

Plagioclase is subhedral to euhedral and it present light sericitization and saussuritization. Some crystals show antiperthitic and mirmekite texture, compositional zoning, deformed and irregular twinning, and inclusions of biotite, zircon, apatite, and rounded quartz.

Quartz presents anhedral habit, slight undulatory extinction and inclusions of biotite, plagioclase, and K-feldspar.

Biotite shows dark brown to light brown pleochroism, subhedral to euhedral form, moderate chloritization and muscovitization, pleochroic halos, and inclusions of zircon, opaque minerals, quartz, and apatite. Some crystals show deformated cleavage and quartz intergrowth.

Orthopyroxene is anhedral, with incolor to light greenish brown pleochroism and it present moderate uralitization into amphibole and biotite. Some crystals show inclusions of biotite, zircon, apatite, quartz, plagioclase, and opaque minerals.

Apatite, allanite, and zircon shows stubby, prismatic, and rounded shaped, usually included in major minerals.

Lithology: Opx-Bt metatonalite

Photographs

A: Charnockite in the outcrop; B: Sample CA-24

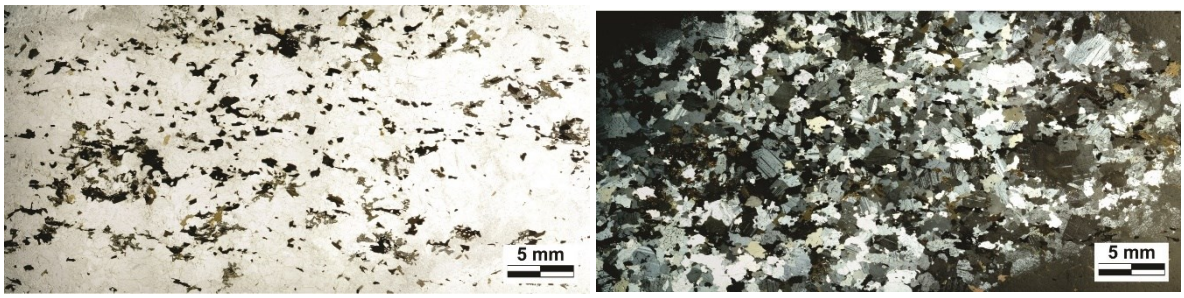

C and D: Photomicrographs showing the main mineralogy and texture.

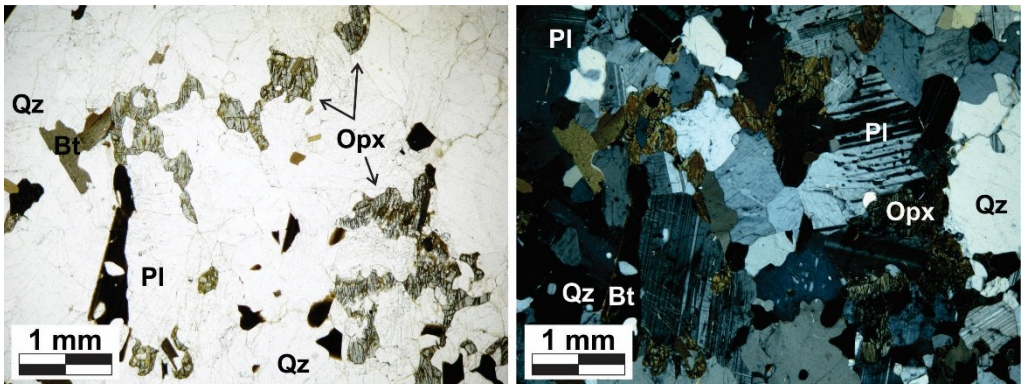

E and F: Photomicrographs showing the main mineralogy and texture.

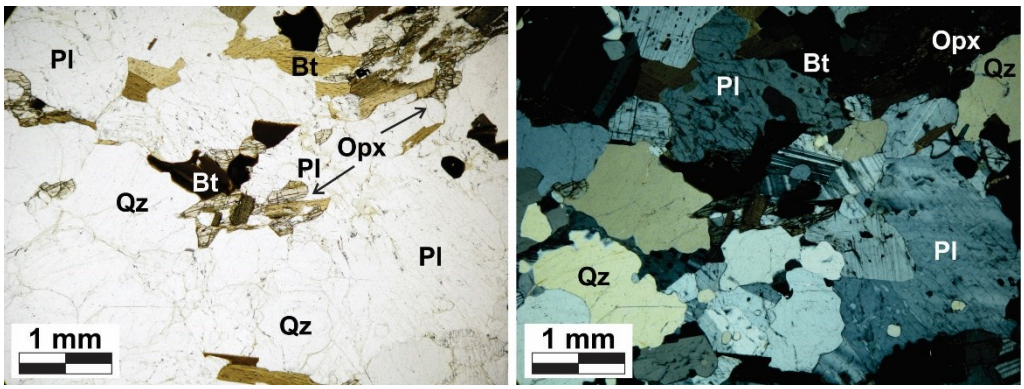

G and H: Photomicrographs showing the main mineralogy and texture.

SHEET OF PETROGRAPHIC DESCRIPTION	
PhD Thesis – Cristina Santos Araujo	
Sample identification: CA-27	**Field identification:** CA-27
Coordinates: -20,171016/-40,500235	**Location:** Santa Leopoldina, Espírito Santo state
Local name: Jequitibá suite	**Lithologic unit:** G1 supersuite, pre-collisional plutonism – Rio Doce Magmatic arc

Sample Description
Greenish gray rock, coarse-grained, with high concentration of biotite (Photograph B). Locally, the minerals are oriented. In the outcrop there are levels ranging from fine to coarse-grained and variations in concentration of mafic and felsic minerals (Photograph A and B).

Lithochemical signature
-

Petrography	
Major minerals	Plagioclase (~30%), amphibole (~25%), biotite (~20%), quartz (~15%)
Accessory minerals	K-feldspar, opaque minerals, zircon, apatite, monazite, titanite, opaque minerals
Alteration minerals	Clay minerals, sericite, muscovite, biotite, chorite, carbonate, opaque minerals

Thin section description and interpretations

The sample presents foliated, medium to coarse-grained, granoblastic to granolepidoblastic textures, with the contacts between the grains being irregular, interlobate, poligonal, and straight (Photographs B). Foliation is defined by major minerals oriented and stretched (Photographs C to H).

Plagioclase is euhedral to anhedral and it present light sericitization and saussuritization. Some crystals show antiperthitic texture, compositional zoning, and irregular twinning, and inclusions of biotite, zircon, apatite, and quartz.

Amphibole is anhedral to subhedral, with brown to green pleochroism and it present light alteration. Some crystals show compositional zoning, twinning, and inclusions of biotite, zircon, apatite, quartz, and opaque minerals.

Biotite shows reddish brown to light brown pleochroism, subhedral to euhedral forms, chloritization and muscovitization, pleochroic halos, and inclusions of zircon, quartz, monazite, and apatite.

Quartz presents anhedral habit, slight undulatory extinction, locality stretched, with inclusions of biotite, and plagioclase.

Apatite, monazite, titanite, and zircon shows stubby, prismatic, and rounded shaped, usually included in major minerals.

Lithology: Amphibolite

Photographs

A: Charnockite in the outcrop; B: Sample CA-27

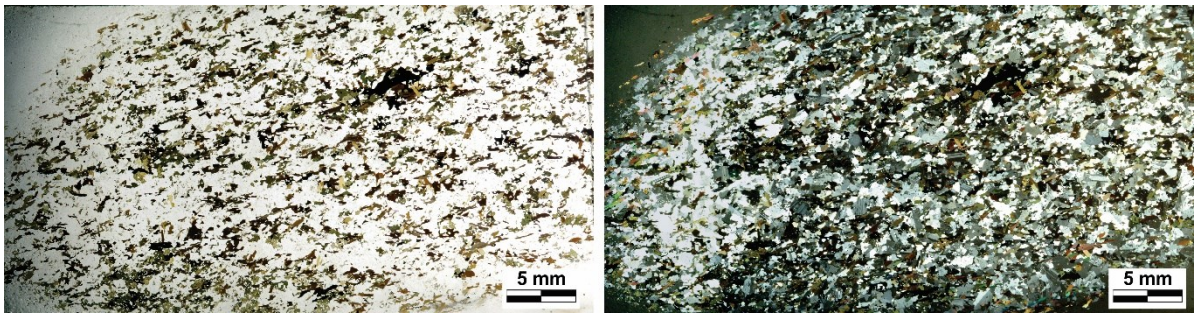

C and D: Photomicrographs showing the main mineralogy and texture.

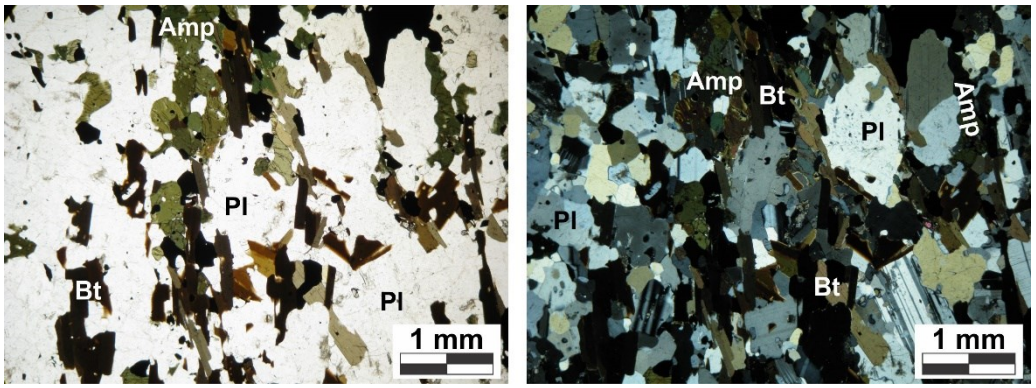

E and F: Photomicrographs showing the main mineralogy and texture.

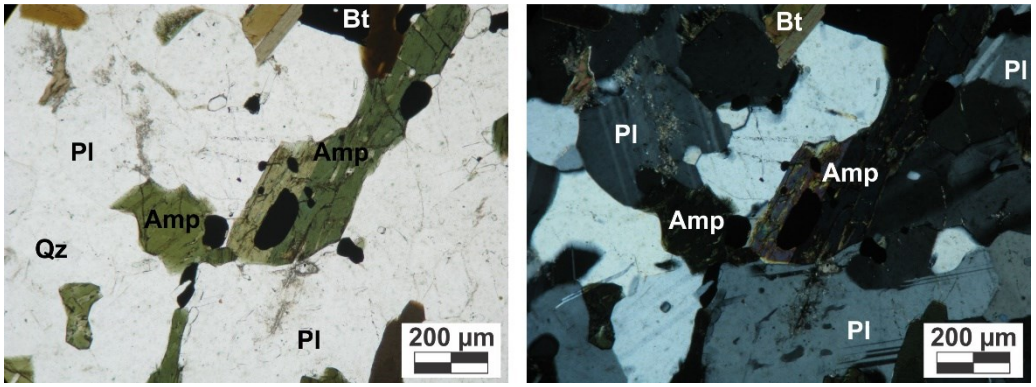

G and H: Photomicrographs showing the main mineralogy and texture.

SHEET OF PETROGRAPHIC DESCRIPTION	
PhD Thesis – Cristina Santos Araujo	
Sample identification: CA-28A	**Field identification:** CA-28
Coordinates: -19,800573/-40,683736	**Location:** Santa Tereza, Espírito Santo state
Local name: Nova Venécia complex	**Lithologic unit:** Nova Venécia complex, back-arc basin
Sample Description	
Migmatitic paragneisses (metatexite) stromatic, laminated to banded, with color variations of blue, dark gray, light brown, and beige being determined by the variation of cordierite, biotite, garnet, quartz, feldspar, sillimanite and accessory minerals (Photographs A and B). The compositional levels range from fine to coarse-grained. Garnet is present in all lithotypes. Some garnet and feldspar crystals have sigmoidal shape.	
Lithochemical signature	
-	
Petrography	
Major minerals	Quartz (~35%), cordierite (~25%), garnet (~10%), K-feldspar (~10%), biotite (~8%), plagioclase (~7%)
Accessory minerals	Opaque minerals, zircon, apatite, monazite, sillimanite, kyanite
Alteration minerals	Sericite, muscovite, clay minerals, carbonate, opaque minerals
Thin section description and interpretations	

The sample presents foliated, medium to coarse-grained, inequigranular, granoblastic to granolepdoblastic textures, with the contacts between the grains being irregular, interlobate, poligonal, and straight. Foliation is defined by ribbonlike deformation bands with flattened and stretched quartz, garnet, feldspars, and cordierite, as well biotite, opaque minerals, and sillimanite oriented. Foliation bypasses quartz and garnet porphyroblasts. Some levels present quartz, cordierite, and feldspar recrystallized (Photographs C to H).

Quartz presents anhedral and subhedral habits, locality recrystallized or in flattened and stretched grains, undulatory extinction and inclusions of biotite, plagioclase, monazite, and apatite.

Cordierite presents anhedral and subhedral habits, some crystals are poikiloblastic, locality recrystallized or in flattened and stretched grains. It presents moderate pinitization, undulatory extinction, pleochroic halos, and inclusions of monazite, zircon, sillimanite, quartz, apatite, opaques minerals, biotite, and K-feldspar. The inclusions of sillimanite, opaque minerals and biotite are oriented according with foliation. It often shows intergrowth with biotite, quartz e K-feldspar.

Poikiloblastic garnet presents subhedral to anhedral habitus, association with cordierite, inclusions of rounded quartz, and biotite, opaque minerals, apatite, monazite, plagioclase, sillimanite, and zircon. Minerals are concentrated around some garnets according to foliation. One crystal has cordierite symplectitic texture.

K-feldspar is microcline and triclinized orthoclase, with anhedral to euhedral forms, locality in flattened and stretched grains, light sericitization, perthitic texture, and biotite, zircon, plagioclase, opaque minerals, and quartz inclusions.

Biotite shows reddish brown to light brown pleochroism, anhedral to euhedral forms, pleochroic halos, and inclusions of opaque minerals, zircon, quartz, monazite, and apatite.

Plagioclase is subhedral to anhedral, commonly elongated according to bands, locality recrystallized, and it present light sericitization and saussuritization. Some crystals show antiperthitic texture, compositional zoning, deformed and irregular twinning, and inclusions of biotite, quartz, and sillimanite.

Sillimanite has granular, acicular and prismatic shape, appearing as trails oriented according to foliation among the essential minerals or included in them, and it is commonly associated with opaque minerals.

Apatite and zircon shows stubby, and prismatic forms, usually included in major minerals.

Monazite shows rounded shape, usually included in major minerals.

Kyanite is anhedral and subhedral, in paragenesis with plagioclase and cordierite.

Lithology: biotite-garnet paragneiss

Photographs

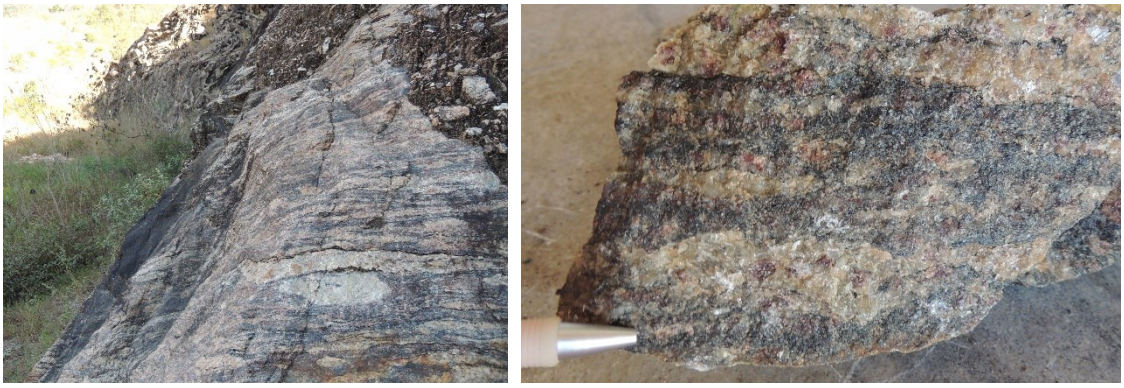

A: Paragneiss in the outcrop; B: Sample CA-28

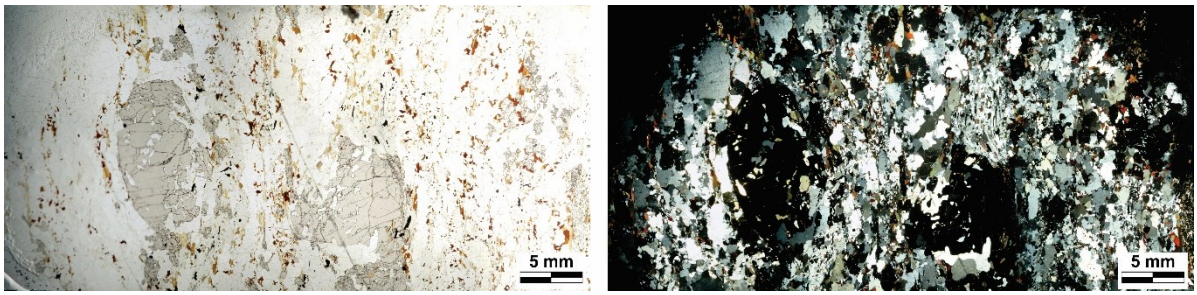

C and D: Photomicrographs showing the main mineralogy and texture.

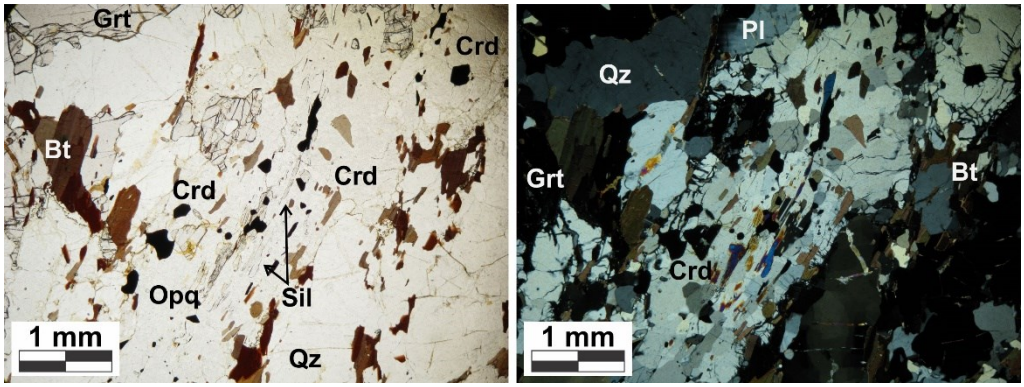

E and F: Photomicrographs showing the main mineralogy and texture.

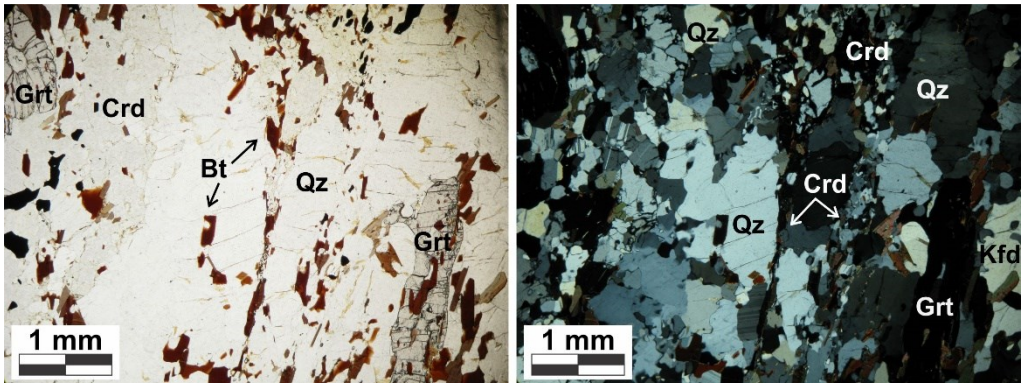

G and H: Photomicrographs showing the main mineralogy and texture.

SHEET OF PETROGRAPHIC DESCRIPTION	
PhD Thesis – Cristina Santos Araujo	
Sample identification: CA-28B	**Field identification:** CA-28
Coordinates: -19,800573/-40,683736	**Location:** Santa Tereza, Espírito Santo state
Local name: Nova Venécia complex	**Lithologic unit:** Nova Venécia complex, back-arc basin

Sample Description

Migmatitic paragneisses (metatexite) stromatic, laminated to banded, with color variations of blue, dark gray, light brown, beige, and red being determined by the variation of cordierite, garnet, biotite, quartz, feldspar, sillimanite and accessory minerals (Photographs A and B). The compositional levels range from fine to coarse-grained. Garnet is present in all lithotypes. Some garnet and feldspar crystals have sigmoidal shape.

Lithochemical signature

-

Petrography

Major minerals	Quartz (~30%), K-feldspar (~25%), plagioclase (~25%), garnet (~10%), biotite (~5%)
Accessory minerals	Cordierite, opaque minerals, zircon, monazite, sillimanite
Alteration minerals	Sericite, clay minerals, carbonate, opaque minerals

Thin section description and interpretations

The sample presents foliated, coarse-grained, inequigranular, granoblastic to granolepdoblastic textures, with the contacts between the grains being irregular, interlobate, poligonal, and straight. Foliation is defined by ribbonlike deformation bands with flattened and stretched quartz, garnet, and feldspars, as well biotite and acicular opaques oriented (Photographs C to G).

Quartz presents anhedral and subhedral habits, locality recrystallized or in flattened and stretched grains, undulatory extinction and inclusions of biotite, K-feldspar, plagioclase, and monazite.

K-feldspar is microcline and triclinized orthoclase, with anhedral to euhedral forms, locality in flattened and stretched grains, light sericitization, perthitic texture, and biotite, sillimanite, zircon, plagioclase, opaque minerals, and quartz inclusions.

Plagioclase is subhedral to anhedral, commonly elongated according to bands, locality recrystallized, and it present light sericitization and saussuritization. Some crystals show antiperthitic and myrmekitic textures, compositional zoning, deformed and irregular twinning, and inclusions of K-feldspar, cordierite, biotite, quartz, and sillimanite.

Poikiloblastic garnet presents subhedral to anhedral habitus, flattened and stretched, inclusions of rounded quartz, and biotite, opaque minerals, monazite, plagioclase, sillimanite, and zircon. Sillimanite are concentrated around some garnets according to foliation.

Biotite shows reddish brown to light brown pleochroism, anhedral to euhedral form, pleochroic halos, and inclusions of zircon, quartz, and monazite.

Cordierite presents flattened and stretched between major minerals, and moderate pinitization.

Sillimanite has granular, acicular and prismatic shapes, appearing included in essential minerals as trails oriented according to foliation.

Zircon shows stubby, and prismatic forms, usually included in major minerals.

Monazite shows rounded shape, usually included in major minerals.

Lithology: biotite-garnet paragneiss

Photographs

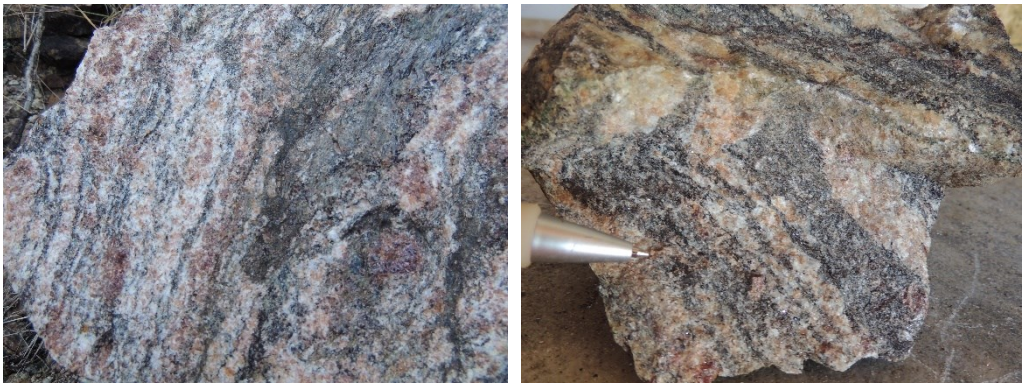

A: Paragneiss in the outcrop; B: Sample CA-28B

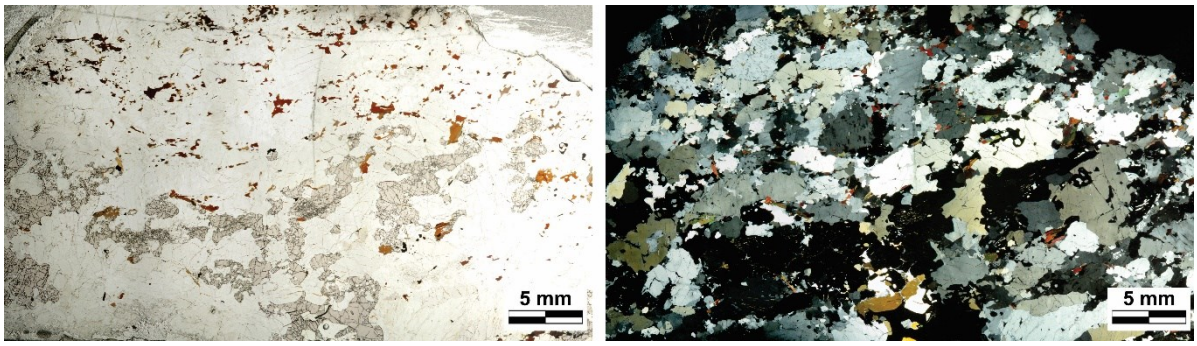

C and D: Photomicrographs showing the main mineralogy and texture.

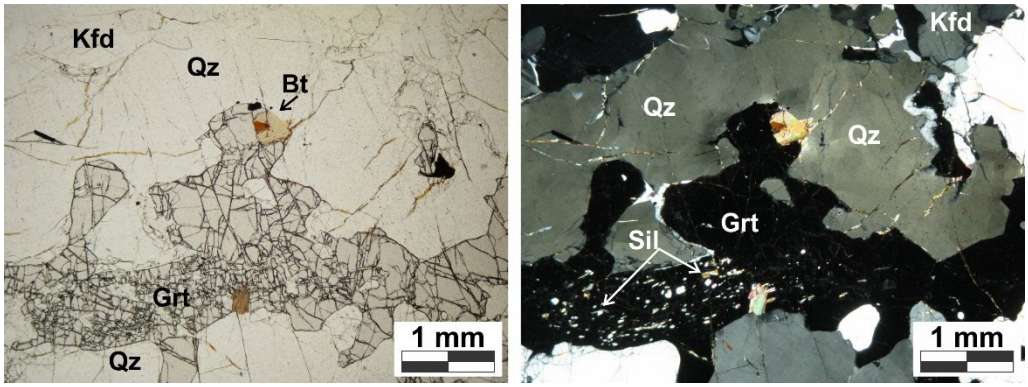

E and F: Photomicrographs showing the main mineralogy and texture.

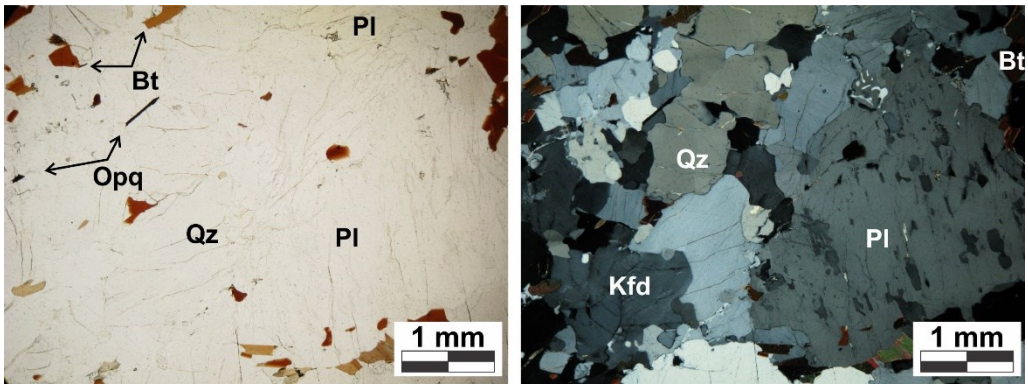

G and H: Photomicrographs showing the main mineralogy and texture.

SHEET OF PETROGRAPHIC DESCRIPTION	
PhD Thesis – Cristina Santos Araujo	
Sample identification: CA-28C	**Field identification:** CA-28
Coordinates: -19,800573/-40,683736	**Location:** Santa Tereza, Espírito Santo state
Local name: Nova Venécia complex	**Lithologic unit:** Nova Venécia complex, back-arc basin
Sample Description	
Light rock, coarse-grained, composed essentially by quartz, feldspar, and euhedral garnet. There are few biotite, mainly around garnet, forming fine levels (Photographs A and B).	
Lithochemical signature	
-	
Petrography	
Major minerals	Plagioclase (~32%), quartz (~30%), garnet (~15%), K-feldspar (~15%), biotite (~3%)
Accessory minerals	Opaque minerals, zircon, monazite
Alteration minerals	Sericite, muscovite, clay minerals, chorite, carbonate, rutile, opaque minerals
Thin section description and interpretations	

The sample is very coarse to coarse-grained, with granoblastic texture, contacts between the grains being irregular to interlobate (Photographs C to H).

Plagioclase is subhedral to anhedral, locality recrystallized or with undulatory extinction, and it present light sericitization and saussuritization. Some crystals show antiperthitic and myrmekitic intergrowths, compositional zoning, deformed and irregular twinning, and inclusions of biotite, plagioclase, quartz, and “micro rock”.

Quartz presents anhedral and subhedral habits, locality recrystallized with undulatory extinction and inclusions of biotite, K-feldspar, plagioclase, zircão, and monazite.

Garnet presents subhedral habitus, inclusions of rounded quartz, and biotite, opaque minerals, monazite, plagioclase, and zircon. Some crystals are surrounded by biotite.

Biotite shows reddish brown to light brown pleochroism, locality deformed, with subhedral to subhedral form, and inclusions of opaque minerals, and quartz.

K-feldspar is microcline and triclinized orthoclase, with anhedral to subhedral forms, light sericitization, perthitic texture, and biotite, zircon, plagioclase, opaque minerals, and quartz inclusions.

Monazite and zircon shows stubby, rounded, and prismatic forms, usually included in major minerals.

Lithology: Leucossome

Photographs

A: Leucossome in the outcrop; B: Sample CA-28C

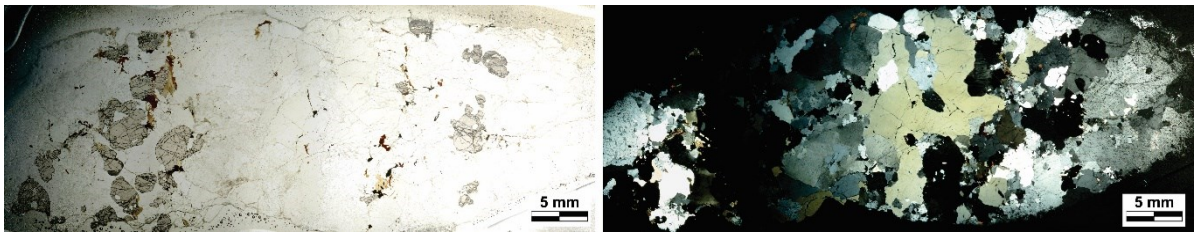

C and D: Photomicrographs showing the main mineralogy and texture.

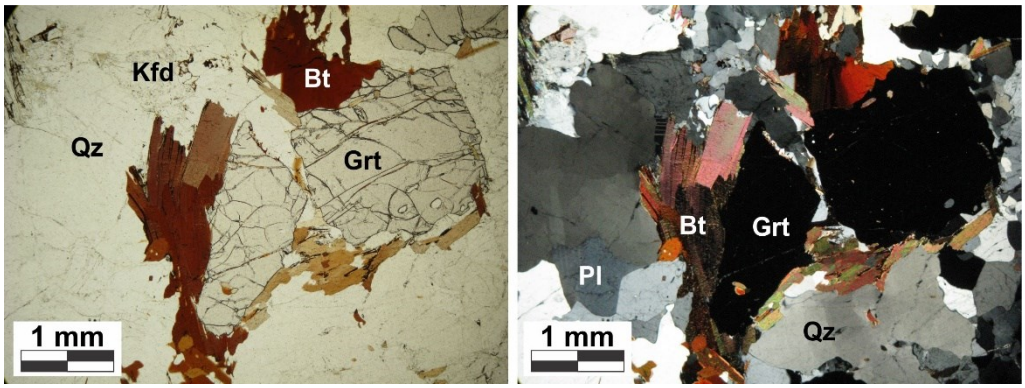

E and F: Photomicrographs showing the main mineralogy and texture.

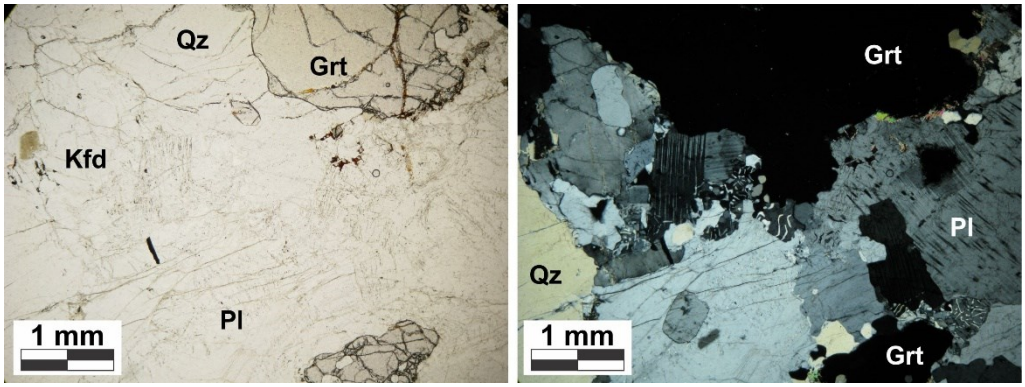

G and H: Photomicrographs showing the main mineralogy and texture.

SHEET OF PETROGRAPHIC DESCRIPTION	
PhD Thesis – Cristina Santos Araujo	
Sample identification: CA-29	**Field identification:** CA-29
Coordinates: -20,09411/-40,561507	**Location:** Santa Leopoldina, Espírito Santo state
Local name: Jequitibá suite	**Lithologic unit:** G1 supersuite, pre-collisional plutonism – Rio Doce Magmatic arc
Sample Description	
Greenish gray rock, fine to medium-grained, with high concentration of biotite in spherical clusters. Locally, the minerals are oriented (Photograph A and B).	
Lithochemical signature	
-	
Petrography	
Major minerals	Plagioclase (~45%), amphibole (~20%), quartz (~10%), biotite (~10%), orthopyroxene (~5%), clinopyroxene (~5%)
Accessory minerals	K-feldspar, opaques minerals, zircon, apatite, epidote
Alteration minerals	Amphibole, biotite, clay minerals, chorite, rutile, carbonate, opaques minerals
Thin section description and interpretations	

The sample is relatively poorly deformed and preserves a magmatic appearance. It present medium-grained, granolepidoblastic texture, with the contacts between the grains being irregular, and interlobate (Photographs B to H).

Plagioclase is subhedral to anhedral and it present light sericitization and saussuritization. Some crystals show antiperthitic texture, compositional zoning, deformed and irregular twinning, and inclusions of biotite, zircon, apatite, opaque minerals, amphibole, and quartz.

Amphibole is horblend, euhedral to anhedral, with greenish brown pleochroism, moderate alteration biotite, and inclusions of biotite, zircon, apatite, quartz, and opaque minerals.

Quartz presents subhedral to anhedral habits, light undulatory extinction, and inclusions of biotite, and plagioclase.

Biotite shows brown pleochroism, subhedral to euhedral form, moderate chloritization, pleochroic halos, and inclusions of zircon, quartz, and apatite.

Clinopyroxene altered to amphibole. Some crystals show compositional zoning,

Apatite and zircon shows stubby, rounded, and prismatic forms, usually included in major minerals.

Lithology: Opx-Bt metatonalite

Photographs

A: Charnockite in the outcrop; B: Sample CA-29

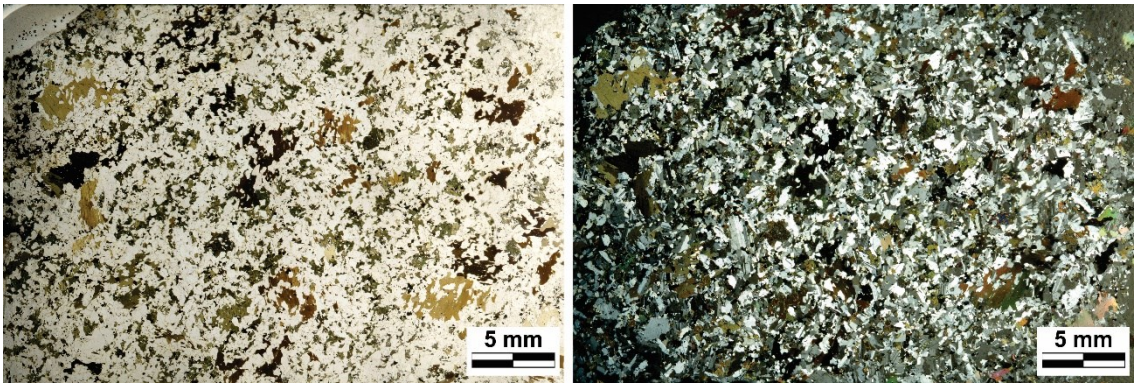

C and D: Photomicrographs showing the main mineralogy and texture.

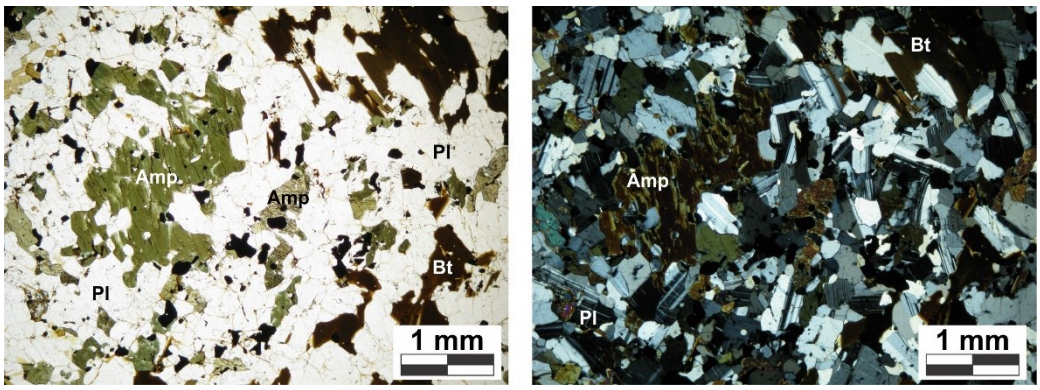

E and F: Photomicrographs showing the main mineralogy and texture.

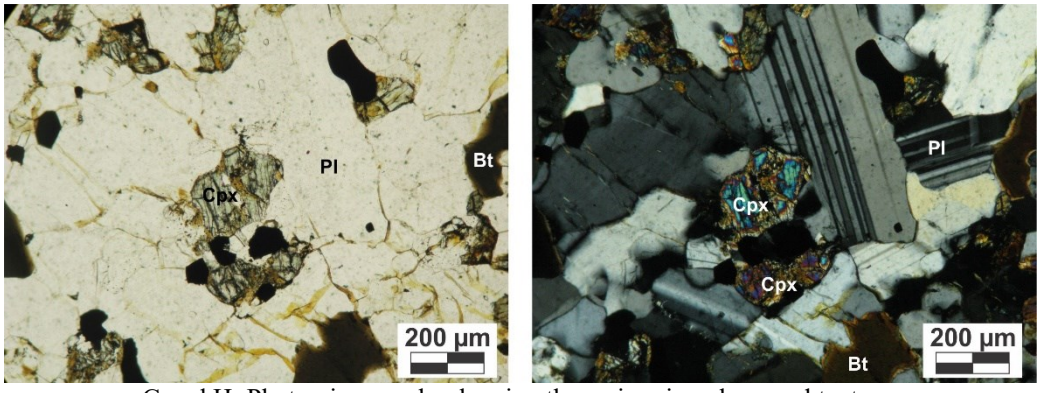

G and H: Photomicrographs showing the main mineralogy and texture.

SHEET OF PETROGRAPHIC DESCRIPTION	
PhD Thesis – Cristina Santos Araujo	
Sample identification: CA-30	**Field identification:** CA-30
Coordinates: -20,114662/-40,577807	**Location:** Santa Leopoldina, Espírito Santo state
Local name: Jequitibá suite	**Lithologic unit:** G1 supersuite, pre-collisional plutonism – Rio Doce Magmatic arc

Sample Description
Foliated biotite granite, light gray, medium-grained, with local small felsic patches coarse-grained (Photograph B). In the outcrop, this lithotype present mafic enclaves and intrude a migmatitic paragneiss (Photograph A).
Lithochemical signature
Magnesian, alkali-calcic, slightly peraluminous, high-K calc-alkaline serie

Petrography	
Major minerals	Plagioclase (~60%), quartz (~15%), biotite (~15%), K-feldspar (~5%)
Accessory minerals	Opaque minerals, zircon, apatite, monazite, allanite
Alteration minerals	Sericite, muscovite, clay minerals, carbonate, opaque minerals

Thin section description and interpretations

The sample is relatively poorly deformed and preserves a magmatic appearance. It present medium-grained, granolepidoblastic texture, with the contacts between the grains being irregular, and interlobate (Photographs B to H).

Plagioclase is subhedral to anhedral, and it present moderate sericitization and saussuritization. Some crystals show antiperthitic and myrmekitic intergrowths, compositional zoning, irregular twinning, and inclusions of biotite, zircon, quartz, apatite, opaque minerals, and monazite.

Quartz presents anhedral habit, undulatory extinction and inclusions of biotite, plagioclase, zircon, and biotite.

Biotite shows dark brown to light brown pleochroism, subhedral to euhedral form, pleochroic halos, and inclusions of zircon, quartz, monazite, and apatite. Some crystals are locally oriented.

K-feldspar is essentially microcline, with anhedral to subhedral forms, light sericitization, perthitic texture, and inclusions of biotite, plagioclase, and quartz.

Apatite and zircon shows stubby, and prismatic forms, usually included in major minerals.

Monazite shows rounded shape, usually included in major minerals.

Lithology: biotite metadiorite

Photographs

A: Biotite metatonalite in the outcrop; B: Sample CA-30

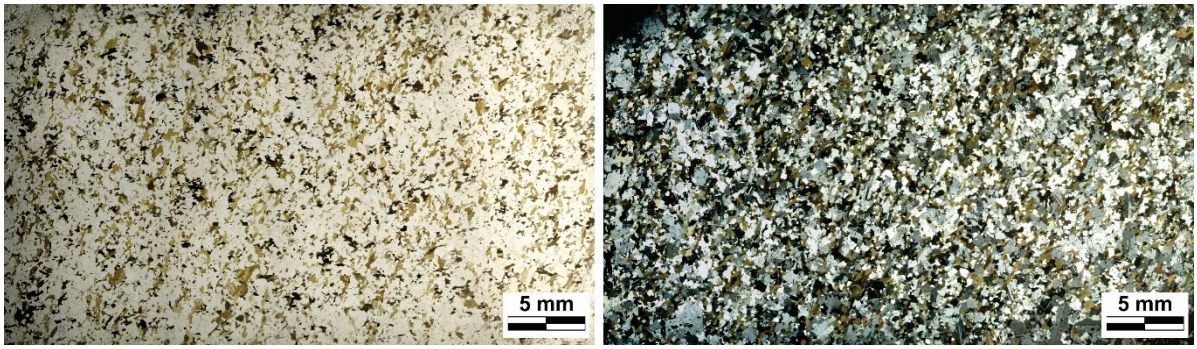

C and D: Photomicrographs showing the main mineralogy and texture.

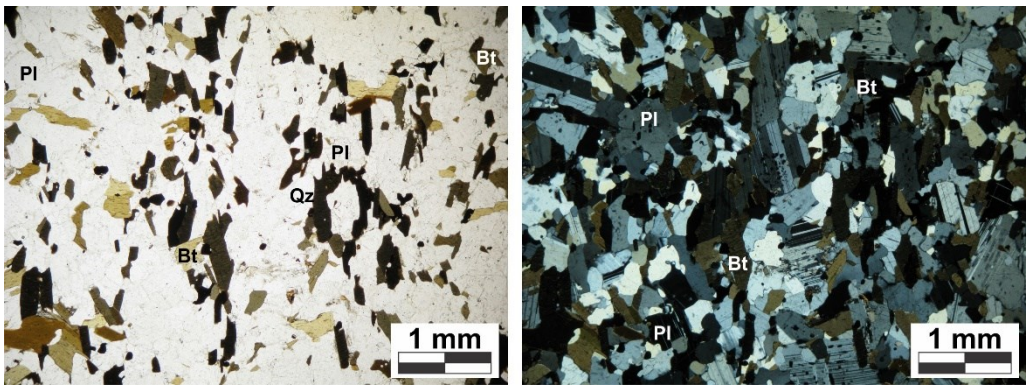

E and F: Photomicrographs showing the main mineralogy and texture.

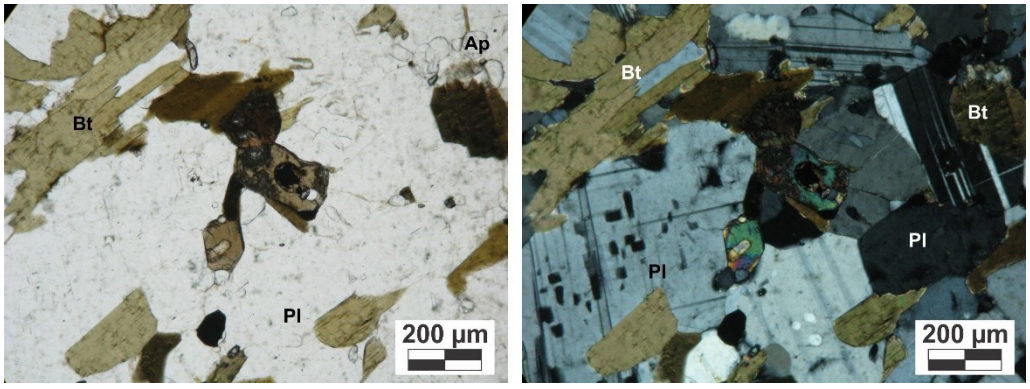

G and H: Photomicrographs showing the main mineralogy and texture.

SHEET OF PETROGRAPHIC DESCRIPTION	
PhD Thesis – Cristina Santos Araujo	
Sample identification: CA-31	**Field identification:** CA-31
Coordinates: -20,046944/-40,699558	**Location:** Santa Maria de Jetibá, Espírito Santo state
Local name: Jequitibá suite	**Lithologic unit:** G1 supersuite, pre-collisional plutonism – Rio Doce Magmatic arc
Sample Description	
Foliated biotite granite with milimetric garnet, light gray, coarse-grained, showing about 15% of mafic minerals and local small felsic patches (Photographs A and B).	
Lithochemical signature	
Magnesian, calcic, slightly peraluminous, calc-alkaline serie	
Petrography	
Major minerals	Plagioclase (~42%), quartz (~30%), K-feldspar (~15%), biotite (~10%), garnet (~1%)
Accessory minerals	Opaque minerals, zircon, apatite, monazite, allanite
Alteration minerals	Sericite, muscovite, clay minerals, chorite
Thin section description and interpretations	

The sample presents foliated, medium to coarse-grained, granoblastic to granolepidoblastic textures, with the contacts between the grains being irregular, poligonal, and straight. Foliation is defined by stretched minerals (Photographs C to H).

Plagioclase is anhedral to euhedral and it present light sericitization and saussuritization. Some crystals show antiperthitic intergrowths, irregular twinning, and inclusions of biotite, zircon, garnet, apatite, and rounded quartz.

Quartz presents anhedral habit, light undulatory extinction and inclusions of biotite, plagioclase, and opaque minerals.

K-feldspar is orthoclase and microcline, with anhedral to euhedral forms, light sericitization, perthitic texture, and biotite, plagioclase, and quartz inclusions.

Biotite shows dark brown to light brown pleochroism, subhedral to euhedral form, moderate chloritization and muscovitization, pleochroic halos, and inclusions of quartz, plagioclase, monazite, and apatite.

Garnet presents subhedral habitus, pink color, inclusions of rounded quartz and apatite.

Apatite and zircon shows stubby, prismatic and acicular forms, usually included in major minerals.

Allanite is incolor to light beige, with rounded shape.

Monazite shows rounded shape, usually included in major minerals.

Lithology: Grt-Bt metagranodiorite

Photographs

A: Foliated biotite granite in the outcrop; B: Sample CA-31

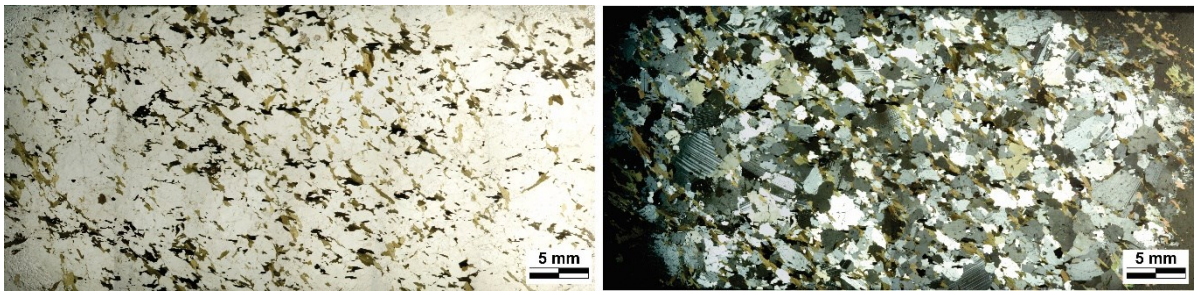

C and D: Photomicrographs showing the main mineralogy and texture.

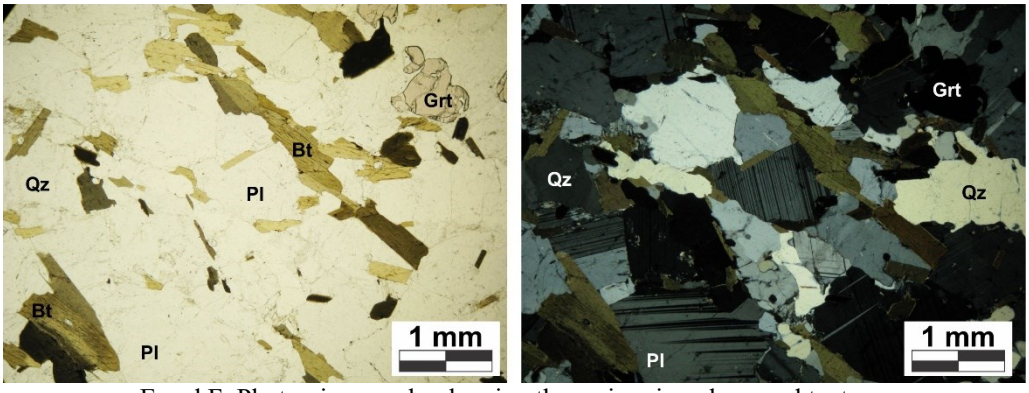

E and F: Photomicrographs showing the main mineralogy and texture.

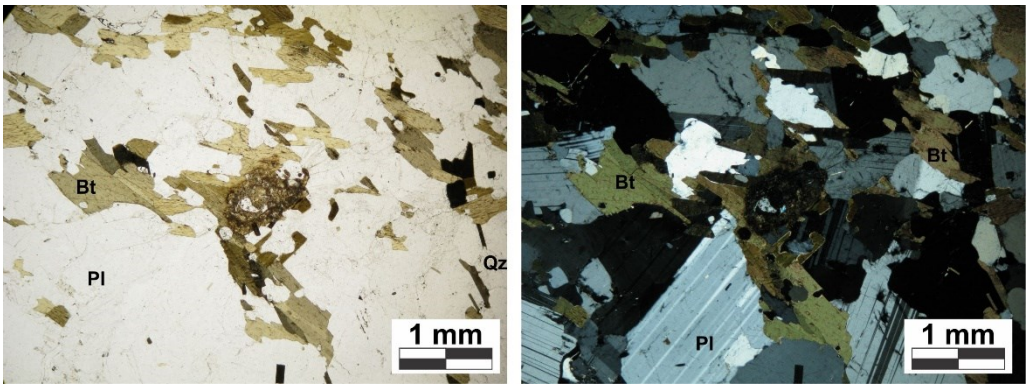

G and H: Photomicrographs showing the main mineralogy and texture.

APPENDIX J - Other contributions

The chapter 11 of the book “Geocronologia e Evolução Tectônica do Continente Sul-Americano: a contribuição de Umberto Giuseppe Cordani”. This book presents the protagonist of Professor Umberto Cordani, from the Institute of Geosciences at USP (Universidade de São Paulo), in his contribution to the knowledge of the tectonic evolution of the South American continent in the last 6 decades, showed in 52 contributions chapters by 90 authors!

The chapter presents an evolution of the geochronological knowledge of the Araçuaí orogen, from the 1960s to 2020.

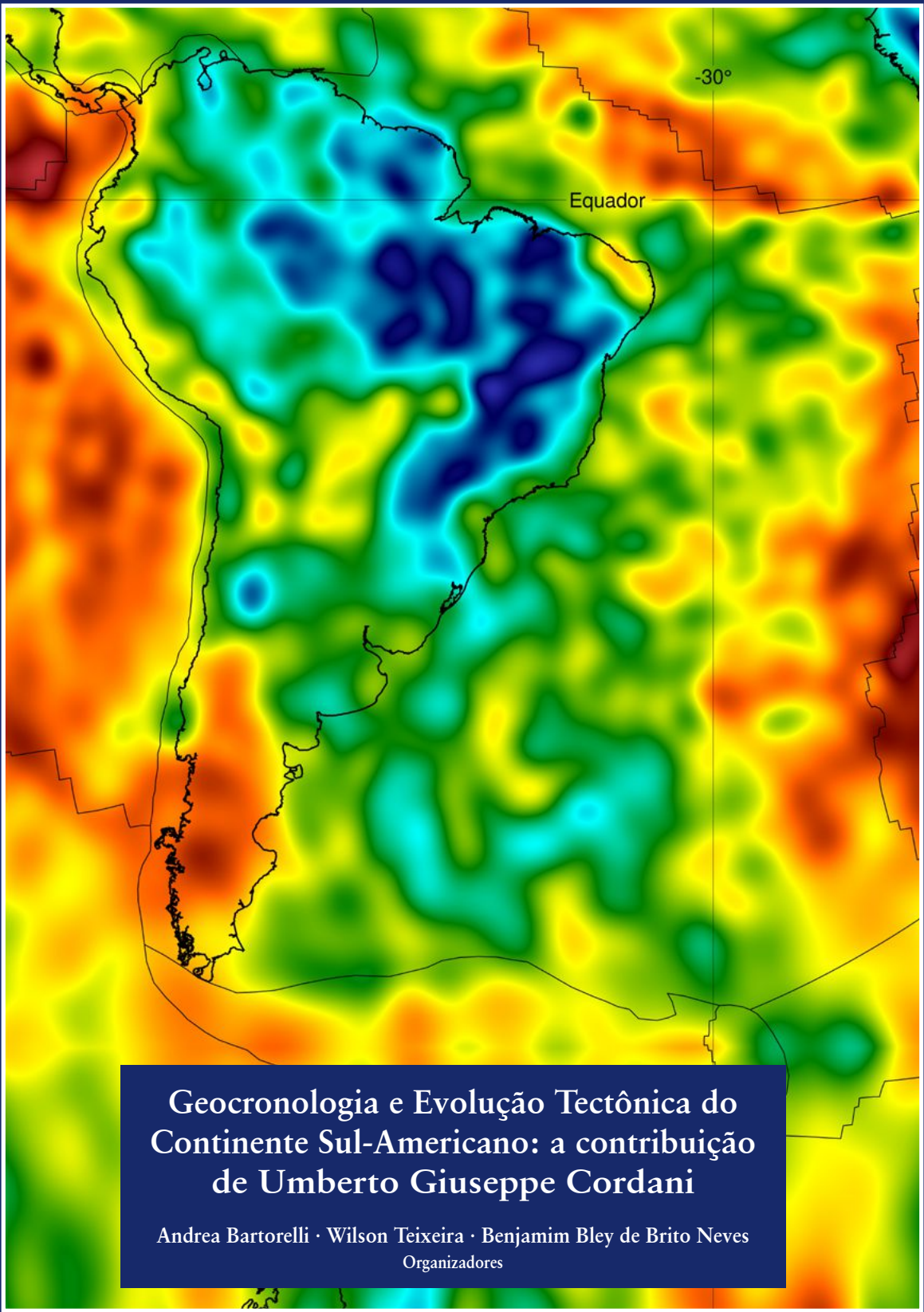

Geocronologia e Evolução Tectônica do Continente Sul-Americano: a contribuição de Umberto Giuseppe Cordani

Andrea Bartorelli · Wilson Teixeira · Benjamim Bley de Brito Neves
Organizadores

ORGANIZAÇÃO
Andrea Bartorelli
Wilson Teixeira
Benjamim Bley de Brito Neves

COORDENAÇÃO EDITORIAL E GRÁFICA
Carlos Cornejo
Silvia Rita dos Santos

PRODUÇÃO GRÁFICA
Solaris Edições e Produções
Culturais e Multimídia Ltda.

PRÉ-IMPRESSÃO
Giclê Fineart Print

IMPRESSÃO E ACABAMENTO
Coan Indústria Gráfica

Dados Internacionais de Catalogação na Publicação (CIP)
(Câmara Brasileira do Livro, SP, Brasil)

Bartorelli, Andrea
Geocronologia e evolução tectônica do Continente Sul-Americano: a contribuição de Umberto Giuseppe Cordani / Andrea Bartorelli, Wilson Teixeira, Benjamim Bley de Brito Neves. – 1. ed. – São Paulo : Solaris Edições Culturais : Andrea Bartorelli, Wilson Teixeira, Benjamim Bley de Brito Neves, 2020.

ISBN 978-65-991526-0-3 (Solarias Edições Culturais)

1. Ciências da terra 2. Cordani, Umberto Giuseppe 3. Geociências 4. Geocronologia 5. Geologia 6. Geologia estrutural – Trabalhos de campo 7. Tectônica I. Teixeira, Wilson. II. Neves, Benjamim Bley de Brito. III. Título

20–38961 CDD-550

Índices para catálogo sistemático:

1. Geociências : Ciências da terra 550

Maria Alice Ferreira – Bibliotecária – CRB-8/7964

Solaris Edições e Produções
Culturais e Multimídia Ltda.
Rua Tavares Bastos, 41 – Perdizes
São Paulo – SP – CEP 05012-020
Fone (11) 3675-6396
E-mail: solarised@terra.com.br
Site: www.solariseditora.com.br

Nota do Editor

Enquanto coordenador editorial e gráfico do livro, agradeço aos organizadores o convite para participar de uma empreitada desta magnitude que, ao sintetizar o conhecimento disponível sobre o assunto, põe a disposição dos interessados uma obra que certamente se tornará um marco e referência ineludível no desenvolvimento de suas pesquisas.

Trata-se de um esforço monumental que, nas suas 6 partes, reúne 52 contribuições, em 4 línguas, com mais de 90 autores nacionais e estrangeiros. Nas suas 728 páginas, o livro contém 645 figuras, entre fotografias, gráficos e tabelas, nele, ficando registrada uma história de mais de seis décadas, com extraordinárias imagens dos protagonistas de valiosos avanços científicos, uma revisão exaustiva e uma posta em dia do conhecimento, com especial destaque para o homenageado.

Foi requerido um enorme esforço de padronização, em consulta permanente com os diversos autores e com os organizadores da obra, na definição de conceitos e termos de uso técnico, afim de aumentar a compreensão do texto e reduzir possíveis ambiguidades.

Fui convidado pelos organizadores porque queriam dar uma feição moderna ao livro, isto é, com excelente qualidade editorial e gráfica, e abundante iconografia, a fim de criar um registro perdurável e ao mesmo tempo atrativo, que, ademais das imagens técnicas, incorporasse retratos dos autores, cenas do trabalho de campo, da participação em eventos e até da convivência, para produzir uma obra que, além dos profundos conhecimentos científicos até aqui atualizados, apresenta uma face humana e bem-humorada.

No desenvolvimento da edição, nos deparamos com um mar de estrangeirismos, arcaísmos técnicos e neologismos, próprios de uma ciência em desenvolvimento, em interação internacional e nas fronteiras do conhecimento.

Houve uma verificação de grafias, toponímicos, datas, siglas e termos em diversas línguas (que incluem espanhol, italiano, latim e inglês), com a padronização de fórmulas e termos técnicos, compondo um glossário e atualizando a ortografia.

Ao excelente e árduo trabalho dos organizadores, num diálogo constante, aportamos diversos critérios e práticas editoriais destinadas a aprimorar a apresentação dos textos e imagens, estas últimas de diversas origens e épocas, em técnicas variadas, muitas das quais exigiram demorado trabalho de digitalização e recuperação.

Eis aqui o resultado!

Carlos Cornejo,
Solaris Edições Culturais.

ANDREA BARTORELLI
WILSON TEIXEIRA
BENJAMIM BLEY DE BRITO NEVES
Organizadores

Geocronologia e Evolução Tectônica do Continente Sul-Americano: a contribuição de Umberto Giuseppe Cordani

1ª edição

ISBN: 978-65-991526-0-3

SOLARIS
Edições Culturais

São Paulo, 2020

Antonio Carlos Pedrosa-Soares.

Carolina Deluca.

Cristina Santos Araujo.

Camila Gradim.

O Orógeno Araçuaí à luz da Geocronologia: um tributo a Umberto Cordani

Antonio Carlos Pedrosa-Soares,
Universidade Federal de Minas Gerais,
Centro de Pesquisa Manoel Teixeira da Costa
(*pedrosasoares@gmail.com*).
Carolina Deluca,
Universidade Federal de Minas Gerais,
Centro de Pesquisa Manoel Teixeira da Costa
(*cdelucam@gmail.com*).
Cristina Santos Araujo,
Universidade Federal de Minas Gerais,
Centro de Pesquisa Manoel Teixeira da Costa
(*crsantosaraujo@gmail.com*).
Camila Gradim,
Universidade Federal de Minas Gerais,
Centro de Pesquisa Manoel Teixeira da Costa
(*gradim_camila@yahoo.com.br*).
Cristiano de Carvalho Lana,
Universidade Federal de Ouro Preto,
Departamento de Geologia
(*cristianodeclana@gmail.com*).
Ivo Dussin,
Universidade Estadual do Rio de Janeiro,
Faculdade de Geologia
(*ivodusin@yahoo.com.br*).
Luiz Carlos da Silva,
Serviço Geológico do Brasil – CPRM
(*luizsilva.cp2012@gmail.com*).
Marly Babinski,
Universidade de São Paulo,
Instituto de Geociências
(*babinski@usp.br*).

1. Introdução

A geocronologia absoluta é um ramo científico resiliente, porque seus métodos analíticos se sucedem rapidamente em busca de resultados radiométricos mais precisos e reprodutíveis, demandando criatividade e produtividade de laboratórios sofisticados e caros, em face de resistências de toda sorte. Resiliente também tem sido Umberto Cordani, cientista e pioneiro da geocronologia absoluta no Brasil, em sua imensa contribuição para o entendimento da evolução geológica da América do Sul e, especificamente, por seu trabalho para a caracterização de um intrigante setor orogênico da região leste-sudeste do Brasil: o Orógeno Araçuaí.

Cristiano de Carvalho Lana.

Ivo Dussin.

Luiz Carlos da Silva.

Marly Babinski.

Dentre as muitas outras contribuições científicas de Cordani, celebradas nos capítulos deste livro, nos coube concretizar a homenagem que aqui se apresenta como uma evolução de conhecimento geocronológico, desde os anos 1960 ao fim da presente década, sem a qual o Orógeno Araçuaí jamais teria sido conceitualmente construído, a muitas mãos, por uma sucessão de descobertas e caracterizações de componentes geotectônicos previsíveis à luz da Teoria da Tectônica de Placas.

Além disso, destacamos a atuação de Cordani na formação de cientistas brasileiros e sua inserção no cenário internacional em decorrência das muitas oportunidades por ele oferecidas a pesquisadores de diversas instituições, e do seu permanente incentivo para que a comunidade geocientífica atuante no Brasil transmita o conhecimento geológico aqui produzido nos mais diversos palcos e mídias das Geociências.

2. Crátons versus orógenos

Na década de 1960, o nascente acervo de dados geocronológicos K-Ar e Rb-Sr deu início a uma nova era no conhecimento do Pré-Cambriano do Brasil. É importante lembrar que a produção de dados geocronológicos sobre amostras do território brasileiro, concentrada no Centro de Pesquisas Geocronológicas (CPGeo) da USP, começou antes mesmo do mapeamento geológico sistemático do território, havendo raras áreas cobertas por mapas articulados (como o Quadrilátero Ferrífero de Minas Gerais). Contudo, nas décadas de 1960 a 1980, a proliferação de idades K-Ar e Rb-Sr pelo território brasileiro foi fundamental para as definições e delimitações dos crátons e faixas orogênicas que compõem o substrato continental, muitas das quais permanecem total a parcialmente válidas até o presente (*vide* Alkmim e Cruz, neste livro).

Àquela época, Cordani participou do artigo de Hurley *et al*. (1967) que demonstrou, com base em dados geocronológicos, a existência de ligações continentais entre América do Sul e África no Pré-Cambriano, sendo uma delas a conexão entre a região leste da Bahia e sua contraparte no Gabão, a qual teria sido poupada de orogenia após *ca*. 2 Ga. Neste contexto, Cordani *et al*. (1968) delinearam uma faixa orogênica brasiliana que delimitaria o Cráton do São Francisco na região fronteiriça entre o sudeste da Bahia e o nordeste de Minas Gerais. Dando continuidade a esta investigação, Cordani obteve dados K-Ar e Rb-Sr de grande número de amostras coletadas na região costeira entre Salvador e Vitória, apresentados e interpretados em sua Tese de Livre Docência (Cordani, 1973), e parcialmente publicados em Torquato e Cordani (1981). Nesta tese aparece a formalização de um limite geocronológico entre o que Cordani definiu como uma faixa orogênica brasiliana, a qual correlacionou à Faixa Ribeira, de Almeida *et al*. (1973), e a região oriental do Cráton do São Francisco, na Bahia (figura 1). Segundo Cordani (1973), este limite geocronológico (ou seja, a

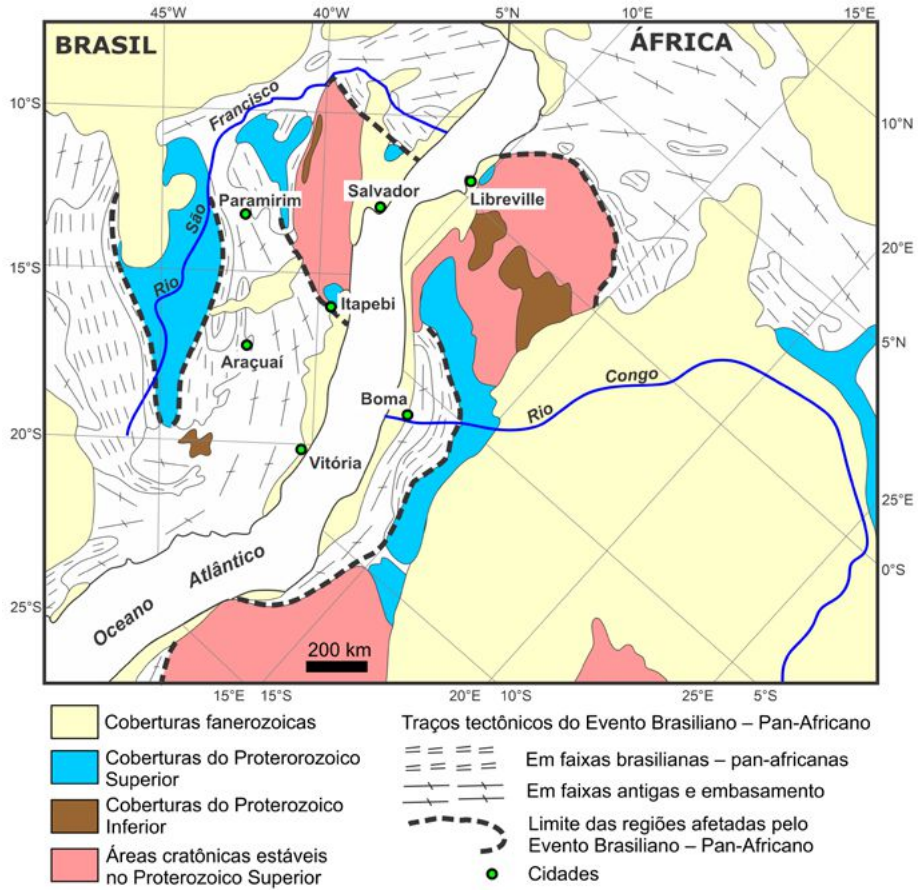

Figura 1: Mapa de correlação geotectônica apresentado por Cordani (2017, adaptado de Cordani, 1973; com cidades acrescentadas para apoio ao texto). A região balizada por Araçuaí, Itapebi e Vitória era considerada como uma faixa orogênica antiga, mas retrabalhada pelo Evento Brasiliano.

fronteira cráton-orógeno) coincidiria com uma importante feição tectônica que denominou Falhamento de Itapebi (uma extensa zona de cisalhamento de direção NW-SE; *cf.* Alkmim *et al.*, 2006), separando o domínio de idades brasilianas, a sul, do domínio de idades mais antigas contido na região cratônica, a norte (figura 1). É importante ressaltar, como mostra a figura 1, que tanto Cordani como os demais autores que abordaram esse tema (*e.g.*, Almeida *et al.*, 1973) consideravam, à época, que a grande maioria das rochas graníticas e de alto grau metamórfico seriam mais antigas ("transamazônicas ou embasamento") e teriam sido apenas retrabalhadas pelo Evento Orogênico Brasiliano. As correlações geológico-geocronológicas com a África, apresentadas por Cordani (1973), consolidaram a importância da ponte continental pré-Atlântica entre as regiões cratônicas de Bahia e Gabão, além de destacar as correspondências entre as faixas orogênicas brasilianas e pan-africanas que limitam estas áreas cratônicas (figura 1). Mas Cordani (1973), retomando o que prenunciou em Cordani *et al.* (1968), voltou sua principal atenção para o recém-definido Cráton do São Francisco (Almeida, 1967; Almeida *et al.*, 1973) e, lançando mão dos marcantes traços estruturais de direção NW-SE e correspondentes idades K-Ar no intervalo 450-650 Ma (Távora *et al.*, 1967), prolongou

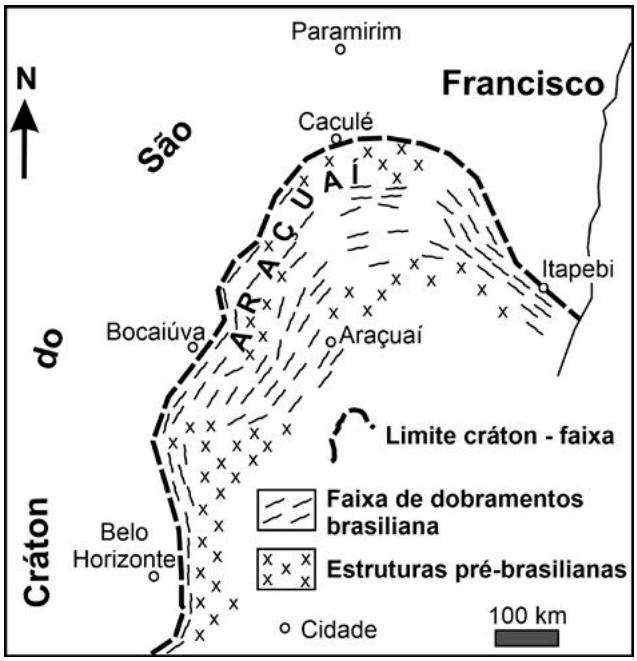

Figura 2: Recorte simplificado do mapa de Almeida (1977), mostrando a delimitação da Faixa de Dobramentos Araçuaí em relação ao Cráton do São Francisco e ao domínio das "estruturas pré-brasilianas".

a faixa orogênica brasiliana da região de Itapebi ao norte de Paramirim, separando o Cráton de Salvador, a leste, do que restou do Cráton do São Francisco, a oeste (figura 1). O trabalho de Cordani se tornou marco de referência no debate sobre a existência de um ou mais crátons na região ocupada pelo Cráton do São Francisco, como está historiado em Alkmim e Cruz (capítulo 3 da primeira parte deste livro).

Em meio à turbulência dos acirrados debates sobre o Cráton do São Francisco, Almeida (1977) fez uma detalhada revisão dos limites cratônicos impostos pelas faixas orogênicas brasilianas, com base nas relações tectônicas e geocronológicas entre unidades brasilianas e aquelas consideradas mais antigas. Assim, Almeida (1977) definiu a Faixa de Dobramentos Araçuaí como marcadora do limite sudeste do Cráton do São Francisco, após caracterizar a ampla curvatura delineada pela trama estrutural brasiliana na região a sul de Caculé (figura 2). Esta curvatura (hoje chamada Saliência do Rio Pardo; Peixoto *et al.*, 2018) se articula, a oeste, com o ramo N-S da Faixa Araçuaí e, a leste, com a Zona de Cisalhamento de Itapebi, o divisor geocronológico que Cordani, em 1973, chamou de Falhamento de Itapebi. É importante lembrar que a definição original da Faixa Araçuaí incluiu apenas o domínio das estruturas brasilianas mostrado na figura 2, pois a região oriental, rica em rochas graníticas e de alto grau metamórfico, continuou sendo considerada como uma unidade geotectônica composta de rochas mais antigas (a Faixa Paraíba ou Ribeira; Cordani *et al.*, 1968; Cordani, 1973; Almeida *et al.*, 1973) que teriam sido apenas retrabalhadas pelo "Ciclo Geotectônico Brasiliano" (Almeida, 1977).

O limite entre a Faixa Araçuaí e o Cráton do São Francisco ficou bem estabelecido a partir de Almeida (1977), tendo sido apenas aprimorado em detalhamentos posteriores (*cf.* Alkmim *et al.*, 2006, 2017). Entretanto, a definição de Almeida (1977) deixou em aberto os limites meridional e oriental da Faixa Araçuaí, causando

frequentes conflitos de nomenclatura na literatura sobre a região, particularmente quanto ao uso dos termos Araçuaí e Ribeira, até que o acúmulo de dados analíticos e a expansão da cobertura de mapas geológicos sistemáticos levassem à revisão dos conceitos e consequente caracterização do Orógeno Araçuaí (ver síntese em Pedrosa-Soares *et al.*, 2007).

3. De faixa de dobramentos a Orógeno Araçuaí

Virada a década de 1970, mas ainda em tempos de geocronologia K-Ar e Rb-Sr, rochas que anteriormente eram consideradas mais antigas passaram a ser cronologicamente redefinidas, ao passo que também avançava o mapeamento geológico dando maior suporte às correlações locais e regionais. De fato, os projetos de mapeamento geológico sistemático da CPRM (*http://geosgb.cprm.gov.br/*) e CODEMIG (*http://www.portalgeologia.com.br/*), executados por equipes próprias ou em parceria com universidades (destacando-se a UFMG, que produziu a cartografia geológica sistemática de cerca de 400.000 km^2 em Minas Gerais e Espírito Santo: *http://cpmtc-igc-ufmg.org/laboratorios6.htm*), acabaram por cobrir toda a região aqui enfocada. Some-se a isto o crescente número de trabalhos publicados, dissertações e teses sobre aquela região.

Em dissertação de mestrado que teve a orientação de Cordani, grande número de corpos graníticos situados no nordeste de Minas Gerais foi cronologicamente organizado em episódios de magmatismo sin- a tardi-tectônico (650-550 Ma), tardi- a pós-tectônico (550-500 Ma) e pós-tectônico a anorogênico (500-450 Ma) por Siga-Junior (1986; *vide* também Siga-Junior *et al.*, 1987), com base em mais de uma centena de datações Rb-Sr e K-Ar, e alguns dados U-Pb. Embora estes intervalos de tempo tenham sido posteriormente revistos em decorrência do crescente acervo de idades U-Pb, o trabalho de Siga-Junior (1986) foi um importante passo para a demonstração de que as rochas graníticas da região a leste de Araçuaí formaram-se durante a Orogenia Brasiliana, não se tratando, portanto, de rochas mais antigas que apenas teriam sido retrabalhadas nesse evento orogênico.

Como um dos temas centrais de seu doutorado, o primeiro autor deste capítulo buscou responder a um desafio contido na definição da Faixa Araçuaí como "geossinclinal alpinótipo" (Almeida, 1977): onde estariam os ofiolitos tão comuns nas faixas orogênicas do tipo alpino? Esta questão foi esclarecida nos trabalhos de Pedrosa-Soares *et al.* (1992, 1998) e Pedrosa-Soares (1995) que, sustentados por mapeamento de detalhe, análises litoquímicas e geoquímica isotópica Sm-Nd, relatam a descoberta de remanescentes ofiolíticos na Faixa Araçuaí, de onde novos achados e estudos recentes de restos oceânicos encontram-se em Queiroga (2010), Peixoto *et al.* (2015) e Amaral *et al.* (2020).

Paralelamente, Figueiredo e Campos-Neto (1993), Nalini-Junior (1997), Nalini-Junior *et al.* (2000a) e Noce *et al.* (2000), lançando mão de dados geocronológicos (inclusive U-Pb e Pb-Pb em zircão), caracterizaram segmentos do Arco Magmático Rio Doce (*vide* síntese em Tedeschi *et al.*, 2016). Embora sem novos dados geocronológicos, o mapeamento sistemático do Projeto Leste cobriu grande parte da região oriental de Minas Gerais, agrupando, com base na trama estrutural, rochas graníticas de tipos I e S de acordo com as fases tectônicas da Orogenia Brasiliana (Pinto *et al.*, 2001).

Assim, ao final da década de 1990, o cenário para a redefinição do conceito de faixa para orógeno estava montado. Então, com base na descoberta de corpos ofiolíticos neoproterozoicos, na identificação dos estágios pré-colisional (Arco Magmático Rio Doce), colisional (rochas graníticas tipo S foliadas e migmatizadas) e pós-colisional (intrusões pós-foliação regional) da evolução brasiliana, e na correlação entre as faixas Araçuaí e Congo Ocidental foi definido o Sistema Orogênico Araçuaí – Congo Ocidental (AWCO) para referir o edifício litotectônico brasiliano – pan-africano confinado à grande reentrância delineada pelos crátons do São Francisco e Congo (Pedrosa-Soares *et al.*, 2001). Portanto, o AWCO engloba um conjunto de componentes geotectônicos que caracterizam um orógeno colisional (rico em granitos tipo S) sucessor de um orógeno acrecionário de margem continental ativa (com arco magmático cálcio-alcalino) que, por sua vez, sucedeu um completo sistema de bacias precursoras, com corpos ofiolíticos e sucessões de margem continental passiva que se seguiram à sedimentação e magmatismo de rifte continental, conforme sumarizado nos itens seguintes deste capítulo e referências bibliográficas neles citadas.

Desde Cordani (1973) e Torquato e Cordani (1981) já se descortinava a característica singular do AWCO, ou seja, sua localização no interior de uma grande reentrância moldada no Cráton São Francisco – Congo. Isto decorre da relação entre os crátons do São Francisco e Congo que permaneceram pelo menos parcialmente ligados desde o evento orogênico do limiar Riaciano – Orosiriano (*ca.* 2,05 Ga) até a abertura do Oceano Atlântico Sul, no Cretáceo, por meio da ponte continental que uniu as regiões de Bahia e Gabão (*vide* síntese em Degler *et al.*, 2018). Este cenário induziu, inicialmente, à interpretação da "Faixa Araçuaí – Congo Ocidental" como exclusivamente ensiálica (*cf.* síntese em Trompette, 2004) até que as descobertas de corpos ofiolíticos, arco magmático e abundante plutonismo tipo S, dentre outros fatos, aportassem novos argumentos para sua reinterpretação. A partir daí, o sistema de bacias precursoras do AWCO passou a ser consistentemente interpretado como um amplo golfo (uma *inland sea-basin* com área mínima de 1 milhão de km^2) parcialmente oceanizado e articulado com aulacógenos (Pedrosa-Soares *et al.*, 2001, 2007, 2008, 2017; Alkmim *et al.*, 2006, 2017; Amaral *et al.*, 2020), mas conectado, via Faixa Ribeira, ao Oceano Adamastor (Cordani *et al.*, 2003; Corrales *et al.*, 2020). Embora largamente cercado pela mesma massa cratônica (o Cráton São Francisco – Congo; ou seja, sem envolvimento de placas distintas), o orógeno colisional resultante (o AWCO) contém corpos ofiolíticos, arco magmático e volumosos plutonismos colisional e pós-colisional. Este edifício colisional singular foi designado como orógeno confinado (Pedrosa-Soares *et al.*, 2001, 2017; Rogers e Santosh, 2004), visando caracterizar um termo intermediário entre os clássicos orógenos colisionais de margem de placa (que têm ofiolitos, arcos magmáticos, e abundantes plutonismos colisional e/ou pós-colisional; *e.g.*, Brasília, Grenvilleano, Himalaias) e os típicos orógenos intracontinentais (ou ensiálicos, os quais são desprovidos de ofiolitos e têm pouco a nenhum magmatismo orogênico; *e.g.*, Alice Springs, Mongolia Altai, Tien Shan).

4. Componentes geotectônicos à luz da geocronologia U-Pb

A sistemática de estudos que levou à definição do Orógeno Araçuaí fundamenta-se na caracterização de componentes geotectônicos e estágios evolutivos à luz da Teoria da Tectônica de Placas (*cf.* Pedrosa-Soares *et al.*, 2001, 2007, 2008, 2017).

Os componentes geotectônicos são representados por produtos (*i.e.*, conjuntos de rochas) originados de processos atuantes durante estágios evolutivos diversos, desde os que se referem ao sistema de bacias precursoras até aqueles que resultam na construção do edifício orogênico. Assim, os conjuntos de rochas que representam rifte continental (*e.g.*, magmatismo bimodal com granitos ferroanos tipo A), margem continental passiva (*e.g.*, sucessões arenito-pelito-carbonato) e assoalho oceânico (*e.g.*, corpos ígneos ofiolíticos) materializam componentes geotectônicos representantes do sistema de bacias precursoras. Por seu turno, arco magmático (magmatismo cálcio-alcalino, magnesiano, tipo I e bacias associadas (que registram contribuição sedimentar provida pelo próprio arco), plutonismo peraluminoso (granitos tipos S), e intrusões tipos A e I representantes de plutonismo tardio representam componentes geotectônicos originados de processos orogênicos. Obviamente, para que cada componente geotectônico possa ser identificado é necessário que as rochas sejam mapeadas e bem caracterizadas em termos petrográficos, litoquímicos e isotópicos. De fato, são grandes os acervos de dados analíticos e de campo, aliados à completa cobertura de mapas geológicos sistemáticos, que sustentam as contribuições de muitos pesquisadores para a identificação dos componentes geotectônicos do Orógeno Araçuaí, simplificadamente ilustrados na figura 3. Este mapa mostra conjuntos de rochas, caracterizadas em campo e laboratório, que compõem os arranjos crono-litotectônicos que contam a evolução do Orógeno Araçuaí.

Se a geocronologia K-Ar e Rb-Sr sustentou, nas décadas de 1960 a 1980, as principais interpretações sobre a evolução geológica da região aqui abordada, foi a partir dos anos 1990 que a tríplice aliança entre mapeamento geológico sistemático, estudos geoquímicos e geocronologia U-Pb implantou os alicerces essenciais para a identificação dos componentes geotectônicos e dos intervalos de tempo a eles associados no Orógeno Araçuaí. Como Cordani atuou em ambos os estágios de produção do conhecimento geocronológico sobre o Orógeno Araçuaí, este capítulo apresenta, em sua homenagem, uma síntese do volumoso acervo de análises de zircão pelos métodos U-Pb (LA-ICP-MS, SHRIMP e TIMS) e Pb-Pb (evaporação), cujos dados foram compilados de um número expressivo de publicações (tabela 1). Esta compilação engloba 5.143 idades, a grande maioria delas obtidas de análises pontuais (*spots* LA-ICP-MS e SHRIMP), incluindo 1.647 idades referentes ao sistema de bacias precursoras (riftes 1 e 2, e margem passiva; figura 4), 1.329 ao magmatismo orogênico (supersuítes G1 a G5; figura 5), 660 aos metamorfismos regional e termal tardio (figura 5), e 1.507 às bacias orogênicas (figura 6). Não se utilizou trabalhos que contêm equívocos e incertezas na classificação de rochas que serviram à extração de zircão ou que apresentam misturas de dados fornecidos por rochas diferentes.

5. O Sistema de Bacias Precursoras

O sistema de bacias precursoras do Orógeno Araçuaí é representado pelas unidades metassedimentares e metavulcânicas do Grupo Macaúbas proximal a transicional, sua unidade distal, a Formação Ribeirão da Folha, e seus correlatos como o Grupo Dom Silvério, o Complexo Jequitinhonha, pacotes metaclásticos com intercalações de metadiamictitos do Vale do Rio Pardo e paragnaisses da Unidade Andrelândia da região de Manhuaçu (figura 3).

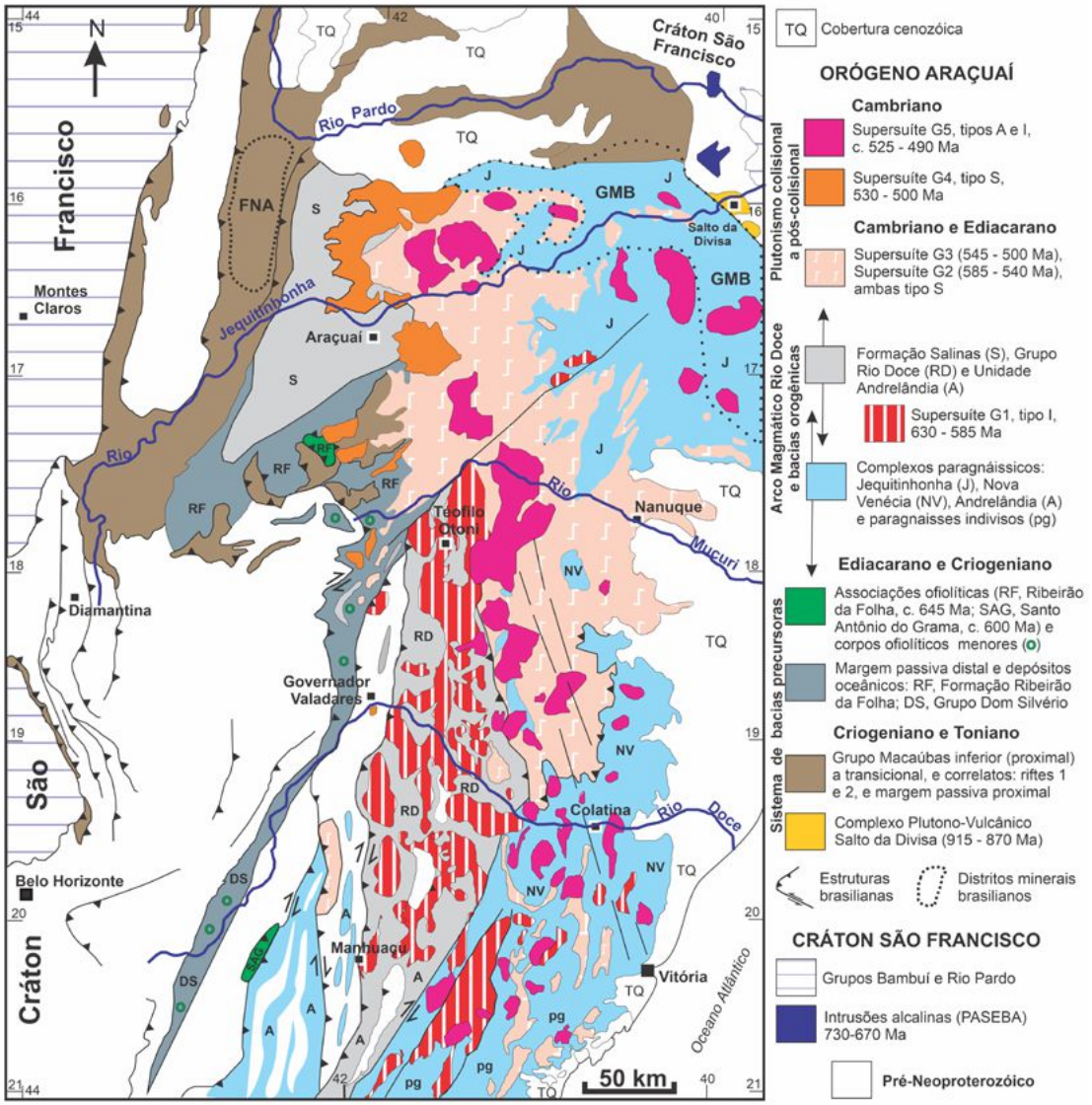

Figura 3: Mapa geológico simplificado do Orógeno Araçuaí (atualizado após Pedrosa-Soares *et al.*, 2007) com indicação de distritos minerais (*cf.* Vilela *et al.*, 2014; para distritos da Província Pegmatítica Oriental do Brasil ver Pedrosa-Soares *et al.*, 2011b).

O Grupo Macaúbas, que tem sido palco de estudos desde o início do século passado (*cf.* Pedrosa-Soares *et al.*, 2011a), está preservado como unidade mais extensa e completa do sistema de bacias precursoras do Orógeno Araçuaí. Este grupo registra dois processos de rifteamento continental na bacia precursora, sendo que o segundo evoluiu para margem passiva e abertura oceânica (Pedrosa-Soares e Alkmim 2011; Kuchenbecker *et al.*, 2015; Amaral *et al.*, 2020). O rifte 1, do Toniano Inferior, inclui as rochas sedimentares e vulcânicas do pacote depositado abaixo dos diamictitos Macaúbas, ou seja, antes do período glacial registrado nesse grupo (Bitencourt *et al.*, 2019; Castro *et al.*, 2019; Souza *et al.*, 2019). O intervalo de idades balizador deste rifteamento toniano (950-880 Ma) está registrado por datações U-Pb (zircão e baddeleyita) de enxames de diques máficos (Dussin, 2017;

BACIAS PRECURSORAS*	BACIAS OROGÊNICAS*	MAGMATISMO OROGÊNICO**	METAMORFISMO***
Rifte 1	**Grupo Rio Doce**	**Supersuíte G1**	**Regional e termal**
Martins *et al.* 2008, Babinski *et al.* 2012, Castro *et al.* 2019, Souza *et al.* 2019, Amaral *et al.* 2020	Vieira 2007, Novo *et al.* 2018, Schannor *et al.* 2019	Nalini Jr. 1997, Paes 1999, Nalini *et al.* 2000, Noce et al. 2000, Silva *et al.* 2005, Figueiredo 2009, Petitgirard *et al.* 2009, Novo *et al.* 2010, Noce *et al.* 2010 e Silva *et al.* 2010 (ambos em Silva *et al.* 2011), Pedrosa-Soares *et al.* 2011b, Mondou *et al.* 2012, Gradim 2013, Novo 2013, Gonçalves *et al.* 2014, 2016, Tedeschi *et al.* 2016	Silva *et al.* 2002, 2011, Noce *et al.* 2010 *in* Silva *et al.* 2011, Gradim 2013, Peixoto *et al.* 2015, Gonçalves *et al.* 2016, Richter *et al.* 2016, Tedeschi *et al.* 2016, Degler *et al.* 2017, 2018, Melo *et al.* 2017, Serrano *et al.* 2018, Castro *et al.* 2019, Araujo *et al.* 2020,
Rifte 2	**Complexo Nova Venécia**	**Supersuíte G2**	
Pedrosa-Soares *et al.* 2000, Babinski *et al.* 2005, 2012, Kuchenbecker *et al.* 2015	Noce *et al.* 2004, Belém 2014, Gradim *et al.* 2014, Richter *et al.* 2016, Araujo *et al.* 2020	Nalini Jr. 1997, Nalini *et al.* 2000, Noce *et al.* 2000, Silva *et al.* 2002, 2011, Vauchez *et al.* 2007, Roncato 2009, Gradim 2013, Peixoto *et al.* 2015, Gonçalves *et al.* 2016, Richter *et al.* 2016, Melo *et al.* 2017, Xavier 2017, Serrano *et al.* 2018, Araujo *et al.* 2020	
Margem Passiva	**Formação Salinas**	**Supersuíte G3**	
Gonçalves-Dias *et al.* 2011, 2016, Peixoto *et al.* 2015, Degler *et al.* 2017, Amaral *et al.* 2020	Kuchenbecker 2014, Peixoto *et al.* 2015, Deluca *et al.* 2019	Silva *et al.* 2007 (*in* Paes *et al.* 2010), Pedrosa-Soares *et al.* 2011b, Gradim 2013	
	Unidade Andrelândia	**Supersuíte G4**	
	Degler *et al.* 2017	Basílio *et al.* 2000, Silva *et al.* 2007 *in* Paes *et al.* 2010, Deluca 2018	
		Supersuíte G5	
		Söllner *et al.* 1991, Mello 2000, Noce *et al.* 2000, Söllner *et al.* 2000, Wiedemann *et al.* 2002, Mendes *et al.* 2005, Silva *et al.* 2005, Petitgirard *et al.* 2009, Gradim 2013, Belém 2014, Campos *et al.* 2016, Gonçalves *et al.* 2016, Xavier 2017, Aranda 2018, Serrano *et al.* 2018, Araujo *et al.* 2020	

Tabela 1: Referências das fontes de compilação de idades de zircão, obtidas pelos métodos U-Pb (LA-ICP-MS, SHRIMP e TIMS) e Pb-Pb (evaporação). Discordância de corte ≤ 10%; *grãos detríticos; **cristais ígneos; ***cristais neoformados e sobrecrescimentos metamórficos em cristais ígneos.

Evans *et al.*, 2015; Chaves *et al.*, 2019), do vulcanismo máfico associado ao Grupo Macaúbas Inferior (Castro *et al.*, 2019; Souza *et al.*, 2019) e do Complexo Plutono–Vulcânico de Salto da Divisa (Silva *et al.*, 2008; Victoria *et al.*, 2019).

Após longo hiato, registrado por discordância regional, inicia-se a evolução do rifte continental 2 até abertura oceânica, do limiar Toniano – Criogeniano ao Ediacarano, incluindo desde: (i) as extensas pilhas de metadiamictitos maciços proximais (ocidentais) até os (ii) espessos pacotes distais portadores de metadiamictitos (fluxos de detritos) estratificados com metarenitos e metapelitos (turbiditos) que passam, vertical e lateralmente, a (iii) sucessões metarenito – metapelito livres de diamictitos, as quais, ainda mais distalmente, dão lugar a (iv) pacotes compostos de xistos peraluminosos (pelitos pelágicos) com intercalações de xistos

grafitosos (*black shales*), metacherts, diopsiditos sulfetados e formações ferríferas (sedimentos químico-exalativos), e metabasaltos com assinatura oceânica, configurando uma bacia que evoluiu de rifte continental para margem passiva associada à instalação de crosta oceânica (Pedrosa-Soares *et al.*, 1992, 1998, 2011a; Queiroga, 2010; Kuchenbecker *et al.,* 2015; Peixoto *et al.,* 2015; Amaral *et al.,* 2020).

O intervalo de idades (730-670 Ma) que se associa ao rifte 2 é dado pelas datações de zircões das intrusões da Província Alcalina do Sul do Estado da Bahia (PASEBA; Teixeira *et al.*, 1997; Rosa *et al.*, 2007) e idades U-Pb (zircão e baddeleyita) de rochas vulcânicas (715-690 Ma) intercaladas em diamictitos da Faixa Congo Ocidental (Straathof, 2011; Thiéblemont *et al.*, 2009). A instalação de crosta oceânica associada à margem passiva sucessora do rifte 2 é balizada pelas idades U-Pb de zircões de plagiogranito (*ca*. 645 Ma) da cunha acrescionária ofiolítica de Ribeirão da Folha (Amaral *et al.*, 2020) e de metagabro (*ca*. 600 Ma) da Suíte Ofiolítica de Santo Antônio do Grama (Queiroga, 2010).

Os estágios evolutivos do sistema de bacias precursoras do Orógeno Araçuaí estão também registrados por grande número de análises U-Pb em grãos detríticos de zircão (figura 4), a começar pelas primeiras idades U-Pb SHRIMP de zircões detríticos do Grupo Macaúbas publicadas em artigo de Pedrosa-Soares, Cordani e Nutman (2000). Os diagramas de idades U-Pb de zircões detríticos mostram uma ampla contribuição de fontes distintas, cobrindo desde o Paleoarqueano até o início do Ediacarano (figura 4), como se espera de um completo sistema de bacias precursoras que evoluiu desde ambientes de rifte continental aos de margem passiva e assoalho oceânico. As fontes arqueanas são minoritárias em todos os diagramas, sugerindo pouca exposição ou escassez de terrenos arqueanos nas regiões que alimentaram

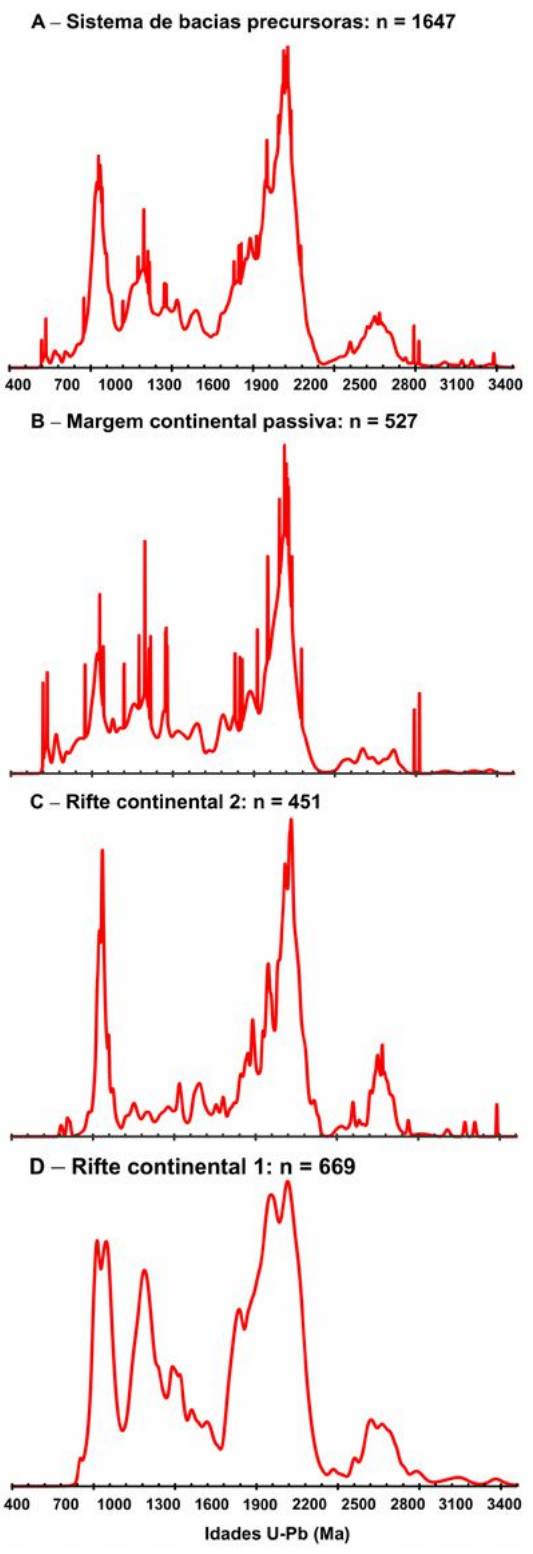

Figura 4: Curvas de densidade de probabilidade representando acervos de idades de grãos detríticos de zircão extraídos de rochas metassedimentares do sistema de bacias precursoras do Orógeno Araçuaí (*cf.* tabela 1).

as bacias (figura 4). Em todos os casos, as maiores contribuições devem-se a fontes com idades em torno de 2,1 Ga, as quais representam importante época de constituição do embasamento do AWCO e região cratônica adjacente, tanto pela formação de arcos magmáticos riacianos quanto pelo retrabalhamento metamórfico-anatético com recristalização de zircões de unidades mais antigas (*cf*. Heilbron *et al.*, 2017; Degler *et al.*, 2018). Outro pico de idades proeminente nos diagramas indica importante atividade magmática produtora de zircão em torno de 900-950 Ma (figura 4). Isto testemunha, como apontado por Pedrosa-Soares, Cordani e Nutman (2000), a contribuição do magmatismo anorogênico do Toniano Inferior também para depósitos sedimentares do próprio rifte 1 (figura 4D), em decorrência da dinâmica das ombreiras e *horsts* internos expostos a soerguimento e erosão contemporâneos ao preenchimento da bacia. O pico em 900-950 Ma diminui significativamente no registro dos depósitos de margem passiva (figura 4B) em contraposição ao aumento da contribuição de outras fontes, indicando que os meios de erosão e transporte de sedimentos atingiram áreas mais amplas e diversificadas. Os diagramas referentes ao rifte 1 e margem continental passiva mostram contribuições significativas de fontes mesoproterozoicas e estaterianas (figura 4D), indicando proveniências desde o Sistema Espinhaço – Chapada Diamantina (Chemale *et al.*, 2012; Magalhães *et al.*, 2018) à Faixa Kibarana (Tack *et al.*, 2010; Degler *et al.*, 2017). No rifte 2 aparecem pequenos picos em torno de 700 Ma (figura 4C), ausentes do diagrama do rifte 1, sugerindo a entrada da contribuição de fontes ígneas criogenianas. Esta contribuição criogeniana aumenta significativamente no estágio de margem passiva que sucede o rifte 2, indicando aporte de sedimentos da Província Alcalina do Sul do Estado da Bahia e de arcos magmáticos situados na Faixa Ribeira (Kuchenbecker *et al.*, 2015; Degler *et al.*, 2017). Idades do fim do Criogeniano e início do Ediacarano sugerem, também, contribuição do Arco Rio Doce para as cunhas acrescionárias com remanescentes ofiolíticos (Peixoto *et al.*, 2015; Amaral *et al.*, 2020).

6. Magmatismo e Metamorfismo Orogênicos

A cobertura de mapas geológicos sistemáticos, produzidos à luz de conceitos atualizados, e o crescente número de dados analíticos levaram à separação dos diferentes conjuntos de rochas ígneas plutônicas (e correspondentes metamórficos) que compõem o núcleo brasiliano do Orógeno Araçuaí, de acordo com suas relações de campo, feições tectono-metamórficas, características mineralógico-petrográficas, assinaturas litoquímicas e isotópicas, e idades de cristalização magmática, resultando em cinco grandes agrupamentos (Pedrosa-Soares *et al.*, 2001) que, após refinamentos e atualizações, são representados pelas supersuítes G1 a G5 (Pedrosa-Soares *et al.*, 2011b; Serrano *et al.*, 2018; Araujo *et al.*, 2020), sumarizadas na tabela 2. As rochas G1 a G5 são diferentes em vários aspectos composicionais e estruturais, os quais remetem para diversos processos petrológicos e tectônicos, envolvendo fontes térmicas variadas e fenômenos geodinâmicos distintos, tais como: processos de geração de arco magmático de margem continental ativa relacionados à dinâmica da subducção de litosfera oceânica (incluindo subducção de dorsal e *slab break-off*), mas com envolvimento majoritário de fusões parciais derivadas do embasamento (em particular dos ortognaisses riacianos, juvenis a moderadamente juvenis, dos complexos Juiz de Fora e Pocrane; *cf.* Degler *et al.*, 2018) na gênese dos magmas tipo I da Supersuíte G1

Supersuíte	G1	G2	G3	G4	G5
Idade (Ma)	630 – 585	585 – 540	545 – 500	530 – 500	525 – 490
Litotipos	dominantemente tonalito a granodiorito, com diorito a gabronorito subordinados, com biotita, anfibólio e/ou clinopiroxênio e/ou ortopiroxênio	biotita-granada sienogranito a álcali-feldspato granito predominantes, com monzogranito a tonalito rico em granada e granito a duas micas subordinados	álcali-feldspato granito a sienogranito com cordierita e/ou granada e/ou sillimanita, livre ou pobre em biotita	granito a duas micas geralmente com granada, associado a granito pegmatóide com turmalina e berilo	álcali-feldspato granito a granodiorito e correspondentes portadores de ortopiroxênio, com enderbito e norito subordinados
Relações de campo	batólitos e *stocks* tonalítico-granodioríticos geralmente ricos em enclaves dioríticos a máficos, com deformação (foliação) dúctil e migmatização; localmente com trama ígnea bem preservada; raros plútons gabronoríticos	batólitos, *stocks,* intrusões estratóides e leucossomas em migmatitos, com deformação (foliação) dúctil, metamorfismo e migmatização, e frequentes xenólitos e restitos de rochas metassedimentares; localmente com trama ígnea bem preservada	veios e bolsões de leucossoma majoritariamente autóctone, e pequenos plútons, livres da foliação regional, geralmente hospedados em migmatitos de granitos G2	intrusões pós-foliação regional, com xenólitos de rochas metassedimentares	intrusões pós-foliação regional, graníticas a charnockíticas ricas em enclaves (autólitos) e feições de misturas de magmas, com eventuais núcleos máficos; intrusões de gabronorito e enderbito mais raras
Assinatura litoquímica	cálcio-alcalina expandida de médio- a alto-K, metaluminosa a fracamente peraluminosa, magnesiana, cálcica a álcali-cálcica.	fortemente a fracamente peraluminosa, cálcio-alcalina a subalcalina	peraluminosa, subalcalina a alcalina de alto-K	peraluminosa, subalcalina (K>Na) a alcalina (Na>K)	metaluminosa a fracamente peraluminosa, alcalina a cálcio-alcalina de alto K-Fe, minoritariamente toleítica
Assinatura isotópica	rocha total: $\varepsilon Nd_{(t)}$ = -4 a -13, idade-modelo Nd = 1,2 a 1,8 Ga; $^{87}Sr/^{86}Sr_{(t)}$ = 0,704 a 0,711; zircão: $\varepsilon Hf_{(t)}$ = +2 a -15, idade-modelo Hf = 1,3 a 1,7 Ga	rocha total: $\varepsilon Nd_{(t)}$ = -5 a -13, idade-modelo Nd = 1,3 a 1,9 Ga, $^{87}Sr/^{86}Sr_{(t)}$ = 0,707 a 0,713; zircão: $\varepsilon Hf_{(t)}$ = -2 a -8, idade-modelo Hf = 1,3 a 1,9 Ga	zircão: $\varepsilon Hf_{(t)}$ = -4 a -10, idade-modelo Hf = 1,3 a 1,7 Ga	$^{87}Sr/^{86}Sr_{(t)}$ = 0,713	rocha total: $\varepsilon Nd_{(t)}$ = -6 a -23, idade-modelo Nd = 1,4 a 2,5 Ga; $^{87}Sr/^{86}Sr_{(t)}$: 0,702 a 0,716; zircão: $\varepsilon Hf_{(t)}$ = -1 a -24, idade-modelo Hf = 1,3 a 2,5 Ga
Tipo genético	tipo I metaluminoso predominante, localmente tipo I peraluminoso	tipo S largamente dominante; localmente tipo I peraluminoso	tipo S	tipo S	tipos A e I
Estágio tectônico	pré-colisional a cedo-colisional; arco magmático (Rio Doce) de margem continental	sin-colisional e tardi-colisional dominantes, localmente pré-colisional tardio	tardi-colisional a pós-colisional	pós-colisional	pós-colisional

Tabela 2: Principais características das supersuítes plutônicas do Orógeno Araçuaí (modificado de Pedrosa-Soares *et al.*, 2011b; Serrano *et al.*, 2018 e Araujo *et al.*, 2020, e referências aí contidas).

(e correspondentes vulcânicos) que constituem o Arco Rio Doce (*e.g.*, Gonçalves *et al.*, 2014, 2016, 2018; Tedeschi *et al.*, 2016); volumosa granitogênese tipo S relacionada essencialmente ao espessamento crustal do estágio colisional, mas em parte ao fim do desenvolvimento do Arco Rio Doce e máximo estiramento na bacia de retroarco ainda na transição dos estágios pré-colisional e sincolisional (Gradim *et al.*, 2014; Richter *et al.*, 2016; Melo *et al.*, 2017), assim como à descompressão regional concomitante à cessação dos esforços tangenciais e passagem para o processo de colapso gravitacional, dos estágios tardi-colisional ao pós-colisional, originando inicialmente a Supersuíte G2, sucedida pela Supersuíte G3 (Pedrosa-Soares *et al.*, 2011b; Gradim *et al.*, 2014); fusão parcial da crosta profunda por ascensão de manto astenosférico (na forma de *hot spot* ou pluma regional) relacionada à delaminação subcrustal durante o processo de colapso gravitacional

no estágio pós-colisional, dando origem às intrusões félsicas tipos A e I, e corpos máficos associados, englobadas na Supersuíte G5 (Campos *et al.*, 2016; Serrano *et al.*, 2018) e, em nível crustal mais raso, à Supersuíte G4 (Deluca, 2018).

Em termos geocronológicos, um significativo acervo de idades de zircão permite delinear com segurança as principais épocas de cristalização magmática e de metamorfismo que ocorreram no núcleo do Orógeno Araçuaí (figura 5). Aqui, Cordani revisitou, quatro décadas após seus estudos pelos métodos K-Ar e Rb-Sr, as rochas gnáissicas e graníticas da região norte do Espírito Santo, contribuindo com dados U-Pb que estão consubstanciados no artigo de Gradim *et al.* (2014).

As 874 idades de cristais de zircão referentes às rochas das supersuítes G1 e G2 delineiam duas curvas bem distintas antes de 585 Ma, mas que tendem a se sobrepor a partir desta idade rumo a valores mais jovens (figura 5). Como previamente indicado por Tedeschi *et al.* (2016), a Supersuíte G1 mostra dois picos principais de maior cristalização de rochas no Arco Rio Doce, o mais antigo em *ca.* 620 Ma e outro, bem mais expressivo, em *ca.* 589 Ma (figura 5). É importante destacar que as idades mais jovens de zircões extraídos de rochas G1 (tipo I) tendem a coincidir com o pico de cristalização magmática dos granitos G2 (tipo S), indicando a forte influência do estágio colisional sobre o Arco Rio Doce que, particularmente em sua parte oriental (*e.g.*, Batólito Baixo Guandu), sofreu metamorfismo e migmatização sin- a tardi-colisionais (Pedrosa-Soares *et al.*, 2011b; Silva *et al.*, 2011; Novo, 2013; Gradim *et al.*, 2014; Tedeschi *et al.*, 2016). A Supersuíte G2, por sua vez, mostra um proeminente pico de cristalização magmática em *ca.* 582 Ma e um pico menor em *ca.* 544 Ma, os quais são dados essencialmente pela distribuição de grande número de idades de *spots* individuais (figura 5). Entretanto, as idades-concórdia de granitos G2 se espalham no intervalo entre *ca.* 590 Ma e *ca.* 540 Ma, com tendência a se concentrar no intervalo 560-570 Ma, ou seja, em torno do pico metamórfico regional de *ca.* 563 Ma (figura 5), provavelmente em decorrência da prolongada influência dos processos metamórfico-anatéticos sobre granitos G2 (Pedrosa-Soares *et al.*, 2011b; Silva *et al.*, 2011; Gradim *et al.*, 2014; Richter *et al.*, 2016; Melo *et al.*, 2017).

Os dados de zircões das rochas G3, G4 e G5 foram tratados em conjunto, uma vez que todas elas se cristalizaram após a foliação regional (que é por elas cortada) e as duas primeiras têm poucas idades disponíveis na literatura (G3: 15 dados e G4: 11) em relação às intrusões G5 (429 idades compiladas). A curva correspondente a G3–G4–G5 se destaca nitidamente das distribuições de idades referentes às supersuítes G1 e G2, mostrando um hiato (um vale) marcante em torno de 545 Ma (figura 5). Os granitos G3 mais velhos (*ca.* 545 Ma, formados por fusão parcial de granito G2 com *ca.* 585 Ma; Gradim *et al.*, 2014) foram contemporâneos dos granitos G2 mais jovens (Richter *et al.*, 2016; Melo *et al.*, 2017), mas a produção de fusões (*melts*) G3 continuou até o clímax do estágio pós-colisional quando se cristalizaram a maior parte das intrusões G5 (Campos *et al.*, 2016; Serrano *et al.*, 2018; Araujo *et al.*, 2020) em torno de 504 Ma (figura 5). Aquele hiato indica marcante diminuição na produção de rochas magmáticas orogênicas, o que também se constata pela avaliação dos intervalos de idades-concórdia das diversas supersuítes, indicando quiescência magmática no intervalo 540-530 Ma e retomada da produção de magmas em torno de 527 Ma (figura 5).

Quanto ao metamorfismo, após tratados apenas os dados de zircão neoformados e de domínios metamórficos em zircões ígneos, verifica-se um pico marcante em *ca.* 563 Ma e outro, menor, em *ca.* 507 Ma, separados por um hiato com vale máximo em torno de

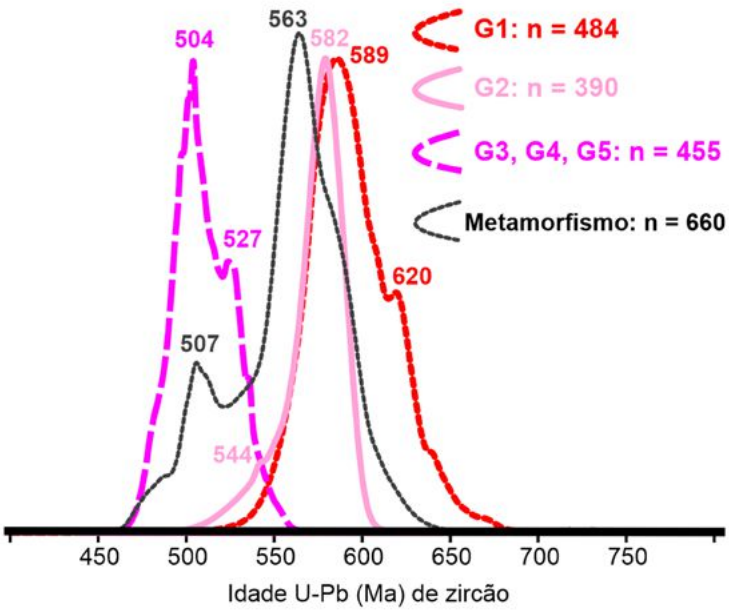

Figura 5: Curvas de densidade de probabilidade representando idades de zircões extraídos de rochas representantes das supersuítes G1 a G5 (tabela 2), formadas nos diversos estágios de magmatismo orogênico brasiliano, e de idades U-Pb dos metamorfismos regional e termal tardio, obtidas de zircões neoformados e sobrecrescimentos metamórficos em zircões ígneos (*cf.* tabela 1).

520 Ma. O primeiro pico (*ca.* 563 Ma) corresponde ao clímax do metamorfismo regional do estágio colisional, sendo equivalente ao intervalo de idades-concórdia de grande parte dos granitos G2 (Pedrosa-Soares *et al.*, 2011; Silva *et al.*, 2011; Gradim *et al.*, 2014; Richter *et al.*, 2016; Melo *et al.*, 2017; Serrano *et al.*, 2018; Araujo *et al.*, 2020). O segundo pico (*ca.* 507 Ma) corresponde ao metamorfismo termal pós-cinemático à foliação regional, contemporâneo do enxame de plútons G4 e G5 (Campos *et al.*, 2016; Deluca, 2018; Serrano *et al.*, 2018; Araujo *et al.*, 2020) e da ampla produção de fluidos que promoveram, no intervalo 515-495 Ma, marcante hidrotermalismo no Orógeno Araçuaí (Gonçalves *et al.*, 2019). É importante lembrar a existência do metamorfismo pré-colisional registrado por Degler *et al.* (2017, 2019) e Vieira *et al.* (2019), o qual, mesmo não marcando um pico bem definido, parece ser o responsável pela protuberância da curva em torno de 600 Ma (figura 5).

7. Bacias Orogênicas

Umberto Cordani, coautor em Lima *et al.* (2002), Gradim *et al.* (2014) e Deluca *et al.* (2019), também participou dos estudos que levaram à descoberta de bacias que se formaram durante estágios da inversão tectônica do Orógeno Araçuaí, quando rochas orogênicas brasilianas expostas à erosão passaram a contribuir com grande quantidade de grãos de zircão para sítios deposicionais parcialmente alimentados pelo Arco Rio Doce e, também, pelo magmatismo colisional (figura 6). De fato, sem a aplicação da geocronologia U-Pb em zircão seria virtualmente impossível distinguir com segurança as bacias precursoras das bacias orogênicas; e foi Cordani

o primeiro a conseguir análises U-Pb SHRIMP para uma unidade, a Formação Salinas (figuras 3 e 6F), que até 2002 era considerada parte da Bacia Macaúbas, mas se tornou um exemplo de bacia orogênica na literatura corrente (*cf*. Lima *et al.*, 2002; Deluca *et al*., 2019, e referências aí contidas). A descoberta de ocorrência da Formação Salinas a noroeste de Governador Valadares (figura 3) ajudou a caracterizar o prisma acrecionário portador de restos ofiolíticos da região de São José da Safira (Peixoto *et al.*, 2015).

Aquela primeira descoberta chamou a atenção para outras candidatas a bacias orogênicas e, também com o apoio de análises U-Pb de grãos detríticos de zircão, foi caracterizada parte da bacia de retroarco representada pelos paragnaisses do Complexo Nova Venécia (figura 3) por Noce *et al*. (2004). Após este trabalho vieram outros que, com muito maior volume de dados geocronológicos U-Pb (figura 6C), confirmaram a natureza orogênica da bacia onde se depositaram os protolitos sedimentares do Complexo Nova Venécia (Gradim *et al*., 2014; Richter *et al*., 2016) e trouxeram dados isotópicos de Hf em zircão que suportam interpretações mais detalhadas sobre proveniência sedimentar e metamorfismo neste complexo paragnáissico (Araujo *et al*., 2020). Sucessivamente, o aporte de dados da geocronologia U-Pb em zircão levou à caracterização do Grupo Rio Doce (figuras 3 e 6B) como cobertura vulcanossedimentar do Arco Magmático Rio Doce (Vieira, 2007; Gonçalves *et al*., 2018; Novo *et al*., 2018; Schannor *et al*., 2019), e à descoberta de depósitos de bacias de ante-arco e intra-arco tectonicamente embaralhados com pacotes sedimentares de bacia precursora, todos representados por paragnaisses da Unidade Andrelândia na região meridional do Orógeno Araçuaí (Degler *et al*., 2017) (figuras 3 e 6D).

O espectro geral de idades para as bacias orogênicas, delineado por 1.507 dados U-Pb, mostra marcante concentração em torno de 600 Ma, sintetizando um conjunto de diagramas que tende à unimodalidade (figuras 6A a 6E). A despeito do proeminente pico em torno de 600 Ma, as idades das fontes de sedimentos das bacias representadas variam significativamente, mas sempre com grande concentração de grãos com idades entre 900 e 600 Ma. Este fato e as variações nas assinaturas isotópicas de Hf dos zircões deste intervalo de idades, desde valores positivos, principalmente em zircões tonianos e criogenianos, a negativos, na maioria dos zircões ediacaranos (Degler *et al*., 2017; Schannor *et al*., 2019; Araujo *et al*., 2020), sugerem que fontes com componentes juvenis, como os arcos magmáticos Serra da Prata (Peixoto *et al*., 2017) e Rio Negro (Tupinambá *et al*., 2012), e corpos ofiolíticos (Queiroga, 2010; Amaral *et al*., 2020), também contribuíram significativamente para o preenchimento das bacias orogênicas, além das fontes crustais ediacaranas relacionadas ao Arco Rio Doce (Tedeschi *et al*., 2016; Corrales *et al*., 2020). Neste sentido, são as rochas metassedimentares do Grupo Rio Doce e da Unidade Andrelândia representantes de bacias intra-arco e ante-arco, que mais contêm zircões juvenis criogenianos e tonianos, sugerindo que os arcos Serra da Prata e Rio Negro já estariam de alguma forma acessíveis aos meios de transporte de sedimentos que alimentaram aquelas bacias antes do crescimento do Arco Rio Doce (*cf*. Degler *et al.,* 2017, 2019; Schannor *et al.,* 2019; Vieira *et al.,* 2019).

Os espectros de idades do Complexo Nova Venécia (figura 6C) e da Formação Salinas (figura 6E) mostram distribuições unimodais relativamente bem concentradas em torno de 600 Ma. Os paragnaisses Nova Venécia registram muita pouca contribuição de fontes mais velhas que 1 Ga, mas os pequenos picos entre 1,9 e 2,1 Ga indicam fontes de sedimentos no embasamento riaciano-orosiriano (Gradim *et al*., 2014; Richter *et al*., 2016; Araujo *et al*., 2020). A Formação Salinas, por sua vez, mostra contribuições signi-

ficativas de fontes mais velhas que 1 Ga segundo padrão de distribuição similar ao do sistema de bacias precursoras (figura 4), mas também apresenta zircões detríticos com idades entre 580 Ma e 545 Ma, indicando a participação de fontes situadas nas áreas hoje dominadas pelos granitos colisionais da Supersuíte G2 (Kuchenbecker, 2014; Deluca *et al.*, 2019).

8. Recursos minerais brasilianos

Além de sua importância petrogenética e geotectônica, o Evento Orogênico Brasiliano foi também profícuo na produção de recursos minerais durante a evolução do Orógeno Araçuaí, no que diz respeito a depósitos minerais relacionados ao metamorfismo regional e magmatismo brasilianos, particularmente os hoje chamados *high-tech minerals* (como grafita e minerais de lítio), além das gemas e minerais industriais, rochas ornamentais e depósitos de ferro (*cf*. Pedrosa-Soares *et al.*, 2011b; Vilela *et al.*, 2014; ver também a plataforma digital Recursos Minerais de Minas Gerais On-Line em *http://recursomineralmg.codemge.com.br/*).

Grandes jazidas e depósitos de grafita do tipo *flake* (lamelar), além de ocorrências de grafita do tipo *lump* (maciça), se formaram a partir da recristalização metamórfica regional, em fácies anfibolito alto a granulito, de sedimentos pelito-carbonosos que constituíram os protolitos dos sillimanita-grafita gnaisses intercalados nos kinzigitos (grafita-sillimanita-cordierita-granada-biotita gnaisses) do Complexo Jequitinhonha e dos sillimanita grafita xistos do Grupo Macaúbas, situados no extremo nordeste do Orógeno Araçuaí, formando o Distrito Grafítico Minas – Bahia (GMB, figura 3). O metamorfismo regional também promoveu a recristalização dos diamictitos anomalamente ricos em ferro do Grupo Macaúbas, transformando-os em forma-

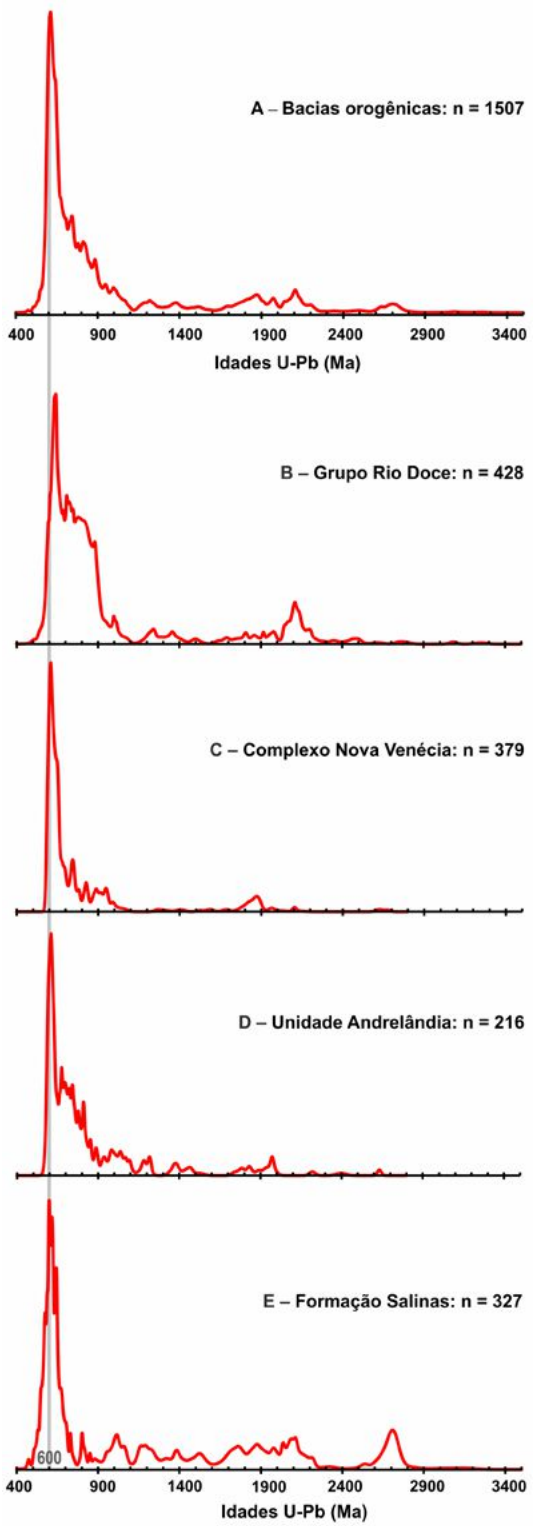

Figura 6: Curvas de densidade de probabilidade representando acervos de idades de grãos de zircão extraídos de rochas metassedimentares e metavulcanoclásticas de bacias orogênicas do Orógeno Araçuaí (*cf.* tabela 1).

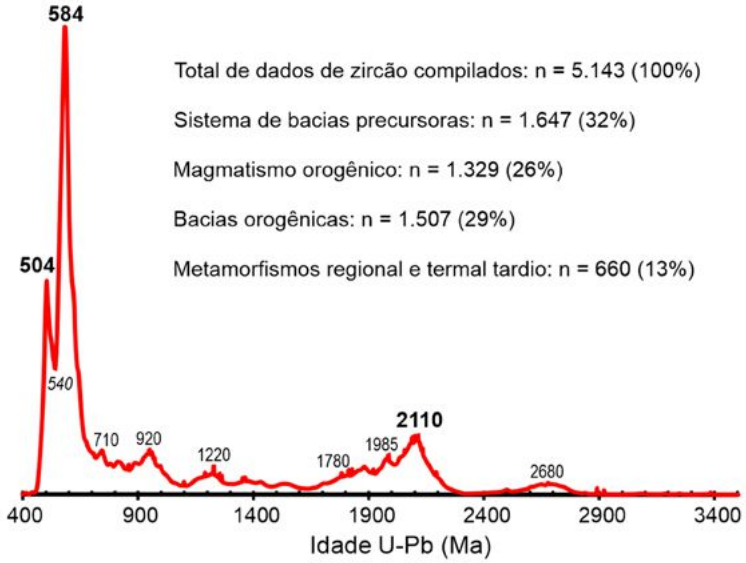

Figura 7: Curva geral de densidade de probabilidade de idades U-Pb de zircão para o Orógeno Araçuaí, com indicação dos principais picos que representam épocas de maior produção de zircão desde o Cambriano ao Arqueano.

ções ferríferas metadiamictíticas, enriquecidas em hematita e/ou magnetita, com teores de Fe total entre 15 e 55%, que constituem o Distrito Ferrífero Nova Aurora (FNA, figura 3).

O magmatismo orogênico produziu enorme quantidade de rochas que servem para materiais de construção, desde rochas ornamentais de alto valor à pedra de talhe. Especialmente no estágio pós-colisional, mas também no estágio colisional, cristalizou-se a enorme quantidade de pegmatitos que constituem a Província Pegmatítica Oriental do Brasil (ver síntese em Pedrosa-Soares *et al.*, 2011b). Os pegmatitos residuais de granitos tipo S da Supersuíte G4, no Distrito Pegmatítico de Araçuaí, e da Supersuíte G2, no Distrito Pegmatítico de Conselheiro Pena, são depósitos de gemas (*e.g.*, turmalinas verde, rosa e/ou azul, morganita, kunzita, citrino e outras variedades de quartzo), minerais de coleção (*e.g.*, fosfatos raros) e minerais para a indústria cerâmica (*e.g.*, feldspatos), mas hoje se destacam principalmente pela produção (na Mina da Cachoeira, da Companhia Brasileira de Lítio, a leste de Araçuaí) e grande potencial para minérios de lítio, essencialmente o espodumênio, um dos mais importantes *high-tech minerals* da atualidade. Os pegmatitos da Supersuíte G4 se caracterizam como fusões residuais da cristalização de magmas graníticos peraluminosos, originados por anatexia de rochas sedimentares pelíticas. Por sua vez, os pegmatitos associados às intrusões G5, em particular aquelas situadas a norte de Teófilo Otoni (figura 3), são os principais produtores de água-marinha e topázio azul a incolor, sendo virtualmente desprovidos de minerais de lítio e pobres a estéreis em turmalinas coradas, em decorrência de sua origem a partir de fusões parciais da crosta profunda. No conjunto, o período de maior produção de pegmatitos residuais mineralizados em gemas e/ou potenciais minérios de lítio situa-se em torno de 500 Ma, correspondendo ao clímax na produção dos magmas pós-colisionais (figuras 3 e 5).

9. Conclusão

As informações históricas e sínteses de dados, aqui apresentadas, demonstram a importância da geocronologia absoluta para a caracterização dos diversos componentes geotectônicos de um orógeno e definição dos estágios tectônicos que marcaram sua

evolução, bem como destacam a contribuição de Umberto Cordani para o conhecimento geológico da região enfocada. Desde a síntese publicada por ocasião da celebração dos 30 anos da definição da Faixa Araçuaí (Pedrosa-Soares *et al.*, 2007, artigo no qual Cordani é coautor) foi enorme o crescimento do conhecimento geocronológico sobre a região do Orógeno Araçuaí, mas permanece a necessidade da produção de mais dados em busca de descobertas, detalhamentos e novas interpretações.

Os padrões de distribuição de idades U-Pb mostram que o Orógeno Araçuaí, a despeito de sua situação paleotectônica singular (confinado a um embainhamento cratônico), teve uma história equivalente à dos clássicos orógenos colisionais de margem de placa, os quais evoluem a partir de sistemas de bacias precursoras complexos (de rifte continental a margem passiva com abertura oceânica), envolvidos em convergência de placas por subducção de litosfera oceânica e, portanto, contêm ofiolito, arco magmático, bacias orogênicas, magmatismos colisional e pós-colisional, e metamorfismos associados. O conjunto de componentes geotectônicos do Orógeno Araçuaí, incluindo bacias precursoras, magmatismos e metamorfismos orogênicos, e bacias orogênicas, está aqui representado por 5.143 idades de zircão, cuja distribuição geral se ilustra na figura 7. Este diagrama sinóptico mostra picos que sintetizam genericamente as épocas de produção de zircão, seja pelos processos ígneos e metamórfico-anatéticos que originaram rochas brasilianas ou por fenômenos similares que atuaram em terrenos mais antigos (figura 7). Assim, o pico em *ca*. 584 Ma sintetiza o magmatismo e metamorfismo na transição dos estágios pré-colisional e colisional, enquanto o pico em *ca*. 504 Ma corresponde ao clímax do magmatismo pós-colisional e metamorfismo termal associado. O vale em *ca*. 540 Ma baliza a quiescência no magmatismo orogênico, marcando a transição entre a cessação dos esforços compressionais e o início da descompressão generalizada que sobrevém com o colapso gravitacional pós-colisional. Os picos mais antigos são todos correlatos de épocas de produção de zircão conhecidas na literatura, como os magmatismos dos riftes 1 (em torno de 920 Ma) e 2 (em *ca*. 710 Ma), registrados no Grupo Macaúbas e rochas ígneas associadas, e os magmatismos anorogênicos relacionados ao Sistema Espinhaço – Chapada Diamantina (*ca*. 1200 Ma e *ca*. 1780 Ma) e crono-correlatos. Por fim, os grandes alimentadores das bacias precursoras são sistemas orogênicos riaciano-orosirianos (1985-2110 Ma) e, em menor parte, unidades do Neoarqueano (*ca*. 2680 Ma) que compõem o embasamento do próprio Orógeno Araçuaí e da região cratônica adjacente, corroborando, mais uma vez, o confinamento do sistema de bacias precursoras e do orógeno dele resultante.

Agradecimentos

Agradecemos à CAPES, CNPq, CODEMIG-CODEMGE, CPRM, FAPEMIG, FAPERJ, FAPESP, FINEP e PETROBRAS-CENPES pelas bolsas de estudo e pesquisa, e recursos para realização de projetos científicos e de mapeamento geológico. Nosso especial agradecimento aos organizadores deste livro (A. Bartorelli, W. Teixeira e B. B. Brito Neves) pelo honroso convite. Este capítulo é um singelo tributo a Umberto Cordani, nosso colaborador em trabalhos sobre temas diversos do Orógeno Araçuaí e, acima de tudo, um permanente incentivador da formação de pesquisadores em Geociências.

Referências

Alkmim F.F., Marshak S., Pedrosa-Soares A.C., Peres G.G., Cruz S.C.P., Whittington A. 2006. Kinematic evolution of the Araçuaí–West Congo orogen in Brazil and Africa: Nutcracker tectonics during the Neoproterozoic assembly of Gondwana. *Precambrian Research*, **149**:43-63.

Alkmim F.F., Kuchenbecker M., Reis H.L.S., Pedrosa-Soares A.C. 2017. The Araçuaí belt. In: Heilbron M., Cordani U.G, Alkmim F.F. (eds.). *São Francisco Craton, Eastern Brazil: Tectonic Genealogy of a Miniature Continent*. Regional Geology Reviews, p. 255-276.

Almeida F.F.M. 1967. *Origem e evolução da Plataforma Brasileira*. DNPM-DGM, Boletim **241**, 36p.

Almeida F.F.M., Amaral G., Cordani U.G., Kawashita K. 1973. The Precambrian evolution of the South American cratonic margin south of the Amazon River. In: Nairn A.E.M. & Stehli F.G (eds). *The Ocean Basins and Margins*, v.1, New York, Plenum Publishing Corp., p. 411-446.

Almeida F.F.M. 1977. O Cráton do São Francisco. *Revista Brasileira de Geociências*, **7**:349-364.

Amaral L., Caxito F.A., Pedrosa-Soares A., Queiroga G., Babinski M., Trindade R., Lana C., Chemale F. 2020. The Ribeirão da Folha ophiolite-bearing accretionary wedge (Araçuaí orogen, SE Brazil): New data for Cryogenian plagiogranite and metasedimentary rocks. *Precambriam Research,* **336**.

Aranda R. 2018. *Petrology of the Afonso Cláudio Intrusive Complex (Espírito Santo State, Araçuaí Orogen): Insights from Petrography, Lithogeochemistry, U-Pb Geochronology and Lu-Hf Isotopes.* Dissertação de Mestrado, Universidade Federal de Minas Gerais, Belo Horizonte, 64 p.

Araujo C., Pedrosa-Soares A., Lana C., Dussin I., Queiroga G., Serrano P., Medeiros-Júnior E. 2020. Zircon in emplacement borders of post-collisional plutons compared to country rocks: A study on morphology, internal texture, U-Th-Pb geochronology and Hf isotopes (Araçuaí orogen, SE Brazil). *Lithos*: 352-353: 105252.

Babinski M., Gradim R.J., Pedrosa-Soares A.C., Alkmim F.F., Noce C.M., Liu D. 2005. Geocronologia U–Pb (SHRIMP) e Sm–Nd de xistos verdes basálticos do Orógeno Araçuaí: Implicações para a idade do Grupo Macaúbas. *Revista Brasileira de Geociências*, **35**:77-81.

Babinski M., Pedrosa-Soares A.C., Trindade R.I.F., Martins M., Noce C.M., Liu D. 2012. Neoproterozoic glacial deposits from the Araçuaí orogen, Brazil: Age, provenance and correlations with the São Francisco craton and West Congo belt. *Gondwana Research,* **21:**451-465.

Basílio M.S., Pedrosa-Soares A.C., Evangelista H.J. 2000. Depósitos de alexandrita de Malacacheta, Minas Gerais. *Geonomos*, **8**:47-54.

Belém J. 2014. *Geoquímica, geocronologia e contexto geotectônico do magmatismo máfico associado ao feixe de fraturas Colatina, Estado do Espírito Santo*. Dissertação de Mestrado, Instituto de Geociências, Universidade Federal de Minas Gerais, Belo Horizonte, 138 p.

Bitencourt C.N., Cruz S.C.P., dos Anjos Cruz V., Pedrosa-Soares A.C., Paquette, J.L., Alkmim A.R., Barbosa J.S.F. 2019. Rifting events in the southern sector of the Paramirim Aulacogen, NE Brazil: new geochronological data and correlations for the São Francisco – Congo paleocontinent. *Precambriam Research*, **326:**417-446.

Campos C.P, Medeiros S.R., Mendes J.C, Pedrosa-Soares A.C., Dussin I., Ludka I.P., Dantas E.L. 2016. Cambro-Ordovician magmatism in the Araçuaí Belt (SE Brazil): Snapshots from a post-collisional event. *Journal of South American Earth Sciences,* **68:**248-268.

Castro M.P., Queiroga G., Martins M., Alkmim F., Pedrosa-Soares A., Dussin I., Souza M.E. 2019. An Early Tonian rifting event affecting the São Francisco-Congo paleocontinent recorded by the Lower Macaúbas Group, Araçuaí Orogen, SE Brazil. *Precambriam Research,* **331**: 105351.

Chaves A.O., Ernst R.E., Söderlund U., Wang X., Naeraa T. 2019. The 920-900-Ma Bahia-Gangila LIP of the São Francisco and Congo cratons and link with Dashigou-Chulan LIP of North China craton: New insights from U-Pb geochronology and geochemistry. *Precambrian Research,* **329:**124-137.

Chemale Jr. F., Dussin I.A., Alkmim F.F., Martins M.S., Queiroga G.N., Armstrong R., Santos M.N. 2012. Unravelling a Proterozoic basin history through detrital zircon geochronology: the case of the Espinhaço Supergroup, Minas Gerais, Brazil. *Gondwana Research*, **22:**200-206.

Cordani U.G., Melcher G.C., Almeida F.F.M. 1968. Outline of the Precambrian Geochronology of South America. *Canadian Journal of Earth Sciences*, **5:**629-632.

Cordani U.G. 1973. *Evolução Geotectônica da Região Costeira do Brasil, entre Salvador e Vitória*. Tese de Livre Docência, Instituto de Geociências, Universidade de São Paulo, São Paulo, 97 p.

Cordani U.G., Brito Neves B.B., D'Agrella M.S., Trindade R.I.F. 2003. Tearing-up Rodinia: the Neoproterozoic paleogeography of South American cratonic fragments. *Terra Nova*, **15**:343-349.

Cordani U.G. 2017. O Cráton do São Francisco e as faixas brasilianas: meio século de avanços. In: Geosudeste 2017, Diamantina, SBG-MG, *Anais*.

Corrales F.F.P., Dussin I.A., Heilbron M., Bruno H., Bersan S., Valeriano C.M., Pedrosa-Soares A.C., Tedeschi M. 2020. Coeval high Ba-Sr arc-related and OIB Neoproterozoic rocks linking pre-collisional magmatism of the Ribeira and Araçuaí orogenic belts, SE-Brazil. *Precambriam Research,* **337:**1-52.

Degler R., Pedrosa-Soares A., Dussin I., Queiroga G., Schulz B. 2017. Contrasting provenance and timing of metamorphism from paragneisses of the Araçuaí-Ribeira orogenic system, Brazil: Hints for Western Gondwana assembly. *Gondwana Research,* **51:**30-50.

Degler R., Pedrosa-Soares A., Novo T., Tedeschi M., Silva L.C., Dussin I., Lana C. 2018. Rhyacian-Orosirian isotopic records from the basement of the Araçuaí-Ribeira orogenic system (SE Brazil): Links in the Congo-São Francisco palaeocontinent. *Precambrian Research,* **317:**179-195.

Degler R., Costa A.G., Pedrosa-Soares A.C., Queiroga G. 2019. High-pressure metamorphism related to suture zone in the Araçuaí orogen (SE Brazil): Further evidence against ensialic models. In: XVII Simpósio Nacional de Estudos Tectônicos, SBG, Bento Gonçalves, *Anais*, p. 124.

Deluca C. 2018. *Evolução do Batólito Itaporé e rochas encaixantes, Orógeno Araçuaí (MG): geoquímica, geocronologia e petrogênese*. Dissertação de Mestrado, Instituto de Geociências, Universidade Federal de Minas Gerais, Belo Horizonte, 116 p.

Deluca C., Pedrosa-Soares A., Lima S., Cordani U., Sato K. 2019. Provenance of the Ediacaran Salinas Formation (Araçuaí Orogen, Brazil): Clues from lithochemical data and zircon U-Pb (SHRIMP) ages of volcanic clasts. *Brazilian Journal of Geology*, **49:**1-19.

Dussin I.A. 2017. *Geocronologia U-Pb e Lu-Hf em zircão, aplicada às bacias proterozóicas*. Moldova, Novas Edições Acadêmicas - ICS Morebooks, 114 p.

Evans D., Trindade R., Catelani E., D'Ágrella-Filho M., Heaman L., Oliveira E., Söderlund U., Ernst R., Smirnov A., Salminen J. 2015. Return to Rodinia? Moderate to high palaeolatitude of the São Francisco-Congo craton at 920 Ma. London. *Geological Society of London Special Publication*, **424:**167-190.

Figueiredo M.C.H. & Campos Neto M.C. 1993. Geochemistry of the Rio Doce magmatic arc, Southeastern Brazil. *Anais da Academia Brasileira de Ciências,* **65:**63-81.

Figueiredo C.M.S. 2009. *O Arco Magmático Brasiliano na conexão entre os orógenos Araçuaí e Ribeira, Região de Muriaé-MG*. Tese de Doutorado, Universidade Federal de Minas Gerais, Belo Horizonte, 103p.

Gonçalves-Dias T., Pedrosa-Soares A.C., Dussin I.A., de Alkmim F.F., Caxito F.A., Silva L.C., Noce C.M. 2011. Idade máxima de sedimentação e proveniência do Complexo Jequitinhonha na área-tipo (Orógeno Araçuaí): primeiros dados U-Pb (La-ICP-MS) de grãos detríticos de zircão. *Geonomos*, **19:**121-130.

Gonçalves-Dias T., Caxito F.A., Pedrosa-Soares A.C., Stevenson R., Dussin I., Silva L.C., Alkmim F., Pimentel M. 2016. Age, provenance and tectonic setting of the high-grade Jequitinhonha Complex, Araçuaí orogen, eastern Brazil. *Brazilian Journal of Geology*, **46:**199-219.

Gonçalves L., Farina F., Lana C., Pedrosa-Soares A.C., Alkmim F., Nalini Jr. H.A. 2014. New U–Pb ages and lithochemical attributes of the Ediacaran Rio Doce magmatic arc, Araçuaí confined orogen, Southeastern Brazil. *Journal of South American Earth Sciences,* **52:**129-148.

Gonçalves L., Alkmim F.F., Pedrosa-Soares A.C., Dussin I.A., Valeriano C.M., Lana C., Tedeschi M. 2016. Granites of the intracontinental termination of a magmatic arc: an example from the Ediacaran Araçuaí orogen, southeastern Brazil. *Gondwana Research*, **36:**439-458.

Gonçalves L., Alkmim F.F., Pedrosa-Soares A.C., Gonçalves C.C., Vieira V. 2018. From the plutonic root to the volcanic roof of a continental magmatic arc: a review of the Neoproterozoic Araçuaí orogen, southeastern Brazil. *International Journal of Earth Science (Geologische Rundschau),* **107:**337-358.

Gonçalves G., Lana C., Buick I., Alkmim F., Scholz R., Queiroga G. 2019. Twenty million years of post-orogenic fluid production and hydrothermal mineralization across the external Araçuaí orogen and adjacent São Francisco Craton, SE Brazil. *Lithos,* **342-343:**557-572.

Gradim C.T. 2013. *Complexo Nova Venécia e magmatismo associado, Orógeno Araçuaí, Estado do Espírito Santo*. Dissertação de Mestrado, Instituto de Geociências, Universidade Federal de Minas Gerais, Belo Horizonte, 123 p.

Gradim C., Roncato J., Pedrosa-Soares A.C., Cordani U.G., Dussin I., Alkmim F.F., Queiroga G., Jacobsohn T., Silva L.C., Babinski M. 2014. The hot back-arc zone of the Araçuaí Orogen, Eastern Brazil: from sedimentation to granite generation. *Brazilian Journal of Geology*, **44:**155-180.

Hurley P.M., Almeida F.F.M., Melcher G.C., Cordani U.G., Rand J.R., Kawashita K., Vandoros P. Pinson W.H., Fairbairn H. 1967. Test of continental drift by comparison of radiometric ages. *Science,* **157:**495-500.

Heilbron M., Cordani U.G, Alkmim F.F. (eds.) 2017. *São Francisco craton, eastern Brazil. Tectonic genealogy of a miniature continent*. Regional Geology Reviews, Switzerland, Springer International Publishing Co, 331 p..

Kuchenbecker M. 2014. *Relações entre coberturas do Cráton do São Francisco e bacias situadas em orógenos marginais: O registro de datações U-Pb de grãos detríticos de zircão e suas implicações geotectônicas.* Tese de Doutorado, Universidade Federal de Minas Gerais, Belo Horizonte, 173p.

Kuchenbecker M., Pedrosa-Soares A.C., Babinski M., Fanning M. 2015. Detrital zircon age patterns and provenance assessment for pre-glacial to post-glacial successions of the Neoproterozoic Macaúbas Group, Araçuaí Orogen, Brazil. *Precambriam Research*, **266:**12-26.

Lima S.A.A., Martins-Neto M.A., Pedrosa-Soares A.C., Cordani U.G., Nutman A. 2002. A Formação Salinas na área-tipo, NE de Minas Gerais: Uma proposta de revisão da estratigrafia da Faixa Araçuaí com base em evidências sedimentares, metamórficas e idades U-Pb SHRIMP. *Revista Brasileira de Geociências*, **32**:491-500.

Magalhães J.R., Pedrosa-Soares A., Dussin I., Müntener O., Pinheiro M.A.P., Silva L.C., Knauer L.G., Bouvier A.S., Baumgartner L. 2018. First Lu-Hf, $\delta^{18}O$ and trace elements in zircon signatures from the Statherian Espinhaço anorogenic province (Eastern Brazil): geotectonic implications of a silicic large igneous province. *Brazilian Journal of Geology,* **48:**735-759.

Martins M., Karfunkel J., Noce C.M., Babinski M., Pedrosa-Soares A.C., Sial A.N., Liu D. 2008. A sequência pré-glacial do Grupo Macaúbas na área-tipo e o registro da abertura do rifte Araçuaí. *Revista Brasileira de Geociências,* **38:**761-772.

Mello F.M. 2000. *Litogeoquímica* e Química Mineral do Maciço *Charnockítico Aimorés-MG*. Tese de Doutorado, Universidade de São Paulo, São Paulo, 167 p.

Melo M.G., Lana C., Stevens G., Pedrosa-Soares A.C., Gerdes A., Alkmin L.A., Nalini Jr. H.A., Alkmim

F.F. 2017. Assessing the isotopic evolution of S-type granites of the Carlos Chagas batholith, SE Brazil: Clues from U-Pb, Hf isotopes, Ti geothermometry and trace element composition of zircon. *Lithos*, **284-285:**730-750.

Mendes J.C., Medeiros S.R., McReath I., De Campos C.M.P. 2005. Cambro-Ordovician magmatism in SE Brazil: U-Pb and Rb-Sr ages, combined with Sr and Nd isotopic data of Charnockitic rocks from the Várzea Alegre complex. *Gondwana Research,* **8:**337-345.

Mondou M., Egydio-Silva M., Vauchez A., Raposo M.I.B., Bruguier O., Oliveira A.F. 2012. Complex, 3D strain patterns in a synkinematic tonalite batholith from the Araçuaí Neoproterozoic orogen (Eastern Brazil): evidence from combined magnetic and isotopic chronology studies. *Journal of Structural Geology,* **39:**158-179.

Nalini H.A. 1997. Caractérisation des suites magmatiques néoprotérozoïques de la région de Conselheiro Pena et Galiléia (Minas Gerais, Brésil): étude géochimique et structurale des suites Galiléia et Urucum et leur relation avec les pegmatites à éléments rares associées. Thèse de Doctorat, École des Mines de Saint-Étienne et École des Mines de Paris, Saint-Étienne, 395 p.

Nalini H.A., Bilal E., Paquette J.L., Pin C., Machado R. 2000a. Geochronologie U-Pb et géochimie isotopique Sr-Nd des granitoides neoproterozoiques des suites Galileia et Urucum, vallée du Rio Doce, Sud -Est du Brésil. *Compte Rendu Academie Science Paris*, **331**:459-466.

Nalini H. A., Bilal E., Correia-Neves J.M. 2000b. Syncollisional peraluminous magmatism in the Rio Doce region: mineralogy, geochemistry and isotopic data of the Urucum suite (eastern Minas Gerais State, Brazil). *Revista Brasileira de Geociências*, **30**:120-125.

Noce C.M., Macambira M.B., Pedrosa-Soares A.C. 2000. Chronology of Neoproterozoic-Cambrian granitic magmatism in the Araçuaí Belt, Eastern Brazil, based on single zircon evaporation dating. *Revista Brasileira de Geociências*, **30**:25-29.

Noce C.M, Pedrosa-Soares A.C., Piuzana D., Armstrong R., Laux J.H., Campos C.M., Medeiros S.R. 2004. Ages of sedimentation of the kinzigitic complex and of a late orogenic thermal episode in the Araçuaí orogen, northern Espírito Santo State, Brazil: Zircon and monazite U-Pb SHRIMP and ID-TIMS data. *Revista Brasileira de Geociências*, **349**:587-592.

Noce C.M., Figueiredo C.M., Novo T.A., Pedrosa-Soares A.C., Alkmim F.F., Silva L.C., Dussin I., Armstrong R. 2010. The southern segment of the Araçuaí magmatic arc (SE Brazil): U-Pb zircon dating and implications for geodynamic reconstructions of the pre-collisional. In: South American Symposium on Isotope Geology. Brasília. *Short papers*, CD-ROM.

Novo T.A., Pedrosa-Soares A.C., Noce C.M., Alkmim F.F., Dussin I.A. 2010. Rochas charnockíticas do sudeste de Minas Gerais: a raiz granulítica do arco magmático do Orógeno Araçuaí. *Revista Brasileira de Geociências,* **40:**573-592.

Novo T.A. 2013. *Caracterização do Complexo Pocrane, magmatismo básico mesoproterozóico e unidades neoproterozóicas do sistema Araçuaí-Ribeira, com ênfase em geocronologia U-Pb (SHRIMP e LA-ICP-MS)*. Tese de Doutorado, Universidade Federal de Minas Gerais, Belo Horizonte, 193 p.

Novo T.A., Pedrosa-Soares A., Vieira V.S., Dussin I., Silva L.C. 2018. The Rio Doce Group revisited: An Ediacaran arc-related volcano-sedimentary basin, Araçuaí orogen (SE Brazil). *Journal of South American Earth Sciences,* **85:**345-361.

Paes V.J.C. 1999. *Geologia e Geoquímica da Região de Alvarenga, Minas Gerais: implicações geotectônicas e metalogenéticas*. Tese de Doutorado, Universidade Federal de Minas Gerais, Belo Horizonte.

Paes V.J.C., Raposo F.O., Pinto C.P., Oliveira F.A.R. (orgs.) 2010. Projeto Jequitinhonha, Estados de Minas Gerais e Bahia: texto explicativo. Geologia e Recursos Minerais das Folhas Comercinho, Jequitinhonha, Almenara, Itaobim, Joaíma e Rio do Prado. Programa Geologia do Brasil. Belo Horizonte, CPRM – Serviço Geológico do Brasil.

Pedrosa-Soares A.C., Noce C.M., Vidal P., Monteiro R., Leonardos O.H. 1992. Toward a new tectonic model for the Late Proterzoic Araçuaí (SE Brazil) - West Congolian (SW Africa) Belt. *Journal of South American Earth Sciences*, **6**:33-47.

Pedrosa-Soares A.C. 1995. *Potencial aurífero do Vale do Araçuaí, Minas Gerais: história da exploração, geologia e controle tectono-metamórfico*. Tese de Doutorado, IG-UnB, Brasília.

Pedrosa-Soares A.C., Vidal P., Leonardos O.H., Brito Neves B.B. 1998. Neoproterozoic oceanic remnants in eastern Brazil: Further evidence and refutation of an exclusively ensialic evolution for the Araçuaí-West Congo orogen. *Geology*, **26**:519-522.

Pedrosa-Soares, A.C. & Wiedemann-Leonardos, C.M. 2000. Evolution of the Araçuaí Belt and its connection to the Ribeira Belt, Eastern Brazil. In: Cordani U.G., Milani E.J., Thomaz-Filho A., Campos D.A. (eds.). *Tectonic Evolution of South America*. São Paulo, Sociedade Brasileira de Geologia, p. 265-285.

Pedrosa-Soares A.C., Cordani U., Nutman A. 2000. Constraining the age of Neoproterozoic glaciation in eastern Brazil: First U-Pb SHRIMP data from detrital zircons. *Revista Brasileira de Geociências*, **30**:58-61.

Pedrosa-Soares A.C., Noce C.M., Wiedemann C.M., Pinto C.P. 2001. The Araçuaí–West Congo orogen in Brazil: An overview of a confined orogen formed during Gondwanland assembly. *Precambrian Research*, **110**:307-323.

Pedrosa-Soares A.C., Noce C.M., Alkmim F.F., Silva L.C., Babinski M., Cordani U.G., Castañeda C. 2007. Orógeno Araçuaí: síntese do conhecimento 30 anos após Almeida 1977. *Geonomos*, **15**:1-16.

Pedrosa-Soares A.C., Alkmim F.F., Tack L., Noce C.M., Babinski M., Silva L.C., Martins-Neto M.A. 2008. Similarities and differences between the Brazilian and African counterparts of the Neoproterozoic Araçuaí-West-Congo orogen. *Geological Society of London Special Publication,* **294:**153-172.

Pedrosa-Soares A.C., Babinski M., Noce C., Martins M., Queiroga G., Vilela F.T. 2011a. The Neoproterozoic Macaúbas Group (Araçuaí orogen, SE Brazil) with emphasis on the diamictite formations. In: Arnaud E., Halverson G. P., Shields-Zhou G. (eds). The Geological

Record of Neoproterozoic Glaciations. *Geological Society of London, Memoir,* **36**(49):523-534.

Pedrosa-Soares A.C., De Campos C.P., Noce C.M., Silva L.C., Novo T., Roncato J., Medeiros S., Castañeda C., Queiroga G., Dantas E., Dussin I., Alkmim F. 2011b. Late Neoproterozoic-Cambrian Granitic Magmatism in the Araçuaí Orogen (Brazil), the Eastern Brazilian Pegmatite Province and Related Mineral Resources. In: Sial, A.N., Bettencourt, J.S., De Campos, C.P., Ferreira, V.P. (eds.), Granite-Related Ore Deposits. *Geological Society of London*, *Special Publication,* **350:**25-51.

Pedrosa-Soares A.C. & Alkmim F.F. 2011. How many rifting events preceded the development of the Araçuaí-West Congo orogen? *Geonomos,* **12:**244-251.

Pedrosa-Soares A.C., Alkmim F.F., Tack L. 2017. From inland-sea basins to confined orogens: An example from the Neoproterozoic Araçuaí-West Congo orogen and implications for Plate Tectonics. In: William Smith Meeting 2017: Plate Tectonics at 50. London, *Abstracts Book*, p. 75-76.

Peixoto C.A., Heilbron M., Ragatky D., Armstrong R., Dantas E., Valeriano C.M., Simonetti A. 2017. Tectonic evolution of the Juvenile Tonian Serra da Prata magmatic arc in the Ribeira belt, SE Brazil: Implications for early west Gondwana amalgamation. *Precambrian Research*, **302:**221-254.

Peixoto E., Pedrosa-Soares A.C., Alkmim F.F., Dussin I.A. 2015. A suture-related accretionary wedge formed in the Neoproterozoic Araçuaí orogen (SE Brazil) during Western Gondwanaland assembly. *Gondwana Research*, **27:**878-896.

Peixoto E., Alkmim F.F., Pedrosa-Soares A. 2018. The Rio Pardo salient, northern Araçuaí orogen: an example of a complex basin-controlled fold-thrust belt curve. Brazilian *Journal of Geology,* **48:**25-49.

Petitgirard S., Vauchez A., Egydio-Silva M., Bruguier O., Camps P., Monié P., Babinski M., Mondou M. 2009. Conflicting structural and geochronological data from the Ibituruna quartz-syenite (SE Brazil): effect of protracted "hot" orogeny and slow cooling rate? *Tectonophysics,* **477:**174-196.

Pinto C.P., Drumond J.B.V., Féboli W.L. (coord.) 2001. *Projeto Leste, Etapas 1 e 2*. Belo Horizonte, CPRM-COMIG, CD-ROM.

Queiroga G.N. 2010. *Caracterização de restos de litosfera oceânica do Orógeno Araçuaí entre os paralelos 17 e 21 S*. Tese de Doutorado, Instituto de Geociências, Universidade Federal de Minas Gerais, Belo Horizonte.

Richter F., Lana C., Steven G., Buick I., Pedrosa-Soares A.C., Alkmim F.F., Cutts K. 2016. Sedimentation, metamorphism and granite generation in a back-arc region: Records from the Ediacaran Nova Venécia Complex (Araçuaí Orogen, Southeastern Brazil). *Precambrian Research,* **272:**78-100.

Rogers J.W. & Santosh M. 2004. *Continents and Supercontinents*. Oxford University Press, 289 p.

Roncato J.G. 2009. *As suítes graníticas tipo-S do norte do Espírito Santo na região das folhas Ecoporanga, Mantena, Montanha e Nova Venécia*. Dissertação de Mestrado, Instituto de Geociências, Universidade Federal de Minas Gerais, Belo Horizonte, 102 p.

Rosa M.L., Conceição H., Macambira M.J.B., Galarza M.A., Cunha M.P., Menezes R.C.L., Marinho M.M., Filho B.E.d.C., Rios D.C. 2007. Neoproterozoic anorogenic magmatism in the Southern Bahia Alkaline Province of NE Brazil: U–Pb and Pb-Pb ages of the blue sodalite syenites. *Lithos,* **97:**88-97.

Schannor M., Lana C., Fonseca M. 2019. São Francisco-Congo Craton break-up delimited by U-Pb-Hf isotopes and trace-elements of zircon from metasediments of the Araçuaí Belt. *Geoscience Frontiers,* **10:**611-628.

Serrano P., Pedrosa-Soares A., Medeiros-Junior E., Fonte-Boa T., Araujo C., Dussin I., Queiroga G., Lana C. 2018. A-type Medina batholith and post-collisional anatexis in the Araçuaí orogen (SE Brazil). *Lithos,* **320-321:**515-536.

Siga-Júnior O. 1986. *A evolução geocronológica da porção nordeste de Minas Gerais, com base em interpretações geocronológicas*. Dissertação de Mestrado, IG-USP, São Paulo, 156 p.

Siga Junior O., Cordani U.G., Basei M.A.S., Teixeira W., Kawashita K., Schmus W.V. 1987. Trabalho Completo - Contribuição ao Estudo Geológico-Geocronológico da Porção Nordeste de Minas Gerais. In: IV Simpósio de Geologia, 1987, Belo Horizonte - MG. *Anais,* v. 7., p. 29-44.

Silva L.C., Armstrong R, Noce C.M., Carneiro M., Pimentel M., Pedrosa-Soares A.C., Leite C., Vieira V.S., Silva M., Paes V., Cardoso-Filho J. 2002. Reavaliação da evolução geológica em terrenos précambrianos brasileiros com base em novos dados U-Pb SHRIMP, parte II: Orógeno Araçuaí, Cinturão Móvel Mineiro e Cráton São Francisco Meridional. *Revista Brasileira de Geociências*, **32**:513-528.

Silva L.C., McNaughton N.J., Armstrong R., Hartmann L., Fletcher I. 2005. The Neoproterozoic Mantiqueira Province and its African connections. *Precambrian Research*, **136**:203-240.

Silva L.C., Pinto C.P., Gomes A.C.B, Paes V. 2007. Geocronologia U-Pb (LA-ICP-MS) e a cronoestratigrafia granítica no segmento NE do Orógeno Araçuaí, MG. In: 10º. Simpósio de Geologia do Sudeste. Diamantina, SBG-MG, *Resumos*.

Silva L.C., Pedrosa-Soares A.C., Teixeira L.R. 2008. Tonian rift-related, A-type continental plutonism in the Araçuaí orogen, Eastern Brazil: new evidences for the breakup stage of the São Francisco-Congo Paleocontinent. *Gondwana Research*, **13:**527-537.

Silva L.C. da, Pedrosa-Soares A., Noce C.M., Pinto C.M., Paes V, J.C., Gonçalves-Dias T., Chemale Jr. F. 2010. LA-ICP-MS and TIMS U-Pb geochronology and the tectonic significance of a number of calc-alkaline and S-type plutons from the Araçuaí Orogen (SE Brazil). In: VII South American Symposium on Isotope Geology. Brasília, *Short Papers*, p. 530-533.

Silva L.C., Pedrosa-Soares A.C., Armstrong R., Noce C.M. 2011. Determinando a duração do período colisional do Orógeno Araçuaí com base em geocronologia U–Pb de alta resolução em zircão: uma contribuição para a história da amalgamação do Gondwana Ocidental. *Geonomos,* **19:**180-197.

Söllner H.S., Lammerer B., Weber-Diefenbach K. 1991. Die Krustenentwicklung in der Küstenregion nördlich von Rio de Janeiro, Brasilien. *Müncher Geologische Hefte*, **4**:1-100.

Söllner F., Lammerer B., Wiedemann-Leonardos C. 2000. Dating the Ribeira Mobile Belt of Brazil. In: Sonderheft, Zeitschrift Angwandte Geologie, p. 245-255.

Souza M.E., Martins M.S., Queiroga G.N., Leite M., Oliveira R.G., Dussin I., Pedrosa-Soares A.C. 2019. Paleoenviroment, sediment provenance and tectonic setting of Tonian basal deposits of the Macaúbas basin system, Araçuaí orogen, southeast Brazil. Journal of *South American Earth Sciences,* **96:**1-19.

Straathof G.B. 2011. *Neoproterozoic Low Latitude Glaciations: An African Perspective*. Tese de Doutorado, Universidade de Edinburgo, Edinburgo, 263 p.

Tack L., Wingate M.T.D., De Waele B., Meert J., Belousova E., Griffin B., Tahon A., Fernandez-Alonso M. 2010. The 1375 Ma Kibaran Event in Central Africa: prominent emplacement of bimodal magmatism under extensional regime. *Precambrian Research* **180:**63-84.

Távora FJ., Cordani UG., Kawashita K. 1967. Determinações de idade K-Ar em rochas da região central da Bahia. In: 21º Congresso Brasileiro de Geologia. Curitiba. SBG, *Anais,* p. 234-244.

Tedeschi M., Novo T., Pedrosa-Soares A., Dussin I., Tassinari C., Silva L.C., Gonçalves L., Alkmim F., Lana C., Figueiredo C., Dantas E., Medeiros S., De Campos C., Corrales F., Heilbron M. 2016. The Ediacaran Rio Doce magmatic arc revisited (Araçuaí-Ribeira orogenic system, SE Brazil). *Journal of South American Earth Sciences,* **68:**167-186.

Teixeira W., Kamo S.L., Arcanjo J.B.A. 1997. U–Pb zircon and baddeleyte age and tectonic interpretation of the Itabuna alkaline suite, São Francisco Craton, Brazil. *Journal of South America Earth Sciences,* **10:**91-98.

Thiéblemont D., Castaing C., Billa M., Bouton P., Préat A. 2009. *Notice explicative de la carte géologique et des ressources minérales de la République gabonaise à 1/1,000,000*. Libreville, Editions DGMG - Ministère des Mines, du Pétrole, des Hydrocarbures, 384 p.

Torquato J.R. & Cordani U.G. 1981. Brazil-Africa geological links. *Earth Science Reviews*, **17**:155-176.

Tupinambá M., Heilbron M., Valeriano C.M., Porto Jr. R., Blanco de Dios F., Machado N., Silva L.G.E., Almeida J.C.H. 2012. Juvenile contribution of the Neoproterozoic Rio Negro magmatic arc (Ribeira Belt, Brazil): implications for western Gondwana amalgamation. *Gondwana Research,* **21:**422-438

Vauchez A., Egydio-Silva M., Babinski M., Tommasi A., Uhlein A., Liu D. 2007. Deformation of a pervasively molten middle crust: insights from the Neoproterozoic Ribeira-Araçuaí orogen (SE Brazil). *Terra Nova*, **19**:278-286.

Victoria A.M., Pedrosa-Soares A., Cruz S.C.P. 2019. Os riftes neoproterozoicos precursores ao Orógeno Araçuaí – Congo Ocidental: atualização dos limites de tempo com base em idades (U-Pb e Pb-Pb) do magmatismo anorogênico. In: XVII Simpósio Nacional de Estudos Tectônicos. Bento Gonçalves, SBG, *Anais*, p. 111.

Vieira V.S. 2007. *Significado do Grupo Rio Doce no Contexto do Orógeno Araçuaí*. Tese de Doutorado, Instituto de Geociências, Universidade Federal de Minas Gerais, Belo Horizonte.

Vieira P.L., Queiroga G.N., Novo T.A., Pedrosa-Soares A.C., Lana C. 2019. Ultrahigh Temperature (UHT) Metamorphic Rocks from the Araçuaí Orogen, Southeastern Brazil: Tectonic implications from petrography, thermobarometry and phase-equilibria modeling. In: XVII Simpósio Nacional de Estudos Tectônicos. Bento Gonçalves, SBG, *Anais,* p.133.

Vilela F.T., Pedrosa-Soares A.C., Carvalho M.T., Arimatéia R., Santos E., Voll E. 2014. Metalogênese da Faixa Araçuaí: O Distrito Ferrífero Nova Aurora (Grupo Macaúbas, Norte de Minas Gerais) no contexto dos recursos minerais do Orógeno Araçuaí. In: Silva M.G., Rocha-Neto M.B., Jost H., Kuyumjian R.M. (orgs.). *Metalogênese das Províncias Tectônicas Brasileiras*, Belo Horizonte, CPRM-Serviço Geológico do Brasil, p. 415-430.

Xavier B.C. 2017. *Relações tectônicas no setor central da Faixa Araçuaí: Análise Estrutural por ASM e Geocronologia U-Pb e Lu-Hf.* Dissertação de Mestrado, Universidade de São Paulo, São Paulo, 123 p.

Wiedemann C.M., Campos C.M., Medeiros S.R., Mendes J.C., Ludka I.P., Moura J.C. 2002. Architecture of late orogenic Plutons in the Araçuaí-Ribeira Folded Belt, Southeast Brazil. *Gondwana Research*, **19**:381-399.